

DARK MATTER

Editors :
J. Audouze
J. Tran Thanh Van

Associated editor :
M. C. Pelletan

XXIIIrd Rencontre de Moriond

Les Arcs, Savoie, France - March 8-15, 1988

DARK MATTER

Series : Moriond Meetings - Astrophysics Session

Copyright 1988 by Editions Frontières
ISBN 2-86332-57-2

All rights reserved. This book, or parts thereof, may not be reproduced in any form or by any means, electronic or mechanical, including photocopying, recording or any information storage and retrieval system now known or to be invented, without written permission from the Publisher.

EDITIONS FRONTIERES

B. P. 33

91192 Gif-sur-Yvette Cedex - France

Printed in Singapore by Kim Hup Lee Printing Co. Pte. Ltd.

18820

iii

Proceedings of the XXIIIrd RENCONTRE DE MORIOND

Series : Moriond Astrophysics Meetings, 1988, Les Arcs, France

Les Arcs, Savoie, France

March 8-15, 1988

DARK MATTER

edited by

J. AUDOUZE

and

J. TRAN THANH VAN

C
E 89 / 215
CERN
BIBLIOTHEQUE
539.12
REN

Editions Frontières

The Astrophysics Session of the Twenty-third Rencontre de Moriond

DARK MATTER

was organized by

J. Audouze
J. Tran Thanh Van

with the active collaboration of :

C. J. Cesarsky
P. Crane
T. Gaisser
D. Hegyi
C. Norman
and J. Truran

AVANT-PROPOS

Cet ouvrage constitue le compte-rendu de l'atelier sur la "Matière Noire" qui s'est tenu aux Arcs en mars 1988 et qui est donc le huitième "Moriond Astrophysics Workshop". Je souhaite souligner le fait que la présence sur le même site des astrophysiciens spécialistes en cosmologie et des physiciens des particules capables de proposer des expériences susceptibles de détecter cette matière "invisible" a donné un caractère tout à fait unique, voire irremplaçable à cette rencontre.

Le livre commence donc par les articles et communications consacrés à la recherche expérimentale des "signatures" de cette matière invisible qui conditionne l'évolution de l'univers dans son ensemble. Après les deux brillants exposés introductifs, une série d'articles permettent de faire le point sur les techniques qui sont envisagées dans cette recherche expérimentale : détecteurs très refroidis, billes supraconductrices, etc.... On peut constater à cette lecture combien les différents projets sont élaborés et prometteurs. Un véritable dialogue sur ces recherches expérimentales s'est donc établi entre les physiciens des particules et les astrophysiciens.

Après le rapport des progrès effectués par les physiciens des particules, c'est au tour des astrophysiciens de faire le point de la situation.

La deuxième partie du livre est consacrée à l'analyse des fonds diffus à différentes énergies ainsi qu'à l'évocation du rôle possible des flux froids de matière dans la constitution de halos galactiques massifs.

Toute recherche de matière sombre passe nécessairement par l'analyse des distributions spatiales des grandes structures de l'Univers. La troisième partie débute par le rapport de quelques travaux observationnels sur ce sujet. Ces contributions sont suivies d'une série d'analyses et d'interprétations statistiques de ces distributions principalement dans le cadre d'univers dominés par la matière sombre froide. Cette partie se termine par une contribution qui passe en revue les déterminations des distributions spatiales des quasars.

La présence de matière sombre doit se signaler à la fois sur le plan local et dans les halos de galaxies. Les contributions rassemblées dans la quatrième partie sont consacrées à ces recherches de matière sombre "locale".

La nucléosynthèse primordiale constitue un moyen particulièrement puissant pour fixer des limites contraignantes sur la densité de matière baryonique. Même lorsque l'on tient compte des inhomogénéités possibles susceptibles d'être induites par la transition quark-hadron évoquée par plusieurs contributions, cette densité reste faible par rapport à celle que l'on peut déduire des modèles dynamiques des grandes structures ou des théories inflationnaires.

Trois sujets intéressent actuellement l'ensemble de la communauté des physiciens des particules et des cosmologistes. Il s'agit des lentilles gravitationnelles, des cordes et solitons ainsi que de l'effet des WIMPS (particules interagissant très faiblement avec la matière ordinaire) sur l'évolution stellaire. Les meilleurs spécialistes sur ces sujets étaient présents à Moriond et ce fut un grand plaisir d'entendre et maintenant de lire leurs contributions.

L'année 1987 fut l'année de la supernova 1987 A. Cette supernova constitue le premier évènement astronomique qui laissa une signature claire dans des détecteurs souterrains. Dans la dernière partie qui lui est consacrée, plusieurs contributions relatent l'usage que l'on peut en faire (ainsi que d'autres supernovae) vis à vis de la détection de cette matière sombre encore mystérieuse.

Cette réunion et j'espère ce livre auront permis de faire le point sur l'un des sujets les plus intéressants de la cosmologie moderne. C'est aussi celui où les astrophysiciens peuvent nouer des collaborations très utiles et fécondes avec les physiciens des particules. Dans l'atmosphère particulièrement chaleureuse des réunions de Moriond le dialogue s'est bien engagé ainsi que le montre ce livre.

Le succès de cette rencontre est indéniablement dû à l'infatigable activité et le talent de J. Tran Thanh Van de savoir faire dialoguer plusieurs communautés scientifiques dans un environnement particulièrement agréable. Les membres du comité scientifique international ont bien voulu continuer à m'aider. Plusieurs de leurs contributions au programme de cette rencontre furent essentielles. Les auteurs des contributions rassemblées ici doivent également être remerciés pour le soin et la célérité avec lesquels il préparèrent leurs manuscrits. Nous avons bénéficié d'une aide financière du CNRS (en particulier à travers le PICS n^o 18) et de la NASA. Je voudrais remercier chaleureusement Marie-Christine Pelletan qui m'a apporté toute son aide à l'organisation de cette rencontre et à l'édition de ce livre sans oublier Lucienne Norry et Nicole Mathieu nos complices de toujours.

Jean AUDOUZE

FOREWORD

This book constitutes the proceedings of the eight Moriond Astrophysics Workshop which took place in March 1988 at Les Arcs and which was devoted to the search of "Dark Matter" in the Universe. I would like to emphasize that the interaction between the astrophysicists specialists in cosmology and particle physicists able to set up some experiments aiming to detect this "invisible" matter confers to this conference its quite unique and unforgettable characteristics.

The book begins with the papers devoted to the experimental search of "signatures" of the dark matter which governs the evolution of the Universe as a whole. After the two brilliant introductory papers, a series of contributions describe the presently considered experimental techniques (cryogenic detectors, supraconducting detectors ...). The reading of this chapter shows how the present experiments are carefully elaborated and most promising. A real dialogue concerning these techniques has been instaurated between particle physicists and astrophysicists.

After the progress report of the particle physicists, the book provide the reader with an updated situation concerning the research in cosmology.

The second part of the book is devoted to the analysis of the backgrounds at different energies such as the possible role of the cooling flows in the constitution of massive galactic halos.

Any search of dark matter implies necessarily the analysis of the spatial distributions of the large scale structures of the Universe. The third part of the book starts with the report of a few observational investigations on this topic. This report is followed by a series of statistical analyses of these distributions. These analyses concern mainly universes filled up with cold dark matter. The last paper of this third part concerns the search of clustering in the spatial distribution of QSOs.

The presence of dark matter should affect the solar neighborhood and related to the existence of galactic haloes. The contributions of the fourth part are devoted to the search of such "local" dark matter.

Primordial nucleosynthesis provides a very powerful tool to set up quite constraining limitations on the overall baryonic density. Even if one takes into account the inhomogeneities in density possibly induced by the Quark-Hadron transition, this baryonic density should be much lower than the overall density deduced from the dynamical models of Universe or the inflationary theories.

Three topics excite most the cosmologists today : they concern gravitational lenses, cosmic strings and solitons such as the effect of WIMPS (weak interacting massive particles) on stellar evolution. The most reputed specialists of these three fields were present at Les Arcs and provided us with their interesting contributions.

1987 is the year of SN 1987. This supernova is indeed the first astronomical event which led to a clear cut signature in underground detectors. The last part of the book is devoted to this outstanding event and especially to its possible use to detect this still mysterious dark matter.

This eight Moriond astrophysics meeting (and hopefully this book) provide an opportunity to think about the future of this most fundamental topic. Astrophysicists are ready to collaborate very tightly with particule physicists to unravel the presence and the nature of dark matter. In the most cheerful atmosphere of the Moriond meetings this dialogue has been instaured in a efficient fashion as shown by this book.

During 1987, four most reputed scientists have passed away. They are L. de Broglie, P.A.M. Dirac, R. Feynman and Y.B. Zeldovich. R. Feynman has had a most critical influence on the evolution of particle physics while Y.B. Zeldovich is considered as one of the fathers of modern cosmology. This is why the scientific committes of the Moriond Rencontres have decided to dedicate the proceedings of the Particle Physics Meeting to the memory of R. Feynman and this one to that of Y.B. Zeldovich. Indeed cosmology is like an orphan after the death of the physicist who founded it as a modern scientific discipline. The concepts of hot and cold dark matter have been invented by him. This is why this book which concerns a question which proceeds directly from his most impressive work is dedicated to his memory. Just after these introductory remarks the reader can consult a short notice written up by A. Szalay.

The success of this eight astrophysics rencontre is due to the overwhelming activity and the spectacular talent of Jean Tran Than Van who is able for years to let several different scientific communities interacting to gather in a most profitable and gratifying surroundings. The members of the scientific committee have been instrumental in building up the program of this rencontre. The authors of the various contributions should be thanked for the care and celerity with which they have produced their manuscripts. Last but not least I would like to extend my warmest recognition to Marie-Christine Pelletan who helped me so much in the organization of this meeting and in the edition of the book. I do not forget Lucienne Norry and Nicole Mathieu who add always and so much to the unique atmosphere of Les Arcs.

Yakov Borisovich ZELDOVICH
(1914-1987)

Ya.B. Zeldovich was one of the most illustrious physicists of the modern era.

He started his scientific career working in physical chemistry at the age of 17. He created a model for the propagation of burning waves and explosions. Later he obtained fundamental results in the theory of shock wave propagation, which was published with Raizer in two volumes that have become standard reference works.

He worked for several years on nuclear physics, then published a series of papers in particle physics, on the theory of weak interactions, lepton charge conservation, prediction of neutral heavy mesons, pseudo-conserved axial currents.

He was the first to point out that accretion onto black holes and neutron stars will lead to emission of X-rays. He had several other important results concerning the physics of black holes and neutron stars.

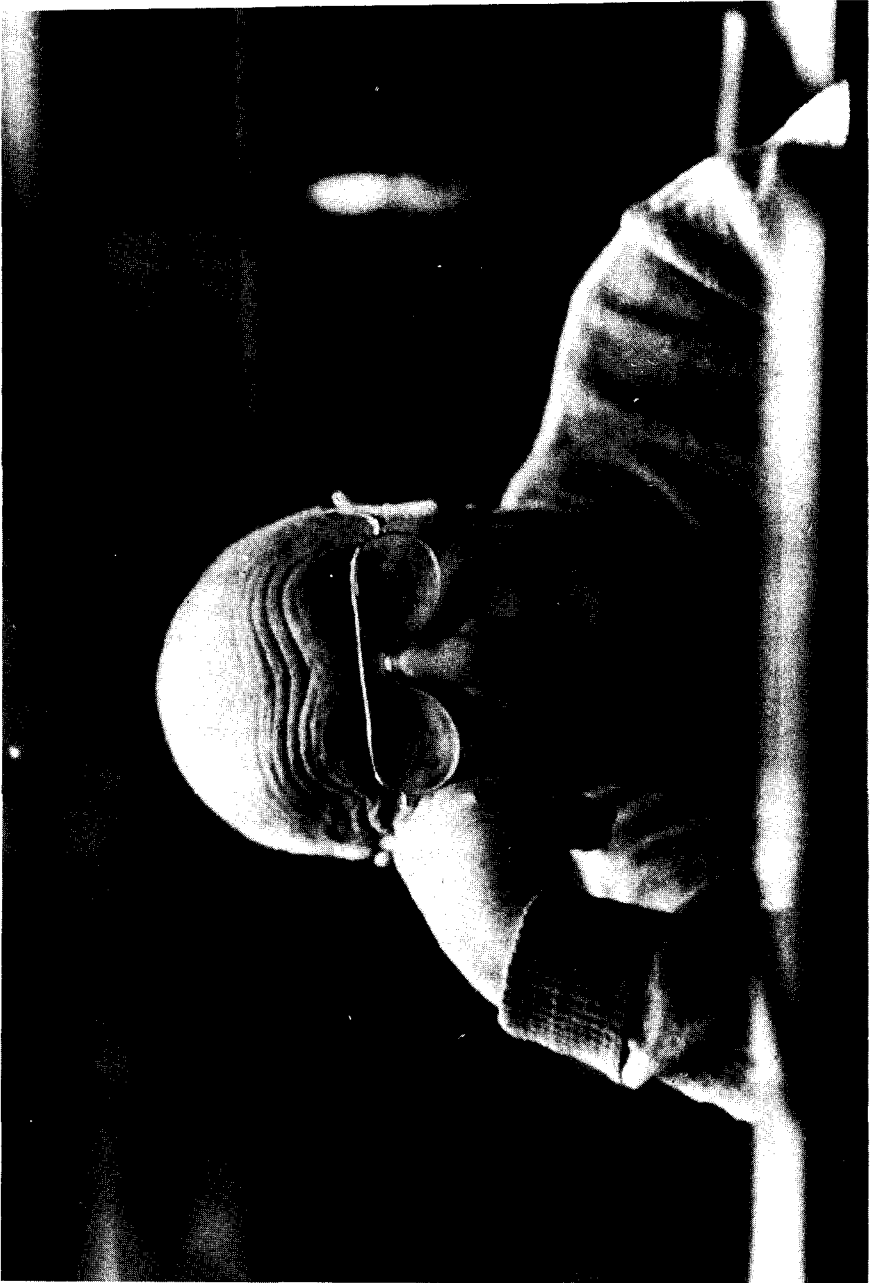
His work in physical cosmology helped enormously to turn it into a real science. He made fundamental connections between particle physics in the early universe and the subsequent stages of evolution. It has been realized over the past few years that as a consequence of inflation the Zeldovich-Harrison spectrum of fluctuations provides an attractive explanation for the origin of large scale structures. He was also one of the first to discuss cosmic strings as an alternate possibility for galaxy formation.

His work on cosmic pancakes and the elegant approximate theory for nonlinear collapse that is recognized as the Zeldovich approximation has generated an enormous advance in our understanding of the large scale structures. His vision of the topology of the universe has guided cosmology for several decades. The collaboration with his student Rashid Sunyaev on the Compton distortions of the microwave background predicted new types of observations, stimulated entire generations of astronomers to pursue these ideas.

He has been a wonderful teacher, sparking with ideas, and igniting everyone around him, to work days and nights on the frontiers of physics. He founded the science of modern cosmology in the Soviet Union. He had a unique career, living through one of the most exciting times in physics ever. His interests spanned the entire range of physics and he left a significant contribution on every subject on which he worked. His papers also reflect his wonderful and warm personality.

The whole physics community, his students, his friends all miss him. Those of us fortunate enough to have had contact with him will never forget his exuberant character and intellectual vigour.

A. SZALAY



CONTENTS

J. AUDOUZE	Avant-propos	v
J. AUDOUZE	Foreword	vii
A. SZALAY	Ya B. Zeldovich	ix
I. SEARCH OF DARK MATTER		1
J. SILK	Strategies for dark matter detection	3
L.M. KRAUSS	Desperately seeking dark matter	23
K.A. OLIVE	Searching for dark matter using underground detectors	33
J. RICH	Direct detection of particle dark matter	43
D.O. CALDWELL, R.M. EISBERG, F.S. GOULDING, D.M. GRUMM, B. SADOULET, A.R. SMITH and M.S. WITHERELL	Dark matter search with a Ge detector	55
B. SADOULET	Detection of dark matter particles with low detectors phonon sensors	63
R.E. LANOU, H.J. MARIS and G.M. SEIDEL	Superfluid helium as a dark matter detector	75
L. GONZALEZ-MESTRES and D. PERRET-GALLIX	Searches for elusive dark matter candidates	85
L. GONZALEZ-MESTRES and D. PERRET-GALLIX	New ideas on the detection of cold dark matter and magnetic monopoles	95
M.A. TARTAGLIA	A search for WIMPS at Fermilab	105
S. DE PANFILIS, A.C. MELISSINOS B. MOSKOWITZ, J. ROGERS, Y. SEMERTZIDIS, W. WUENSCH, H. HALAMA, A. PRODELL, W. FOWLER, F. NEZRICK	Intermediate results from an experiment to detect galactic axions	113

II. BACKGROUNDS AND COOLING FLOWS		121
Y. REPHAEI and G. SMOOT	Cosmological implications from recent spectral measurements of the microwave background radiation	123
R.A. DALY	Implications of the 1 to 10 MeV gamma ray background : a determination of Ω_{\bullet} or a new particle ?	133
K.M. ASHMAN and B.J. CARR	Are dark galactic halos made by cooling flows ?	141
III. LARGE SCALE DISTRIBUTIONS		149
L.N. DA COSTA and P.S. PELLEGRINI	Large scale distribution of galaxies in the southern galactic CAP	151
T.X. THUAN	A 21-cm redshift survey and the large scale distribution of dwarf galaxies	161
P. CRANE and W.C. SASLAW	Gravitational clustering of galaxies in the CfA slice	171
R. SCHAEFFER	The galaxy and matter distribution in the non-linear regime	177
M. LACHIEZE-REY	The statistics of galaxies : beyond correlation functions	187
S. MAUROGORDATO and M. LACHIEZE-REY	Segregations in the galaxy distribution	199
F.R. BOUCHET	Non-linear scale invariance in a cold-dark-matter universe	205
S. COLAFRANCESCO, F. LUCCHIN and S. MATARRESE	The multiplicity function in a cold dark matter universe	211
D. KUNTH	Quasar clustering and cosmology : observational status	219
IV. DARK MATTER IN GALAXIES AND HALOS		229
E. ATHANASSOULA	The effects of baryonic infall on the halo mass distribution in disk galaxies	231
A.C. ROBIN, M. CREZE, and O. BIENAYME	An upper limit to the local dark matter or the missing "missing mass"	239
G.J. MATHEWS, J.J. COWAN, and D.N. SCHRAMM	Evolution of heavy-element abundances in the galactic halo and disk	251

V. DARK MATTER AND PRIMORDIAL NUCLEOSYNTHESIS		259
J.W. HAYWOOD and D.J. HEGYI	A measurement of the primordial abundance using μ Cassiopeiae	261
S. VAUCLAIR	On the primordial Lithium abundance	269
J. AUDOUZE, P. DELBOURGO-SALVADOR and P. SALATI	Primordial nucleosynthesis and particle physics	277
H. REEVES	Lithium and the nature of dark matter	287
G.M. FULLER, G.J. MATHEWS and C.R. ALCOCK	Generation of fluctuations from the quark-hadron transition in the early universe	303
G.J. MATHEWS, G.M. FULLER, C.R. ALCOCK and T. KAJINO	The evolution of baryon number density fluctuations before, during and after primordial nucleosynthesis	319
K.A. OLIVE	On the magnitude of baryon density fluctuations in the quark-hadron transition	329
VI. GRAVITATIONAL LENSES		337
L. NOTTALE	Dark matter and gravitational lensing	339
E.L. TURNER	Dark matter in gravitational lenses	347
R.J. NEMIROFF and A. DEKEL	Probability of elongated galaxy images from cluster lensing	355
VII. STRINGS AND SOLITONS		359
F.R. BOUCHET and D.P. BENNETT	Dynamical evolution of cosmic strings	361
A.L. MELOTT	Glowing hot dark matter with or without strings attached	373
T. PIRAN, J. ORLOFF, and F. ENGLERT	Fundamental cosmic strings and large scale structure formation	381
S.M. BARR	Limiting currents in fermionic conducting cosmic strings	389
G. GELMINI	Solitogenesis, can non topological solitons be the dark matter	393

VIII. STELLAR EVOLUTION AND DARK MATTER (WIMPS)		401
P. SALATI	A stellar probe of dark matter annihilation in galactic nuclei	403
A. BOUQUET, J. KAPLAN, F. MARTIN and P. SALATI	WIMPS and stellar structure	413
D.N. SPERGEL and D.O. RICHSTONE	Realistic halo models and the detection of WIMPS	419
IX. DARK MATTER, SN 1987A AND OTHER SUPERNOVAE		427
J. VAN DER VELDE	Possible evidence for dark matter from SN 1987A	429
A. DAR and S. DADO	Neutrinos properties and the neutrino bursts from SN 1987A	441
T. PIRAN and D. SPERGEL	The neutrino signals from SN 1987A	453
S.A. BLUDMAN and P.J. SCHINDER	General features of neutrino explosion dynamics revealed by supernova 1987A	461
R. SCHAEFFER	Comments on SN 1987A	471
J.P. CHIEZE	Simulation of neutrino transport in supernovae	477
S.A. BLUDMAN	Theoretical mechanisms for type II explosion dynamics	487
Author Index		495
List of Participants		497

I. SEARCH OF DARK MATTER

STRATEGIES FOR DARK MATTER DETECTION

Joseph Silk
Astronomy Department
University of California
Berkeley, CA 94720
USA

ABSTRACT

The present status of alternative forms of dark matter, both baryonic and non-baryonic, is reviewed. Alternative arguments are presented for the predominance of either cold dark matter (CDM) or of baryonic dark matter (BDM). Strategies are described for dark matter detection, both for dark matter that consists of weakly interacting relic particles and for dark matter that consists of dark stellar remnants.

1. Introduction

Dark matter candidates vary in mass over the range $10^{26\pm 40}$ GeV. The particle physics domain of weakly interacting elementary particle candidates spans 10^{-14} GeV (the axion) to 10^{19} GeV (Planck mass relics, such as monopoles), whereas the astrophysical regime ranges from 10^{40} GeV (10^{16} gm, the mass of a stable mini-black hole) to $\gtrsim 10^{66}$ GeV ($10^9 M_\odot$ corresponds to the mass of black holes believed to be lurking in active galactic nuclei). Needless to say, most of this mass range is unexplored. More to the point, perhaps, it is also unmotivated. This review will discuss some of the dark matter candidates for which there is at least a modest amount of theoretical prejudice.

One distinction between the particle physics and the astrophysical candidates is that the existence of (some of) the latter is not in question, but we have virtually no means of estimating their contribution to Ω with any confidence, whereas for the former, we have elegant techniques for computing their abundance although their very existence is largely a question of faith at present. I shall summarize here the arguments for both non-baryonic and baryonic dark matter, and describe the key observational strategies that promise to resolve this problem.

2. The Case For Non-Baryonic Dark Matter

The evidence for non-baryonic dark matter rests on four arguments, no one of which is compelling, but which collectively provide a strong case.

A. The standard cosmological model of the Big Bang requires $\Omega = 1 + Kt/t_0$, where t_0 is the present epoch ($t_0 = 2/3H_0$ if $\Omega = 1$ and K , a measure of curvature, is observationally bounded by $-0.9 \leq K \leq 1$). Inflation results in a flat universe with $|K| \lesssim 10^{-4}$. The amplitude of K is fitted empirically by normalization of the inflation-amplified quantum fluctuations to the observed large-scale structure, together with the inflationary prediction of a scale-invariant gaussian fluctuation spectrum. Inflation does not require that Ω consists of non-baryonic matter. However complementary arguments do constrain the baryonic component.

B. The microwave background is uniform, over angular scales from $1'$ to 90° to better than $\delta T/T \lesssim 10^{-4}$. If large-scale structure has developed by gravitational instability from primordial adiabatic fluctuations, there should be temperature fluctuations induced at last scattering (when $z \sim 1000$). The fact that these are not seen at a level $\delta T/T \sim 10^{-4}$ suffices to rule out a baryon-dominated universe¹⁾, since baryonic fluctuations only undergo growth by a factor $\delta\rho/\rho \propto (1+z)^{-1}$ on galactic scales after matter-radiation decoupling

at $z \sim 1000$. One would expect $\delta T/T \sim 10^{-3}$ in order for galaxies to have formed by $z \sim 5$, say. In a non-baryonic matter-dominated universe, fluctuation growth is initiated much earlier, at the epoch of matter-radiation equality $1+z = 4 \times 10^4 \Omega h^2$, if $\Omega \sim 1$. There is also weak (logarithmic) growth in the radiation-dominated era on subgalactic scales. The net effect is that one predicts $\delta T/T \sim 10^{-5}(\Omega h)^{-1}$. Reducing Ω limits the period over which gravity can aid fluctuation growth to $1+z \lesssim \Omega^{-1}$. The microwave background uniformity therefore requires non-baryonic matter with $\Omega h \gtrsim 0.2$. This lower bound is valid for adiabatic fluctuations, if we adopt the inflationary prediction of a scale-invariant spectrum. A steeper spectrum weakens this limit; however, a purely baryonic universe containing adiabatic fluctuations is untenable for *any* power-law fluctuation power spectrum. With isothermal or isocurvature fluctuations, a purely baryonic universe is tenable provided that the initial fluctuation spectrum is sufficiently steep.

C. Primordial synthesis of ${}^4\text{He}$, ${}^2\text{H}$, ${}^3\text{He}$, and ${}^7\text{Li}$ directly involves the baryonic components and requires $\Omega_b h^2 \simeq 0.03$ to within about a factor of two in order for consistency with the observations of these light elements. Ω_b is bounded both from below, otherwise excessive ${}^7\text{Li}$ is produced, and from above, in order to synthesize enough ${}^2\text{H}$ and not overproduce ${}^4\text{He}$. This, of course, assumes the standard Big Bang nucleosynthesis model.²⁾

D. Numerical simulations of large-scale structure³⁾ have provided an attractive explanation of several observable, and hitherto unexplained, characteristic properties, provided that the universe is dominated by cold dark matter (CDM), which is defined to be a weakly interacting and cold component of the mass distribution. The leading candidate for CDM is any generic, stable, weakly interacting particle, which has been non-relativistic since $T \gg 1$ MeV. Most candidates (in particular, those I will discuss here) have masses m_x in the 1-100 GeV range; the invisible axion with $m_a \approx 10^{-5}$ eV is the only exception. Popular candidates include the lightest supersymmetric partner of known particles: this may be the photino, higgsino, or gravitino in current models. Since weak interactions play a negligible role in thermal equilibrium at $T < 1$ MeV, any remnant CDM, which inevitably was thermally produced in the Big Bang at $T \gtrsim m_x$, must have negligible velocity dispersion in the matter-dominated era, $T \lesssim 10$ eV. Hence during this epoch of galaxy and cluster formation, CDM clusters freely on all scales of astrophysical interest. The simulations generally require that $\Omega > 0.1$ (and usually take $\Omega = 1$) in order to provide an acceptable match to such features of the galaxy distribution as the galaxy correlation function, galaxy-galaxy relative velocities, the structure of galaxy halos, galaxy rotation

curves, the luminosity functions of galaxies and of galaxy clusters, and the distribution of galaxy clusters and voids.

Arguments A, B and D support a value $\Omega \sim 1$, whereas C tells us that the dark matter associated with Ω should be non-baryonic if we are to preserve the simplest Big Bang nucleosynthesis model. Since neither hot nor unstable dark matter have hitherto led to satisfactory models of large-scale structure, I shall focus in the remainder of this discussion on CDM, and in particular on massive weakly interacting relics. Of course, cosmic strings offer a possible means of providing primordial seeds, that may help resurrect hot dark matter: however, the most recent numerical simulations suggest that strings cannot account for the cluster-cluster correlations.⁴⁾ This failure to help with one of the outstanding large-scale structure problems removes much of the motivation for pursuing cosmic string scenarios.

3. Massive Weakly Interacting Relics

Remarkably, one can calculate precisely how much CDM survives today, if one knows the particle properties. The problem, of course, is that we have no evidence at present that such particles exist. Lack of evidence has never deterred theorists, however, and in fact has motivated an alternative approach. This goes as follows. Let us assume that CDM exists in a specified amount: then one appeals to cosmology to infer the interaction strength of the dark matter candidate. This “hands-off” approach leads to specific predictions for observing dark matter candidates, and, in particular, for designing experiments.

The argument goes as follows.^{5,6)} At $T > m_x$, the number density of x -particles is $n_x \sim n_\gamma$. As the temperature drops below m_x , x -particle creation gradually ceases, and the number density is suppressed by a Boltzmann factor:

$$n_x \sim n_\gamma y^{3/2} \exp(-y), \quad (1)$$

where $y \equiv m_x/T$. Expression (1) becomes invalid once the annihilation rate becomes slower than the Hubble expansion rate. It tells us that this occurs at a temperature which depends very weakly (logarithmically) on the particle annihilation cross-section. For typical weak interaction rates, one expects $\langle\sigma v\rangle_{ann} \sim 10^{-26} \text{ cm}^3\text{s}^{-1}$. One finds that freeze-out occurs at $y_f \simeq 20$ or $T_f \equiv m_x/20$, after which the comoving density remains constant.

The number of cold relics is given by equating the annihilation rate to the expansion rate at T_f , or

$$n_x \langle\sigma v\rangle_{ann} \sim H. \quad (2)$$

Since $n_x \propto T^3$ and $H \propto T^2$, this yields an expression for the mass-density in terms of the annihilation rate that is approximately independent of particle mass: $\rho_x \equiv n_x m_x \propto \langle \sigma v \rangle_{ann}^{-1}$. A precise value for ρ_x in units of the critical density for closure of the universe $3H_0^2/8\pi G$, where $H_0 \equiv 100h \text{ km s}^{-1}\text{Mpc}^{-1}$, with $0.5 \lesssim h \lesssim 1$, is Hubble's constant, is given by

$$\Omega_x = 0.96 \langle \sigma v \rangle_{26}^{-1} h^{-2} y_{20} f. \quad (3)$$

Here $\langle \sigma v \rangle_{26} \equiv \langle \sigma v \rangle_{ann}/10^{-26} \text{ cm}^3 \text{ s}^{-1}$, $y_{20} \equiv (y_f/20)$ and $f \simeq 1$ is a factor which includes a temperature correction to the annihilation cross-section and allowance for uncertainty in the number of relativistic species present at freeze-out. It is a completely unexpected coincidence that for typical weak interaction cross-sections ($\sigma \sim 10^{-36} \text{ cm}^2$), the density of surviving relics (with mass in the 1 - 10 GeV range) yields ⁷⁻¹¹⁾ $\Omega_x \sim O(1)$.

4. Direct Detection

Provided that $\Omega_x \gtrsim 0.03$, CDM provides a natural candidate for the content of the dark halo of our galaxy. The dark halo density in the solar neighborhood is known from modelling of the galactic rotation curve to be between 0.03 and 0.3 GeV cm^{-3} . One therefore expects a local flux of dark matter particles of at least $10^6 m_x^{-1} \text{ cm}^{-2} \text{ s}^{-1}$ (with m_x in GeV). Such a flux is measurable in a laboratory bolometric detector by virtue of elastic scattering with suitable target nuclei. The energy deposition is of order¹²⁾

$$m_x^2 M_{target} v^2 (1 - \cos \theta) (m_x + M_{target})^{-2} \sim 100 \text{ eV}$$

for a silicon target. The elastic cross-section ($xp \rightarrow xp, xn \rightarrow xn$) is at least $\sigma_{el} \sim 10^{-38} \text{ cm}^2$ for a particle with annihilation cross-section $\sigma_{ann} \sim 10^{-36} \text{ cm}^2$, and may be enhanced by as much as a factor of ~ 100 if spin-independent interactions are important (as for heavy neutrinos, for example). The velocity refers to the relative velocity between the earth and the halo particles, and the forward peaking means that seasonal modulation can be important in enhancing a signal.

5. Detection via annihilations

Majorana-mass candidates for CDM annihilate with a cross-section corresponding to the low energy limit of the early universe annihilation cross-section, itself known once Ω_x is specified. The relevant mass range is generally 1-20 GeV. For Dirac particles, the cross-section is nearly energy-independent, and is large ($\sim 10^{-36} \text{ cm}^2$); for Majorana particles, a typical cross-section is $\sim 10^{-38} \text{ cm}^2$. For generic candidates (photino, higgsino, etc.) other than the scalar neutrino, the annihilation products consist of heavy quarks

that decay into $\nu\bar{\nu}, e^+e^-, p\bar{p}$, and γ -rays. To obtain a more precise estimate of their flux and spectrum, one has to specify the dark matter candidate. For example, for the popular supersymmetric candidate, the photino, one has¹³⁾

$$\langle\sigma v\rangle(T_f) \propto m_{sf}^{-4}(m_f^2 + m_{\tilde{\gamma}}^2),$$

where m_{sf} denotes the scalar fermion mass and m_f represents the mass of fermions into which the annihilation channels proceed. Applying (3), this yields

$$\Omega h^2 \simeq 0.25(m_{sf}/60 \text{ GeV})^4(4 \text{ GeV}/m_{\tilde{\gamma}})^{4/3}.$$

The experimental lower bound $m_{sf} \gtrsim 60 \text{ GeV}$ requires $m_{\tilde{\gamma}} \gtrsim 4 \text{ GeV}$. Note also that $\langle\sigma v\rangle(T=0) \propto m_{sf}^{-4}$, so that theories which have very massive scalars, as in phenomenological superstring models, result in massive ($\gg 10 \text{ GeV}$) photinos. For candidates in the 1 – 100 GeV range, the annihilation products are potentially detectable in at least four distinct environments.

5.1 Annihilations in the halo: energetic antiprotons

Charged particles produced by annihilations accumulate in the galactic halo, trapped by magnetic confinement for $\tau_p \sim 10^8 \text{ yr}$. The rarest stable charged particle annihilation product is the \bar{p} , and its production energy is expected to be $\sim 0.2m_x$. One, therefore, expects a potential cosmic ray \bar{p} signature of CDM.¹⁴⁾ The predicted flux is proportional to the cosmic ray confinement time–scale τ_p , to n_x^2 , and to approximately $m_{\tilde{\gamma}}^{-1}$ if the photino is the dark matter candidate. The only competing source is from high energy ($\gtrsim 7 \text{ GeV}$) protons colliding with interstellar atoms to produce occasional \bar{p} secondaries that are, however, kinematically suppressed below several GeV. Low energy cosmic ray \bar{p} should therefore provide a clean signature of halo CDM, especially if the data allow sufficient energy resolution to separate the secondary contribution. Unfortunately, two experiments flown in August 1987 failed to confirm Buffington's¹⁵⁾ measurement of low energy \bar{p} . The upper limit set by Ahlen *et al.*¹⁶⁾ was a factor 7 below the earlier claim of a \bar{p}/p detection over the demodulated interstellar energy range 700 – 1135 MeV. The uncertainties in the various factors that go into predicting the \bar{p} flux mean that one cannot derive any useful limits on $\tilde{\gamma}$ or any other halo dark matter candidates.¹⁷⁾

5.2 Annihilations in the galactic bulge: gamma rays

The γ -ray annihilation luminosity from the galactic halo may be approximated by

$$L_\gamma = N_x n_x (\sigma_{ann} v)^{-1} \zeta,$$

where N_x is the total number of halo dark matter particles, n_x is the mean density, and ζ is the γ -ray multiplicity (γ 's per annihilation).¹⁸⁾ With N_x corresponding to $10^{12}M_\odot$, one finds $\langle n_x \sigma_{ann} v \rangle^{-1} \simeq 10^{19}$ yr and $L_\gamma \equiv 10^{41} \text{s}^{-1} \zeta (\text{GeV}/m_x)$. At the earth, this amounts to only about one percent of the isotropic gamma ray background above 100 MeV. Anisotropy may help enhance the halo signal; it will also be more significant relative to the isotropic background at high energies (above 1 GeV) if $m_x \gtrsim 10$ GeV, although diffuse galactic disk emission may be a source of confusion.

The galactic bulge also provides a potential γ -ray source. One should not necessarily assume that the galactic spheroid (with characteristic r^{-3} density profile and core radius ~ 100 pc) is necessarily 100% baryonic matter. Formation of the galaxy would inevitably entrain some dark matter, and we do not understand its formation so well that one can dismiss the possibility of a dense dark matter core that formed in the early universe around which the galaxy accreted. The bulge of our galaxy contains a mass $\sim 6 \times 10^8 M_\odot$ within a core-radius ~ 100 pc, and the inferred mean annihilation time $\langle n_x \sigma_{ann} v \rangle^{-1} \simeq 5 \times 10^{22} \text{s}$ leads to a γ -ray luminosity $L_\gamma \simeq 10^{42} \text{s}^{-1} \zeta (\text{GeV}/m_x) f_{b,x}$, where $f_{b,x}$ is the fraction of the bulge mass in the form of CDM. This is observable if $f_{b,x} \sim 1$, and one can even limit¹⁹⁾ $f_{b,x}$ to $\lesssim 0.1$ using COS-B data for some bulge models and dark matter candidates with $m_x \lesssim 10$ GeV.

Unfortunately there is little direct evidence for an enhanced mass-to-light ratio in our own galactic bulge. The situation in M31 is more intriguing, however. Recent high resolution observations²⁰⁾ of the innermost core of M31 find a high ratio of mass-to-luminosity within the central 2 pc or so. The inferred mass within this region is $\sim 10^7 M_\odot$. While a central black hole offers one possible explanation, a dark matter core is also viable: the inferred annihilation time is $\langle n_x \sigma_{ann} v \rangle^{-1} \simeq 10^{18} \text{s}$, and the γ -ray luminosity is $\sim 10^{46} \text{s}^{-1} \zeta m_x^{-1}$. Since the annihilation spectrum of gamma rays turns out to have a different signature from other gamma ray sources, this could lead to an interesting cold dark matter signature, if indeed CDM accumulates in the cores of galaxies.

5.3 Annihilations in the sun: high energy neutrinos

As the sun orbits the galaxy, it traps halo dark matter. Particles impact the solar surface, the impact rate being boosted by gravitational focussing, and elastic scattering with protons and other nuclei guarantees that they remain and settle in the sun provided that²¹⁾ $m_x > 4$ GeV. Lighter x -particles evaporate before accumulating in the solar core. The solar trapping rate is

$$\Gamma_T = 7 \times 10^{28} m_x^{-1} (\rho_h / 0.3 \text{ GeV cm}^{-3}) v_{300}^{-1} f_E,$$

where $v_{300} \equiv v_x/300 \text{ km s}^{-1}$ is the average velocity of a halo cosmion near the sun and f_E is the trapping probability per incoming particle. According to Srednicki *et al.*²²⁾,

$$f_E = (0.18 Y_p \sigma_{el,p} / 10^{-36} \text{ cm}^2) \min \left\{ 1, 43 m_p m_x (m_p^2 + m_x^2)^{-1} v_{300}^2 \right\}$$

allows for incoming particles to be scattered and energetically trapped.

The equilibrium abundance is inferred by equating annihilation and trapping rates. Annihilations in the solar core yield high energy neutrinos that escape. These may be detectable at the earth given the rapid decline of atmospheric neutrinos with increasing energy. Indeed, Ng *et al.*²³⁾ find that the predicted high energy neutrino solar flux of $\sim 10 m_x^{-1} \text{ cm}^{-2} \text{ s}^{-1} \text{ GeV}^{-1}$ for sneutrinos already exceeds IMB bounds, although photinos, producing neutrinos at about one percent of this rate, are not presently constrained.

5.4 Annihilations in stars

Cosmions efficiently transport energy in stellar cores by virtue of their long mean free paths. A specific choice of cosmion parameters can be designed to reduce the solar neutrino flux by flattening the temperature gradient in the solar core.²⁴⁾ These cosmions do not annihilate in the solar core, and accumulate over the lifetime of the sun. A large elastic scattering cross-section ($\sigma_{el} \sim 10^{-36} \text{ cm}^2$) is required in order to build up a sufficient abundance. Examples of such cosmions are the magnino²⁵⁾ and a fourth-generation Dirac neutrino.²⁶⁾ Provided the particle mass exceeds $\sim 4 \text{ GeV}$, evaporation does not occur, and once trapped, the cosmions remain in the core of the sun and of other solar mass stars. This may have interesting implications for the evolution of a star in its helium-burning phase if convection were suppressed because of cosmion energy transport. According to Renzini,²⁷⁾ this leads to a reduction in the horizontal branch (HB) lifetime that would affect the observed number of horizontal branch stars in globular star clusters. Spergel and Faulkner²⁸⁾ disputed this conclusion, but Bouquet *et al.*²⁹⁾ have recently self-consistently included main-sequence capture of cosmions to demonstrate that magninos with mass $\gtrsim 8 \text{ GeV}$, equal to the evaporation mass for HB stars, are excluded. Other particles with larger elastic cross-sections on He, such as fourth generation massive neutrinos, would modify HB populations only in old stellar populations subject to a much larger flux of dark matter than in the solar neighborhood, as might occur, for example, in globular clusters in the inner galaxy or in nearby dwarf spheroidal galaxies.

More conventional candidates for CDM, such as Majorana particles with spin-dependent cross-sections, do not normally modify stellar evolution. Extreme environments

are possible, however, in which the energy input from cold dark matter annihilations overwhelms the nuclear energy source. This would happen in low mass stars which form within a dense dark matter cloud that might exist in the nucleus of a galaxy. Collapse of galactic nuclei in the early universe plausibly leads to aggregations of dark matter with central density up to $\sim 10^6 M_\odot \text{pc}^{-3}$. Even at such a high density, the annihilation time-scale exceeds a Hubble time, and such dark matter clouds would severely modify the evolution of lower main sequence stars. Salati and Silk³⁰⁾ find that such stars would swell up along the Hayashi track, and most likely undergo collisions with other stars and consequently disrupt. This sequence of events, while speculative, could be responsible for eventual formation of massive black holes in dense dark matter clouds within galactic nuclei.

6. The Case for Baryonic Dark Matter

I will now don my astronomer's cap, and make an equally powerful case that the prevalent form of dark matter is baryonic. The arguments for baryonic dark matter (BDM) may be summarized as follows.

6.1 Direct determination of Ω

Ω is nowhere measured to be unity. Two recent results which report that $\Omega \simeq 1$ are subject to unknown amounts of systematic error. These results are based on measurement of the overdensity in a sample of IRAS galaxies extending to $\sim 100 \text{ Mpc}$,³⁰⁾ and on determination of the volume element by obtaining crude redshifts for galaxies out to $z \sim 0.7$ ³²⁾. The problem with the first test is that the IRAS sample is biased towards star-forming field galaxies and biased against the most nearby (and therefore extended) galaxies that are expected to dominate any signal; the problem with the second test is that adequate calibration of the redshift technique has not yet been possible. Work in progress should improve the accuracy of these determinations of Ω .

Direct determinations of Ω by dynamical measurements do not provide any unambiguous support for $\Omega > 0.1$. One can summarize these determinations in terms of the ratio of mass, measured by spectroscopic determinations of velocity, to blue-band luminosity within a specified scale, both measured in solar units.³³⁾ One finds that a distribution of old stars, characteristic of the spheroid of a spiral or an elliptical galaxy, weighs in at $M/L \simeq 10h$ with M in M_\odot and L in L_\odot . Spirals typically have $M/L \sim 3h$ within their luminous confines. The relevant scale is about 10 kpc for these measurements. Dark halos of spirals, probed by rotation curves, extend to at least $\sim 50 \text{ kpc}$, within which $M/L \simeq 50h$. The largest M/L values are measured for groups and clusters of galaxies over $\sim 1 \text{ Mpc}$,

and for superclusters, over ~ 10 Mpc. Both statistical measures of clustering and galaxy peculiar velocities probe scales up to ~ 50 Mpc. One can say with some confidence that between ~ 1 Mpc and ~ 10 Mpc, the measured M/L is about $300h$. On larger scales, it is very uncertain.

These results may be compared with the mass–luminosity ratio required for closure. The mean luminosity density in luminous galaxies³⁴⁾ of $1.2 \times 10^8 h L_\odot \text{ Mpc}^{-3}$ can be expressed in terms of the mean mass density $\Omega(3H_0^2/8\pi G)$ as a mass–luminosity ratio $M/L = 2300\Omega h$. We conclude that luminous matter in ordinary stars amounts to about 0.005 of the critical value, whereas all dynamically measured matter accounts for $\Omega \simeq 0.1 - 0.2$. Dark matter therefore amounts to about 30 times the luminous stellar (and gas) content of galaxies. It could only be 150 times larger with $\Omega = 1$ if its distribution were uniform over scales up to 10 Mpc.

6.2 BDM candidates exist

Astrophysical candidates for dark baryonic matter include white dwarfs, brown dwarfs, neutron stars and black holes. One cannot predict the abundance of any of these objects with any degree of certainty. White dwarfs are only observable for $\sim 10^{10}$ yr, after which they become black dwarfs. Prolific neutron star or white dwarf production would almost certainly be accompanied by excessive heavy element synthesis.³⁵⁾ The evidence for the existence of black holes is highly compelling: their formation is most likely to result in considerable ejection of enriched matter unless their mass exceeds about $300 M_\odot$. However, the remaining options, black holes, of mass $\gtrsim 100 M_\odot$, or brown dwarfs, of mass $< 0.08 M_\odot$, the hydrogen–burning threshold, are much more difficult to constrain.³⁶⁾ One usually resorts to plausibility arguments: for example if even one percent of the matter forming these high or low mass stars were to form solar mass stars, one would not be producing sufficiently black dark matter, or if the efficiency of forming these objects out of primordial gas clouds were fifty percent or less, one would have excessive amounts of gas remaining behind, which would be detectable.

6.3 Primordial nucleosynthesis requires BDM

Up to 90 percent of the dynamically determined Ω may be dark baryonic matter. Primordial nucleosynthesis overproduces²⁰⁾ ${}^2\text{H} + {}^3\text{He}$ unless $\Omega_b > 0.011h^{-2}$ and³⁷⁾ ${}^7\text{Li}$ unless $\Omega_b > 0.007h^{-2}$ whereas $\Omega_{lum} \simeq 0.005$. Acceptance of a Big Bang origin for ${}^7\text{Li}$ requires there to be at least three times more dark than luminous baryons.

6.4 Are dark halos flattened?

Observations of planetary nebulae in the halo of NGC 5128 have been used³⁸⁾ to study the rotation curve in the outer regions of this elliptical galaxy. Preliminary indications, based on two survey fields, indicate that the rotation curve is flat, asymptoting at about 100 km s^{-1} at a distance of 20 kpc. However, the velocity dispersion of these stars, treated as test particle probes of the dark halo, appears to decline precipitously outside about 15 kpc. If confirmed, this result would provide evidence that the geometry of the dark halo is that of a cold flattened disk, rather than that of a hot spheroid. BDM could plausibly form such a mass distribution, whereas CDM could not. Warm dark matter of non-baryonic nature is an alternative possibility, but presently lacks much particle physics motivation.

6.5 Cluster cooling flows

More than 20 galaxy clusters have been found to contain gas cooling flows, generally observed by central peaks in the x-ray surface brightness profiles centered on the brightest galaxy in the cluster core, and in the best-studied cases revealing x-ray and optical line emission over a range of excitation temperatures.³⁹⁾ The inferred electron densities and temperatures lead to estimates of cooling time-scales that are less than a Hubble time, and the inferred mass flow rates span the range from $\sim 20 M_{\odot} \text{ yr}^{-1}$ in the case of Virgo to $\sim 300 M_{\odot} \text{ yr}^{-1}$ for Perseus. This is sufficient to form a galaxy mass in stars over a Hubble time, yet the observed star formation rates in the central galaxies amount to at most 10% of these accretion rates, if the stars are assumed to form with the conventional mass function observed in the solar neighborhood. The mass-luminosity ratio associated with the mass deposited from the cooling flow over a Hubble time must substantially exceed that measured for an old stellar population in the luminous core of the central galaxy. This has led to the speculation that the cooling flows preferentially form very low mass stars or even “Jupiters”.^{40,41)} One cannot yet rule out other possibilities, however: for example, the mass deposition at large radii ($\sim 100 \text{ kpc}$) into stars with a conventional initial mass function (IMF) would result in too low a surface brightness to be detectable.⁴²⁾

6.6 Disk dark matter?

If the galactic disk contains a significant component of dark matter, this would provide strong evidence for its baryonic nature. Observational evidence is in conflict, however, on the amount of disk dark matter. On the one hand, Bahcall’s analysis⁴³⁾ of a sample of F stars within 200 pc of the galactic plane results in a local volume density

of $0.18 M_{\odot}\text{pc}^{-3}$, only half of which is accounted for by known stars and gas. However data at a larger scale height are necessary to unambiguously constrain the total surface density, and a recent study by Kuijken and Gilmore⁴⁴⁾ of K dwarfs out to ~ 7 kpc finds a surface density of $46(\pm 7) M_{\odot}\text{pc}^{-2}$ which can be fully accounted for in terms of luminous matter. The dark halo has a local density of $0.011 M_{\odot}\text{pc}^{-3}$, and accounts for about 50% of the local radial acceleration in modelling the galactic rotation velocity in the solar neighborhood. There is still a puzzle, however, in reconciling the observed luminous matter volume density of $0.1 M_{\odot}\text{pc}^{-3}$ with that determined dynamically. One possibility is that the shortfall could be due to uncertainty in the poorly known local gas density averaged over the solar circle: gas accounts for about 50% of the local volume density but only 15% of the local surface density.

7. Compact Stellar Remnants as BDM

The obvious form of BDM is in compact remnants of massive stars. Because stars of mass $\gtrsim 2 M_{\odot}$ are sufficiently short-lived (lifetime $\lesssim 10^9$ yr), they could have formed in great numbers early in galactic history, and littered the galactic halo with their dark remnants, as white dwarfs, neutron stars or black holes. This conjecture is notoriously difficult to quantify. Let me summarize the arguments both for and against compact stellar remnants as BDM.

7.1 Starbursts

Regions of intense star-forming activity appear to be deficient in low mass stars.⁴⁵⁾ A nearby example is 30 Doradus in the Large Magellanic Cloud. Extreme objects such as Arp 220 are starburst galaxies, where the star formation is inferred from the far infrared flux to exceed several hundred solar masses per year within a central region less than a kiloparsec across. Such an elevated star formation rate clearly cannot last for more than $\sim 10^8$ yr, but still suffices to use up so much of the available gas that the stellar mass function must be massive star-dominated. Massive stars, especially OB stars, can recycle gas efficiently and increase the star formation efficiency by about an order of magnitude, from the value of a few percent typical of the solar neighborhood, to fifty percent or more. Evidently, compact remnants are being formed in starburst galaxies at a rate per unit mass that is two orders of magnitude or more larger than in the solar vicinity at present. Direct evidence of a high supernova rate is seen in the dust-shrouded nucleus of M82, where radio supernova remnants are inferred to be produced at a rate of several per decade. Gas longevity is generally a problem in spiral galaxies, unless regions of active star formation are assumed to be preferentially, but not exclusively, forming massive stars.⁴⁶⁾

7.2 Protogalaxies

During the process of formation of the spheroidal components of galaxies, star formation is inferred to have been a very efficient process, otherwise a dissipative disk would have formed. In fact, one can estimate the required rate of protogalactic star formation, and it is similar to what is observed in extreme starburst systems. The circumstantial evidence therefore points to an initial mass function during protogalactic spheroid formation that was enhanced in massive stars.

7.3 Chemical evolution

A related but independent argument comes from studying the chemical evolution of disk galaxies, and in particular, of the solar neighborhood. The paucity of low metallicity G dwarfs in the disk of our galaxy implies efficient early enrichment: enhancement of massive star formation provides a possible, but not unique, resolution of this problem.^{47,48)} For example, enhanced effective yields could also be due to more efficient metal production by low metallicity stars or to continuing infall to the galactic disk of unenriched gas.⁴⁷⁾

7.4 Initial mass function

An indication that massive star formation once proceeded at a different, and presumably greater, rate than presently observed comes from studying the initial stellar mass function (IMF). This is the distribution by mass of all stars that have ever formed. For stars of mass $\lesssim 1 M_{\odot}$, this is observed directly when one measures the luminosity function in the solar neighborhood, but for massive short-lived stars, one has to adopt a model for the past rate of star formation. One finds that, regardless of whether the past rate is constant with time or enhanced, a kink remains in the IMF between 1 and $2 M_{\odot}$.⁴⁵⁾ This discontinuity is presumed to be a relic of a time-dependent formation rate for massive stars that differs from the formation rate of low mass stars: alternatively, one would have to postulate an IMF which coincidentally possesses a kink corresponding to stellar masses appropriate to lifetimes of several gigayears, a possibility that seems somewhat contrived.

7.5 Spectral distortions in the cosmic background radiation

The recently reported deviations from a blackbody spectrum in the cosmic microwave background radiation⁵⁰⁾ have led to considerable speculation about possible explanations. The excess energy, relative to the 2.7 K blackbody spectrum, amounts to about 10% of the microwave radiation density, or equivalent to $\Omega_{\text{excess}} \approx 10^{-5}$. The most conservative assumption about the origin of this distortion is that it represents reprocessed

stellar energy, either injected as a heat source into the intergalactic medium, which then partially Comptonizes the incident blackbody background photons, or due to protogalactic starlight absorbed and reemitted by dust grains. Even if one of these processes is completely efficient at redistributing the nuclear energy source into the far infrared, the requirement on the mass fraction in evolved massive stars presumed to form at some redshift z_* amounts to $\Omega_* \sim 10^{-2}(1 + z_*)$. One needs $z_* \gtrsim 10$ if the distortions are produced by dust reprocessing to obtain sufficient optical depth⁵¹⁾, which leads us to conclude in this case that at least 10% of the mass density in a flat universe must have been converted into massive stars. The remnants of these stars, whether compact objects or in the form of intergalactic gas, provide a plausible form of dark matter. If predominantly gas, this dark matter is dynamically significant only in the intergalactic medium and in the outer regions of galaxy clusters, and not in galaxy halos nor probably in galaxy groups. However, if in compact remnants, the inferred amount of BDM suffices to account for all observations of dark matter.

7.6 Over-enrichment: a problem with BDM?

Massive stars are likely to overproduce heavy elements if their remnants account for the putative dark matter in the galactic disk, let alone that in galaxy halos or clusters. Larson⁴⁷⁾ tackled this problem by advocating that the IMF was suppressed at high as well as at low masses in the early galaxy. As already mentioned, the BDM hypothesis requires the low mass cut-off to exceed $\sim 2M_\odot$, otherwise the stars would be observable today. At the high mass end, only primordial stars above about $12M_\odot$ have an appreciable nucleosynthetic yield. For a metallicity below $\sim 10^{-3}$ that of the sun, helium shell flashes and the ensuing wind-driven mass loss are suppressed⁵²⁾ for intermediate mass stars.⁵³⁾ Metal production by stars between 2 and $16M_\odot$, forming at a greatly enhanced rate during the first 2 gigayears or so after the disk formed, can account for the chemical evolution of the old disk stars. However a significant steepening of the IMF above $\sim 16M_\odot$ is necessary to avoid overproduction of oxygen if stellar remnants are to account for $\sim 0.05 M_\odot \text{pc}^{-3}$ of dark matter in the solar vicinity.

Old halo stars are enhanced in oxygen relative to iron (which is believed to be produced by low mass stars in Type I supernovae): this may provide an additional indication of an early IMF dominated by massive star formation, although other explanations, notably appealing to the time-delay in Fe synthesis, are possible. It may be that the inadequacy of our modelling of Type I supernovae prevents us from obtaining any reliable yields for massive stars.

The situation is much more extreme if the entire halo is to be formed from massive star remnants. By requiring the old disk to not exceed a metallicity of $Z_D \sim 0.1 Z_\odot \sim 2 \times 10^{-3}$, and with a typical yield (assuming 50% of the processed core is ejected) of $Z_y \approx 0.1$ for a $25 M_\odot$ star⁵⁴⁾, one can infer that dark halos containing, say, $\Omega_{halo} \approx 0.05$, while $\Omega_{lum} \approx 0.005$, could only contain a mass fraction of about $f_{BDM} = Z_y^{-1} Z_D (\Omega_{lum}/\Omega_{halo}) \approx 2 \times 10^{-3}$ in the form of BDM.³⁵⁾ This estimate assumes that only one generation of massive star formation has occurred. Use of a more realistic massive star IMF would increase f_{BDM} by a factor of 2 or so, and recycling would also increase the lock-up fraction in dark remnants. However the discrepancy is so great that it seems clear that dark halos cannot consist of ordinary stellar remnants. Only by increasing the typical stellar mass to $\gtrsim 200 M_\odot$, so that little ejection of processed material occurs or by restricting it to be $\lesssim 15 M_\odot$, where yields are low, is it feasible to have the halo consist of BDM.

8. An observational Test for BDM

If our halo consists of BDM, then compact stellar remnants are our best guess as to its nature. In this case, one would expect white dwarfs to be a substantial, even if not a dominant, component of the halo. The sharp turn-down in the luminosity function of local white dwarfs below⁵⁵⁾ $\log(L/L_\odot) \approx -4.5$ suggests that a search for halo white dwarfs may be feasible. The turn-down is so abrupt that it is not due to the onset of rapid cooling associated with crystallization.^{56,57)} Rather, it must be associated with the formation of the disk. This means that white dwarfs which formed prior to disk formation should be visible at $\log(L/L_\odot) < -4.5$. The Luyten proper motion survey, used to identify the faintest local white dwarfs, is only complete to an apparent magnitude $M_v = 18$, the shortfall setting in at $M_v = 16$. Use of modern techniques should enable one to develop future catalogs that go several magnitudes deeper. The hypothesis that the dark halo consists of stellar remnants may be testable. Exclusion of white dwarfs as a significant contributor to halo dark matter would narrow the remaining window of mass for normal stars ($0.1 - 100 M_\odot$) to the implausible range of only $\sim 8 - 12 M_\odot$.

9. Conclusions

An equally plausible case can be that halo is dominated either by BDM or by CDM. The arguments against BDM are not insuperable, and the strongest of these, primordial nucleosynthesis of ^2H , only argues against $\Omega = 1$ in BDM. If one merely requires the halo

to consist of BDM, then one can perhaps appeal to HDM, or at least some form of dark matter that is not CDM, to satisfy the inflationary requirement that $\Omega = 1$. CDM and a BDM-dominated halo seem incompatible, at least from a cosmologist's perspective, since it is difficult to prevent CDM from collapsing on galactic and subgalactic scales.

There are several arguments that weaken, but do not destroy, the case for a CDM-dominated halo. CDM has had great success in leading to a theory of galaxy halo formation and galaxy clustering. Problems arise on larger scales, however. In particular one has to confront four distinct observations, confirmation of any one of which would probably be fatal for CDM.

A. Dark halos around spiral galaxies may terminate at ~ 50 kpc according to studies of the dwarf satellites of the Milky Way⁵⁸⁾ galaxy and of lensing distortions of distant field galaxies that are produced by intervening dark halos.⁵⁹⁾

B. The clustering of galaxy clusters⁶⁰⁾ amounts to an enhancement of the strength of cluster correlations relative to galaxy-galaxy correlations by a factor of at least 20 on scales of 10 – 20 Mpc.

C. Large-scale bulk motions have been reported,⁶¹⁾ averaged over scales of up to 50 Mpc, that amount to ~ 600 km s⁻¹ in the reference frame of the cosmic microwave background radiation. This is in addition to the motion of the Local Group with similar amplitude, inferred from the dipole anisotropy of the background radiation.

D. Temperature fluctuations have been measured⁶²⁾ in the cosmic microwave background over 8° at a strength of about $\delta T/T \simeq 5 \times 10^{-5}$.

None of these observations can yet be considered to be definitive. For example, coherent (over several Mpc) zero-point variations in the correlation between velocity dispersion and luminosity of giant ellipticals, a correlation for which there is no accepted explanation, would induce distance errors, which would in turn be interpreted, erroneously, as coherent peculiar velocities. Also, the enhanced cluster-cluster correlations may be partly due to a selection effect that preferentially picks out close pairs of clusters in projection.

However, it is fair to say that the CDM theory makes unambiguous predictions. Normalization of the inflationary scale-invariant, gaussian, fluctuation spectrum to the galaxy luminosity function leads to predictions of large-scale power. One infers $\delta\rho/\rho$ as a function of scale, and one can straightforwardly calculate the various observables such as peculiar velocity and $\delta T/T$. Biasing, or appeal to rare fluctuations on large scales, helps accentuate the density contrast and produces large voids, as observed. Indeed, biasing on

galactic scales is essential to account for the concentration of light relative to the dark matter. However, this effectively lowers the mean amplitude of the dark matter power spectrum relative to that of the luminous matter, thereby compounding the difficulties in producing sufficient large-scale power to obtain observable peculiar velocities and microwave background temperature fluctuations.⁶³⁾ Indeed, the value of $\delta T/T$ predicted even by unbiased CDM is an order of magnitude below the recently reported value⁶²⁾ over $\sim 8^\circ$. Nevertheless, one may conclude that until definitive confirmation of these various results is forthcoming, CDM merits serious attention because of its many successes on scales below ~ 10 Mpc. These include accounting for galaxy correlations, galaxy groups and clusters, galaxy peculiar velocities, galaxy rotation curves, and the structure of galaxy halos.

Accelerator experiments, one hopes, will eventually confirm the existence of a weakly interacting massive particle candidate, if CDM is the dominant form of matter in the universe. If such a particle exists, and is stable, then we can calculate its abundance at the present epoch. A most exciting prospect is that bolometric laboratory experiments are now capable of direct searches for generic CDM candidates in the halo. However, astronomers need not despair: they have much to do. The search for annihilation products of Majorana candidates requires a coordinated attack, involving x - and γ -ray astronomy, neutrino astronomy, cosmic ray astrophysics, ultraviolet astronomy, and microwave astronomy. The microwave background holds vital clues as to the nature of the dark matter. Moreover if BDM prevails, then the search for dim white dwarfs should acquire the highest priority. The rate of current progress encourages one to believe that we shall make considerable progress over the next decade in resolving the outstanding problem of astrophysics today: the nature of the prevalent form of matter in the universe.

ACKNOWLEDGEMENTS

I gratefully acknowledge many discussions with my collaborators K. Freese, G. Raffelt, P. Salati and D. Seckel. This research has been supported in part by DOE, NSF, and by CalSpace.

REFERENCES

1. Wilson, M.L., *Ap.J.*, **273**, 2 (1983).
2. Yang, J. *et al.*, *Ap.J.*, **281**, 493 (1984).
3. White, S., Frenk, C., Davis, M., Efstathiou, G., *Ap.J.*, **313**, 505 (1987).
4. Bennett, D. and Bouchet, F., *Phys. Rev. Lett.*, **60**, 257 (1988).
5. Zel'dovich, Ya. B., *Adv. Astron. Astrophys.*, **3**, 241 (1965).
6. Chiu, H.-Y., *Phys. Rev. Lett.*, **17**, 712 (1966).
7. Dicus, D.A., Kolb, E.W. and Teplitz, V., *Phys. Rev. Lett.*, **39**, 168 (1977).
8. Hut, P., *Phys. Rev. Lett.*, **69B**, 85 (1977).
9. Lee, B.W. and Weinberg, S., *Phys. Rev. Lett.*, **39**, 165 (1977).
10. Sato, K. and Kobayashi, M., *Prog. Theor. Phys.*, **58**, 1775 (1977).
11. Vysotskii, M.I., Dolgov, A.D. and Zel'dovich, Ya. B., *JETP Lett.*, **26**, 188 (1977).
12. Goodman, M. and Witten, E., *Phys. Rev. D.*, **31**, 3059 (1985).
13. Goldberg, H., *Phys. Rev. Lett.*, **50**, 1419 (1983).
14. Silk, J. and Srednicki, M., *Phys. Rev. Lett.*, **53**, 624 (1984).
15. Buffington, A. *et al.*, *Ap.J.*, **248**, 1179 (1981).
16. Ahlen, S. *et al.*, *Phys. Rev. Lett.* (in press).
17. Ellis, J., Flores, R., Freese, K., Ritz, S., Seckel, D. and Silk, J., preprint (1988).
18. Stecker, F.W., *Phys. Lett.*, **201B**, 529 (1988).
19. Silk, J. and Bloemen, H., *Ap.J. Lett.*, **313**, 47 (1987).
20. Kormendy, J., *Ap.J.*, **328**, 28 (1988).
21. Gould, A., *Ap.J.*, **321**, 569 (1987).
22. Srednicki, M., Olive, K., and Silk, J., *Nucl. Phys. B*, **279**, 804 (1987).
23. Ng, K., Olive, K. and Srednicki, M., *Phys. Lett.*, **188B**, 138 (1987).
24. Spergel, D. and Press, W., *Ap.J.*, **294**, 663 (1985).
25. Raby, S. and West, G., *Phys. Lett.*, **194B**, 557 (1987).
26. Raby, S. and West, G., *Phys. Lett.*, **202B**, 47 (1988).
27. Renzini, A., *Astr. Ap.*, **171**, 121 (1987).
28. Spergel, D. and Faulkner J., preprint (1988).
29. Bouquet, A. *et al.* preprint (1988).
30. Salati, P. and Silk, J., *Ap.J.* (in press, 1988).
31. Yahil, A., Walker, D. and Rowan-Robinson, M., *Ap. J.*, **301**, L1 (1988).
32. Loh, E. and Spillar, E., *Ap. J. Lett.*, **307**, L1 (1986).
33. Faber, S. and Gallagher, J., *Ann. Revs. Astron. Ap.*, **17**, 135 (1979).

34. Davis, M. and Huchra, J., *Ap.J.*, **254**, 437 (1982).
35. Carr, B.J., Bond, J.R. and Arnett, W.D., *Ap.J.*, **277**, 445 (1984).
36. Hegyi, D. and Olive, K., *Ap. J.*, **303**, 56 (1986).
37. Kawano, L., Schramm, D. and Steigman, G., *Ap.J.*, **327**, 750 (1988).
38. Ford, H.C. *et al.*, I.A.U. Symposium **131** (in press) (1988).
39. Jones, C. and Forman, W., *Ap.J.*, **276**, 38 (1984).
40. Fabian, A., Nulsen, P. and Carizares, C., *M.N.R.A.S.*, **201**, 933 (1982).
41. Sarazin, C.L. and O'Connell, R.W., *Ap.J.*, **268**, 552 (1983).
42. Silk, J., Djorgovski, S., Wyse, R. and Bruzual, G., *Ap.J.*, **307**, 415 (1986).
43. Bahcall, J.N., *Ap.J.*, **276**, 169 (1984).
44. Kuijken, K. and Gilmore, G., *Nature* (in press) (1988).
45. Scalo, J., *Fund. Cosm. Phys.*, **11**, 1 (1986).
46. Silk, J. in Comets to Cosmology, ed. A. Lawrence (Berlin: Springer), p. 297 (1988).
47. Larson, R.D., *Mon. Not. Roy. Astr. Soc.*, **218**, 409 (1986).
48. Wyse, R. and Silk, J., *Ap. J. Letters*, **313**, L11 (1987).
49. Lacey, C. and Fall, S.D.M., *Ap.J.*, **290**, 154 (1985).
50. Matsumoto, T. *et al.*, *Ap.J.* (in press) (1988).
51. Hayakawa, S. *et al.*, *P.A.S.J.*, **39**, 941 (1987).
52. Fujimoto, M.Y. *et al.*, *Ap.J.*, **287**, 749 (1984).
53. Chieffi, A. and Tornambé, A., *Ap.J.*, **287**, 745 (1984).
54. Woosley, S. and Weaver, T., *Ann. Rev. Astr. Ap.*, **24**, 205 (1986).
55. Winget, D.J. *et al.*, *Ap. J. Lett.*, **315**, L77 (1987).
56. Lamb, D.Q. and Van Horn, H.M., *Ap.J.*, **200**, 306 (1975).
57. Iben, I. and Tutukov, A., *Ap.J.*, **282**, 615 (1984).
58. Little, B. and Tremain, S., *Ap. J.*, **320**, 493 (1987).
59. Tyson, A. in Dark Matter in the Universe, ed. J. Knapp and J. Kormendy (Dordrecht: D. Reidel), p. 315 (1987).
60. Bahcall, N. and Soneira, R.M., *Ap. J.*, **277**, 27 (1984).
61. Dressler, A. *et al.*, *Ap. J. Letter*, **313**, L37 (1987).
62. Davies, R.D. *et al.*, *Nature*, **326**, 462 (1987).
63. Vittorio, N. and Silk, J., *Ap. J. Lett.*, **293**, L1 (1985).

Desperately Seeking Dark Matter

Lawrence M. Krauss
Departments of Physics and Astronomy
Yale University
New Haven CT 06511



ABSTRACT

I provide an overview, from a particle physics perspective, of the candidates, and prospects for detecting dark matter.

I. INTRODUCTION

Last year at this time I presented the case for non-baryonic dark matter.¹ At this meeting I have been asked to provide an overview, from a particle physics perspective, of the candidates and prospects for detecting dark matter. Thus, I have the chance to finish the lecture I began a year ago.

I will first review rather generally the various candidates which have been proposed to constitute dark matter in the universe. As even a cursory analysis reveals, these candidates differ greatly in their properties. In spite of this, I will suggest that the mechanisms by which these widely differing particles might become dark matter fall under one of three different types, which I will then describe. Once we understand the mechanisms for generating dark matter, the means by which we might detect it are then more easily introduced. I will conclude by describing briefly the range of experiments which have been proposed to detect dark matter.

2. THE CANDIDATES:

In table 1 I list the current rogues gallery of what I call "standard" exotic cold dark matter candidates. To make it to this hit parade, a candidate must (a) have been around for more than a year, and more importantly (b) have been proposed for other than astrophysical purposes, i.e. responding to "legitimate" particle physics concerns.

Table 1: Standard Exotic Dark Matter Candidates

Particle	Mass for $\Omega=1$	Simplest Model?	Existing Bounds ^b (A=astro; D=direct)
Neutrino	≈ 30 eV	no	$\nu_e < O(20)$ eV (A,D)
Axion	$\approx 10^{-5}$ eV	no	$m < 10^{-2}-10^{-3}$ eV (A)
WIMPS:			
(a) Neutrinos:			
Dirac	≈ 2 GeV	no	$m < O(15-20)$ GeV? (D)
Majorana	≈ 5 GeV	no	
(b) SUSY:			
Photino	$\approx 1-50$ GeV	yes?	
Sneutrino	> 100 MeV	yes?	ruled out? (D)
Millicharge			
Shadow matter?	?	no	ruled out? (D)
Monopoles	?	?	

Scanning the table one notes a few important features. First, cold dark matter candidates vary widely in their mass, ranging from axions of 10^{-5} eV to monopoles of 10^{16} GeV or solitons which may be astrophysical in size. It is worthwhile noting that among the entire managerie, with the exception of perhaps SUSY models, the parameter range which results in a significant dark matter density for the particles listed is not "natural". By this I mean that if you locked a particle theorist in a room and asked her to invent any of these models, she would not have any particular reason to choose their masses to be in the range which is necessary to make them dark matter contenders. On the other hand, the parameters listed are not "unnatural". No a priori argument suggests they could not arise.

Finally, and most important, all of the candidates listed have either indirect bounds on them from independent astrophysical arguments, or direct limits from terrestrial experiments. It is this last feature which is most exciting. The virtue of imagining that the galactic halo dark matter resides in the form of elementary particles, is that the dark matter is then not just "out there" but is also streaming through this room. Experiments are now underway to probe directly for dark matter in the lab using a variety of techniques which I shall mention and which will be reviewed in this volume. Thus, over the course of the next 2-3 years, all of the candidates on the present hit parade may either be ruled out, or better yet, one may be detected.

II. DARK MATTER GENERATION: MECHANISMS

I suggest that one can categorize under three general themes the diverse mechanisms suggested thus far by which exotic elementary particles might become sufficiently abundant to dominate the mass density of the universe today. Such particles are either

(a) *Born to be Dark Matter*

or (b) *Achieve Dark Matterdom.*

or (c) *Have Dark Matterdom thrust upon them.*

I will now proceed to review each of these alternatives.

(a) *Born to be Dark:* This category is comprised of particles which, with little or no dynamics, by virtue of their very existence, come to dominate the energy density of the universe today. Nevertheless the exact manner in which this comes about can vary significantly. I describe here two important prototypical examples.

(i) Thermal production -- the neutrino paradigm: Light neutrinos were the first

among the non-baryonic candidates for dark matter to be taken seriously. There is good reason for this. First, we know neutrinos exist. Second, the same primordial nucleosynthesis calculations which predict so well the abundance of light elements in the universe guarantee that there is a cosmic neutrino background of roughly the same number density as photons today. The prescription goes as follows: Anything which is in thermal equilibrium at times when its mass is negligible compared to the temperature will have a thermal number density roughly equal to that of photons, by equipartition. Say these particles remain in thermal equilibrium until late enough that almost all massive particles that eventually dump their energy by annihilation into the relativistic particle bath have done so. Then if these particles go out of thermal equilibrium later, but still when the temperature exceeds their mass, equipartition still guarantees that there will be roughly the same number of these particles around today as photons in the cosmic background. Such is the case for light neutrinos, whose interactions decouple around 1 MeV, after all massive particles but electrons have dumped their rest energy into photons. Now the rest is easy. There are roughly 100 photons/cm³ in the microwave background today. With a temperature of about 3K, their energy accounts for about 10⁻⁵ of closure density today. Hence, just allow the neutrino, or whatever, mass to be about 10⁵ times 3K ($\approx 10^{-4}$ eV), or about 10 eV, and poof, you have an $\Omega=1$ universe².

(ii) Coherent production -- the axion paradigm: A much trickier way for particles to be born as dark matter is not to produce them thermally, but straight out of stored vacuum energy density. If this vacuum energy does not get converted by the present time, then it remains as the famous cosmological constant, which is perhaps the darkest way to close the universe. However, various mechanisms exist for converting such energy harmlessly at late times to an energy density of real particles. Here's one: Imagine any parabolic scalar field potential which is zero at the origin and rises upward. The second derivative at the origin gives the mass for the particles created by the field. The lowest energy configuration for such a field involves zero expectation value, or no density of particles in the vacuum. However, if the curvature is very small, then it costs very little energy to move up the potential energy curve. One can then easily imagine that after some inflationary epoch we happen to find ourselves in a universe which has inflated out of a region in which a non-zero vacuum energy in such particles had arisen. Due to inflation, all but the zero momentum, or spatially uniform configuration of this field has damped away. What happens next? Well the expectation value for a field is a classical quantity, so you just solve the classical field equations for the field to predict its evolution. In an expanding universe with Hubble parameter H , the evolution equation for a massive, minimally coupled scalar field is:

$$\ddot{\phi} - 3H\dot{\phi} + m^2\phi = 0 \quad (1)$$

Now this equation is trivial to solve in the two regimes where either $3H \gg m$, or $3H \ll m$. In the former case, the solution is a constant. Physically this is easy to understand. The lifetime of the universe is inversely proportional to the expansion rate H . If H is large, the lifetime is shorter than the classical period of oscillation in the parabolic potential, which is of order m^{-1} . Hence the field has not had time to "roll" down the hill. As long as this is the case, it is straightforward to show that the energy density in the field remains constant over time. In fact we don't even have to do this, since it is clear that this constant field VEV is nothing other than a cosmological term, which of course remains constant. Now once m is comparable to H the field begins to oscillate in the well, and one can then easily show that the energy density begins to redshift like standard massive field energy, i.e. like R^{-3} (where R is the scale factor of the universe.).

If you think about this, you will see what a miracle it produces. As long as the field energy remains constant, even a very small initial energy density will grow in relation to radiation, with a ratio which goes as R^4 (since the radiation density is redshifting like R^{-4}). This relative growth continues until a time inversely proportional to the particle's mass, at which time the field redshifts like normal matter. Thus, the smaller the particle mass, the greater the energy density remaining today compared to photons and baryons, even if only a miniscule extra energy density was necessary at early times to begin the whole process! This process is exactly the type of thing which occurs for axions in an inflationary scenario. Explicit calculations yield³:

$$\rho_{\text{axion}}/\rho_{\text{critical}} = k (10^{-5} \text{ eV}/m_{\text{axion}})^{3/2} \quad (2)$$

where k is a constant presumed to be of order 1.

Note two important differences between scenarios (i) and (ii). The latter produces a non-relativistic background of particles even though their mass may be small compared to the temperature of radiation today. Also, their energy is coherent, and not thermal, so that only a narrow band around the the frequency associated with their rest mass contains power.

(b) Dark Matter the Hard Way...Earning It (WIMPS): The first prototype WIMP (weakly interacting massive particle) is a neutrino heavier than 1 MeV (the temperature at which the weak interactions decouple). Now the situation is slightly different than before. At very early times things are still the same with all particles

being in thermal equilibrium with equal number densities. However, once the temperature drops below the neutrino mass, as long as it is still in equilibrium, its number density will drop compared to photons with a Boltzmann factor; $n_\nu/n_\gamma \approx \exp(-m_\nu/kT)$. This process will continue until the neutrino density becomes sufficiently sparse that annihilation can no longer compete with expansion. Here's where the dynamics enters! One must solve the Boltzmann rate equation to determine the time of "freeze-out" at which the neutrino to photon ratio freezes out. This has become known as the Lee-Weinberg bound, although it may have been done earlier by others, and it certainly has been done since by many...⁴. The numerical result is that a closure density of neutrinos results for:

$$m_\nu \approx 2 \text{ GeV (Dirac } \nu\text{'s)}^4; m_\nu \approx 5 \text{ GeV (Majorana } \nu\text{'s)}^5.$$

Now who ordered such neutrino masses? Well, while it is difficult to answer this question, there is a model in which such a situation arises more or less naturally: low energy supergravity (LES)⁶. The argument goes as follows: We don't observe the supersymmetric particles of ordinary matter at ordinary energies. Thus supersymmetry is broken. At what scale does this occur? Well, one scale where we know symmetry breaks is the weak interaction scale, of order M_W . Thus supersymmetric particles might have masses of this order. However in LES models the lightest SUSY particle is both stable, and has a mass of order $\alpha M_W \approx$ one or a few tens of GeV.⁶ This particle behaves exactly like a heavy neutrino, since its interactions with normal matter involve exchange of particles of mass of order M_W . It also has a mass in the range given above. Ta Da! (Of course such models have other cosmological problems, but I won't go into them here.)

(c) Dark Matter by force: There are again two prototypes which are forced to become dark matter due to factors beyond the purvey of mere dynamics.

(i) The monopole, or "topological" paradigm: Imagine the same type of potential I mentioned earlier, but with a little bump at the origin. Now the field would definitely prefer to have a non-zero VEV (costing no energy). However, if there is no inflation, then different regions of the presently observable universe will have been causally disconnected at all earlier times. In particular, at the time when the field relaxes to its VEV, it will take different values in different regions. Depending on the topology of the locus of minima of the potential, it is possible to force the field to go through zero VEV at some points in space to avoid singularities. (Like vortices in a superconductor) The topology of the vacuum determines what form the resultant local non-zero energy density gets trapped in: domain wall (Z_2), strings ($U(1)$), monopoles ($O(3)$ etc..). Some of these are disastrous and some harmless.

Some lead to dark matter today....

An alternative to such topological obstructions are non-topological remnants. Here many examples have been suggested: Quark Nuggets⁷, Q-Balls⁸, etc. The idea for all of these is essentially the same. If the Hamiltonian for the field is such that a local non-zero VEV configuration of radius R has energy that goes like:

$$E \approx Q/R + AR^2 + BR^3, \quad (3)$$

where Q,A,B, are constants, then it possible, depending on their values, for stable configurations to arise. Whether they are actually created in the early universe is another question.

(ii) Asymmetries: The final method for making non-baryonic dark matter involves a kind of numerology based on our experience with baryons. One of the most important numbers in cosmology is the baryon to photon ratio. This number, of order 10^{-9} , presumably results from a baryon-antibaryon asymmetry. If this were not the case, then the strong interactions are strong enough so that all the baryons would have annihilated into photons by today (see mechanism (b)). Now, the density of baryons today is about 1-20% of critical. Thus, if we give some other hypothetical particle an initial asymmetry comparable to that of baryons (perhaps this is natural....), then independent of its annihilation cross section, if its mass is about 5-100 times that of the proton, then it will close the universe today. Such mechanisms have been proposed just to avoid constraints on particles whose number density today depends on their interaction cross sections. (mechanism (b)).

There you have it. Choose your favorite and make a model, and maybe some experimentalist will probe it by one of the methods I mention below.

III. DETECTION:

If the galactic halo dark matter is non-baryonic, what are the parameters for detection? Well, the halo density in the region of the sun has been suggested⁹ to be

$$\rho \approx .3 \text{ GeV/cm}^3.$$

Assuming some virialized galactic velocity distribution of such particles then their mean velocity is expected to be of order

$$v \approx 300 \text{ km/sec} = 10^{-3} c.$$

Having these two numbers, you just have to plug in your favorite particle mass to find out the flux of such particles at the earth's surface. Once you have this, you need only calculate an interaction cross section to determine the energy deposit in an ideal detector. The numbers turn out to be rather daunting. For example:

<u>Candidate</u>	<u>Max Energy Deposit</u>	<u>Power Deposit</u>
axions	10^{-5} eV	10^{-24} Watts/m ³
WIMPS	$10 \cdot 10^4$ eV	10^{-19} Watts/kg.

These energies and this kind of power deposit require special low background detectors if such particles are to be observed. Nevertheless detectors have been proposed and are being built. I will review the detection prospects for WIMPS and axions briefly below.

(A) WIMPs: One first might think it is just plain impossible to detect these guys. After all, the cross section for scattering of massless neutrinos of keV energies on protons is of order $\sigma \approx G_F^2 E^2 \approx 10^{-50}$ cm². This results in a mean free path of about 10^8 light years in matter! However, as Goodman and Witten¹⁰ were the first to point out, this estimate is vastly in error. For massive neutrinos, the cross section is cut off by the mass, not the energy, so that for GeV scale particles scattering on protons, $\sigma \approx G_F^2 M^2 \approx 10^{-38}$ cm², 12 orders of magnitude larger. The mean free path is now more like 10^{13} cm.

One's first thought might be to find a detector of this size, and strange as this may sound, in a manner of speaking this is what I proposed¹¹ shortly after their paper. Namely, the Sun has a radius of $\approx 10^{11}$ cm, and an escape velocity from its core comparable to the galactic virial velocity, so that one might expect that WIMPS could be captured by the Sun.

So what?

Well, in the first place, it looked for a few days like this might solve the solar neutrino problem^{11,12}, by producing densities in the Sun's core of these particles which might mediate heat transfers which could cool the core¹³. Unfortunately, annihilation inside the sun of these particles with their antiparticles will in general keep the numbers far too small¹⁴. While this may be bad news for SNU's, it is good news for particle physicists, because among the annihilation products will be light neutrinos which can escape the sun, and interact inside proton decay detectors with just the right energies to be seen¹⁵! Limits on WIMPs from the absence of such an indirect signal are now available¹⁶ and will be discussed at this meeting.

However, forgetting indirect detection, the interaction cross sections mentioned above are much larger than reactor neutrinos-- which we can detect-- so it was first suggested¹⁰ that proposed "neutrino" detectors^{17,18} might be sensitive to WIMPs. In fact many such detectors (and new ones..) are now being designed, as you will hear at this meeting. It turns out that the energy deposit in existing low background double

beta decay detectors is probably measurable, as Caldwell will describe here¹⁹.

There are two slight wrinkles which have been raised recently: (1) It turns out that the interaction cross section of photinos off nuclei depends on a quantity which has probably recently been measured by the EMC collaboration at CERN, of all places. It seems this quantity is about a factor of 4 smaller than previously thought^{20,21}, but the good news is that it is much larger off neutrons than one would have guessed before. (2) WIMPS trapped in the earth can also give a direct signal. (see ref. 21 for the implications of both of these).

The cryogenic detectors which have been proposed to detect WIMPS are ingenious, and much of this meeting is devoted to discussing them. Suffice it to say here that within a year or two we might know something definitive....

(B) AXIONS: Axions are much more weakly interacting than WIMPs, but one should not give up hope. After all, gravitons are much more weakly interacting still, and we detect the gravitational force all the time....using coherence. The fact that the axion background is coherent over large volumes suggest one might couple axions coherently to a background detector in the lab. This was first proposed by Sikivie²², who exploited the coupling of axions to electromagnetic fields. Basically the $a\mathbf{E}\cdot\mathbf{B}$ coupling allows axions to turn into photons in the presence of a background magnetic field with the right spatial distribution. Thus what one proposes to build is an "axion radio": i.e. tune in a large Q microwave cavity to the axion frequency, and find photons where there were none before. This is not so easy. Calculations by myself and colleagues²³ suggest the task is very daunting. Nevertheless, brave experimenters have recently produced limits within one order of magnitude away from the predicted axion signal²⁴. There is hope....

Thus we may be on the threshold of a wonderful new discovery, unprecedented in its importance for both cosmology and astrophysics. Or else, all of the premises on which these experiments are based are wrong....

^aAlso Visiting Scientist, Harvard Smithsonian CFA. Research supported in part by the DOE and by a Presidential Young Investigator Award.

References:

1. L.M.Krauss, in *The Standard Model, The Supernova 1987a*, ed. by J. Tran Thanh Van, Editions Frontieres (Gif Sur Yvette, 1987)
2. This was originally presented by R. Cowsik, Phys. Rev. Lett. 39, 784 (1977)
3. For reviews and refs, see L.M.Krauss, in *High Energy Physics 1985*, ed by M.

- Bowick and F. Gürsey, World Scientific (Singapore 1985), or J.E. Kim, Phys. Rep. 150, 1 (1987)
4. For a review see G. Steigman, Ann. Rev. Nucl. Part. Sci. 29, 313 (1979)
 5. L.M.Krauss, Phys. Lett. 128B, 37 (1983)
 6. For a review see J. Polchinski, in *Inner Space, Outer Space*, Ed. by E. W. Kolb et al, University of Chicago, (Chicago 1986)
 7. E. Witten, Phys. Rev. D30, 272 (1984)
 8. S. Coleman, Nucl. Phys. B262, 263 (1985)
 9. see for example M. S. Turner, Phys. Rev. D33, 889 (1986)
 10. M.W. Goodman and E. Witten, Phys. Rev. D31, 3259 (1985)
 11. L. M. Krauss, Harvard Preprint HUTP-85/A008a (1985) unpublished
 12. see for example W. H. Press, and D.N. Spergel, Ap. J. 296, 679 (1985)
 13. see for example J. Faulkner and R. Gilliland, Ap. J. 299, 994 (1985)
 14. L.M.Krauss et al., Ap. J. 299, 1001 (1985)
 15. see for example M. Srednicki, K. Olive and J. Silk, Nucl. Phys. B279, 804 (1987)
 16. see for example J. LoSecco et al., Phys. Lett. B188, 388 (1987)
 17. A. K. Drukier and L. Stodolsky, Phys. Rev. D30, 2295 (1985)
 18. B. Cabrera, L.M. Krauss and F. Wilczek, Phys. Rev. Lett. 55, 25 (1985)
 19. D. Caldwell, these proceedings
 20. J. Ellis, R. A. Flores, and S. Ritz, Phys. Lett. B198, 393 (1987)
 21. L.M.Krauss and P. Romanelli, Yale preprint YCTP-P3-88, submitted to Phys. Rev. Lett.
 22. P. Sikivie, Phys. Rev. Lett. 51, 1415 (1983)
 23. L. M. Krauss, J. Moody, D. Morris and F. Wilczek, Phys. Rev. Lett. 55, 1797 (1985)
 24. University of Rochester Preprint 1988.

SEARCHING FOR DARK MATTER USING UNDERGROUND DETECTORS

Keith A. Olive
School of Physics and Astronomy
University of Minnesota
Minneapolis, MN 55455 USA

ABSTRACT

The possibility of detecting cold dark matter by searching for high energy ($E_\nu \geq 1$ GeV) neutrinos produced by dark matter annihilations in the sun using underground detectors is reviewed. The best current limits available come from combining data from the IMB, Kamioka and Frejus detectors.

The thought that we know extremely little about perhaps as much as 90% of the overall mass of the Universe is troubling. At this meeting, we have heard many reasons for believing in the existence of dark matter. On galactic scales there is evidence from rotation curves for an extended dark halo. On cosmological scales, present theories of galaxy formation and inflation imply that the ratio of the overall mass density to the critical closure density $\rho/\rho_c = \Omega = 1$. On the other hand, big bang nucleosynthesis¹⁾ restricts the portion of Ω in baryons $\Omega_b \leq 0.15$, leaving the rest necessarily in the form of non-baryonic dark matter.

Although experimental searches for dark matter are taking place, to date only limits on candidate particle properties exist. At this meeting, we have heard several talks on direct searches for dark matter²⁾. In this contribution, I will discuss the prospects of an indirect search looking for high energy neutrinos in underground proton decay-type detectors produced by dark matter annihilations in the sun³⁻¹¹⁾. Experimental data for these searches exists¹²⁻¹⁵⁾ and the best limits are found by combining these data samples^{7,8)}.

In addition to the big bang nucleosynthesis constraint on Ω_b , there are strong reasons why we believe that the dark matter must be non-baryonic¹⁶⁾. There are of course many such candidates available from particle physics¹⁷⁾. Among these only the neutrino is a known-to-exist particle. If its mass is less than $O(100\text{eV})$, it would be a so-called hot dark matter particle in that at the time of perturbation growth for galaxy formation, it was still relativistic. A particle which was non-relativistic at this time is called a cold dark matter candidate. These include, heavy neutrinos ($m_\nu \geq O(\text{few}) \text{ GeV}$), photinos/higgsinos, sneutrinos and axions. Unlike the case for heavy neutrinos, which in general we would not expect to be stable, supersymmetric theories nearly always predict the existence of one stable massive particle¹⁸⁾ making one of the supersymmetric candidates (in my view) highly favorable as cold dark matter.

While the cosmological abundance of neutrinos depends only on the neutrino mass (because the annihilation is mediated by W and Z exchange) the abundance of photinos is controlled by both the photino mass and the unknown scalar fermion masses which mediate annihilations. This means that for (almost) any $m_{\tilde{\nu}}$ $\Omega_{\tilde{\nu}}$ can be set equal to one by an appropriate choice of a sfermion mass^{19;18)}, $m_{\tilde{F}}$. Indeed by combining current experimental limits on $m_{\tilde{F}}$, one finds²⁰⁾ a lower bound on $m_{\tilde{\gamma}} > 6 \text{ GeV}$ (for $\Omega(h/0.5)^2 \leq 1$) and in addition if $m_{\tilde{\gamma}} \leq 10 \text{ GeV}$ then $\Omega(h/0.5)^2 \geq 0.1$ implying that photinos would make a significant contribution to the overall mass density.

Assuming the existence of dark matter and assuming that the dark matter is responsible for the observed flat rotation curves of galaxies it is possible to estimate the mass density of dark matter in an isothermal halo,

$$\rho = \frac{v_r^2}{4\pi G} \left(\frac{1}{a^2 + r^2} \right) = 0.07 \text{ GeV cm}^{-3} \left(\frac{v_{100}^2}{a_{10}^2 + r_{10}^2} \right) \quad (1)$$

where $v_r = 100 v_{100} \text{ km s}^{-1}$ is the galactic rotation velocity, $a = 10a_{10} \text{ kpc}$ is some core radius for the halo and $r = 10 r_{10} \text{ kpc}$ is the distance from the galactic center to the sun. Typical values are $v_{100} \approx 2.4$, $r_{10} \approx 1$ and $a_{10} \approx 0.6$ so that $\rho = 0.3 \text{ GeV cm}^{-3}$. Dark matter particles in the solar neighborhood may be trapped²¹⁾ in the sun as they pass through and elastically scatter. Numerically, the trapping rate is^{21,4)}

$$\Gamma_t \approx 10^{29} \text{ s}^{-1} (n_x / 0.3 \text{ cm}^{-3}) (300 \text{ kms}^{-1} / \bar{v}) (1 \text{ GeV} / m_x) (\sigma_E / 10^{-36} \text{ cm}^2) \quad (2)$$

where n_x is the dark matter abundance in the solar neighborhood, \bar{v} is the R.M.S. velocity of X in the halo and σ_E is the elastic scattering cross-section.

The abundance of dark matter particles in the sun is controlled by annihilations^{3,22)} and evaporation^{23,21,9)} which is negligible for $m_x \geq 3 \text{ GeV}$. Although the annihilations make it difficult²²⁾ to resolve to the solar neutrino problem by heat transfer²³⁾ they open up a possibility for detecting a signature of the presence³⁾ of dark matter. The products of these annihilations are high energy neutrinos. In particular, we will be interested in looking for the prompt neutrinos in reactions such as^{5,6)}



It is then straightforward to calculate the differential flux of neutrinos produced in this way⁶⁾

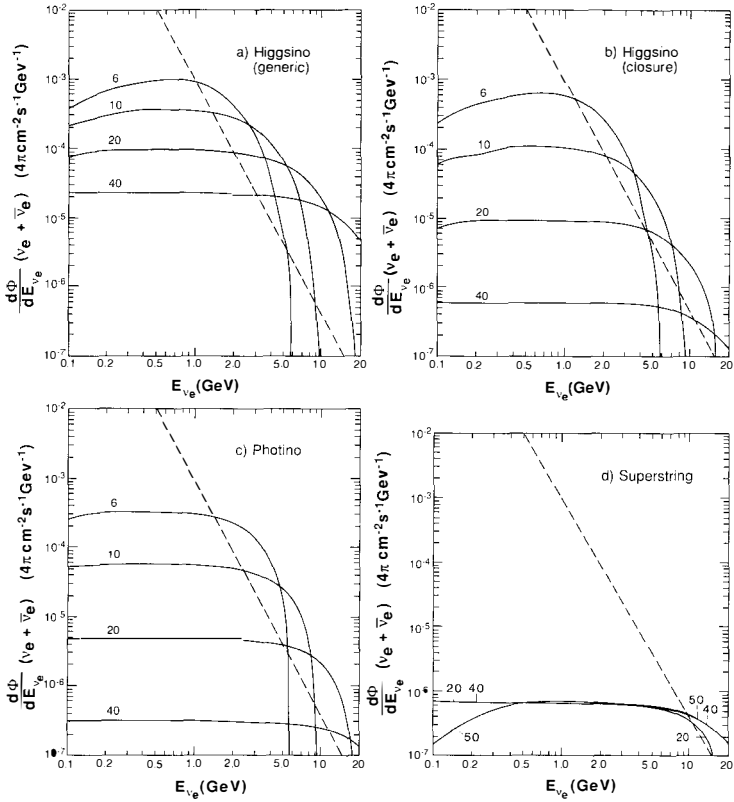
$$\frac{d\Phi}{dE_\nu} = \sum_f \frac{1}{4\pi d^2} \frac{\Gamma_f B_f}{\Gamma_f} \frac{1}{\Gamma_f} \frac{d\Gamma_f}{dE_\nu} \quad (4)$$

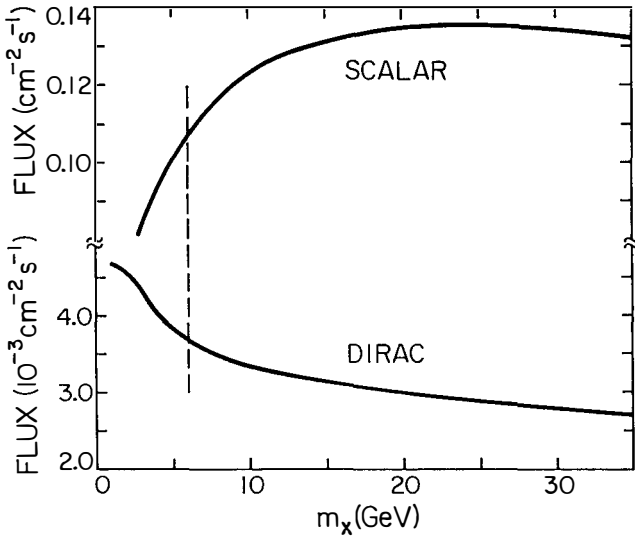
where $d = 1 \text{ A.U.}$, B_f is the branching ratio for $f \rightarrow f' + \bar{l} + \nu_l$ and Γ_f is the decay rate for the same process. We can now compare eq. (4) with the differential flux of atmospheric neutrinos produced by cosmic rays²⁴⁾. In the figures⁶⁾, the differential neutrino flux for a) (generic) higgsinos (these are equivalent to Majorana mass neutrinos, i.e. their abundance is completely determined by their mass); b) (closure) higgsinos (their abundance can always be adjusted so that $\Omega = 1$); c) photinos; and d) also shown is a typical candidate from superstring inspired theories²⁵⁾.

Indicated on the figures, is the mass of each particle in the range 6-40 GeV (a-c) and 20-50 GeV (d). The dashed line is the atmospheric background flux

of ν_e 's within 30° of the sun. Also shown is the total flux of monochromatic neutrinos⁴⁾ for the Dirac mass neutrinos and sneutrinos. The differential flux for these particles is just

$$\frac{d\Phi}{dE} = \Phi\delta(E - m_\chi). \quad (5)$$





In order to make the comparison between the calculated dark matter induced flux and the background we must compute an event rate

$$\bar{S} \propto \int dE V_F(E) \sigma_\nu(E) \frac{d\Phi}{dE_\nu} \quad (6)$$

for neutrinos from the sun, where V_F is the fiducial volume of the detector and σ_ν is the neutrino cross-section in the detector. A similar computation is done for the atmospheric background rate \bar{A} . We also distinguish between three types of events⁸⁾: 1) contained events with $1\text{ GeV} \leq E_\nu \leq 2\text{ GeV}$; 2) neutrino events with $E_\nu > 2\text{ GeV}$ producing through-going muons; and 3) contained events with $E_\nu \geq 2\text{ GeV}$.

Data for each of these event types exists. For case 1), IMB¹²⁾ reports 11 events within 30° of the sun out of a total of 89 events. The 90% confidence level statistical upper limit on the ratio $r = \bar{S}/\bar{A}$ is $r < 0.14^{7,8)}$. For case 2), IMB¹²⁾ reports 2 through going muon events within 8° of the sun out of a total of 187 events yielding $r < 0.024$ at the 90% confidence level. Finally for case 3), IMB¹²⁾ reports 0 events out of 10 within 30° of the sun for $r < 0.23$; Kamioka¹³⁾ reports 0 events out of 23 for $r < 0.10$ and Frejus¹⁴⁾ reports 0 events out of 24 with $r < 0.096$.

Because the data is still statistics limited, the best limit for contained events with $E_\nu \geq 2$ GeV comes from combining the data yielding⁸⁾

$$r < 0.040$$

(7)

In the tables, the calculated values of r are shown⁸⁾.

Table 1. Photinos

$m_{\tilde{\gamma}}$ (GeV)	r (Case 1)	r (Case 2)	r (Case 3)
4	0.11	0.014	0.097
6	0.032	0.015	0.077
10	0.0067	0.016	0.054
20	—	0.0066	0.013
40	—	0.0023	0.0023
limit	0.14	0.024	0.040

Table 2. Higgsinos

$m_{\tilde{H}}$ (GeV)	r (Case 1)	r (Case 2)	r (Case 3)
6	0.045	0.0091	0.052
10	0.0084	0.010	0.040
20	—	0.0057	0.012
40	—	0.0023	0.0025
limit	0.14	0.024	0.040

Table 3. Majorana neutrinos

m_{ν^M} (GeV)	r (Case 1)	r (Case 2)	r (Case 3)
6	0.055	0.011	0.064
10	0.023	0.028	0.11
20	0.0058	0.051	0.11
40	—	0.078	0.082
limit	0.14	0.024	0.040

Table 4. Dirac neutrinos

m_{ν^D} (GeV)	r (Case 1)	r (Case 2)	r (Case 3)
4	—	0.022	0.087
6	—	0.044	0.12
10	—	0.10	0.17
20	—	0.30	0.24
40	—	0.70	0.28
limit	0.14	0.024	0.040

Table 5. Scalar electron neutrinos

$m_{\tilde{\nu}_e}$ (GeV)	r (Case 1)	r (Case 2)	r (Case 3)
4	—	—	3.7
6	—	—	6.3
10	—	—	11.
20	—	—	20.
40	—	—	26.
limit	0.14	0.024	0.040

Table 6. Scalar muon neutrinos

$m_{\tilde{\nu}_\mu}$ (GeV)	r (Case 1)	r (Case 2)	r (Case 3)
4	—	0.50	1.4
6	—	1.3	2.3
10	—	3.8	4.1
20	—	13.	9.5
40	—	35.	18.
limit	0.14	0.024	0.040

Before discussing the limits we can set based on this data, it is worthwhile to remind the reader of the uncertainties in the analyses. These were discussed in detail in ref. 7. The largest uncertainty comes from astrophysics because the trapping rate $\Gamma_t \propto n_x / \tilde{v}$. If we naively take the limits $1.75 \leq v_{100} \leq 2.6$, $0.8 \leq r_{10} \leq 1$, and $0 \leq a_{10} \leq 2.5$ ($\tilde{v} = \sqrt{3/2} v_r$)

$$0.14 \leq \left(\frac{n}{0.3 \text{cm}^{-3}} \right) \left(\frac{300 \text{ kms}^{-1}}{\tilde{v}} \right) \leq 2.3 \quad (8)$$

implying the signal could be lowered as much as by a factor of 7. However Flores²⁶⁾ has argued that conservative lower limit on ρ_x might be 0.2 GeVcm^{-3} implying a smaller uncertainty. Other factors to be taken into account are fragmentation effects¹⁰⁾, couplings to protons¹¹⁾ and properties of the halo²⁷⁾.

Keeping in mind the uncertainties, we can obtain the following limits on cold dark matter candidates with $m_x \geq 3 \text{ GeV}$:

photinos:	$m_{\tilde{\gamma}} \geq 15 \text{ GeV}$
Higgsinos:	$m_{\tilde{H}} \geq 10 \text{ GeV}$
Majorano Neutrinos:	excluded as dark matter
Dirac Neutrinos:	excluded as dark matter
e, μ sneutrinos:	excluded

One should be very aware however that with the exception of the sneutrinos all limits are within a factor of 2-3 of being acceptable so conservatively we can conclude only the sneutrinos are excluded.

In summary, limits based on the (non) detection of high energy neutrinos from the sun due to the annihilation of cold dark matter candidates are available. Future experiments and data are likely to greatly improve these limits or (hopefully) find a signature.

ACKNOWLEDGEMENTS

Much of the work described here was done in collaboration with J. Hagelin, K.W. Ng, J. Silk and M. Srednicki. Research was supported in part by DOE grant DE-AC02-83ER040105 and by a Presidential Young Investigator Award.

REFERENCES

1. J. Yang, M.S. Turner, G. Steigman, D.N. Schramm and K.A. Olive, Ap. J. 281, (1984)493.
2. J. Rich, D. Caldwell, B. Sadoulet, L. Gonzales-Mestres, D. Perret-Gallix and R. Lanou, these proceedings.
3. J. Silk, K.A. Olive and M. Srednicki, Phys. Rev. Lett. 55, (1985)257.
4. M. Srednicki, K.A. Olive and J. Silk, Nucl. Phys. B279, (1987)804.
5. T.K. Gaisser, G. Steigman and S. Tilar, Phys. Rev. D34, (1986)2206.
6. J. Hagelin, K.W. Ng and K.A. Olive, Phys. Lett. 180B, (1986)375.
7. K.W. Ng, K.A. Olive and M. Srednicki, Phys. Lett. 188B, (1987)138.
8. K.A. Olive and M. Srednicki, Phys. Lett B (in press) 1988.
9. K. Greist and D. Seckel, Nucl. Phys. B283, (1987)681.
10. S. Ritz and D. Seckel, CERN preprint TH-4627 (1987).
11. J. Ellis, R.A. Flores and S. Ritz, CERN preprint TH-4812 (1987).
12. IMB Collaboration: J. LoSecco et al, Phys. Lett. 188B, (1987)388.
13. Kamioka Collaboration: Y. Totsuka, University of Tokyo preprint UT-ICEPP-87-02 (1987).
14. Frejus Collaboration: B. Kuznik, Orsay preprint LAL 87-21 (1987).
15. D. Casper, M. Takita and B. Kuznik, these proceedings.
16. D. Hegyi and K.A. Olive, Phys. Lett. 126B, (1983)28 and Ap. J. 303, (1986)56.

17. see e.g. L. Krauss, these proceedings.
18. J. Ellis, J. Hagelin, D.V. Nanopoulos, K.A. Olive and M. Srednicki, Nucl. Phys. B238, (1984)453.
19. H. Goldberg, Phys. Rev. Lett. 50, (1983)1419.
L.M. Krauss, Nucl. Phys. B227, (1983)556.
20. K.A. Olive, J. Silk and M. Srednicki, in Proceedings of the Theoretical Workshop on Cosmology and Particle Physics ed. I. Hinchliffe (World Scientific Press, Singapore 1997) p. 148.
21. W.H. Press and D.N. Spergel, Ap. J. 296, (1985)67;
A. Gould, Ap. J. 321, (1987)571.
22. K. Freese, D.N. Spergel and W.H. Press, Ap. J. 299, (1986)1001.
23. G. Steigman, C. Sarazin, H. Quintana and J. Faulkner, A.J. 83, (1978)1050; D.N. Spergel and W.H. Press, Ap. J. 294, (1985)663.
24. see e.g. D.H. Perkins, Ann. Rev. Nucl. Part. Sci. 34, (1984)1.
25. B. Campbell, J. Ellis, K. Enqvist, D.V. Nanopoulos, J. Hagelin and K.A. Olive, Phys. Lett. 173B, (1986)270.
26. R. Flores, CERN preprint TH-4736(1987).
27. D. Spergel, these proceedings.

Direct Detection of Particle Dark Matter

J. Rich
DPhPE, CEN Saclay
91191 Gif-sur-Yvette, France



Abstract

We discuss in general terms the problem of detecting and identifying weakly-interacting particles in our galactic halo via the observation of nuclei recoiling from elastic scatters. Emphasis is placed on experimental signatures and on detector requirements as to size, energy sensitivity and background. The problems are illustrated with three popular dark-matter candidates: heavy Dirac neutrinos, supersymmetric photinos, and cosmions (particles invented to solve the solar-neutrino problem). Recent progress in the construction of suitable detectors is discussed.

1 Introduction

The idea that our galaxy is surrounded and pervaded by a gravitationally-trapped gas of weakly-interacting massive particles is an attractive hypothesis that is not without strong theoretical and observational motivation [1]. Three years ago, Goodman and Witten [2] suggested that such particles could be directly detected by observing nuclei recoiling from elastic scatters. Recoil energies are small, 0.01-100 keV, with rates in the range of events/day for kilogram size targets. The Goodman-Witten program then presents a challenge to modern low-energy calorimetry.

Possible detection techniques were first reviewed by Smith [3] and more recently by Sadoulet [4]. In this review, we will concentrate on the general requirements for detectors of weakly-interacting dark-matter candidates with masses in the GeV range, e.g. heavy Dirac and Majorana neutrinos, photinos, and cosmions (particles invented to solve the solar-neutrino problem). Astrophysical signatures for such particles, i.e., the presence of dark matter annihilation products in cosmic radiation, was discussed in this conference by Olive [5] and by the various experimental groups involved [6]. Detection of other types of particle dark matter, e.g. axions, monopoles, and quark nuggets, was discussed in this conference by Gonzalez-Mestres [7].

2 Kinematics and Experimental Signatures

In a collision of a (dark-matter) particle of mass m_x and velocity $v(= \beta c)$ with a stationary nucleus of mass m_N , the nucleus will receive a kinetic energy E given by

$$E = m_N c^2 \beta^2 (1 - \cos \theta) \left[\frac{m_x}{m_N + m_x} \right]^2 \quad (1)$$

where θ is the center of mass scattering angle. For a given m_N the observed distribution of recoil energy is determined by m_x (unknown) and the distributions of β and θ . The hypothesis that the particles are gravitationally trapped in the galaxy constrains the particles to have, like the Earth, velocities of order $10^{-3}c$. One generally assumes [8,9,10] that the halo particles have a quasi-Boltzmannian velocity distribution with $v_{rms} \approx 270 km/sec$ and that the solar system moves through this distribution on its circular galactic orbit with $v_c \approx 220 km/sec$. Because of the Earth's movement about the sun, the Earth's velocity with respect to the dark matter has an annual modulation of $\pm 15 km/sec$.

As for the distribution of θ , most dark-matter candidates scatter via the exchange of heavy particles so the low energy total cross section is independent of v and isotropic in the center-of-mass. Under these assumptions, the observed distribution E will be the roughly exponential distribution shown in figure 1. The average value of E is a function of m_x and m_N :

$$\langle E \rangle \approx 2keV \frac{m_N}{1GeV} \left[\frac{m_x}{m_N + m_x} \right]^2 \quad (2)$$

Also shown in figure 1 is the seasonal modulation of the distribution resulting from the Earth's movement about the solar system. The effect is about 15% at $E = \langle E \rangle$.

For large nuclei, the assumption of isotropic scattering is false because of the nuclear elastic form factor [11]. This gives a differential scattering cross section that is proportional to $\exp(-E/E_{coh})$, where E_{coh} is a function of the radius, R , of the nucleus:

$$E_{coh} = \frac{3\hbar^2}{2m_N R^2} = 300keV \left(\frac{20}{A}\right)^{5/3} \quad (3)$$

where in the last form we have used $R \approx 1.2A^{1/3}fm$. The exponential form factor will not significantly affect the form of the observed (already exponential) recoil spectrum. However, for nuclei heavier than silicon and m_z not too small, it will strongly change the average value of E , the reciprocal of which is now given approximately by the sum of the reciprocals of E_{coh} and $\langle E \rangle$ as given by eq. 2 .

Ignoring the form factor, equation 2 says that for a given nucleus, $\langle E \rangle$ is proportional to m_z for $m_z \ll m_N$ and reaches an asymptotic value for $m_z \gg m_N$. A given detector will, then, be sensitive only to particle masses greater than a value determined by its energy threshold.

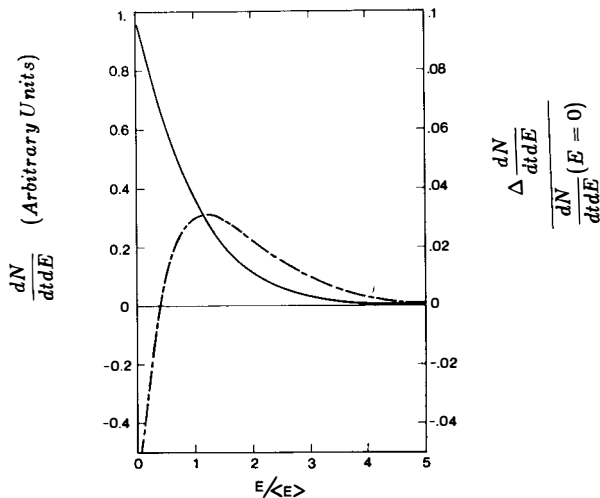


Figure 1: The average differential scattering spectrum (solid line, arbitrary scale) as a function of $E/\langle E \rangle$. and the difference between the maximum (May) and minimum (Nov.) differential rates (dash-dot line, right scale).

For a given m_x equation 2 shows that $\langle E \rangle$ rises linearly for $m_N \ll m_x$, reaches a broad maximum at $m_N = m_x$, and then falls like m_N^{-1} . By using several targets, one can then determine m_x and the mean velocity (which determines $\langle E \rangle$ for the optimal nucleus). Unfortunately, for m_x greater than 20 GeV, the spectrum for the optimal nucleus is strongly affected by the nuclear form factor, so the mass cannot be measured by this method.

One can, in principle, identify a signal as due to dark matter by using the above kinematical characteristics to distinguish it from background due to the ambient radioactivity (see the next section). This would require one to use several nuclear targets and/or to have sufficient statistics to see the seasonal modulation. An even stronger signature would come from the strong correlation of the recoil direction of the nucleus with the direction of the Earth's galactic motion, a point recently emphasized by Spergel [10]. Unfortunately, there are no existing detectors that can measure the direction of recoiling nuclei in the keV range, though some speculations have been put forward [3,12].

If one merely wants to set limits on the presence of various dark matter candidates, one needs only to compare the counting rate of one's detector with that calculated for the dark-matter candidate. We turn, therefore, to questions of background and event rates.

3 Background

For purely calorimetric techniques, background for dark-matter scattering will come from Compton-, beta-, and photo-electrons due to the ambient radioactivity. In the keV range, the lowest rate for such processes is near 1 event $(\text{kg-day-keV})^{-1}$ [11,13].

4 Event Rates and Present Limits

The normalization of the differential scattering rate (figure 1) is simply related to the $v \rightarrow 0$ limit of the elastic scattering cross section on the target nucleus, σ , the reduced mass of the particle-nucleus system, m_{red} , the local number density of halo particles, ρ/m_x , and the average value of particle inverse velocity, $\langle v^{-1} \rangle$ (in the Earth-frame):

$$m_N^{-1} \frac{dN}{dt dE}(E=0) = \frac{1}{2} \frac{\sigma}{m_{red}^2} \frac{\rho}{m_x} \langle v^{-1} \rangle \quad (4)$$

Estimates of ρ tend to be near $0.4 \text{ GeV}/\text{cm}^3$ [1], and for the galactic model discussed above, $\langle v^{-1} \rangle^{-1} \approx 260 \text{ km}/\text{sec}$. Dark-matter candidates are distinguished by their values of σ/m_{red}^2 and m_x .

For weakly interacting particles, σ is proportional to m_{red}^2 and to a series of factors determined by the interaction strength and the nature of the couplings

[14]. For particles with vector couplings, σ for a heavy nucleus will be of the form:

$$\sigma \approx \frac{G^2}{2\pi} m_{red}^2 C^2 \quad (5)$$

where G is the strength of the particles couplings to nucleons and C is a linear function of the number of protons, Z , and the number of neutrons, N , in the nucleus. This linearity reflects the fact that for vector couplings, the scattering amplitudes on individual nucleons add coherently to give a cross section much greater than the cross section on individual nucleons. For heavy Dirac neutrinos with normal Weinberg-Salam-Glashow couplings, G is equal to the Fermi constant, G_F , and C^2 is nearly equal to $N^2/2$ [2,11]. Supersymmetric scalar-neutrinos have similar couplings.

If the particle's couplings are purely axial-vector, the scattering amplitude on individual nucleons will be proportional to the nucleon spin and will cancel for paired nucleons. For N -even, Z -even nuclei (the majority of terrestrial nuclei) one almost always has complete pairing and $\sigma = 0$. For nuclei with one unpaired neutron (N -odd, Z -even) or one unpaired proton (N -even, Z -odd), σ takes the form [14,17]

$$\sigma \approx G^2 m_{red}^2 \lambda^2 J(J+1) \quad (6)$$

where J is the nuclear spin and λ is a factor of order unity determined by the orbital quantum numbers of the unpaired nucleon. G is the interaction strength that may depend on whether there is an unpaired neutron or unpaired proton. For Majorana neutrinos, G is of order G_F for both neutrons and protons. For photinos scattering by the exchange of scalar-quarks of mass m_{sq} , G is proportional to e^2/m_{sq}^2 , with a constant or proportionality of order unity for protons [15,16]. Since the neutron is uncharged, one would naively expect a much smaller constant for neutrons [15,16]. It has been argued [16,17] that recent results on the spin-dependent structure function of the proton [20] indicate that the photino has a coupling to neutrons that is larger than expected and a coupling to protons that is smaller than expected. This belief has, however, been contested [19].

Concerning m_z , galactic models require only that the particles be heavier than a few tens of eV. However, for Dirac and Majorana neutrinos and for photinos, the mass and couplings determine, via the annihilation cross section, the mean cosmological density, Ω_x . This quantity is usually assumed to be within an order of magnitude of the closure density, which defines a range of interesting masses and couplings [17,18,22].

Unlike these "standard particles", cosmions [21] have masses and couplings that are chosen so that they are captured in the sun at rate that solves the solar-neutrino problem: $G \approx 10G_F$ and $4GeV < m_z < 10GeV$. Since only the cross section on protons is determined by astrophysical arguments, they may have either vector or axial vector couplings in any proportion.

Figure 2 shows (σ/m_{red}^2) vs m_z for a variety of dark matter- target combinations. The curve " $\nu_D - Ge$ " refers to Dirac neutrinos scattering on germanium.

Curves for other targets can be found by scaling by N^2 . The range of masses corresponds to Ω_ν within an order of magnitude of the closure density [18]. The curve " $\tilde{\gamma} - p$ " (" $\tilde{\gamma} - n$ ") refers to photino scattering on typical odd-Z (odd-N) nuclei. The cross sections were taken from reference [17]. (In both cases the most optimistic cross sections were used; for $\tilde{\gamma} - p$ ($\tilde{\gamma} - n$) the cross section could be a factor 4 (factor 100) smaller.) The scalar-quark masses were chosen for each m_x to make $\Omega_{\tilde{\chi}} h_{1/2}^2 = 1$ [22]. (Degenerate scalar fermions are assumed.) The cross section is inversely proportional to the assumed Ω . The curve "C-Si" refers to cosmion scattering on silicon assuming a cross section proportional to Z^2 . The curve "C-p" refers to cosmion scattering on typical odd-Z nuclei assuming only axial-vector couplings.

Putting some nominal particle physics and cosmological values into equation 4, we get the following differential rate per unit target mass:

$$\frac{1000 N_A}{A} \frac{dN}{dt dE} (E=0) = 2.8 (\text{kg} \cdot \text{day} \cdot \text{keV})^{-1} \times \left[\frac{\sigma/m_{red}^2}{G_F^2/2\pi} \right] \left[\frac{1 \text{ GeV}}{m_x} \right] \left[\frac{\rho}{.4 \text{ GeV}/\text{cm}^3} \right] \left[\frac{220 \text{ km/sec}}{v_c} \right] \quad (7)$$

Contours of equal differential rate are shown as the dashed lines in figure 2.

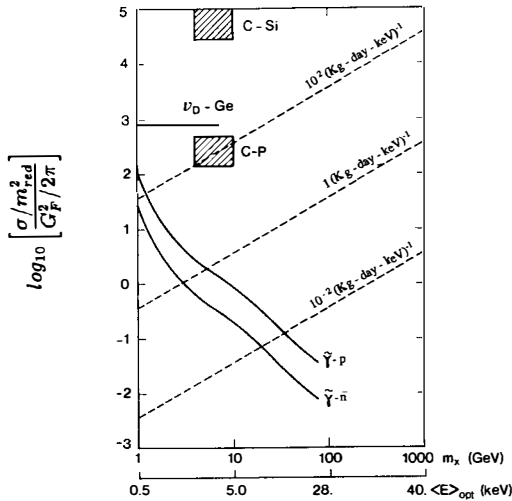


Figure 2: σ/m_{red}^2 vs m_x for several particle-nucleus combinations as explained in the text. The diagonal dashed lines show the differential rate using equation (7). The second horizontal scale shows $\langle E \rangle$ for the optimal nucleus using equations (2) and (3).

An experiment can place limits on the bracketed quantities in equation 7 by comparing, over their range of sensitivity, the calculated rate with the observed rate. The limit will depend on m_x since this quantity, in addition to m_N determines $\langle E \rangle$. Figure 3 shows the limits from the Germanium experiment of reference [11] (for improved limits, see [13]). For large m_x , the excluded range follows the contour for 1 event $(\text{kg}\cdot\text{day}\cdot\text{keV})^{-1}$ since for large masses, the experiment is sensitive to most of the recoil spectrum (see the bottom scale). For smaller masses, the sensitivity decreases because $\langle E \rangle$ becomes smaller than the experimental threshold, $\approx 20\text{keV}$. Below 10 GeV, the experiment has no sensitivity.

If we had used a galactic model with a smaller $\langle v^{-1} \rangle^{-1}$, the limits at large m_x would have been better but would not have extended down to such low values of m_x .

Also shown in figure 3 are the contours for photino and Dirac neutrinos scattering on germanium assuming $\rho = .4\text{GeV}/\text{cm}^3$. The experiment rules out a wide range of mass for Dirac neutrinos but not in the range where such particles are expected to be cosmologically important. For photinos, the experiment has low sensitivity because of the low isotopic content of ^{73}Ge (7.76 percent) and "high" background. The experiment has no sensitivity at all to cosmions because of their low mass.

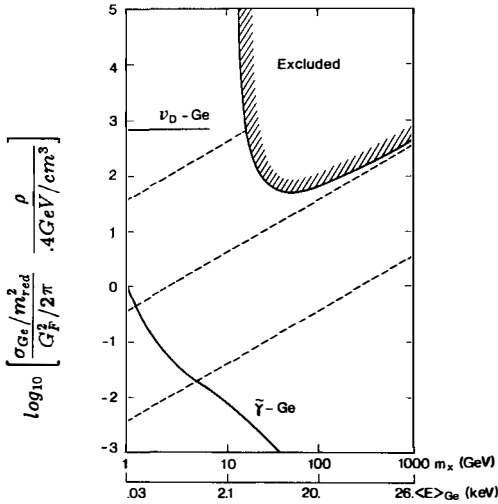


Figure 3: The limits on interaction strength and local density as a function of m_x from the germanium experiment of reference [11]. The dashed lines show the differential rate as in figure 2. The second horizontal scale shows $\langle E \rangle$ as calculated from equations (2) and (3).

5 Future Detector Requirements

From figure 3, it is clear that there are two general requirements for future dark-matter detectors. For dark-matter candidates with vector couplings, we need to become sensitive to lower mass particles. This implies going to lower mass nuclei and lower energy thresholds with respect to Ge semiconductor detectors. In both respects, silicon, either as a semiconductor or, in the future, as a phonon detector (see the next section) is probably the best bet for fast progress [30].

For particles with only spin-dependent couplings, the primary problem is one of background, since the rates are generally below the $1 \text{ (kg day keV)}^{-1}$ now obtainable with germanium detectors. It may be difficult to lower this figure with existing detectors where much effort has already gone into the exploitation of construction materials with very low radioactivity. One can search for dark matter somewhat below the background by using the anticipated seasonal modulation [8,9]. A big reduction in background for silicon and germanium detectors could also come about by detecting, in addition to e^- -hole pairs, the phonons produced by the recoiling nucleus, since the ratio between the two excitations is expected to be different for electrons and nuclei.

The most important progress must come through the development of targets of different nuclear composition. As for germanium, a detector enriched in ^{73}Ge could be more than ten times more sensitive to majorana particles than present germanium detectors. Unfortunately, isotope enrichment is very expensive. The development of targets based on odd- Z materials is essential if we are to investigate those Majorana particles that couple primarily to protons. This is the case with photinos and even more so for cosmions whose characteristics are defined by their couplings to protons.

As for detector size, the requirements are relatively modest, at least if one is willing to accept many cells. Figure 4 shows, for Dirac neutrinos and photinos, the detector size and threshold required for 1 event/day, assuming 1000 cells. Also shown are the performance of some existing detectors. Detectors with a low enough threshold to see Dirac neutrinos already exist, but they are, for the moment, not massive enough to get a sufficient rate. For photinos, silicon and germanium semiconductor detectors have sufficient size (assuming photinos couple to neutrons). This just emphasizes again that the problem here is one of background.

6 A Catalog of Possible Detectors

One does not detect recoiling nuclei, but rather things made by recoiling nuclei. Table 1 shows a list of such things. For the moment, only detectors of e^- -hole pairs (germanium and silicon semiconductors) have yielded useful limits on some dark matter candidates. Detectors of phonons (bolometers), randomized spins (magnetic bolometers) and broken Cooper pairs (superconducting tunnel junctions) have yielded impressive first results that are shown in figure 4. Detectors observing rotons in ^4He or phase transitions in superconducting grains or wires

are, for the moment, interesting ideas that have yet to be developed. Scintillators and gas detectors are classic detectors but it is far from clear that the signal due to recoiling nuclei is sufficient for them to be used in dark-matter searches. Which, if any of these techniques, will prove to be the best for dark matter detection is an open question.

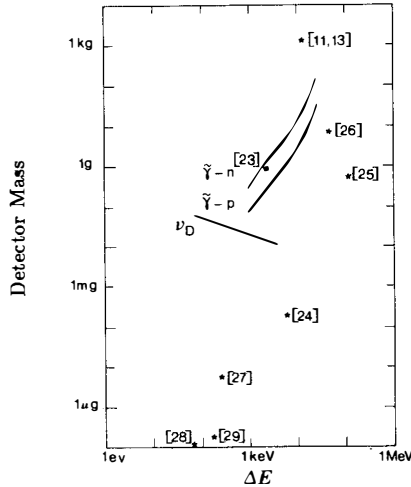


Figure 4: Detector mass and energy sensitivity required for 0.001 event/day for Dirac neutrinos ($1 \text{ GeV} < m_x < 10 \text{ GeV}$) on silicon and for $\Omega = 1$ photinos ($2 \text{ GeV} < m_x < 80 \text{ GeV}$) on the optimal odd-Z or odd-N nucleus. The references refer to existing detectors and the type of detector can be read from table 1.

Table 1: Some things that are made by recoiling nuclei.

thing	medium	reference
e^- -hole pairs	semiconductors	
	germanium	[11,13]
	silicon	[23,30]
phonons	crystals	[31,24,25,27,39]
randomized spins	magnetically polarized media	[26]
broken Cooper pairs	superconductors	[28,29,32]
rotons	superfluid ^4He	[33]
phase transitions	small superconductors	[34,35,36,37]
scintillation	scintillators	[38,36]
e^- -ion pairs	gases	[12]

Acknowledgements : It is a pleasure to thank the following people for conversations concerning various aspects of this review: A. de Bellefon N. Booth, M. Chapellier, G. Chardin, N. Coron, J. Ellis, F. v. Feilitzsch, E. Fiorini, L. Gonzalez-Mestres, L. Krauss, D. Perret-Gallix, B. Sadoulet, A. Schuhl, J. Silk, P. Smith, M. Spiro, C. Tao, and G. Tarlé.

References

- [1] J.Silk, in these proceedings
L.Krauss, in these proceedings.
- [2] M.W.Goodman and E.Witten, Phys.Rev. D31 (1985) 3059.
- [3] P.F.Smith, Rutherford-Appleton Lab preprint RAL-86-029.
- [4] B.Sadoulet, Lawrence-Berkeley Lab preprint LBL-24302.
- [5] K.Olive, in these proceedings.
- [6] D.Casper, in these proceedings;
G.Kuznik, in these proceedings;
M.Takita, in these proceedings.
- [7] L.Gonzalez-Mestres, in these proceedings.
- [8] A.K.Drukier, K.Freese and D.N.Spergel, Phys.Rev. D33 (1986) 3495.
- [9] K.Freese, J.Freedman and A.Gould, SLAC preprint SLAC-PUB-4427 (1987).
- [10] D.N. Spergel, Phys.Rev. D37 (1988) 1353.
- [11] S.P.Ahlen, F.T.Avignone III, R.L.Brodzinski, A.K.Drukier, G.Gelmini and D.N.Spergel, Phys.Lett.B195 (1987) 603.
- [12] J.Rich and M.Spiro, Saclay report DPhPE88-04 (1988).
- [13] D.O.Caldwell in New and Exotic Phenomena edited by O.Fackler and J.Tran Thanh Van (Editions Frontieres, Gif-sur-Yvette, France,1987);
D.O.Caldwell, in these proceedings.
- [14] I.Wasserman, Phys.Rev. D33 (1986) 2071.
- [15] G.L.Kane and I.Kani, Nucl.Phys. B277 (1986) 525.
- [16] J.Ellis, R.A.Flores and S.Ritz, Phys. Lett. B198 (1987) 393.
- [17] J.Ellis and R.A.Flores, CERN preprint CERN-TH.4911/87.
- [18] E.W.Kolb and K.A.Olive, Phys.Rev. D34 (1986) 2531.
- [19] F.E.Close and R.G.Roberts, Phys.Rev.Lett. 60 (1988) 1471.
- [20] P.B. Renton et al., Oxford Univ. preprint 88/87.
- [21] J.Faulkner and R.L.Gilliland, Astrophys.J. 299 (1985) 994;
D.N.Spergel and W.H.Press, Astrophys.J. 294 (1985) 663;
W.H.Press and D.N.Spergel, Astrophys.J. 296 (1985) 679;
R.L.Gilliland et al., Astrophys.J. 306 (1986) 703.

- [22] T.K.Gaisser, G.Steigman and S.Tilav, *Phys.Rev.* D34 (1986) 2206.
- [23] J.Rich, R.Rocchia and M.Spiro, *Phys.Lett.B* 194 (1987) 173.
- [24] Th.Peterreins, F.Pröbst, F. von Feilitzsch, R.L.Mössbauer and H.Kraus, *Phys. Lett. B* 202 (1988) 161.
- [25] A.Alessandrolo, D.V.Camin, E.Fiorini and A.Giuliani, *Phys.Lett. B* 202 (1988) 611.
- [26] M.Bühler and E.Umlauf, *Europhys. Lett.* 5 (1988) 297.
- [27] D.McCammon, S.H.Moseley, J.C.Mather and R.F.Mushotzky, *J.Appl.Phys* 56 (1984) 1263.
- [28] D.Twerenbold and A.Zehnder, *J.Appl.Phys.* 61 (1986) 1.
- [29] H.Krauss et al., *Europhys.Lett.* 1 (1986) 161.
- [30] B.Sadoulet, J.Rich, M.Spiro and D.O.Caldwell, *Astrophs.J.* 324 (1988) L75.
- [31] B.Cabrera, L.M.Krauss and F.Wilczek, *Phys.Rev.Lett.* 55 (1985) 25.
- [32] N.E.Booth, Oxford University report 93/87 (1987).
- [33] R.E.Lanou, H.J.Maris and G.M.Seidel, *Phys.Rev.Lett.* 58 (1987) 2498; R.E.Lanou, in these proceedings.
- [34] A.Drukier and L.Stodolsky, *Phys.Rev.* D30 (1984) 2295.
- [35] W.Seidel, L.Oberauer and F.v.Feilitzsch, *Rev.Sci. Instrum.* 58 (1987) 1471.
- [36] D.Perret-Gallix, in these proceedings.
- [37] P.F.Smith, *Z.Phys.C* 31 (1986) 265.
- [38] D.J.Ficenec et al., *Phys.Rev.* D36 (1987) 311.
- [39] B.Sadoulet, in these proceedings.

DARK MATTER SEARCH WITH A Ge DETECTOR

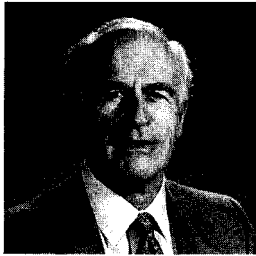
UCSB-LBL-UCB Collaboration

D.O. Caldwell,¹ R.M. Eisberg,¹ F.S. Goulding,² D.M. Grumm,¹ B. Sadoulet,³
A.R. Smith,² and M.S. Witherell¹

Presented by

David O. Caldwell

Department of Physics, University of California, Santa Barbara, CA. 93106

**Abstract**

A very low background Ge detector used to search for double beta decay has yielded new restrictions on candidates for cold dark matter particles in the halo of our galaxy. Particles with $\beta = 10^{-3}c$ with respect to the earth and having spin-independent interactions would scatter coherently from Ge nuclei. From the observed counting rate at low energies Dirac neutrinos constituting all of dark matter are excluded for masses between 12 GeV/c^2 and 1.4 TeV/c^2 . Better limits are set on magninos ($< 11 \text{ GeV}/c^2$) and cosmions ($< 9 \text{ GeV}/c^2$), proposed massive particles which also explain the solar neutrino problem and which interact more strongly with Ge. In addition, millicharged shadow matter is ruled out as the main form of dark matter.

¹ Department of Physics, University of California, Santa Barbara, CA. 93106

² Lawrence Berkeley Laboratory, Berkeley, CA. 94720

³ Department of Physics, University of California, Berkeley, CA 94720

Since perhaps 90% of matter is detected only through its gravitational interactions, knowledge of what constitutes this dark matter would have widespread importance for astrophysics and cosmology. As it is unlikely¹⁾ that dark matter consists of particles as they are known in the Standard Model, the discovery of their nature would also point the way to important new particle physics. Useful constraints on candidates for dark matter can already be set by apparatus used to search for neutrinoless double beta decay. In order to approach lifetime limits²⁾ on this process in ^{76}Ge of 10^{24} years, it has been necessary to take extreme measures to reduce backgrounds. When the energy threshold for the Ge detectors is made as low as possible, the resulting background rates can be used to set limits on the scattering of the dark matter candidates from the Ge nuclei.³⁾ Limits on some specific models for dark matter, and some more general constraints on dark matter are obtained from measurements with the UCSB/LBL double beta decay detector.⁴⁾

The apparatus has been described elsewhere,⁴⁾ but some relevant features will be mentioned. Up to 8 Ge detectors have been used for double beta decay, but the data of concern here comes from just one detector of about 160 cm^3 fiducial volume (0.9 kg). The Ge detectors were enclosed in a cavity formed by ten blocks of NaI (Tl) scintillator of 15-cm thickness. Compton scattering, which provides the main source of radioactivity background at low energies, is suppressed not only by the vetoing of the scattered γ in the NaI or another Ge detector, but also because many of the γ 's come from cascade decays, and the detection of one of these other γ 's would also eliminate the event. The threshold at 30 keV ionization energy for the NaI counters is high enough that the small energy deposits by the dark matter candidates do not cause a veto signal, except for the case of large cross section. The NaI detectors are surrounded by borated polyethylene to degrade and capture neutrons and then a 20-cm shield of 99.999% pure virgin lead.

Much effort has been devoted to finding materials of low radioactivity and to developing fabrication procedures to reduce the amount of such materials. In order also to avoid losing γ 's before they could be vetoed, it was particularly necessary to keep structural material to a minimum inside the NaI cavity and to have that used of as low an atomic number, Z , as possible.

When the apparatus was constructed, the emphasis was on achieving low background near 2.041 MeV, the region to be searched for a peak from neutrinoless double beta decay in ^{76}Ge . However, when it was decided to look for dark matter, we found that there was a rapidly rising background below about 400 keV. This was due to the presence of about half a gram of In, which has a 486 keV β^- with a half-life of 4×10^{14} years! When the In was replaced by Au in one detector, the background for that detector became flat down to about 14 keV at a level of $\frac{1}{2}$ count/keV \cdot kg \cdot day, except for some X-ray peaks. A part of that spectrum is shown in Fig. 1, and it will be noticed that at lower energies the counting rate rises due mainly to

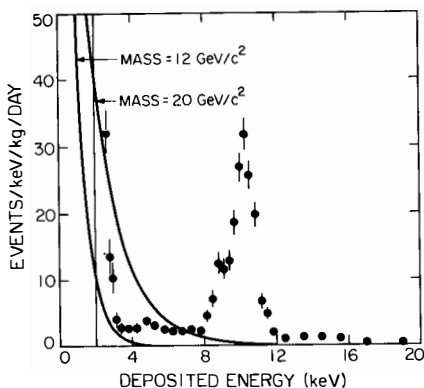


Fig. 1. Ionization energy detected at the low end of the operating range of one Ge counter in a four-week run. Below the Ga and Zn X-ray peaks the noise is almost flat until 3 keV. The threshold was set at 2.0 keV. The two curves show the contributions expected for particles of mass 12 and 20 GeV/c^2 , which interact via Z^0 exchange. Taking into account the almost flat background in the 3 to 8 keV region, the 12 GeV/c^2 curve is ruled out at the 95% confidence level.

Ga (10.4 keV), and a little to Zn (9.7 keV) X-ray peaks which result from the $^{68}\text{Ge} - ^{68}\text{Ga}$ decay chains coming from radioactivity induced by cosmic rays when the Ge was above ground.²⁾ The counting rate drop at the low end of the X-ray peaks begins to be off-set by the rapidly rising noise rate which currently limits measurements to about 3 keV. Although further improvements will occur, we already have lower backgrounds in the low energy region than have heretofore been available. Hence, we have utilized those data to set useful limits on several dark matter candidates.

An interesting speculation⁵⁾ which has motivation from string theory is that another world may occupy the space in which we live and that this shadow universe interacts with us only gravitationally. However, Holdom⁶⁾ pointed out that if any particle, no matter how heavy, exists connecting the two universes, then the shadow universe has a massless photon which mixes with our photon, providing a way in which shadow photons can interact with us through a very weak electric charge. Goldberg and Hall⁷⁾ investigated whether such

millicharged shadow matter could be a candidate for dark matter and found that it was possible, despite constraints from cosmology, galactic astrophysics, and Ge detector counting rates⁸⁾ at the surface and at a depth of 4000 m.w.e. However, our experiment gives a rate about $\frac{1}{3}$ that of the PNL/USC experiment⁸⁾ in the relevant range of ionization energies (20–150 keV) and is at a depth of only 600 m.w.e. In order that too few particles survive to that depth to be counted at the observed background rates, their cross section (and hence the shadow proton mass) has to be so large that it exceeds other constraints, eliminating this as a dark matter candidate.

Another candidate for dark matter is the class of weakly interacting massive particles (WIMPs) which interact via Z^0 exchange. This vectorial, spin-independent interaction is coherent in a nucleus and so depends on the square of the number of neutrons, N^2 . If the coupling of these particles is similar to that of Dirac neutrinos and their mass is greater than a few GeV/c^2 , the resulting large annihilation cross section necessitates at masses above a few GeV/c^2 particle-antiparticle asymmetry for them to be responsible for all of dark matter.⁹⁾ An asymmetry similar to that of baryons would require a mass of the order of 10 GeV.

For such a particle of mass m scattering from a Ge nucleus of mass M , the average energy deposition at low energy is $\langle E_d \rangle = m^2 M \langle v^2 \rangle / (m + M)^2$, where $\langle v^2 \rangle$ is the mean square speed of m . For these low values of E_d , the recoiling nucleus ionizes very inefficiently and gives an ionization signal much smaller ($\sim \frac{1}{4}$) than that of an electron of the same kinetic energy. Fortunately, accurate measurements¹⁰⁾ of this ionization efficiency have been made by neutron scattering in Ge down to an equivalent electron energy of 2 keV ($E_d \approx 10$ keV), and the results agree very well with the theory of Lindhard, et al.¹¹⁾ It is the equivalent electron energy which is plotted in Fig. 1.

To compare the measured rates in Fig. 1 with the spectrum expected for a given mass of Dirac neutrino from the halo of our galaxy, we took a halo density of $0.3 \text{ GeV}/\text{cm}^3$, which is $5.3 \times 10^{-25} \text{ g}/\text{cm}^3$, and a Maxwellian velocity distribution with a root mean square average of 270 km/s without any truncation (which could exist if the galaxy escape velocity were relatively low). For the relevant period (March) we assumed the velocity of the earth with respect to the halo to be 230 km/s. Using the known³⁾ interaction cross section and

the parametrization of Lindhard's model¹¹⁾ by Robinson,¹²⁾ the solid curves of Fig. 1 were generated for several values of m . If we assume a flat background in the region 3–8 keV, masses above 12 GeV/ c^2 are excluded. The mass value is actually double valued for a fixed halo density, so there is an upper bound of 1.4 TeV for the region of excluded masses. If we decrease the halo density by 30%, the lower mass limit increases from 12.0 to 12.5 GeV/ c^2 . Changing the r.m.s. velocity to 240 km/s increases the limit to 12.2 GeV/ c^2 .

There is an interesting variant on the standard Dirac neutrino which Raby and West have proposed¹³⁾ in order to have the same particle not only be the main component of dark matter but also explain the solar neutrino problem. This apparent deficit of ^8B neutrinos coming from the sun¹⁴⁾ could be explained¹⁵⁾ by WIMPs being trapped in the sun and transporting energy from the core to larger solar radii, thereby slightly cooling the central region from which most of the neutrinos originate. This mechanism requires cross sections with protons of about 10^{-36} cm², a low enough annihilation rate, and masses roughly in the range of 4 to 15 GeV/ c^2 . Below 4 GeV/ c^2 the particles evaporate too rapidly from the surface and above about 15 GeV/ c^2 they do not travel far enough from the core to cool it efficiently. Such particles could also explain¹⁵⁾ the discrepancy between observations of solar oscillations and the standard solar model, but the required properties are not possessed by conventional or even previously proposed particles.¹⁶⁾ The Raby-West¹³⁾ solution is to postulate a fourth-generation Dirac neutrino, called a magnino, since it would have a large magnetic moment arising from the existence nearby in mass of its charged partner and associated Higgs particle. The resulting electromagnetic interaction with protons has an appropriate cross section $\sim 10^{-36}$ cm², two orders of magnitude longer than the weak interaction cross section. For a heavy nucleus like Ge, however, the electromagnetic interaction becomes only comparable to the weak interaction. In addition, the interference term becomes model dependent, since it involves the charge radius, r , and magnetic moment, μ , of the magnino. With parameters ($\mu = 1/8\pi^2$, $r^2 = \mu^2/8m^2$, where $m =$ magnino mass) suggested by Raby and West, the resulting mass limit is 11 GeV/ c^2 , which is not very different from that for a particle with only weak interactions. Although the statement is often made that WIMPs with cross sections large enough to account for the solar neutrino problem should be easy to detect in laboratory

experiments, this model at least shows that that is not necessarily so. However, as the mass of either the incident particle or the target nucleus is diminished, the relative effect of the electromagnetic interaction becomes more important.

In contrast, there are models for WIMPs to solve the solar neutrino problem in which the large cross section on protons is reflected in a large cross section on Ge as well. These include the cosmion of Gelmini, Hall, and Lin,¹⁷⁾

which interacts with light quarks via a heavy colored scalar, another fourth-generation neutrino of Raby and West,¹⁸⁾ which has a stronger interaction because of a light neutral Higgs, and the neutrino from broken E_6 of Ross and Segrè,¹⁹⁾ which gets its needed interaction from an addition Z' . A single mass limit of $< 9 \text{ GeV}/c^2$ is determined from the data for all of these models because the cross sections are large enough so that the limit is set by the kinematic threshold.

Since such models may be ephemeral, it is important to display the results of this experiment in a way which may have wider eventual application. Such information is shown in Fig.

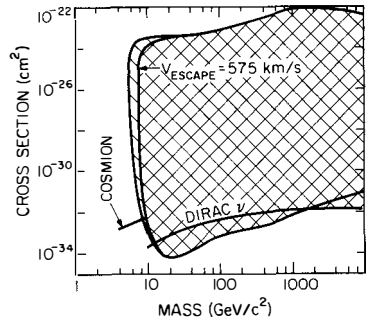


Fig. 2. Mass exclusion plot for particular cross sections for the interaction with Ge (or for the upper boundary, with the earth) using data from the present experiment. The larger shaded region is excluded if the escape velocity is infinite; the smaller region if the escape velocity is 575 km/s. All limits are 2σ . The curve near the bottom of the plot shows the cross section as a function of mass for a Dirac neutrino. The short line with the label cosmion shows the expected cross section for cosmions with mass between 4 and 9 GeV/c^2 .

2, which is an exclusion plot in dark particle mass vs. interaction cross section above the detector. In the region of large masses, the upper limit on cross section corresponds to the case in which the energy deposition in the NaI is sufficient to veto the event. At lower masses, particles with a large enough cross section are slowed before they reach the apparatus so that they produce insufficient recoil energy to be observed. The left edge of the exclusion region is determined by the data near threshold. Note the small difference in this region which occurs if a 575 km/s escape velocity is assumed to truncate the Maxwellian velocity distribution. The lower edge rising with mass comes from a combination of the decreasing number density

of the incident particles (since the mass density of the halo is fixed) and of an increasing contribution of the background due to the widening of the expected energy distribution. We have taken into account the loss of coherence at high masses, assuming a radius of $4 \cdot 10^{-13}$ cm for the Ge nucleus. Above about 50 GeV mass the background at energies above the Ga X-ray is setting the limit. At high masses, the lower limit is proportional to mass. All mass limits given here are at the two standard deviation level. In all cases the usual assumption has been made that the considered particles constitute all of dark matter.

Fig. 2 shows that existing Ge detectors set useful limits on dark matter candidates. We have shown here that one class of proposed dark matter, millicharged shadow matter, is effectively eliminated and that the masses of particles with an initial asymmetry in the universe, such as Dirac neutrinos, magninos, and cosmions, are being constrained. While the present apparatus will give improved results after some time, more promising is the development of Si detectors which can cover the full range (down to 4 GeV) of interest for WIMPs which could also solve the solar neutrino problem.²⁰⁾

This work was supported in part by the U.S. Department of Energy, and the results could not have been obtained without the invaluable help of D.L. Hale, D.A. Landis, N.W. Madden, and R.H. Pehl. One of us (DOC) thanks the von Humboldt Foundation for a U.S. Senior Scientist Award utilized during the preparation of this paper.

REFERENCES

- 1) D. Hegyi and K.A. Olive, *Phys. Lett.* , B126, 28 (1983); J. Yang et al., *Ap. J.* **281**, 493 (1984); G.R. Blumenthal et al., *Nature* **311**, 517 (1984).
- 2) D.O. Caldwell et al., *Phys. Rev. Lett.* , 59, 419 (1987).
- 3) M.W. Goodman and E. Witten, *Phys. Rev. D* , 31, 3059 (1985).
- 4) F.S. Goulding et al., *IEEE Trans. Nucl. Sci.* NS-**31**, 285 (1984); and *IEEE Trans. Nucl. Sci.* NS-**32**, 463 (1985); D.O. Caldwell et al., *Phys. Rev. Lett.* , 54, 281 (1985); and *Phys. Rev. D* , 33, 2737 (1986).
- 5) D.J. Gross et al., *Phys. Rev. Lett.* , 54, 502 (1985).
- 6) R. Holdom, *Phys. Lett.* , B166 (196,) 1985.
- 7) H. Goldberg and L.J. Hall, *Phys. Lett.* , B174 (151,) 1986.
- 8) S.P. Ahlen et al., *Phys. Lett.* , B195, 603 (1987).

- 9) E.W. Kolb and K.A. Olive, *Phys. Rev. D* , 33 (1202), 1986; K. Greist and D. Seckel, *Nuc. Phys.* **B283**, 681 (1987).
- 10) C. Chasman in "Penetration of Charged Particles in Matter—A Symposium", National Academy of Sciences (1970), p. 16 and references therein.
- 11) J. Lindhard et al., Kgl. Dan. Vidensk. Selsk., *Mat.-Fys. Medd.* **33**, 10 and 14 (1963).
- 12) M.T. Robinson in "Nuclear Fusion Reactors", ed. by J.L. Hall and J.H.C. Maple, British Nucl. Energy Soc., London (1970), p. 364.
- 13) S. Raby and G.B. West, *Nucl. Phys.* **B292**, 793 (1987); *Phys. Lett.* , B194, 557 (1987); and *Phys. Lett.* , B200, 547 (1988).
- 14) J.K. Rowley, B.T. Cleveland, and R. Davis, Jr. in "Solar Neutrinos and Neutrino Astronomy", ed. by M.L. Cherry et al., AIP Conf. Proc. 126, Am. Inst. of Physics, New York (1985), p. 1.
- 15) J. Faulkner and R.L. Gilliland, *Ap. J.* **299**, 994 (1985); L.M. Krause, Harvard University preprint HUTP-85/A008a (1985, unpublished); W.H. Press and D.N. Spergel, *Ap. J.* **296**, 679 (1985); R.L. Gilliland, J. Faulkner, W.H. Press, and D.N. Spergel, *Ap. J.* **306**, 703 (1986).
- 16) L.M. Krause et al., *Ap. J.* **299**, 1001 (1985); J. Silk, K. Olive, and M. Srednicki, *Phys. Rev. Lett.* , 55, 257 (1985).
- 17) G.B. Gelmini, L.J. Hall, and M.J. Lin, *Nucl. Phys.* **B281**, 726 (1987).
- 18) S. Raby and G.B. West, *Phys. Lett.* , B202, 47 (1988).
- 19) G.G. Ross and G.C. Segrè, *Phys. Lett.* , B197, 45 (1987).
- 20) B. Sadoulet, J. Rich, M. Spiro, and D.O. Caldwell, *Ap. J. (Letters)* **324**, 75 (1988).

DETECTION OF DARK MATTER PARTICLES WITH LOW
TEMPERATURE PHONON SENSORS

Bernard Sadoulet
Department of Physics
University of California
Berkeley, California 94720
USA



ABSTRACT

Taking as an example our development effort in Berkeley, I discuss for nonspecialists (Astronomers and Particle Physicists) the promises of phonon sensing at low temperature for the detection of dark matter particles and the difficulties faced.

1. MOTIVATIONS

The hypothesis that dark matter is made out of exotic particles not yet discovered at accelerators is rather natural¹⁾, and specific enough to allow a direct experimental test²⁾. But as Rich has shown at this workshop³⁾, it is necessary to reach both lower thresholds and lower backgrounds that are presently available. The fundamental nature of the problem justifies a strong experimental development, and two directions are being explored:

- On the one hand, one could attempt to improve ionization detectors. Caldwell⁴⁾ discussed at this workshop the results obtained with solid state detectors and the developments which are being started. Low pressure gas detectors may also be promising^{3,5)}.

- On the other hand, many groups are launching development of cryogenic particle detectors⁶⁾. In the dark matter context, it is hoped that both smaller thresholds and lower backgrounds than conventional technologies allow, can be obtained.

The hope of reaching lower thresholds stems from the fact that much smaller quanta (broken Cooper pairs or phonons) are used in these detectors. Low thresholds are mainly interesting for investigating the low mass region of $2-4 \text{ GeV}/c^2$, which is not excluded by accelerators⁷⁾ and not accessible easily to ionization detectors. Another possible application of low thresholds is for the detection of dark matter particles trapped in the earth ^{8,2)}. If their mass is right ($\approx 12 \text{ GeV}/c^2$), then their flux at the surface is enhanced and a 1 gram detector sensitive to 10 eV deposition would detect a few events per day!

In my mind, a more important justification for the development of cryogenic detectors is that at least some of the proposed techniques are able to provide much smaller background. It is obvious from Caldwell's discussion that it is essential to obtain the followings:

- a good spectral resolution in order to exclude X-ray lines and to recognize the spectral shape and the annual modulation expected for a positive signal.

- some position resolution to exclude short range radioactive products from the experimental surroundings.

In addition, it would be extremely useful to have additional handles:

- a wide variety of materials to check the behaviour of both the signal and the background. Note also that, at least in naive models⁹⁾, Majorana particles are expected to interact only with targets having nuclear spins¹⁸⁾.

- an unambiguous signature that the interaction occurred on a nucleus.

The main background is expected ultimately to be Compton scattering in electrons by stray γ -rays¹¹⁾, and β from radiogenically produced materials such as tritium. If one could measure simultaneously both the ionization and the amount of heat deposited^{12,11)}, one could then recognize a nuclear recoil and reject these background contributions.

- directionality; Since the sun velocity is of the same order of magnitude as that of dark matter particles, they are expected to come mainly from one direction¹³⁾.

Although it is unclear whether the phonon distribution will remember the direction of the initial particle, with phonons detectors, it may be possible to reach in particular, most of these objectives. This has been the main motivation behind the effort of our group in Berkeley. Other types of cryogenic detectors have been proposed for dark matter detection and are reviewed in reference 6). Perret-Gallix¹⁴⁾ discussed the potentialities of superconducting granules at this workshop. We limit our remarks to the phonon detectors.

2. AN EXISTENCE PROOF: LOW TEMPERATURE CALORIMETRY.

The hope that phonon detectors can indeed do the job is further boosted by the recent success of low temperature calorimetry.

2.1 Calorimetry and Bolometry

Calorimetry is probably the oldest method for measuring a deposition of energy. The rise of temperature of an isolated system in which an energy ΔE is dumped is given by

$$\Delta T = \frac{\Delta E}{C}$$

where C is the system's heat capacity. For an insulator, the heat capacity behaves as T^3 (Debye law), as the temperature T approaches the absolute zero. Thus for low enough temperature, the sensitivity could be excellent.

This method has long been used by infrared astronomers to detect the infrared light from a star. In their case, the technique is known as bolometry since an energy flux is measured. The temperature is usually measured with a thermistor. A small bias current develops a voltage difference across it which is sensed by a FET amplifier.

As early as 1974, Niinikoski and Udo¹⁵⁾ suggested that this technique could be used for the detection of particles. This concept has been marvelously established by the work of McCammon, Moseley, and Mather¹⁶⁾. They have achieved a resolution of 17.4 eV FWHM for 6 keV X-rays, and the base line fluctuations are only 13 eV, a very impressive value which indicates the possibility of thresholds of the order of 30 eV!

2.2 Naive Extrapolation to Larger Sample.

The only problem with the last result is that it was obtained with a crystal of 10^{-5} g, far from the kilogram of detection needed for a dark matter search.

However, at least superficially, it is possible to extrapolate this method to much larger samples. Mather and co-workers¹⁷⁾ have shown that the noise is ultimately limited by the thermal noise (both the energy fluctuation of the crystal and the Johnson noise of the thermistor) and is given by

$$\delta E = \xi \sqrt{k T^2 C}$$

where ξ is a constant depending on the sensitivity of the thermistor, and is of the order of 2.5 for the best ones currently available. But for an insulator

$$C \sim T^3 M$$

where M is the mass of the sample and the T^3 is predicted by the Debye law.

Therefore

$$\delta E \sim \xi T^{5/2} M^{1/2}$$

and if ξ is a constant (that is the thermistor efficiency does not decrease with temperature), if the Debye law is valid and if no other contribution dominates the noise, it is possible to compensate a large increase in mass by a much smaller decrease in temperature.

Extrapolating naively in this way¹⁸), and starting from the heat capacity that McCammon et al. have measured for their detection at 100 mK, we conclude that it could be possible to have 100 eV threshold with crystals of 300g of boron, 200g of silicon, or 100g of germanium at 15 mK. Even taking the experimental characteristics of the thermistors, that we have measured at 20 mK, 50g of boron should achieve this threshold. Let us emphasize again that this assumes the absence of any deviation from the Debye law and of any excess noise!

3. A TYPICAL ITINERARY

Fascinated by those numbers, our Berkeley group started enthusiastically experimenting with these low temperature calorimeters. We were not the only ones nor the first ones, but our trajectory is fairly typical of the experience of other groups who have started similar developments for dark matter searches (Cabrera and co-workers at Stanford, Lanou and collaborators at Brown University, E. Fiorini et al. in Milano, and P. Smith and co-workers at Rutherford). As such, the following description may be informative for groups attracted by the subject!

I began to gather a cross disciplinary team of people able to spend (for most of them) a small amount of their time on this interesting problem: E. E. Haller, a material physicist who brought to the team his knowledge of Solid State Physics and his know-how with Neutron Transmutation Doped thermistors; A. Lange, an infrared astronomer and an expert in bolometry; and two particle physicists R. Ross and H. Steiner.

My students and I knew nothing about low temperatures. We started to train ourselves at 1.3K^o (with a pumped ⁴He cryostat). Using the same type of bolometers used by infrared astronomers, Ning Wang, a graduate student, could relatively easily observe α pulses, and over time we improved the signal to noise.

This experience showed us clearly the need to have state of the art amplifiers. We embarked then to develop a low noise FET which could work in a 4K environment. Carol Stanton, an undergraduate, succeeded in obtaining $1 \text{ nV}/\sqrt{\text{Hz}}$ for a 3 mW dissipation and a total input capacitance of 15 pF.

Meanwhile, we borrowed time on existing dilution refrigerations. Profs. Packard and Clarke in the Physics Department offered us to run parasitically in their fridges. This led us to quickly discover the problems of very low temperatures and of our devices. For instance, RF shielding (not available in Packard's fridge) proved absolutely essential for devices of the sensitivity we were using, and we have also learned many tricks of the trade. In the process, we started to identify the fundamental difficulties of the enterprise that are summarized below in section 4.

But in spite of the kindness and patient help of our hosts, it became clear that no fast progress was possible without having our own low temperature facility, adapted and dedicated to our project. With the help of the University, we bought a dilution refrigerator from Oxford Instruments. Tom Shutt, a graduate student, began to design and construct a Faraday cage and a gas system, and a year later we are nearly operational.

The experience of Fiorini, for instance, closely parallels this trajectory a few months before us. And it is when his team finally had its own fridge working that rapid progress was made. They have observed¹⁹⁾, for instance, an α spectrum with 0.7g of germanium, and at the time of this writing they have a 10g calorimeter. The noise is still large (50keV FWHM) because of thermistors and electronics which are not optimized, but these devices clearly show great promise!

4. A DEVELOPMENT AT THE FRONTIER OF SOLID STATE PHYSICS

Although the practical problems linked to starting up and operating at low temperature should not be underestimated (it took us two years to reach our present status), the fundamental problems we are facing are of another nature. The behavior of

the detectors we are trying to build depends critically on phenomena, which are at the frontier of the understanding in Solid State Physics. We will sketch two examples. Interested readers will find a more technical discussion in reference 20).

4.1 Are the phonons ballistic?

Even the small energy deposited by dark matter particles is huge compared to the typical energies in the crystal, and the initial interaction creates a "fireball" which expands and cools off. It leads to optical phonons which down-convert eventually to transverse phonons. The energy of these, in turn, gradually decreases to an energy corresponding to the crystal temperature. However at low temperature, as well known to Solid State physicists²¹⁾, the phonon lifetime in the bulk of the crystal increases as the inverse of the 5th power of their energy and for practical time scales, they stop thermalizing at an energy of 1 meV, or an effective temperature of 10 K, much higher than that of the crystal. Such phonons are called "ballistic" since they travel in straight lines with mean free path of the order of 1 cm and scatter on impurities, the different isotopes and surfaces.

This description contrasts sharply with the picture that we painted in section 2, where we assumed implicitly a complete thermalization of the phonons. Therefore the scaling laws that we gave are presumably unrealistic. But is it so bad to deal with phonons out of equilibrium? As first emphasized by Cabrera and coworkers²²⁾, there may be a number of advantages⁶⁾:

- If phonons stay at high energy, we indeed could use higher threshold detectors, such as aluminum tunnel junction²³⁾ or superconducting strips²⁴⁾. Experimentally, such an assertion has been unambiguously proven by the von Feilisch group²⁵⁾. Even for thermistors, the higher energy of the phonons may improve their coupling to the sensor²⁰⁾.

- If the sensor is not sensitive to thermal phonons, the heat capacity of the sample is irrelevant in determining the fluctuations of the detected energy. The crystal then acts as a phonon guide and very large detectors may be possible.

- Last, but not least, there is the remote possibility that the phonon flux may remember the initial direction of the incoming particle. After all, the initial momentum has to be conserved²⁶⁾, and may introduce some asymmetry if the down conversion process is not dominated by umklapp processes which transfer the momentum to the crystal as a whole. This would be an exceptional signature for dark matter detection¹³⁾.

However, using these properties would impose the requirement of not thermalizing unduly the phonons, for instance on surfaces, crystal defects or the interfaces between the crystal and the sensor. These problems are extremely difficult, and, unfortunately, are at the present frontier of Solid State Physics²⁷⁾.

In a contribution to this workshop²⁸⁾, R. Lanou gives another example of the use of sophisticated Solid State phenomena, rotons in ⁴He liquid.

4.2 The Phonon Coupling Mechanism in the Sensor.

Many problems are also encountered in the understanding of the sensor.

Let us take, for instance, the example of our Neutron Transmutation Doped germanium thermistors²⁹⁾. In a series of experiments, around 20 mK, we have tried to characterize their behaviour^{30,20)}, and have found the following:

- They indeed display a very fast resistance dependence on temperature. Between 20 mK and 70 mK, their resistance (extrapolated at zero bias current) changes by 5 orders of magnitude.

- Unfortunately, a resistance cannot be measured without a current and as soon as we apply a current, the resistance decreases greatly and the devices severely lose their sensitivity. The carriers in the crystal (holes in our case) become hot for very low biasing power.

- We have been trying to understand the origin of this phenomena, which is to some extent present in all semiconductor doped thermistors¹⁶⁾. Our tests point to the possibility of decoupling between the carriers and the (thermal) phonons. If this is the

case, it is indeed very bad news, since we would like to use these detectors as phonon sensors!

- The situation may be saved by the lack of thermalization of phonons mentioned in section 4.1. Theoretical reasons²⁰⁾ lead us to believe that high energy phonons will not encounter this decoupling problem. The α and 60 keV pulses that we observe in our samples have very fast rise times (limited by our electronics), as is expected for good coupling. This does not constitute, however, an unambiguous proof for that process, and we are actively trying to obtain better experimental evidence. Our problem is that not very much is known on these processes as hot carriers and electron-phonon decoupling phenomena are at the forefront of Solid State Physics. Again, this is typical and if we had chosen to describe the development of tunnel junctions, we would have encountered similar fundamental problems of Solid State Physics³¹⁾.

5. CONCLUSIONS

We seem to have drifted far from our scientific quest on the nature of dark matter. However, the full testing of the hypothesis that dark matter is made of particles requires very sophisticated instrumentation, able of detecting weak energy deposition and providing the signatures necessary to distinguish the signal from the background.

Cryogenic detectors are good candidates for this important and challenging job. It is too early to know whether they will succeed. From our remarks, it should be clear, however, that in order to develop them it is necessary to master hosts of practical and Solid State Physics problems. It will clearly be a long haul, but the experimental challenges are fascinating. In addition to dark matter searches, there are many promising applications⁶⁾. And the fundamental nature of our initial scientific question certainly deserves a large amount of effort.

This work is partially supported by the U.S. Department of Energy, contract No. DE-AC03-76SF00098.

References

- 1) Silk ,J., this volume.
- 2) Krauss,L., this volume.
- 3) Rich,J., this volume.
- 4) Caldwell,D.O., this volume.
- 5) Rich,J. and Spiro,M., Saclay preprint 1987
- 6) For a review see e.g. Sadoulet,B., "Cryogenic Detectors of Particles:Hopes and Challenges",IEEE Trans. on Nucl. Sci.,NS-36, 543(1988).
- 7) Griest,K. and Sadoulet,B., "Model independence of interaction rates of dark matter particles", In preparation.
- 8) Freeze,K. and Freeman,J., In preparation.
- 9) Griest,K., "Direct Detection of Neutralino Dark Matter", Submitted to Phys.Rev.Lett.,(1988).
- 10) Goodman, M.W. and Witten, E., "Detectability of certain dark-matter candidates", Phys.Rev.D.,31, 3059(1985).
- 11) Sadoulet,B., "Prospects for detecting dark matter particles by elastic scattering", in Proceedings of the Texas Symposium on Relativistic Astrophysics, Chicago, Dec 14-19,1986, Ulmer,M.L., Editor,(World Scientific, Singapore) p. 260(1987).
- 12) Krauss, L. and Srednicki,M. and Wilczek,F., "Solar System Constraints on Dark Matter Candidates", Phys. Rev.,D33, 2079(1986).
- 13) Spergel, D.N., "The Motion of the Earth and the Detection of WIMPS", Astrophysics Preprint Series,IASSNS-AST 87/2, (1987)
- 14) Perret-Gallix,D., this volume.
- 15) Niinikoski, T. O. and Udo, F., CERN preprint,(1974).
- 16) McCammon,D. et al., "Thermal Detectors for High Resolution Spectroscopy", Proc. 18th Int. Conf. on Low Temperature Physics, Kyoto,1987 Jap. Journal of Appl. Phys.,26, Supplement 26-3, (1987).
- 17) Moseley, S.H. and Mather, J.C. and McCammon, D., "Thermal Detectors as X-Ray Spectrometers", J.Appl.Phys.,56(5), 1257(1984).
Mather, J.C., "Bolometer Noise: Nonequilibrium Theory", Applied Optics,21, 1125(1982).
Mather, J.C., "Bolometers: ultimate sensitivity, optimization, and amplifier coupling", Applied Optics,23, No4, 584(1984).
- 18) Cabrera, B. and Krauss, L.M. and Wilczek, F., "Bolometric Detection of Neutrinos", Phys. Rev. Lett.,55, 25(1985).
- 19) Alessandrello,A. and Camin,D.V., Fiorini,E. and Giuliani,A., "Construction of a Massive Germanium Thermal Detector for Experiments on Rare Decays", Phys.Lett. B,202, 611(1988).
- 20) Sadoulet,B., "Phonon Detection with Semiconductor Thermistors", in Proceedings of European Workshop on Low Temperature Devices for the Detection of Low Energy Neutrinos and Dark Matter, Annecy (LAPP) France, May 2-6 1988, In press, (1988).
- 21) Maris, H.J., "Design of Phonon Detectors for Neutrinos", Fifth International Conference on Phonon Scattering in Condensed Matter, Urbana, Illinois, June 2-6, (1986).
- 22) Cabrera, B. and Martoff, J. and Neuhauser, B., "Acoustic Detection of Single Particles", Stanford University, (1986).
- 23) Neuhauser, B. and Cabrera, B. et al., "Acoustic Detection of Single Particles for Neutrino Experiments and Dark Matter Searches", 1986 Applied Superconductivity Conference, Baltimore, Maryland, (1986).
- 24) Neuhauser, B. and Cabrera, B. and Martoff, C.J. et al., "Phonon-Mediated Detection of Alpha Particles with Aluminum Transition Edge Sensors", Proc. 18th Int.Conf.on Low Temperature Physics, Kyoto Jap. Journ. of Applied Physics,26, (1987).

- 25) Peterreins, T.H. et al., "A new detector of Nuclear Radiation Based on Ballistic Phonon Propagation in a Single Crystal at Low Temperatures", Phys. Lett. B, 202, 161 (1988).
- 26) Based on a remark made by Mark Davis in a brainstorming discussion.
- 27) See for instance the Proceedings of the Fourth and Fifth International Conference on Phonon Scattering in Condensed Matter, Springer Verlag
- 28) Lanou, R., this volume.
- 29) Haller, E.E., "Physics and Design of Advanced Infrared Bolometers and Photoconductors" IR Physics, 25, 257 (1985).
- 30) Wang, N. et al., "A 20mK Temperature sensor", IEEE Trans. in Nuclear Science, NS 35, 55 (1988).
- 31) See e.g. Booth, N.E., "Quasiparticle trapping and the quasiparticle multiplier", Apl. Phys. Lett., 50, 293 (1987).

SUPERFLUID HELIUM AS A DARK MATTER DETECTOR

R. E. Lanou, H. J. Maris, & G. M. Seidel
Department of Physics
Brown University
Providence, Rhode Island 02912
USA
(Presented by R. E. Lanou)



ABSTRACT

The properties of liquid helium-four at temperatures in the vicinity of 100 mK suggest that it might be a suitable medium from which to construct a detector for certain types of dark matter. Among these properties are freedom from contaminants producing background and a high multiplicity of carriers (rotons) produced in energy deposition. It is suggested that there are processes available in helium which may permit discrimination between recoil nuclei and electronic of equal energy deposit.

I. INTRODUCTION

A severe experimental challenge has been posed if dark matter is elementary particle in nature and weakly coupled to ordinary matter. The combination of flux, cross section and low kinetic energy of these particles leads to expectations of low event rates and low energy deposits in any detector. Consequently a suitable detector for such dark matter should possess a low content of intrinsic or spallation produced radioactivity, a low energy threshold, good energy resolution, good sensitivity (size vs. rate), a choice of integer or half integer spin targets, real time detection and good signal to noise discrimination.

The design choices for any detector for this purpose depend on optimization of these competing requirements. It is unlikely that they will all be realized in a single type of detector; no doubt there will be needed several complementary ones. At this conference, in the joint session with the Electroweak Workshop, we heard¹ about some of the detector developments which are furthest along. Most are based upon solid state devices utilizing interaction with a lattice through ionization or phonons or superheat.

Recently, we have begun work on a calorimetric method² which is quite different from any of those previously discussed. It is based upon the properties of liquid ${}^4\text{He}$ and its bulk excitations at very low temperatures. Our original motivation has been to develop a device suitable for studying the spectra of solar neutrinos down to the very lowest energies — that is, those of the p-p and ${}^7\text{Be}$ reactions. Such a solar detector consisting of 10 tons of ${}^4\text{He}$ would collect 20 events per day from those two reactions.

The same properties of superfluid helium which make it useful for solar neutrinos should make it an excellent candidate for dark matter searches; however, the scale could be much smaller — typically, less than 5 kilograms might produce 100 events per day.

II. CALORIMETRY OF SUPERFLUID ${}^4\text{He}$

The properties of ${}^4\text{He}$ superfluid although widely studied and understood through a very active community of distinguished workers until fifteen years ago,³ do not seem to have found their way into being part of the everyday knowledge and bag of tricks of the rest of us — particle and astrophysicists especially. These properties of a macroscopic quantum fluid are surprising, beautiful and some familiarity with them is essential for a critical hearing of the proposal to use them for detecting neutrinos or dark matter. Consequently, I hope you will bear with me while I (a particle physicist) digress to share with you my elementary understanding of the nature of ${}^4\text{He}$ superfluid.

In general terms, ${}^4\text{He}$ is attractive because it is inexpensive (\sim \$5 per liter), clean, quiet and simple. ${}^4\text{He}$ at low temperature (< 100 mK) is the purest material known. All other atomic species freeze out as helium remains liquid to absolute zero at equilibrium pressure. ${}^3\text{He}$ content can be reduced to one part in 10^{13} . When energy is deposited in ${}^4\text{He}$ superfluid most of the energy appears in the bulk excitations known as phonons and rotons. As is described below, it is the rotons which will be of primary interest to us; they constitute a high multiplicity population of stable carriers which lead to real time detection with the promise of good energy resolution.

Radioactive backgrounds are the principal limitations on solar neutrino and dark matter experiments. This background can be thought of as having three sources: a) a long-lived radioactive isotopes *intrinsic* to the detector medium (such as ${}^{115}\text{In}$ in indium detectors⁴⁾), b) long-lived isotopes made *cosmogenically* while the materials are above ground (such as ${}^3\text{H}$ and ${}^{22}\text{Na}$ in silicon detectors⁵⁾) and c) neutrons and gammas (Compton recoils) from the *environment*.⁶⁾ Helium has no natural radioactive isotopes and its first excited state is very high — 21 MeV. Neutrons from the environment are easily controlled and so the chief concern for any helium detector are gammas generated in its container and its immediate shielding. The extensive use of copper in double beta decay experiments⁷⁾ provides reliable numbers for expected gamma rates from a copper dewar (a natural material for helium containment). These rates seem to be quite manageable (0.09 decays/min/kg).

If a neutrino or dark matter candidate interacts with the atoms of a helium detector there will be a recoil — typically an electron or an entire nucleus — and it is the kinetic energy of the recoil which we must detect and measure. These energies are very small ranging from a few kilovolts to electron volts.

How does one measure such energy deposited hermetically in bulk material? The classical macroscopic temperature rise calorimetry is not a promising one. The excess energy deposited, ΔE , in a mass, M , of specific heat, C , yields a temperature rise $\Delta T = \Delta E/CM$. The specific heat at low temperature is proportional to $\left(\frac{T}{\theta_D}\right)^3$, where the Debye temperature for helium is $\theta_D = 25.9^\circ\text{K}$ which results in too low a temperature rise to detect in the quantities of ${}^4\text{He}$ required unless infinitesimal segmentation were utilized. Even such a draconian solution would not provide adequate energy resolution.

Fortunately, there exists a microscopic approach which suggests an elegant solution. The recoiling particle deposits most of its energy into the form of bulk excitations (phonons and rotons) in less than 10^{-6} sec. Only about 0.7 milli-electron volts (meV) are required to make the majority (Fig. 1b) of these carriers so a one kilovolt

recoil would produce $\sim 10^6$ such carriers thus leading to good statistical resolution $[\Delta E/E = \sqrt{10^6} \times (.7\text{meV}/1\text{KeV}) \simeq 0.1\%]$. These carriers propagate ballistically at about 100 m/sec which, if they can be efficiently collected, permit real time detection and measurement of deposited energy.

To understand the nature and origin of these carriers (rotons) we must look at the microscopic properties of helium. As helium is cooled it undergoes a phase transition at 2.1°K (the “ λ -point”) into a condensed boson liquid of effectively zero viscosity. It has a density of 0.141 gm/cc in a rather open structure. The He-He interaction potential strongly repels at separations of $\sim 2.7\text{\AA}$ and is weakly attractive at greater distances. We might then think of the He atoms as spheres $\sim 1\text{\AA}$ radii randomly sited on “equilibrium” centers of $\sim 3\text{\AA}$. At very low temperatures the atoms move easily from these sites; small vibrations and larger displacements which constitute the bulk excitations are quantized^{8]} and are the carriers we call phonons and rotons. Their distinctions from each other are determined by the dispersion curve which constrains their possible energies and momenta (see Fig. 1a). There are both similarities and important differences to the dispersion relation for excitations on a solid lattice. Figure 2 illustrates the case for a one dimensional uniform spacing. Helium differs in that it obeys boson symmetries and has inexact 3-D spacing. This dispersion curve has been well established by neutron scattering experiments. The roton minimum occurring approximately at $2(\text{\AA})^{-1}$ can be thought of crudely as equivalent to the minimum at $2\pi/a$ of Fig. 2. These phonons/rotons themselves constitute a boson gas within the boson liquid and they can decay and interact with each other if there are enough of them at a given equilibrium temperature. The temperature dependence of these equilibrium populations is strong — n (phonons) $\propto T^3$ and n (rotons) $\propto e^{-\frac{\pi}{\Delta}}$. As can be seen from Fig. 1a, the so called roton region is the very non-linear one at high momentum and energy (characterized by an energy gap $\Delta \simeq 8^\circ\text{K}$ or 0.7 meV) thus they are forbidden to decay freely due to energy-momentum conservation. Consequently, if the equilibrium temperature of the liquid is low enough, non-equilibrium rotons suddenly produced (e.g., due to a recoil) will be stable and propagate ballistically^{9]} at about 100 m/sec. At 100 mK — a temperature low enough for the above conditions to obtain yet high enough not to require a cryogenic tour-de-force — it is useful to remind ourselves that this is indeed a very “quiet” medium with an average atomic kinetic energy of $\sim 10\mu\text{eV}$ and an equilibrium vapor pressure such that there are only 10^{-12} atoms/cc above the liquid.

III. USE AS A PARTICLE DETECTOR

The challenge then is to collect these rotons in a realistic device. Figure 3 illus-

trates in a schematic way one method of proceeding. Briefly (see Ref. 2 for details) the sequence of events would be as follows: a) kinetic energy of the recoil from an interaction is converted to mechanical excitations in the helium,^{10]} b) the large population of rotons propagate ballistically to the free surface, c) at the free surface 1/3 of the rotons^{11]} knock-out ${}^4\text{He}$ atoms, d) the ${}^4\text{He}$ atoms, via a large van der Waals interaction^{12]}, are physisorbed onto the surface of thin silicon wafers suspended a few millimeters above the surface, e) in a few milliseconds the binding energy released into the silicon results in a measurable temperature rise (θ_D (silicon) = 636°K). An energy amplification of about a factor 3 occurs in this sequence — a non-essential but convenient feature. The ultimate energy resolution achievable by this technique will probably depend upon how well geometric effects and losses at the walls can be controlled. Deferring other practical matters of construction for a moment, what about the scale of such a technique for use in a dark matter search?

We take the standard “assumptions” concerning dark matter if it is elementary particle-like: a density of 0.4 GeV/cc, a mean velocity of 300 km-sec⁻¹, interaction cross sections coherently off nuclei^{13]} of $\simeq 10^{-38} \text{ cm}^2$, an annual rate modulation of 2-7%^{14]}. The maximum recoil energies are given by $E_{max} = 2n^2 M_{hc} (\beta)^2 / (n + 1)^2$ where $n = m(\text{dark})/M(\text{helium})$. If a threshold of 0.5 keV is assumed and a minimum of 5 events/day (corresponds to a mass of 30 GeV/c²) as a practical limit, then a volume of 20 liter (2.8 kg) would produce 80 events/day at the lower mass limit of 2 GeV/c². The recoil energy maximum deposits range from 0.8 KeV to 5 KeV. Backgrounds are expected^{1]} to be mainly Compton scattering of gamma rays originating from spallation products in the copper^{7]} dewar. We estimate these at about 35/day. This might be considered a minimal example since a solar neutrino detector of 10 tons appears feasible — in fact, should a dark matter experiment by this technique prove successful dark matter as a background would swamp the solar neutrino experiment!

Goodman and Witten (Ref. 13) have emphasized the value of having targets with different intrinsic spins. ${}^4\text{He}$ would be a spin zero candidate but unfortunately half integer spin ${}^3\text{He}$ does not support a population of stable rotons.

Sadoulet and others^{15]} have emphasized the potential importance of the ability to discriminate between equal energy deposits caused by different deposition mechanisms. Specifically, it would be valuable to separate energy deposition primarily by ionization in the case of Compton recoils as opposed to deposition by slowly moving recoil nuclei which produce little ionization. The unusual properties of drifting ions in liquid helium may provide the ability to make this discrimination. Positive ions form a stable, dimer which polarizes the immediate surrounding medium; the result-

ing forces are such as to solidify the medium out to a radius of $\sim 7\text{\AA}$ encompassing a mass of about 40 atoms.^{16]} There is no stable, negative bound state; the weak He-He interaction and the strong electron-electron repulsion contributes to the free electron being contained in a "bubble" of $\sim 16\text{\AA}$ by displacing about 160 atoms.^{17]} When drifted in even modest electric fields (200V/cm) these rather large structures contribute complex mobilities. There is a critical velocity which, if exceeded in fluid flow or object motion, causes production of excitations in liquid helium and consequently the drifting ions reach terminal velocities (Fig. 4a). These excitations are rotons and ring vortices and the drifting ions radiate them continuously (Fig. 4b) at rates which depend upon conditions of field strength, pressure and temperature.^{18]} Dependences on these variables are complex but well measured^{18]} and moderately but not thoroughly understood; the critical velocities are of the order of several tens of meters/sec. Thus, the energy of a charge moving through an electric field can be converted into energy within the liquid helium and depending on the number of charges produced could be substantially larger than the kinetic energy of the original recoil event. While if the helium is pressurized above 12 bar the energy produced by the moving charges is in the form of rotons, at zero pressure required by our present detection scheme, the energy is in the form of ring vortices.

The ability to initiate, amplify and control a signature unique to the charge carriers would be a powerful mechanism to distinguish between Compton and nuclear recoils. Figure 5a and 5b illustrate crudely the basis. The dark matter detector might contain a static electric field across its volume. Roton from the initial recoil deposition would be received first; rotons (or vortices if detectable^{19]}) from drifted charges would arrive later and much amplified (perhaps by as much as factor $10^5 - 10^6$). If, as expected, Compton and low energy helium recoils have significantly different fractions of their deposition in ionization then the time-amplitude correlation of the rotons'/vortices' pulse might permit an event-by-event separation method.

In conclusion, there are many promising possibilities in the application of superfluid ^4He as a medium for very low energy calorimetry. Nearly all physical principles on which these suggestions are based have been established and are in the literature; no new technology is required to exploit them. On the other hand, detailed quantitative information is lacking in several areas and various tests leading to whether such devices are feasible or not must be carried out. To this end we have recently been funded by the U.S. Department of Energy to carry out such tests. We expect to begin construction of the necessary research and development apparatus in the next few months.

REFERENCES

1. B. Sadoulet, "Phonon Detectors for Dark Matter"; J. Rich, "Direct Detection of Dark Matter Particles"; D. Caldwell, "New Limits on Dark Matter with Ge Detectors"; L. Gonzales-Mestres, "Search for Exotic Dark Matter"; all in these Proceedings.
2. R. E. Lanou, H. J. Maris, G. M. Seidel, *Phys. Rev. Lett.* **58**, 2498 (1987); further aspects are discussed in R. Lanou, H. Maris, G. M. Seidel, "Low Temperature Detectors for Neutrinos and Dark Matter", p. 150, Editors K. Pretzl, N. Schmitz, L. Stodolsky, Springer-Verlag (1987) and in "Neutrino Masses and Neutrino Astrophysics", p. 391, Editors V. Barger, et al (World Scientific, 1987).
3. See for example: A. L. Fetter in "Physics of Liquid and Solid Helium" (Vol. I). Editors: K. Bennemann and J. Ketterson, Wiley-Interscience (1976); J. Wilks in "Liquid and Solid Helium", Clarendon Press (Oxford) (1967).
4. R. S. Raghavan, *Phys. Rev. Lett.* **37**, 259 (1976).
5. C. J. Martoff, *Science* **237**, 507 (1987).
6. A. Rindi et al, INFN (Frascati), Preprint LNF-86/16R (April 1986) and LNF-86/1 (R) (January 1986); G. T. Ewan et al, Sudbury Neutrino Observatory Proposal, Report # SNO-87-12 (1987).
7. R. Brodzinski et al, Pacific Northwest Laboratory Report #PNL-SA-14244 (1987); F. Avignone et al, *Phys. Rev. Lett.* **54** 2309 (1985); P. Fisher, Proceedings of XXI Rencontre de Moriond, Tignes, France (1986); D. Caldwell, private communication.
8. R. P. Feynman, *Phys. Rev.* **91**, 1301 (1953); *Phys. Rev.* **94**, 262 (1954); R. P. Feynman and M. Cohen, *Phys. Rev.* **102**, 1189 (1956).
9. S. Balibar et al, *Phys. Rev.* **B18**, 3096 (1978); H. Maris and R. Cline, *Phys. Rev.* **B23**, 3308 (1981).
10. See for example: L. Meyer and F. Reif, *Phys. Rev.* **123**, 727 (1961); G. W. Rayfield, *Phys. Rev. Lett.* **16**, 934 (1966).
11. A. Wyatt, *Physica* **126B**, 392 (1984); F. Hope, *Phys. Rev. Lett.* **52**, 1528 (1984).
12. See for example: R. Lucchese and J. C. Tully, *Surf. Sci.* **137**, 570 (1984); M. Cardillo (ATT-Bell Labs), private communication.
13. M. Goodman and E. Witten, *Phys. Rev.* **31D**, 3059 (1985).

14. K. Freese, J. Frieman and A. Gould, SLAC preprint #SLAC-PUB-4427 (submitted to Phys. Rev. D, Sept. 87); D. Spergel, Inst. for Advanced Study preprint #IASSNS-AST87/2.
15. B. Sadoulet, Proceedings of 13th Texas Symposium on Relativistic Astrophysics. Editor: M. Ulmer (World Scientific Pub. 1987), p. 260.
16. L. Pauling, "The Chemical Bond", Cornell Univ. Press (1967) p. 189; K. Atkins, Phys. Rev. **116**, 1339 (1959) and Ref. 3 above.
17. E. Haloier and J. Midtdal, Proc. Phys. Soc. **A68**, 815 (1955); G. Careri et al, Nuovo Cimento **15**, 774 (1960) and Ref. 3 above.
18. See for example: R. Bowley et al, Phil Trans. R. Soc. Lond. **A307**, 201 (1982); T. Ellis and P. McClintock, *ibid.* **A315**, 259 (1985) and references therein; P. Hendry et al, Phys. Rev. Lett. **60**, 604 (1988).
19. G. Gamota and M. Barmatz, Phys. Rev. Lett. **22**, 874 (1969).

Fig. 1 a) Dispersion curve for liquid helium at low temperature
b) Density of states.

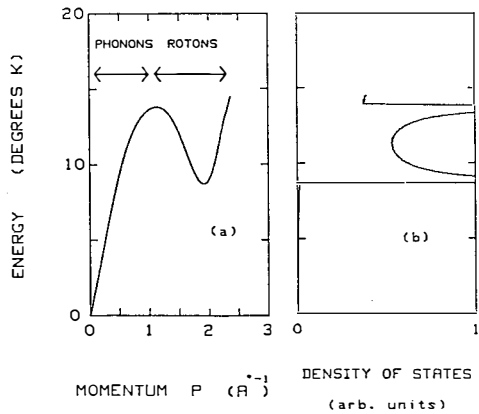
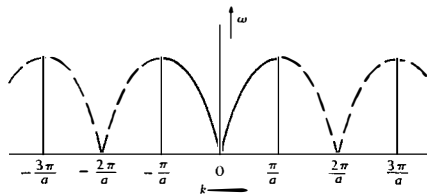


Fig. 2 Dispersion curve for one dimensional lattice.



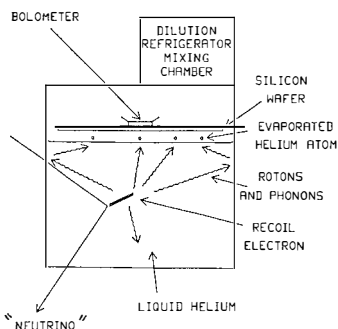
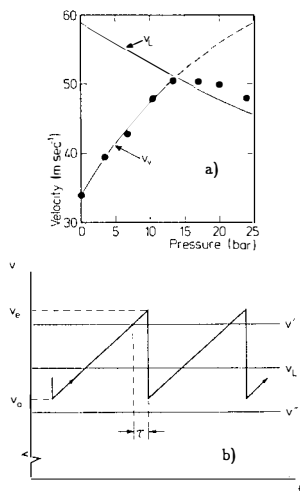


Fig. 3 Schematic of principle for detection of dark matter and neutrinos.

Fig. 4 a) Pressure variation of ion terminal velocities in helium due to emission of rotons (v_L) or vortices (v_v). b) Velocity trajectory of an ion showing successive periods of acceleration by an electric field followed by instantaneous recoil after roton emission. After Bowley and Sheard P.R. 16D, 244 (1977).

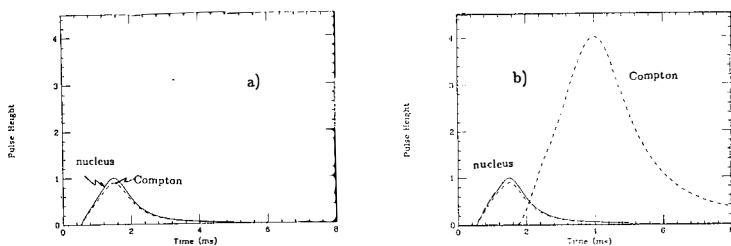


Fig. 5 Schematic of pulse height vs. time a) for rotons generated by recoil in helium with no electric field, b) for rotons/vortices generated by recoil with an electric field to accelerate ions.

SEARCHES FOR ELUSIVE DARK MATTER CANDIDATES**L. GONZALEZ-MESTRES, D. PERRET-GALLIX****L.A.P.P. ANNECY****B.P. 909, Chemin de Bellevue, Annecy-le-Vieux, 74019 cedex FRANCE****Abstract:**

We present a brief review of searches for dark matter candidates not expected to present the large event rates characteristic of heavy Dirac neutrinos (coherent scattering off nuclei) or cosmions (special interactions). Present bounds and current experiments are reviewed, and possible new detection techniques are described. Particular emphasis is put on the problems related to the detection of Majorana fermions, for which no obvious technique exists by now.

1. INTRODUCTION

Non baryonic dark matter candidates are being the object of growing interest from the experimental point of view, as techniques that may eventually detect such particles are currently being developed.

A halo of non-baryonic dark matter would have an approximate density $\rho \sim 0.3 \text{ GeV/cm}^3$, leading to a particle density $n \approx 0.3/m_\chi \text{ GeV/cm}^3$, where m_χ is the dark matter particle mass. With a speed $v \sim 10^{-3} c$, such particles would present appreciable fluxes and are expected to lead to observable effects. However, the detection of the main dark matter candidates turns out to be very difficult. This is the subject of the present talk.

2. NEUTRINOS AND MAGNINOS

Present experimental bounds on the electron neutrino mass give: $m_\nu < 18\text{-}32\text{eV}$ [1]. Detection of non-relativistic light neutrinos is an extremely hard task. If they were clustered in the galactic halo, they would have a kinetic energy $\leq 10^{-4} \text{ eV}$, which is close to the excitation energy of a single quasiparticle in ordinary superconductors. Furthermore, at such energies, neutrino cross sections are expected to be rather small. If light neutrinos are Dirac fermions, their long wavelength would lead to comparatively large cross sections for coherent scattering and interaction with phonons may be worth considering. In such case, rather than trying to detect neutrinos individually, the right strategy may be to look for some collective effect (e.g., heat leaks in future very low temperature devices [2]). Several laboratory experiments to detect cosmological light neutrinos have been proposed in the past [3], but some of them have been refuted [4] and those which turned out to be correct lead to too small effects.

Heavy neutrinos ($m_\nu \geq 3 \text{ GeV}$) arise from new families of fermions, $SU(2)_L \otimes SU(2)_R$ models or superstring theories. On general grounds, there is no obvious reason why they should be stable, but they may eventually carry a new conserved quantum number.

The magnino [5] is a Dirac neutrino carrying a conserved number (to prevent unwanted annihilation rates) and an anomalous magnetic moment (to bring a sufficiently large scattering cross-section $\sigma \approx 10^2 \sigma_{\text{weak}}$). Then, with a mass in the range of 4 to 10 GeV and a magnetic moment $\approx 10^{-2}$, the magnino can reproduce the requirements of the cosmion model. The magnino is basically a new sequential neutrino associated to a heavy charged lepton. Therefore, its existence can in principle be checked by accelerator experiments.

Heavy Dirac neutrinos, as well as magninos, are the most accessible dark matter candidates for present and forthcoming experiments, due to the comparatively large cross sections involved. The basic detection principles, as well as present bounds, have been covered by J. Rich and D.O. Caldwell at this session.

3. AXIONS

For a theoretical discussion of axions, we refer the reader to the introductory talk by L. Kraus.

Axion emission would accelerate energy losses from helium burning stars, which leads to the bound [6]: $m_a \leq 10^{-2}$ eV. On the other hand, the cosmological bound $\Omega_a \leq 1$ brings [7]: $m_a \geq 10^{-5}$ eV. These numbers illustrate the difficulty to detect a non-relativistic cosmic axion.

The key mechanism for axion detection lies in the coupling $a \rightarrow \gamma\gamma$ coming from axion- π^0 mixing, with a strength $\sim \alpha/\pi f_a$ (f_a = axion coupling from pseudoscalar field expectation value). Defining the coupling constant $g_{a\gamma\gamma}$ from the lagrangian:

$$\mathcal{L}_{a\gamma\gamma} = - g_{a\gamma\gamma}/4\pi (\vec{E} \cdot \vec{B}) a \quad \{1\}$$

where \vec{E} and \vec{B} are the electromagnetic field and a the axion field, the Peccei-Quinn theory gives:

$$g_{a\gamma\gamma} \simeq 1.1 \times 10^{-34} \text{ MeV}^{1/2} \text{ cm}^{3/2} m_a/(10^{-5} \text{ eV})$$

Sikivie [8] proposed to detect cosmic axions by $a \rightarrow \gamma$ conversion in the presence of a strongly inhomogeneous magnetic field. The energy of the produced γ is then the total energy of the incoming axion. Therefore, the main signature for cosmic axions would be a very narrow signal in frequency, where the finite width would be due to the axion kinetic energy $\approx 2 \times 10^{-6} m_a$. Using a variable frequency cavity, tuned to a given value of the axion mass, one can attempt to progressively explore the relevant domain of proposed axion masses. This amounts to covering the frequency range 1-10³ GHz by successive narrow band experiments.

Recently, a search for cosmic axions along these lines has been started at BNL [9], at ~ 1 GHz frequencies. The experiment (BNL-Rochester-FNAL Collaboration) used a 6.6 T superconducting magnet and a copper cavity at liquid helium temperature. The resonant frequency could be tuned in the range 1.09 GHz $< f < 1.22$ GHz, with an operating Q of 9×10^4 and a bandwidth of 13 kHz. The axion mass for such frequencies varies in the range $4.5 \mu\text{eV} < m_a < 5.0 \mu\text{eV}$ and the intrinsic bandwidth of the axion signal would be ~ 130 Hz. No signature for axions was found, and the obtained upper bound is: $g_{a\gamma\gamma} < 10^{-33} \text{ MeV}^{1/2} \text{ cm}^{3/2}$ for $m_a \approx 5 \times 10^{-6}$ eV, assuming 100% of the galactic dark matter to be made of such axions. This bound lies 50 times above the value predicted by the Peccei-Quinn theory. The BNL experiment provides an encouraging start point for more ambitious searches. Updated results, covering the range, $5 \mu\text{eV} < m_a < 12 \mu\text{eV}$, are being presented by W. Wuensch at the Dark Matter Workshop. A second group, in Florida [10] is planning a similar experimental program.

If axions are trapped in the solar system, and thermalized by its central core, they can reach earth with an energy of the order of the sun central temperature ($E \sim 1$ keV). Then, if they interact with matter, they can be detected by cryogenic calorimetric techniques. It has indeed been shown [11] that axion-photon conversion in atoms yields acceptable cross-sections (axioelectric effect) leading to a few events/

Kg.day. The feasibility of such an experiment is then mainly related to the development of recently proposed low temperature detectors.

In the meantime, double β germanium detectors [12, 13] have been used to provide some interesting upper bounds on solar axions. The PNL/USC group [12] developed a 135 cc intrinsic Ge detector with the lowest background ever achieved in the keV energy region and a threshold at $E \approx 4$ keV. Installed at a water equivalent depth of 4000 meters in the Homestake mine, it brought upper bounds allowing to exclude the range $f_a \leq 0.5 \times 10^7$ GeV. Theory favors: 10^9 GeV $< f_a < 10^{12}$ GeV. In order to reach cosmological bounds and cover the full spectrum of solar axions, two obvious requirements appear: a) background should still be lowered in order to reach sensitivity to the expected solar axion flux; b) the energy threshold should be set an order of magnitude lower, which justifies the development of cryogenic devices.

4. WEAKLY INTERACTING MASSIVE PARTICLES

The lightest supersymmetric particle (LSP) is often considered to be stable by R-parity conservation. Gravitinos and scalar neutrinos are not the LSP in most models [14], the main candidates being the photino ($\tilde{\gamma}$) and the higgsino (\tilde{H}). One often has $m_{\tilde{H}} > m_{\tilde{\gamma}}$, which makes the photino the most popular LSP. The photino mass is rather model dependent, and present studies concern mainly the range 5 GeV $< m_{\tilde{\gamma}} < 100$ GeV, for which $\Omega_{\tilde{\gamma}} \approx 1$ appears to come out quite naturally.

Astrophysical detection of galactic WIMP was proposed by Goodman and Witten [16] using the recoil energy of scattered nuclei. For a WIMP of kinetic energy E ($\approx 10^{-6}$ m) scattering a nucleus of mass M , the maximum recoil energy is:

$$T_{\max} = 4 m M E / (M + m)^2 \quad \{2\}$$

For a reaction producing an excited nucleus of mass $M' = M + \Delta M$, the relevant formulae can be found in [15]. WIMP weak cross-sections with nuclei can be cast in three different categories:

4.1 Coherent scattering.

Coherent scattering appears if a non-relativistic particle of well defined weak hypercharge interacts with a nucleus through the isoscalar components of the Z^0 current. The condition for coherent scattering is that the wavelength defined by momentum transfer be larger than the size of the nucleus. The relevant matrix element is:

$$\mathcal{M} = 4 \sqrt{2} G_F J^0_{\text{WIMP}} J^0_{\text{TARGET}} \quad \{3\}$$

If the WIMP is a fermion, we get:

$$J^0_{\text{WIMP}} = 1/4 (Y_L + Y_R) \quad \{4\}$$

where Y_L (Y_R) is the weak hypercharges of the left (right) components of the WIMP. For a Majorana neutrino, $J^0_{\text{WIMP}} = 0$ and there is no coherent scattering.

On the contrary, s-neutrinos and Dirac neutrinos interact coherently with nuclei (see talks by D. Caldwell and J. Rich).

4.2 Spin-dependent interactions.

This is the case for galactic photinos interacting with nuclei through the exchange of a scalar quark. The nonrelativistic limit of the relevant Feynman diagram is equivalent to the exchange of a space-like pseudovector current. Then, assuming that valence quarks carry most of the spin of the nucleon, the nucleon couplings are proportional to [16]:

$$\begin{aligned} \langle p | \vec{u} \vec{\gamma} \gamma_5 u | p \rangle &= (1 + g_A) \langle p | \vec{S} | p \rangle \\ \langle p | \vec{d} \vec{\gamma} \gamma_5 d | p \rangle &= (1 - g_A) \langle p | \vec{S} | p \rangle \\ \langle n | \vec{u} \vec{\gamma} \gamma_5 u | n \rangle &= (1 - g_A) \langle n | \vec{S} | n \rangle \\ \langle n | \vec{d} \vec{\gamma} \gamma_5 d | n \rangle &= (1 + g_A) \langle n | \vec{S} | n \rangle \end{aligned}$$

where experimentally $g_A \simeq 1.2$. Therefore, a u-quark in a proton or a d-quark in a neutron would have a larger matrix element than the converse case. Furthermore, the complete diagrams carry twice the coupling $qq\tilde{\gamma}$, which is proportional to the charge of the interacting quark. It would then follow [16, 17] that photino searches should be made with even-odd nuclei carrying an odd number of protons.

This conclusion has been recently reconsidered at the light of EMC data [18, 19] which suggest that a sizeable part of the nucleon spin is carried by sea quarks. If this is the case even for low values of Q (the momentum transfer), the above estimates should be seriously modified and a wide range of target elements could be used for dark matter detection. EMC data were taken at $Q^2 \geq 3 \text{ GeV}^2$, and there has been some controversy [20] on their interpretation and validity at $Q^2 \simeq 0$. Recent theoretical work [21] based on the Skyrme model at large N_c (number of colors) seems to support the EMC statements.

In any case, spin-dependent interactions of WIMP with nuclei are likely to lead to event rates of $\approx 10^{-2}$ events/Kg.day, whereas the best background rate of germanium detectors at the relevant energies is of 1 event/keV.Kg.day. This is likely to be the main obstacle to the detection of galactic Majorana fermions.

4.3 Inelastic scattering.

For particles that do not scatter coherently off nuclei, Goodman and Witten proposed the use of special target nuclei where the matrix elements for the transition to excited states may be as important as those of elastic scattering. Then, besides the recoil energy, it would be possible to detect a γ ray coming from the decay of the excited state. The main drawback is our lack of knowledge of the actual nuclear wave functions and matrix elements.

In spite of its not well known cross-sections (a priori quite small), inelastic scattering may in some cases provide a specific signature (delayed time coincidence) which appears potentially able to reject severe backgrounds. As will be seen later, this may turn out to be a crucial point even if very large detectors are likely to be required. A systematic investigation of all possible target nuclei for inelastic scat-

tering, with reliable calculations of the relevant matrix elements, is urgently required. Recent estimates [22] seem to indicate that cross sections for inelastic scattering are actually very small. For isotopes allowing for a delayed time coincidence, 10 ton detectors are needed to reach a rate of the order of 1 event/day. Assuming that such detectors can be built, with high sensitivity and low background, the delayed time coincidence should in principle still allow for a clean identification of dark matter events. Such gigantic experiments will obviously have to be the last step of dark matter searches.

5. DETECTION TECHNIQUES FOR WIMP

For a WIMP mass of 1 GeV (100 GeV), dark matter detectors should be sensitive to ≤ 1 keV (100 keV) deposit of energy if a target of mass $M = m$ is used. Since the last requirement cannot be fulfilled a priori (the WIMP mass is unknown), a threshold two orders of magnitude lower (10 to 100 eV) would be the ultimate goal for a universal WIMP detector. This naturally hints to the development of low temperature devices. However, more conventional detectors have already provided some interesting bounds [23, 24] and are still being proposed for further experiments (see talks by J. Rich and D. Caldwell, as well as references [15, 25]).

Cryogenic detectors are by now the preferred "next generation devices" since they should naturally provide the required low threshold and energy resolution. Things may actually not be so simple, and it should be kept in mind that low temperature devices are still at the level of feasibility studies. Among the proposed techniques are:

5.1 Crystal calorimeters [26].

They are often called "bolometers" by astronomers, who use small calorimeters to detect very low energy γ 's. Actually, the same expression is also used for superconducting devices [27]. Assuming that the intrinsic limit on the performance of a crystal bolometer is given by energy fluctuations, a commonly used expression [28] is:

$$\Delta E \approx 2.5 (kT^2C)^{1/2} \quad \{5\}$$

where C is the heat capacity of the bolometric system (crystal + sensor). Taking $C \approx \alpha MT^3$ where M the mass of the crystal, the $T^{5/2} M^{1/2}$ dependence of ΔE from {5} suggests that it may be possible to obtain high sensitivity for comparatively large detectors if size is compensated by a decrease in working temperature. This technique is dealt with at length by J. Rich and B. Sadoulet in the present session.

5.2 Superconducting tunneling junctions (STJ).

STJ exhibit potentially an energy resolution (and threshold) in the meV range, which corresponds to the energy gap Δ of conventional superconductors. Existing prototypes [29, 30, 31] are made of Sn-SnO-Sn and Nb-NbO-Pb junctions. They have been found to exhibit an excitation energy ϵ of 30 to 400 meV per quasiparticle, where the lowest value [29] corresponds to a Sn-SnO-Sn junction at 300 mK. In the last case, an energy resolution of 0.7% was obtained for 6 KeV γ 's

It must be realized, however, that the above performances come from small junctions (10^{-4} cm²). Large surface junctions have never been tested, but tunneling time is expected to increase linearly with the junction thickness. The best sensitivity is obtained at comparatively low temperatures [29, 30], but the recombination time increases as $\exp(\Delta/kT)$. Although tunneling junctions are certainly very performant at the scale of small detectors, it remains to be shown that their size can be increased in a satisfactory way. The growing technological effort in such devices should provide basic improvements in the years to come.

5.3 Superheated superconducting granules (SSG).

The initial idea originates from members of the Orsay Group on Superconductivity [32], who proposed to use as particle detectors colloids of metastable type I superconducting granules previously developed by J. Feder [33]. Irradiation results with a low energy electron beam were subsequently made in Rennes [34]. Although sensitivity to ionizing particles was demonstrated, SSG were at that time judged unable to provide the required sensitivity and energy resolution to compete with the most performant particle detectors. Attempts to build devices for X-ray imaging [35] and transition radiation detection [36] failed, but real time electronic was developed by A. Hrisoho (LAL, Orsay), allowing for the first time to read granules individually. Subsequently, the use of SSG was proposed for several applications at the cross-disciplinary frontier between particle physics and astrophysics [37]. Recent studies [38] suggest that, at least in their conventional version, SSG fail to provide the required performances needed for dark matter detection.

We have recently proposed [25] a new way for SSG development based on a the concept of "amplification by thermal micro-avalanche". With a better handling of heat exchanges in the detector, and working at temperatures where the released latent heat is slightly positive, the new scenario is particularly relevant for dark matter detection, since: a) the detector response to WIMP interactions is no longer reduced to a single granule flip, therefore energy resolution can be obtained ; b) the dielectric material surrounding the granules becomes itself an active target (e.g., hydrogen target). Obviously, much more experimental work on the new version of SSG is required. If the basic physics of the micro-avalanche scenario works as expected, SSG are likely to provide the best suited cryogenic detector for large volume experiments.

6. QUARK NUGGETS

Witten [39] proposed that quarks may form dense stable states where u, d and s quarks fill a Fermi sea up to very high values of the baryon number. Then, the gain in Fermi energy may eventually make the s quark stable inside a heavy nugget.

The interaction of cosmic quark nuggets (nuclearites) with matter has been discussed at length [40] and they turn out to be detectable in real time experiments [41] for masses in the range $10^{-13} \text{g} < m < 1 \text{g}$. Assuming that nuclearites are gravitationally dominant, present real time experiments exclude $m < 10^{-7} \text{g}$. The 10^4m^2 underground MACRO detector [42] will be sensitive to much smaller fluxes, allowing to exclude nuclearite masses up to $m < 10^{-2} \text{g}$.

Nuclearites lighter than 10^{-10} g would be trapped in earth, and could be detected using heavy ion beams [43], the crucial point being that strange quark matter is expected to form bound states with ordinary matter. Searches along this line are being performed [44], but no positive result has by now been reported.

Finally, very heavy nuclearites ($m > 1\text{g}$) would leave macroscopic tracks on rock and geological searches are possible [45]. Again, no candidate has been found, but more searches are required to cover such small fluxes.

7. MONOPOLES

In spite of its apparent exoticity, the monopole problem is a fundamental issue in modern physics, for the existence of magnetic charges would naturally complete the dual symmetry of Maxwell's equations. Monopoles which are non-perturbative solutions of grand-unified Yang-Mills theories [46] may have been formed in the early universe. They are not genuine dark matter candidates if Parker's bound [47] is to be believed. Bounds on monopole flux from the persistence of neutron stars are even more stringent [48] if monopoles are assumed [49] to catalyze baryon decay. The cosmological implications of a precise knowledge of the monopole flux (if any) would be extremely important.

MACRO [42] provides a large area experiment able to detect fast monopoles, but it is unclear what lower bound on the monopole speed should be associated to data obtained with conventional techniques. Recent studies [50] suggest that the MACRO detector may be sensitive to monopoles with $\beta > 6 \times 10^{-4}$. However, the interaction of slow monopoles with matter is not fully understood, and current estimates rely at some point on theoretical calculations or extrapolations not derived directly from first principles.

Induction experiments [51] have by now reported two candidates, but none of them is firmly established. Superconducting detectors (induction loops [52] or SSG [53]) are the only proposed techniques for "all beta" monopole detection. Induction experiments provide the only monopole search where the signal is a direct consequence of first principles (Faraday's law). They are likely to reach only comparatively small areas, because of the cost of SQUID technology. Also, background is likely to become more and more severe as the detector size increases. SSG may provide a natural way to escape such problems, since large signals and high background rejection are naturally expected [38].

8. CONCLUSION.

Dark matter, if it exists at all, may indeed be made of non-relativistic particles, but its nature remains completely unknown. If light neutrinos (hot dark matter) are the right answer, their detection in the laboratory will be the greatest challenge ever faced by particle physics and astrophysics. The success of such an experiment would in turn be one of the most fundamental results in the recent history of science. Axions and some WIMP candidates look by now easier to detect, but we just do not know whether such particles exist at all. Furthermore, the most prominent WIMP candidate, the photino, poses rather severe background problems and requires quite sophisticated detection techniques, even if cryogenic detectors reach successfully the required sensitivity and energy resolution.

References

- [1] See, for instance, L. Di Lella in "A Unified View of the Macro- and the Micro-Cosmos". Ed. A. de Rujula, P. Shaver and D.V. Nanopoulos, World Scientific Pub. 1987
- [2] For a discussion of the potentialities of existing cryogenic devices, see T.O. Niinikoski, Proceedings of the "Rencontre sur la Masse Cachée dans l'Univers et la Matière Noire" July 1987, to be Published by Annales de Physique (France).
- [3] L. Stodolsky, Phys. Rev. Lett. 34, 110 (1974).
- [4] P. Langacker, J.P. Leveille and J. Sheiman, Phys. Rev. D27, 1228 (1983).
- [5] S. Raby and G. West, Phys. Lett. B194, 457 (1987)
- [6] D. Dicus, E. Kolb, V. Teplitz and Wagoner Phys. Rev. D22, 839 (1978).
M. Fukugita, S. Watamura and M. Yoshimura, Phys. Rev. Lett 48, 1522 (1982).
- [7] L. Abbot and P. Sikivie, Phys. Lett. 120B 133 (1983).
M. Dine and W. Fischler, Phys. Lett. 120B 137 (1983).
J. Preskill, M. Wise and F. Wilczek, Phys. Lett. 120B 127 (1983).
- [8] P. Sikivie, Phys. Rev. Lett. 51 1415 (1983).
- [9] S. de Paolis et al. Contribution to Telemark IV Neutrino Mass and Neutrino Astrophysics, Ashland WI March 16-18 1987.
B.E. Moskowitz et al., NIM A264, 98 (1988).
- [10] University of Florida Development Project (1986).
S.I. Cho et al., Contribution to LT-18, Kyoto 1987.
- [11] S. Dimopoulos, G.D. Starkman and B.W. Lynn, Mod. Phys. Lett. 1, 491 (1986).
- [12] F.T. Avignone III et al., Phys. Rev. D35, 2753 (1987).
- [13] D. O. Caldwell, NIM A264, 106 (1988).
- [14] See, for instance, J. Ellis, CERN preprint TH 4840/87.
- [15] L. Gonzalez-Mestres and D. Perret-Gallix, preprint LAPP-EXP-87-03, to be published in the Proceedings of the "Rencontre sur la Masse cachée dans l'Univers et la Matière Noire".
- [16] M.W. Goodman and E. Witten, Phys. Rev. D312 3059 (1985).
- [17] A.K. Drukier, K. Freese and D. N. Spergel, Phys. Rev. D33, 3495 (1986).
- [18] EMC Collaboration, as reported by T. Sloan at the EPS Conference on High Energy Physics, Uppsala 1987.
- [19] J. Ellis and R. Flores, Cern preprint TH-4911 (1987).
- [20] F.E. Close and R.G. Roberts, Preprint RAL-88-007 (1988).
- [21] S.J. Brodsky, J. Ellis and M. Karliner, CERN and SLAC preprint january 1988.
- [22] J. Ellis, R. Flores and J.D. Lewin, in preparation.
- [23] S.P. Ahlen, F.T. Avignone III, R.L. Brodzinski, A.K. Drukier, G. Gelmini and D.N. Spergel, Harvard center for Astrophysics Preprint 2292 (1986).
- [24] D. O. Caldwell, R.M. Eisberg, D.M. Granum, M.S. Witherell, F.S. Goulding and R. Smith, preprint UCSB-HEP-87-3.
- [25] L. Gonzalez-Mestres and D. Perret-Gallix, Proceedings of this Dark Matter Meeting.
- [26] S. Simon, Nature 135 763 (1935).
T.O. Niinikoski, in "Liquid and Solid Helium" (Halsted, New York 1975), p.145.
- [27] I.A. Khrebtov, Pribory i Tekhnika Eksperimenta 4, 5 (1984).
- [28] S.H. Moseley, J.C. Mather and D. Mc Cammon, J. Appl. Phys. 56 1257 (1984) and references therein. "Single Particles", Stanford 1986.
- [29] D. Twerenbold, Europhysics Letters 1, 209 (1985).
- [30] M. Kurakado, J. Appl. Phys. 55 3185 (1984) and Phys. Rev B34, 7748 (1986).
- [31] A. Barone, S. Destefano and K.E. Gray, NIM A235, 254 (1985).

- [32] H. Bernas, J.P. Burger, G. Deutscher, C. Valette and S.J. Williamson, *Phys. Lett.* 24A, 721 (1967). C. Valette, Thesis (1971).
- [33] J. Feder, S.R. Kiser and F. Rothwarf, *Phys. Rev. Lett.* 17, 87 (1966).
- [34] J. Blot, Y. Pellan, J.C. Pineau and J. Rosenblatt, *J. Appl. Phys.* 45, 1429 (1974).
- [35] C. Valette and G. Waysand, "Détecteur Supraconducteur de Rayons Gamma à résolution intrinsèque submillimétrique", Orsay 1976.
- [36] A.K. Drukier, C. Valette, G. Waysand, L.C.L. Yuan and F. Peters, *Lett. al Nuovo Cimento* 14, 300 (1975).
A.K. Drukier and L.C.L. Yuan, *Nuclear Instruments and Methods* 138, 213 (1976).
- [37] For a recent update see: L. Gonzalez-Mestres, D. Perret-Gallix in "A Unified View of the Macro- and the Micro-Cosmos".
- [38] L. Gonzalez-Mestres and D. Perret-Gallix, in "Low Temperature Detectors for Neutrinos and Dark Matter", Ed. K. Pretzl, N. Schmitz and L. Stodolsky, Springer-Verlag 1987.
L. Gonzalez-Mestres and D. Perret-Gallix, Proceedings of the Workshop on Superconductive Particle Detectors, Villa Gualino (Torino), October 1987, to be published by World Scientific Pub.
- [39] E. Witten, *Phys. Rev.* D30, 279 (1984).
- [40] A. de Rujula, *Nucl. Phys.* A434 605 (1985).
A. de Rujula and S.L. Glashow, *Nature* 312, 734 (1984).
- [41] K. Nakamura, H. Horie, T. Takahashi and T. Tanimori, *Phys. Lett.* 161B, 417 (1985).
- [42] See, for instance, B.C. Barish for the MACRO Collaboration, Proceedings of the EPS Conference on High-Energy Physics, Uppsala 1987.
- [43] E. Farhi and R.L. Jaffe, *Phys. Rev.* D32, 2452 (1985).
- [44] D. Elmore et al., "A search for anomalously heavy isotopes of low Z nuclei", Univ. of Michigan preprint 1986.
- [45] P.B. Price and M.H. Salamon, in Proceedings of the XIXth ICRC, La Jolla, 1985. Cui Huanhua, O. Eugster, Ke Wei, P. Le Coultre and Tang Xiaowei, preprint IHEP Beijing-Univ. Bern-IHEP Zürich 1988.
- [46] E.N. Parker, *Ap. J.* 160 383 (1970).
M.S. Turner, E.N. Parker and T.J. Bogdan, *Phys. Rev.* D26 1296 (1982).
- [47] See, for instance, the Proceedings of the Monopole Meeting, Trieste 1981, Ed. N.S. Craigie, P. Goddard and W. Nahm, World Scientific Pub.
- [48] E.W. Kolb, S. Colgate and J.A. Harvey, *Phys. Rev. Lett.* 49 1373 (1982).
S. Dimopoulos, J. Preskill and F. Wilczek, *Phys. Rev. Lett.* 119B 320 (1982).
- [49] V.A. Rubakov, *ZhETF Pis'ma* 33, 658 (1981).
- [50] D.J. Ficenec, S.P. Ahlen, A.A. Marin, J.A. Musser and G. Tarlé, *Phys. Rev.* D36, 311 (1987).
- [51] See, for instance: B. Cabrera, Proceedings of the Moriond Meeting on Massive Neutrinos, January 1986, Ed. J. Tran Thanh Van. D. Caplin, Proceedings of the Moriond Meeting on New and Exotic Phenomena, January 1987, Ed. J. Tran Thanh Van.
- [52] See, for instance, D. Fryberger, Proceedings of the Applied Superconductivity Conference, San Diego, September 1984.
- [53] L. Gonzalez-Mestres and D. Perret-Gallix, Proceedings of Underground Physics 85, *Nuovo Cimento* 9C, (1986).

**NEW IDEAS ON THE DETECTION OF COLD DARK MATTER
AND MAGNETIC MONOPOLES**

L. GONZALEZ-MESTRES and D. PERRET-GALLIX

L.A.P.P.

B.P. 909, Chemin de Bellevue, Annecy-le-Vieux, 74019 cedex FRANCE

Abstract:

Superheated superconducting granules (SSG) provide several interesting targets for cold dark matter detection, not only through coherent scattering off nuclei, but also for Majorana fermions through spin-spin interactions. The concept of "localized micro-avalanche" should introduce crucial improvements in SSG devices and, eventually, make feasible a cold dark matter detector based on nucleus recoil. Recent results on the metastability of very large granules also suggest that a SSG large area monopole detector may be feasible, if the theoretically conjectured detection principle (destruction of the superheated state by two injected flux quanta) is checked experimentally.

We also consider the use of special crystal scintillators to detect Majorana fermions through inelastic scattering.

1. SUPERHEATED SUPERCONDUCTING GRANULES

Superheated superconducting granules [1] were proposed for particle detection [2] by a Orsay group [3,4] and further studied in Rennes [5], where irradiation tests with a low energy electron beam were first performed. Subsequent attempts to build transition radiation detectors [6] or X-ray imaging devices [7] failed. The two main problems related to the use of SSG detectors have been until now the following:

- a. Very small grains are required if the detector has to be sensitive to minimum ionizing particles, which leads to small electronic signals.
- b. SSG may be used for the detection of low energy particles, which deposit most of their energy on a short path. But then energy resolution is rather poor and the electronic signal remains comparatively small.

For a dark matter experiment, the main problem of SSG is the presumed absence of energy resolution. The recoil energy of a single nucleus thermalizes in a single grain and, in the conventional scenario, the detector response is a single grain flip. Therefore, it is usually believed that SSG detectors are only threshold detectors as far as nucleus recoil is concerned. Furthermore, the dispersion in grain size makes such threshold a rather ill-defined quantity. In these conditions, SSG should to our opinion be discarded as a dark matter detector.

In spite of such drawbacks, SSG have the basic advantage of being an active target detector that can be instrumented with a simple X-Y read-out system, optimizing the ratio between the number of electronic channels and the size of the detector elementary cell. Typically, 10^5 channels allow for segmentation into 10^7 elementary cells. With fast and sensitive electronics, time resolution can be rather good since the flipping time of very small granules is expected to be fast (less than 1 nsec for a $1\mu\text{m}$ diameter grain). These are crucial points for background rejection in experiments involving time delayed coincidences, and may prove relevant for the detection of galactic Majorana fermions. Furthermore, SSG are not "very low temperature" devices, that must be operated at 50 mK or so. We actually expect, in case of success, to be able to perform all proposed experiments at ^3He or ^4He temperatures (between 0.3 and 4.2 K). Then, SSG would be the best suited cryogenic detector for large volume experiments. Also, the sensitivity of existing prototypes is at least as good as predicted by naive theoretical calculations (global heating). The detection of ^{55}Fe 6 keV γ 's with comparatively large grains ($10\mu\text{m} < \phi$, diameter, $< 25\mu\text{m}$) has recently been demonstrated [8], even if the efficiency is rather low. In this case, a local heating mechanism is obviously at work. All irradiation experiments [9, 10] have clearly confirmed the principle of grain flipping by particle energy deposition. Such considerations justify further efforts to improve the performance of detectors based on SSG, through a better understanding of their basic properties.

Another possible application of SSG is the detection of superheavy magnetic monopoles [11, 12] through a velocity independent effect. As a magnetic monopole

crosses a superheated superconducting granule, it leaves behind two flux quanta injected into the sample. The ends of the flux tube create nucleation centers of the normal state on the surface of the grain, so that in most cases the granule should flip instantaneously from superconducting to normal state. SSG may in this way provide a real time, track detector with a high background rejection due to the use of large granules (30 to 100 μm in diameter). SSG would also give a large signal that can be read with conventional electronics (several large granules would flip in each elementary cell crossed by the monopole), and seem better suited than induction loops to reach comparatively large surfaces.

2. AMPLIFICATION BY THERMAL MICRO-AVALANCHE

It was first noticed by the Garching group [13] that, at very low temperature, the latent heat released by the flip of a single granule can spread to the surrounding granules and produce new flips. This appeared in a rather spectacular way when, working with Cd granules at $T < 300$ mK, the whole detector was seen to collapse under the effect of a thermal avalanche. We performed tests with Sn granules at $T > 450$ mK and found no avalanche effect. Both data can actually be understood in a simple model [8, 9], whose results are as follows:

- a. The superconducting to normal state latent heat can be positive only in the case of superheating and at $t_T = T/T_C$ (reduced temperature) less than a critical value.
- b. When going down in temperature from the point where q^ℓ (latent heat per unit volume) = 0, a domain is found where thermal avalanches remain localized instead of spreading to the whole detector. One then has a local amplification effect to be discussed later on.
- c. If t_T is set below this domain, q^ℓ becomes too large and the SSG detector cannot be operated because of the global thermal avalanche.

The localized micro-avalanche can be described as follows. Let H_{test} be the value of H_0 (applied magnetic field) at which the detector operates, δH a small sweep in H_0 setting a small threshold, V the volume of detector reached by heat propagation and V_{flip} the total volume of granules having changed state due to the particle interaction. For a point-like deposit of energy ΔE , we assume V to be the volume of a isothermal sphere of radius $R(t) \approx 2(Dt)^{1/2}$ (t = time, D = detector heat diffusion coefficient). Taking for all granules a universal dependence of the effective superheated critical field in terms of temperature:

$$H_{\text{Sh}}^{\text{eff}}(T) \approx H_{\text{Sh}}^{\text{eff}}(0) f(T) \quad \{1\}$$

we can write a relation between the increase of temperature ΔT inside the isothermal hot sphere, and the equivalent threshold in magnetic field ΔH [2]:

$$\Delta H = H_{\text{test}} [f(T) - f(T + \Delta T)] [f(T + \Delta T)]^{-1} \quad \{2\}$$

The rate of granules changing state at a distance R from the interaction point is given by:

$$dV_{\text{flip}}/dV = \int_{H_{\text{test}} + \delta H}^{H_{\text{test}} + \Delta H} d\psi/dH_0 dH_0 \quad \{3\}$$

Where ψ is the filling factor in volume and $d\psi/dH_0$ the differential superheating curve in filling factor [2, 8].

Finally, ΔT is related to ΔE , V_{flip} and V through the equation:

$$\Delta E + V_{\text{flip}} q^\ell = V \int_T^{T+\Delta T} c_{\text{det}} dT' \quad \{4\}$$

where c_{det} is the average specific heat of the SSG colloid. A first consequence of equations {1-4} is that ΔE simply sets an overall scale for volume, time and distance in the evolution of a localized micro-avalanche. This can be seen writing:

$$x = V \Delta E^{-1} , y = V_{\text{flip}} \Delta E^{-1} \quad \{5\}$$

Then, expressing the above equations in terms of x and y removes all explicit dependence on ΔE . If the total flipping volume $V_{\text{flip}}(t=\infty)$ is finite, one has: $\Delta\Phi$ (signal in magnetic flux) $\propto \Delta E$, whereas the maximum of the signal in voltage is reached in a time $\tau \propto (\Delta E)^{2/3}$ and is proportional to $(\Delta E)^{1/3}$. Amplification by localized micro-avalanche preserves the proportionality of the signal in magnetic flux and can be used to improve the response to low energy particles. For a minimum ionizing particle, the relation $\Delta\Phi \propto \Delta E$ remains, but the rise time τ depends only on the detector parameters. Then, studying in detail the shape of the signal, it is possible to get an insight on the nature of the interaction.

Using very small granules (about $1\mu\text{m}$ diameter), the new concept of localized thermal micro-avalanche would allow to:

- a. Increase the electronic signal by one or two orders of magnitude;
- b. Obtain a better linearity for very low energy particles (e.g. the 116 keV γ produced in the ^{115}In solar neutrino experiment first proposed by Raghavan [14]) and lower the energy threshold by the use of very small granules;
- c. Eliminate problems related to the lack of uniformity in grain size;
- d. Produce, for the first time in a SSG detector, a linear response to the recoil energy of a nucleus (e.g., dark matter detection);
- e. Use the dielectric material as an active target (e.g., hydrogen target for dark matter searches).

Fig.1 shows the solution of {1-4} in a simplified version of the SSG Ga detector ($T_c = 1.09$) for dark matter searches (nucleus recoil), with $\psi = 0.3$, at $t_T = 0.5$. The

detector response at $\delta H/H_{\text{test}} = 0.005$ for several values of the deposit of energy is exhibited through V_{flip} in terms of V . Even at $q^{\ell} = 0$, the solution of {1}-{4} differs from the conventional SSG scenario in that the detector response does not stop at the granule(s) where the energy was deposited by the incident particle. Heat keeps propagating in the detector, and it can be shown analytically that $V_{\text{flip}}(t=\infty)$ diverges logarithmically in t as $\delta H \rightarrow 0$. When $q^{\ell} > 0$, this divergence becomes power-like but remains regularized by the cutoff δH if q^{ℓ} does not exceed a certain value. If q^{ℓ} is too large, one gets asymptotically $dV_{\text{flip}}/dV \propto V^{\alpha}$, with $\alpha > 0$, and a global avalanche is produced.

To a first approximation, time propagation can be described taking for the heat diffusion coefficient of the colloid that of the dielectric material. For $\psi < 0.3$, this is known to be correct within a factor of 2 [15]. Also, at the beginning of the micro-avalanche phenomenon, Kapitza resistances can play a significant role. We have checked that, using Varnish GE 7031 [9] and taking a standard value of Kapitza resistivity for this material [16], heat exchanges between granules and the dielectric would occur in about 10 nsec. In 200 nsec (the time resolution required for a In solar neutrino experiment), a point like deposit of heat would have spread to a radius of about 30 μm . For dark matter detection through elastic scattering, time resolution is less crucial and it should be possible to work with dielectric materials that conduct heat more slowly (therefore allowing for a more efficient heat transfer between the granules and the dielectric).

If inelastic scattering with ^{119}Sn is used [17], the situation becomes difficult since the lifetime of the 24 keV excited state is only of 18 nsec. Perhaps a shorter micro-avalanche (smaller q^{ℓ} and V_{flip} , in an optimized composite medium) would allow for the use of very fast voltage amplifiers [18].

Fig. 2a shows a sample of $10 \mu\text{m} < \phi < 25 \mu\text{m}$ Sn granules in GE Varnish 7031, at a comparatively low filling factor. We have started an experimental study of Sn grains - GE varnish composite materials at ^3He temperatures, in order to check the validity of the micro - avalanche scenario.

3. PRESENT STATUS OF THE MONOPOLE PROJECT

The case for monopole detection with SSG has been considerably improved by our recent experimental results on the metastability of very large granules made with low purity materials [8]. Our main conclusions are:

a) Adding impurities to the pure metal indeed shortens the flipping time of grains without spoiling metastability (although the superheated critical field decreases for impurity levels larger than 0.1%). We have observed normal superheating curves for tin granules with impurity levels between 0.1 and 1%. Fast enough flipping times were always observed, having in mind the requirement of large voltage signals and good time resolution (to measure velocity) for a monopole detector.

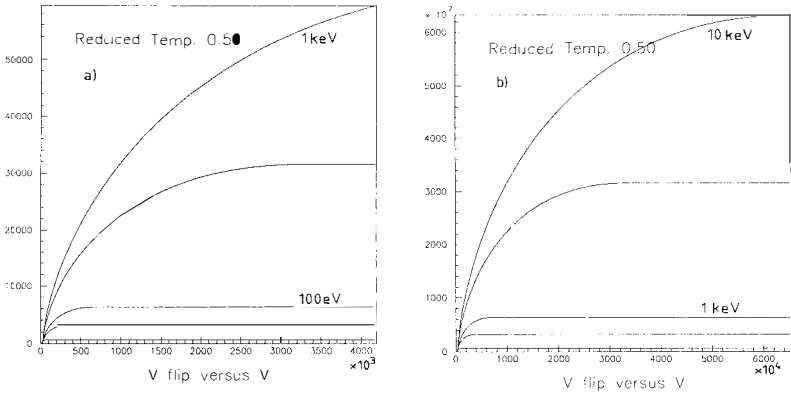


Fig.1 : V_{flip} versus V at $\delta H/H_{\text{test}} = 0.005$ for: a) $\Delta E = 10, 50, 100, 500$ and 1000 eV ; b) $\Delta E = 0.1, 0.5, 1, 5$ and 10 keV. All volumes are given in μm^3 .

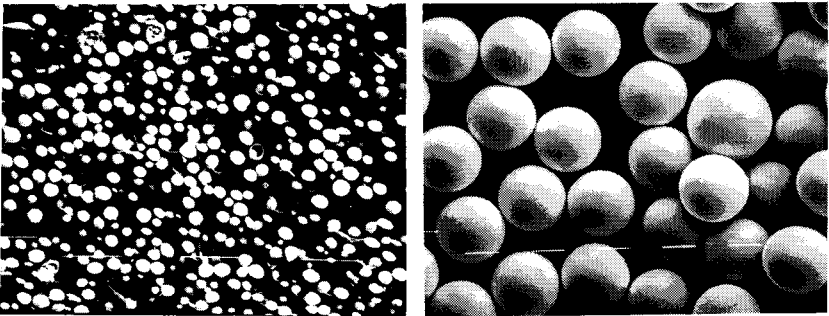


Fig.2 : Left: $\text{Sn}_{99}\text{Sb}_1$ granules ($10 \mu\text{m} < \phi < 25 \mu\text{m}$) in GE Varnish 7031 ; Right: $200 \mu\text{m}$ diameter Sn_{998} grains prepared in He atmosphere.

b) Samples of very large granules prepared by industrial procedures (EXTRAMET [19], BILLITON [20]) exhibit superheating at reasonable values of the applied field. This is particularly encouraging for large area experiments, where several tons of grains would be required (EXTRAMET can at present produce ≈ 5 Kg/hour of Sn grains).

As an example, superheating was still observed for 200 to 400 μm diameter granules prepared by BILLITON with an alloy $\text{Sn}_{99}\text{Sb}_1$. These granules give electronic signals with risetimes of less than 300 ns. When irradiated, they turned out to be sensitive to 6 keV γ 's (local heating at the surface leading to nucleation). Such results are extremely encouraging for the feasibility study of a SSG monopole detector, since very large granules can be used without spoiling time resolution. In the expression for flipping time: $\tau \sim R^2 \rho^{-1}$ (R = radius, ρ = normal state resistivity), the increase in grain size is compensated by a higher impurity rate [12]. Furthermore, the irradiation result obtained with ^{55}Fe γ 's indicates that a local surface phenomenon can indeed flip a large superheated grain. A possibility to perform the SSG monopole experiment at liquid helium temperature (4.2 K), would be to use β -Ga spheres. The feasibility of collections of metastable granules involving only this phase of gallium ($T_c = 5.9$ K) was demonstrated long ago by Feder and Parr [21]. As a more conventional solution (working at superfluid helium temperatures), Fig. 2b shows a collection of ≈ 200 μm 998 pure Sn grains produced by EXTRAMET in a He atmosphere. They exhibit good metastability properties, and so do smaller grains from the same producer.

The main concern for the monopole project is at present to perform an experimental test of the detection principle itself (i.e., check the incompatibility between the superheated state and the presence of two flux quanta injected into the sample). This is a highly nontrivial solid state experiment, and is likely to require a long term specific study.

4. DEDICATED SCINTILLATING CRYSTALS

Inorganic scintillating crystals, like SSG devices, fall into the group of target detectors. A large amount of target element can be found in some crystals, still remaining transparent to scintillating light. Developing new scintillating crystals, based on compounds of specific target elements is not a simple task. Some examples can be found in [22], where indium borate has been proposed for neutrino detection. Photon cross-sections may be quite dependent on the target nucleus and therefore using a large variety of target elements may help to get a better dark matter signature. We are here confronted with the problem of detecting a very low energy deposition. Scintillating crystals have been shown to be sensitive to low energy γ 's down to 800 eV [23]. Cooling down crystals and photomultipliers can in some cases increase by one or two orders of magnitude the light yield, still reducing the background. An applied electric field may also for some compounds enhance the light output and even help to obtain some directionality information. Two cases deserve particular attention:

4.1 Coherent scattering for scalars and Dirac fermions

Depending on the masses of the WIMP and target elements, the event rates range from a few to several thousands per kg and per day. Adapting the mass of the target nucleus to the explored mass range for the WIMPs, a higher recoil energy can be obtained (about $10^{-6}m_{\text{WIMP}}$). Not much is known about light yield from recoiling heavy ions, however 300 keV ^{12}C ions have been detected and one observes an increase at low energy (< 1 MeV) of the relative pulse height per unit energy [24]. Clearly, specific studies and experiments should be performed to investigate the low energy scintillation light yield from recoiling nuclei.

4.2 Inelastic scattering for Majorana fermions

The natural way to reject background would be to detect, in a time delayed coincidence, the recoil of an excited nucleus followed by the γ ray associated to its decay to the ground state. However, the cross-sections here seem [17] much smaller than previously suggested [25]. ^{187}Os ($E_\gamma = 9.8$ keV) has a lifetime of 2.4 nsec and may bring an event per ton and per day. It would provide the smallest detector, but a very difficult time delayed coincidence. Rare earths (^{149}Sm , τ lifetime = 7.6 ns for $E_\gamma = 23$ keV ; ^{151}Eu , $\tau = 9.5$ ns for $E_\gamma = 22$ keV) allow in principle to produce scintillating crystals with a high light yield but require 30 tons of detector for 1 event/day. The above mentioned ^{119}Sn leads to 10 tons for 1 event/day, but allows for more comfortable delayed coincidences. Unfortunately, it is not obvious whether conventional detectors would be able to incorporate ^{57}Fe ($\tau \simeq 98$ ns , similar event rate). In spite of such extremely low rates, detectors based on inelastic scattering may indeed be able to reject background if the recoil energy turns out to be detectable and the delayed time coincidence can be observed. A detailed study of the basic properties of detectors (scintillators, semiconductors, SSG,...) incorporating specific target elements must be performed in order to eventually find a suitable inelastic scattering detector for galactic Majorana fermions. The case for conventional techniques (as compared to cryogenic detectors) may improve in the future, if high energy experiments provide more stringent lower bounds on the masses of supersymmetric particles, for a heavier WIMP would carry a larger kinetic energy.

5. CONCLUSION AND COMMENTS

The improved version of SSG may provide a leap forward in the feasibility study of a dark matter detector based on recoil energy. A ^{119}Sn inelastic scattering detector seems much more problematic, and in any case belongs to a later generation of dark matter experiments. Monopole detection with SSG remains extremely tempting, but the crucial point is to check experimentally the validity of the proposed detection principle.

For inelastic scattering, no good solution exists by now, but dedicated scintillating crystals may be worth considering if they can see the nucleus recoil and if they are fast enough to observe the delayed time coincidence. In any case, this is the most ambitious part of dark matter searches and should not be considered as a short term goal.

Acknowledgments

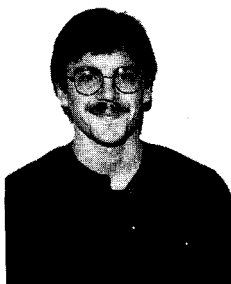
We are grateful to John Ellis and Ricardo Flores for kindly communicating, prior to publication, some interesting results on inelastic scattering of WIMP off nuclei.

References

- [1] J. Feder, S.R. Kiser and F. Rothwarf Phys. Rev. Lett. 17, 87 (1966).
- [2] For an updated introduction, see: L. Gonzalez-Mestres and D. Perret-Gallix, in "A unified view of the Macro- and the Micro-Cosmos", World Scientific Pub. 1987.
- [3] H. Bernas, J.P. Burger, G. Deutscher, C. Valette and S.J. Williamson, Phys. Lett. 24A, 721 (1967).
- [4] C. Valette, Thesis Orsay 1971.
- [5] J. Blot, Y. Pellan, J.C. Pineau and J. Rosenblatt, J. Appl. Phys. 45, 1429 (1974).
- [6] A.K. Drukier, C. Valette, G. Waysand, L.C.L. Yuan and F. Peters, Lettere al Nuovo Cimento 14, 300 (1975); A.K. Drukier and L.C.L. Yuan, Nucl. Instrum. and Methods 138, 213 (1976).
- [7] C. Valette and G. Waysand, "Décteur supraconducteur de rayons gamma a résolution intrinseque submillimétrique", Orsay 1976; D. Hueber, Thesis Orsay 1980.
- [8] L. Gonzalez-Mestres and D. Perret-Gallix in "Low Temperature Detectors for Neutrinos and Dark Matter", Springer-Verlag 1987.
- [9] L. Gonzalez-Mestres and D. Perret-Gallix, Preprint LAPP-EXP-87-08 (1987), to be published in the Proceedings of the Workshop on Superconductive Particle Detectors, Torino 1987.
- [10] K. Pretzl, preprint MPI-PAE/Exp.El. 187 (1987), to be published in the same Proceedings.
- [11] L. Gonzalez-Mestres and D. Perret-Gallix, Proceedings of the Moriond Meeting on Massive Neutrinos, January 1984, Ed. Frontiers.
- [12] L. Gonzalez-Mestres and D. Perret-Gallix, Proceedings of Underground Physics 85, Nuovo Cimento 9C, 573 (1986).
- [13] F. Von Feilitzsch, T. Hertrich, H. Kraus, L. Oberauer, Th. Peterreins, F. Probst and W. Seidel, in "Low Temperature Detectors for Neutrinos and Dark Matter", Springer-Verlag 1987.
- [14] R. S. Raghavan, Phys. Rev. Lett. 37, 259 (1976).
- [15] R.H. Davis, Int. J. Thermophys. 7, 609 (1986).
- [16] O. Lounasmaa, "Experimental Techniques and Methods Below 1K", Academic Press 1974.
- [17] J. Ellis, R. Flores and J.D. Lewin, CERN preprint TH-5040 in preparation.
- [18] Voltage amplifiers for SSG readout have been developed at LPC (College de France). First presented by R. Bruere-Dawson at the Meeting on Superconductive Devices for Neutrino Astronomy, Strasbourg December 1984.
- [19] EXTRAMET, 24A rue de la Résistance, 74 Annemasse (Haute-Savoie, FRANCE).
- [20] BILLITON WITMETAAL FRANCE, 48 - 58 rue Alfred Dequéant, 92 Nanterre.
- [21] H. Parr and J. Feder, Phys. Rev. B7, 166 (1973).
- [22] L. Gonzalez-Mestres and D. Perret-Gallix, LAPP-EXP-87-03 (1987). To be published in the Proceedings of the "Rencontre sur la Masse Cachée dans l'Univers et la Matière Noire", Annecy (LAPP) July 1987.
- [23] M.F. McCann and K.M. Smith, Nucl. Inst. and Meth. 65, 173 (1968).
- [24] J.B. Birks, Theory and Practice of Scintillation Counters, Pergamon Press 1964.
- [25] M.W. Goodman and E. Witten, Phys. Rev. D31, 3059 (1986).

A SEARCH FOR WIMPS AT FERMLAB

Michael A. Tartaglia
Department of Physics and Astronomy
Michigan State University
East Lansing, MI 48824-1116
USA



ABSTRACT

We have instrumented the FMMF fine-grained neutrino detector at Fermilab with high-resolution scintillation timing counters to search by Time-Of-Flight for Weakly Interacting Massive Particles (WIMPs) in the Tevatron neutrino beam. In a recent exposure of about $5 \cdot 10^{17}$ 800 GeV protons on target, we accumulated a sample of nearly 10^5 fiducial interactions, and recorded a comparable number of test-beam calibration interactions. We describe this search experiment here in detail, and give a preliminary review of the detector performance.

INTRODUCTION

The Standard Big-Bang Model of Cosmology ^{1]} has enjoyed a fruitful relationship with Particle Physics in the last few years. The solution to one of the current fundamental problems in Cosmology -- the so-called Dark Matter problem -- may come, at least in part, from the Particle Physics sector ^{2]}. Meanwhile, on the front lines of Particle research, the discovery of something "unexpected" is eagerly sought to provide more clues toward the understanding of mass generation and Nature's fundamental symmetries. A number of theoretical extrapolations ^{3]} from the Standard Electro-Weak Model ^{4]}, suggest the possibility of heavy neutrinos or other massive particles with weak interaction strength that could contribute to the Dark Mass, and so provide some incentive to search in this realm.

This experiment attempts to produce these prospective new particles by heating a target (or beam dump) with 800 GeV protons from the Fermilab Tevatron, and then detecting their interactions or decays in a large, finely segmented neutrino detector ^{5]}. The search makes use of a Time-Of-Flight (TOF) technique ^{6]} to distinguish massive from (nearly) massless states in the Tevatron neutrino beam/dump, and is therefore qualitatively different from previous neutrino beam dump searches of this type ^{7]}. In particular, the particle mass, as opposed to its interactions or decays, will be the discriminator that identifies, in a model-independent way (since we measure all "visible" leptonic and hadronic final states), the presence of new Physics. Furthermore, if the timing resolution is 1 ns or better, one can perform a search with essentially no background. The properties of such a particle, if found, can be investigated further by exploiting the powerful pattern recognition capabilities and good energy and angle resolutions of the existing detector.

In addition to the new approach, the experiment was motivated to explore the new kinematic regime at the Tevatron with an increase in available center-of-mass energy over previous (400 GeV) fixed-target experiments, from $\sqrt{s} = 27.4$ GeV to $\sqrt{s} = 38.8$ GeV. The quadrupole-focus design of the neutrino beamline, shown in Figure 1, makes two line-of-sight sources at different distances simultaneously available for study; namely, the one-interaction length Beryllium primary target at 1615 meters, and the secondary pion/kaon/proton on Aluminum beam dump at 1065 meters from the detector. Also, due to the existence of a well-instrumented test beam facility (Figure 1), it was possible to continuously calibrate the TOF system to measure resolutions and systematic effects.

The E733 experiment is a collaboration of Fermilab, MSU, MIT and U. of Florida personnel, and it first recorded Tevatron (anti) neutrino data in 1985 to study production of dimuons. The TOF technique was first considered as an option for the Prompt Neutral Lepton Facility experiments ^{8]}, and was approved to run in the 1987 Wide Band Beam exposure. The TOF data were recorded from June, 1987 to February, 1988, and about 2/3 of these have been studied so far in a first analysis pass.

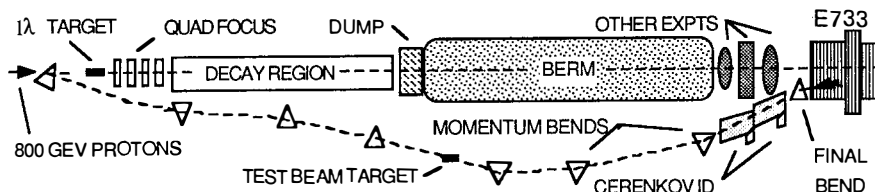


Figure 1. Schematic plan view of Neutrino and Calibration beamlines.

TECHNIQUE

This time-of-flight search is possible because of the bunched time-structure of the Tevatron beam: protons are constrained to be in "buckets" of about 1 ns width (FWHM) and spaced by 18.83 ns, due to the 53.1 MHz RF-frequency of acceleration. The protons extracted from the accelerator therefore hit a target every 18.83 ns, producing secondary pions and kaons from which the neutrino beam is derived. A relativistic particle of mass M and momentum P will take longer than a massless particle at the same momentum to reach the detector at a distance L away from the production point, with the time difference ΔT given by

$$\Delta T = (L/2c) \cdot (cM/P)^2, \quad (\text{Eq. 1})$$

where c is the speed of light. The nearly massless secondaries and neutrinos remain in phase with the RF clock, while "heavy" particles will arrive at the detector with a measureable phase delay. Experimentally, one must measure precisely the "arrival time" of each event with respect to the accelerator RF clock signal. The neutrino event times will be clustered in peaks separated by the RF clock period, where the peak width, σ_t , depends upon the width of the proton buckets and the resolution of the detector timing system.

One can define a search region between the buckets where no events should appear: assuming Gaussian resolutions, there should be less than one event in 10^5 whose deviation from the mean peak position is more than 4 standard deviations, σ_t . The search region is therefore a window of width

$$18.83 - 8 \cdot \sigma_t, \quad \text{for } \sigma_t < 2.4 \text{ ns.} \quad (\text{Eq. 2})$$

From preliminary analysis of the calibration data obtained, it appears that a resolution of about 1 ns will be achievable. The detailed shape of the resolution function may be an important consideration, and the resolution shape will be determined from the calibration data, for which comparable event statistics to the neutrino data have been collected.

One does not know from which RF bucket an event arose, so the measured deviation from the peak position, $\Delta \tau$, can be offset from ΔT by an integer multiple of the clock period. So $\Delta \tau$ represents a lower limit on ΔT . Furthermore, the visible energy deposited by an interacting or decaying particle will, in general, be less than the total energy. From Equation (1), these considerations imply that one determines a lower bound on the mass of the new particle. Below about 10 GeV energy deposition, the trigger is not fully efficient. This establishes the

smallest detectable mass (largest $\gamma = E/Mc^2$): from Equation (1) with $\Delta\tau = \Delta T = 4\sigma_t$, and assuming $\sigma_t = 1$ ns, this corresponds to 0.4 GeV/c² from the target, and 0.5 GeV/c² from the dump. Particles with lifetimes τ much shorter than $\tau = L/\gamma c = 10^{-7}$ seconds will decay before reaching the detector.

INSTRUMENTATION

To obtain precise timing information for as many low-bias events as possible, we installed an array of large area scintillation counters, arranged to cover the calorimeter fiducial volume. As illustrated by an event picture in Figure 2, the array contained a total of 16 scintillation counters, each 2m x 0.3m x 2 cm, mounted in 4 "structural boundary" stations; the stations are separated by 2.5 interaction lengths (λ) = 17.5 radiation lengths (χ) of material. The vertical positions were staggered from station to station, leaving no projected gaps in coverage. Each counter was instrumented with phototubes at both ends, and cable lengths were adjusted so that signals caused by beam particles, moving at c , would arrive simultaneously to the trigger and timing electronics.

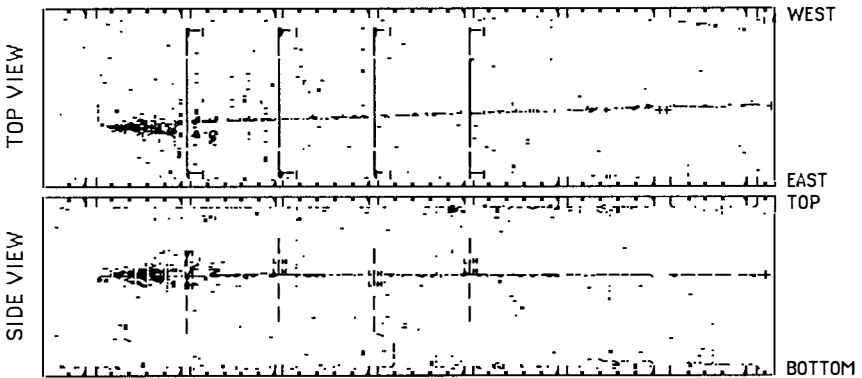


Figure 2. A charged current neutrino interaction, seen with flash chambers in orthogonal projections, traverses the Time-Of-Flight scintillator array. Time measurements are flagged in the side view as L=low, H=high level threshold, positioned with East below and West above. Pulse height bars are drawn in the top view, in vertical order.

Timing information was recorded for all detector events** in which at least two phototubes from the same side (East or West) of the detector had pulse heights above a low threshold level. This condition, the second phototube pulse crossing threshold, formed a "clock start" signal for digitizing all event times. The accelerator RF signal was processed to generate a "clock stop" signal every four RF clock cycles. Each (delayed) phototube pulse also generated two "clock stop" signals, one for each of two separate threshold

* Previously occupied by liquid scintillator tanks, used to trigger on Cosmic Rays.

** Of neutrino interactions with a fiducial vertex found, 94% have TOF data.

levels; the pulse height from each phototube was also recorded. In what follows, we consider only the information contained in the former channel, the RF CLOCK TIME, T_{RF} , representing the time between the clock start and the RF clock stop. The final analysis will, of course, utilize all of the available information.

The consequence of using long scintillators in this timing scheme is that the "raw" T_{RF} depends upon where the ionization occurs along the triggering counter; the clock start will be delayed after the particle traversal by the time it takes for light to reach the phototube. This is easily seen for the case of test beam interactions: The test beam particles traverse a consistent trajectory through the detector, with some phase relative to the RF clock. However, hadron showers are broader than muons, so the clock starts slightly sooner on average than for muons, and the mean T_{RF} is shifted. Fluctuations in the shower edge position lead to a broadening of T_{RF} for hadrons, as do bremsstrahlung and delta radiations, to a lesser extent, for muons. Figure 3 shows the RF CLOCK TIME distributions for large statistics samples of 250 GeV test beam muons and hadrons. It is encouraging that the resolutions are about the required level of 1 ns, without having made any corrections to the data. It is anticipated that the resolutions will be improved by using the high resolution flash chamber information to locate the ionization, and correct the raw times on an event by event basis. It is also encouraging that the region between the peaks, shown enlarged in Figure 4 for 250 GeV hadrons, is relatively devoid of events out of time, at the level of about one in 9000; the small low-time tail is due to contamination by low-energy events as yet unfiltered from the hadron sample.

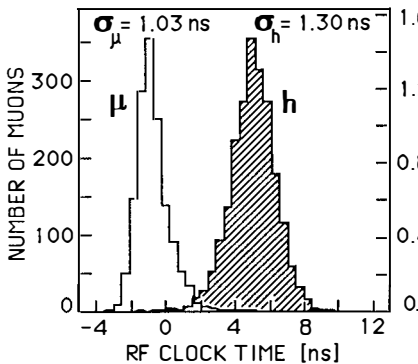


Figure 3. RF peaks for 2133 muons and 9154 hadrons at 250 GeV.

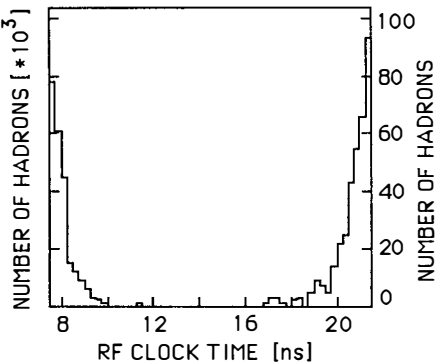


Figure 4. Signal region between RF peaks for 250 GeV hadrons.

The long-term performance of the system is illustrated in Figure 5, by showing the program-found T_{RF} peak positions, for program-classified muon and hadron event types, as a function of time early in the run. Both 250 and 50 GeV data are shown, with each point corresponding to data from one tape. Several features are consistent with expectations: the average shower width appears to be greater at the higher energy; also, changing the penetration depth (before showering) introduces shifts, because the trigger scintillator cuts

a shifted average shower profile. Other shifts occurred, as expected, when certain equipment changes were made, and when the test beam angle was altered. The accelerator RF signal is quite stable, but appears to drift slowly at the level of about 0.5 ns, and in a completely measurable and correctable way. In the time period following the epoch shown, a variety of test beam studies were made over an energy range from 25 GeV to 300 GeV, and encompassing a range of bend angles at each energy setting.

For neutrino interactions that occur over the entire fiducial volume, and have a wide range of visible energies deposited, the raw T_{RF} distribution is rather broad at $\sigma_t = 3$ ns. The process of correcting for the event position and energy is now under study. There is at least one class of events, those with an isolated muon traversal of a scintillator, in which the event time can be cleanly resolved, and so provide an internal check upon the event time as measured from the shower information. Indeed, such events are likely to lead to the first physics results from the search experiment.

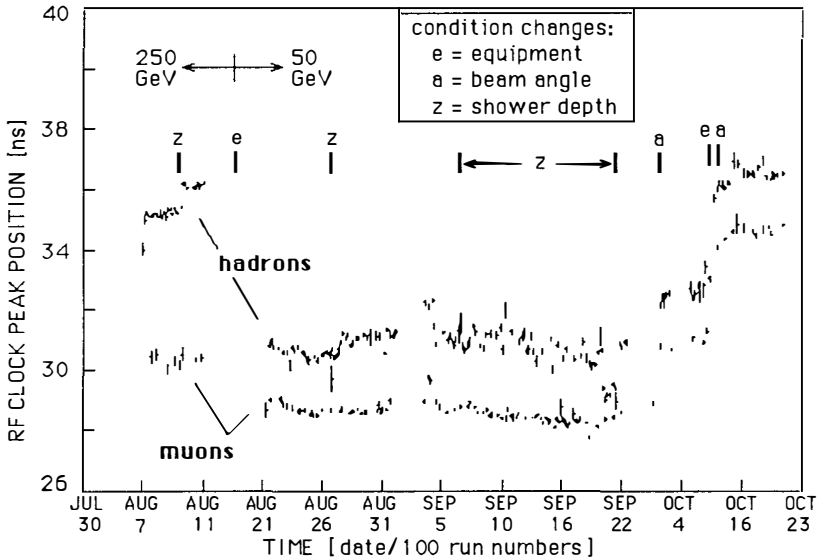


Figure 5. RF clock peak position versus time during the run, for 250 GeV and 50 GeV muons and hadrons.

PROSPECTS

The number of WIMPs, N_{new} , that may be detected can be written as a product of factors,

$$N_{new} = N_{prod} \cdot P_{det} \\ = \{(\alpha_{live} \cdot N_{pot} \cdot N_{T/A}) \cdot (\sigma \cdot BR)_{prod} \cdot \phi_{geom}\} \cdot P_{det}, \quad (\text{Eq. 3})$$

where N_{prod} is the number of produced WIMPs that traverse the live detector, and P_{det} is the probability for detecting an interaction or decay. The average detector live fraction, α_{live} ,

was about 40%, and the beam intensity integrated to about $(5.3 \cdot 10^{17}) \cdot (4/3) = 7 \cdot 10^{17}$ protons on target+dump, with $N_{T/A} \approx 4.5 \cdot 10^{25}$ target nucleons/cm². The geometrical acceptance, Φ_{geom} , is the production-weighted solid angle fraction subtended by the detector; if we assume x - and p_T - spectra typical of heavy quark production^{9]}, we find $\Phi_{\text{geom}} \approx 10^{-3}$. The factor of production cross section times final-state branching fraction, $(\sigma \cdot \text{BR})_{\text{prod}}$, may be calculated in specific models.

The probability of detecting any produced WIMPs depends on the detection efficiency, \mathcal{E}_{det} , and on whether they a) interact (if stable), or b) decay:

$$\text{a) } P_{\text{det}} = N_{\text{fidT/A}} \cdot \sigma_{\text{int}} \cdot \mathcal{E}_{\text{det}}, \quad \text{b) } P_{\text{det}} = P_{\text{decay}} \cdot \mathcal{E}_{\text{det}}, \quad (\text{Eq. 4})$$

where σ_{int} is the interaction cross section, P_{decay} is the probability that the particle survives to, and decays within the fiducial volume, and $N_{\text{fidT/A}}$ is the number of fiducial target nucleons per unit area = $8 \cdot 10^{26}$ /cm². The detection efficiency, i.e., the fraction of WIMPs that fall within the signal region (with 10 GeV visible energy), also depends upon the production spectrum; under the assumption made above, we expect that $\mathcal{E}_{\text{det}} > 0.1$ (although this is a function of σ_1). Combining equations (3) and (4), a measured upper limit of N_{new} would impose a constraint on new particles given roughly by

$$(\sigma \cdot \text{BR})_{\text{prod}} \cdot \sigma_{\text{int}} \leq N_{\text{new}} / \{1.0 \cdot 10^{66} \text{ /cm}^4\} \quad (\text{Eq. 5})$$

Note that attenuation in the berm becomes important for $\sigma_{\text{int}} \geq 10^{31}$ cm².

We have investigated what limits might be obtained on the existence of unstable heavy neutrinos that arise from heavy quark decays. In particular, we have applied the analysis of Gronau, Leung, and Rosner^{10]} (GLR) to the case of D meson production and decay into electron-type heavy neutrinos. In this model, the production and decay of heavy neutrinos are calculated in terms of the neutrino mass and the square of a mixing angle, $|U|^2$. GLR have analysed the CHARM beam dump experiment^{7]}, a calculation which we use as a benchmark for comparison. Figure 6 shows the region that this experiment will exclude, if in fact no "decays" are observed in a 10 m decay region, as tagged by this TOF system with 1 ns resolution. The CHARM limit is more exclusive by virtue of greater accumulated proton intensity; however the TOF limit will exclude a region that encompasses all visible decay modes, so is independent of assumptions about the decay branching ratios made in the GLR analysis of CHARM.

CONCLUSION

In conclusion, we have begun a new search for Weakly Interacting particles at the Tevatron, using Time-Of-Flight to identify massive particles in a neutrino beam. A preliminary analysis of calibration data shows the viability of the search: uncorrected resolutions are close to the anticipated 1 ns resolution goal, the signal region appears uncontaminated by tail events or "out of bucket" protons, and the RF clock signal has a stable phase relation to the beam over long time periods. In the future, all recorded times will be used to construct a consistent "event time", and straightforward corrections based

on flash chamber ionization information will be applied to the "raw times". Internal consistency checks on the neutrino analysis are possible using a sample of events containing a clean muon measurement.

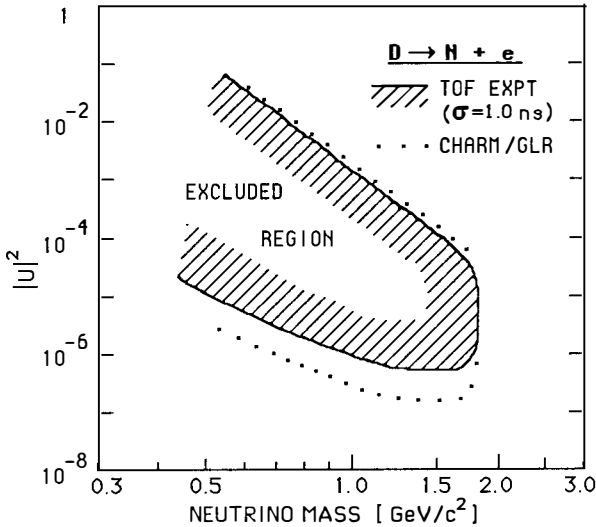


Figure 6. Mixing angle squared versus mass, excluded regions for heavy neutrino decay (following GLR¹⁰ analysis)

REFERENCES

- 1] S. Weinberg in *The First Three Minutes*, Bantam Books, 1977.
- 2] See, for example, L. Krauss, this conference.
- 3] For a recent review, see F. Gilman, *Comments Nucl. & Part. Phys.* 16(1986)231; for SUSY, see G.R.Farrar, P.Fayet, *Phys. Lett.* 76B(1978)575.
- 4] S.Weinberg, *Phys. Rev. Lett.* 19(1967)1264; A.Salam, in *Nobel Symp. no.8, Elementary Particle Theory*, ed. N. Svartholm, 1968; S.Glashow, *Nucl. Phys.* 22(1961)579.
- 5] F.Taylor *et al.*, *IEEE Trans. Nucl. Sci* 27(1980)30; D.Bogert *et al.*, *ibid.* 29(1982)363 M.Tartaglia *et al.*, in *Proceedings of the Gas Calorimetry Workshop II*, Fermilab, 1985, p259; J.Womersley *et al.*, *Nucl. Instrum. & Methods* A267(1988)49.
- 6] J.Appel *et al.*, *Phys. Rev. Lett.* 32(1974)430; R.Gustafson *et al.*, *Phys. Rev. Lett.* 37(1976)474; G.Kalbfleisch *et al.*, *Phys. Rev. Lett.* 36(1976)837; *ibid.* 43(1979)1361; R.Shrock, *Phys. Rev. Lett.* 40(1978)1688.
- 7] R.C.Ball, *et al.*, *Phys. Rev. Lett.* 51(1983)743; F.Bergsma *et al.*, CHARM collaboration, *Phys. Lett.* 128B(1983)361; A. Cooper *et al.*, BEBC collaboration, *Phys. Lett.* 160B(1985)212.
- 8] M. Tartaglia, in *Workshop on Beam Dump Physics and Beam Dump Designs*, (copies of transparencies), Fermilab, April 4-5, 1986.
- 9] We assume $d^3\sigma/dp^3 \approx (1-x)^4 e^{-2M_L}$, where $M_L = (p_\perp^2 + M_N^2)^{1/2}$; (see Ref. 10).
- 10] M.Gronau, C.N.Leung, J.Rosner, *Phys. Rev.* D29(1984)2539.

INTERMEDIATE RESULTS FROM AN EXPERIMENT TO DETECT GALACTIC AXIONS

S. DePanfilis, A. C. Melissinos, B. Moskowitz, J. Rogers, Y. Semertzidis and W. Wuensch
Department of Physics and Astronomy, University of Rochester, Rochester, New York 14627

H. Halama and A. Prodell
Brookhaven National Laboratory, Upton, New York 11973

W. Fowler and F. Nezrick
Fermi National Accelerator Laboratory, Batavia Illinois 60510

Paper presented by W. Wuensch



ABSTRACT:

An experiment has been underway to search for galactic axions using an electromagnetic cavity detector. Since the mass of the axion is not known it is necessary to search over a range of masses. Limits on the abundance and coupling of axions are presented in a mass range of $4.5 < m_a < 12 \times 10^{-6}$ eV to be less than between $(g_{a\gamma\gamma})^2 \rho_a < 1.4 - 6 \times 10^{-41}$. The theoretical prediction is $(g_{a\gamma\gamma})^2 \rho_a \sim 3.9 \times 10^{-4}$. This mass range has not been excluded by previous experiments or by astrophysical constraints.

INTRODUCTION:

At Brookhaven National Laboratory we have been conducting an experiment which seeks to directly determine whether axions compose the halo of dark matter in our galaxy¹. The extremely weak coupling of low mass axions, known as "invisible axions"², make them prime cold dark matter candidates. The original motivation for the axion is particle physics, interestingly independent from later astrophysical considerations. We shall describe this motivation, a scheme to detect dark matter axions, and the results produced so far from an experiment based on such a scheme.

The QCD Lagrangian contains a term $\theta G^{\mu\nu} G_{\mu\nu}$ which violates CP. However there has been no observed CP violation in the strong interaction, in particular from measurement of the electric dipole moment of the neutron and a limit of $\theta < 10^{-9}$ has been placed. To explain naturally why θ should be so small but not zero Peccei and Quinn³ introduced a global symmetry (PQ) which is spontaneously broken in the theory. As a result θ becomes a dynamic variable oscillating about zero in a potential defined by the energy scale F_a at which the symmetry is broken. Weinberg⁴ and Wilczek⁴ pointed out that the breaking of the PQ symmetry should give rise to a pseudoscalar Goldstone boson, dubbed the axion. The mass of the particle is not given by the theory but is related to F_a

$$m_a = \frac{\sqrt{2} F_\pi m_\pi}{F_a}$$

where $F_\pi = 93$ MeV and $m_\pi = 135$ MeV.

F_a was originally thought to equal the weak symmetry breaking scale, $F_{\text{weak}} = 100$ GeV which corresponds to an axion mass of 10^5 eV. However, accelerator experiments have failed to detect axions with mass greater than 200 keV. Subsequently models for lighter axions with consequently weaker couplings have been proposed. The existence of such axions has been severely constrained by a number of astrophysical arguments. Very light axions, $m_a < 10^{-5}$ eV would have been produced in such abundance in the early universe that they would now overclose it. Analysis of stellar evolution and of supernova SN1987a further restricts the mass of the axion to lie outside the range of 10^{-3} to 10^5 eV. These limits are summarized graphically in figure 1.⁵ Conspicuously on this graph is a gap from 10^{-5} to 10^{-3} eV.

Axions in this mass range have been described by Dine, Fischler, and Srednicki². Their model predicts a coupling to fermions and, through a triangle graph, to two photons (figure

2). The coupling is extremely weak so the life time of the axion is extremely long, over 10^{40} years. For this reason, the axion is an extremely interesting dark matter candidate. Axions should have been produced in the early universe and later condensed into the galaxies. Of course, as is true for all good dark matter candidates, such axions are rather hard to see. In spite of the weak coupling, it is possible to enhance the decay $a \rightarrow \gamma\gamma$.

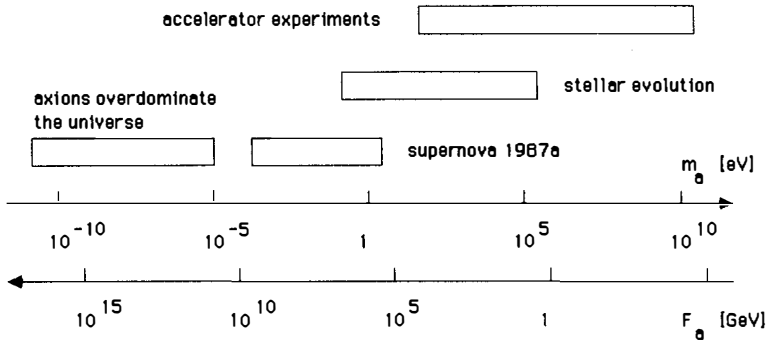


Figure 1, Constrains on the mass of the axion

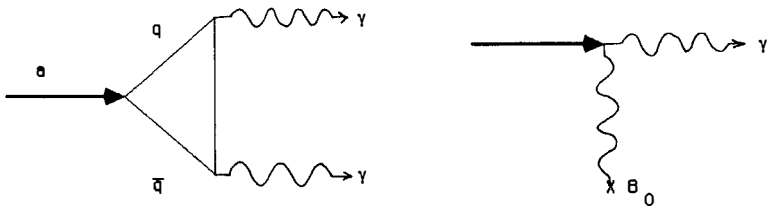


Figure 2, The coupling of the axion to two photons

THE DETECTION SCHEME:

As proposed by Sikivie ⁶, axions could be converted into photons in the presence of an intense electromagnetic field via the Primakoff effect. The interaction Lagrangian is

$$L_{int} = -\left(\frac{g}{4\pi}\right) E \cdot B \phi_a$$

where E and B are the electric and magnetic fields respectively and ϕ_a is the axion field. The

coupling constant is given by

$$g_{a\gamma\gamma} = m_a \frac{e^2}{\hbar c} \frac{(\hbar c)^{2/3}}{f_n m_n} (\sqrt{2\pi})^{-1}$$

The decay signal can be further enhanced by placing a high Q microwave cavity in the magnetic field. If tuned correctly, the photon produced in the decay of the axion becomes an excitation of the cavity resonance. It is expected that axions which compose the galactic halo move with velocities similar to those of luminous galactic objects. This velocity is typically $\beta \sim 10^{-3}$, so very little spread is expected in the energy spectrum of the axions, $E_\gamma \sim m_a(1 + \beta^2/2)$. A more detailed calculation⁷ predicts a full width of the converted photon line of $\Gamma_a \sim 3 \times 10^{-7} m_a$. It is the narrowness of this line which makes the detection of axions possible and defines their experimental signature. It also makes detection difficult, in a way, since one must sweep the tune of the (narrow) microwave cavity to search for a narrow signal of unknown frequency (because the mass of the axion is only broadly constrained). Our experiment will scan a mass range of $4.5 < m_a < 25 \times 10^{-6} \text{ eV}$ or corresponding photon frequencies $1 < f_a < 6 \text{ GHz}$. Our apologies to those used to other units, we will refer to the mass of the axion by its converted photon frequency for the rest of the paper.

EXPECTED SIGNAL STRENGTH:

When the electromagnetic-axion interaction Lagrangian given earlier is solved for a cavity in a magnetic field given the presence of axions, the expected signal power available to the detector is

$$P_a = \frac{1}{2} \left(\frac{g_{a\gamma\gamma}}{m_a} \right)^2 \langle \rho_a \rangle \omega Q [\epsilon_0 (cB_0)^2] V G_J^2$$

where,

$\langle \rho_a \rangle$	local dark matter density, 300 MeV/cm^3
f	cavity (axion) frequency
B_0	average field from the magnet
V	volume of the cavity

Q_L loaded cavity Q, $Q_L = Q_0/2$ at critical coupling

G_j^2 form factor $E B d^3 x$, implies use of TM_{010} mode.

Rewriting this in terms of parameters which are typical of those in the experiment

$$P_a = (3.44 \times 10^{-24} \text{ W}) \left(\frac{\langle p_a \rangle}{300 \text{ MeV/cm}^3} \right) \left(\frac{f}{1 \text{ GHz}} \right) \left(\frac{V}{10^4 \text{ cm}^3} \right) \left(\frac{Q_L}{10^5} \right) \left(\frac{G_j^2}{0.7} \right)$$

In particular,

$$\begin{aligned} &= 3.29 \times 10^{-24} \text{ W} \\ &= .6 \text{ mK (assuming a 400 Hz wide axion)} \\ &= 3 \text{ photons per second} \end{aligned}$$

There are two significant noise sources in the experiment: thermal noise from the cavity which has a temperature of 4.2 K, and the amplifier which has an equivalent noise temperature of typically 10 K. This gives a total noise temperature of 14.2 K, much higher than the expected signal strength of .6 mK. To see such a small signal extensive averaging is clearly necessary. It is this need to average which limits the rate at which one can scan through frequency in an experiment of this type. Typical sweep rates result in 250,000 averages of a given frequency channel and consequently produce a noise reduction of a factor 500 and effective noise temperature of 30 mK. This unfortunately is more than the expected signal strength but represents our best efforts so far. The exact signal to noise produced is a function of frequency as many experimental parameters change with frequency.

THE EXPERIMENT:

Since the expected signal strength is proportional to the square of the magnetic field it is important that the field be as high as possible. This experiment uses an 8.7 Tesla superconducting magnet with a 6 inch diameter by 16 inch long bore. Placed inside of the bore is a copper right circular cylindrical microwave cavity. As has been stated the strength of the signal is proportional to the Q of the cavity. Upon cooling the conductivity of copper increases. Measurement of Q in our cavities when cooled from 293K to 4.2K have produced increases of Q of a factor of 5. Although the DC conductivity for the copper used in the cavities increases by a factor 170^8 the Q in the microwave range is limited to the observed values by the anomalous skin effect. Measurements indicate that we have arrived to within 75% of the theoretically maximum Q.

In addition to confirming a bit of solid state physics these Q results are gratifying to us in that they indicate that we have been able to produce a series of high quality cavities over a wide range of frequencies. The cavities are machined from high purity copper, electropolished, and electron beam welded or compressed together with flanges.

Tuning is accomplished by inserting a dielectric rod along the central axis of the cavity effectively increasing the volume of the cavity and lowering its resonant frequency. Sapphire was chosen for the dielectric because of its high dielectric constant, 10, and low microwave absorption (insignificant compared to the losses in the cavities themselves). The TM_{010} can be tuned 15-20% in this way. In order to cover from 1 to 6 GHz, a factor 6, it is necessary to construct many cavities.

Power is coupled out of the cavity by means of a critically coupled loop antenna. The first stage of the detection electronics is an ultralow noise cryogenic amplifier. The amplifiers are based on a design 3 stage GASFET transistor design developed by the National Radio Astronomy Observatory⁹. Originally designed for operation around 1.5 GHz, the amplifiers have been constructed and modified by our group to function from 1 to 4 GHz¹⁰. Like the cavities the amplifiers have limited bandwidths, approximately 20%. Minimum noise temperatures of 8K near 1GHz and 11K near 2.5GHz have been realized. A microwave circulator is placed between the cryogenic amplifier and the microwave cavity in order to minimize the noise temperature of the amplifier. The noise performance of an amplifier is dependant on the source impedance the amplifier sees and is usually optimized for 50Ω ¹¹. The impedance of a cavity near resonance is a strong function of frequency: the circulator provides a constant 50Ω load. After the cryogenic amplifier the signal exits the dewar and is further amplified by a room temperature microwave amplifier. The signal is then superheterodyned to a frequency of 20 to 50 KHz where it is finally detected in a 64-channel multiplexer whose channel bandwidth is 400 Hz and logged by the data acquisition computer. Figures 3 and 4 show schematic drawings of the apparatus.

During data taking the cavity resonant frequency is continuously changed by withdrawing the sapphire rod from the cavity slowly with a precise machine screw mechanism mounted on the top of the dewar. The frequency tuning rate is typically one multiplexer channel width per second and the time to withdraw the rod the full 16 inches is approximately 10 days. Every 50 seconds the cavity frequency is measured, the current sweep rate is calculated and the first rf local oscillator is set to track the cavity. Data is read out continuously from the multiplexer by the acquisition computer. Every 30 minutes data taking is briefly halted, various calibrations and diagnostic measurements are made and the data are transferred to the communications computer. From there the data are sent to a Vax computer for final analysis.

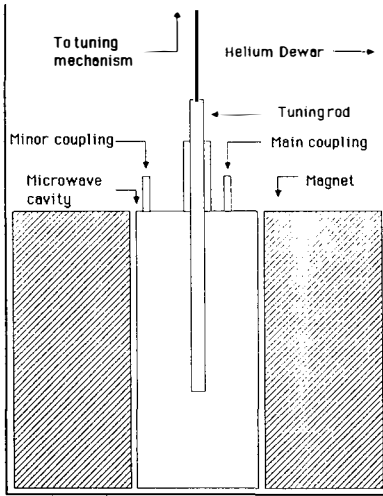


Figure 3, Cavity and magnet.

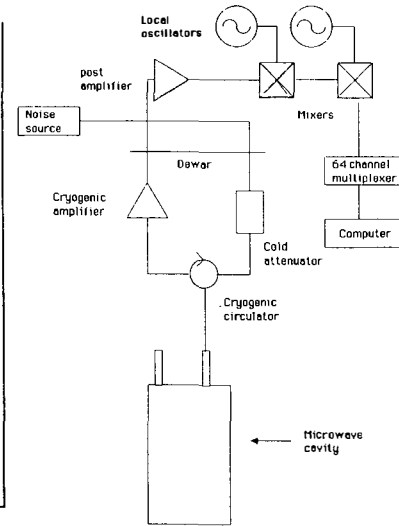


Figure 4, Detection electronics

DATA AND LIMITS WHICH HAVE BEEN PLACED:

On a larger scale data taking consists of a series of runs using different cavity-amplifier combinations. Each cavity tuning range is swept over twice. The data are an averaged power spectrum with channel bandwidth equal to the multiplexer channel bandwidth. For every channel the deviation from the local mean power is normalized by the local statistical fluctuations. The data from the two sweeps are compared and frequency channels which have large statistical deviations, above 4σ , in coincidence in both sweeps are rechecked with the apparatus. Suspect peaks have been found in the data and have been eliminated because of their independence on magnetic field and cavity tune when rechecked. The sources have been microwave radiation from the data acquisition computer and other microwave synthesizers in the lab. During data taking peaks are periodically injected into the cavity through its minor coupling port to test the dynamic range of the apparatus and to test the peak finding algorithm the off line analysis computer program.

In this way nearly all of the frequency range 1.1 to 2.5 GHz has been covered. The axion has not been found by our experiment but limits on the product of coupling and abundance have been produced. They are represented graphically in figure 8. Data is currently being taken in the two small gaps in this range which remain. After this we plan to continue the search up to a frequency of 6 GHz. Amplifiers and cavities in the new range are now under construction and test. This work was supported by the DOE.

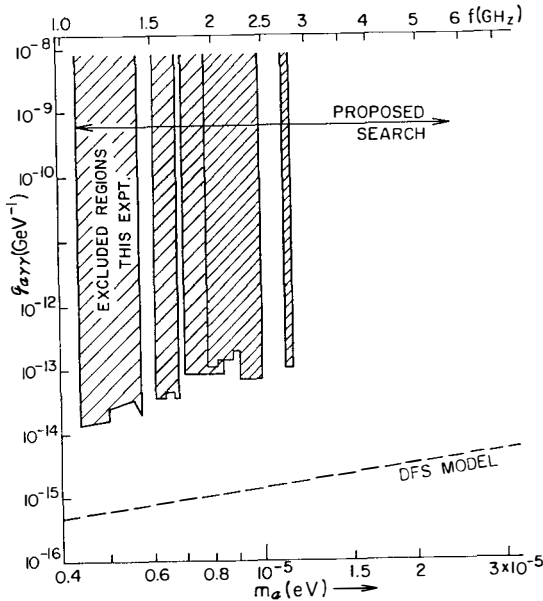


Figure 5, Limits on axion coupling assuming 300 MeV/cm^3

- ¹ S. DePanfilis et. al., Phys. Rev. Lett. **59**, 839 (1987).
- ² M. Dine, W. Fischler, and M. Srednicki, Phys. Lett. **104B**, 199 (1981); J. Kim, Phys. Rev. Lett. **43**, 103 (1979).
- ³ R. D. Peccei and H. Quinn, Phys. Rev. Lett. **38**, 1440 (1977).
- ⁴ S. Weinberg, Phys. Rev. Lett. **40**, 223 (1978); F. Wilczek, Phys. Rev. Lett. **40**, 279 (1978).
- ⁵ Thanks to G. Raffelt for the form of this figure.
- ⁶ P. Sikivie, Phys. Rev. Lett. **51**, 1415 (1983), Phys. Rev. Lett. **52**, 695 (1984).
- ⁷ L. Krauss, J. Moody, F. Wilczek, and D. E. Morris, Phys. Rev. Lett. **55**, 1797 (1985).
- ⁸ J. Rogers et. al., University of Rochester preprint UR 1043 (1988).
- ⁹ S. Weinreb, D. Fenstermacher, and R. Harris, National Radio Astronomy Observatory Internal Report No. 220, (1981).
- ¹⁰ S. DePanfilis and J. Rogers, IEEE Trans. on Microwave Theory and Tech. **36**, 607 (1988).
- ¹¹ B. Moskowitz and J. Rogers, Nucl. Instr. and Meth. in Phys. Resch. **A264**, 445 (1988).

II. BACKGROUNDS AND COOLING FLOWS

COSMOLOGICAL IMPLICATIONS FROM RECENT SPECTRAL MEASUREMENTS
OF THE MICROWAVE BACKGROUND RADIATION

Yoel Rephaeli
School of Physics and Astronomy
Tel Aviv University
Tel Aviv 69978
Israel

and

George Smoot
Space Sciences and Lawrence Berkeley Laboratories
University of California
Berkeley, CA 94720
USA

ABSTRACT

We discuss the results of an analysis of recent spectral measurements of the Cosmic Microwave Background (CMB) radiation in the frequency range 0.6-624 GHz. The most recent Nagoya-Berkeley submillimeter measurements constitute an excess emission at a level of 8% with respect to a $T=2.74\pm 0.02$ K Planckian, which is the best fit to the rest of the data base. The degree of this excess limits energy released by various (conjectured) processes in the early universe to be less than 1%. Perhaps the simplest interpretation is that the CMB spectrum has been Comptonized by hot intergalactic gas. We discuss the relevance of this possibility to a thermal origin of the cosmic X-ray background.

I. INTRODUCTION

The nature of the CMB and its dominance over other (cosmic) radiation fields make it a uniquely important cosmological and astrophysical probe. Its spectral and spatial characters are unparalleled as sources of information on (e.g.) the processes of energy injection into the CMB by the primordial plasma, and on galaxy formation. Indeed, CMB anisotropy has been intensely studied both observationally and theoretically.

In recent years it has become possible to perform high sensitivity measurements of the CMB spectrum. The 1987 high altitude rocket experiment of Matsumoto et al.¹⁾ has yielded what are claimed to be the most accurate submillimeter measurements made to date. These results are very important in that they not only allow a precise determination of the CMB temperature, T_0 , but also give substantial evidence for the long hypothesized possibility that the submillimetric spectrum may not have a pure Planckian shape.

We have analyzed²⁾ all recent spectral measurements in the frequency range 0.6-624 GHz. Here, we briefly report the results of this analysis and some of its cosmological implications.

II. RECENT SPECTRAL CMB MEASUREMENTS

Recent spectral CMB measurements are summarized in our paper (Smoot et al.²⁾. These include all measurements³⁻¹³⁾ at 19 different frequencies in the range 0.6-624 GHz. The most recent CMB measurements are those of Matsumoto et al.¹⁾ at 259, 423, and 624 GHz (in their channels 1, 2, and 3, respectively). The latter measurements are very recent (and perhaps not yet well known); the following is a brief description of the essential features of this experiment. A radiometer, which was flown on a rocket to a maximal altitude of 317 km, collected radiation in 6 frequency channels. Measurements were made starting 100 s after launch at an altitude of about 200 km. The optical spin axis precessed such that the radiometer was directed along lines of sights at galactic latitudes $b=18^\circ-48^\circ$. Only data in the first three channels, centered on 1160μ , 709μ , and 481μ did not show any modulation with galactic latitude. The measured flux in the 4th channel, centered on 262μ , did indicate some modulation, yielding an

upper limit on the CMB intensity at this wavelength. Emission at higher frequencies is dominated by interstellar dust; data at the other two channels do indeed show significant modulation with the changing value of b .

Excluding the Matsumoto et al.¹⁾ measurements, the available data are well fit by a Planckian with a temperature of 2.74 ± 0.02 K, which is plotted in Figure 1. Also shown are the rocket measurements (with 1σ error bars) in channels 1-3, and the upper limit from the channel 4 datum. A fit of all the data set, including the rocket measurements, by a Planckian is unacceptable, as can be (qualitatively) seen from Figure 1.

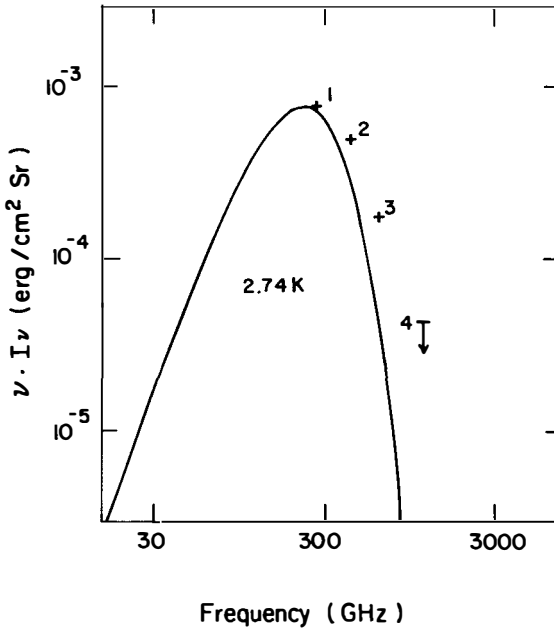


Figure 1

The best-fit 2.74 K Planckian and the Matsumoto et al.¹⁾ data in channels 1-4.

III. COMPTON-BREMSSTRAHLUNG DISTORTIONS OF THE CMB SPECTRUM

Research on spectral deviations from a pure Planckian form has begun soon after the detection of the CMB. Processes which have been conjectured to cause distortions in the Wien side of the spectrum fall in three categories: Heating of the radiation through interactions with hot gas, thermal emission from cosmological dust, and radiative decay of various dark matter candidates. Here, we will only investigate distortions of the CMB spectrum due to processes in hot gas. We will briefly discuss the other two possibilities in the next section.

The interaction of the CMB radiation with the heated-up matter in the Universe has attracted most attention. Hot gas affects the CMB spectrum through Compton scattering and bremsstrahlung emission and absorption. Detailed theoretical analyses had been carried out starting with Weymann⁴⁾, and Zeldovich and Sunyaev⁵⁾. Statistical fits of Comptonized spectra to the results of ever growing number of measurements have been performed (see, e.g., Danese and De Zotti⁶⁾ and references therein). The results of such fits always led to upper limits on the degree of Comptonization of the spectrum. The most recent measurements¹⁾ are the strongest evidence yet for a distorted spectrum, and it is natural to consider first the possibility that the measured distortion has its origin in energy release into the matter. The nature of this distortion depends very much on the epoch during which the gas had been heated. In the following, we summarize the results of our²⁾ recent analysis which is based on previous^{15,17)} calculations.

If heating occurs sufficiently early at epochs $z > 10^6$, when there still is tight coupling between matter and radiation, then the spectrum preserves its exact Planckian form. Equilibrium between matter and radiation is attained through bremsstrahlung emission and absorption, and Compton scattering. The net result of an energy release into the plasma is an increase in the radiation temperature. Bremsstrahlung has a steep redshift dependence, due to the proportionality of the emissivity to n^2 , where n is the gas density. Thus, heating at redshifts $z < 10^6$ no longer results in a Planckian spectrum at all frequencies. The spectrum has this form only at low frequencies, for which bremsstrahlung absorption is still effective. At higher frequencies, the spectrum has a Bose-Einstein form, with

positive chemical potential, μ , which depends on frequency. At very high frequencies, μ attains a constant value, μ_0 , which is a measure of the relative energy, $\Delta\epsilon/\epsilon$, injected into the radiation field. An approximate relation is $\mu_0 \approx 1.4 \cdot \Delta\epsilon/\epsilon$.

When the electron density is low enough that Compton scattering is not sufficiently effective in coupling radiation and matter, a Bose-Einstein spectrum is no longer attained. This occurs at a characteristic redshift,

$$z_a \approx 3.8 \cdot 10^4 \Omega_b^{-1/2} h^{-1}, \quad (1)$$

where Ω_b is the baryonic mass fraction in units of the closure density, and h is the Hubble constant in units of $50 \text{ km s}^{-1} \text{ Mpc}^{-1}$. Heating at redshifts $z < z_a$ results in a spectrum which is different from the above two basic distributions. It is characterized by enhanced emission in the far Rayleigh-Jeans (R-J), due to bremsstrahlung, and reduced emission in the middle R-J region. Compton scattering preserves the number of photons, so its effect is the transfer of photons from the R-J to the Wien side of the spectrum. This is sometimes referred to as Comptonization, although Thomsonization is a more appropriate term when the electrons are non-relativistic. Generally speaking, energy injection into the matter at sufficiently late epochs, when bremsstrahlung ceases to be important, leads to a Comptonized spectrum. If the electron temperature, T_e , is low enough that first order (in kT_e/mc^2) relativistic corrections can be ignored, then the spectrum is determined by the parameter,

$$u = \int [k(T_e - T)/mc^2] \cdot n_e \sigma_T c dt. \quad (2)$$

In this equation, T is the radiation temperature, n_e is the electron density, σ_T is the Thomson cross section, and the integral is over cosmological time, from the present to the time of heating. When $T_e \gg T$, $u \rightarrow y$, which is the usual Comptonization parameter.

A description of a Comptonized Planckian in terms of u (or y) is valid only when the scattering process can be adequately treated by the Kompaneets¹⁸⁾ equation. The latter is essentially a diffusion equation, valid only for large optical depths to (Compton) scattering, τ . If heating of the gas was recent, τ is small, and a more detailed calculation of the frequency redistribution function is required.

Another complication may arise if the gas is heated to a very high temperature, such that relativistic corrections cannot be ignored. A calculation of the spectrum in these limits had been carried out by Wright¹⁹).

IV. RESULTS AND DISCUSSION

In our²⁾ analysis of the measurements we have allowed for distortions of all types mentioned above, by taking various values of the heating redshift, z_h . Fitting the data set to a Bose-Einstein spectrum results in an upper limit to the energy injected into the CMB, $\Delta\epsilon/\epsilon \leq 0.01$ for $\Omega_b \cdot h^2 \leq 1$. This, obviously, constrains all sources of energy release into the CMB. In particular, the conjecture that galaxy formation may have been initiated by turbulent motions in the primordial plasma²⁰⁾, is probably ruled out by this (low value of the) upper limit.

We next attempted fits of the data to Comptonized spectra for a few values of $z_h \leq 10^4$. These fits are plotted in Figure 2; also indicated are the equivalent thermodynamic temperatures corresponding to the measured data set; (the measurements are shown according to their type). Curves a,b, and d are the fits to Comptonized spectra, whereas curve c is a fit to a Bose-Einstein spectrum with a chemical potential $\mu_0 = 0.0117$, $\Omega_b \cdot h^2 = 0.1$, and $T = 2.925$ K.

A particularly interesting and important possibility is the heating of the intergalactic medium (IGM) to very high temperatures at recent epochs. This possibility has been considered in connection with what is perhaps the most basic outstanding issue in X-ray astronomy - the origin of the Cosmic X-ray Background (CXB; for a recent review, see Boldt²¹⁾). The observed spectrum can be well fit by thermal bremsstrahlung from $O(10^8$ K) gas with a value of Ω_b of few tenths²²⁾. An IGM with these properties can Comptonize the CMB spectrum, and it is important to know if the submillimetric excess is from such a hot gas. The most recent analysis of a hot IGM origin for the CXB is that of Guilbert and Fabian²³⁾. These authors conclude that the residual (i.e., after subtraction of the contributions of known classes of sources) CXB spectrum can be well fit by a hot IGM if $\Omega_b > 0.22$, and $kT_e \sim 36(1+z_h)$ keV, with $3 \leq z_h \leq 6$. The predicted CMB spectral distortion is estimated to be less than that corresponding to $u = 0.018$. Our best fit

value for u ($=y$ in this high T_e limit) is 0.020 ± 0.002 for z_h in this interval. Thus, the observed excess is consistent with a thermal IG origin for the CXB. Strictly speaking, however, the representation of the Compton distortion in terms of u may not be adequate in the limit of small optical thickness to Compton scattering, or when relativistic corrections are not negligible. For $T_e(10^9 \text{ K})$, the first order relativistic correction has to be taken into account¹⁹.

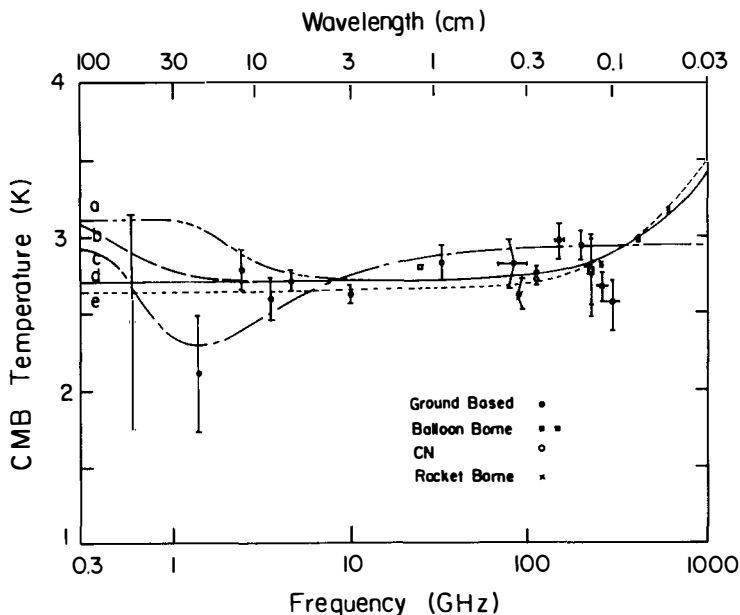


Figure 2

Data and model spectra of the CMB. The models have parameters:

(a) $\Omega_b h^2 = 1.0$, $T = 2.811 \text{ K}$, $u = 0.0200$, $z_h = 4000$;

(b) $\Omega_b h^2 = 0.1$, $T = 2.813 \text{ K}$, $u = 0.0201$, $z_h = 10000$;

(c) $\Omega_b h^2 = 0.1$, $T = 2.925 \text{ K}$, $\mu_e = 0.0117$;

(d) $\Omega_b h^2 = 0.1$, $T = 2.814 \text{ K}$, $u = 0.0201$, $z_h = 1000$.

(e) Semi-relativistic calculation adopted from Wright¹⁹.

This model corresponds approximately to $u = 0.03$, $T = 2.82 \text{ K}$, and an electron temperature of $1.5 \cdot 10^9 \text{ K}$.

We have used the analysis by Wright¹⁹⁾ to obtain a fit to the data. Doing so led to the fit which is described by curve e in Figure 2. It corresponds to $u=0.03$, $T=2.82$ K, and $T_e \approx 1.5 \cdot 10^9$ K. We conclude that the data is not inconsistent with hot IG origin for the CXB even if the required value of T_e necessitates a semi-relativistic calculation of the Comptonized spectrum. It should be noted, however, that the goodness of fits of high frequency excess emission by semi-relativistic Comptonized spectra is quite sensitive to data in the 200-300 μ range. First, emission from interstellar dust is not yet dominant in this region. Second, the semi-relativistic calculation yields a distorted spectrum which flattens out, so it is very important to determine the exact behavior of the measured spectrum at such wavelengths. The current upper limit at 262 μ is not tight enough to rule out an IGM with the above best-fit properties²³⁾ as an origin for the excess emission. This conclusion is contrary to that reached by Hayakawa et al.²⁴⁾. In any case, the observed excess emission can be due to hot IGM, even if it does not have the required properties for it to (also) produce the CXB. More extensive and exact analysis is required in order to determine the baryonic mass fraction of the Universe from the X-ray and submillimeter data. Obviously, it will be extremely important if the value of Ω_b will turn out to be higher than 0.19, which is the nucleosynthesis upper limit.

As mentioned in the Introduction, high frequency deviations of the CMB spectrum from a Planck curve can, in principle, be also due to radiative decay of (weakly interacting) particles which may dominate the mass density in the Universe. This possibility has been considered by various authors; in particular, Silk and Stebbins²⁵⁾ have deduced limits on the properties of dark matter candidates from allowing relative deviations in the CMB spectrum of up to 10% in energy density. As this degree of distortion is within the (now) observed value, their deductions should be valid.

Thermal emission from dust as origin of the observed excess has been considered by Hayakawa et al.²⁵⁾. These authors find that silicate-like grains with radii in the range 0.03-0.3 μ , heated at the redshift interval 15-20 to temperatures $T_d=3.55(1+z)$ K, can account for the observed distortion. The required cosmological dust density (in units of the closure value) is estimated to be 10^{-5} .

REFERENCES

1. T. Matsumoto, S. Hayakawa, H. Matsuo, H. Murakami, S. Sato, A.E. Lange, and P.L. Richards, *Astrophys. J. (Lett.)*, in press.
2. G. Smoot, S.M. Levin, C. Witebsky, G. De Amici, and Y. Rephaeli, *Astrophys. J.*, in press.
3. G. Sironi et al., in *Proceedings of the 13th Texas Symposium on Relativistic Astrophysics (1987)*.
4. S.M. Levin et al., *Astrophys. J.*, submitted (1987).
5. G. Sironi, and G. Bonelli, *Astrophys. J.*, 311, 418 (1986).
6. G. De Amici et al., *Astrophys. J.*, submitted (1987).
7. N. Mandolesi et al., *Astrophys. J.*, 310, 561 (1986).
8. G. Smoot et al., *Astrophys. J. (Letters)*, 317, L45 (1987).
9. D.G. Johnson, and D.T. Wilkinson, *Astrophys. J. (Letters)*, 313, L1 (1986).
10. G. Smoot et al., *Societa Italiana di Fisica, Conference Proceedings*, 1, 27 (1985).
11. D.M. Meyer, and M. Jura, *Astrophys. J.*, 297, 119 (1985).
12. P. Crane, D.J. Hegyi, N. Mandolesi, and A.C. Danks, *Astrophys. J.*, 309, 822 (1986).
13. J.B. Peterson, P.L. Richards, and T. Timusk, *Phys. Rev. Lett.*, 55, 332 (1985).
14. R. Weymann, *Astrophys. J.*, 145, 560 (1966).
15. Y.B. Zeldovich, and R.A. Sunyaev, *Astrophys. Space Sci.*, 4, 301 (1969).
16. L. Danese, and G. De Zotti, *Astron. Astrophys.*, 84, 364 (1980).
17. R.A. Sunyaev, and Y.B. Zeldovich, *Astrophys. Space Sci.*, 7, 20 (1970).
18. A.S. Kompaneets, *Soviet Phys. JETP*, 4, 730 (1957).
19. E.L. Wright, *Astrophys. J.*, 232, 348 (1979).
20. L.M. Ozernoy, and A.D. Chernin, *Soviet Astron. AJ*, 11, 907 (1967).
21. E. Boldt, *Phys. Reports*, 146, 215 (1987).
22. F. Marshall et al., *Astrophys. J.*, 235, 4 (1980).
23. P. Guilbert, and A. Fabian, *Mon. Not. R. Astron. Soc.*, 220, 439 (1986).
24. S. Hayakawa, T. Matsumoto, H. Matsuo, H. Murakami, S. Sato, A.E. Lange, and P.L. Richards, *Astron. Soc. Japan*, in press.
25. J. Silk, and A. Stebbins, *Astrophys. J.*, 269, 1 (1983).

IMPLICATIONS OF THE 1 TO 10 MEV GAMMA-RAY BACKGROUND:
A DETERMINATION OF Ω_0 OR A NEW PARTICLE?

Ruth A. Daly
Institute of Astronomy
Madingley Road
Cambridge CB3 0HA
England



ABSTRACT

Monoenergetic photons resulting from the decay of an unstable particle produce an observable spectrum because photons produced at different times are redshifted to different energies. It has been shown¹⁾ that the 1 to 10 MeV Gamma-Ray background is very well fitted by monoenergetic photons produced at a decay rate while the universe was young ($z_d \gtrsim 3$). The fit constrains the energy of the decay photon, the decay rate, and the number density of particles whose decay produces the photons. If the photons comprising the 1 to 10 MeV shoulder are produced by a decay (as suggested by the observations), then they may result from either the radioactive decay of an unstable isotope or from the decay of a previously unidentified particle. If the photons result from a radioactive decay, the fit to the spectrum may be used to determine Ω_0 , the current ratio of the average mass-energy density in the universe to the critical value.

I. INTRODUCTION

The X and Gamma-ray backgrounds are extragalactic, isotropic backgrounds extending from a few keV to greater than 100 MeV. It is quite likely that they contain a wealth of information, although interpreting these backgrounds to extract this information has not proven to be entirely straight forward. Indeed, there is still no consensus as to the origin(s) of any part of these backgrounds.

The X and Gamma-ray backgrounds are comprised of three primary features. One of these is a nonpower-law feature known as the 1 to 10 MeV shoulder.^{2,3)} Several mechanisms to produce this feature have been suggested, all of which are fairly exotic: neutral pion decay,⁴⁾ matter-antimatter annihilation,⁵⁾ positronium annihilation from accreting objects,⁶⁾ and the decay of a long lived SUSY particle.⁷⁾ It has been shown¹⁾ that monoenergetic photons produced while the universe was young ($z_d \gtrsim 3$, where z_d is the redshift at which the age of the universe is equal to the lifetime of the unstable particle), at a decay rate, fit the observed feature extremely well.

We briefly review the spectrum expected from monoenergetic, cosmologically redshifted photons, and compare this spectrum with that of the 1 to 10 MeV gamma-ray background (see section II). If the photons comprising the 1 to 10 MeV gamma-ray background are produced by a decay, there are far reaching implications, as discussed in section III. A summary is presented in section IV.

II. THE CALCULATED SPECTRUM AND THE DATA

The calculated spectrum of photons is presented and compared with the observations; a more detailed derivation of the calculated spectrum and comparison with the data has been presented elsewhere.¹⁾

Suppose that there is an unstable particle, m , with average number density n_m , lifetime τ , which, upon decay, produces a monoenergetic photon of energy E_γ for some fraction b of the decays. The rate at which photons are produced is:

$$\frac{dn_\gamma}{dt} = -b \frac{dn_m}{dt} = b \frac{n_m}{\tau} = \frac{b n_{0m} (1+z)^3 e^{-t/\tau}}{\tau}, \quad (1)$$

where n_{0m} is the initial (set at $t \ll \tau$) number density of m scaled to the current epoch, and t is the age of the universe at redshift z . The expected spectrum of photons $dn_{0\gamma}/dE_0$ is given by:

$$\frac{dn_{0\gamma}}{dE_0} = \frac{dn_{0\gamma}}{dt} \frac{dt}{dz} \frac{dz}{dE_0}, \quad (2)$$

where $dn_{0\gamma} = dn_\gamma (1+z)^{-3}$ is the differential number density of decay photons at a redshift of zero and $E_0 = E_\gamma(1+z)^{-1}$ is the energy the decay photon has at a redshift of zero. Using these relations and assuming the universe is matter dominated, Einstein-de Sitter ($\Lambda = 0$, $\Omega_0 = 1.0$) so that $t = t_0(1+z)^{-3/2}$, t_0 being the current age of the universe, the spectrum of photons which will be observed at a redshift of zero from monoenergetic photons produced at a decay rate is:

$$\frac{dn_{0\gamma}}{dE_0} = k_m E_0^{1/2} e^{-(k_\gamma E_0)^{3/2}} \quad (3)$$

where $k_m = 1.5 b n_{0m} k_\gamma^{3/2}$, $k_\gamma^{-1} = E_\gamma(1+z_d)^{-1}$, and z_d is the redshift at which the age of the universe is τ . If the universe is radiation-dominated during the decay

epoch a similar result is obtained:¹⁾ $dn_{0\gamma} \propto E_0 e^{-(k_\gamma E_0)^2}$. The calculated spectrum (3) is compared with the observed spectrum²⁾; we note that the underlying power-law has been taken into account.¹⁾ The parameters k_m and k_γ are adjusted until the best fit to the data is obtained. Figure 1 shows the best fit, calculated spectrum (solid line) and the observed data points (points with one sigma error bars); the best fit is accurate to the 99% confidence level and is obtained for $k_\gamma^{-1} \simeq 2.5 \text{ MeV}$ and $k_m(c/4\pi) \simeq 0.0035 \text{ photons MeV}^{-3/2} \text{ cm}^{-2} \text{ s}^{-1} \text{ sr}^{-1}$.

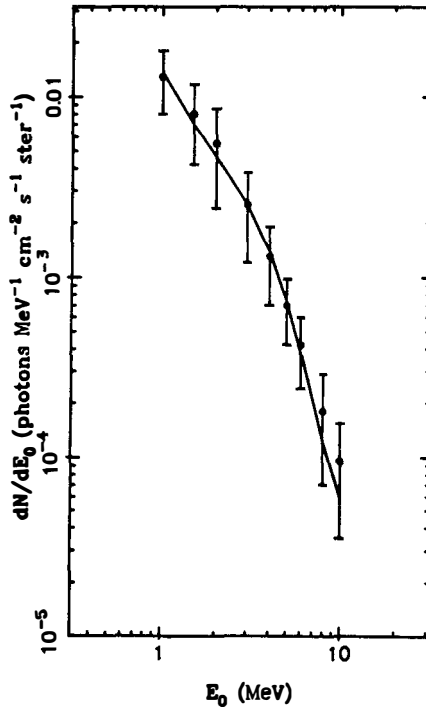


Figure 1. Comparison of the calculated and observed spectrum of the 1 to 10 MeV shoulder. The solid line shows the sum of the calculated spectrum and the underlying power-law (which has been detailed elsewhere^{1,2)}) for a matter-dominated, Einstein-de Sitter universe with $k_\gamma^{-1} \simeq 2.5 \text{ MeV}$ and $ck_m/4\pi \simeq 0.0035 \text{ photons MeV}^{-3/2} \text{ cm}^{-2} \text{ s}^{-1} \text{ sr}^{-1}$. The observed intensities are denoted by points with 1σ error bars. The fit is accurate to the 99% confidence level.

III. IMPLICATIONS

The excellent fit obtained suggests that the photons comprising the 1 to 10 MeV gamma-ray background result from a decay. It is possible that a population of massive stars (population III stars) produced a long lived, radioactive isotope at a time $t \ll \tau$, and the radioactive decay of this isotope leads to the production of high energy ($E_\gamma \gtrsim 8 - 10 \text{ MeV}$) photons. The fit to the observed spectrum implies that $k_\gamma^{-1} \simeq 2.5 \text{ MeV}$ or

$$E_\gamma \simeq 2.5 (1 + z_d) \text{ MeV}. \quad (4)$$

For a matter-dominated, Einstein-de Sitter universe, this translates to:

$$E_\gamma \simeq 2.5 \left(\frac{t_0}{\tau} \right)^{2/3} \text{ MeV}, \quad (5)$$

where t_0 is the age of the universe at the current epoch. If a radioactive isotope is identified which roughly satisfies (5), and if it can be shown that it is viable for population III stars to produce this isotope with the required abundance (with an average number density scaled to the current epoch of $^1) \sim 4 \times 10^{-12} \text{ cm}^{-3}$), then we may infer that the photons comprising the 1 to 10 MeV gamma-ray background may result from the radioactive decay of this isotope. In this case Ω_0 (the present mass-energy density of the universe relative to the critical value) may be determined in the following manner. If the age of the universe is known at a specific redshift, then q_0 and hence Ω_0 may be determined, although the value of Ω_0 thus obtained will dependent on the current value of the Hubble constant. If an unstable isotope is identified as described above, then E_γ and τ would be known. The fit to the observed spectrum yields $E_\gamma \simeq 2.5(1+z_d)\text{MeV}$, hence $(1+z_d)$ would be specified. But $(1+z_d)$

is the redshift at which the age of the universe is τ . Hence, we would know that at a specific redshift, $(1 + z_d)$, the age of the universe is τ : therefore ρ_0 and hence Ω_0 may be determined. Since $E_\gamma \gtrsim (8 - 10)MeV$ ¹⁾ and since $E_\gamma \simeq 2.5(1 + z_d)MeV$, we expect $(1 + z_d) \lesssim 4$ or 5 so that E_γ is not unreasonably large. A likely radioactive candidate would have $E_\gamma \simeq 10 MeV$, $\tau \sim 1.5 \times 10^9$ years.

A consideration which argues against this possibility (Martin Rees, private communication) is that a corresponding high-energy, gamma-ray line from radioactive debris produced by supernova in our own galaxy is not observed. However, the radioactive debris from population III stars need not be identical to that from stars which have undergone a supernova in our galaxy in the past $\sim 10^9$ years.

It is possible that the photons result not from a radioactive decay, but from the decay of a previously unidentified, unstable particle. In this case the fit to the observed spectrum yields a relationship between the energy of the photon produced by the decay and the lifetime of the unstable particle (via equation (5)). Additional relationships between the branching ratio b , the mass m , and the initial mass-energy density (or annihilation cross section) of the unstable particle may be obtained from the fit to the observed spectrum.¹⁾

IV. SUMMARY

The 1 to 10 MeV gamma-ray background is very well fitted by cosmologically redshifted, monoenergetic photons produced at a decay rate while the universe was young ($z_d \gtrsim 3$). The photons could result from the radioactive decay of an unstable isotope produced at a time $t \ll \tau$ by a generation of population III stars. An approximate relationship between the energy of the photon produced by the decay,

E_γ , and the lifetime characterizing the decay, τ , is: $E_\gamma \simeq 2.5(t_0/\tau)^{2/3} MeV$ where t_0 is the current age of the universe, $t_0 \simeq (1 - 2) \times 10^{10} years$. Simple arguments¹⁾ indicate that $E_\gamma \gtrsim (8 - 10) MeV$, hence $\tau \lesssim few \times 10^9 years$. If a radioactive isotope is identified which has approximately the right E_γ and τ (i.e. they must approximately satisfy equation (5)), and if it can be shown that this isotope may be produced by population III stars with approximately the right abundance (average number density at a redshift of zero of ¹⁾ $\sim 4 \times 10^{-12} cm^{-3}$), then a determination of q_0 and hence Ω_0 follows, although Ω_0 thus determined is not independent of the current value of Hubble's constant. Ω_0 would be determined in the following way: if E_γ is known then $(1 + z_d)$ may be inferred from the fit to the observed spectrum. Since τ would be known, the specific age of the universe, τ , at the specific redshift, $(1 + z_d)$, would be known. Hence, Ω_0 could be deduced.

Another possibility is that the feature results from the decay of a previously unidentified, unstable particle. In this case the fit to the observed spectrum leads to a series of relationships between the energy of the photon produced by the decay, E_γ , the lifetime of the unstable particle, τ , the branching ratio, b , and the initial mass-energy density of the particle relative to the critical density Ω_m (as discussed in detail elsewhere¹⁾). Interpreting the 1 to 10 MeV gamma-ray background as photons produced at a decay rate while the universe was young ($t \lesssim few \times 10^9 years$) may prove to have important consequences for either cosmology or particle physics.

I would like to acknowledge helpful conversations with Alvaro de Rujula, George Fuller, Martin Rees, James Rich, and David Spergel. This work was supported by a NATO-NSF Fellowship, grant No. RCD-8751127.

REFERENCES

- 1) Daly, R.A. 1988, *Ap. J. (Letters)*, **324**, L47.
- 2) Schönfelder, V., Graser, U., and Daugherty, J. 1977, *Ap. J.*, **217**, 306.
- 3) Rothschild, R.E., Mushotzky, R.F., Baity W.A., Gruber, D.E., Matteson, J.L., and Peterson, L.E. 1983, *Ap. J.*, **269**, 423.
- 4) Stecker, F.W. 1971, *Cosmic Gamma Rays* (NASA SP-249), p.209.
- 5) Stecker, F.W., Morgan, D.L., and Bredekamp, J. 1971, *Phys. Rev. Letters*, **27**, 1469.
- 6) Heffernan, D.M., and Liboff, R.L. 1984, *Physics Letters*, Vol. **101A**, No. 5-6, p. 305.
- 7) Olive, K.A., and Silk, J. 1985, *Phys. Rev. Letters*, **55**, 2362.

ARE DARK GALACTIC HALOS MADE BY COOLING FLOWS?

K. M. Ashman and B. J. Carr
School of Mathematical Sciences
Queen Mary College
London E1 4NS
UNITED KINGDOM

**ABSTRACT**

Primordial nucleosynthesis arguments suggest that most of the baryons in the Universe are dark. This possibility is strengthened by the observation that cluster cooling flows process gas into baryonic dark matter. We argue that observed cooling flows are the endpoint of a process that began at pregalactic epochs, and present a model in which the majority of baryonic matter forms clusters of Jupiters. These objects undergo gravitational clustering to eventually form galactic halos.

1. INTRODUCTION

The inflationary scenario¹⁾ and cosmological aesthetics suggest that we live in an $\Omega = 1$ universe, so that the majority of matter must be dark. Primordial nucleosynthesis calculations constrain the baryonic density, Ω_b , to the range²⁾ $0.014 < \Omega_b h^2 < 0.035$ ($h = H_0/100 \text{ km s}^{-1} \text{ Mpc}^{-1}$), with $0.5 < h < 1$ observationally. Since Ω_b falls short of the critical density, non-baryonic dark matter must be invoked to produce an $\Omega = 1$ universe. The popular trend is to keep the number of forms of dark matter as small as possible by assuming that essentially all baryons are luminous. Consequently, the nature of the dark matter has become reduced to a discussion of the relative merits of various "exotic" particles, whereas the idea of baryonic dark matter has been largely ignored.

While this argument has a certain simplistic appeal, it is difficult to reconcile with observation. The density of visible baryons is $\Omega_v \sim 0.01$ or less³⁾, so if all baryons are luminous the above constraints on Ω_b require that h is around unity. However, if one wants the Universe to be older than the globular clusters⁴⁾, h must be around 0.5; in this case $\Omega_b \sim 0.1$ and most baryons are dark. This raises the possibility that galactic halos, which have a density $\Omega_h \sim 0.1$, and the cluster dark matter, with a density $\Omega_c \sim 0.1-0.3$, are baryonic. We concentrate on the question of the halo dark matter, but note that at least *some* of the dark matter in clusters must be the disrupted remnants of these halos.

There are various constraints on the *form* that baryons in galactic halos can take. Hot gas generates too many X-rays⁵⁾, low mass stars are ruled out by source counts limits⁶⁾, and other stellar remnants are excluded by nucleosynthesis and background light constraints⁷⁾. The only possible options seem to be either *jupiters* or the *black hole* remnants of massive stars. The usual argument against these possibilities is that the "standard" stellar initial mass function (IMF) produces too few of these objects. However, in the next Section we will present evidence that jupiters can be formed with high efficiency in at least some circumstances.

2. COOLING FLOWS IN CLUSTERS OF GALAXIES

X-ray observations show that most clusters of galaxies contain hot intracluster gas with a temperature of around 10^8 K . In many cases the emission is centrally peaked, indicating a high gas density and thus a short cooling time⁸⁾. In clusters where the cooling time, t_c , is less than the Hubble time, t_H , one expects the cooling gas to be flowing inwards, driven by the pressure of the outlying uncooled gas. Since the cooling time of the gas exceeds the sound-crossing time, t_f , the flow is quasi-static. These "cooling flows" are usually centred on massive cD galaxies. The observational evidence for cooling flows has been reviewed elsewhere^{8,9)}, and includes X-ray emission from

relatively low temperature gas ($T \sim 10^6\text{--}10^7\text{K}$), optical emission from 10^4K gas and inverted temperature gradients.

The mass flow rate, \dot{M} , can be obtained from $L = H\dot{M}$, where L is the X-ray luminosity and H is the enthalpy. This yields typical values of $10^2 M_{\odot}\text{yr}^{-1}$ and exceptional ones of $10^3 M_{\odot}\text{yr}^{-1}$ (ref 10). In fact, since the luminosity is measured as a function of radial distance r within the flow, one can also deduce $\dot{M}(r)$. Observations indicate that the flow rate increases with radius, implying that mass is being deposited throughout the flow⁸⁾. Constraints on the mass in cool gas in cooling flows⁸⁾ imply that most of the material is forming stars, but if the stars form with a standard IMF the accreting galaxies should be bluer and brighter. The colours and luminosities of these galaxies can be reproduced if typically 1% of the cooling gas forms stars with the standard IMF, while the other 99% goes into dark matter¹⁰⁾. In some cases more than 10% of gas participates in "normal" star formation¹⁰⁾, but it is apparent that the mass-to-light ratio of objects forming in cooling flows is much higher than in other star forming regions. Since the mass in cool gas is constrained, this dark matter must either be low mass stars or jupiters. Present results¹¹⁾ indicate that the average stellar mass forming in cooling flows must be below $0.2M_{\odot}$, so while stars with masses just above the hydrogen-burning limit ($0.08M_{\odot}$) are not ruled out, the jupiter option is favoured.

There have been several objections to the idea that cooling flows produce baryonic dark matter^{12,13)}. A common criticism is that any heating mechanism that operates in cooling flows will reduce \dot{M} and could thereby permit a standard IMF. Such a view seems to stem from an obsession with the standard IMF, but is difficult to sustain. For instance, if supernovae are the heat source, limits on the numbers of supernovae in cooling flows indicate that the effect on \dot{M} would be negligible⁸⁾. The most important evidence in support of cooling flows is that cooling gas *is* observed, and that the amount of gas at relatively low temperature is just that expected from the observed \dot{M} (ref 9).

It is difficult to avoid the conclusion that cooling flows produce baryonic dark matter, but the physical mechanism responsible for the cooling flow IMF is uncertain. One suggestion is that the high pressure reduces the Jeans mass and hence the stellar fragment mass^{14,15)}. Typically, pressures in cooling flows are $10^5\text{--}10^6\text{cm}^{-3}\text{K}$, greater by about 10^2 than in star forming regions in our Galaxy, so the Jeans mass is lower by an order of magnitude. The quasi-static nature of cooling flows ensures that these high pressures are maintained as the gas cools. Other factors that have been considered include the lack of dust and molecules⁸⁾ and the possibility that star forming regions in cooling flows are significantly smaller than the Giant Molecular Clouds where massive stars form⁹⁾.

The fact that the origin of the cooling flow IMF is poorly understood has led some to reject the considerable evidence that baryonic dark matter is being formed. While this situation is admittedly undesirable, it should be stressed that the origin of the standard

IMF is also unclear. It is worth noting that since the star formation rates in cooling flows greatly exceed those in "normal" star forming regions, one could regard the standard IMF as the curiosity!

Cluster cooling flows cannot directly solve any of the dark matter problems since they are restricted to the central regions of clusters of galaxies. In the next Section we take the empirical properties of cooling flows that may be responsible for jupiter formation, the high pressure and quasi-static nature, and argue that similar conditions occur at earlier epochs, so that baryonic dark matter will be formed more extensively.

3. PREGALACTIC AND PROTOGALACTIC COOLING FLOWS

To investigate the possibility that cooling flows occur at earlier epochs we require a model for the formation of large-scale structure. This allows us to calculate the density and temperature of the gas in virialized objects, from which we can find the pressure and establish if the flow is quasi-static. Here we present some general results, the detailed calculations having been given elsewhere¹⁶⁾.

We concentrate on the hierarchical clustering scenario^{17,18)} with particular reference to the "cold dark matter" variant¹⁹⁾, since it currently gives the best fit to the observed large-scale structure of the Universe. In this picture, the first objects to virialize have relatively low masses of around $10^6 M_\odot$. As the universe evolves, more massive objects virialize and structure is built from the "bottom up" through gravitational clustering. For gas in a bound cloud to fragment into stars, a necessary condition is that it cools within a Hubble time, otherwise the gas is disrupted as the next stage of the hierarchy virializes. Since a characteristic of a cooling flow is that the gas is quasi-static, we must look for conditions where $t_f < t_c < t_H$.

We model the gas density profile of a virialized cloud by a "core" of constant density to a radius $r = a$, plus a power law fall-off to a truncation radius R . By further assuming that the gas is isothermal we find that there are three possible cases (see Figure 1). (i) $t_c(r) < t_f(r)$ everywhere: the entire cloud fragments rapidly with little global collapse and the gas pressure is therefore not maintained. In this case we do not expect a cooling flow (however, see ref 20 and Section 4 below). (ii) $t_c(r) > t_f(r)$ everywhere: this is the situation in cluster cooling flows, although in clusters the cooling flow lies entirely within the core. This can arise since the density within the cores of clusters decreases slightly with radius, whereas in our model the density is assumed constant. Only a small fraction of the gas is processed through a cooling flow unless the core radius is large. (iii) $t_c(a) < t_f(a)$, $t_c(R) > t_f(R)$: in this case, all the gas between r_c^{\min} and r_c^{\max} in Figure 1 undergoes quasi-static flow and cools within a Hubble time, so if the pressure in the gas is sufficiently high we expect jupiters to form.

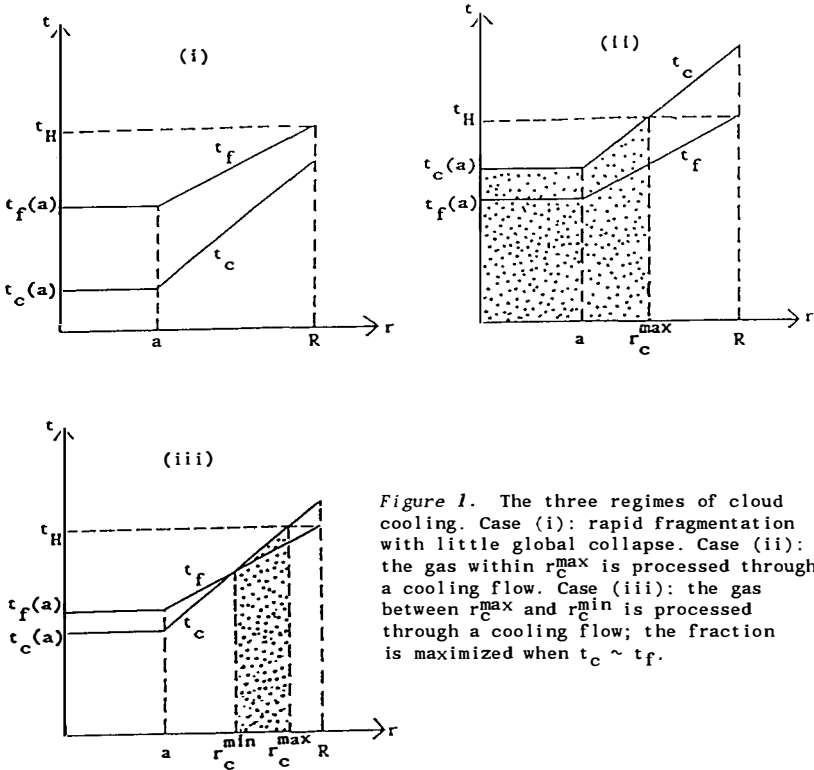


Figure 1. The three regimes of cloud cooling. Case (i): rapid fragmentation with little global collapse. Case (ii): the gas within r_c^{\max} is processed through a cooling flow. Case (iii): the gas between r_c^{\max} and r_c^{\min} is processed through a cooling flow; the fraction is maximized when $t_c \sim t_f$.

The fraction of the gas that satisfies $t_f(r) < t_c(r) < t_H(r)$ is maximized when the *mean* cooling and free-fall times of the gas cloud are comparable; that is $t_c \sim t_f$. We refer to this as a *pervasive pregalactic cooling flow* (PPCF). The precise relationship between t_c and t_f depends on the slope of the density profile power law and the timescale of disruption, which can differ somewhat from the Hubble time¹⁶). In Figure 2 we have plotted $t_c = t_f$ in the (M, z) plane, as well as the line of constant pressure $P = 10^5 \text{cm}^{-3} \text{K}$, comparable to pressures in cluster cooling flows. Regions that lie above this line should be at sufficiently high pressures to produce jupiters. We have also shown the line $M(z)$ which represents the trajectory of virializing clouds in the cold dark matter scenario. [The situation is rather more complex than this since the first objects to form arise from the high- σ peaks of the fluctuation spectrum. The details are beyond the

scope of the present work, but are addressed in a separate paper²¹.) When $M(z)$ intersects the line $t_c = t_f$, we expect PPCFs to occur, so Figure 2 shows that there are two relevant epochs and mass scales. The high-mass scale is around $10^{11} M_\odot$ and occurs at a redshift of $z \sim 10$. The low-mass case is rather ambiguous since it depends on the dominant cooling mechanism. Molecular hydrogen is the most important coolant below about $10^4 K$, but the mass fraction of H_2 is difficult to predict. The low-mass portion of the line $t_c = t_f$ in Figure 2 represents a compromise where the H_2 fraction is determined by the residual ionization of the Universe²²). Destruction of H_2 moves the line to the right, whereas increased production of H_2 via shocks moves the line to the left¹⁹). The typical mass scale for the low-mass PPCF is around $10^6 M_\odot$.

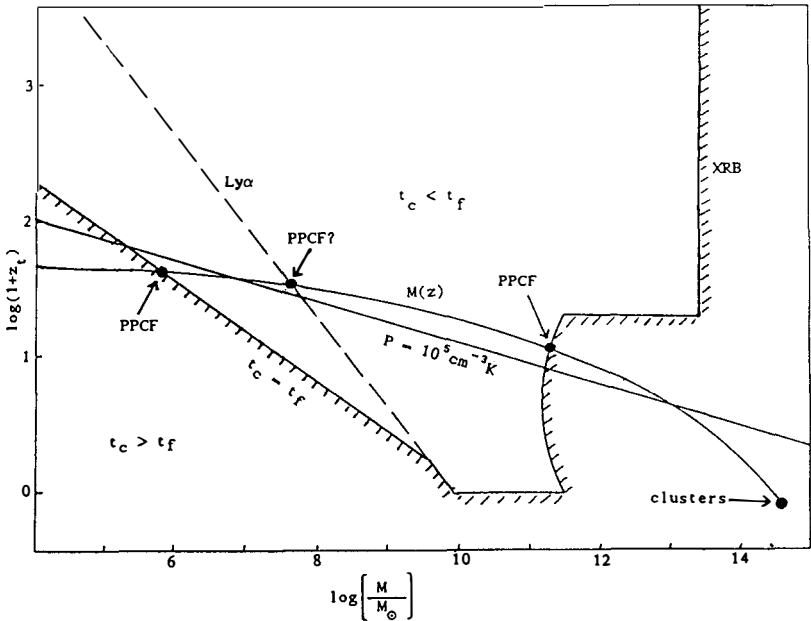


Figure 2. Evolution of clouds of mass M binding at a redshift z_t in the hierarchical clustering scenario. Clouds within the hatched region $t_c < t_f$ can cool on a Hubble time. PPCFs occur when the binding trajectory $M(z)$ crosses the line $t_c = t_f$. If primordial H_2 is completely destroyed the low-mass PPCF occurs when $M(z)$ crosses the broken line representing $t_c = t_f$ for $Ly\alpha$ cooling. The vertical line represents constraints on the mass of cooling flows obtained from background light considerations (see ref 16).

From Figure 2 it is apparent that the pressures in PPCFs in the cold dark matter scenario are sufficiently high for jupiters to be formed; that is, $M(z)$ intersects $t_c = t_f$ above or close to the line $P = 10^5 \text{cm}^{-3} \text{K}$. It is also probable that the more important PPCF is the low-mass one, since at this epoch one expects all the baryons in the universe to be gaseous. One consequence of our model in the cold dark matter scenario is that we predict substantial amounts of baryonic dark in clusters with masses around $10^6 M_\odot$. These clusters end up in galactic halos.

We have carried out similar calculations¹⁶⁾ in the pancake scenario²³⁾ and explosion scenario²⁴⁻²⁶⁾. These two pictures lead to similar results, since in both cases gas is compressed into massive "sheets". We have found that the pressure in the sheets can be high ($P > 10^5 \text{cm}^{-3} \text{K}$) and that the gas flow may be quasi-static, so that baryonic dark matter may form in both scenarios. The scale on which the dark matter is clumped depends on the cooling mechanism, but can be as low as $10^6 M_\odot$ if H_2 cooling is dominant.

4. DISCUSSION

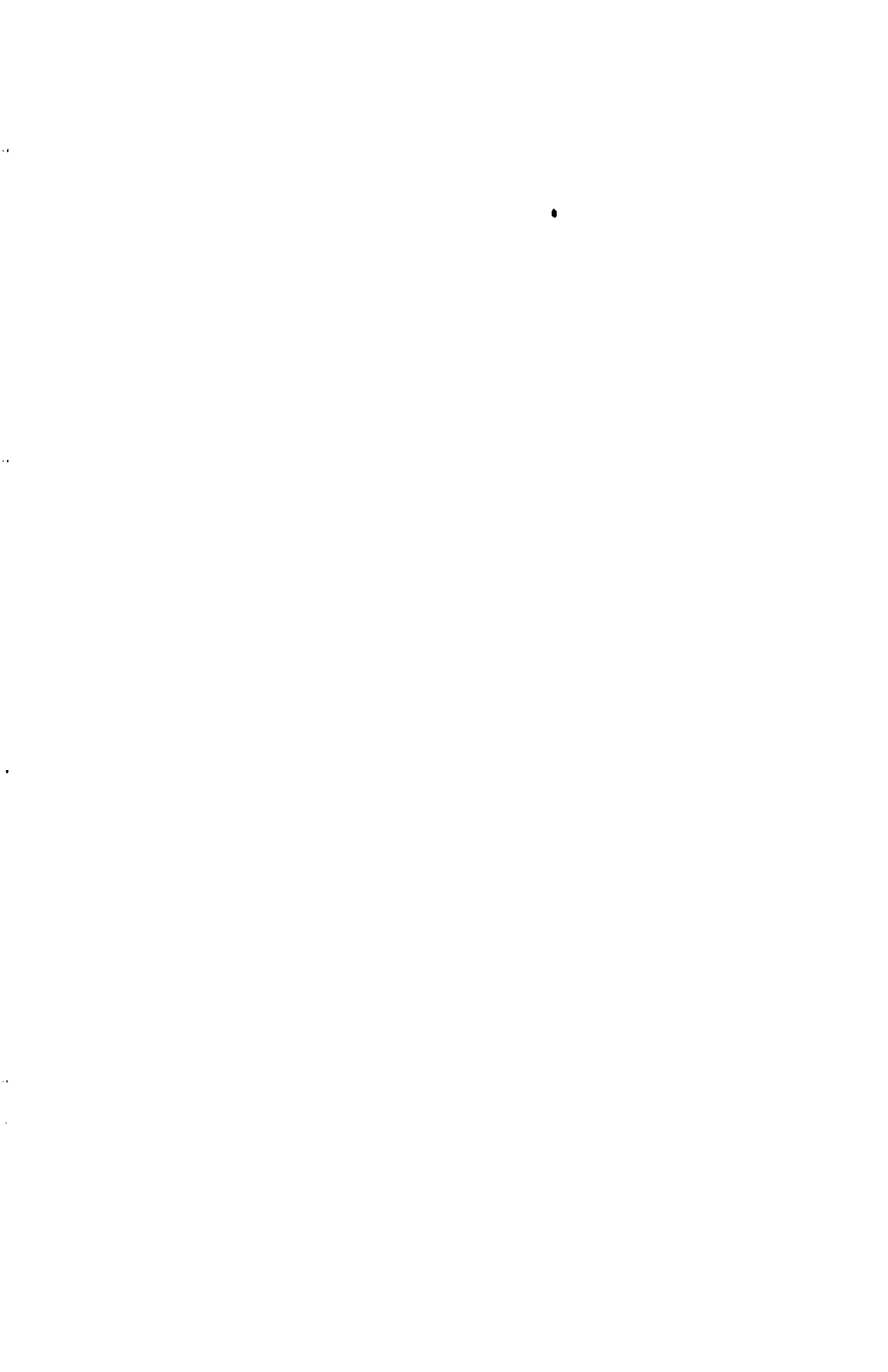
Although our simple picture suggests that a large fraction of gas can be processed through a cooling flow only when clouds lie close to the cooling curve, there are various ways in which baryonic dark matter can be produced throughout the cooling region ($t_c < t_f$ in Figure 2). Since the first objects to form deplete the gas density, the ratio t_c/t_f of the gas increases, thereby extending the $t_c \sim t_f$ regime into the cooling region. Another possibility is that, even when $t_c < t_f$, the gas develops a two-phase structure with cool clouds embedded in a hot medium. $t_c \sim t_f$ could be preserved in the hot gas, in which case high pressure would be maintained as in the quasi-static flows discussed above. This picture is similar to the Fall-Rees²⁷⁾ theory of globular cluster formation. In fact, a recent modification to this theory²⁰⁾ predicts that globular cluster formation should be accompanied by the formation of clusters of jupiters with masses up to about $10^6 M_\odot$, the total mass in dark clusters exceeding that in globular clusters by about two orders of magnitude.

One of the most important predictions of the cooling flow model is that the dark matter in galactic halos should reside in clusters of jupiters, with masses typically around $10^6 M_\odot$. Possible observational evidence is provided by the heating of the Galactic disc, which can be explained by such objects²⁸⁾. There has also been a claim for the detection of a dark cluster in the Galactic halo with a mass of about $10^6 M_\odot$ ²⁹⁾. A further point of interest is that considerations of gravitational lensing by galactic halos has led to the tentative conclusion that the dark matter is clumped on mass-scales between $3 \times 10^4 M_\odot$ and $3 \times 10^7 M_\odot$ ³⁰⁾.

REFERENCES

1. Guth, A., 1981. *Phys. Rev. D* **23**, 347.
2. Yang, J., Turner, M.S., Steigman, G., Schramm, D.N. & Olive, K.A., 1984. *Astrophys. J.*, **281**, 493.
3. Faber, S.M. & Gallagher, J.S., 1979. *Ann. Rev. Astron. Astrophys.*, **17**, 135.
4. Tayler, R.J., 1986. *Q. Jl. R. astr. Soc.*, **27**, 367.
5. Hegyi, D.J., 1984. In *Proceedings Of The Third Moriond Astrophysics Meeting*, ed. Audouze, J. & Tran Thanh Van, J., (Reidel, Dordrecht) p.149.
6. Gilmore, G. & Hewitt, P., 1983. *Nature*, **306**, 669.
7. McDowell, J., 1986. *Mon. Not. R. astr. Soc.*, **223**, 763.
8. Fabian, A.C., Nulsen, P.E.J. & Canizares, C.R., 1984. *Nature*, **310**, 733.
9. Fabian, A.C., 1987. In *Proceedings Of The 22nd Moriond Astrophysics Meeting*, ed. Thuan, T.X., Montmerle, T. & Tran Thanh Van, J., (Editions Frontieres, France).
10. Johnstone, R.M., Fabian, A.C. & Nulsen, P.E.J., 1987. *Mon. Not. R. astr. Soc.*, **224**, 75.
11. Arnaud, K.A. Gilmore, G., 1986. *Mon. Not. R. astr. Soc.*, **220**, 759.
12. Silk, J., Djorgovski, S., Wyse, R.F.G. & Gustavo, A.B., 1986. *Astrophys. J.*, **307**, 415.
13. Rephaeli, Y., 1987. *Mon. Not. R. astr. Soc.*, **225**, 851.
14. Fabian, A.C., Nulsen, P.E.J. & Canizares, C.R., 1982. *Mon. Not. R. astr. Soc.*, **201**, 933.
15. Sarazin, C.L. & O'Connell, R.W., 1983. *Astrophys. J.*, **268**, 552.
16. Ashman, K.M. & Carr, B.J., 1988. *Mon. Not. R. astr. Soc.*, in press.
17. Peebles, P.J.E. & Dicke, R.H., 1968. *Astrophys. J.*, **154**, 891.
18. White, S.D.M. & Rees, M.J., 1978. *Mon. Not. R. astr. Soc.*, **183**, 341.
19. Blumenthal, G.R., Faber, S.M., Primack, J.R. & Rees, M.J., 1984. *Nature*, **311**, 517.
20. Ashman, K.M., 1988. *Preprint*.
21. Ashman, K.M. & Carr, B.J., 1988. *Preprint*.
22. Couchman, H.M.P. & Rees, M.J., 1986. *Mon. Not. R. astr. Soc.*, **221**, 53.
23. Zeldovich, Ya. B., 1970. *Astr. Astrophys.*, **5**, 84.
24. Ostriker, J.P. & Cowie, L.L., 1981. *Astrophys. J. Lett.*, **243**, L127.
25. Ikeuchi, S., 1981. *Pub. Astron. Soc. Japan*, **33**, 211.
26. Allen, A.J. & Carr, B.J., 1988. *Preprint*.
27. Fall, S.M. & Rees, M.J., 1985. *Astrophys. J.*, **298**, 18.
28. Carr, B.J. & Lacey, C.G., 1987. *Astrophys. J.*, **316**, 23.
29. Sommer-Larsen, J. & Christensen, J.P., 1987. *Mon. Not. R. astr. Soc.*, **225**, 499.
30. Subramanian, K. & Chitre, S.M., 1987. *Astrophys. J.*, **313**, 13.

III. LARGE SCALE DISTRIBUTIONS



**LARGE-SCALE DISTRIBUTION OF GALAXIES
IN THE SOUTHERN GALACTIC CAP**

L. Nicolaci da Costa and P. S. Pellegrini
Departamento de Astronomia
CNPq/Observatorio Nacional
Rio de Janeiro
Brasil

ABSTRACT

We have recently extended the Southern Sky Redshift Survey (SSRS) both in angular coverage and depth. In the first case we have nearly completed a survey of galaxies northwards of $\delta = -17.5^\circ$, extending the SSRS to the southern limit of the CfA Redshift Survey at $\delta = -2.5^\circ$, for galactic latitudes south of $b = -30^\circ$. Completion of this extension allows us to examine the large-scale distribution of galaxies in the Southern Galactic Cap over a contiguous area of 3.13 steradians, in particular, the extent of some of the structures observed in the region covered by the SSRS. In the second case we have carried out a deeper survey in the region $-40^\circ \leq \delta \leq -30^\circ$, to probe in more detail the structures and voids previously detected in this strip. Here we present a preliminary discussion of our findings.

I. INTRODUCTION

The present decade has been marked by the completion of several extensive redshift surveys (see ref. 1 for a recent review). The results from these various efforts have been responsible for major changes in our ideas about the nature of the three-dimensional galaxy distribution and have been the driving force for recent theoretical work on the origin of large scale structures in the universe.

The clustering properties of galaxies have been studied using different observational strategies such as: 1) surveys of small angular regions of the sky to very faint magnitude limits, like those being conducted by Kirshner and collaborators²⁾ in the Bootes void and by Koo and collaborators³⁾ to probe evolutionary effects of galaxy clustering; 2) wide-angle surveys of relatively small declination strips like the CfA slice survey⁴⁾ and CfA Redshift Survey extension (CfA2)⁵⁾; 3) moderately deep large angular scale surveys like the CfA Redshift Survey (CfA1)⁶⁾, the Arecibo Survey⁷⁾ and the Southern Sky Redshift Survey (SSRS)⁸⁾. These surveys provide complementary information and their contributions to the large-scale structure studies have been recently reviewed by Geller⁹⁾. Nearby wide-angle surveys are particularly important since they are essential for: 1) estimating the universal mean galaxy density, although fainter samples may be required for a more reliable estimate¹⁰⁾; 2) measuring the velocity flow field, in conjunction with data from other surveys; 3) searching for evidences of biased galaxy formation; 4) testing models for the origin of large-scale structures by means of direct comparisons with results of N-body simulations.

A major finding from the CfA1 survey was that the sizes of the largest structures observed were comparable to the effective survey depth indicating the need to extend it both in depth and sky coverage. As a consequence, over the past 6 years several groups have been working on systematic surveys of the southern

skies, some of which have already been completed like the SSRS and others that are still ongoing such as the Supergalactic Plane Redshift Survey¹²⁾. The main motivations for surveying the southern sky are that it provides a statistically independent sample that can be compared with the CfA1 to address the "fair sample" issue and, particularly in the Southern Galactic Cap, it avoids the large concentration of galaxies associated with the Virgo cluster, thus allowing for a clearer view of the low-contrast structures. An optically selected southern sample can also be used to improve the computation of the peculiar velocity of the Local Group induced by matter in our surroundings, complementing the recent works using the IRAS sample¹³⁾, as well as to search for evidence, at low galactic latitudes, of a large concentration of mass as proposed by the Great Attractor model¹⁴⁾. However, a serious drawback for southern surveys is still the lack of a photometric catalog of galaxies from which well-defined samples can be drawn. This also prevents the construction of a homogeneous optical catalog of the whole sky. Hopefully, this situation will be resolved in the near future.

From the existing nearby surveys in both hemispheres several important characteristics about the galaxy distribution can be inferred: galaxies lie on relatively thin (≈ 5 to $10 h^{-1}$ Mpc, $H_0 = 100h$ km/s/Mpc), sheet-like structures that delineate vast regions devoid of bright galaxies^{4),8)}; voids can be large, with sizes up to $60h^{-1}$ Mpc; large voids may be common both nearby and at large distances^{2),4),11)}. These properties are now relatively well-established and must be explained by viable theoretical models. Here we present further evidences that corroborate these findings, based on the results of surveys we have recently completed in the southern hemisphere.

II. THE SOUTHERN GALACTIC CAP (SGC)

Below galactic latitude $b = -30^\circ$, the SSRS covers the region south of $\delta = -17.5^\circ$, while the southern portion of CfA1 surveys the region north of $\delta = -2.5^\circ$. This leaves an uncovered strip of 0.55 steradians in the SGC. In order to complete a survey of the whole southern cap we have been carrying out, over the past few years, a redshift survey of galaxies in the declination band mentioned above. This sample includes about 450 galaxies with $m_B \approx 14.5$ drawn from the Morphological Catalog of Galaxies (MCG)¹⁵⁾. The magnitudes were taken from the MCG, adding 0.5 mag to transform them into the same system adopted in the CfA1¹⁶⁾. The sample is nearly complete and enable us to construct a magnitude-limited sample for the entire southern galactic cap from a merge of the Zwicky¹⁷⁾-MCG-ESO/Uppsala¹⁸⁾ catalogs down to $m_B \approx 14.5$. Magnitudes for galaxies in the region of the SSRS were estimated from mean relations between diameters and magnitudes, calibrated using galaxies in the ESO/Uppsala catalog with available information (see ref. 19 for further details). The final sample consists of 2372 galaxies covering the entire southern galactic cap south of $b = -30^\circ$.

The importance of the SGC sample is that it enables the investigation of a continuous area of 3.13 steradians of the SGC, 1.7 times the sky coverage of the CfA1 and SSRS. This larger and continuous coverage allows us to explore the extent of some of the main features of the galaxy distribution detected in the SSRS region. In figure 1 we present a subset of the galaxy distribution in the same cartesian coordinate system adopted in the SSRS, showing projections onto the x-y plane of galaxies within $10h^{-1}$ Mpc thick slabs. In the figure only the northernmost slabs in the interval $10 < z < 30h^{-1}$ Mpc are shown for both the SSRS and the SGC. A detailed discussion of the characteristics of the SGC sample will be presented elsewhere²⁰⁾. Here we would only like to stress that by including the

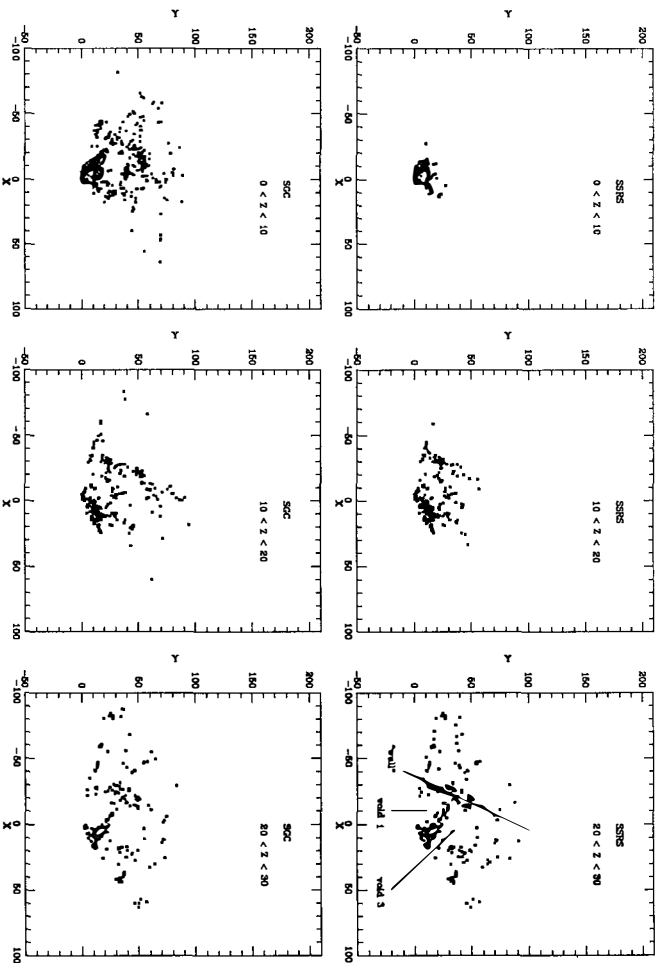


Figure 1. Distribution of galaxies with velocities less than 10000 km/s in a Cartesian coordinate system defined in ref 8), projected in consecutive slices, $10h^{-1}$ Mpc thick, from $z = 0$ to $30h^{-1}$ Mpc. SSRS and SGC samples are indicated in the panels.

MCG data we can now examine structures in the z direction over scales comparable to those along the x - y plane, corresponding to an effective gain of roughly $30h^{-1}$ Mpc in the z direction. From the inspection of these maps we find that all of the main structures detected in the SSRS region extend to the north, among which the main wall and voids 1 and 3 described in the SSRS. The implication of the extended survey is that most of the structures visible inside the survey volume appear coherent over scales greater than $50h^{-1}$ Mpc reaching up to $80h^{-1}$ Mpc. Although coherent these structures are not uniform, with breaches over scales of 10 to $20h^{-1}$ Mpc. They are also quite flat with the ratio of the intermediate to the largest dimension being typically 0.8, while the ratio of shortest to the longest dimension ranges from 0.1 to 0.2. In the southern galactic cap we identify at least 6 of these flat structures, although some are near the borders²⁰⁾. We also note that we find no prominent clusters at the intersection of the walls. The only noticeable virial distortions observed are those associated with the foreground clusters of Eridanus and Fornax. Some degree of sub-clustering is found within the walls with the centers of small groups tracing fairly well the large structures.

This larger sky coverage also allows to examine the properties of voids over larger scales. In fact, detailed inspection of the voids indicates that they gradually change their shapes (note how voids 1 and 3 evolve below $z = 10h^{-1}$ Mpc), sometimes tenuous features cut across them and holes in the surrounding walls connect what apparently are different voids. This general behavior is at least suggestive of a sponge-like topology²¹⁾. This impression is consistent with the quantitative analysis of the void properties in the SSRS region²²⁾ which indicates that: voids seem to have very irregular shapes; most low-density regions become connected at a density contrast of about 25% of the mean density and only one large void is detected within the SSRS region, with a equivalent radius $> 30h^{-1}$ Mpc; the smoothed galaxy density function seems to have a sponge-like topology

with the low-density regions being multiply connected.

III. SOUTHERN SLICE SURVEY

We have also extended the SSRS in depth concentrating observations in the region $-40^\circ \leq \delta \leq -30^\circ$, $b \leq -30^\circ$ comprising an area of $135^\circ \times 10^\circ$. In the first phase we considered only morphological types with $T \leq 3$ (E-Sb) down to $m_B \approx 15.1$. The sample, which consists of 489 galaxies, is complete and includes 250 galaxies in addition to those observed in the SSRS.

In figure 2 we plot the observed velocity versus right ascension of galaxies in the strip mentioned above with $v < 12000$ km/s. A striking result is that no new

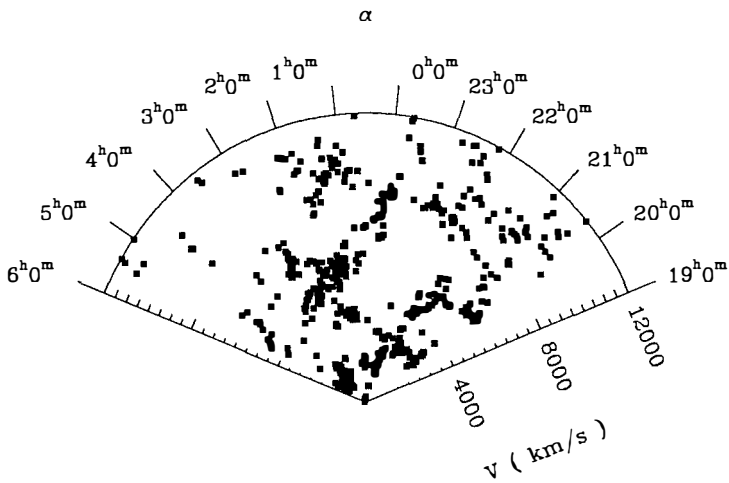


Figure 2. Observed velocities versus right ascension for galaxies with velocities less than 12000 km/s.

galaxy falls within the volume of the main void detected in the SSRS (void 3), while the far side of this void which was barely discernible becomes well-defined, being associated with an elongated structure which extends over $100h^{-1}$ Mpc at about 10000 km/s. From the deeper sample we also identify an adjacent void with dimensions comparable to void 3, which is separated from it by the "main" wall of the SSRS. These preliminary results, that will be reported in more detail elsewhere²³⁾ give additional support to the idea that vast voids may be a common feature of the galaxy distribution¹¹⁾. However, this must be confirmed by deeper surveys, which should include all morphological types.

VI. FINAL REMARKS

A general pattern of the galaxy distribution seems to be emerging from the various nearby wide-angle surveys efforts. Galaxies lie primarily on large, coherent planar structures that intersect each other at sharp corners and nearly surround vast voids; large voids with sizes up to $60h^{-1}$ seem to be common; voids seem to be interconnected, as expected for a sponge-like topology. However, the size of the largest inhomogeneity of the galaxy distribution is still unconstrained indicating the need for deeper redshift surveys⁹⁾. Towards this goal a galaxy sample is being generated from plate scans²⁴⁾ of the southern hemisphere and we intend to extend our southern slice survey down to $m_B = 15.5$ for all morphological types, in collaboration with the CfA.

ACKNOWLEDGMENTS

We thank our collaborators J. Huchra, D. Latham and C. Willmer for allowing us to

use the data before publication. We also thank M. Geller for useful discussions. Some of our data were obtained in the Complejo Astronomico El Leoncito, Argentina. We acknowledge the help of H. Levato, J. H. Calderon and the entire argentine staff.

REFERENCES

- 1) Huchra, J. P., and Geller, M., J. 1986, 13th Texas Symposium on Relativistic Astrophysics, Ed. M. Ulmer (World Scientific: Singapore).
- 2) Kirshner, R. P., Oemler, A., Schechter, P. L. and Shectman, S. A. 1987, Ap. J., 314, 493.
- 3) Koo, D., Kron, R., and Szalay, A. 1986, 13th Texas Symposium on Relativistic Astrophysics, Ed. M. Ulmer (World Scientific: Singapore).
- 4) de Lapparent, V., Geller, M. and Huchra, J. P. 1986, Ap. J. (Letters), 302, L1.
- 5) Geller, M. J., Huchra, J. P. and de Lapparent, V. 1987, IAU Symp. 1 2 4 ,
Observational Cosmology, ed. A. Hewitt, G. Burbidge and L. Z. Fang (Dordrecht: Reidel), p. 301.
- 6) Huchra, J. P., Davis, M., Latham, D. and Tonry, J. 1983, Ap. J. Suppl., 52, 89.
- 7) Giovanelli, R., Haynes, M. and Chincarini, G. L. 1986, Ap. J., 300, 77.
- 8) da Costa, L. N., Pellegrini, P. S., Nunes, M. A., Willmer, C. and Latham, D. W. 1984, A. J., 89, 1310.
- 9) Geller, M. J. 1988, "17th Advanced Course in Astronomy and Astrophysics, Saas-Fee, Switzerland, in press.
- 10) de Lapparent, V., Geller, M. and Huchra, J. P. 1988, preprint.
- 11) Postman, M., Huchra, J. P. and Geller, M. J. 1986, A. J. 92, 1238.
- 12) Dressler, A. 1988, preprint.
- 13) Strauss, M., and Davis, M. 1987, IAU Symp. 130, Large Scale Structure in the Universe, eds. J. Audouze and A. Szalay (Dordrecht: Reidel)
- 14) Lynden-Bell, D., Faber, S. M., Burstein, D., Davies, R. L., Dressler, A., Terlevich, R. J., Wegner, G. 1988, preprint.
- 15) Vorontsov-Velyaminov, B. A. and Arhipova, V. P. 1963-68, Morphological Catalogue of Galaxies (Moscow) Parts 2 to 4.
- 16) Huchra, J. P. 1985, private communication.
- 17) Zwicky, F., Herzog, E., Wild, P., Karpowicz, M., and Kowal, C. T. 1961-68, Catalogue of Galaxies and Clusters of Galaxies (Pasadena: California Institute of Technology)
- 18) Lauberts, A. 1982, The ESO/Uppsala Survey of the ESO(B) Atlas (Munche: European Southern Observatory).
- 19) Pellegrini, P. S. 1988, Ph D. thesis, Observatório Nacional.
- 20) Pellegrini, P. S., da Costa, L. N., Huchra, J. P., Latham, D. W., and Willmer, C. 1988, in preparation.
- 21) Gott, J. R., Melott, A. L. and Dickinson, M. 1986, Ap. J., 306, 341.
- 22) Pellegrini, P. S., da Costa, L. N., and de Carvalho, R., 1988, in preparation.
- 23) da Costa, L. N., Pellegrini, P. S., Willmer, C., and Latham, D. W., 1988, in preparation.
- 24) Geller, M. J., and Kurtz, M., private communication.

**A 21-CM REDSHIFT SURVEY AND
THE LARGE SCALE DISTRIBUTION OF DWARF GALAXIES**

Trinh X. Thuan

Astronomy Department, University of Virginia
Charlottesville, VA 22903, USA

and

Institut d'Astrophysique de Paris, CNRS, France

and

Service d'Astrophysique,
Centre d'Etudes Nucléaires de Saclay, France



The first results of an all-sky 21-cm redshift survey of all 1849 galaxies north of $-2^{\circ}30'$ classified as dwarf, magellanic irregular or irregular by Nilson in the Uppsala General Catalog are presented. The detection rate is $\sim 85\%$. The survey reveals a broad continuum of galaxies with absolute blue luminosities ranging from -13 to -21 . Thus the sample contains not only bona fide dwarf galaxies ($M_B > -16$) but also luminous low-surface-brightness (LSB) systems ($M_B < -16$).

Detailed comparison of the spatial distributions of dwarf and bright galaxies shows that there is no difference between the two distributions. Dwarf galaxies do not fill the voids seen in the bright galaxy distribution. This rules out a certain class of biased galaxy formation theories. If biasing occurs, the dark matter which is in the voids cannot be traced by dwarf and LSB galaxies, and biasing must be equally effective for both bright and faint galaxies.

The dwarf redshift sample has been used in conjunction with other redshift samples to measure the topology of the universe out to $\sim 21\,000\text{ km s}^{-1}$. The universe shows a sponge-like topology, which implies random phase Gaussian initial density fluctuations. This topology is inconsistent with explosive amplification or cosmic string galaxy formation models. The cold dark matter model with $\Omega=1$ and $H=50\text{ km s}^{-1}\text{ Mpc}^{-1}$ fits best the topology of the universe on different length scales.

I. INTRODUCTION

Recent extensive redshift surveys^{1,2)} of thousands of galaxies have permitted a start on unraveling the three-dimensional distribution of galaxies. They have revealed an extraordinary landscape where galaxies appear to trace out long filamentary structures reaching dimensions of up to ~ 50 Mpc (we adopt throughout a Hubble constant of $75 \text{ km s}^{-1} \text{ Mpc}^{-1}$) or bubble-like structures, with sharp edges and typical diameters of ~ 30 Mpc, leaving large voids completely empty of bright galaxies^{3,4)}. However, all existing major redshift surveys suffer from a serious selection effect which may have important consequences on analyses of galaxy clustering : they all miss the very small low-surface-brightness (LSB) dwarf galaxies.

The Center for Astrophysics¹⁾ (CfA) survey is magnitude-limited and cuts off at $m_{pg} = 14.5$. The majority (more than 90 %) of the LSB dwarf galaxies are fainter than 14.5 and would not be included in such a survey. The HI survey of Fisher and Tully²⁾ only included galaxies with a diameter larger than 2 arcminutes and contained only ~ 200 dwarf galaxies out of a total of ~ 2000 galaxies. More than 90 % of the dwarf galaxies have diameters less than 2 arcminutes and again would not be included in such a survey.

It is not clear at present that bright galaxies are reliable tracers of the mass distribution in the Universe. The currently popular theories of biased galaxy formation⁵⁾ propose that bright galaxies form only in regions of very high density contrast and thus are not fair tracers of the mass distribution on very large scales. Furthermore, inflationary cosmologies which demand that the mass density parameter Ω be equal to 1 require that severe biasing exists in order to be consistent with the observations that Ω (luminous matter) ~ 0.01 and Ω (luminous + dark baryonic matter) ~ 0.2 . Since the latter value is obtained from observations of the motions of bright galaxies in clusters, this suggests that the dark matter which may constitute the remaining 80 % of the mass of the universe is not associated with bright galaxies in clusters and may be more uniformly distributed, filling in the voids seen in the bright galaxy distribution.

Are we having a "biased" view of the universe because we have not surveyed the sky to a faint enough surface brightness level ? Are the voids filled with LSB dwarf galaxies ? There have been several attempts^{6,7)} to study the clustering properties of galaxies as a function of surface brightness but the results have been inconclusive because of the lack of complete redshift data. In order to provide a definitive answer to these questions, I have undertaken (with S.E. Schneider joining the effort in 1986) in the last several years a complete redshift survey of all northern dwarf galaxies catalogued by Nilson⁸⁾. Section II describes the survey. Section III discusses the spatial distribution of dwarf galaxies as compared to that of bright galaxies. Section IV presents some preliminary results concerning the topology of the universe using the dwarf sample in combination

with other galaxy redshift samples.

II. THE 21-CM DWARF GALAXY REDSHIFT SURVEY

The redshift survey consisted of all galaxies classified by Nilson⁸⁾ in the Uppsala General Catalog (UGC) as dwarf, magellanic irregular or irregular galaxies, 1849 galaxies out of a total of $\sim 13\,000$ galaxies of all morphological types in the UGC. The sample thus defined avoided the selection effects against dwarf galaxies present in previous redshift surveys: the UGC is a diameter-limited catalogue (it lists all galaxies with a blue diameter larger than 1 arcminute visible on the Palomar Sky Survey Prints and north of $\delta = -2^{\circ} 30'$) and thus does not discriminate against faint low-surface-brightness dwarf galaxies. Moreover, its lower diameter limit of 1 arcminute permitted to include many more small dwarf galaxies than the Fisher-Tully catalogue.

To carry out the dwarf redshift survey, the 21cm line was used. Dwarf galaxies are often characterized by a very low surface brightness ($S \sim 25.5 \text{ mag arcsec}^{-2}$) which makes their optical study very difficult and time-consuming. Fortunately, the magellanic and irregular dwarfs often contain significant amounts of neutral hydrogen⁹⁾ ($\sim 10^8 M_{\odot}$) which makes them easily detectable (~ 5 minutes of integration) with existing radio telescopes. The dwarf redshift survey was carried out using the Arecibo 305m telescope for galaxies with $0^{\circ} \leq \delta \leq 36^{\circ}$ and the Green Bank 100m telescope for galaxies with $-2.5^{\circ} \leq \delta < 0^{\circ}$ and $\delta > 36^{\circ}$. The velocity search range was from -400 to $10\,000 \text{ kms}^{-1}$. The survey was finished in April 1986, yielding a detection rate of $\sim 90\%$ for the sample in the Arecibo declination range and of $\sim 80\%$ for the sample in the Green Bank declination range. Of the 1849 galaxies which were observed, only 283 galaxies were not detected, either because they have a velocity beyond the search range, or they have an HI flux below the flux limit of the telescope, or both. A list of 150 dwarf redshifts has already been published⁹⁾. Additional redshifts in a specific region of the sky (the CfA slice of the universe⁴⁾) have also been recently published¹⁰⁾. The very high detection rate in 21cm of the Nilson dwarf sample implies that there is a strong bias in the Nilson catalog for HI-rich dwarfs, i.e. for magellanic or irregular dwarfs. Dwarf ellipticals which do not contain neutral hydrogen have a lower surface brightness and are not easily seen on the Palomar Sky Survey Prints.

The vast amount of data is being organized into a catalog¹¹⁾ which will contain a total of ~ 1800 entries for dwarf galaxies, giving for each galaxy an accurate HI flux (or an upper limit), velocity and velocity width. In addition, the catalog will contain photographic magnitudes for all galaxies. Most ($\sim 80\%$) of the galaxies in our sample are too faint to be included in the Zwicky catalog¹²⁾ whose limiting magnitude is 15.5. Photographic magnitudes of the dwarf galaxies can be obtained to $\sim 0.5 \text{ mag}$ by estimating the surface brightness of each galaxy on the Palomar Sky Survey Prints and

multiplying by their area⁹). This catalog is the best one can assemble for the moment for LSB dwarf galaxies at northern declinations ($\delta \geq -2^{\circ} 30'$), until the ongoing deeper Palomar Schmidt survey on III aJ plates, which will undoubtedly pick up many more dwarf galaxies, is made available (unless the higher surface brightness of the San Diego sky foils any attempt to go deeper).

The catalog is also very complete for small galaxies. If V is the volume of the sphere whose radius is the distance to the object and V_m is the volume of the sphere whose radius is the maximum distance to which a galaxy can be moved to and still be in the sample, i.e. still possess a blue angular diameter greater than 1 arcminute, then the mean $\langle V/V_m \rangle = 0.453$ for all dwarf galaxies larger than 1 arcminute, very close to the value of 0.5 expected for an uniform distribution in Euclidian space of a complete sample of galaxies¹³). There are no large variations in the counts of dwarf galaxies from plate to plate, suggesting that Nilson did a very careful job in cataloguing these galaxies and that the small plate variations in the Palomar Sky Survey do not play a dominant effect in their identification. Moreover, because we have systematically observed every dwarf galaxy in the Nilson catalog, there will be no systematic effect introduced by redshift incompleteness as a function of position in sky. Galactic extinction effects and radio telescope sensitivity effects can be modeled and taken into account, when deriving a selection function for the catalog. This selection function is needed to compute such statistics as the dwarf–dwarf spatial autocorrelation function or the dwarf–bright galaxy cross–correlation function.

Figure 1a shows the redshift distribution of the Nilson magellanic and dwarf galaxies in the Arecibo declination range ($0^{\circ} \leq \delta \leq 36^{\circ}$). Galaxies are detected up to velocities near the 10 000 km s⁻¹ upper limit of the velocity search range. It is clear that the completeness of the sample drops off drastically beyond 5000 km s⁻¹ due to the flux decrease of distant galaxies. It is also clear that the galaxies classified by Nilson as “dwarf” or “magellanic–type” are not all bona fide dwarf galaxies. Galaxies in the high velocity tail ($v \geq 6000$ km s⁻¹) have absolute photographic magnitudes of -19 or smaller and cannot be properly labeled dwarf galaxies.

The selection criteria of “low surface brightness” and “little or no central concentration”, which Nilson⁸) used to identify dwarf galaxies, have isolated a broad continuum of galaxies with absolute blue luminosities, ranging from ~ -13 to ~ -21 , from the “true” dwarf galaxies to more luminous and very low surface brightness systems. Thuan and Seitzer¹³), studying a subsample of ~ 150 galaxies, and dividing, for convenience, the data into a “dwarf” (those galaxies fainter than -16) and “non dwarf” sample ($M_{pg} < -16$), found that dwarf galaxies have a smaller hydrogen width ($\Delta v_{20} \sim 100$ km s⁻¹), contain less hydrogen ($M_H \sim 10^8 M_{\odot}$), and are less massive ($M_T \sim 10^9 M_{\odot}$) than the non–dwarf LSB galaxies ($\Delta v_{20} \sim 250$ km s⁻¹, $M_H \sim 10^9 M_{\odot}$, $M_T \sim 10^{10} M_{\odot}$). With respect to the total galaxy population, non–dwarf LSB galaxies are relatively rare: they

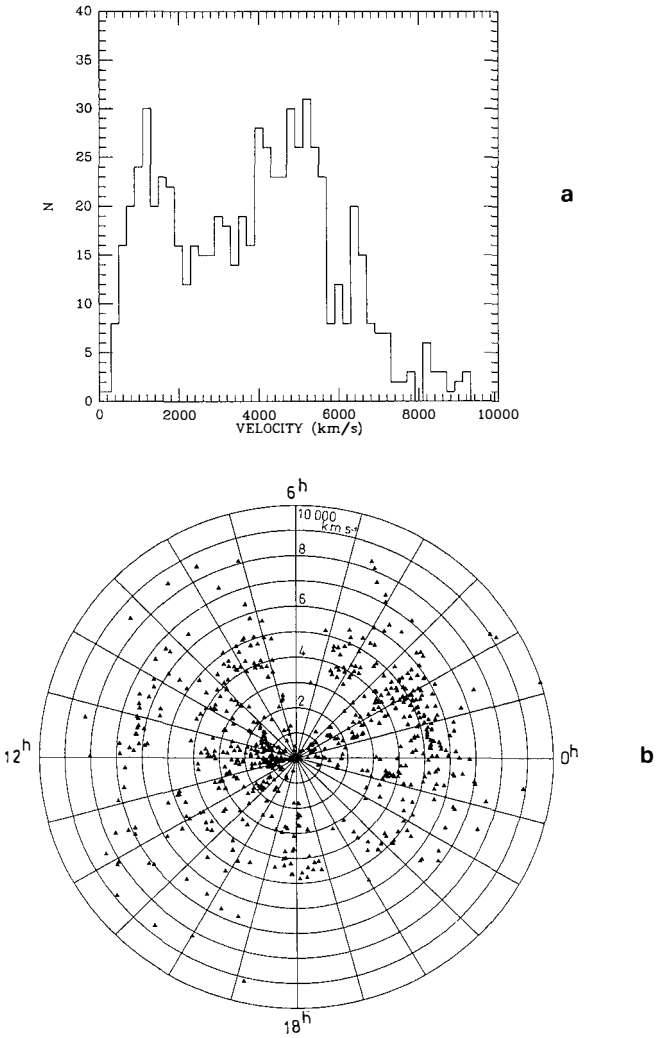


Figure 1. The Arecibo ($0 \leq \delta \leq 36^\circ$) dwarf and low-surface brightness galaxy sample. a) histogram of observed heliocentric velocities. b) wedge diagram of observed heliocentric velocity vs. right ascension. The velocity circles go from 0 to $10\,000 \text{ km s}^{-1}$ in intervals of 1000 km s^{-1} .

constitute only $\sim 10\%$ of all field galaxies at $M_B = -19$ and $\sim 1\%$ of all galaxies at $M_B = -20$.¹³⁾ In the following, we shall refer to non-dwarf galaxies as “LSB galaxies”.

III. DWARF GALAXIES DO NOT FILL IN VOIDS

Figure 1b shows the all-sky spatial distribution of dwarf and LSB galaxies in the declination range accessible to the Arecibo telescope from 0 to 36° , in a wedge diagram of observed heliocentric velocity versus right ascension. The velocity circles go from 0 to $10\,000\text{ km s}^{-1}$, in intervals of 1000 km s^{-1} . It is clear from figure 1b that the spatial distribution of dwarf and LSB galaxies with $-21 \leq M_B \leq -13$ is not uniform, that it shows structures with several large voids extending several thousands of km s^{-1} across, and prominent concentrations of galaxies, especially the ones at $\sim 1200\text{ km s}^{-1}$ and $9\text{h} \leq \alpha \leq 13\text{h}$ and at $\sim 5000\text{ km s}^{-1}$ and between 23h and 3h in right ascension. These structure are also evident from figure 1a, where there are two large velocity peaks at $\sim 1200\text{ km s}^{-1}$ and $\sim 5000\text{ km s}^{-1}$. There structures are well-known from studies of the bright galaxy distribution, the first one being the Virgo cluster and the second one being the Perseus–Pisces supercluster. Thus even a very coarse look at the three-dimensional distribution of galaxies tells us that dwarf and LSB galaxies trace out very similar structures to the ones traced out by bright galaxies and that they do not appear to fill in the voids seen in the bright galaxy distribution.

The comparison can be made more precise by plotting the dwarf and LSB galaxies on top of the bright galaxies. This was done by Thuan, Gott and Schneider¹⁰⁾ in a small region of the sky, the CfA slice ($8\text{h} \leq \alpha \leq 17\text{h}$, $26^\circ 5' < \delta \leq 32^\circ 5'$) of de Lapparent, Geller and Huchra⁴⁾. These authors obtained redshifts for all Zwicky galaxies brighter than 15.5 in this region of space and found that they appear to be on the surfaces of “bubble-like” structures with sharp edges. Using our complete redshift sample of 58 Nilson dwarf and LSB galaxies in the slice, we find that these (open circles) also lie on the structures delineated by the high surface brightness (HSB) galaxies (crosses) and are just as narrowly confined to the bright galaxy structures as the bright galaxies themselves (figure 2a). They do not fill in the voids. There is no dependence on absolute magnitude. The dwarf galaxies ($-16 < M_B < -13$) adhere just as closely to the structures outlined by the HSB galaxies as do the non-dwarf LSB galaxies with $M_B < -16$. I have also analyzed the 6° slice above ($8\text{h} \leq \alpha \leq 17\text{h}$, $32^\circ 5' < \delta \leq 38^\circ 5'$) in the same fashion. The bright galaxies are now represented by open circles and the dwarf and LSB galaxies by crosses (figure 2b). The above conclusions are reinforced: there is no difference between the bright and dwarf galaxy distributions. Eder et al.¹⁴⁾, analyzing the spatial distribution of dwarf irregular galaxies in the vicinity of a nearby ($\alpha \sim 1\text{h}$, $\delta \sim 15^\circ$, $v \sim 3500\text{ km s}^{-1}$) void, also reached similar conclusions.

The result that dwarf and LSB galaxies do not fill the voids seen in the bright galaxy distribution rules out a certain class of biased galaxy formation theories which propose

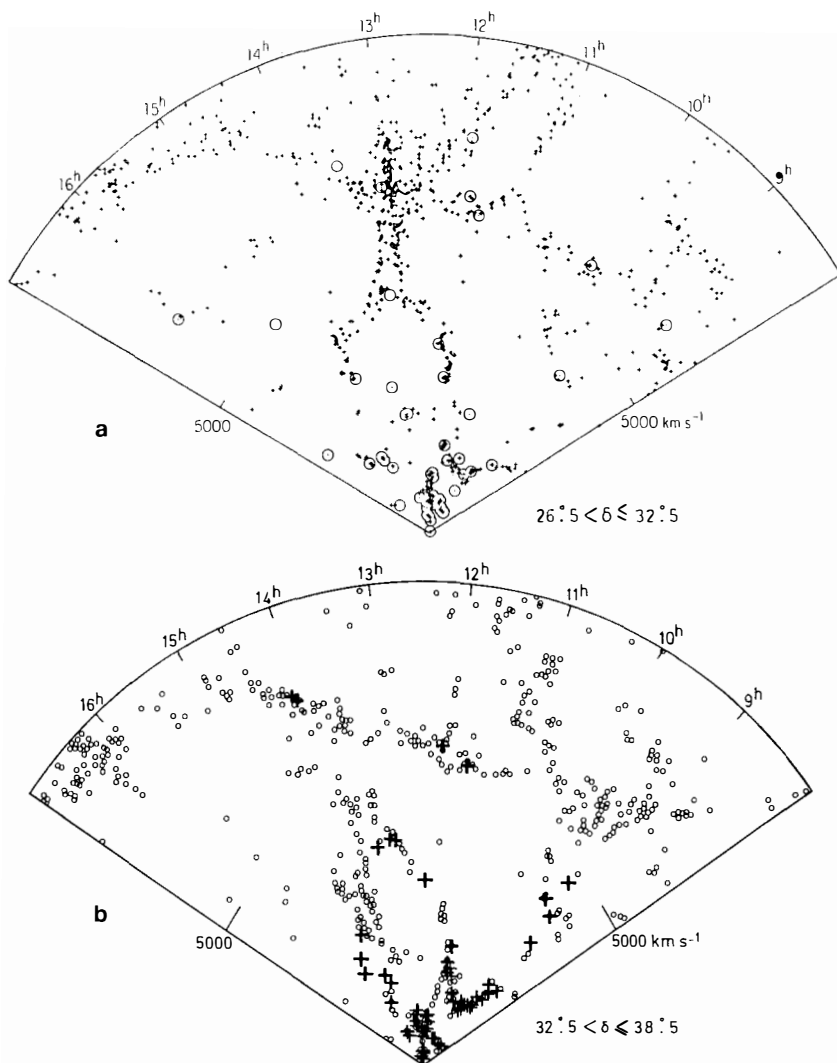


Figure 2. a) Comparison between the spatial distribution of dwarf and LSB galaxies (open circles) and that of bright ($m_{pg} \leq 15.5$) galaxies (crosses) in the CfA slice⁴⁾ ($8^{\text{h}} \leq \alpha \leq 17^{\text{h}}$, $26^{\circ}.5 < \delta \leq 32^{\circ}.5$). There is no difference between the bright and dwarf galaxy distributions. b) Same as in figure 2a, but for the 6th slice above ($8^{\text{h}} \leq \alpha \leq 17^{\text{h}}$, $32^{\circ}.5 < \delta \leq 38^{\circ}.5$). Bright galaxies are open circles and crosses are dwarf and LSB galaxies.

that LSB dwarfs originate from typical ($\sim 1\sigma$) density perturbations in contrast to the normal, brighter HSB galaxies which can only form from the highest density peaks ($\sim 2-3\sigma$). In these theories, dwarfs trace the mass while bright normal galaxies trace the light⁵). They predict explicitly that dwarfs should be present everywhere, including in the voids, and that differences in the distribution of HSB and LSB galaxies should begin to appear at $M_B > -17$ and be strong at $M_B \sim -15$, in contradiction to the data presented here. If biasing ideas are correct, the dark matter which is in the voids cannot be traced by dwarf and LSB galaxies with absolute blue magnitudes as faint as -13 .

IV. THE TOPOLOGY OF THE UNIVERSE

Cold dark matter (CDM), $\Omega=1$, biased models have been remarkably successful in reproducing the appearance of the CfA slice¹⁵). It is the biasing effect in these models which makes the voids so completely clear of galaxies. The results described here imply that, if biasing is operating, it must be equally effective for both HSB and LSB galaxies. Another scheme for naturally producing large voids clear of all galaxies is the explosive galaxy formation scenario¹⁶).

Is there a way to distinguish between models with such radically different initial conditions? A promising method is the quantitative measure of the three-dimensional topology of the universe developed by J.R. Gott and his collaborators¹⁷). In collaboration with J.R. Gott, J. Miller and S. Schneider, I have begun to use the previously described dwarf redshift sample in conjunction with other redshift samples such as the CFA sample¹), the Fisher-Tully sample²), the Perseus-Pisces sample¹⁸) and the nearby Abell cluster sample¹⁹) to measure the topology of the universe. These different redshift samples probe different depths. The dwarf and Fisher-Tully samples can be used to form complete volume-limited samples out to 3000 km s^{-1} , the CfA survey out to 5000 km s^{-1} , the Perseus-Pisces sample out to $\sim 12000 \text{ km s}^{-1}$ and the Abell sample out to $\sim 21000 \text{ km s}^{-1}$.

The galaxy distribution in each redshift sample is smoothed by Fourier convolution with a Gaussian function to obtain a continuous density function. The smoothing length needs to be 2 to 3 times the mean galaxy separation. Numerical simulations show that this is required to recover the initial topology from the present evolved state²⁰). Constant density surfaces are then drawn which divide each galaxy sample into high and low-density regions which occupy equal volumes, (the surfaces are called "median" sponges) and the topology of these surfaces is measured. For all the redshift samples which were analyzed, there were neither high density peaks nor isolated voids. Rather, the high and low-density regions are always completely connected and interlocking: the universe, at least out to $\sim 21000 \text{ km s}^{-1}$, has a sponge-like topology. The quantitative measure of the topology confirms this conclusion. The topology analysis thus does not support the suggestion by de Lapparent et al.⁴) that the universe may possess a

“bubble-like” topology. This suggestion, based on the visual impression of a small region of the universe (figure 2a) may be misleading. Already in the contiguous 6^0 slice above (figure 2b), “bubble-like” structures are much less evident. Rather, a sponge-like topology with interconnected low and high-density regions, appears to provide a more adequate description.

A sponge-like topology arises naturally when structures develop gravitationally from initial density fluctuations with random phases. In a random phase distribution, the high and low-density regions are treated on an equal basis and are topologically indistinguishable. This situation only occurs in a sponge. Thus, the observed sponge-like topology of the universe out to $\sim 21000 \text{ km s}^{-1}$ appears to favor Gaussian initial conditions and rule out non random phase scenarios such as the explosive amplification¹⁶⁾ or cosmic string²¹⁾ galaxy formation models.

Because our redshift samples reach different depths, we can measure the topology of the universe (i.e. the number of holes per unit volume in a median sponge-like surface) as a function of smoothing length. The topology-smoothing length relationship depends directly on the nature of the power spectrum $P(k)$ of the initial density fluctuations. If we adopt a power-law form $P(k) \propto k^n$ for the power spectrum, then our topology results are most consistent with an universe dominated by cold dark matter (CDM), with $\Omega h = 0.5$ (i.e. $\Omega = 1$, $H = 50 \text{ km s}^{-1} \text{ Mpc}^{-1}$). The spectrum changes smoothly from an $n \sim -3$ power law on small scales to an $n \sim 1$ power law on large scales.

In summary, the topology analysis of our dwarf redshift sample in combination with other redshift samples probing the universe out to $\sim 21000 \text{ km s}^{-1}$, shows that the universe has a sponge-like structure, which implies random phase Gaussian initial density fluctuations. The CDM model with $\Omega = 1$ and $H = 50 \text{ km s}^{-1} \text{ Mpc}^{-1}$ fits best the topology of the universe on different length scales.

Acknowledgements

I thank J.R. Gott, J. Miller and S.E. Schneider for allowing me to present preliminary results from our joint work. I acknowledge partial financial support from a Fulbright fellowship and thank the hospitality of the Institut d’Astrophysique de Paris and the Service d’Astrophysique at the Centre d’Etudes Nucléaires de Saclay in France.

REFERENCES

- 1) Huchra, J., Davis, M., Latham, D. and Tonry, J. 1983, Ap. J. Suppl., 52, 89
- 2) Fisher, J.R. and Tully, R.B. 1981, Ap. J. Suppl., 47, 139

- 3) Gregory, S.A., Thompson, L.A. and Tifft, W.G. 1981, Ap. J. 243, 411
- 4) de Lapparent, V., Geller, M.J. and Huchra, J.P. 1986, Ap. J. (Letters), 302, L1
- 5) Dekel, A. and Silk, J. 1986, Ap. J., 303, 39
- 6) Davis, M. and Djorgovski, S. 1985, Ap. J., 299, 15
- 7) Bothun, G.D., Beers, T.C., Mould, J.R. and Huchra, J.P. 1986, Ap.J., 308, 510
- 8) Nilson, P. 1973, Uppsala Astr. Obs. Ann., Vol. 6 (Uppsala General Catalog of Galaxies)
- 9) Thuan, T.X. and Seitzer, P.O. 1979, Ap.J., 231, 327
- 10) Thuan, T.X., Gott, J.R. and Schneider, S.E. 1987, Ap. J. (Letters), 315, L93
- 11) Thuan, T.X. and Schneider, S.E., in preparation
- 12) Zwicky, F., Herzog, E., Wild, P., Karpowicz, M. and Kowal, C.T. 1961-1968, Catalog of Galaxies and of clusters of galaxies, vols. I-VI, (Pasadena : California Institute of Technology).
- 13) Thuan, T.X. and Seitzer, P.O. 1979, Ap. J., 231, 680
- 14) Eder, J.A., Schombert, J.M., Oemler, A. and Dekel, A., 1988, preprint
- 15) White, S.D.M., Frenk, C.S., Davis, M. and Efstathiou, G. 1987, Ap. J., 313, 505
- 16) Ostriker, J.P. and Cowie, L.L. 1981, Ap. J. (Letters), 243, L127 ; Ikeuchi, S. 1981, Publ. Astr. Soc. Japan, 33, 221
- 17) Gott, J.R., Melott, A.L. and Dickinson, M. 1986, Ap. J., 306, 341
- 18) Haynes, M.P., Giovanelli, R., Starosta, B.M. and Magri, C. 1988, A.J., 95, 607
- 19) Hoessel, J.G., Gunn, J.E. and Thuan, T.X. 1980, Ap.J., 241, 486
- 20) Hamilton, A.J.S., Gott, J.R. and Weinberg, D. 1986, Ap. J., 309, 1
- 21) Vilenkin, A. 1985, Phys. Rept, 121, 263

GRAVITATIONAL CLUSTERING OF GALAXIES IN THE CfA SLICE

Philippe Crane
European Southern Observatory
Munich, West Germany

and

William C. Saslaw
Department of Astronomy
University of Virginia
Charlottesville, Va., USA

Abstract

The clustering properties of the galaxies in the CfA slice have been analyzed by comparing the properties of the neighbor distributions to the predictions of gravitational clustering theory. The agreement is excellent and implies that the observed structures can be explained by gravitational effects alone and do not require exotic explanations.

1. Introduction

The study of structures on the scales of the order of megaparsecs is one of the few tools available to observational cosmologists probing the dynamics and mass density of the Universe. The subject has a rich history and the collection of the required data is currently one of the most actively pursued programs of optical observers.

A recent compilation of the positions and redshifts for galaxies in the so-called CfA slice¹ has revealed new and fascinating structures in the three dimensional distribution of galaxies. The CfA slice data is for the sample of 1099 galaxies listed by Zwicky et al.² in the region $8^h \lesssim \alpha \lesssim 17^h$ and for $26:5 \lesssim \delta \lesssim 32:5$ with $m_B \lesssim 15.5$. Although the original analysis of these data was descriptive, it has provoked considerable discussion, speculation, and controversy.

We present here a quantitative analysis of the galaxies in the CfA slice using data taken directly from the lists of Zwicky et al.². The analysis compares the predicted probability distribution function for gravitating systems detected by Saslaw and Hamilton³ with the distributions of angular distances from a random point to the n^{th} nearest galaxy. A crucial point in this analysis is that the predicted distribution function has the same form in 2 and 3 dimensions^{4,5}. Thus similar information on the gravitational clustering is contained in the 2 dimensional analysis as in the 3 dimensional analysis even though certain details may be lost in the 2 dimensional data.

2. Analysis

Saslaw and Hamilton³ have derived the probability distribution function for finding N galaxies in a volume V under the assumption that the galaxies interact gravitationally and evolve through a series of quasi-equilibrium states. The probability function is:

$$f_V(N) = \frac{\bar{N}(b+1)}{N!} [\bar{N}(1-b)+Nb]^{N-1} e^{-\bar{N}(1-b)-Nb} \quad (1)$$

where

$$\bar{N} = \bar{n}V$$

$$b = -\frac{W}{2K} \quad (2)$$

Here \bar{n} is the average volume number density of galaxies and b is the ratio of the gravitational correlation energy, W , among galaxies to twice their kinetic energy of peculiar motion. For a two dimensional distribution such as analyzed here, n becomes the average surface density of galaxies and V becomes A the area, but b retains its meaning.

The procedures described in Crane and Saslaw⁶ for generating and analyzing the neighbor distributions in terms of the function $f_N(\theta)$ have been used here. $f_N(\theta)$ is the probability distribution function for finding a 2 dimensional area $\pi\theta^2$ which contains N galaxies. For example, $f_0(\theta)$ is the void distribution and $f_1(\theta)$ is the distribution of the nearest neighbor distances.

Five hundred randomly chosen points were selected in the region to be analyzed and the histograms of the angular distances from each point to the first, second, third, etc neighbor provided an estimate of the function $f_N(\theta)$ for $N = 0, 1, 2, \dots, 5$. These histograms were then fit to the predicted distribution function to determine a value for b defined in Eq. 2.

In addition to the CfA slice as defined above, two slices above the CfA slice in declination, one below it, and the center of the CfA slice which contains the Coma cluster were analyzed. Table 1 summarizes these results and includes the previous results⁶ for the entire Zwicky catalog. Table 1 contains the values of b for the various samples as well as the most probable angle, θ , containing at least N galaxies.

Figure 1 shows plots of the derived histograms for the CfA slice and of the fitted function $f_N(\theta)$. As is evident in the figure and confirmed by the χ^2 values for the fits, the predicted function $f_N(\theta)$ is an accurate description of the histograms.

Table 1: Summary of fitting results

Sample	N=0		N=1		N=3		N=5	
	b	θ	b	θ	b	θ	b	θ
21-26	0.58	0.60	1.00	0.68	1.70	0.75	2.00	
Center of CfA slice	0.68	0.63	0.70	0.73	1.25	0.77	1.80	
27-32 (CfA slice)	0.63	0.58	0.70	0.68	1.50	0.73	2.10	
33-39	0.60	0.59	1.25	0.69	1.70	0.74	2.00	
39-45	0.56	0.54	0.80	0.66	1.70	0.68	2.45	
Zwicky Catalog	0.63	0.68	1.20	0.71	1.60	0.75	2.20	

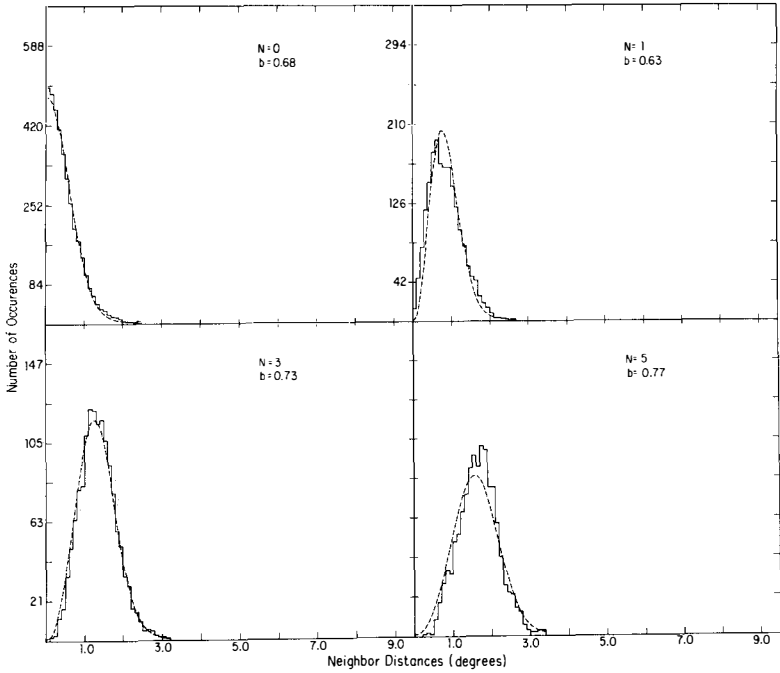


Figure 1: Plot of the histograms for $N=0,1,3,5$. The dotted lines are the fitted function $f_N(0)$.

3. Discussion

The rather simple analysis presented here conclusively demonstrates that the nature of the clustering of galaxies in the CfA slice is not significantly different than for the neighboring strips or the Zwicky catalog as a whole. The mean angles, θ , are smaller in the CfA slice. Nevertheless, the CfA slice is not peculiar relative to other similar slices as determined by the good agreement of the data with the predictions of the $f_N(0)$ statistic.

If the physical premises from which $f_N(0)$ has been derived are correct, then the close agreement between the data and the predictions imply that the observed clustering in the CfA slice, the neighboring slices and in the Zwicky catalog are dominated by gravitational effects. Exotic explanations (see ref. 5 for a summary) of the structure are not required.

References

1. deLapparent, V., Geller, M.J., and Huchra, J.P., 1986, *Ap.J. (Letters)* **302**, L1.
2. Zwicky, F., Herzog, E., Karpowicz, M., and Kowal, C.T., 1961-1968, *Catalog of Galaxies and of Clusters of Galaxies*, Vols. 1-6 (Pasadena: California Institute of Technology).
3. Saslaw, W.C., and Hamilton, A.J.S., 1984, *Ap.J.*, **276**, 13.
4. Itoh, M., Inagaki, S., and Saslaw, W.C., 1988, *Ap.J.*, in press August 1988.
5. Saslaw, W.C., and Crane, P., 1988, *Ap.J. (Letters)*, submitted.
6. Crane, P., and Saslaw, W.C., 1986, *Ap.J.* **301**, 1.

THE GALAXY AND MATTER DISTRIBUTION IN THE NON-LINEAR REGIME

Richard SCHAEFFER
Service de Physique Théorique[†] de Saclay,
91191 Gif-sur-Yvette Cedex, FRANCE



Non-linear structures are seen to be present in the Universe at nearly any scale : galaxies at the sub-Mpc scale, clusters and voids at scales ranging from 1 to 10, possibly 100 Mpc. These structures arise from initial conditions in the early universe that we are having difficulties in finding out. They arise also from the non-linear behaviour of gravitationally interacting matter inhomogeneities. It is of primordial importance to be able to disentangle the presently observed properties of the galaxy distribution that are due to non-linearity from those that are genuine tracers of the initial conditions. The matter (or galaxy) distribution may be described in terms of correlation functions , not only the usual 2-body correlations, but those of arbitrary order. We start from the suggestion of Peebles (1980) that the observed power-law behaviour of the 2-body correlation function may be explained by some "virialization" process. This in turn implies that the N-body correlation function also are powers-laws. In a series of papers (Schaeffer 1984, 1985, 1987a and b, Balian and Schaeffer 1988a,b,c,d, Schaeffer and Silk 1988) we have explored the consequences of this behaviour, and obtained predictions for the probability of holes, the galaxy and cluster luminosity functions, and more generally on the probability distribution of galaxy counts in a cell of any size, on the fractal distribution of galaxies and matter as well as on the cluster distribution in the past leading to an estimate of their X-ray emission and of the fluctuations they introduce in the microwave background.

[†] *Laboratoire de l'Institut de Recherche Fondamentale du Commissariat à l'Energie Atomique*

Theoretical scale-invariant distribution

The starting point is the two-body correlation function (Davis and Peebles 1983)

$$\xi(r) \sim (r/r_0)^{-\gamma}, \quad r_0 = 5h^{-1}\text{Mpc}, \quad \gamma = 1.8 \quad (1)$$

and the assumption that the N^{th} order function obeys

$$\xi_N(\lambda r_1, \dots, \lambda r_N) = \lambda^{-N(\gamma-1)} \xi_N(r_1, \dots, r_N) \quad (2)$$

From the knowledge of the N -body correlation functions one is able (White 1979) to deduce the probability of having no galaxy in a given volume

$$P_0(V) = \exp \sum_{N=1}^{\infty} \frac{(-)^N n^N}{N!} \int_V d^3 r_1 \dots \int_V d^3 r_N \xi_N(r_1, \dots, r_N) \quad (3)$$

where n is the number density of galaxies (or small pieces of matter if the matter distribution is to be considered). By successive derivations with respect to n , the probability of finding N objects in V is readily obtained

$$P_N(V) = \frac{(-)^N}{N!} n^N \frac{d^N}{dn^N} P_0(V) \quad (4)$$

In case ξ_N obeys the scaling relation, equ.2, P_0 can be expressed (Balian and Schaeffer 1988c)

$$P_0(V) = \exp \frac{\varphi(N_c)}{\bar{\xi}}$$

$$\varphi(y) = \sum (-)^N S_N y^N \quad (5)$$

$$\bar{\xi} = \int_V d^3 r_1 \int d^3 r_2 \xi(r_{1,2})$$

$$N_c = nV\bar{\xi}$$

Determination of $\varphi(y)$

The galaxy distribution and the counts in cell are thus determined by an unknown function $\varphi(y)$, or by the coefficients S_N of its series expansion. Early arguments were given (Schaeffer 1984) that S_N should not strongly decrease with N , and was more likely to be growing with N :

$$S_N \sim \mu^N \quad (6)$$

This was first for conjectured for simplicity in the structure of ξ_N as a symmetrized product of $N-1$ functions $\xi(r_{i,j})$, and then seen to be necessary (Schaeffer 1985 and 1987a) in order to explain the relatively large number of rich Abell clusters, that decreases only exponentially with luminosity. It implies that the N -body correlation functions grow as $N!$ More specifically (Balian and Schaeffer 1988c), the data require S_N to behave as

$$S_N \sim (1/y_s)^N, \quad y_s \sim 0.1 \quad (7)$$

A rapid decrease of S_N , on the other hand, would lead to a severe discrepancy. For instance $S_N \sim 1/N!$ implies a luminosity function decreasing as $(L/L_c)^{-L/L_c}$ instead of $e^{-y_s L/L_c}$ that is a many order of magnitude too small for rich Abell clusters ($L \sim 100L_c$). Surprisingly enough the calculation of S_N by Fry (1984) from the exact gravitational (BBGKY) equations of motion cannot explain the Abell cluster abundance. This difficulty was partly resolved when Hamilton (1988) found an error in the latter calculation of S_N and, from an approximate solution of the BBGKY equation, deduced that S_N should be about constant for large N , much closer to the behaviour, equ.7, required by the data. This, however, is still not sufficient since $S_N \sim \text{cst}$ would underestimate $L_* = L_c/y_s$ by a factor $1/y_s \sim 10$, and still lead to much too rapid a decrease of the luminosity function.

The original determination (Schaeffer 1984) of $\varphi(y)$ used the (two-dimensional) probability for having no galaxy in a given angular sector, as determined by Sharp (1981) from the Zwicky catalog. It lead to $\mu \sim 3-12$, close to the estimate (7) deduced from Abell clusters. The function $\varphi(y)$ should be nearly the same (Schaeffer 1984 and 1987b) at two and three dimensions, and the CFA data provided a much more precise determination (Bouchet and Lachieze-Rey 1986, Maurogordato and Lachieze-Rey 1987) of the function φ , that turned out to be consistent with the early 2-dimensional determination. The form (5) of P_0 thus is compatible with the large scale 3-dimensional statistics.

Scaling of the counts in cell (Balian and Schaeffer 1988b,c)

From eqs.4-5, the probability for finding N galaxies can be deduced. Firstly a bound on $\varphi(y)$ can be obtained from the fact that these probabilities take necessarily values between 0 and 1. It can be shown this way that φ must behave as a power-law for large y (times some possible logarithmic factors)

$$\varphi(y) \sim a y^{1-\omega}, \quad 0 \leq \omega \leq 1 \quad (8)$$

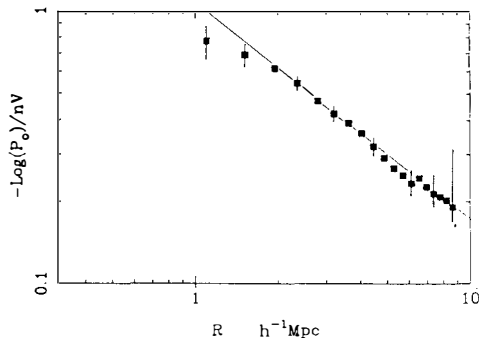


Fig. 1 From Alimi et al (1988) Probability of holes extracted from the CFA catalogue and compared to the power-law predicted (Balian and Schaeffer 1988) by the theory.

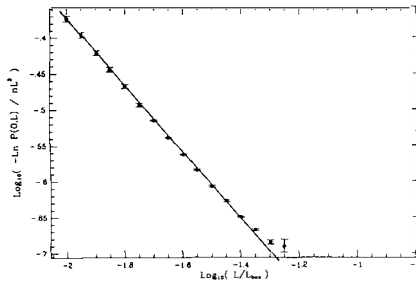


Fig. 2 From Bouchet et al. (1988). Probability of holes extracted from the Cold Dark Matter simulations (Davis et al. 1985) and compared to the power-law predicted (Balian and Schaeffer 1988) by the theory.

This was subsequently checked (Alimi, Blanchard, Schaeffer 1988) against the CFA data (Fig.1), that indeed lead to the predicted behaviour. The latter is already apparent in the earlier determinations of P_0 from the CFA (Bouchet and Lachieze-Rey 1986, Maurogordato and Lachieze-Rey 1987), but had not been noticed. The value of ω implied by the power-law behaviour of $\ln P_0$ as a function of the volume V depends on the value of γ , equ.1, that is chosen, that varies somewhat from sample to sample and even with scale, $\bar{\xi}$ being not exactly a power-law :

$$\omega_{obs} \sim 0.4 - 0.7 \tag{9}$$

An examination (Bouchet, Schaeffer, Davis 1988, Bouchet, this conference) of the numerical simulations with Cold Dark Matter initial shows (Fig.2) also that φ is a power-law, with

$$\omega_{CDM} \approx 0.45 \tag{10}$$

The prediction (8) then seem well verified.

Another prediction can be made using solely the relation (2). For

$$N \gg N_V = N_c \bar{\xi}^{-1/1-\omega} \tag{11}$$

The probability $P_N(V)$ obeys a scaling relation, in the sense that

$$\frac{N_c^2}{nV} P_N(V) = h(N/N_c) \tag{12}$$

is not a function of the quantities N , n , V and $\bar{\xi}$ separately, but a function $h(N/N_c)$ of the unique variable N/N_c , that can be calculated once $\varphi(y)$ is known. The mass function can be deduced (Schaeffer 1987a) from P_N and has the same scaling, and so for the luminosity function :

$$\begin{aligned} \frac{L_c^2}{\rho_L} \eta(L)dL &= H(L/L_c)dL \\ L_c &= \rho_L \bar{V} \bar{\xi} \end{aligned} \tag{13}$$

Most interesting, the properties of φ allow us to deduce the behaviour of

P_N and $\eta(L)$, which is the same, for small and large values of N/N_c or L/L_c . At large N or L

$$\begin{aligned} P_N &\sim e^{-y_8 N/N_c} \\ \eta(L) &\sim e^{-y_8 L/L_c} \end{aligned} \quad (14)$$

At small N or L

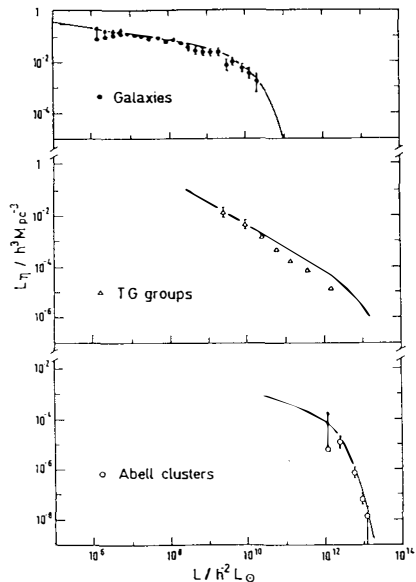
$$\begin{aligned} P_N &\sim (N/N_c)^{2+\omega} \\ \eta(L) &\sim (L/L_c)^{2+\omega} \end{aligned} \quad (15)$$

This is very reminiscent of the Schechter form of the galaxy luminosity function, as well as of the current parametrisations of the cluster luminosity function. Assuming galaxies correspond to a constant radius, independent of the luminosity we get the relation between ω and the parameter α of the Schechter function

$$\omega = 2 + \alpha \quad (16)$$

consistent with the values of ω , eqs.9 and 10, obtained from observations. Using the Schechter function to obtain H , from the relation between the radius $R_G \sim 0.05$ Mpc of a galaxy and the Abell radius $R_A = 1.5h^{-1}$ Mpc we then get a prediction for the cluster luminosity function using the proper scaling of $N_c(R)$. A similar calculation can be made for Turner-Gott groups. Both are seen to match the data fairly well (Fig.3), showing again that the scale-invariance of the correlation functions is readily built in the data. We have also shown that there is a cut-off at the faint end, precisely at $N \sim N_V (L = L_V \equiv L_c \bar{\xi}^{-1/1-\omega})$.

Fig. 3 From Balian and Schaeffer (1988). Theoretical predictions for the luminosity function of TG groups and Abell clusters using the scaling, eq. 13, to relate the latter to the galaxy luminosity function. This scaling is implied by the power-law behaviour, eq. 2, of the many-body correlation function.



Fractal dimensions of the galaxy distribution (Balian and Schaeffer 1988a,b,d)

The counts in cells can be used to determine the fractal dimensions of the galaxy distribution. Fractals are very common in nature (Mandelbrot 1971), but there is a large number of fractal dimensions and fractal indices. The simplest fractal has only one "fractal" dimension that can be obtained in several ways. The number of neighbour of a given point (here, a galaxy) within a cell of volume ℓ^3 behaves in this case as

$$N_{nb} \propto A(\alpha) \ell^\alpha \quad (17)$$

α is a fractal index, it does not play the role of a dimension. On the other hand, the number of cells which contain a number of particles that behaves as α a power of ℓ that is between α and $\alpha + d\alpha$ may itself be a power-law

$$N_\alpha = B(\alpha) \ell^{-f(\alpha)} d\alpha \quad (18)$$

The exponent $f(\alpha)$ is the dimension of the set of cells whose content behaves as ℓ^α , as can be easily seen by trying to cover a lign or a surface with cells of size ℓ^3 .

A third way of defining a fractal indices is to consider the probability p for a cell to be occupied, estimated from the number of points it contains divided by the total number of points, and by forming

$$C_q = \sum_i p_i^q \quad (19)$$

where the sum runs over all occupied cells. Whenever C_q is a power-law of ℓ , from

$$C_q \propto A_q \ell^{(q-1)D_q} \quad (20)$$

fractal indices D_q can be defined. For a simple fractal $\alpha = f(\alpha) = D_q$ are the same and take a unique value which is called the fractal dimension of the system. A multi fractal (Henschel and Procacia 1983) has a whole distribution of indices. Relations exist between α , $F(\alpha)$ and D_q . For instance, there is a theorem that was thought to be general that D_q must be a decreasing function of q .

For $q = 0$, D_0 is usually called the Hausdorff dimension and D_2 the correlation dimension. The above property implies $D_0 \geq D_2$ which is verified in all known fractal systems. From the definition (19) for C_q and calculating the latter by using (17) for the number of points that a cell contains, one gets the relations

$$\alpha = \frac{d}{dq} (q-1)D_q, \quad f(\alpha) = \alpha q - (q-1)D_q \quad (21)$$

The fractal indices exist only provided the corresponding N_{nb} , N_α or C_q are power laws of ℓ . They are then defined as

$$\alpha = \frac{\partial \ln N_{nb}}{\partial \ln \ell}, \quad F(\alpha) = \frac{\partial \ln N_\alpha}{\partial \ln \ell}, \quad D_q = \frac{1}{q-1} \frac{\partial \ln C_q}{\partial \ln \ell} \quad (22)$$

It has been customary to use a more approximate definition by taking the

ratio of the logarithms that are more easy to compute, for instance D_q is usually replaced by

$$\tilde{D}_q = \frac{1}{q-1} \frac{\ln C_q}{\ln \ell} \quad (23)$$

that is equivalent to (21) provided the coefficient A_q is of order unity. However, the very essence of the fractal dimensions is the power-law behaviour of (17,18,19). For most fractal systems, the latter holds over a limited range of values of ℓ : there is always a lower as well as an upper cut-off at which these power laws break down. For some other systems, there is no lower or upper scale.

The average number of neighbours of a galaxy behaves according to (1) as $n\ell^3 + n\ell^{3-\gamma}\ell_0^\gamma$, so for $\ell \ll \ell_0$ we expect the galaxy distribution to exhibit a fractal behaviour and $\alpha = 3 - \gamma$ to be one of the fractal indices. It is readily seen from (1) that there is an upper scale $\ell_0 \approx 2r_0$ above which this fractal behaviour no longer holds. Also a lower scale, that might be much smaller than the galaxy size, is expected. Whether this index $3 - \gamma$ is the only one can be seen by calculating the distribution of values of α , and the other fractal indices $f(\alpha)$ and D_q . These values were extracted from the CFA catalog by Jones et al. (1988) who found, by using the definition (23), that D_q is a decreasing function of q , as expected, that all values of α between 0.6 (large q) and 2.6 (small q) are possible whereas $f(\alpha)$ can take values between 0 and 1.5, the galaxy distribution being thus a multifractal. We have calculated these indices. When we use the approximate definition (23), we find similar results. The fractal indices obtained this way, however, do not correspond to the power-laws of (17,18,20), because the definitions (23) and (22) are not equivalent in this case, the one giving the fractal exponents being (22), not (23). The calculation of these exponents gives a function D_q that increase with q (the proof for it to be decreasing relying on (23) that does not give D_q in this case). The Hausdorff dimension is found to be $(3 - \gamma)\omega$ and the correlation dimension $3 - \gamma$. From (8), we see that the galaxy distribution corresponds to $D_0 \leq D_2$, and is seen to be the first known system to exhibit this reversed behaviour. The calculation of α and $f(\alpha)$ shows that the galaxies do not form a multifractal, only two values of α being statistically significant

$$\alpha = 0, \quad f(\alpha) = (3 - \gamma)\omega \quad (24)$$

corresponding to cells containing isolated galaxies and clusters and

$$\alpha = 3 - \gamma, \quad f(\alpha) = 3 - \gamma \quad (25)$$

corresponding to cells contained within a cluster. The galaxy distribution thus forms a bifractal system (intermediate values of α may exist, but are not statistically significant in the sense they do not modify the power-law behaviour of C_q , that is the values of D_q). The direct check of these predictions against observations is difficult, the definition (22) being much less suited for computational purpose. It may be possible using large numerical simulations and is presently undertaken by Bouchet et al. (1988) -see the contribution presented at this meeting-

Cluster evolution (Schaeffer and Silk 1988)

The "virialization" argument that has been used (Peebles 1980) to advocate for power-law N -body correlation functions also leads to a well-defined redshift dependence of these correlation functions.

Predictions for the galaxy and cluster distribution in the past can thus be

made using

$$\xi(r) = (1+z)^{-(3-\gamma)} (r_{\text{com}}/r_0)^{-\gamma} \quad (26)$$

and $\xi_N \propto (1+z)^{-(N-1)(3-\gamma)}$. Relation (26) holds as long as ξ is given by the non-linear equations of motion. Numerical simulations (Davis et al. 1985) show that as long as the correlation function is small, and given by linear theory, practically no clusters are present. But as soon as it turns non linear, it grows very rapidly and evolves very soon according to (26). It is then possible to use the previous results to calculate the evolution of the distribution of virialized clusters up to some (possibly scale-dependent) redshift z_{NL} where the correlation functions turn non-linear.

The cluster luminosity function is qualitatively the same as for galaxies (eq.17) : a power-law behaviour at the faint end, with an exponential cut-off. Using a radius $R \sim L^{1/3}/(1+z)$ that ensures that the density contrast is larger than say, 200 and so that the cluster is virialized, L/L_c is changed into $(L/L_{c\ell})^{\gamma/3}$ since $L_c \propto R^{3-\gamma}$ and $H(L/L_c)$ into another function $H_{c\ell}(L/L_{c\ell})$. The typical cluster luminosity thus scales as

$$L_{c\ell}^* = 1.2 \cdot 10^{12} (1+z)^{-3(3-\gamma)/\gamma} h^{-2} L_{\odot}. \quad (27)$$

Eq.(27) is the non-linear analogue of the typical luminosity derived by (Kaiser 1986) from linear theory, but in this improved calculation we obtain a very large spread of L around the value (27). For $L \ll L_{c\ell}^*$, the distribution is a power-law, for $L \gg L_{c\ell}^*$ it has an exponential cut-off.

The X-ray luminosity function can be calculated in the same way. Assuming that the electron density of the intergalactic gas scales as the optical luminosity density, L_x scales as $T^{1/2} L^2 R^{-3}$ where T is the virial temperature. For virialized clusters, L/L_c can be written as $(L_x/L_x^*)^{\gamma/4}$ with a typical X-ray luminosity

$$L_x^* = 1.8 \cdot 10^{43} (1+z)^{(15\gamma-24)/2\gamma} \text{erg}^{-1} \quad (28)$$

with again a very large spread around this values. Note that this luminosity increases nearly as $1+z$ with redshift. This is at variance with the predictions (Kaiser 1986) based on linear theory that lead to a value of L_x^* that decreases, and is a genuine non-linear effect. The radius of the typical cluster is

$$R_{c\ell}^* \sim 1.7 (1+z)^{-\frac{3}{\gamma}} h^{-1} \text{Mpc} \quad (29)$$

that decreases faster than $(1+z)^{-1}$. The typical cluster thus stays quite hot, its temperature

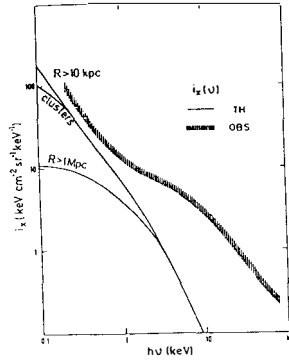
$$T_{c\ell}^* \sim 1.8 \cdot 10^7 (1+z)^{-3(2-\gamma)/\gamma} \text{K} \quad (30)$$

decreasing very slowly at high redshift, although an additional factor $1+z_{\text{due}}$ to the general expansion is to be added to (30).

The total X-ray emission is very large at the smaller (<1 keV) frequencies, due to the large number of small objects and the high temperature of the typical cluster even at large redshift. The integrated X-ray background (Fig.4) depends weakly on the redshift z_{NL} at which the universe turns non-linear. It is somewhat more sensitive to the smallest cluster that may contain hot gaz. Assuming that all objects with

$R > 100$ kpc did not cool, we see that clusters contribute a large fraction of the observed X-ray background in the sub-keV region.

Fig. 4 From Schaeffer and Silk (1988). Calculation of the X-ray background due to virialized clusters, using the luminosity function implied by the power-law, eq. 2, behaviour of the many-body correlation function and the redshift dependence, eq. 26, of the latter that this behaviour implies.



Clusters containing hot gas also shift the microwave background temperature (Sunyaev and Zeldovich 1981). From $\Delta T/T \sim T_0 g_{\text{e}z} R$, we obtain a mean diminution along a line of sight, $y = \sum_{\text{clusters}} (\Delta T/T)$ that is comparable to the shift $\Delta T/T \sim 3 \cdot 10^{-5}$ produced by an Abell richness class II cluster. This is because of the contribution from many (typically ~ 5) small clusters that are present along any line of sight. This induces large fluctuations at the minute-arc scale, also of the order of $3 \cdot 10^{-5}$, and similar size residual fluctuations, independent of angle, at the 4.5 resolution of the Uson-Wilkinson experiment, provided all clusters with $R > 100$ kpc contain hot gas.

REFERENCES

- Alimi J., Blanchard A., Schaeffer R., 1988, in preparation
Balian R., Schaeffer R., 1988a, *Compte Rendus Acad. Sciences* 306, série II, 689.
Balian R., Schaeffer R., 1988b, submitted to *Ap. J. Lett.*
Balian R., Schaeffer R., 1988c, submitted to *A.A.*
Balian R., Schaeffer R., 1988d, in preparation for *A.A.*
Bouchet F., Lachieze-Rey M., 1986, *Ap. J. Lett.* 302, L37
Bouchet F., Schaeffer R., Davis M., 1988, in preparation
Davis M., Efstathiou G., Frenk C., White S.D.M., 1985, *Ap. J.* 292, 371
Davis M., Peebles P.J.E., 1983, *Ap. J.* 267, 465
Hamilton A.J.S., 1988, to be published
Jones B.J.T., Martinez Y.J., Saar E., Einasto J., 1988, to be published
Kaiser N., 1986, *M.N.R.A.S.* 222, 373
Mandelbrot B., 1977, *Fractals : Form, chance and Dimensions*
Maurogordato S., Lachieze-Rey M., 1987, *Ap. J.* 320, 13
Peebles P.J.E., 1980, *The large Scale Structure of the Universe* (Princeton: Princeton University Press)
Schaeffer R., 1984, *A.A. Lett.* 134, L15
Schaeffer R., 1985, *A.A. Lett.* 144, L1
Schaeffer R., 1987a, *A.A. Lett.* 180, L5
Schaeffer R., 1987b, *A.A. Lett.* 181, L23
Schaeffer R., Silk J., 1988, *Ap. J.* 333, in press
Sharp N., 1981, *M.N.R.A.S.* 195, 857
Sunyaev R., Zeldovich Ya.B., 1981, *Ap. Sp. Phys. Rev.*, 1, 1
Uson J.M., Wilkinson D.T., 1984, *Ap. J. Lett.* 272, L1
White S.D.M., 1979, *M.N.R.A.S.* 186, 145

THE STATISTICS OF GALAXIES : BEYOND CORRELATION FUNCTIONS

Marc Lachièze-Rey

Service d'Astrophysique

CEN-SACLAY

91191 GIF sur YVETTE CEDEX, FRANCE

ABSTRACT

I mention some normalization problems encountered when estimating the 2-point correlation functions in samples of galaxies of different average densities. I present some aspects of the void probability function as a statistical indicator, free of such normalization problems. Finally i suggest a new statistical approach to give an account in a synthetic way of those aspects of the galaxy distribution that a conventional method is unable to characterize.

I - Introduction

The study of the distribution of galaxies in space is an increasing field of development, with the main motivations of checking the different models for galaxy and large scale structure formation. A large amount of work has been devoted to establish the predictions of the scenarios for galaxy formation, like for instance biased formation with cold dark matter, so that they can be compared with observation. I will concentrate here on the spatial organization of the galaxies, as a point distribution in space, and to the tools for characterizing its statistics. These tools are mainly used for comparison of the real distribution with statistical models, for instance those characterizing initial conditions properly evolved (or preserved if it can be assumed that it is so), as well as the results of dynamical analytical calculations or numerical simulations. These tools can be also used for the comparison between different samples of galaxies, for instance in the purpose to detect a possible morphology, or luminosity segregation, as predicted by some models of galaxy formation; or to check if the clustering properties of galaxies do vary in space. Up to now the most widely used statistical tool has been, mainly for practical reasons, the 2 point correlation function (hereafter cf). However, this approach is very near from reaching its limitations, for different reasons, and there is a need for other and complementary indicators; after some remarks concerning the use of cf (II), and having presented the void probability function (hereafter vpf) which has shown to be an efficient tool (III), I will suggest new kinds of possible approaches for the next future.

II - Correlation functions.

A definition of 2 point cf, in the purpose of studying the galaxy distribution, can be found for instance in Peebles (1980). I will refer principally to the probabilistic definition, which is of practical use and has been the most widely employed in the context of astrophysics : the estimations of cf encountered in the literature are based on measurements of these probabilities for some defined samples of galaxies (the catalogs).

The main result, that cf can be described by a power law with exponent -1.8 , and correlation length about $5 h^{-1}$ Mpc, is well known.

There is however no general agreement concerning the level of the cf at scales larger than about $10 h^{-1}$ Mpc, so that this statistical tool appears, for the moment, mainly useful in the non linear range from .5 to $10 h^{-1}$ Mpc. Concerning mainly the non linear behaviour development of perturbations (which can be hardly calculated), the observed form of ξ is rather used as a kind of normalization for the numerical simulations : any simulation of a process generating large structure must give, at first order, the right spatial density, and at second order, the right 2 point cf etc. By the way we know that this constraint is not trivial since it led to reject simple scenarii for galaxy formation with hot or cold dark matter and to include the hypothesis of biasing.

Other indicators have been used, like cf of higher order, or the moment distributions associated, but they are of the same "family" . Since it is expected in some models of galaxy formation that luminosity or morphology segregation is present in the galaxy distribution, there is a hope that cf could be an efficient tool for testing such effects. On the other hand, it has been reported (Einasto, 1985) that the estimation of cf seems to vary with the size of the sample under study. Such an effect has been invoked by Calzetti et al. (1987) to suggest a fractal character of the galaxy distribution. I will criticize these approaches below by showing that normalization effects are a source of difficulties.

Normalization of the 2-point correlation function

Any measurement of ξ is performed by counting pairs of galaxies in the catalog, and then dividing the result by a corresponding number for an uniform Poisson distribution. This number is in fact introduced as the best way to estimate the volume sampled; it is generally measured from a realization of a random distribution, or calculated analytically. In any case, establishing this number of pairs requires to assign a value to n_r , the spatial point density of this random catalog. This is due to the fact that the probabilistic definition of ξ is a conditional one : $(1 + \xi) n_r^2 dV_1 dV_2$ is the probability for finding both an object in dV_1 and another in dV_2 , with the (implicit) assumption that the probability to find one galaxy in dV is $n_r dV$. This necessity of choosing a value for n_r acts as a normalization for calculating ξ . In fact it is easy to show that if normalization is changed from n_r to n_r' , the estimation of ξ changes from ξ to $\xi * n_r / n_r'$.

This is not a priori a difficult situation. The result is

normalization dependent, but we only have to choose the right normalization. For instance, if we try to estimate the absolute value of the cf of galaxies, we want to use, as normalization density n_r , the spatial density of the galaxies in the universe. The natural way to estimate this latter is to take the largest sample available (for instance the CfA for a 3-dimensional analysis), to count the galaxies and, dividing by the volume, to get an estimation n_{CfA} . Then we count the pairs, we normalize by $n_r = n_{CfA}$ and get ξ_{CfA} . Can we then claim to have measured universal values? Concerning the density, the question is: are they still density fluctuations at the scale of our sample? (By this we mean the size of a complete sample extracted from it, let say of typical size about 40 Mpc). We know that large voids do exist at this scale, and even at larger scale. So that our sample itself is almost certainly contained inside a fluctuation, probably of order not very much smaller than 1. Thus we cannot claim that n_{CfA} is a good estimate of n .

What about ξ ? The use of n_{CfA} for normalization (what other value is available?) leads to an estimate ξ_i (i for intrinsic). If we had the true value n_u of the galaxy density in the universe (but by which mean?), we would estimate $\xi_e = \xi_i * n_{CfA} / n_u$ (e for extrinsic). Even in this case, we would not be able to claim that ξ_e is the right estimation of ξ since ξ may also fluctuate like n (unless we can demonstrate that it does not). To resolve this question it would be useful to have an other catalog similar the CfA (like for instance in the south hemisphere) to estimate the order of magnitude of the fluctuations: independent estimations of n and ξ would be made, and compared to those of the CfA.

The same problems are present at smaller scale, even with a stronger level of fluctuations. They appear when we examine subsamples of the existing catalogs, since we know that these subsamples (smaller than the CfA) cannot be fair samples of the universe, and that the density fluctuates from one to the other (by the effect of voids, or superclusters for instance). This is the case when we search for differential effects (like luminosity segregation) since this implies precisely to examine subsamples with different characteristics.

For instance, we have made such a study inside the CfA catalog (see the paper by Maurogordato in this volume): we consider different (complete) subsamples with different shapes, sizes, and locations. As an effect of fluctuations, they have different intrinsic densities n_{i1} , n_{i2}, \dots (intrinsic density means only the number of galaxies divided by the volume of the subsamples).

However, for a given sample, the "conventional" normalization (that we will call "extrinsic") requires to use, as a value for n_r , not the effective density n_i of the subsample, but the average value n_e (e for extrinsic), characterizing the large scale distribution. In a smooth distribution, it is expected that different samples defined with the same selection criteria have effective densities of about the same value, not very different from n_e (i.e that they are realizations of a homogeneous statistical process). If the samples are of different luminosities, it is expected that their densities can be calculated from a common luminosity function.

But the reality is very different from this ideal situation ; different samples defined with the same selection criteria have very different values of n_i , as it is easy to check ; and the values of n_i for subsamples of bright and faint galaxies do not reflect any universal luminosity function (see for instance Maurogordato and Lachieze-Rey, 1987 and 1988, hereafter ML1 and ML2). In such a disordered situation, the utility of the extrinsic normalization can be questioned.

There is an other possibility for normalization, although it does not correspond to the true definition of the cf, as given by Peebles (but the Peebles definition implicitly requires an homogeneity of n , which is not the case). This "intrinsic" normalization assigns to n_r the intrinsic value n_i , as it is measured in the sample. It has the advantage of requiring no hypothesis concerning the true density, or luminosity function, of galaxies in the universe, but to be entirely pursued from the available data.

Of course the 2 quantities ξ_i and ξ_e , calculated using the 2 normalizations do not measure the same thing. According to the definition, ξ_e is the "true" cf, but the question is to know if it gives the desired information, or if ξ_i is more convenient. A first answer could be that neither of both is really convenient. For instance Alimi and Blanchard (1988) remarked that, although ξ_i or ξ_e are normalization dependent, the product $(1+\xi) * n$ is not (although this is only true if ξ is estimated by their method) and can be used as a statistical indicator. We will show below that the VPF is also normalization independent. However the large use of ξ in the literature justifies to discuss the validity of ξ_e and ξ_i as possible statistical indicators. As a contribution to the debate, I present below a toy model as an illustration of the problem.

A toy model

Let us for instance imagine an idealized situation, and assume that we know some statistical process able to distribute points in space, with an homogeneous 2 point correlation function ξ . We can generate, for instance, two samples, 1 and 2, with different densities n_{i1} and n_{i2} ($n_{i2} > n_{i1}$), but, by definition, with the same correlation functions. Suppose now that we are interested in measuring the statistical properties of these samples (considered as two realizations of the given statistical process), seen as fluctuations around a mean value n_e (averaged over a collection of such samples). If we now count the pairs in the 2 samples, there will of course be more pairs in the densest sample, just by the density effect. Using the extrinsic normalization, we can immediately infer that $\xi_{e2} > \xi_{e1}$, more precisely that $(1+\xi_{e1})/n_{i1} = (1+\xi_{e2})/n_{i2}$ since $1+\xi_e$ is, in this case, proportional to the number of pairs. Thus the extrinsic normalization gives us no chance to recognize that the 2 samples are two realizations of the same process, that they are, in some sense, similarly clustered. In fact a large part of the information contained in ξ_e is already contained in the knowledge of n for the sample (since n is still fluctuating at this scale). For the intrinsic estimation, this is not the case and we would find that $\xi_{i1} = \xi_{i2}$.

We should note at this point that other prescriptions for calculating ξ could even lead to worse situations for the extrinsic normalization. For instance, if the number of pairs in the random catalog (used for normalization) is not calculated using the points were they are galaxies in the real catalog, but where are the galaxies in this random catalog, then we have: $(1+\xi_{e1})/(n_{i1} * n_{i1}) = (1+\xi_{e2})/(n_{i2} * n_{i2})$.

This is also the case if the normalization for the random catalog is calculated analytically with the density n_e . Thus if we try to recover the results that the different samples are different realizations of an unique process, the usefull quantity is ξ_i (or the indicators mentionned before). ξ_e gives us a mixed information, already partially contained in the knowledge of the density of the sample. Since, in any case, the average density n must be known in order to use the extrinsic normalization, there is no big advantage to use it.

The Void Probability function

It is known that the complete knowledge of a statistical process is contained in the hierarchy of correlation functions; the density and the 2 point cf are the first and second order quantities in this hierarchy. Although the 3, 4 and 5 points have been estimated, there is no chance to go any further in a direct way. But it has been shown by White (1979) that the VPF contain information of higher degree in the hierarchy and is, in this sense, complementary to the cf. Concerning normalization properties, the VPF does not seem, at first sight, very attractive since it depends on both the volume and the density ; the 2 point cf, conversely, depends only on the volume, not on the density, at least in principle. But the situation is in fact much more favorable if we use not $\phi(V)$ as a function of the volume but the quantity $\chi = \log \phi/n V$ as a function of the variable $q = n V \langle \xi \rangle$. For distributions obeying to what has been called the scaling invariance property (see for instance Schaeffer, 1987), the function $\chi(q)$ is independent on the density. We have shown (ML1, ML2) that the galaxy distribution obeys to this scaling invariance, so that $\chi(q)$ is a usefull indicator. This property was predicted by Schaeffer on the basis of hierarchical models. But we have also shown (ML2) that, if χ shares with the cf the property of beeing density independent, it has the advantage of beeing also normalization independent. This allowed us to derive results concerning the segregations mentionned before, independently of the normalization. These results are presented elsewhere in this volume. One of the striking facts is that the apparent existence of a segregation in clustering properties, as measured by the correlation functions, does not imply a corresponding segregation as measured by the VPF. For instance we have shown that samples containing different galaxy morphological types, or of different sizes, have different values of 2-point cf (although the sign and the level of the differences depend on the adopted normalization), although there are no differences in the VPF. Conversely, the luminosity segregation is apparent with both indicators. This clearly indicates that cf and VPF do not measure the same kind of clustering properties. The main interest of the study with the VPF was to allow to establish the property of scale invariance .

How to characterize the galaxy distribution ?

The 2-point (and the small order) of give information at the lowest order in the hierarchy. But it becomes increasingly clear that some features of the galaxy distribution cannot be accounted for by such

indicators. This is the case for the presence of voids, the possible organization of galaxies in elongated (filaments) or flattened (pancakes) structures. Although such structures are usually referred to at scales of the order or greater than supercluster size, it is more and more apparent that such features are present even at smaller scales. We can think for instance to a network of bubbles, as it appears at least qualitatively from the visual appearance of the CfA catalog (de Lapparent et al. 1986), or as it is predicted by models or explosive galaxy formation.

If the galaxies are really distributed in such a way, it is of great interest to characterize quantitatively the features of this network : the dimensionality, the connectivity properties, the sharpness of the edges, etc. It is clear that the language of cf is unadapted for such a task. Moreover, the presence of such features is very difficult, for the moment, to predict from dynamical studies. One reason is that there is no widely accepted statistical method to characterize such effects. In the last years, new types of analysis have been applied to the study of the galaxy distribution, with more or less success. The VPF can be considered as a first step in this way since it includes information at all orders. For instance the fact that scale invariance can be shown from it is very encouraging. Other methods are percolation (Shandarin and Zeldovich, 1986), analysis in terms of fractals or multifractals (Jones et al, 1987, Schaeffer and Balian, 1988), topology analysis (Gott et al., 1986, Melott et al., 1988), tessellation (Icke and van de Weygaert, 1987), and probably many others of which the author is unaware. The problem is that these different indicators give different kinds of information, not easy to compare between themselves, or with the prediction of a dynamical model. There is no general agreement concerning one type of analysis like the one which developed around the use of cf ; so that it appears necessary to develop a method of analysis allowing to characterize the different aspects of the spatial distribution of galaxies, including the most striking to the eye, as well as to synthetize them in a common formalism, which ideally could be related to some dynamical processes .

IIII - The cluster aggregation approach

The universe, as it appears from recent observational results, is an highly structured, but also highly disordered medium. This is the reason of the difficulties encountered with a conventional statistical

approach. Since the statistics of disordered media is an increasingly well studied field in physics, it is tempting to try to adapt its methods for the study of the universe (remember that the use of cf also resulted from the adaptation of techniques from a very different field to astrophysics). This is already the case for the use of fractal analysis which, mainly developed in microscopic statistics, is becoming increasingly used in astrophysics. I will here suggest a new approach, also derived from the study of disordered media. More precisely, this approach is derived both from the study of percolation clusters, and from the dynamics of the so called "cluster aggregation", and gelification models.

This approach is rapidly presented below. Its main interest lies in two points. First it suggest an analysis able to characterize features of unconventional statistics (those which seems to be present in the galaxy distribution and that conventional indicators are unable to take into account). It appears also a priori very convenient for a synthetic approach since it can be related to the others indicators used up to now: the link with the VPF is very straightforward. The connexion with fractals can be said to be contained in the method, since the objects defined during this analysis are themselves fractal: different kinds of fractal dimensions are very easy to extract from the analysis. The link with the percolation studies is also very natural since the method is adapted from the study of percolation clusters. It is also expected that the information concerning the topology is contained in this approach; this seems natural since the method is very sensitive to the topology of the distribution and posses some common characteristics with the topology analysis already developed by Gott et al. (1986). The quantitative relations remain however to be calculated.

Additionally, this approach concerns the variation of clustering properties of galaxy groups and clusters with their richness. Although such studies have been made for various cases (like comparison of the cf between galaxies and clusters, or between clusters of different richness classes), the analysis presented here deals with it in a more systematic and synthetic way.

The method

I will present here only the gross features of the methods. Further details will be given in a next paper. Starting from the distribution of points to be studied, we create a geometrical object by the following

rule : given a length L (the "scale variable"), we "fill up" the space around each point of the distribution, up to distance L . In other words, we consider a distribution of spheres of radius L , and having for center every point of the distribution. Some of these spheres are isolated, some other are in contact or intersect. These latter are said to form a cluster. The new object created is therefore the reunion of clusters and of isolated spheres (which can be considered as clusters of multiplicity 1). Each cluster will be characterized by the volume V that it occupies in space. Of course the volume of a cluster of multiplicity 1 is $4 \pi L^3/3$ but the volume of a cluster of multiplicity k is between this value and k times this value. We will be interested in the distribution of clusters, as a function of the volumes V . Of course the definitions of clusters depend on the scale L , and also the distribution function, so that this latter can be written as a function of the 2 variables : $N(L, V)$.

We propose the use of $N(L,V)$ as a statistical indicator. First of all, there is no special difficulty for its calculation, like those encountered for instance in the calculation of cf , because of normalization problems ; we have already developed a code in such a purpose. In addition, it can be expected that the predictions for a gaussian distribution (useful as a reference) are not too difficult to calculate analytically.

It is very straightforward to express the link with the VPF and this will be presented in a subsequent paper. More peculiar are the links with fractal analysis. I will not detail those here but only point out that the geometrical object that we have defined is of the same nature as the percolation cluster for a given distribution, although it is more rich since it contains information not only concerning the percolation cluster, i.e. the largest cluster in the sample, but also clusters of all sizes (Stanley et al., 1986). However it is relevant to use for its study the same tools than for percolation studies, i.e. the whole serie of different fractal dimensions (Stanley et al., 1986). Our purpose here is not to promote this use, but rather to remark that the conversion from one langage to an other is possible and that all properties expressed in the langage of fractals, can also be expressed by the use of N , and, in our sense, in a more synthetic way. Of course it also results that all percolation properties are contained in N . If we remember that percolation as a statistical tool was criticized for the reason that it had not very convenient scaling properties, it is worth to remember that the aggregation analysis gives additional information concerning the

dimensionality (or dimensionallities) of the distribution : this is very encouraging since, precisely, the "scaling" difficulties for the percolation analysis came from the fact that the dimensionality of the distribution under study is not necessarily 3 (in a 3-dimensional analysis).

Of course many benefits of this method come from the work already done by different authors with the same formalism, although in a very different context. A similar quantity has been introduced for the purpose of studying the so-called cluster aggregation models (Kolb et al., 1986). In this latter case, a dynamical process is considered, where the clusters (defined in a very similar way than above) grow dynamically with the time t . In fact the dynamics of these models implies that the sizes of the clusters increase with t , so that the parameter t can be regarded as playing about the role played by L in our analysis. This analogy suggests many developments useful for the analysis of the point statistics. For instance, a scaling can be applied to the distribution under study so that the evolution of $N(L,V)$ with L mimick the cluster aggregation dynamics, i.e. the time evolution for this model (in fact we must compare the evolutions of the scaled quantities). This is only an analogy but it can be hoped that it will unveal some details of the dynamics underlying the galaxy distribution. In any case, this analogy suggest to use the same formalism as for the cluster aggregation models.

There is a succesful kinetic equation to decribe this dynamics, namely the Smoluchowski equation, allowing to follow the time evolution of N with time. A similar equation can be used in our case to depict the behaviour of N with the variable L . Although we will not suggest for the moment any dynamical analogy, there is no doubt that this can be very fruitful in the future: in the case of the cluster aggregation model, the relevant physics is contained in the so called "kernel" K of the equation and we can think that the kernel derived for the Smoluchowski equation for the point distribution also contains the important features of the statistics. This suggets that K could be a more fundamental indicator than N .

Finally, since these statistical methods are derived from dynamical models, there is a hope that the link may be done with dynamical models of galaxy formation. This will certainly require that we are able to express the dynamics in a new language but, even if we do not accept this approach, this conclusion seems to be unescapable : it is more and more apparent that some important characteristics of the process of galaxy, or

structure formation cannot be expressed by the usual dynamical calculations. It would be, for instance, very interesting to extract some characteristics of the distribution which are conserved (or, at least, whose evolution can be followed) during the non linear evolution. Such properties are probably of topological, or dimensional nature; in any case they probably are in a range whose description is appropriate by the language introduced here.

REFERENCES

- Alimi J. M. and Blanchard A., 1988, preprint
- Calzetti D., Giavalisco M., and Ruffini R., 1987, Submitted to A.A.
- de Lapparent V., Geller M. J., and Huchra J., 1986, Ap.J. letters, 302, L1
- Einasto J., Klypin A. A., and Saar E., 1986, M.N.R.A.S., 219, 457
- Gott J. R., Melott A. L., and Dickinson, 1986, Ap.J., 306, 341
- Icke V. and van de Weygaert R., 1987, A.A. 184, 16
- Jones B. J. T., Martinez, V. J., Saar E., and Einasto J., Nordita preprint 87/28 A
- Kolb M., Botet R., Jullien R. and Herrmann J., 1986, in Growth and Form, fractal and non fractal patterns in physics, NATO ASI series E n0 100, Stanley and Ostrowsky ed, Martinus Nijhoff publishers, Dordrecht, p 222
- Mauger S. and Lachieze-Rey M., 1987, Ap. J., 320, 13 (ML1)
- Mauger S. and Lachieze-Rey M., 1988, in preparation, (ML2)
- Melott J. A., Weinberg D. H. and Gott J. R. III, 1988, Ap. J., 328, 50
- Peebles P.J.E., 1980, The large scale structure of The Universe, Princeton University Press
- Schaeffer R., 1987, A.A. letters, 181. L23
- Schaeffer R., and Balian R. 1988,
- Shandarin S.F. and Zeldovich Ya.B., 1986, in Cosmology, Astrophysics, and Fundamental Physics, proc of the 2nd ESO-CERN symposium, Setti and Van Hove ed.
- Stanley H. E., 1986, in Growth and Form, fractal and non fractal patterns in physics, NATO ASI series E n0 100, Stanley and Ostrowsky ed, Martinus Nijhoff publishers, Dordrecht, p 21
- White S.D., 1979, M.N.R.A.S. 186, 145

SEGREGATIONS IN THE GALAXY DISTRIBUTION

by

Sophie Maurogordato and Marc Lachieze-Rey**Service d'astrophysique du CEN Saclay France**

and

DAEC Observatoire de Paris Meudon France**Abstract**

Facing with observational evidence of large voids in the galaxy distribution, a new statistical indicator is developed which allows a quantification of voids properties at each scale of work. A systematic analysis of the Center for Astrophysics redshift survey allows to compare the statistical properties versus the size and location of the sub-sample tested, the luminosity class and morphological type involved, and a confrontation with theoretical models. A "scaling invariance" will be evidenced in the distribution.

The void probability function (hereafter V.P.F) was shown to be a very promising statistical tool as it can infer information about high order correlation functions which are not available from observation above order four. After its mathematical interest was developed by White in 1979, models were constructed to give it an analytical form, as did Schaeffer (1984) and Fry (1984). It was then applied to large surveys in order to extract the information directly from the data. We will try to summarize the different points in which the V.P.F has brought substantial conclusions

A lot of theoretical models are built on the "scaling hypothesis" i.e. the n-point correlation function $\xi^{(N)}$ is a sum of n-1 products of the 2-point correlation functions.

$$\xi^{(N)}(x_1, x_2, \dots, x_N) = \sum_{a_N} Q_N \sum_l \prod_{N-1} \xi(x_1, x_2)$$

The first sum is done over a_N different types of "tree graphs" and the product over the l symmetries (Schaeffer 1984). Fry (1986) reviewed these models as "hierarchical". This hypothesis was shown to be true for the data until $n=3$ above which noise predomines. R.Schaeffer (1984) showed this hypothesis to imply a scaling relation for the V.P.F. The function χ defined as its logarithm normalized to the Poisson value, $\chi(V) = \text{Log}(P_0(V))/nV$ would then only depend on the variable $q = nV < \xi >$. In order to test this property, we built from a sample of the CfA catalog (Huchra et.al 1983), children subsamples by selecting at random a fraction of galaxies. So we tested the same distribution with the same statistical properties only differing by the value of density. The result, showing a good agreement between all curves $\chi = f(q)$, argues strongly in favour of the previous "hierarchical" models. This representation, therefore independant of density, allows us to compare the properties of samples with different density in the CfA.

We confronted then the data from the CfA with several estimations from theoretical models : Fry's one who derives the value of the n-point correlation amplitude from the BBGKY hierarchy, and Schaeffer's analytical expression deduced from a statistical model. Jensen and Szalay (1986) derived from the theory of biased galaxy formation a relation between unreduced n-point correlation functions versus two-point ones :

$$1 + w_\nu^{(N)} = (1 + \xi_\nu)^{N-1}$$

This relation contradicts the scaling hypothesis. The analytical expressions for the V.P.F are compared with the data from the CfA catalog, showing best agreement for "hierarchical" models and particularly Schaeffer's one (Maugorodato and Lachièze-Rey 1987). For testing more complex effects, comparing statistical indicators for subsamples of different intrinsic properties, size, location, it is fundamental to get rid of normalization effects (Maugorodato and Lachièze-Rey 1988). There were shown to be drastic for correlation functions which directly depends on the mean density as: $1 + \xi = C n^{-1}$, so an over-estimation of density should appear as a spurious under-clustering (Blanchard and Alimi 1988) . The representation χ versus $q = nV < \xi >$ has the advantage of not depending too much on normalization as $n(1 + \xi)$ is constant.

Recent literature has inflated about the "spatial" variation of statistics. As Einasto et.al(1986) show the correlation length to be proportional to the size of the sample, it was soon interpreted by Calzetti et.al (1987) as a fractal property. We tested this effect for bright galaxies of absolute magnitude $M < -18.5$ and selected therefore four samples volume-limited respectively to 20, 25, 32, 40 h^{-1} Mpc. When normalizing ξ by the intrinsic density of the sample, or by a mean theoretical density deduced by integration of the luminosity function in the distribution, this effect is reversed. However, in both cases of normalization, the scaling invariance previously shown for the V.P.F remains valid when changing the depth and location of the sample as shown in Fig.1.

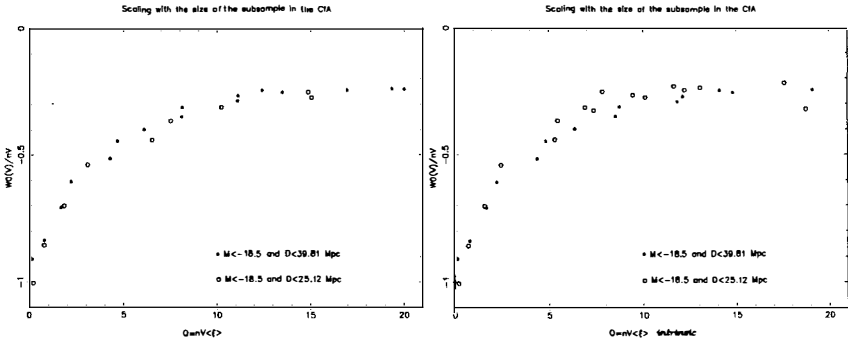


Fig 1: Scaling with the size of the subsample in the CfA: χ versus $q = nV \langle \xi \rangle$ for two subsamples of the CfA involving bright galaxies with $M < -18.5$ distance-limited to 25.12 Mpc (circles) and 39.81 Mpc (stars) with both normalizations.

One can test if statistical indicators varies with the luminosity class considered. Both normalizations are used again for calculating the correlation functions, showing once more different results. Different luminosity classes were tested in the *same volume* so that we can assume inhomogeneities will not affect them in a different way. The difficulty to use an external density comes from the bad accuracy on luminosity function under $M=-17$. Using the intrinsic density does not allow us to conclude on any segregation, although external one shows an over correlation for bright galaxies. In order to be free of these inhomogeneity problems, the V.P.F was calculated for two subsamples in the same volume, with the same intrinsic density, only differing by their luminosity class. It shows an *over-clustering of brighter galaxies against fainter ones*. This luminosity segregation can directly be explained by the biased galaxy formation models.

It is not a revelation to show a clustering segregation with morphological type as correlation functions calculated separately for elliptical, lenticular, and spiral galaxies in the CfA limited to 40 Mpc and including magnitudes lower than -18.5, show unambiguously. The same effect is shown when expressing the V.P.F as a function of the mean number of particles. The real striking fact is that, *in spite of their clustering differences, the representation $\chi(q)$ is identical. The scaling relation resists then to the strong morphological effect.*(Fig.2)

As tri-dimensionnal surveys are up to now, strongly affected by inhomogeneities as the nearby Virgo cluster, which infers normalization problems, the question is to know how much the conclusions can be extended to the whole real distribution. Applying this method to a bi-dimensionnal deep survey (Slezak et.al 1988) magnitude-limited to $m_B = 18$ allowed us to compare with the results obtained by Bouchet and Lachieze-Rey with the CfA up to $m_B = 14.5$ (Fig.3). The scaling invariance is there verified up to a depth of $182.5h^{-1}$ Mpc (Maugordato et.al 1988).

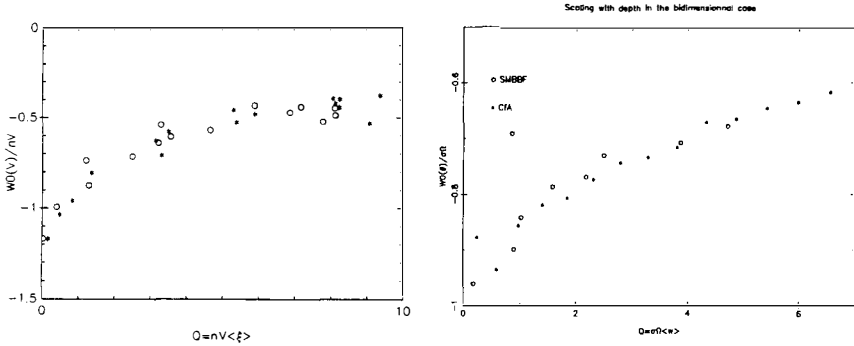


Fig 2:Scaling with morphological type in the CfA: χ versus $q = nV \langle \xi \rangle$ for two subsamples of the CfA involving bright galaxies with $M < -18.5$ distance-limited to 39.81 Mpc differing by their morphological type:ellipticals and lenticulars (circles) and spirals (stars).

Fig 3: Scaling with depth in bidimensionnal surveys: χ versus $q = \sigma \omega \langle w(\theta) \rangle$ for CfA (stars) and SMBBF (circles).

Conclusion

The representation of the void probability function by the function $\chi(q)$ was shown to be independant of the size and location of the sample, and of the morphological type of galaxies. Moreover it seems to hold with the depth of sample. This result, joined to direct comparison to prediction from theoretical models, favours the so-called "hierarchical models". Luminosity effects shown by the V.F.F need deeper surveys to be entangled from any non-fair sample effect. If confirmed, it would be a great argument for biased galaxy formation scenarios.

References

- Blanchard,A. and Alimi,J.M. 1988, *private communication*.
- Bouchet, F. R., and Lachièze-Rey, M. 1986, *Astrophys J. Lett.*, **302**, L37.
- Calzetti,D.,Giavalesco,M. and Ruffini,R. 1987, *submitted to Astron. and Astrophys.* .
- Einasto,J.,Klypin,A.A. and Saar,E. 1986, *M.N.R.A.S*, **219**, 45.
- Fry,J.,N. 1984, *Astrophys. J.(Letters)*, **277**, L5.
- Fry,J.,N. 1986, *Astrophys. J.(Letters)*, **306**, 358.
- Hamilton, A.J.S., Saslaw, W.C.,and Thuan, T.X 1985, *Astrophys. J.*, **297**, 37.
- Huchra, J., Davis, M., Latham, D. ,Tonry, J. 1983, *Astrophys. J.(supplts)*, **52**, 89.
- Maurogordato, S., and Lachièze-Rey, M. 1987, *Astrophys. J.*, **320**, 13.
- Maurogordato, S., and Lachièze-Rey, M. 1988, *submitted to Astrophys. J.*.
- Maurogordato, S., Lachièze-Rey, M. and Bouchet,F. 1988, *submitted to Astron. and Astrophys. (Letters)*.
- Peebles, P. J. E. 1980, *The Large Scale Structure of the Universe*, Princeton University Press, Princeton.
- Schaeffer, R. 1984, *Astron and Astrophys. Lett*, **134**, L1.
- Slezak, E., Mars, G., Bijaoui, A., Balkowski, C., and Fontanelli, P., *to be published in Astronomy and Astrophysics(Supplement Series)*.
- White, S. D. M. 1979, *M. N. R. A. S.*, **186**, 145.

**NON-LINEAR SCALE INVARIANCE
IN A COLD-DARK-MATTER UNIVERSE**

FRANÇOIS R. BOUCHET

Department of Astronomy, University of California, Berkeley,
and The Institute of Geophysics and Planetary Physics, Lawrence Livermore National Laboratory, Livermore;
on leave from The Centre de Physique Théorique de l'Ecole Polytechnique, Palaiseau, France,
and from The Institut d'Astrophysique de Paris, Paris, France.



ABSTRACT

The observed decomposition of the lowest ($N = 3, 4$) N -point correlation functions in symmetrized $(N - 1)$ products of two-point correlation functions suggest the possibility that the Universe may obey a specific scale invariance, at least in some range. Assuming that this scale invariance is strictly verified for all N , some specific predictions concerning the void probability function P_0 , and more generally the count probabilities P_N , as well as the fractal dimensions of the system can be made (see Schaeffer, this volume). In this *Progress Report*, we investigate the possibility that the non-linear evolution in a CDM Universe indeed leads to such a scale invariance. First of all, we determine the count probabilities in a "galaxy" catalog generated with a P^3M simulation code by Davis and Efstathiou¹⁾. We then proceed to check some of the expected scaling model predictions concerning the volume size and the count number dependence. Although still preliminary, our results are consistent with the the scale invariance predictions. We also compute some fractal properties of the sample. The distribution appears to be essentially a bifractal, with dimensions 0 and $3 - \gamma$, where γ is the index of the power-law which describes the two-point correlation function. This simply means that the number of objects either does not change with the size l of the sampled volume $v \propto l^3$ (dimension 0 corresponding to voids or field galaxies), or changes according to $l^{3-\gamma}$ (for galaxies in clusters). The other cases are not determinant for the global properties. The volume of field galaxies varies approximately as $l^{1/2}$ and the volume of cluster galaxies varies as $l^{3-\gamma}$.

The statistical description of a system of \mathcal{N} objects is complete if one knows, for instance, the (reduced) N -point correlation function $f_N(\mathbf{x}_1, \mathbf{x}_2, \dots, \mathbf{x}_N)$, for all $N \leq \mathcal{N}$. The function f_N embodies the information concerning the clustering properties of N objects. The galaxy distribution has long been characterized by its two-point correlation function $\xi(x)$ ($\xi(|\mathbf{x}_1 - \mathbf{x}_2|) \equiv f_2(\mathbf{x}_1, \mathbf{x}_2)$), which was shown to be a power law of index $\gamma \simeq 1.8$ over a wide range of scales²⁾. The N -point correlation functions for $N = 3, 4$ have also been measured³⁾; they are compatible with a decomposition in an $(N-1)$ product (and *not* with an N product) suitably symmetrized of two-point correlation functions, in the regime where $\xi > 1$, *i.e.* $x \lesssim 5Mpc$). The existence of tight clusters of many galaxies indicates that correlations for much larger N may also be very strong. Since the determination of the f_N is increasingly difficult for larger N , such a complete description is unattainable, and alternatives might prove useful.

Another description is provided by the functions $P_N(v)$ which are the probabilities of finding N objects in a volume v . The description is also complete if, again, the functions are known for all $N \leq \mathcal{N}$. Nevertheless, at small N , the f_N and P_N provide complementary informations, as can be seen by considering $P_0(v)$, since White⁴⁾ showed that for an homogeneous sample of mean density n

$$P_0(v) = e^{\chi(v)}, \quad \chi(v) = \sum_N \frac{(-n)^N}{N!} \int_v d^3x_1 d^3x_2 \dots d^3x_N f_N. \quad (1)$$

Thus P_0 at short scale is sensitive to the correlation functions at all orders (and $\chi(v) = -nv$ if the sample is uncorrelated). Furthermore, this void probability function alone may also offer a complete statistical description, provided its dependence on the system density n is also known. One can then use $P_0(n, v)$ as a generating function, and the P_N are obtained by successive derivatives with respect to the density

$$P_N(v) = (-n)^N \frac{d^N P_0(n, v)}{dn^N}. \quad (2)$$

In practice though, the density dependence might prove hard to measure with sufficient accuracy.

Let us now assume that the distribution possesses the following scale invariance

$$f_N(\lambda \mathbf{x}_1, \lambda \mathbf{x}_2, \dots, \lambda \mathbf{x}_N) = \lambda^{-\gamma(N-1)} f_N(\mathbf{x}_1, \mathbf{x}_2, \dots, \mathbf{x}_N), \text{ for all } N \leq \mathcal{N}. \quad (3)$$

Balian and Schaeffer⁵⁾ showed that $\sigma(n, v)$, which characterizes the departure of P_0 from the Poisson one ($P_0(n, v) = e^{-nv\sigma(n, v)}$), then depends on a unique scaling variable N_c , which is the average number of clustered particles (above the mean) inside the volume v

$$\sigma(n, v) \equiv \sigma(N_c), \text{ with } N_c = nv\bar{\xi}, \text{ and } \bar{\xi}(v) = \int_v \frac{d^3x_1}{v} \frac{d^3x_2}{v} \xi(|\mathbf{x}_1 - \mathbf{x}_2|). \quad (4)$$

For cubic volumes of side l ($v = l^3$), $\bar{\xi}(l) = (l/l_0)^{-\gamma}$, with $l_0 \simeq 2.4x_0$, x_0 being the correlation length defined by $\xi(x_0) = 1$. **THUS $\xi(l)$ AND $\sigma(l)$ ALONE PROVIDE A COMPLETE DESCRIPTION OF SUCH A SCALE INVARIANT SYSTEM.** By using Eq. 2, detailed

predictions concerning the statistical properties of the system can be made. These predictions depend on the specific scale invariance assumed, *i.e.* they depend on the fact that λ in Eq. 3 is raised to the power $N - 1$, and not to the power N as in usual statistical systems.

Before proceeding any further, let us note at this point that the sole dependence of σ on N_c has already been checked in 2D galaxy catalogs^{6,7}, and in 3D catalogs^{8,9} (see also Maurogordato, this volume). When measured in different samples with different densities, $\sigma(n, v)$ does appear to be a universal function of the scaling variable N_c . For more detailed predictions, it becomes increasingly difficult to separate the effect of small number statistics, catalog incompleteness, and morphology and luminosity effects from a possible discrepancy with the scale invariant model. In this *Progress Report*, we investigate the possibility that the non-linear evolution in a Cold-Dark-Matter (CDM) Universe does generate such a short-scale invariance.

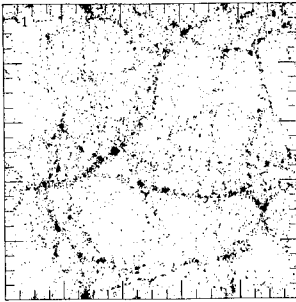


Figure 1

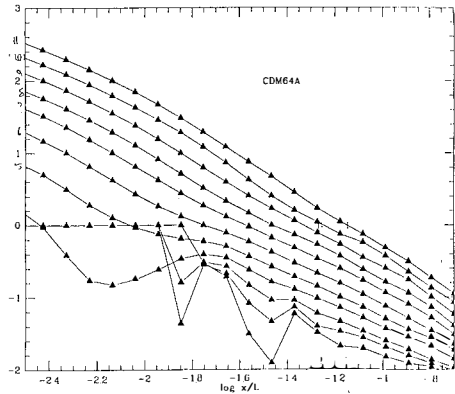


Figure 2

The sample we analyze (Fig. 1) is the result of a numerical simulation¹⁾ using the P^3M technique to evolve 262,144 particles laid down according to CDM initial conditions. The force smoothing length ϵ was $1/600^{\text{th}}$ of the simulation cube side L . The simulation was stopped when γ had approximately the right value, after an expansion factor of 8. This sets the length of the box at 64 Mpc (with $H=50$ km/s), and the particle's mass at $7 \times 10^{10} M_{\odot}$. We express in the following all lengths in units of L . One might picture this unbiased sample as a very complete galaxy catalog extending down to small galaxies. We note that in this simulation $x_0 \simeq 10^{-1.25}$ (so $l_0 \simeq 10^{-0.9}$). Also, the slope γ of the two-point correlation function is not quite constant: it varies from about 1.6 for $-2.4 < \text{Log}_{10} l < -2$, to about 2.4 for $-1.8 < \text{Log}_{10} l < -1.4$ (Fig. 2). Unless otherwise specified, we used an average value $\gamma = 2$. Nevertheless the slope variations are expected to lead to some discrepancies with the scale invariance predictions. Although this is a limitation of the simulations, they have the advantage of providing well-defined samples, devoid of the observational bias aforementioned.

We now turn to a brief description of some predictions of the scale invariance model. The full predictions are in Balian and Schaeffer⁵). First of all, one expects that $\sigma(N_c)$ be a simple power law of N_c

$$\sigma(N_c) \propto N_c^{-\omega} \propto l^{-(3-\gamma)\omega}, \quad 0 \leq \omega \leq 1, \quad (5)$$

at scales small enough that the scaling applies (roughly $l < l_0$), but large enough when compared to the mean intracluster separation l_c (defined by $N_c(l_c) = 1$, i.e. $l_c = l_0(nl_0^3)^{-1/(3-\gamma)} \simeq 10^{-3.7}$ in our sample). At smaller scales $l < l_c$ (but $\ll \epsilon \simeq 10^{-2.8}$), one expects a Poisson behaviour ($\sigma \equiv 1$). The value of the parameter ω is not fixed by the theory. Nevertheless, once ω has been measured, the predictions for the count probabilities at $l \ll l_v$ (with $P_0(l_v) = 1/e$) are

$$\text{if } 1 \lesssim N \ll N_c(l), \quad P_N(l) = a(N) l^{3-(3-\gamma)\omega}, \quad \text{with } a(N) \propto N^{-2+\omega} \text{ if } 1 \ll N \ll N_c(l), \quad (6)$$

$$\text{and if } N \gg N_c(l), \quad P_N(l) \propto \frac{1}{N_c \xi} e^{-y_s(N/N_c)}. \quad (7)$$

A fit to the Abell clusters luminosity function suggests that y_s should be of the order of 0.1.

Let us now consider the fractal dimension α such that the number of objects $N(l)$ in a box of size l scales as l^α . Since α may not be everywhere the same, one needs to characterize the relative proportion N_α of boxes which scales like α . It is convenient to use the function $f(\alpha)$ defined by $N_\alpha \propto l^{-f(\alpha)}$, so that $f(\alpha)$ is the fractal dimension of the volume occupied by the population of dimension α . This "spectrum" $f(\alpha)$ is related to the P_N by the following relations

$$f(\alpha) = \alpha q - \tau, \quad \alpha = \frac{d\tau}{dq}, \quad \text{where } \tau(q) = \frac{\partial \ln C_q}{\partial \ln l}, \quad \text{and } C_q(l) \propto l^{-3} \sum_{N=1}^N N^q P_N(l). \quad (8)$$

The assumption of scale invariance leads to the prediction that there should be two statistically significant populations: the isolated galaxies with $\alpha = 0$ and $f(0) = (3 - \gamma)\omega$, and those in clusters with $\alpha = 3 - \gamma$, and $f(3 - \gamma) = 3 - \gamma$. In other words, the system should be essentially a bifractal.

We start by computing the P_N for $0 \leq N \leq 5$, in the CDM sample and in a Poisson catalog with the same density (Fig. 3-a & 3-b). This is done by laying down cubic grids of various mesh size l . We record the occupation numbers, and accumulate the results on grids offset by different amounts to improve the statistics. As expected, the void probability in the correlated CDM sample is much larger than in the random one. We can then obtain $\sigma = -\ln P_0/nv$ as a function of l (Fig. 4). First of all, we verify (upper curve) that σ is indeed unity for the Poisson catalog. Second we see that σ behaves as predicted as a power law (lower curve), and we measure $(3 - \gamma)\omega \simeq 0.45 \sim \omega$ (cf. Eq. 5), which is surprisingly close from the value $(3 - \gamma)\omega \simeq 0.55$ (but $\gamma = 1.8$) obtained by Bouchet and Lachièze-Rey⁷) in the 2D CfA catalog. We can now check the l dependence (at $l \ll l_v \simeq 10^{-1.6}$) in Eq. 6. We see in Fig. 3-a that the P_N are described by power laws, with an index which is approximately constant with N , as expected. But the predicted value of the slope which is $3 - (3 - \gamma)\omega \simeq 2.55$ (dashed line) is accurately obeyed only by P_1 at $l < 10^{-2.2}$, where $N_c \simeq 25$. Since this prediction

holds for $N \ll N_c$, this suggests that 2 cannot be considered small enough as compared to 25 for the quantitative prediction to be accurate (but 1 is fine).

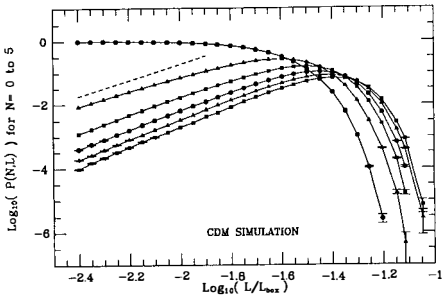


Figure 3-a

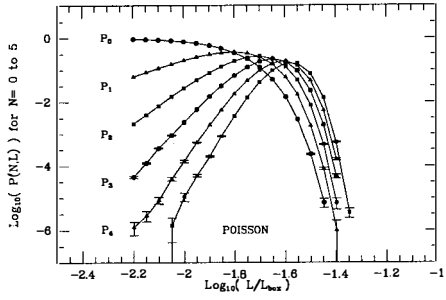


Figure 3-b

In order to check the N -dependence of the count probabilities, we computed all the non-zero P_N , for four different mesh sizes l (Fig. 5). For small N (Eq. 6), we expect the probability to vary as $N^{-2+\omega}$ in the range $1 \ll N \ll N_c(l)$ (and $-2 + \omega \simeq -1.55$). The actual slope is quite steeper (~ -2.5). This is nevertheless not too surprising, since the inequalities to satisfy are even stricter than for the l dependence. On the other hand we do see the predicted exponential decay at large N (Fig. 6). Furthermore, all the measured slopes $s(l)$ are described by the expression $s(l) = -y_s/N_c$, with a common value $y_s \sim 0.25$. Although larger, the measured value is in the ballpark of the expected one ($y_s \sim .1$). The sample thus exhibits a behavior that closely follows the expected one in the scale invariant model. Further studies will be required (using different sample densities and thus N_c) to determine if quantitative discrepancies are real or not.

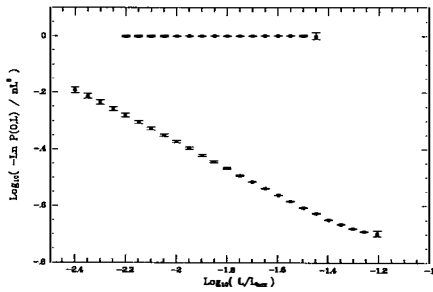


Figure 4

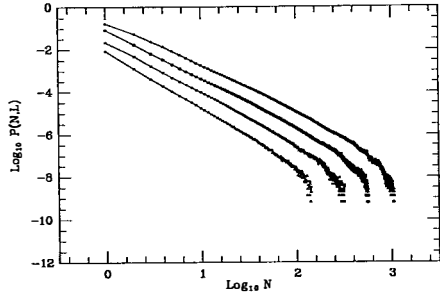


Figure 5

Finally, we computed the $f(\alpha)$ after Eqs. 8 (a different approach may be found in Jones *et al.* ¹⁰). We start by computing the $C_q(l)$. At large N , the terms appearing in the $C_q(l)$ sums

behave as $N^q e^{-y_s N/N_c}$, which begins to decrease when N obeys $y_s N/N_c > q$. Thus we cannot trust our calculations for values of q larger than $y_s N_{max}(l)/N_c(l)$, where $N_{max}(l)$ is the largest value for which we measured $P_N(l)$. With our present number of iterations, this means that we cannot compute the $C_q(l)$ accurately for $q \gtrsim 3$. The spectrum we derive (for $-6 < q$ by increment of 0.25) is shown in Fig. 7. Even though our estimated error bars are quite large, the results are consistent with an essentially bifractal behaviour, the $f(\alpha)$ spectrum exhibiting, as expected in the scale invariant model, two accumulation points around $\alpha = 0$ and 1.5 ± 0.25 ($\sim 3 - \gamma$), with appropriate amplitudes.

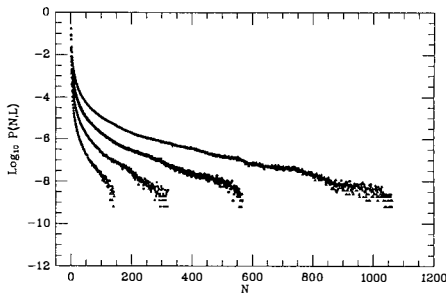


Figure 6

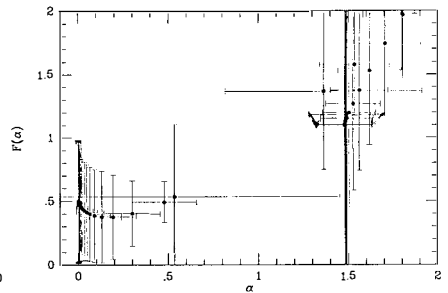


Figure 7

In conclusion, our results, though preliminary, lend support to the hypothesis that the non-linear evolution in a CDM Universe does yield a system whose behaviour is well predicted by the scale invariant model. In particular, the sample appears to be essentially a bifractal. In the future, it will be extremely interesting to assess the significance of the quantitative discrepancies we sometimes noticed. It is interesting to note that this specific scale invariance, if further confirmed, will single the gravitating system out of all other known statistical systems.

This ongoing work is done in collaboration with R. Schaeffer (CEA-CEN Saclay), and M. Davis (Berkeley Astronomy department). It was supported in part by the Theoretical Astrophysics Center at the University of California at Berkeley, and under the auspices of the U.S. Department of Energy by Lawrence Livermore National Laboratory under contract No. W-7405-Eng-48.

REFERENCES

- 1) Davis, M., and Efstathiou, G. 1987 To be published in the Proceedings of the Vatican study week on "Large Scale Motions in the Universe".
- 2) Groth, E., and Peebles, P. J. E. 1977, *Astrophys. J.*, **217**, 385.
- 3) Fry, J., and Peebles, P. J. E. 1978, *Astrophys. J.*, **221**, 19.
- 4) White, S. D. M. 1979, *Mon. Not. Roy. Astr. Soc.*, **186**, 145.
- 5) Balian, R., and Schaeffer, R. 1988, To be published in *Astron. & Astrophys.*
- 6) Sharp, N. 1981, *Mon. Not. Roy. Astr. Soc.*, **195**, 857.
- 7) Bouchet, F. R., and Lachièze-Rey, M. 1986, *Astrophys. J. Lett.*, **302**, L37.
- 8) Hamilton, A. J. S. 1985, *Astrophys. J. Lett.*, **292**, L35.
- 9) Manroghorato, S., and Lachièze-Rey, M. 1987, *Astrophys. J.*, **320**, 13.
- 10) Jones B.J.T., Martinez, V.J., Saar, E., and Einasto J. 1987, *Nordita preprint*.

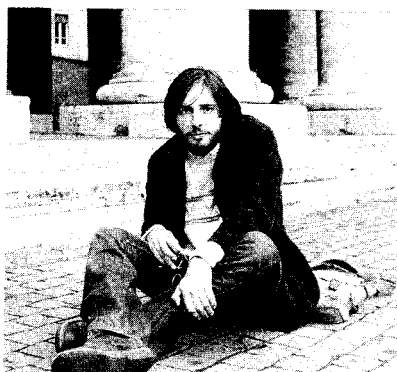
THE MULTIPLICITY FUNCTION IN A COLD DARK MATTER UNIVERSE

S. Colafrancesco

Dip. di Astronomia, Università di Padova, Italy.

F. Lucchin and S. Matarrese

Dip. di Fisica 'G. Galilei', Università di Padova, Italy.



ABSTRACT

The mass multiplicity function (m.m.f.) in a Cold Dark Matter scenario is considered within the hierarchical scenario for the origin of bound systems, from galaxies to groups and eventually to richer and richer clusters, for different statistical distributions of primordial density perturbations. The resulting m.m.f. is compared with the original one derived by Press and Schechter for a primordial power law variance $\sigma_M \propto M^{-(1/2+n/\beta)}$ with the assumption of a constant value for the spectral index n .

The evolutionary behaviour of the predicted multiplicity function is explored and the associated time scales are computed; the features of the rate of production and/or destruction of objects is considered in the source function.

We test the predictions from our multiplicity function with the existing data on the optical luminosity function for groups and clusters of galaxies: this extends from $10^{10} \div 10^{14} L_{\odot}$, even if it is not reliable especially in the group region. These data seem to require a primordial scale free spectrum with $n \lesssim 1$ and a considerable *bias* factor $b \simeq 2$: the possibility of non gaussian hierarchical statistics are not excluded.

1 INTRODUCTION

The clustering of galaxies could be extensively studied using the correlation functions (of higher and higher order) (Peebles 1980); an alternative analysis takes the hint to explore the statistical properties of the coagulation of the galaxian *seeds* into richer and richer aggregates: groups and clusters of galaxies. The latter approach goes on through the construction of a multiplicity function (Press and Schechter 1974, Gott and Turner 1977) which is defined as the number density of independent collapsed systems with mass between M and $M + dM$.

Once a multiplicity function has been obtained, the relative luminosity function can be derived, and its integrals, the counts and the redshift distributions, can be computed using standard relations (Weinberg 1972).

The assessment of a luminosity function depends not only on the statistical distribution of the mass perturbations but also on the physics of the considered systems. In fact, following Cavaliere and Colafrancesco (1988), in the case of the X-ray sources associated with clusters of galaxies, their luminosity function is obtained as a solution of a continuity equation (Cavaliere, Morrison and Wood 1971)

$$\frac{\partial N}{\partial t} = S - \frac{\partial(N\dot{L})}{\partial L}, \quad (1)$$

while in the optical range the same quantity reflects the behaviour of the m.m.f. $N(M, z)$

$$N(L, z) = N(M, z) \frac{dM}{dL}, \quad (2)$$

and the relation between M and L in the mass range $10^{13} \div 10^{15} M_{\odot}$ is

$$\left\langle \frac{M}{L} \right\rangle \sim 100 \div 300 \quad (3)$$

(see, e.g., Blumenthal et al. 1984). At present we are interested in this latter case: the next step is the construction of a m.m.f. .

2 THE MULTIPLICITY FUNCTION: A THEORETICAL APPROACH

The comoving multiplicity function in its general form can be written down as (Lucchin and Matarrese 1988)

$$N(M, z) = (1 + f) \frac{\rho_{bgr}}{M} \left| \frac{dP_{>\epsilon_c}}{d\sigma(M, z)} \right| \left| \frac{d\sigma(M, z)}{dM} \right|, \quad (4)$$

where $\rho_{bgr} = \rho_c \Omega_o$ is the background density of the universe and the factor f takes into account the infall of material induced by the growth of the perturbations: in the limit of complete infall $f = 1$.

The statistical distribution of the initial overdensities, $p(\delta)$, is considered through the quantity

$$P_{>\epsilon_c} = \int_{\delta_c}^{\infty} d\delta p(\delta). \quad (5)$$

We first consider hierarchical statistics (see, e.g., Fry 1984). The general form of $P_{>\epsilon_c}$ is

$$P_{>\epsilon_c} = (2\pi)^{-1/2} \frac{\sigma_M}{\delta_c} C(\delta_c) \exp(-\delta_c^2 B(\delta_c) / 2\sigma_M^2) \quad (6)$$

and the following constraints hold $C(\delta_c) > 0$, $0 < B(\delta_c) < 1$; different hierarchical distributions are characterized by different choices of the functions $C(\delta_c)$ and $B(\delta_c)$ (Lucchin and Matarrese 1988).

For δ_c we take into account values in the range $\delta_c = 1 \div 1.7$, depending on the presence of non-linear effects in the considered systems.

Among non-hierarchical statistics we shall only consider the Peebles model (Peebles 1983) for which

$$\frac{dP_{>\delta_c}}{d\sigma} \simeq (2\pi)^{-1/2} \frac{1}{\sigma_M} \left(1 + 4 \frac{\delta_c^2}{\sigma_M^2}\right)^{-1/4} \exp\left(-\left(1 + 4 \frac{\delta_c^2}{\sigma_M^2}\right)^{1/2}/2\right) \quad (7)$$

approximately holds (Lucchin and Matarrese 1988). The variance

$$\sigma^2(M, z) = (1+z)^{-2} \frac{C}{2\pi^2} \int_0^\infty dk k^{2+n} T^2(k) W^2(kR), \quad (8)$$

normalized as $\sigma^2(M, z)_{8Mpc} = 1/b^2$, where b is the *biasing* factor, contains all the informations on the time evolution of the m.m.f..

The primordial index n takes values in the range $n \gtrsim 0.5$ to ensure the *bottom-up* behaviour for the collapse of the fluctuations (Vittorio, Matarrese and Lucchin 1988).

The primordial fluctuation spectrum in the adiabatic Cold Dark Matter scenario is assumed to be modified by a transfer function (Davis et al. 1985)

$$T(k) = \frac{1}{1 + ak + bk^{3/2} + ck^2}, \quad (9)$$

with $a = 1.7(\Omega_0 h^2)^{-1} Mpc$, $b = 9(\Omega_0 h^2)^{-3/2} Mpc^{3/2}$, $c = (\Omega_0 h^2)^{-2} Mpc^2$. Cosmological parameters are $h = H_0/100$ km/s Mpc and $\Omega_0 = 1$.

A *top-hat* filtering

$$W(x) = \frac{3}{x^3} (\text{sen}x - x \text{cos}x) \quad (10)$$

(with $x = kR$) has been used.

In order to give prominence to the effects of the CDM scenario and to those of the statistics we explore the differences between the m.m.f. that we presently derive and the one firstly derived by Press and Schechter (1974) in its original and adapted form [simple Hierarchical Clustering Scenario (H.C.S.), see Cavaliere and Colafrancesco 1988]. The major differences appear in the source function, $S(M, t)$

$$S(M, t) = \frac{dN(M, t)}{dt}. \quad (11)$$

For hierarchical distributions the source function reads

$$S(M, t) \propto N(M, t) \frac{1}{t} \left[\frac{\delta_c^2}{\sigma_M^2} B(\delta_c) - 1 \right], \quad (12)$$

and a similar expression is obtained in non-hierarchical scenarios.

As Fig.1 shows, the source term and the relative m.m.f. respectively for CDM spectrum and simple HCS differ drastically: this is essentially due to the use of a constant index $n = 1$ for the simple HCS. An effective index $n_{eff} \simeq -1 \div -1.5$ is needed to recover an agreement between the two scenarios in the considered luminosity range ($L_V/L_* \sim 0.01 \div 10$):

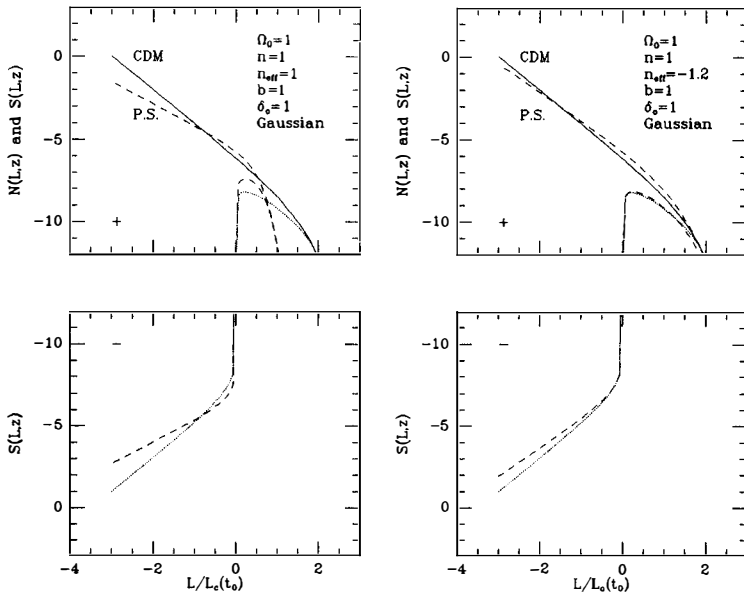


Fig. 1 The source function and the relative multiplicity function in CDM and simple HCS; parameters are given on the right.

this confirm the results previously founded by variuos authors (Kaiser 1986, Cavaliere and Colafrancesco 1988).

The use of power law spectra with $\sigma(M) \sim M^{-(1/2+n/6)}$, correctly normalized to the observed variance (corresponding to the collapse of a mass $M_c(t_0) \approx 10^{15} M_\odot$, at the present epoch), would reflect in the following situation: the collapse of higher mass systems is inhibited: their number density is lower than in the CDM case.

If the real mass spectrum has a curvature, the Press - Schechter rendition could provide a good representation of the cosmogonic effects only with a choice of the effective index n_{eff} appropriate to the considered mass range: moreover, this balance results more and more difficult where the curvature of the spectrum is greater, i.e., in the range $10^{13} \div 10^{15} M_\odot$ on which we are particularly interested. Based on these considerations Cavaliere and Colafrancesco found a best value of $n_{eff} \approx -1.2$.

In the following we shall consider the full mass spectrum in attempting to derive the optical luminosity function (l.f.) of groups and clusters of galaxies.

3 THE LUMINOSITY FUNCTION OF CLUSTERS OF GALAXIES

The luminosity function for groups and clusters of galaxies can be now constructed. Generally speaking, the X-ray case requires the additional information on the Intra Cluster Plasma physics: this has been widely explored by Cavaliere and Colafrancesco (1988) and

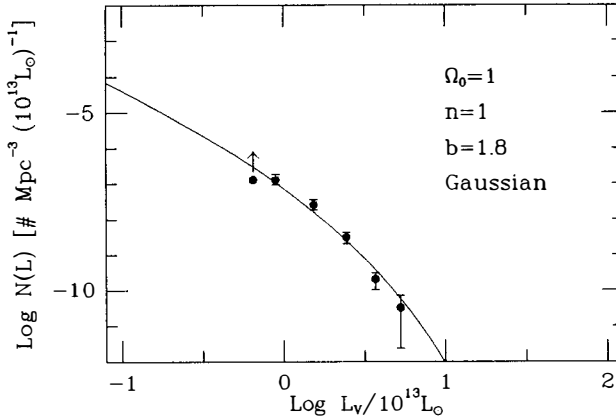


Fig. 2 The local luminosity function for $R \geq 1$ Abell clusters; data from Bahcall 1979. The fit is obtained with a $b = 1.8$ biasing factor

Cavaliere, Colafrancesco, Lucchin and Matarrese (1988 in preparation).

In the optical band the distribution of galaxies inside the systems is the only information as $\langle M/L \rangle \sim \text{const.}$ and the observed l.f. could provide a direct test for the models of the m.m.f.

In the construction of the l.f. our fiducial parameters are $L_* \approx 10^{13} L_{\odot}$, corresponding to $M_c(t_0) \approx 10^{15} M_{\odot}$, when we adopt a value $\langle \frac{\Delta M}{L} \rangle \sim 100$.

Fig.2 shows that the local l.f. for Abell clusters is reproduced by our model with $b \simeq 1.8$ and $n \simeq 1$.

The extrapolation of this model to the Turner-Gott (1976) (hereafter T.G.) groups region cannot fit the data: however, these data may suffer a number of uncertainties, namely:

- the possible relative normalization effects that could exist between the two different surveys, the Abell's one, that is distance limited, and the T.-G. one, that is magnitude limited;
- the identification procedure for the T.-G. groups, that is based on a purely statistical rule in which the contamination of the background galaxies could play a crucial role;
- due to this effect, the total luminosities for groups of galaxies may change by a considerable factor. Besides this, also the luminosities for rich Abell clusters could vary because of a lack of a tight correlation between L_V and the richness R .

To these sources of uncertainties we must add, following Bahcall (1979), the presence of possible incompleteness effects as well as the data error estimates.

Nevertheless, based on the fairly good fit to the rich cluster l.f., we may study the effects of cosmogonical parameters and of the statistics of the fluctuations on the observable distribution. Fig.3 shows the effect of different values of biasing on the same gaussian l.f.: the effects of non-gaussian hierarchical statistics reproduces at least qualitatively an *anti-biasing* behaviour that tends to flatten the l.f. at its bright end.

A different normalization of the l.f. in non-gaussian scenarios could reproduce the T.-G. group distribution but not the sharp cutoff in the region of the Abell clusters, $L_V \gtrsim 10^{13} L_{\odot}$

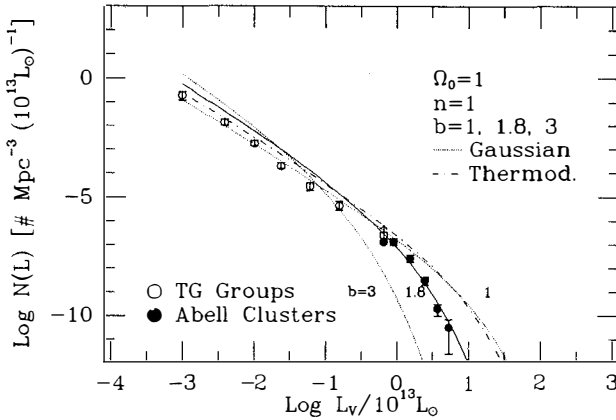


Fig. 3 The effects of bias and non-gaussian hierarchical statistics on the luminosity function; b varies from 3 to 1 from left to right. The dot-dashed curve corresponds to the Thermodynamic model (Saslaw and Hamilton 1984) and is given as an example of non-gaussian hierarchical statistic.

(Fig.2).

The evolutionary behaviour of the l.f. is shown in Fig.4: note that in CDM scenarios the evolution of the l.f. is faster than that predicted by simple HCS, essentially due to the curvature of the fluctuation spectrum that allows smaller and smaller masses to collapse on shorter time scales

$$M_c(t) \propto t^{2/3 a_{eff}}, \quad (13)$$

where $a_{eff} = (1/2 + n_{eff}/6)$. The presence of biasing increases the evolutionary rate simulating a "fast return to the past", while non-gaussian hierarchical features slow down this rate.

The evolutionary time scale for the m.m.f., $\tau \equiv N(M,t) / |S(M,t)|$, is shown in Fig.5: from this graph the dynamics of the present model for the hierarchical clustering is also easily recognized.

4 CONCLUSIONS

Based mostly on the present rich clusters luminosity function, our main conclusions are the following:

- i) the CDM scenario with a moderate biasing prescription $b \lesssim 2$ seems to reproduce the distribution of rich ($R \geq 1$) Abell Clusters;
- ii) the inclusion of a higher overdensity threshold ($\delta_c > 1.5$) tends to increase the curvature of the bright end of the m.m.f., and for this reason, a lower bias factor is then required in order to match the observations;
- iii) the extension of the data about the local l.f. toward lower luminosities could provide strong constraints on the spectrum ($n_p \approx 0.5 \div 1$) and to the possible cosmogonical scenarios;

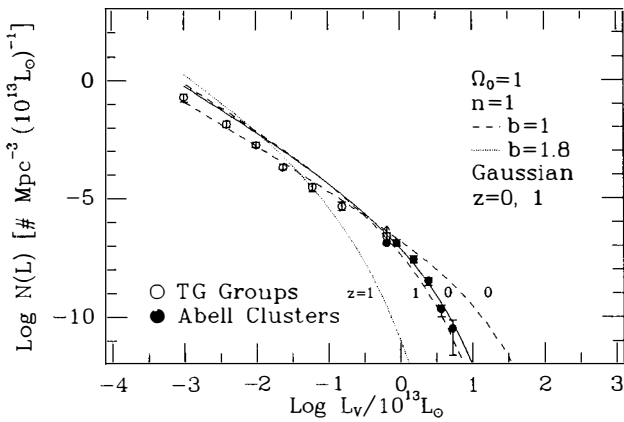


Fig. 4 Predicted luminosity function evolutions for a gaussian statistics with (dotted-continuous curve) and without biasing (dashed curves).

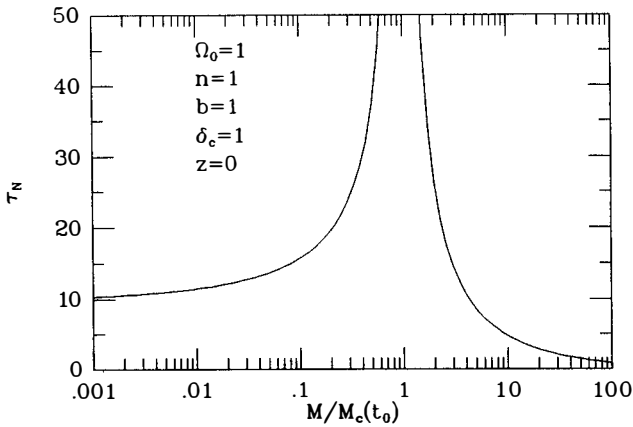


Fig. 5 The evolutionary time scale τ_S of the multiplicity function vs mass: the presence of the asymptote identifies the characteristic mass $M_c(t)$ which characterizes the assumed hierarchical clustering model.

iv) the evolution into the look-back time of the m.m.f. would provide quite strong tests for biasing and for statistical effects.

According to our results, a better knowledge of the local luminosity function both in the optical and in the X-ray band (see Cavaliere and Colafrancesco 1988b in preparation), would provide useful informations and tight constraints to cosmogonical and statistical effects.

Acknowledgements. We thank A. Cavaliere for many stimulating discussions and suggestions in improving the presentation of this work. A special thank to M.C. Pelletan for her kindness in satisfying any requirement for this publication.

REFERENCES

- Abell, G.O. 1958, *Ap. J. Suppl.*, **3**, 211.
 Bahcall, N.A., 1979, *Ap. J.*, **232**, 689.
 Blumenthal, G.R. et al. 1984, *Nature*, **311**, 517.
 Cavaliere, A. Morrison, P. Wood, K. 1971, *Ap. J.*, **170**, 223.
 Cavaliere, A. Danese, L. and De Zotti, G. 1977, *Ap. J.*, **296**, 402.
 Cavaliere, A., and Colafrancesco, S. 1988, *Ap. J.*, *in press*.
 Cavaliere, A., Colafrancesco, S., Lucchin, F., and Matarrese, S. 1988, in preparation.
 Davis, M., Efstathiou, G.G., Frenk, C.S., and White, S.D.M. 1985, *Ap. J.*, **292**, 371.
 Fry, J.N. 1984, *Ap. J.*, **279**, 499.
 Gott, J.R. and Turner, E.L. 1977, *Ap. J.*, **216**, 357.
 Lucchin, F., and Matarrese, S. 1988, *Ap. J.*, *in press*.
 Peebles, P.J. 1980, *The Large Scale Structure of the Universe*, (Princeton Univ. Press).
 Peebles, P.J. 1983, *Ap. J.*, **274**, 1.
 Press, W.H. and Schechter, P. 1974, *Ap. J.*, **187**, 425.
 Saslaw, W.C., and Hamilton, J.S. 1984, *Ap. J.*, **276**, 13.
 Turner, E.L., and Gott, J.R. 1976, *Ap. J. Suppl.*, **32**, 409.
 Vittorio, N., Matarrese, S., and Lucchin, F. 1988, *Ap. J.*, **328**, 69.
 Weinberg, S. 1972, *Gravitation and Cosmology: Principles and Application of the General Theory of Relativity* (New York: Wiley).

QUASAR CLUSTERING AND COSMOLOGY : OBSERVATIONAL STATUS**Daniel Kunth****Institut d'Astrophysique de Paris, CNRS
98bis, bd Arago F-75014 Paris****ABSTRACT**

The importance of quasars as probes to underline large-scale structures of the Universe is emphasized . Recent work on quasar clustering detection is discussed . The methods used to detect and characterize quasar clustering are analysed and compared within each other . The possible evolution with redshift of quasar clustering at small-scale separation is discussed and compared to other types of clustering at low and high redshift. Figures are given of typical survey sizes needed to significantly improve the present observational status.

INTRODUCTION

The characterisation of large-scale structures in the Universe and the understanding of their evolution are of great interest for cosmology. This is relevant for the presence and composition of dark matter, in particular on scales at which fluctuations growth is still linear and brings interesting clues for the galaxy formation scenario. One of our hopes is to constrain the epoch at which galaxies are formed and decide whether large structures develop from isothermal or adiabatic fluctuations or any variation on these themes. Since quasars are by now, essentially the only so intrinsically bright objects to be seen beyond $z=1$ and up to z larger than 4, they fill the gap between the universe as seen today and the early universe as observed from the microwave background radiation at $z \sim 1500$. If we thus consider quasars as good tracers of baryonic matter, one can use them over a large range in redshift to study large structures and their evolution over most of the universe lifetime.

DETECTING QUASAR CLUSTERING

The steep luminosity function of quasar and their scarcity are the main observational difficulties for quasar clustering detection. Indeed quasars brighter than 20 and 21 have a surface density of only 8 and $20/h^2$ respectively, whereas a typical supercluster of few tens of Mpc will cover about 30 arcmin. on the sky at $z=2$. Moreover to achieve a 3-dimensional analysis, redshifts must be obtained to better than $\Delta z \simeq 0.01$ since at $z \sim 2$ an 0.01 uncertainty in Δz corresponds to about $10 h^{-1}$ Mpc.

The first attempt to detect quasar clustering is due to Osmer (1981) and Webster (1982) who analysed complete samples but restricted to less than hundred objects. The low surface density of these samples hampered from drawing any concluding statement about quasar separation at small scales. On the other hand firmer limits have been set on correlations at scales larger than $100 h^{-1}$ Mpc. Major surveys have been achieved these recent years, in particular an "avalanche" of papers have discussed at length two types of data sets. A first category deals with complete samples of typically $100 \div 300$ objects down to limiting magnitudes close to 21. Second an attempt has been made to analyse general catalogues that are large (more than 3000 objects) but inhomogeneous by nature. A summary of the most recent papers devoted to the subject is given by Shaver (1988,a,b).

CHARACTERIZING QUASAR CLUSTERING

The most widely used method to characterize quasar clustering is based on the derivation of the 2 points correlation function $\xi(r)$ such that

$$N_p = N(1 + \xi(r))$$

where N_p is the number of pairs of a given r separation in the sample under investigation and N is the number of pairs of the same separation obtained from a random sample. It is required that random samples, generated by Monte-Carlo techniques be subject to the same selection effects than the observed sample. An alternative technique applied to the Véron catalogue was devised by Shaver (1984) to predominantly investigate small scales clustering and consists of considering pairs of small redshift differences separately from those of large differences. Kruszewski (1988a) using the same data corrected for inhomogeneities by assuming a particular parametric form of them. Both authors find that on scales from 0.1 to roughly $10 \text{ h}^{-1} \text{ Mpc}$ the correlation function was similar to the galaxy-galaxy correlation function at present epoch. Kruszewski further points out that ξ evolves with redshift in the sense that no clustering is seen beyond $z=1.5$ while it increases toward lower redshifts becoming almost as large as that of rich clusters of galaxies. Application of the scrambling technique to the Véron catalogue by Anderson, Kunth and Sargent (1988) gives consistent results with those of Shaver and Kruszewski. By adding up distinct homogeneous samples Iovino and Shaver (1988) detect clustering on comoving scales $\leq 10 \text{ h}^{-1} \text{ Mpc}$ at 5σ level. A similar finding is tentatively reported by Shanks et al. (1988) who find QSO clustering at a stronger level than that expected for galaxies on a simple 'stable' model for galaxy clustering evolution. When all the results are assembled, most studies do comfort the view that at small separations a positive signal comes from quasars of low redshift. This is illustrated in Figure 1 taken from Shaver (1987). As a function of redshift the amplitude of the quasar correlation function at $10 \text{ h}^{-1} \text{ Mpc}$ increases rapidly with decreasing z , more rapidly than that of galaxies assuming stable clustering and similar to that of present epoch of radio galaxies. However large uncertainties are still present, since very few pairs are contained in the lower separation bins. At larger scales Shanks et al. (1988) derive an observed correlation function close to zero consistent with an homogeneous Universe where QSOs well map the baryonic mass distribution.

ANALYSIS OF QUASAR CLUSTERING DETECTION METHODS

The scrambling technique : it is generally postulated that generated random samples have the same global properties as the observed surveys but are known to be unclustered. Anderson et al. (1988) have examined the Véron Catalogue using a modification of the "scrambling" technique employed by Osmer (1981). This technique generates artificial quasar catalogues by randomly permuting redshift in the original catalogue. The underlying assumption is that selection effects in z are independent from α and δ . However Anderson et al. (1988) show that this assumption does not always hold and

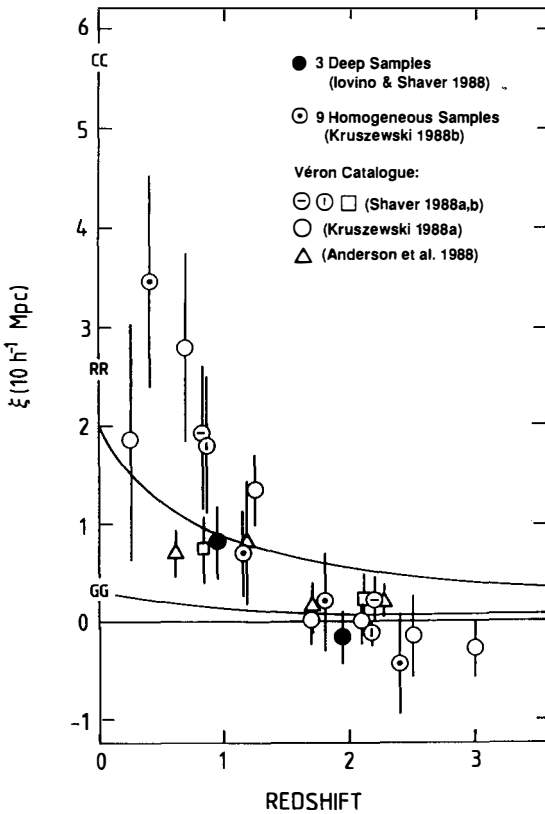


Figure 1 : Amplitude of the quasar correlation function at $10 h^{-1}$ Mpc as a function of redshift taken from Shaver (1988a) from different studies as indicated . On the left axis are positioned the amplitudes of the correlation function at low redshift for galaxies (GG), clusters(CC) and radio galaxies (RR). The two curves show the expected evolution for stable clustering.

leads to overestimate the correlation function ξ at all separations . Since the quasar distribution in a catalogue such as the Véron's cannot express as a product

$$\phi(\alpha, \delta, z) = \phi(\alpha, \delta)\phi(z) \quad (3)$$

a situation such as the one sketched in Figure 2 may occur. In such an example, containing 2 disconnected regions, scrambling scatters points outside the observed domain. The density of the scrambling catalogue is therefore reduced , leading to overestimating the correlation function. To reduce the magnitude of this effect Anderson et al. have divided the Véron catalogue into several shells in redshift and scrambled each shell separately. They find that quasars cluster on a scale of $9 \text{ h}^{-1} \text{ Mpc}$ and 2.6 ± 1.1 times that among galaxies. Moreover in agreement with Shaver's results this effect occurs in the redshift interval $0.3 < z < 1.4$ and not at large z . However, by dividing the sample in smaller cells clustering is once again produced by a small number of pairs and yet possible systematic errors are not completely ruled out . More work is being done to demonstrate the validity of the scramble technique : we are applying the technique to the CFA galaxies and compare our results with those obtained by other method analysis (Moutarde et al.1988)

Using homogeneous samples is in principle a far more secure procedure except for the small number of quasars involved . Table 1 summarizes results obtained by Iovino and Shaver (1988) by combining 3 independent data sets. Clustering is also dominant

Table 1 : Homogeneous samples studied in Iovino and Shaver (1988). The table illustrates the typical survey sizes that are used at present for quasar clustering studies. The total number of quasars is a strong function of the limiting magnitude. The total number of pairs is indicated with $10 \text{ h}^{-1} \text{ Mpc}$ separation as well as the number of expected pairs.

Authors (*)	m_{lim}	n_{qso}	n_{pairs}	$n_{expected}$	area (\square^2)
Crampton et al (1987)	20.5	125			5.2
Boyle (1986)	20.9	171			4
Barbieri et al. (1988)	19.5	80			10
Total =		376			19.2
z < 1.5			15	4.7	
z > 1.5			5	4	

(*): references in Iovino and Shaver (1988)

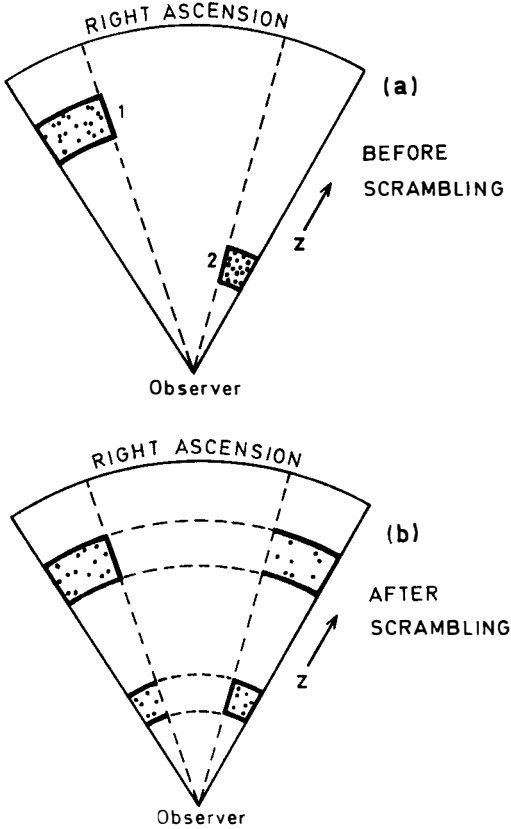


Figure 2 : A example showing two disconnected regions in an (α ,redshift) plane (2a) . Scrambling only redshifts while preserving the positions scatters points outside these regions and lowers the mean density of the scrambled catalogue (2b). this results in an overestimation of the clustering.

on a scale of $10 h^{-1} \text{ Mpc}^{-1}$. However their results are based on the detection on very few pairs : 15 are detected at $z < 1.5$ against 5 expected from Poisson statistics. Again a lack of clustering is noteworthy at $z > 1.5$. Recent analysis from Iovino et al.(1988) and based on larger samples establishes beyond doubt clustering among the quasar population at a 5.5σ level . More work will now be devoted to investigate the evolution of such an effect and its dependence with other parameters such as quasar luminosity and/or radio properties. Caution must be made with respect to a possible contamination of lensed pairs the number of which should increase with redshift.

WHAT DOES QUASAR CLUSTERING TELL US ?

It is now widely accepted that quasars are associated with baryonic matter. Before discussing the significance of quasar clustering to the evolution of large structures in general one must elucidate the relationship between quasars and other objects and their interplay with their own environment. Recent IRAS studies suggest that ultraluminous objects have Seyfert spectra and that they evolve into classical optical quasars. Distinction between different classes of AGN is predominantly related to the interstellar medium surrounding the source (Sanders et al. 1988). At low redshift direct imaging has now shown that quasars are nested in the center of ordinary galaxies. Close association with galaxies — sometimes clearly interacting (Bothun et al.1982) — or clusters are numerous (Shaver 1987). Yee (1987 and references therein) emphasizes that radio quasars tend to correlate with galaxies much stronger than radio quiet do consistently with the picture in which AGN are more numerous in clusters of high redshift (Dressler et al. 1985).

Less of such direct connections are available at high redshift. However quasar absorption lines permit to study the evolution of the correlation redshift much beyond where typical galaxies are directly observed. Heavy elements systems that contain strong lines due to H and heavier elements are shown to arise in a tenuous gas of near solar composition. Sargent and Steidel (1988) have shown that heavy elements redshift are strongly clustered on a scale from 200 to 600 km s^{-1} . Occasionally studies of common heavy elements absorption redshift in pairs of quasars offer some indication of large scale distribution in the clustering of the absorbers (Sargent 1987). Some views differ on how to interpret cases of common absorption systems in quasars. They could be due to either galaxies that are members of intervening clusters or superclusters or originate from extended halos of single galaxies. In either cases substantial masses on large scales are implied. The wide quasar pair Q1037–2704 and Q1038–2712 discovered by Jakobsen et al. (1986) has been discussed at length by many authors (Bohuski and Weedman 1979, Sargent and Steidel 1987). The most plausible explanation for the occurrence of several common absorption redshifts in this quasar pair is that the two lines of sight traverse a large scale distribution of galaxies that belongs to a supercluster viewed from

a particular rare direction. Some doubts remain that common absorptions could simply arise from chance coincidence (Cristiani et al. 1987, Robertson 1987).

The nature of the absorbers that give rise to the Ly α forest is still a matter of debate. Some arguments have been given that they are associated with gas-rich dwarf galaxies that show less clustering than normal galaxies do. Carswell and Rees (1987) have argued that the flat correlation function of the Ly α clouds implies that there is no evidence for voids such as the ones visible in the local distribution of galaxies. This suggestion has recently been strengthened and modelled by Iovino, Pierre and Shaver (1988). Webb and Carswell (1988) report weak clustering at $z=2$ with some indication for rapid evolution since no such clustering is detected at $z=3$.

Clustering is revealed among a wide variety of objects. Many of them show strong redshift dependence in their overall properties but the observational data is not secure enough to allow any further comparison with theoretical predictions.

CONCLUSION AND PROSPECTS

Oort (1981) has emphasized the reasons why superclusters should be detected at $z=2.5$ if they bear some resemblance with those known at present epoch. At $z=0$ no quasar are known to be associated with optically found clusters or superclusters because quasar space density is far too low. Indeed at $z=2.5$ the situation differs markedly. Following Schmidt and Green (1983) models one finds about 2000 to 3000 quasars per Gpc³ brighter than -23.5 and -24.5 respectively. Assuming an overdensity of 10 in the matter distribution a supercluster of $100 h^{-1}$ Mpc size ($q_0=0.5$) would nest about 10 quasars per magnitude interval between -23 and -28 . Superclusters should therefore be detected. I believe that not enough data has been accumulated for this purpose yet. Only chance discoveries or deep searches around known galaxies have provided us with few clear cases (Oort et al. 1981). Anderson et al. (1988) have estimated that magnitude limited samples should aim to $B \geq 21$ to keep surveys of reasonable sizes and get enough quasars per single large supercluster.

As a crude estimate, 60 square degrees must be surveyed down to a limiting magnitude of 21 to obtain about 50 pairs with separations of less than $10 h^{-1}$ Mpc. This figure is somewhat pessimistic because both clustering and density variations with redshift will increase the number of pairs.

REFERENCES

- Anderson, N., Kunth, D., Sargent, W.L.W. : 1988, *Astron. J.* 95,644
- Bohuski, T.J., Weedman, D.W. : 1979, *Astrophys. J.* 231, 653
- Bothun, G.D., Mould, J.R., Heckman, T., Balick, B., Schommer, R.A., Kristian, J. : 1982, *Astron. J.* 87,1621
- Carswell, R.F., Rees, M.J. : 1987 *Mon. Not. R. Astr. Soc.* 224, 13
- Cristiani, S., Danziger, I.J., Shaver, P.A. : 1987 *Mon. Not. R. Astr. Soc.* 227,639
- Dressler, A., Gunn, J.E., Schneider, D.P. : 1985 *Astrophys. J.* 294, 70
- Iovino, A., Shaver, P.A. : 1987, in *Evolution of Large Scale Structures in the Universe*, IAU Symp. 130 ; eds J. Audouze, M.C. Pelletan & A. Szalay ; Reidel, Dordrecht
- Iovino, A., Shaver, P.A., Osmer, P.S., Hewitt, P., Crampton, D., Cowley, A.P., Hartwick, F.D.A., Barbieri, C., Cristiani, S.: 1988, in "Large-Scale Structure and Motions in the Universe"; eds G.Giuricin et al. ;Reidel,Dordrecht
- Iovino, A., Pierre, M., Shaver, P.: 1988, in "Large-Scale Structure and Motions in the Universe"; eds G.Giuricin et al. ;Reidel,Dordrecht
- Jakobsen, P., Perryman, M.A.C., Ulrich, M.H., Macchetto, F., and di Serego Alighieri, S.: 1986 *Astrophys. J. (Letters)* 303, L27
- Kruszewski, A. : 1988a, preprint
- Kruszewski, A. : 1988b, *Acta Astr.*, in press
- Moutarde F.,Kunth,D.,Lachize-Rey,M.:1988,in preparation
- Oort, J.H., Arp, H., de Ruiter, H. : 1981, *Astron. Astrophys.* 95, 7
- Oort, J.H. : 1983, in *Quasars and Gravitational Lenses (24th Liège Int. Astrophys. Colloq.)*, p. 301
- Osmer, P.S. : 1981, *Astrophys. J.* 247, 762
- Robertson, J.G. : 1987, *Mon. Not. R. Astr. Soc.* 227,639
- Sanders, D.B., Soifer, B.T., Elias, J.H., Neugebauer, G. and Matthews, K., 1988, IRAS preprint n^o 0034
- Sargent, W.L.W. : 1987,in IAU Symposium n^o 124, *Observational cosmology*,ed. A. Hewitt,G.Burbidge,and L.Z.Fang(Dordrecht:Reidel),p.777.
- Sargent, W.L.W., Steidel, C. : 1987,*Ap.J.*,322,142.
- Sargent, W.L.W., Steidel, C. : 1988, preprint
- Shanks, T., Fong, R., Boyle B.J., Peterson, B.A.:1987:*Mon. Not. R. Astron. Soc.* 227, 739
- Shaver, P. : 1984, *Astron. Astrophys.* 136, L9
- Shaver, P. : 1988a,in "The Post-Recombination Universe" (NATO ASI) ,in press
- Shaver, P. : 1988b,in "Optical Surveys for Quasars " (ed. P.Osmer), P.A.S.P.,in press

Schmidt, M., Green, R.F. : 1983, *Astrophys. J.* 269, 352

Véron-Cetty, M.-P., Véron, Ph. : 1987, *ESO Scientific Report* n° 5

Webb, J.K., Carswell, R.F., 1988 in preparation

Webster, A. : 1982, *Mon. Not. R. Astron. Soc.* 199, 683

Yee, H.K.C. : 1987, in *Observational Cosmology*, Eds. A. Hewitt, G. Burbidge, L.-Z. Fang ; Reidel, p. 685

IV. DARK MATTER IN GALAXIES AND HALOS

THE EFFECTS OF BARYONIC INFALL ON THE HALO MASS DISTRIBUTION IN DISK
GALAXIES

E. Athanassoula
Observatoire de Marseille
2, Place Le Verrier
13248 Marseille cedex 04
France

ABSTRACT

Simple numerical simulations are used to study the effects of baryonic infall on the halo mass distribution in disk galaxies. Three populations are used: stars and gas, which are closely coupled through star formation, mass loss, cooling and heating, and a halo population which interacts only gravitationally. For several values of the star-gas coupling parameters and initial halo configurations we find final configurations with flat rotation curves. Some of them are maximum disk solutions with asymmetries suppressed (no $m = 1$ solutions), and some of them have such strong halos that bisymmetric disturbances are suppressed (no $m = 2$ solutions).

1. INFALL SCENARIO

The observed rotation curves of spiral galaxies are flat or rising, and seem devoid of features which demarcate clearly the visible disk from the invisible halo contribution. This, as discussed by Bahcall and Casertano (1985), argues for a conspiracy between these two components, and might be explained by considering their mutual gravitation interaction and settling down in a common gravitational potential during the formation process of a galaxy.

In the framework of the infall scenario of galaxy formation, suggested initially by White and Rees (1978), the dissipative material collapses in a pre-existing potential well formed by the halo material. Let us start with a protogalaxy composed of a homogeneous mixture of a fraction F of dissipative baryons and a fraction $1-F$ of non dissipative dark matter. As the dissipative material collapses, the non-dissipative material, which will be the dark halo, necessarily responds. Ryden and Gunn (1984, 1987) proposed a semianalytic model to calculate the halo response. They assume that the dark matter is drawn inwards sufficiently slowly that the adiabatic invariants are conserved and that the disk does not respond to the change of mass distribution in the halo. However their results show a predominance of the halo in the central parts (cf. their Fig. 13-15). Blumenthal et al. (1985) introduced one more assumption, namely that the orbits of the halo particles are circular or near circular, thereby permitting simple analytical solutions to the problem. We will hereafter refer to this as the circular adiabatic approximation. For the examples given in their Fig. 1 the final halo rotation curve is of the order of, or exceeds, the disk rotation curve at every radius.

The resulting models are thus in disagreement with the commonly accepted disk/halo decompositions, which show a predominance of the baryonic mass in the central parts. Using constraints from the swing amplifier theory Athanassoula et al. (1987) introduced two decompositions: the "no $m = 1$ " and the "no $m = 2$ ". If a disk has more mass than the "no $m = 1$ " solution it will allow the growth of $m = 1$ components or asymmetries, while if it has less than the "no $m = 2$ " it

will not allow two armed spirals. All maximum disk or "no $m = 1$ " decompositions are dominated by the baryonic mass distribution in the central parts, and the halo and disk mass become equal at a radius which is of the order of the de Vaucouleurs radius (Athanasoula et al., 1987). Comparison of such decompositions with the adiabatic approximation models shows that the latter are not maximum disk or "no $m = 1$ " solutions. Flores (1988) concluded that the results of the infall scenario are incompatible with the standard maximum disk solutions. I will argue here that it is more correct to say that the assumptions of the circular adiabatic model are incompatible with the maximum disk hypothesis.

Barnes (1986) and van Albada and Sancisi (1986) have used N body simulations to follow the response of a halo to a slowly growing disk. Unfortunately in their simulations the disk is considered as rigid, which makes the conspiracy somewhat onesided. Barnes (1986) found that the orbits of the particles in his simulations have large radial excursions. For such orbits one would expect lesser response than for circular ones and indeed Barnes shows that the analytical circular adiabatic model may overestimate the halo response by as much as a factor of 2, compared to his simulations. Furthermore, to particles on orbits reaching far out, the disk potential looks not far from spherical and thus the approximation used in the analytical approach of replacing the disk by the equivalent spherical mass distribution is more or less justified.

2. NUMERICAL SIMULATIONS

In order to follow the collapse of the baryons and its effects on the halo and test whether the maximum disk models can be compatible with the infall scenario, I ran numerical simulations, using a 1D hydrodynamic scheme developed for a different project in collaboration with K.H. Prendergast and S. Morin. In many aspects it follows the scheme described by Chiang and Prendergast (1985). I will give here only a very brief description of it, more information being contained in a forthcoming paper.

Since the gas and the stars do not have the same behaviour, the

numerical simulations of the infall and consequent halo contraction use three components, namely a halo population, stars and gas. The treatment is selfconsistent and, when heating and cooling are not included, conservative. Stars are formed out of gas according to a Schmidt-type law, and stars eject gas during their lifetime. The interstellar medium is heated from the ejecta and cooled by radiation. The halo component contributes only to the total gravitational force. The final mass distribution is determined by the competition between cooling and star formation. In real collapses angular momentum would be also of importance. However this is not accounted for in the simulations, since a fully 3D problem is at present beyond the scope of our code.

The protogalaxy is in all simulations a homogeneous mixture of a fraction F of gas and a fraction $1-F$ of non dissipative halo material within an isothermal sphere of core radius r_c . Its outer boundary is taken to be reflecting so that I do not need to assume an outer radius for the halo. This configuration is in equilibrium even after 34 free fall times.

One typical example is given in Fig. 1. This has $F = 0.1$ and initial $r_c = 0.42$ times the radial extent of the simulation. The inverse of its cooling rate is one third of the initial free fall time. Its heating rate is twice its cooling rate and its mass loss rate a quarter of that. The star formation rate varies with time and position, since it is proportional to the gas density. At the beginning of the run the star formation rate is five times as high as the cooling rate at the center of the galaxy and half the cooling rate in the outer parts.

Fig. 1 shows the "rotation curves" of the three components for equally spaced times covering in total roughly 27 initial free fall times. The velocities are calculated simply from $u_j = \sqrt{GM_j(r)}/r$ where $M_j(r)$ the mass of a given component within a radius r , and $j = 1, 2$ or 3 . The upper panel corresponds to the stellar population. As stars are formed from the gas the corresponding rotation curves rise monotonically with time to reach at the end of the simulation the short dashed line. The second panel corresponds to the gas. Its initial configuration is rather extended and has been plotted with a long dashed line. The gas collapses fast so that the maximum of the rotation curve moves sharply inwards. At the same time stars are formed out of the gas so that the

total mass in gas diminishes rapidly. At the end of the simulation roughly 95 % of the initial gas is in the form of stars. The third panel corresponds to the halo and shows clearly the inward contraction it has undergone. It is interesting to note that this is somewhat more rapid in the initial phases, where most of the baryonic mass is still in the form of rapidly collapsing gas. It is thus not correct to distinguish an initial phase of rapid collapse of the gas followed by a more gradual phase of adiabatic infall of the halo material, since the two are simultaneous. It is clear that the stimulation has not reached stationarity, but evolution at the end is slow, so I stopped the simulation. The lowermost panel gives the total rotation curve as a function of time. It is a very nice example of how, starting with a slowly rising rotation curve, one can end up with one which is flat. The rotation curve stays flat a least till $16 r_{\max}$, where r_{\max} is the radius of the maximum of the stellar rotation curve.

The relative contribution of each of the three components can be seen clearly in Fig. 2. The dot-dashed line gives the halo contribution, the long dashed line corresponds to the gaseous component and the short dashed line to the stars. The total rotation curve is given by a solid line. Note that within $2.5 r_{\max}$ the disk material dominates, while further out the halo takes over. This is definitely a maximum disk solution, and shows that the latter is well compatible with the infall scenario. Furthermore this example is in no way unique, and maximum disk or "no $m = 1$ " solutions have been found in many of the simulations.

These simulations have a large number of free parameters. Apart from the two describing the initial isothermal sphere (e.g. its central density ρ_0 and its core radius r_c) there is the fraction F of gas at the beginning of the run, the rates for star formation, gas loss, heating and cooling, and the exponent p for the Schmidt law. Other parameters could be introduced if more sophisticated heating, cooling, star formation and mass loss laws were introduced. For some combinations the end result was not at all a flat rotation curve, so that these would be dismissed as unphysical. I have made about 60 runs sofar, a number which does not permit to cover even superficially the whole parameter space but is big enough to give a feeling for the influence of some of the parameters. For example if the star formation rate was too low the final

Figure 1 (next page): Rotation curves a) due to the stellar, b) the gaseous, c) the halo component and d) the total mass distribution at 9 moments of the run. The rotation curves corresponding to the last moment of the run are plotted with a short dashed line, and the initial gaseous rotation curve with a long dashed line.

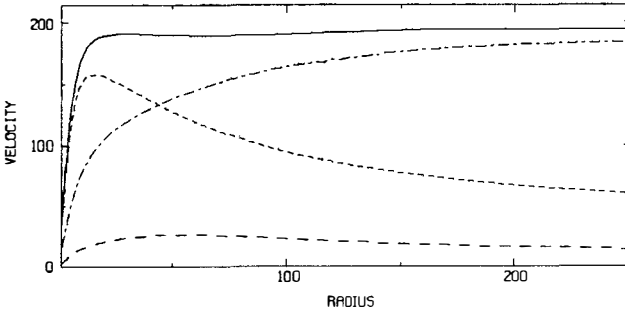
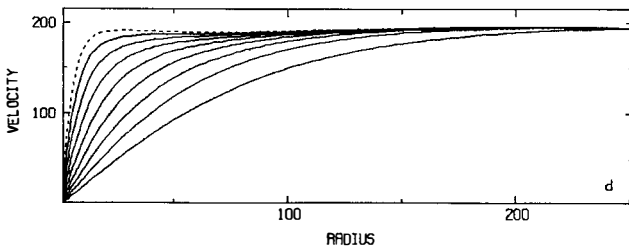
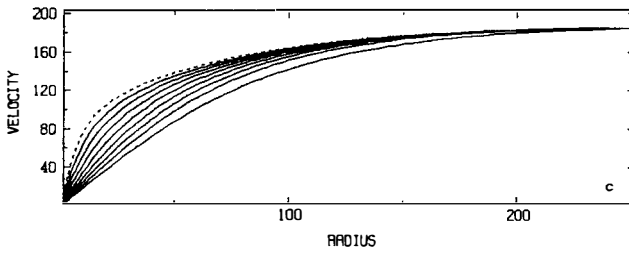
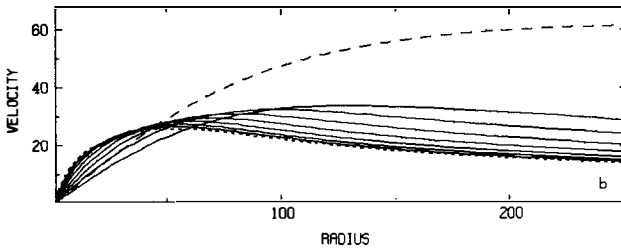
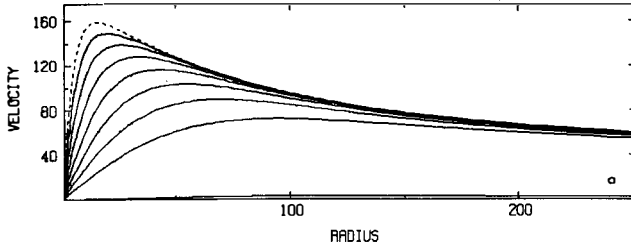


Figure 2 : Relative contribution of each of the three components to the total rotation curve.



gas and star configuration could be described as one fat baryon in the center. Amidst the simulations whose final result was a flat rotation curve both maximum disk or "no $m = 1$ " solutions and "no $m = 2$ " solutions could be found.

The results of these simulations can be also used to check the accuracy of the circular adiabatic approximation, which overestimates the response of the halo. This, as could be expected, is more pronounced for high disk to halo mass ratios than for low ones, and for flat rotation curves compared to slowly rising ones. Within a few disk scale lengths from the center the differences between the halo rotation curve calculated from the simulation and that resulting from the circular adiabatic approximation may be as high as 30 - 40 %. This leads to discrepancies of the corresponding halo masses of up to a factor of two, in good agreement with the results by Barnes (1986). The differences of the slopes of the halo rotation curves can, however, be much higher than a factor of two, and may even have different signs. The same holds for the slopes of the total rotation curves.

REFERENCES

- Athanassoula E., Bosma A. and Papaioannou S. 1987, *Astron. and Astrophys.* 179, 23
- Bahcall J. and Casertano S. 1985, *Ap. J.* 293, L7
- Barnes J.E. 1986, in "Nearly Normal Galaxies", Ed. S.M. Faber, p. 154
- Blumenthal G., Faber S., Flores R. and Primack J. 1985, *Ap. J.* 301, 27
- Chiang W.H. and Prendergast K.H. 1985, *Ap. J.* 297, 507
- Flores R. 1988, in "Evolution of large scale structures in the universe", Ed. J. Audouze and A. Szalay, in press; and CERN/TH.4756/87
- Ryden B. and Gunn J. 1984, *Bull. AAS.* 16, 487
- Ryden B. and Gunn J. 1987, *Ap. J.* 318, 15
- Van Albada T. and Sancisi R. 1986, *Phil. Trans. R. Soc. London*, 320, 15
- White S. and Rees M. 1978, *MNRAS* 183, 341

AN UPPER LIMIT TO THE LOCAL DARK MATTER OR THE MISSING "MISSING MASS"

A.C. Robin, M. Crézé, O. Bienaymé
Observatoire de Besançon
CNRS UA 040389
F-25044 BESANCON CEDEX
FRANCE



ABSTRACT

From a stellar population model based on evolution theory we build a self consistent dynamical model of the Galaxy through the Boltzmann and Poisson equation. We show that comparisons of model predictions with general star counts give strong constraints on the dynamical mass density in the solar neighbourhood. A best fit solution is obtained with a model including a small unseen-mass disc of density $.01 M_{\odot} \text{pc}^{-3}$ and 600 pc scale height. The total *dynamical* mass density in the solar neighbourhood ranges between $.09$ and $.12 M_{\odot} \text{pc}^{-3}$. These values are well compatible with published estimation of the *observed* local mass.

These values conflict with the large amount of unseen mass derived by Bahcall. So we reanalyze the density data he used, based on spectral type surveys by Uppgren. We discuss the fit of Bahcall's density models on the original Uppgren star count data through the classical Bok's $m\text{-log}\pi$ table. We show that, due to the poor statistics and non poissonian fluctuations of observed counts, most Bahcall models are compatible with the data (including models without unseen mass as well as the ones with large amounts of missing mass). The $m\text{-log}\pi$ method is shown to provide estimates of the density that are significantly biased towards getting too much missing mass.

I- INTRODUCTION

The determination of the mass density in the solar neighbourhood is one of the first tests about the existence and the composition of dark matter. Locally it is possible to measure the potential to which stars are submitted and then to dynamically determine the local mass density. On the other hand, assuming the contributions of all observed objects one gets the seen mass density. After the pioneering works of Oort^{1,2)} and Hill³⁾ on the local stellar dynamics some evidence was found that the dynamical mass was larger than the observed one.

The total observed mass density is composed as follows⁴⁾ :

- Interstellar matter (ISM): $0.04 M_{\odot} \text{pc}^{-3}$, which includes neutral hydrogen (.021), molecular hydrogen⁵⁾ (0.007), helium (0.01) and interstellar dust⁶⁾ (0.002). Sanders et al.⁷⁾ report a larger value ($.05 M_{\odot} \text{pc}^{-3}$) for the total ISM density. The uncertainties in deriving the HII density from CO observations may be as large as a factor 2 and apply to the major contributor to the ISM mass density. Hence the adopted $0.04 M_{\odot} \text{pc}^{-3}$ should be considered as a low estimate.

- Stars: We have recently synthesized stellar contributions in a global model. According to this model disc stars contribute to the local mass density for a value of $.044 M_{\odot} \text{pc}^{-3}$. Halo stars make a negligible part. The synthetic model of the Galaxy is described below.

Most determinations of the local dynamical mass density are based on the same method: A spectral type survey toward the galactic poles provides homogeneous star samples to be used as density tracers. Together with an estimation of their velocity distribution such samples give constraints to the K_z force. They give access to the local density, and to some extent to the z density distribution of the whole mass^{2,4,8,9,10)}. These approaches are limited by the size of the star samples and the difficulty of satisfying a proper "homogeneity" criteria. A detailed track of such works can be found in the successive reports of IAU commission 33¹¹⁾. Estimations of the dynamical mass density obtained through this method range between 0.08 and .25. This leaves room to a large amount of missing mass as well as none. Most recently Hill et al.⁴⁾ obtained $.14 M_{\odot} \text{pc}^{-3}$, and Bahcall^{9,10)} obtained values ranging between .18 and .23. These latter values imply that at least half the total mass density is not seen in the solar neighbourhood (the so-called *missing mass*. For comparison let us remind that the local density of the massive corona - the *dark matter*- imposed by the shape of the rotation curve is no more than $.01 M_{\odot} \text{pc}^{-3}$). Actually complete precision studies are seldom associated to these estimations. We show in Sect. 5 and in Cr ez e et al.²⁾ that errors are larger than usually emphasized.

We describe here a new method to measure the vertical scale heights of the disc stars and therefore to constrain the vertical potential. The observational constraint is provided by general star counts of magnitude ranging between 6 and 22, towards various galactic directions. This method is shown to give strong constraints on the density and scale height of an hypothetical disc of missing mass.

We use a synthetic model of galactic stellar populations described in Robin and Crézé¹³). This model was based on three main ingredients: (a) a distribution of ages for the various stellar species in the solar neighbourhood, derived from considerations on star formation and galaxy evolution; (b) an age-velocity dispersion relation derived from kinematic studies; (c) a velocity distribution/density law relation resulting from the Oort potential. In order to achieve dynamical consistency we now drop hypothesis (c) and do not impose any a priori shape of the galactic potential towards the galactic poles: the stellar mass density distributions generated by the population model are supplemented by interstellar matter and unseen mass contributions (including corona, bulge, and hypothetical unseen mass disc). All these mass components, entered into the Poisson equation, impose a potential. Corona and bulge parameters are adjusted until the potential produces an acceptable rotation curve. The new potential combined with the above quoted velocity dispersions in the Boltzmann equation, produces a modified density distribution for each stellar component. The process is iterated until the mass model stabilizes thus producing a self-consistent solution.

A series of self-consistent mass models has been generated under different hypotheses on the unseen disc component. Two types of observational constraints are used in order to discriminate acceptable models:

- Density distribution of all stellar components are used to predict general star counts. The predicted counts in magnitude and colour are then compared to observations over a wide range of magnitude (V from 6 to 22). The goodness of fit is estimated using a likelihood computation scheme. These comparisons mainly constrain the mass distribution perpendicular to the galactic plane.
- The potentials generate rotation curves which are also compared with observations. This comparison mainly constrains the central bulge and the corona mass distribution.

In Sect. 2 we summarize the philosophy and main ingredients of the stellar population model. In Sect. 3 we describe the mass model and the resolution of the equations to get dynamical self consistency. In Sect. 4 we show how general star counts strongly constrain the disc scale heights and consequently the potential and are consistent with no missing mass disc in the solar neighbourhood. In Sect. 5 we reexamine previous attempts to determine the K_z force, we compute the statistical errors and show that data used so far in such analysis in the magnitude range within which homogeneity and completeness can be assessed are unable to produce definitive conclusions on the existence or non existence of a local missing mass disc.

2. THE MODEL OF POPULATION SYNTHESIS

2.1 Mainsprings

Any attempt to predict the apparent distribution of observable properties of stars in a given field of view is based on the equation of stellar statistics :

$$\mathcal{A}(m) = \int \phi(M) \rho(r) \omega r^2 dr \quad (1)$$

$\mathcal{A}(m)$ is the number of stars with apparent magnitude m in the solid angle ω , M the absolute magnitude and r the heliocentric distance. Since the density $\rho(r)$ as well as the luminosity function $\phi(M)$ may be extremely different depending on population, equation (1) breaks in a sum of components with different ρ and ϕ .

Equation (1) is commonly used as an integral equation for $\rho(r)$. Solving this equation involves a number of numerical problems^{14,15}). The synthetic approach consists in making assumptions on both ρ and ϕ for all components and then attempting to reproduce $\mathcal{A}(m)$ by trial and errors. In order to reduce ambiguities, observations in various galactic fields, using different filters and combining different kinds of information (magnitudes, colours, proper motions, radial velocities, etc.) are used.

Our specific approach is based on outsets directly derived from current pictures of galactic evolution : stars born at the same epoch of galactic life have been formed out of similar interstellar medium, their space and velocity distributions reflect a common dynamical history, while their mass distribution at birth (Initial mass function) defines the way they have spread in the HR diagram.

On these grounds, we first try to define a distribution $\phi(M_{\text{bol}}, T_{\text{eff}}, \text{Age})$ of the number of stars per cubic parsec in a given cell of the HR diagram, with ages in a given range, near the Sun. ϕ , if perfectly known, would define the stellar content in the solar neighbourhood. Chemical composition is introduced in the same way through the relative frequency of stars with a given metal content Z , $\psi(Z, \text{Age})$. ψ is allowed to vary along a galactic radius. Since the age is a driving parameter of density distributions as well, it will govern the process of deriving how many stars of each kind are to be expected everywhere in the galaxy.

Once the distribution of intrinsic properties of stars in the solar neighbourhood is specified, numbers of stars with similar properties throughout the galaxy can be obtained provided that the density $\rho(r, l, b, \text{Age})$ is known.

$$N = \psi \phi \rho r^2 \cos b dl db dr \quad (2)$$

The coordinates r , l , b , and intrinsic properties of stars near this point being fixed, one can derive their contribution to observations from the earth in any specified pass band (assuming that necessary calibrations are available). It is worth noting that usual ambiguities in deriving intrinsic parameters from photometric measurements vanish here. Then a trivial integration along any specified line of sight can be performed using a step method.

Extinction is taken into account by using a space distribution of the absorbing material scaled to a mean density of diffuse interstellar dust near the sun. Detected inhomogeneities can be introduced as well.

2.2. Ingredients

2.2.1. Age distribution of disc stars

We have used the Rocca-Volmerange evolution model^{16,17}): A 3-slope Initial Mass Function, stellar birth rate proportional to the mass of gas, one zone with instantaneous recycling. Starting with a given mass of gas, stars are formed according to the stellar birth rate and they evolve along standard evolutionary tracks. After 10 billion years of evolution we get the number of stars in each bin of the 3 dimensional HR diagram. It produces the function $\phi(M_{\text{bol}}, \text{Log}T_{\text{eff}}, \text{Age})$ for the disc stars.

The luminosity function derived by Wielen^{18,19}) from the catalogues of Gliese^{20,21}) is our most direct access to the luminosity distribution of stars in the solar neighbourhood. We use it as an overall marginal constraint to our function. The Michigan Catalogue^{22,23,24}) is used to derive the absolute magnitude spectral type distribution of stars of magnitude $-2 \leq M_V \leq 2$.

2.2.2. Spheroid

The luminosity function has been adopted from the mean globular cluster luminosity function from Da Costa²⁵) for stars brighter than $M_V = 6$. It includes the so called globular cluster feature (i.e. a significant dip between $M_V = 2$ and 4.5). It has been extended faintwards parallele to the Wielen luminosity function 0.21 bluer in B-V. Comparisons to remote star counts lead to give to the spheroid stars a $1.4 \cdot 10^{-4}$ stars pc^{-3} local density.

2.2.3. Intermediate population

The typical sequence used for this population is the one of the relatively metal rich globular cluster 47Tuc with a density normalization of 1.6% of the disc. This value is not yet well constrained by star counts and could be change by a factor of 2.

3. GETTING DYNAMICAL CONSISTENCY

3.1 The mass model

The model of stellar populations allows to build a mass model of the Galaxy as follows: we compute the contribution to the potential of the stellar components using standard mass-luminosity relation. To these components we add :

- A disc of interstellar matter (ISM) with a double-exponential density law. The ISM radial distribution is assumed to be similar to that of the young disc with scale length 4500 pc. We adopt a local density $0.04 M_{\odot} \text{pc}^{-3}$ and scale height 140 pc, in agreement with Spitzer's determination²⁶) (respectively $0.045 M_{\odot} \text{pc}^{-3}$ and 125 pc).
- A central bulge modeled by a point mass. The precise shape of the bulge is poorly known and is usually deduced from HI or CO rotation curve in the innermost part of the Galaxy.
- A corona of matter (the "dark halo"). This component is needed to explain flat rotation curves at large radii in spiral galaxies²⁷). Evidence for such a component is more indirect in the case of our own Galaxy (escape velocity of stars, velocity dispersion of spheroid material^{28,29}) and uncertainties in modeling the mass and distribution of the unseen coronal

matter are accordingly larger. The core radius r_c and the central density ρ_c are constrained by the rotation curve.

- An Unseen-Mass Disc (hereafter UMD) is added to take into account the unseen matter in the solar neighbourhood suggested by Oort. The adopted ρ_{umd} density law is a double exponential with scale length 4500 pc. The local density ρ_{umd} is allowed to vary between 0 and $0.12 M_{\odot} \text{pc}^{-3}$ and the scale height h_{umd} between 200 and 1000 pc. Dynamical models involving a wide range of UMD were tested. A set of representative models have been given in Table 2 of Bienaymé et al³⁰). Outside this range of parameters models give too massive a UMD incompatible with the rotation curve or/and are unable to match observed star counts (see Sect. 4). We have also tried different functional forms for the UMD. These latter forms do not play a critical role in potential computations.

3.2 Dynamical constraints

Each set of UMD parameters ($\rho_{\text{umd}}/h_{\text{umd}}$) produces a different galactic mass model. For each model the remaining free parameters are set by dynamical constraints : (1) the observed rotation curve defines the bulge and corona characteristics, (2) the first order moment of the collisionless Boltzmann equation defines the thicknesses of each of the stellar discs.

3.2.1. Constraints from the rotation curve

In a first step we give numerical estimates for the unknown quantities M_B , ρ_c , r_c (bulge and corona parameters), and disc thicknesses (i.e. eccentricities), and we adopt one of the UMD's from the set. We numerically solve the Poisson equation. We thus obtain a first guess of the potential $\Phi(r,z)$ and the radial force $K_z(r, z)$. Data are taken from Caldwell et al.³¹) assuming $R_{\odot} = 8.5$ kpc and a circular velocity at the solar radius $V_{\odot} = 220 \text{ kms}^{-1}$. Corona and bulge parameters are then determined by fitting the predicted rotation curve to the data. We obtain a new potential that satisfies the first dynamical constraint and use it in the Boltzmann equation.

3.2.2 Constraints from the Boltzmann equation

The first order moment of the collisionless Boltzmann equation for an isothermal stellar population with mass density $\rho(r,z)$ and a mean velocity dispersion σ_w can be expressed as³²) :

$$-\Phi(r,z) + \Phi(r,0) = \sigma_w^2 \ln(\rho(r,z) / \rho(r,0)) \quad (3)$$

where we have neglected the cross terms $\langle V_r V_z \rangle$ assuming radial and vertical motions to be decoupled. This approximation limits the validity of Eq. (3) to $z = \pm 1$ kpc above the galactic plane for $r = R_{\odot}$. Equation (3) is valid for each stellar disc component old enough for its velocity distribution to have achieved relaxation, to an isothermal state. For this reason the youngest stellar component (age $< 10^9$ yr) is not bound to satisfy Eq (3) and its axis ratio has been fixed to 0.014. We use an age - σ_w relation adapted from Mayor³³). Playing with the disc thicknesses, we adjust the disc density distributions until Eq. (3) is accurately satisfied, at least within 1 kpc out of the galactic plane at the solar galactic radius.

Since we solve Poisson and Boltzmann equation separately we do not obtain a potential satisfying both constraints. So we come back to the rotation curve to fit again the bulge and corona parameters. We iterate the process (figure 1) until the potential and the parameter changes get small enough (less than 1%). The process converges in two or three iterations.

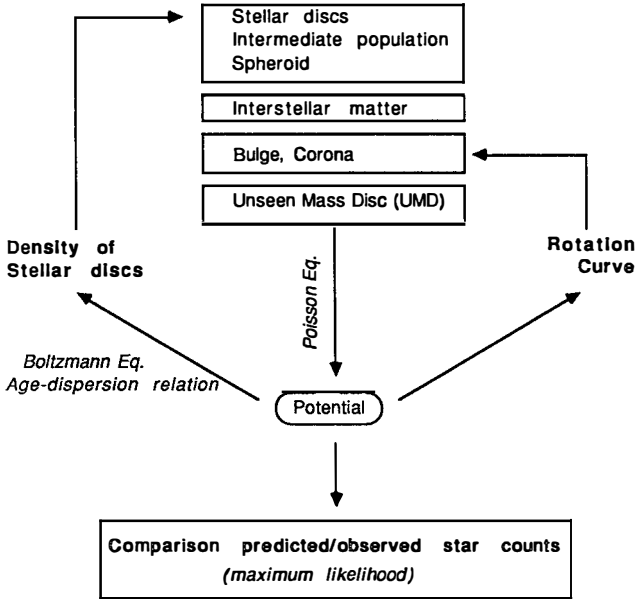


Figure 1: Scheme of the method used to get a self consistent galaxy model constrained by the rotation curve and general star counts.

4. CONSTRAINTS FROM GENERAL STAR COUNTS

So far we have obtained a set of dynamically consistent models differing from each other by the density and thickness of the UMD and consequently by the shape of the old disc subcomponents, and by the corona. The star count predictions from different models will be different due to their scale heights and ellipticities. The resulting set of models is used to compute star counts. Comparison to observational data leads to reject unreliable models, i.e. unacceptable UMD hypotheses.

4.1. Observational data

Observations used to constrain the model cover a wide range of magnitude (from 6 to 22 in V) and a set of directions at high and intermediate latitudes (galactic poles, Aquarius and Serpens ($l = 37^\circ$, $b = \pm 51^\circ$), SA68 ($l = 111^\circ$, $b = 46^\circ$), SA94 ($l = 175.3^\circ$, $b = 49.3^\circ$)).

Data are from the data base of the Centre de Données Stellaires (CDS) for bright stars and various authors^{34,35,36,37,38,39,40} for stars fainter than 9.

4.2. Method

For each model we compute the likelihood of the whole set of data under the hypothesis that this model is correct. The maximum likelihood method is described in Appendix C of Bienaymé et al³⁰). It gives the best estimates and rejection limits.

Considering all data the maximum likelihood is obtained with the model with a UMD of 0.01 local mass density and 600 pc scale height. The acceptable range lies between no UMD at all and a UMD density $0.03 M_{\odot} \text{pc}^{-3}$. Scale heights of the exponential unseen mass component range between 300 and 800 pc, its surface density between 0 and $24 M_{\odot} \text{pc}^{-2}$.

Table 1 summarizes the mass density and surface density of all components in the case of the best fit model. The age-velocity dispersion relation is also given for the stellar discs. Details of the fitting procedure and comparison to star counts are extensively given in Bienaymé et al³⁰).

Table 1. Mass density and surface density of all components of the best fit model in the solar neighbourhood (* indicates sum without the corona).

Population	Mass density $M_{\odot} \text{pc}^{-3}$	Surface density $M_{\odot} \text{pc}^{-2}$	Velocity dispersion km s^{-1}
Disc <i>age (Gyr)</i>			
0-0.15	7.40 E-04	0.092	6.
0.15-1	6.78 E-03	2.397	10.
1-2	3.93 E-03	2.261	14.
2-3	4.47 E-03	3.710	18.5
3-5	5.42 E-03	5.878	23.
5-7	7.02 E-03	8.402	25.
7-10	1.52 E-02	18.197	25.
Total stellar disc	4.36 E-02	40.937	
Intermediate pop.	5.28 E-05	0.158	
Spheroid	5.28 E-06	0.155	
Interstellar matter	4.00 E-02	11.2	
Corona	7.90 E-03		
Unseen mass disc	0 - 0.03	0. - 24.	
TOTAL	0.092 - 0.12 0.084 - 0.11*	52.0 - 76.0*	

5. UNCERTAINTIES ON BAHCALL DETERMINATION

The result described above conflicts with the large amount of missing mass derived by Bahcall^{9,10}) in a reinvestigation of density laws produced by Uppgren^{41,42}) for F dwarfs

and K giants on the basis of spectral type survey. We suspected that the discrepancy was due to a drastic overconfidence placed on the constraint imposed by Uggren star counts on the density law : Bahcall did not directly use star counts as constraints to his models, he used densities derived from smoothed counts by other investigators through the $m\text{-log}\pi$ table. He emphasized that Poisson fluctuations were negligible compared to systematic uncertainties. We show that, due to the poor statistics and non poissonian fluctuations of observed counts, most of Bahcall's models are compatible with the data (including models without unseen mass as well as the ones with large amounts of missing mass).

5.1 The data

The data under consideration come from a spectral survey on objective-prism spectra by Uggren^{41,42}) in the north galactic polar cap. The survey covers 134 square degrees for F dwarf sample and 396 for K giants. The shape of the density law of homogeneous sample towards the galactic poles is expected to provide a tracer of the potential.

K giant samples offer several advantages: being intrinsically bright, they can be used to trace the potential away from the galactic plane. Furthermore being old on average, even a substantial age mixture does not alter drastically the velocity dispersion. However, beyond 500 pc off the galactic plane, unrecognized Population II giants may contribute to the giant star counts. Other difficulties arise from the fact that the local giant density is so small that the zero point of the density law cannot be easily estimated, and that the absolute magnitude of K0 to K5 giants is poorly known due to the difficulty of getting good parallaxes for a significant number of these stars.

F dwarfs are more numerous locally and their calibration seems well established. However to get a better statistics we have to consider spectral types F5 and F8 altogether although the density law of each type separately indicates that they have not exactly the same scale height⁴). The second point is that Bahcall used smoothed Uggren's data such that Poissonian uncertainties cannot be taken into account.

Another independant K giant sample has been recently observed⁴³) towards the south galactic pole within 81 square degrees. Although it is in a smaller area than Uggren's, and subject to the same contamination by population II stars, it is still worth using for a $m\text{-log}\pi$ determination of the density law.

5.2 Bahcall densities versus Uggren counts

Uggren derived the density law from his star counts assuming that the luminosity function is known. This is currently achieved through the classical $m\text{-log}\pi$ table⁴⁴) after smoothing the $\mathcal{A}(m)$ curve. The method is equivalent to integrating numerically the equation of stellar statistics (eq. (1)) in the case of an homogeneous sample.

Bahcall fitted his model densities to Uggren's densities obtained by this method. In the following we reverse the process and introduce Bahcall density models in equation (1) so as to compute predicted counts. These counts are then directly compared to raw star counts. We also keep all Bahcall's hypotheses concerning the luminosity function and the density

laws: each law corresponds to a potential derived under each assumed unseen mass disc proportional to the observed disc density. Models differ from each others through the proportionality factor P from $P=0.0$ to $P=2.0$. The luminosity function is a gaussian defined by a mean magnitude and a dispersion.

$m\text{-log}\pi$ tables allow to get the star counts $\mathcal{A}(m)$ deduced from Bahcall models with various missing mass. Detailed description of the method can be found in Cr ez e et al¹²).

To compare model predictions with observed counts, we use the maximum likelihood method. We applied this method to derive F dwarf count predictions from 3 Bahcall models with missing mass parameters $P= 0.0, 0.97$ and 2.0 corresponding to a local mass density $0.1, 0.2$ and $0.3 M_{\odot} \text{pc}^{-3}$ respectively. For K giants we only apply to models $P=0.5$ and 1.5 since density laws for others were not published by Bahcall. Bahcall decided to limit his fit to 200 pc for F dwarfs and 600 pc for K giants. He stated that beyond these limits the samples may be substantially contaminated by higher velocity stars. Consequently only stars brighter than $B= 10$ actually contribute to the fit.

In the case of F dwarf sample we obtain high likelihood values for the models 0.0 and 0.97 while the model $P=2.0$ is completely ruled out. On figure 2a, Upgren's raw data are compared with Bahcall model between magnitudes 6 and 10 . Error bars on raw data are only 1 sigma Poisson error. It shows that the only points that really constrain the fit are at magnitude $B=9.5$ and 10 .

In the case of K giants figure 2b show the comparison between Bahcall models and Upgren and McNeil samples respectively. Error bars are even larger and both Bahcall models with $P=0.5$ and $P=1.5$ are compatible with the data.

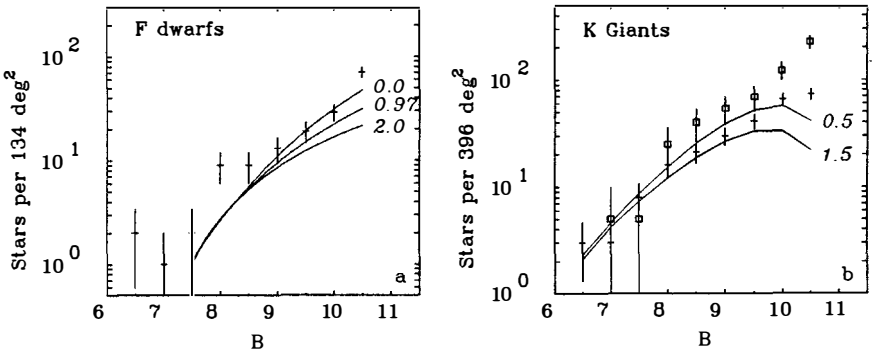


Figure 2: Comparison of star counts with Bahcall models with various missing mass : (a) F dwarf data from Upgren and missing mass models $P=0, 0.97$ and 2 . (b) K giant data from Upgren (plus signs) and McNeil (squares) and missing mass models $P=0.5$ and 1.5 . Error bars account for 1 sigma of Poisson statistics.

To be able to put quantitative error bars on the estimation of the missing mass from those samples, we made a simulation to estimate the probability distribution of the actual parent density law given a star count sample. The detailed process is described in Cr ez e et

al.12). The probability distribution has been found asymmetric such that the estimation of a best fit model is biased towards lower scale heights i.e. towards more missing mass. However the dispersion of this distribution is so large that any Bahcall model from no missing mass to 150 % of missing mass are compatible with the data.

Another important lesson of these numerical experiments is that simulated counts, although based on realistic hypotheses and including random observation errors are far more regular than actual ones. This means that real samples are not just random achievements of the parent laws we are trying to find. There are certainly selection effects and incompleteness effects and possibly failures in discriminating spectral classes or irregular systematic errors in the magnitude scale which make the result even more uncertain.

Thus we conclude that there is very little information relevant to the mass density in the galactic plane available in this F dwarf sample and even less in the K giant ones. Finally there is no real conflict between Bahcall's results if we take into account the uncertainties and the much more severe constraints derived from general star counts, supporting the conclusion of little or no missing mass in the disc.

6. CONCLUSION

The quite small value of missing mass in the solar neighbourhood deduced from our galaxy model is well inside uncertainties on the observed mass density, specially on the interstellar matter. We have set an upper limit to the local density of any disc-like dark matter. Anyway it does not rule out hypotheses of any kind of dark matter in the galactic halo. Our model includes such a dark corona necessary to fit a flat rotation curve. The local density of this spherical corona is small ($.008 M_{\odot} \text{pc}^{-3}$). The effect produced by a small Unseen Mass Disc is similar to the one we would get from a flattened corona.

Some new evolution models have been made recently by Larson⁴⁵) among others to account for the large amount of missing mass claimed by Bahcall. This model creates dark matter in the form of very cool white dwarfs using a bimodal initial mass function with decreasing Star Formation Rate for the high mass mode and a fast white dwarf cooling time. Our result rules out this scenario.

REFERENCES

- 1) Oort, J.H., 1932, *Bull. Astr. Inst. Netherlands* **6**, 249.
- 2) Oort, J.H., 1960, *Bull. Astr. Inst. Netherlands* **15**, 45.
- 3) Hill, G., 1960, *Bull. Astr. Inst. Netherlands* **15**, 1.
- 4) Hill, G., Hilditch, R.W., Barnes, J.V., 1979, *Mon. Not. R. Astron. Soc.* **186**, 813.
- 5) Savage, B.D., Bohlin, R.C., Drake, J.F., Budich, W, 1977, *Astrophys. J.* **216**, 291
- 6) Allen, C.W., 1973, *Astrophysical Quantities*, 3rd Edition, The Athlone Press, University of London.
- 7) Sanders, D.B., Solomon, P.M., Scoville, N.Z., 1984, *Astrophys. J.* **276**, 182
- 8) Turon-Lacarrieu, C., 1971, *Astron. Astrophys.* **14**, 95

- 9) Bahcall, J.N., 1984, *Astrophys. J.* **276**, 169
- 10) Bahcall, J.N., 1984, *Astrophys. J.* **287**, 926
- 11) Wielen, R., 1986, *Mitt. Astron. Rech. Instit. Heidelberg Ser. A*, n° 176 (report I.A.U. Commission 33)
- 12) Crézé, M, Robin, A.C., Bienaymé, O., 1988, Besançon Observatory preprint
- 13) Robin, A.C., Crézé, M., 1986, *Astron. Astrophys.* **157**, 71
- 14) Turon-Lacarrière, C., 1977, *Highlights of Astronomy* **4**, part II, 79
- 15) Ochsenbein F., Bischoff M., 1982, Automated data retrieval in Astronomy, IAU Coll. **64**, p. 211, Jaschek and Heintz Ed.
- 16) Rocca-Volmerange, B., Lequeux, J., Maucherat-Joubert, M., 1981, *Astron. Astrophys.* **104**, 177
- 17) Vangioni-Flam, E., 1980, Thèse de doctorat de Spécialité, Université Paris VII
- 18) Wielen, R., 1974, *Highlights of Astronomy* **3**, 395
- 19) Wielen, R., Jahreiss, H., Krüger, R., 1983, IAU Coll. **76**, The Nearby Stars and the Stellar Luminosity Function, Eds. A.G.D. Philip and A.R. Uppgren, p. 163
- 20) Gliese, W., 1969, Catalogue of Nearby Stars, *Veröff. Astr. Rech. Inst Heidelberg* **22**, 1
- 21) Gliese, W., Jahreiss, H., 1979, *Astron. Astrophys. Suppl. Ser.* **38**, 423
- 22) Houk N., Cowley, A.P., 1975, Michigan Catalogue of Two-Dimensional Spectral Types for the HD stars Vol. 1, Univ. Michigan, Ann Arbor.
- 23) Houk N., 1978, Michigan Catalogue of Two-Dimensional Spectral Types for the HD stars Vol. 2, Univ. Michigan, Ann Arbor.
- 24) Houk N., 1982, Michigan Catalogue of Two-Dimensional Spectral Types for the HD stars Vol. 3, Univ. Michigan, Ann Arbor.
- 25) Da Costa, G.S., 1982, *Astron. J.* **87**, 990
- 26) Spitzer, L. Jr, 1978, Physical Processes in the Interstellar medium, ch. 11, Wiley (New York)
- 27) Bosma, A. 1978, Thesis, University of Groningen
- 28) Hartwick, F.D.A., Sargent, W.L.W., 1978, *Astrophys. J.* **221**, 512
- 29) Lynden-Bell, D., Cannon, R.D., Godwin, P.J., 1983, *Monthly Not. Roy. Astron. Soc.* **204**, 87p
- 30) Bienaymé, O., Robin, A.C., Crézé, M., 1987, *Astron. Astrophys.* **180**, 94.
- 31) Caldwell, J.A.R., Ostriker, J.P., 1981, *Astrophys. J.* **251**, 61
- 32) Mihalas, D., 1968, Galactic Structure, Freeman (San Francisco)
- 33) Mayor, M., 1974, *Astron. Astrophys.* **32**, 321
- 34) Bok, B.J., Basinski, J., 1964, *Memoirs Mt Stromlo Obs.* **16**, 1
- 35) Chiu, L.-T.G., 1980, *Astrophys. J. Suppl.* **44**, 31
- 36) Kron, R.G., 1980, *Astrophys. J.; Suppl.* **43**, 305
- 37) Koo, D.C., Kron, R.G., 1982, *Astron. Astrophys.* **105**, 107
- 38) Tritton, K.P., Morton, D.C., 1984, *Monthly Not. Roy. Astron. Soc.* **209**, 429
- 39) Gilmore, G., Reid, N., Hewett, P., 1985, *Monthly Not. Roy. Astron. Soc.* **213**, 257
- 40) Friel, E.D., Cudworth, K.L., 1986, *Astron. J.* **91**, 293
- 41) Uppgren, A.R., 1962, *Astron. J.* **67**, 37.
- 42) Uppgren, A.R., 1963, *Astron. J.* **68**, 194.
- 43) McNeil, R.C., 1986, *Astron. J.* **92**, 335.
- 44) Bok, B.J., 1937, The distribution of stars in Space, University of Chicago Press.
- 45) Larson, R.B., 1986, *Monthly Not. Roy. Astron. Soc.* **218**, 409

EVOLUTION OF HEAVY-ELEMENT ABUNDANCES IN THE GALACTIC HALO AND DISK

G. J. MATHEWS

Lawrence Livermore National Laboratory, Livermore, CA 94550 USA

J. J. COWAN

Department of Physics and Astronomy, University of Oklahoma
Norman, OK 73019 USA

and

Harvard-Smithsonian Center for Astrophysics, Cambridge, MA 02138 USA

and

D. N. SCHRAMM

Department of Astronomy and Astrophysics, University of Chicago
Chicago, IL 60637 USA

ABSTRACT

The constraints on the universal energy density and cosmological constant from cosmochronological ages and the Hubble age are reviewed. Observational evidence for the galactic chemical evolution of the heavy-element chronometers is described in the context of numerical models. The viability of the recently discovered Th/Nd stellar chronometer is discussed, along with the suggestion that high r-process abundances in metal-poor stars may have resulted from a primordial r-process, as may be required by some inhomogeneous cosmologies.

I. INTRODUCTION

The evolution of heavy-element abundances is connected with the dark matter theme of this conference in two ways. On the one hand, the heavy-element abundances provide cosmochronological ages which when compared to the Hubble age yield an independent indicator of the value for present universal energy density, and hence the total amount of dark matter¹⁾. On the other hand, as we have already heard at this conference²⁾, cosmological models in which the universe is presently closed by baryonic dark matter require that primordial nucleosynthesis occur in an inhomogeneous environment. In such environments, the constraints from observed light elemental abundances can be satisfied. However, the preliminary results from these models seem to indicate that at least some heavy-element (r-process) nucleosynthesis is unavoidable. Regarding both of these points, considerable data has accumulated recently³⁻⁶⁾ which significantly clarifies the history of the galactic abundances of heavy elements and even provides⁷⁾ for a new stellar nuclear cosmochronometer. This paper discusses heavy element galactic chemical evolution in the context of these data.

II. NUCLEOCOSMOCHRONOLOGY AND DARK MATTER

The connection between nucleocosmochronology and the universal energy density has recently been reviewed in detail¹⁾. The essential connection is simply obtained from the Friedman equation for the universal expansion rate (or inverse Hubble time, T_0) in the present matter-dominated epoch, which we write as

$$H_0^2 = \frac{1}{T_0^2} = \left[\frac{\dot{R}}{R} \right]^2 = \frac{8}{3} \pi G \rho_c (\Omega + \lambda) - \frac{kc^2}{R^2} \quad (1)$$

where H_0 is the present value of the Hubble constant, R is the scale factor, ρ_c is the critical mass-energy density necessary to close the universe, Ω is the ratio of the present baryon density to the critical density, λ corresponds to a cosmological constant in units of the critical density, and $k = 0, \pm 1$ is the curvature parameter. (For the purposes

of this discussion, we neglect speculation on any contribution from nonbaryonic dark matter.)

Inflationary cosmology requires that $\Omega + \lambda = 1$, *i.e.* $k = 0$. With this constraint, there are simple analytic relations¹⁾ between the ratio of elapsed time to Hubble time, t_0/T_0 , and Ω :

$$\Omega < 1, \quad \lambda > 0; \quad t_0/T_0 = \frac{2}{3(1-\Omega)^{1/2}} \tanh^{-1}(1-\Omega)^{1/2} > 2/3 \quad (2a)$$

$$\Omega = 1, \quad \lambda = 0; \quad t_0/T_0 = 2/3 \quad (2b)$$

$$\Omega > 1, \quad \lambda < 0; \quad t_0/T_0 = \frac{2}{3(\Omega-1)^{1/2}} \tan^{-1}(\Omega-1)^{1/2} < 2/3 \quad (2c)$$

Estimates of the age of the universe based on actinide chronometers range from 10 to 20 Gyr^{8,9)}. The uncertainty in the chronometric age can be traced in large part to uncertainties in the nuclear binding energies, fission properties, and the beta-decay strength function for nuclei near the termination of the r-process path, as well as the uncertainty in the galactic chemical evolution parameters described here.

As far as nuclear properties are concerned, we note that recent calculations^{8,10)} which utilize a more consistent set of beta-decay strength functions and fission barriers favor a lower galactic age (*c.f.* 11.0 ± 1.6 Gyr¹⁾; 13.5 ± 1.2 Gyr¹⁰⁾). With a chronometric age for the universe of 10 – 15 Gyr and a Hubble constant of 58 ± 5 km sec⁻¹ Mpc⁻¹ from SNI light curves¹⁾, the ratio of chronometric time to Hubble time becomes $t_0 H_0 = t_0/T_0 = 0.6-0.9$ for which $0.1 < \Omega < 1.5$ from Eqs. (2a-c). Note, however, that other determinations of the Hubble constant from SNI's¹¹⁾ and SNII's¹²⁾, including SN1987A, deduce a larger uncertainty, $H_0 = 60 \pm 15$ km sec⁻¹ Mpc⁻¹. This larger uncertainty would imply a larger range for Ω .

III. Th/Nd COSMOCHRONOLOGY

The lower limit to the present value of Ω is set by the upper limit to the galactic age. Therefore we were particularly intrigued by the recent observations of Butcher⁷⁾ of the Th/Nd line ratios in G-dwarfs. These data represent the first measurement of an actinide chronometer outside the solar system. They were interpreted in Butcher⁷⁾ to represent an upper limit of 9.6 Gyr to the galactic age. However, that conclusion was obtained by assuming equal production functions for Th and Nd and a linear approximation to the variation of Th/Nd with time. We have reanalyzed these data in the context of numerical separable galactic chemical evolution models which explicitly take into account the different nucleosynthetic origins of Th (r-process) and Nd (50% s-process + 50% r-process), as well as the loss of Th and Nd from the interstellar medium due to star formation and radioactive decay. We use the Miller-Scalo¹³⁾ initial mass function and variable infall rates of extragalactic material depleted in heavy elements. Figure 1 shows an example¹⁴⁾ of numerical models for different galactic ages. Depending upon whether or not we include the secondary dependence of s-process Nd on the preexisting Fe abundance, we deduce 3σ upper limits to the galactic age of 13 to 18 Gyr. Thus, the galactic age is not constrained by these data to be less than 10 Gyr nor is Ω required to be ~ 1 .

IV. IS THERE EVIDENCE FOR A PRIMORDIAL r-PROCESS?

Finally, we consider the question of whether there is any evidence in observed abundances for a primordial r-process as suggested^{2,15)} in recent studies of inhomogeneous cosmologies. Figure 2 shows the observed³⁻⁶⁾ correlation of the Eu abundance with the Fe abundance for metal-poor stars in the halo. Since $\sim 95\%$ ¹⁶⁻¹⁷⁾ of the Eu in the solar system is of r-process origin, this correlation roughly corresponds to the behavior of pure r-process material relative to Fe over the history of the Galaxy. Also shown for comparison is a prediction of this correlation for an evolutionary model with a constant

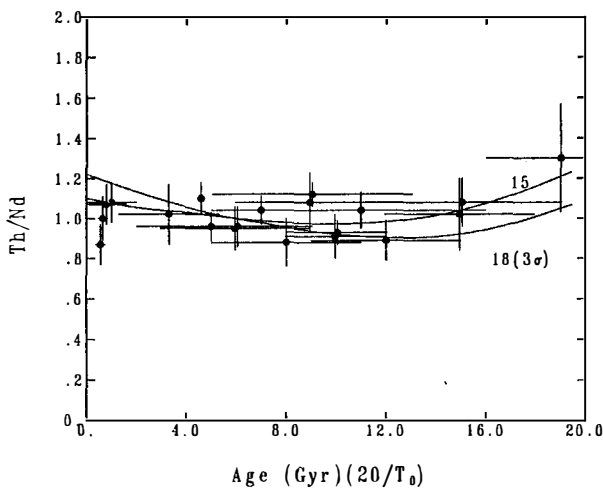


Fig. 2. Observed³⁻⁶ [Eu/H] versus [Fe/H] (points) compared with a numerical calculation (line).

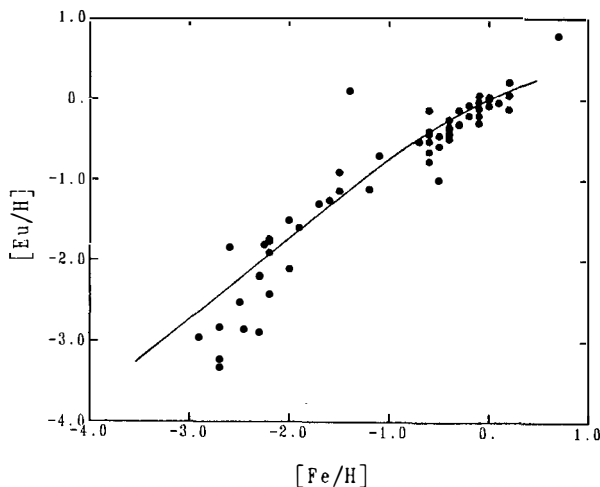


Fig. 1. Calculated (lines) Th/Nd line ratios compared with observations⁷⁾ (points) as a function of apparent stellar age. The upper line is the highest age, 15 Gyr, for which the fit to the data gives a reduced $\chi^2 \leq 1$. The lower line is the 3σ upper limit to the galactic age, 18 Gyr.

star formation rate, no extragalactic infall, and an age of 15 Gyr. To estimate the Fe evolution, the rate of Type I supernovae is taken to be proportional to the accumulated total mass of C-O white dwarf remnants. It is also assumed that SNII's have contributed to half of the solar system Fe abundance¹⁸⁾. The presence of significant primordial r-process material would correspond to a deviation of the data *above* the calculated line when the Fe abundance is small. If anything, the data tend to indicate a deviation *below* the line for $[\text{Fe}/\text{H}] \lesssim -2$. This would seem to indicate that any pregalactic nucleosynthesis of heavy elements probably did not produce an excess of r-process elements relative to Fe.

V. CONCLUSIONS

We have summarized the dependence of the present day value of Ω on the ratio of galactic age to Hubble age. We find that the present cosmochronometers, including stellar Th/Nd, are consistent with $\Omega \sim 0.1 - 1.5$ in a universe with $\Omega + \lambda = 1$. Furthermore, there is no evidence for a primordial enhancement of r-process elements relative to iron as predicted by some models of inhomogeneous cosmologies.

VI. ACKNOWLEDGEMENTS

The authors acknowledge useful correspondence with H. R. Butcher, D. D. Clayton and W. A. Fowler. Work performed in part under auspices of the U. S. Department of Energy at Lawrence Livermore National Laboratory under contract number W-7405-ENG-48, and supported in part by NSF grant AST-8521705. J.J.C. acknowledges support from NASA grant NGR 22-007-272 and Smithsonian Institutional funds.

REFERENCES

- 1) Fowler, W. A., *Q. J. R. Astr. Soc.* **28**, 87 (1987).
- 2) Mathews, G. J., Fuller, G. M., Alcock, C. R. and Kajino, T., (this conference proceedings) (1988).

- 3) Sneden, C., Pilachowski, C. A., Gilroy, K. K. and Cowan, J. J., in *The Impact of High S/N Spectroscopy on Stellar Physics*, I A U Symposium **132**, eds. G. Cayrel and M. Spite, (Dordrecht:Reidel), in press (1988).
- 4) Gilroy, K. K., Sneden, C., Pilachowski, C. A. and Cowan, J. J., *Astrophys. J.* **327**, 298 (1988).
- 5) Butcher, H. R., *Astrophys. J.* **199**, 710 (1975).
- 6) Luck R. E. and Bond, H. E., *Astrophys. J.* **292**, 559 (1985).
- 7) Butcher, H. R., *Nature* **328**, 127 (1987).
- 8) Cowan, J. J., Thielemann, F.-K. and Truran, J. W., in *Origin and Distribution of the Elements*, ed. G. J. Mathews, (World Scientific:Singapore), pp. 556-574 (1988).
- 9) Meyer, B. S. and Schramm, D. N., *Astrophys. J.* **311**, 406 (1986).
- 10) Cowan, J. J., Thielemann, F.-K. and Truran, J. W., *Astrophys. J.* **323**, 543 (1987).
- 11) Arnett, W.D., Branch, D., and Wheeler, J.C., *Nature* **314**, 337 (1985).
- 12) Branch, D., *Ap. J. (Letters)* **320**, L23 (1987).
- 13) Miller, G. E. and Scalo, J. M., *Astrophys. J. Suppl.* **41**, 513 (1979).
- 14) Mathews, G. J. and Schramm, D. N., *Astrophys. J.* **324**, L67 (1988).
- 15) Applegate, J. H., Hogan, C. J. and Scherrer, R. J., *Astrophys. J.*, in press (1988).
- 16) Cameron, A. G. W., in *Essays in Nuclear Astrophysics*, eds. C. A. Barnes, D. D. Clayton and D. N. Schramm, (Cambridge:Cambridge University Press), p. 23 (1982).
- 17) Howard, W. M., Mathews, G. J., Takahashi, K. and Ward, R. A., *Astrophys. J.* **309**, 633 (1986).
- 18) Matteucci, F., in *Origin and Distribution of the Elements*, ed. G. J. Mathews, (World Scientific:Singapore), pp. 186-198 (1988).

V. DARK MATTER AND PRIMORDIAL NUCLEOSYNTHESIS

**A MEASUREMENT OF THE PRIMORDIAL HELIUM ABUNDANCE
USING μ -CASSIOPEIAE**

James W. Haywood and Dennis J. Hegyi
Department of Physics
The University of Michigan
Ann Arbor, MI 48109
U.S.A.



Abstract

Speckle interferometric observations of the Population II astrometric binary star μ -Cassiopeiae have been made at four different epochs with a direct imaging CCD system. Using the available orbital data on the system, the masses of the stars have been found to be $M_P = 0.728 \pm 0.049 M_\odot$ and $M_S = 0.171 \pm 0.008 M_\odot$. Application of the theoretical mass-luminosity law to the primary yields a helium abundance of 0.23 ± 0.05 by mass for an assumed system age of 14 billion years.

Almost forty years ago, Gamow first considered the possibility that a hot big bang universe would synthesize an appreciable amount of helium. Twenty years later, Peebles carried out the first modern calculation of the primordial helium abundance, the amount of helium synthesized in the big bang. In addition, he calculated the production of deuterium and ^3He . Since that time, many others have calculated the primordial helium abundance adding additional reactions to calculate the production of heavier elements, most notably ^7Li , and by generally varying physical parameters in the calculation to test the sensitivity of the calculated helium abundance to the various uncertainties. From these studies, it has been found that Y_p , the calculated helium abundance by mass, is sensitive only to the present baryon density and to the number of light neutrinos (or more generally to the relativistic energy density at the time of nucleosynthesis).

From the point of view of the Moriond meeting on Dark Matter, any helium abundance measurement sets an upper limit on the primordial abundance; it is extremely difficult to destroy helium, though helium can be synthesized in stars. Thus, to determine the amount of dark matter in the universe, it is necessary to subtract the mass density in baryonic matter from the total energy density of the universe obtained from dynamical arguments (see, for example, Low and Spillar (1987)) or from some other method which can be used to determine the total energy density of the universe.

While there have been many discussions of the primordial helium abundance in the literature and several reviews on the subject (Pagel 1982), there is no consensus on the best value of Y_p . At present, it is generally thought that the best estimates of Y_p have been obtained from measurements of extragalactic HII regions since such measurements have impressively small random errors, but, the size of the systematic errors may be large. For example, Ferland (1986) has presented arguments based on collisional excitation of helium which he claims reduces a typical measured helium

abundance obtained from an extragalactic HII region of $Y_P \simeq 0.23$, to as low as $Y_P \simeq 0.19$. This corresponds to $\Omega_{\text{baryon}} \sim 0.001$ which is about a factor of ten lower than the lower limit on Ω_{baryon} obtained from X-ray observations which must be due to free-free transitions in baryonic matter. Thus, because of the importance of measurements of the primordial helium abundance it is quite desirable to obtain accurate measurements of Y_P using a variety of methods to access the presence of unknown systematic errors. Unfortunately, it has been difficult to carry this out because there are very few approaches which appear to be capable of providing an accurate value for Y_P .

One approach, however, which holds promise and which we have been pursuing is the application of the theoretical stellar mass-luminosity law to an old Population II star. From this approach, the helium abundance of a star can be obtained from the star's luminosity, metal abundance, and mass. In order to determine a stellar mass, a star must be a member of a nearby binary system. In the near future, there is only one nearby Population II binary star to which this approach may be applied, namely, the astrometric binary μ -Cassiopeiae. Two separate orbits have been determined for the motion of the bright primary star about the center of mass of a two body system. In principle, one measurement which can resolve the faint companion star so that the distance between the primary and secondary can be measured to high precision would yield the masses. The experimental problem has been that there is a large difference in intensity between the two components, $\Delta m_v \sim 6.5$, and the stars are close together with a separation ranging from $\sim 0.3 - 1.5$ arc seconds through the orbit.

If earth-based telescopes were capable of achieving diffraction limited imaging, it would be relatively easy to resolve μ -Cassiopeiae. It is the inhomogeneities in the earth's atmosphere which distort incoming plane waves to the extent that typical stellar images have characteristic sizes of ~ 2 arc seconds which makes it difficult to

resolve the components. Consequently, we have used speckle interferometric techniques which make it possible to obtain information at the high spatial frequencies characteristic of diffraction images. We have used integration times of ~ 40 ms to resolve μ -Cassiopeiae.

Our basic observational approach has been to correct for differential refraction in the earth's atmosphere and to image an enlarged stellar image on a CCD. Considering the imaging system in more detail, light first enters a filter with a pass-band of about 1000 \AA centered at about 8000 \AA . At this wavelength the ratio of intensities between the components is more favorable, $\Delta m_{8000} \sim 5$. Then the light passes through a lens located one focal length below the first telescope focus so that parallel light exits the lens. Next, the light passes through two prisms set at 180° with respect to one another so that the total dispersion of the two prisms is zero. Rotating one prism with respect to the other leads to a net dispersion which is adjusted to compensate for the dispersion of the atmosphere. The reason the light was made parallel was to minimize the chromatic aberration of the prisms. The final element of the optical system is another lens which images the parallel light on a 64×64 pixel corner of an RCA 512×320 CCD nearest the readout amplifier to reduce the smearing due to multiple charge transfer. A magnification of three matched the diffraction scale of the McGraw-Hill 1.3 m telescope operating at $f/13.5$ to the $30\mu \times 30\mu$ pixels of the CCD.

Observations of μ -Cassiopeiae and several nearby single calibration stars were made at four epochs between 1983.71 and 1985.84 at 810 and 858 nm. The images were flatfielded using a twilight flatfield and the two dimensional power spectrum of each binary image and nearby calibration star image was computed. The power spectra for each image of the binary, and correspondingly, the calibration star, were added together to increase the signal to noise ratio of each object.

It is worth understanding why adding the power spectrum of the images causes

the signal to add coherently while adding the actual images is much less effective. To describe how a plane wave distorted by the inhomogeneities in the earth's atmosphere is imaged, it is convenient to expand the distorted wavefront in terms of plane waves of different angular momenta. The image of a plane wave is a diffraction pattern. Thus, plane waves of different angular momenta correspond to plane waves incident on the telescope from different directions so they form images in different places in the focal plane of the telescope. Thus, at one instant the image of the primary of μ -Cassiopeiae is a superposition of many diffraction patterns each of which is called a "speckle". Next to each speckle of the primary star is a speckle due to the faint companion star with an angular separation corresponding to the angular separation of the components of the binary star. Because the two stars are close together, their light travels through almost the same atmospheric path so that images of the two stars suffer similar distortions; thus, the images of the two components of the binary star always maintain the same angular separation.

Continuing with the reason for taking the power spectrum, we note that the Fourier transform of a speckle from the primary stellar component is the same as that for the corresponding image of the secondary star (the images have similar shapes) except for a phase factor due to the angular separation between the stars. On the other hand, different speckle pairs have different phase factors with respect to one another. By taking the power spectrum, the phase shift of the speckle pair is eliminated and the relative phase shift of the speckle of the primary star relative to the corresponding speckle of the secondary leads to an interference term with a frequency which is inversely proportional to the separation between the two stars. Consequently, by adding together the power spectrum of each frame, the information regarding the separation between the stellar components adds coherently. The reason for taking exposures of a nearby companion star is to determine the functional form of the factor which multiplies the inference term so that the frequency

of the inference term can be extracted more precisely. In terms of our data analysis, we have fit the average power spectrum of the nearby calibration single star with a 10 parameter fit which we have used as the starting point for a 22 parameter fit to the average power spectrum of the binary star divided by the average power spectrum of the calibration star.

To gain confidence with the imaging system and to develop the data analysis procedure, we observed several calibration binary star systems from McAlister and Hartkopf (1983). The average ratio of our separation to the observations of McAlister *et al.* (1987) is 1.002 ± 0.015 and the average difference between our position angles is $-0.7^\circ \pm 0.2^\circ$. The brightness ratio between the components of the calibration binaries ranged from 0^m to $1^m.8$ and the separations ranged from 0.694 to 1.458 arc seconds.

The astrometric orbits of Lippincott (1981) and Russell and Gatewood (1984) when combined with our observations yielded inconsistent sets of masses for the components of μ -Cassiopeiae. The most significant difference between the two astrometric orbits is the position of the periastron relative to the line of nodes, the angle ω . The parameter ω appears to be particularly sensitive to systematic errors. Consequently, we decided to fit the relative orbit data and separately, each of the two astrometric orbits using ω and the semimajor axis of the relative orbit as fitting parameters. For this procedure, the fit to Lippincott's orbit yielded $a = 0.986 \pm 0.025$ arc seconds and $\omega = 332.1^\circ \pm 1.9^\circ$, and the fit to Russell and Gatewood's orbit yielded $a = 1.033 \pm 0.024$ arc seconds and $\omega = 332.3^\circ \pm 1.7^\circ$. The values obtained for ω are in excellent agreement while those obtained for a are in reasonable agreement. In addition, fitting any parameter of the astrometric orbit other than ω makes it impossible to bring the orbits into agreement. With these values, Lippincott's data yielded masses $M_P = 0.734 \pm 0.063 M_\odot$ and $M_S = 0.174 \pm 0.010 M_\odot$ while Russell and Gatewood's data yielded $M_P = 0.719 \pm 0.077 M_\odot$ and $M_S = 0.163 \pm 0.015 M_\odot$.

The weighted average of the masses of the components are $M_P = 0.728 \pm 0.049 M_\odot$ and $M_S = 0.171 \pm 0.008 M_\odot$.

The Helium Abundance

The next step in the procedure to determine the helium abundance of the primary of μ -Cassiopeiae is to obtain its luminosity. Based on the data of Carney and Aaronson (1979), we find the star's bolometric magnitude to be 5.54 ± 0.02 using Lippincott's parallax and 5.62 ± 0.06 using Russell and Gatewood's parallax.

The last parameter which must be obtained to determine the helium abundance is the metal abundance of μ -Cassiopeiae. The two most recently determined metal abundances for μ -Cassiopeiae (Tomkin and Lambert 1980, Perrin *et al.* 1977) yielded an average metal abundance $Z = 0.0021 \pm 0.0005$. Using this metal abundance with the mass of the primary and luminosity obtained from each of the orbits and an interpolation formula fit to the models of Vandenberg (1985) and Vandenberg and Bell (1985), we have calculated the weighted average helium abundance of the primary for the two orbits for ages ranging between 14 and 20 billion years. For an age of 14 billion years, the helium abundance is 0.230 ± 0.052 and decreases to 0.197 ± 0.055 for an age of 20 billion years. While the deduced helium abundance is consistent with big bang calculations (Yang *et al.* 1984), the errors are not as small as one might hope. It will be necessary to obtain more accurate orbital data before the errors in the measured helium abundance can be reduced.

Nevertheless, one correction to the calculated helium abundance that is worth making, is correcting for the helium produced during galactic evolution which was injected into the gas from which μ -Cassiopeiae formed. Pagel, Terlevich and Melnick (1986) estimate the correction due to galactic enrichment to be $\Delta Y = -5Z$. For μ -Cassiopeiae, to the accuracy worth discussing, this reduces the deduced helium abundance by -0.01 .

Regarding the subject of this Moriond conference, the dark matter content of the universe, the 1σ upper limit on the primordial helium abundance, is $Y_{\text{primordial}} \lesssim 0.28$ for a galactic age of 13×10^9 yr and for $\Omega = 1$, and is not sufficiently low to require any dark matter. On the other hand, even without additional supporting evidence, the best estimate of the helium abundance is suggestive that there may be substantial amounts of dark matter.

We would like to thank the AFOSR for their support for this research through Grant AFOSR-85-09120.

References

1. Carney, B.W., and Aaronson, M., *A. J.* 84, 867 (1979).
2. Ferland, G.J., *Ap. J. (Letters)* 310, L67 (1986).
3. Lippincott, S.L., *Ap. J.* 248, 1053 (1981).
4. Loh, E.D., and Spillar, E.J., *Ap. J. (Letters)* 307, L1 (1986).
5. McAlister, H.A., and Hartkopf, W.I., *P.A.S.P.* 95, 778 (1983).
6. McAlister, H.A., Hartkopf, W.I., Hutter, D.J., and Franz, O.G., *A. J.* 93, 688 (1987).
7. Pagel, B.E.J., *Philos. Trans. R. Soc. London Ser. A* 307, 17 (1982).
8. Pagel, B.E.J., Terlevich, R.J., and Melnick, J., *P.A.S.P.* 98, 1005 (1986).
9. Perrin, M.N., Hejlesen, P.M., Cayrel de Strobel, G., and Cayrel, R., *Astr. Ap.* 54, 779 (1977).
10. Russell, J.L. and Gatewood, G., *P.A.S.P.* 96, 429 (1984).
11. Tomkin, J. and Lambert, D.L., *Ap. J.* 235, 925 (1980).
12. Vandenberg, D.A., *Ap. J. Suppl.* 58, 711 (1985).
13. Vandenberg, D.A. and Bell, R.A., *Ap. J. Suppl.* 58, 561 (1985).
14. Yang, J., Turner, M.S., Steigman, G., Schramm, D.N., and Olive, K.A., *Ap. J.* 281, 493 (1984).

ON THE PRIMORDIAL LITHIUM ABUNDANCE

Sylvie VAUCLAIR
Observatoire Midi-Pyrénées
14, avenue Edouard Belin
Toulouse, France

ABSTRACT

The lithium depletion due to rotation-induced turbulence is studied for halo stars in the frame of Zahn's theory of instabilities in rotating stars. The lithium abundance observed in these stars ($\frac{Li}{H} = 10^{-10}$) may be the primordial one, only if no depletion occurred during 15 billion years in these stars. This needs a fine tuning of turbulence under the outer convection zone. It is not excluded, but it is also not excluded that depletion occurred, so that the primordial abundance may lie between 10^{-10} and 10^{-9} .

The lithium primordial abundance brings one of the most severe constraints on the parameters which govern the first minutes of the universe (see papers by Audouze and by Reeves, this conference). This primordial abundance is still a subject of debate. The maximum lithium abundance observed in young galactic clusters is $\frac{Li}{H} = 10^{-9}$ (e.g., Boesgaard and Tripicco 1986, Boesgaard, Budge and Ramsay 1988, Hobbs and Pilachowski, 1986a and b, Pilachowski, Booth and Hobbs 1988). This result suggests that young stars were all born with this lithium abundance, and that it has been depleted in some of them. On the other hand Spite and Spite 1982 and Spite, Maillard and Spite 1984 observed that the maximum lithium abundance in halo stars was $\frac{Li}{H} = 10^{-10}$. This result has further been confirmed by several authors (Boesgaard 1985, Rebolo, Molero and Beckman 1988, Hobbs and Duncan 1987). Most astronomers now refer to this value as the primordial lithium abundance, for the basic reason that it is remarkably constant in halo stars (except for depletion in the cool G stars), while it seems at first sight that depletion effects would lead to a large dispersion. I will show in this paper that this is not always true: the nuclear destruction of lithium due to rotation-induced turbulence may lead to similar depletion in stars of different masses, provided that they have had the same rotation history.

As shown by Zahn 1983, 1984 and 1987a,b, the thermal imbalance induced by stellar rotation leads to meridional circulation and differential rotation which give rise to horizontal shear flow instabilities (the vertical ones being damped out by the density stratification). The resulting 2-D turbulence decays into 3-D turbulence at small scales, which in turn leads to mixing.

In the barotropic approximation and assuming a small differential rotation, the turbulent diffusion coefficient takes the form :

$$D_T \simeq \frac{\Omega^2 r^6}{G^2 (\nabla_{ad} - \nabla_{rad})} \frac{L}{M^3} \left(1 - \frac{\Omega^2}{2\pi G \rho} \right) P_2(\cos\theta) \quad (1)$$

where L and M are the stellar luminosity and mass, ∇_{ad} and ∇_{rad} the adiabatic and radiative gradient $\left(\frac{\partial \ln P}{\partial \ln T} \right)$ in the stellar gas at radius r , $P_2(\cos\theta)$ the usual Legendre polynomial, and Ω the angular rotational velocity. The negative term $\frac{\Omega^2}{2\pi G \rho}$ comes from the classical expression for the local energy density due to thermal imbalance. This term may become larger than one at low densities, where the centrifugal effects take over the

gravitational ones in the stellar deviation from spherical symmetry (Von Zeipel 1924). It is always smaller than one under the outer convection zones of main-sequence halo stars.

For a first approximation the lithium nuclear destruction is treated in a step model, lithium being completely destroyed at radius r_{NB} and not destroyed above. With the W.K.B. approximation (see Baglin, Morel and Schatzman 1985), the variation of the lithium abundance with time in the convection zone is supposed to vary as :

$$N(Li) = N_o(Li) e^{-\lambda t} \quad (2)$$

assuming the negative term negligible in eq. (1), and with averaged Ω , $\nabla_{ad} - \nabla_{rad}$ and $P_2(\cos\theta)$, λ comes out as :

$$\lambda = \frac{\gamma \Omega^2}{(\nabla_{ad} - \nabla_{rad})} \left(\frac{r_{NB}}{r_{\odot}} \right)^4 \frac{\beta^4}{(\beta^2 - 1)^2} \frac{L_*/L_{\odot}}{(M_*/M_{\odot})^3} y r^{-1} \quad (3)$$

with $\beta = r_{CZ}/r_{NB}$ where r_{CZ} is the radius at the bottom of the convection zone, and γ is a factor of order 0.1. The variation of Ω with time (rotational braking) is not introduced here. The interest of the present analytical formulation is to show the physics. The variation of λ with β is interesting to discuss. If β is close to one (deep convection zone), λ is large and the lithium nuclear destruction is rapid in the convection zone. If β increases (going from G to F stars) λ decreases and the lithium nuclear destruction is less effective. However the slope of the variation of λ with β also decreases, so that the change in the lithium abundance due to the regression of the convection zone is less and less pronounced. This result is simply due to the fact that the added radiative layer is mixed by turbulence in a time scale which is short compared to the layers underneath. This effect creates a "plateau" shape of the lithium abundances (Fig. 1).

Computations of lithium nuclear destruction have been done in halo stars using Van den Berg 1983 evolutionary tracks for 0.7 and 0.8 M_{\odot} with $Y = 0.2$ and $Z = 10^{-4}$. The extrapolation values given by Van den Berg have been used to obtain parameters for evolutionary tracks with $\alpha = 1.9$. Three model envelopes have been computed with these parameters for 0.7 M_{\odot} (ages 0.297, 4.047 and 13.481 billion years) and four for 0.8 M_{\odot} (ages 0.197, 3.187, 9.276 and 13.448 billion years). The lithium nuclear destruction

has been deduced by interpolation in the two cases for 4, 9 and 15 billion years. The numerical factor in eq. (2) has been adjusted for a best fit with the observations at 15 billion years, which leads to an average rotation velocity of 10 km s^{-1} . The rotation velocity of halo stars is not known from observations except for HD 13095 where it is only about 1.6 km s^{-1} (Noyes et al. 1984), but it may have been larger in the past. The interesting result here is that the lithium depletion is parallel along the two tracks. As already mentioned, a plateau appears naturally in this frame work because of the rapid increase of the turbulent diffusion coefficient with radius. The increase of $\frac{L}{M^3}$ for hotter stars balances the remaining effect. Also shown on Fig. 1 (arrow) is the effective temperature for stars in which lithium is completely destroyed (the bottom of the convection zone reaches the nuclear destruction layer in the zero age main sequence model). This occurs for stars of about $0.6 M_{\odot}$.

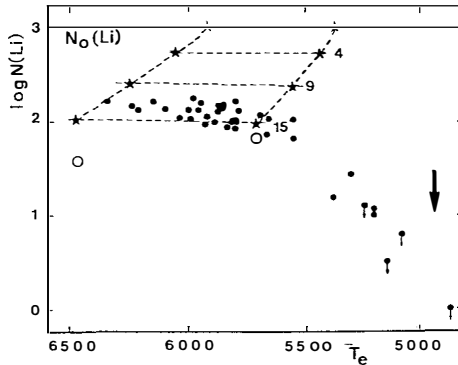


FIGURE 1. — Lithium nuclear burning in Population II stars, computed in Van den Berg 1983 evolutionary tracks for 0.70 and 0.80 solar masses, with $\alpha = 1.9$ and an initial abundance $\frac{Li}{H} = 10^{-9}$. The stars show the computed lithium abundances after 4, 9 and 15 billion years. The arrow shows the effective temperature for which lithium is completely destroyed in the convection zone. The circles represent the theoretical values of the lithium abundance obtained by gravitational diffusion, in case of an initial abundance of 10^{-10} and no turbulence under the convection zone. The points represent Spite and Spite 1982 and Rebolo, Molaro and Beckman 1987 observations.

These computations have been done with the hypothesis that all the stars had the same average rotation velocity, the same age and the same metallicity. These points have to be discussed. The weakest point of this theory is the strong constraint needed on the rotation velocity. The dispersion in the rotation velocity for G stars of

a given effective temperature must be less than 10%, for the dispersion in the lithium abundance not to exceed 20% as observed in the "plateau" (Spite and Spite, 1982 and 1986). Recent measurements of rotation periods in G stars from the observations of activity show a remarkably low dispersion for a given spectral type (Duncan et al 1984, Rebolo and Beckman 1987, Radick et al 1987). This leads to the idea of a self regulating braking mechanism, which would take place early in the stellar life (see also Endal and Sofia 1981).

Let us now discuss the problem of age and metallicity. Rebolo, Molaro and Beckman 1988 have shown that the $\frac{Li}{H}$ abundance is constant for stars with $\left[\frac{Fe}{H}\right]$ less than (- 1.0) while for larger metallicities its upper value increases, the dispersion becoming larger and larger. These characteristics would show quite a different behavior if plotted against time. The current observations of metallicity versus age in old stars show that the iron abundance has reached a value within a factor 10 of the present value in less than one billion year (e.g. Twarog 1980). Then $\left[\frac{Fe}{H}\right]$ increased somewhat linearly with time in the Galaxy. The constant Li abundance found by Rebolo, Molaro and Beckman between $\left[\frac{Fe}{H}\right] = -3.5$ to -1.0 is due to a stretching of the scale. If plotted against time all these points would appear clustered at the same abscissa. The fact that the lithium value appears as unique for halo stars while a dispersion is observed for young stars is due to the interval in effective temperature chosen by the authors to be represented on their figure 3 ($T_{eff} > 5500^{\circ}K$). Due to opacity effects, the distance between the bottom of the convection zone and the nuclear burning layer is larger in low metallicity stars than in high metallicity stars of the same effective temperature. For T_{eff} larger than 5500 K low metallicity stars are in the "plateau" domain so that their G side depletion domain is not included.

Now the question arises whether the opposite hypothesis, (namely that the primordial lithium abundance is that of halo stars and that this abundance has remained unchanged during 15 billion years, except for the coolest ones) is possible. Computations of lithium gravitational settling have been done along the same evolutionary tracks, with an initial lithium abundance of $\frac{Li}{H} = 10^{-10}$ and with the assumption of no turbulence under the convection zone. Results are given in Fig. 1: lithium should have been depleted by a factor 3 on the hot part of the plateau (see also Michaud, Fontaine

and Beaudet 1984). However, as shown by Vauclair et al 1978, a turbulent diffusion coefficient larger than 10 times the gravitational one would prevent this depletion. Here the gravitational diffusion coefficient is of order one $\text{cm}^2.\text{s}^{-1}$. On the other hand, the turbulent diffusion coefficient needed to destroy lithium by a factor 10 (as in the preceding computations) is of order 10^4 at the bottom of the convection zone. For a lithium destruction of less than 10%, D_T must be smaller than 10^3 . So it is possible that the lithium abundance has not evolved with time if the turbulent diffusion at the bottom of the convection zone has remained between 10 and $10^3 \text{cm}^2.\text{s}^{-1}$. Numerical computations of lithium destruction introduced in an evolutionary sequence with a rotation braking law will help in getting further. The necessity of reproducing correctly the depletion domain on the cool side of the plateau will bring constraints on D_T . An observational test of the lithium primordial abundance could be found in measurements of the $\frac{{}^6\text{Li}}{{}^9\text{Be}}$ ratio. In case of no nuclear destruction we expect for this ratio the spallation value (≈ 4.5). For a ${}^7\text{Li}$ destruction by a factor 10, ${}^6\text{Li}$ would be depleted by more than 5 orders of magnitude while ${}^9\text{Be}$ would be depleted by less than a factor 2. For a ${}^7\text{Li}$ destruction smaller than 20% ${}^6\text{Li}$ could not be depleted by more than 70% ($\frac{{}^6\text{Li}}{{}^9\text{Be}} \geq 1.3$). Unfortunately, while Be has been detected in some metal deficient stars with $\frac{\text{Be}}{\text{H}} \approx 10^{-12}$ (Rebolo et al 1988), only upper limits have yet been found for ${}^6\text{Li}$ (Maurice et al 1984), leading to $\frac{{}^6\text{Li}}{{}^9\text{Be}} \leq 5$. More precise observations of these elements would be very interesting in that respect.

References

- BAGLIN, A., MOREL, P.J., SCHATZMAN, E. 1985 *Astr. Ap.* **149**, 309
 BOESGAARD, A.M. 1985, *Publ. A.S.P.* **97**, 784
 BOESGAARD, A.M., BUDGE, K.G., RAMSAY, M.E. 1988, preprint
 BOESGAARD, A.M., TRIPICCO, M.J. 1986, *Ap. J.* **303**, 724
 DUNCAN, D.K., BALIUNAS, S.L., NOYES, R.W., VAUGHAN, A.H., FRAZER, J., LANNING, H.H. 1984, *Publ. A.S.P.* **96**, 707
 ENDAL, A.S., SOFIA, S. 1981, *Ap. J.* **243**, 625
 HOBBS, L.M., DUNCAN, D.K. 1987, *Ap. J.* **317**, 796
 HOBBS, L.M., PILACHOWSKI, C.A. 1986a, *Ap. J.* **309**, L17
 HOBBS, L.M., PILACHOWSKI, C.A. 1986b, *Ap. J.* **311**, l37
 MAURICE, E., SPITE, F., SPITE, M. 1984, *Astr. Ap.* **132**, 278
 MICHAUD, G., FONTAINE, G., BEAUDET, G. 1984, *Ap. J.* **282**, 206

- NOYES, R.W., WEISS, N.O., VAUGHAN, A.H., 1984, *Ap.J.*, **287**, 769
- PILACHOWSKI, C.A., BOOTH, J., HOBBS, L.M. 1988, preprint
- RADICK, R.R., THOMPSON, D.T., LOCKWOOD, G.W., DUNCAN, D.K., BAGGETT, W.E. 1987, *Ap. J.* **321**, 459
- REBOLO, R., BECKMAN, J.E. 1987, in *IAU Symp. 132 The Impact of Very High S/N Spectroscopy on Stellar Physics*, ed. G. Cayrel de Strobel and M. Spite
- REBOLO, R., MOLARO, P., ABIA, C., BECKMAN, J.E. 1988, Preprint
- REBOLO, R., MOLARO, P., BECKMAN, J.E. 1988, *Astr. Ap.*, **192**, 192
- SPITE, F., SPITE, M. 1982, *Astr. Ap.* **115**, 357
- SPITE, F., SPITE, M. 1986, *Astr. Ap.* **163**, 140
- SPITE, M., MAILLARD, J.P., SPITE, F. 1984, *Astr. Ap.* **141**, 56
- TWAROG, B.A. 1980, *Ap. J.* **242**, 242
- VANDENBERG, D.A. 1983, *Ap. J. Suppl.* **51**, 29
- VAUCLAIR, S., VAUCLAIR, G., SCHATZMAN, E., MICHAUD, G. 1978, *ApJ* **223**, 567
- VON ZEIPEL, H. 1924, *M.N.R.A.S.* **84**, 665
- ZAHN, J.P. 1983, in *Astrophys. Processes in Upper Main Sequence Stars*, ed. A. Maeder and B. Hanck (publ. Observatoire de Genève) p. 253
- ZAHN, J.P. 1984, in *Proc. 25th Liège Intern Astrophys. coll.* (Publ. Université de Liège) p. 407
- ZAHN, J.P. 1987a, in *The Internal Solar Angular Velocity*, ed. B.R. Durney and S. Sofia, Reidel, Dordrecht, p. 201
- ZAHN, J.P. 1987b, Course given at the "Les Houches" summer school
- ZAPPALA, R.R. 1972, *Ap. J.* **172**, 57

PRIMORDIAL NUCLEOSYNTHESIS AND PARTICLE PHYSICS

Jean Audouze¹, Pascale Delbourgo-Salvador² and Pierre Salati³

1 — Institut d'Astrophysique de Paris, CNRS
98bis, bd Arago F-75014 Paris

2 — CEA Bruyères-Le-Châtel, France

3 — LAPP Annecy le Vieux, France
and Department of Astronomy, Univ. of California, Berkeley USA



ABSTRACT

After the presentation of a brief review of the standard models of primordial nucleosynthesis which reproduce quite well the abundances of the lightest elements (D, ³He, ⁴He and ⁷Li) it is argued here that these nucleosynthetic processes can impose quite valuable constraints on several aspects of particle physics.

These constraints concern

- (i) the number of neutrino (lepton) families which is basically limited by the primordial abundance of ⁴He.
- (ii) the mass and life time of non baryonic massive and unstable particles (neutrinos, gravitinos, photinos ...) which would decay by producing large fluxes of energetic photons able in turn to partly photodesintegrate the nuclei of the very light elements.
- (iii) the physics of the Quark-Hadron phase transition. As seen here, the primordial abundance of ⁷Li restricts quite drastically the density contrast resulting from this first order transition. Consequently valuable constraints on the temperature at which quarks transform into hadrons and the so-called quark bag constant can be deduced from the ⁷Li abundance determination.

1. INTRODUCTION

The cosmological relevance of the primordial Big Bang nucleosynthesis (BBN) and the overwhelming success of the standard simple models have been emphasized in many papers : see e.g. Audouze, (1987a and b) and Boesgaard and Steigman (1985). It is well known that these models reproduce well the primordial abundances of D, ^3He , ^4He and ^7Li and provide interesting constraints on the baryonic density such that $\Omega_B \sim 0.1$ (i.e. the baryonic cosmological parameter being ~ 0.1 of the critical value) and on the maximum number of neutrino (lepton) families (3–4). A quick summary of the present situation regarding the abundances of the lightest elements and the standard models of primordial nucleosynthesis is provided in section 2.

The purpose of this paper is to emphasize further constraints on some aspects of particle physics which can be deduced from the comparison between the abundance predictions of these nucleosynthetic models and the “primordial” abundances of the lightest elements. Many attempts have indeed be made recently to reconcile the predictions of the primordial nucleosynthesis with some higher values of the baryonic density.

These attempts belong to two categories : either one assumes the existence of unstable massive particles which could decay into high energy photons. These photons would trigger the partial photodisintegration of ^4He and ^7Li which are overabundant in an $\Omega_b \geq 1$ universe into D and ^3He which could be depleted. Several candidates have been considered massive neutrinos and gravitinos by Audouze et al. (1985) and photinos by Salati et al. (1987). Section 3 outlines some of the conclusions of these two investigations.

May be the most exciting attempt to reconcile a value of Ω_b as large as 1 with the predictions regarding the abundances of the very light elements is to consider the effects of the Quark–Hadron phase transition on the homogeneity of the universe at the time of nucleosynthesis. As recalled in section 4 (see also Fuller, Mathews and Reeves, this book), the ^7Li abundance constitute a very severe constraint on such scenarios (section 4 and conclusion).

2. THE STANDARD MODELS OF EARLY NUCLEOSYNTHESIS

The standard BBN models have been reviewed recently many times. We will only recall here that they are simple in the sense that the following assumptions are made (i) the Universe was “born” from a very dense and hot phase (Big Bang) leading to a statistical equilibrium between the existing particles (ii) the Universe is homogeneous and isotropic and its expansion is governed by General Relativity (GR) with a cosmological constant $\Lambda=0$ * (iii) the Universe is asymmetric (the matter density is much higher

* Should Λ be > 0 during the time of nucleosynthesis the expansion would be more rapid inducing a larger production of ^4He which seems to be infirmed by the present observations. There is still a possibility of constructing models of Universe with $\Lambda \neq 0$ which are compatible with the BBN requirements (Sato, 1988).

than that of antimatter) and the baryon density parameter $\eta_{10} = 10^{10} n_B/n_\gamma$ lies between 1 and 10. The present baryonic density in the Universe is $\rho_B = 6.64 \cdot 10^{-32} \eta_{10} (T/2.7)^3 \text{ g cm}^{-3}$. T is the actual temperature of the background radiation, while the baryonic cosmological parameter $\Omega_B = \rho_B/\rho_c$ (ρ_c being the critical density) ; $\Omega_B = 3.5 \cdot 10^{-3} \eta_{10} h^{-2} (T/2.7)^3$ with $h = (H_0/100)$, where the Hubble constant H_0 is expressed in $\text{km s}^{-1} \text{ Mpc}^{-1}$ (iv) The leptons are not degenerate and the chemical potential of neutrinos is very small.

The two crucial parameters which govern the outcome of nucleosynthesis are (i) the baryonic density of the Universe described in terms of the parameter η_{10} and (ii) the number of neutrino (lepton) flavors. From the comparison between the abundances evaluated from such models and those derived from the observations (see e.g. Audouze 1987b who reviewed the possible values of the primordial abundances of the lightest elements) $\Omega_b \sim 0.1$ and $N_\nu \sim 3-4$ (fig. 1). We notice that the agreement between the primordial abundances of the light elements and the predictions coming from the standard BBN model requires some careful "fine tuning". As shown in figure 1, adapted from Yang et al. (1984) and discussed at some length in Audouze (1987b), the only value of $\eta = n_B/n_\gamma$ consistent with $X(^4\text{He}) = Y < 0.25$ and $(D + ^3\text{He})/H \leq 10^{-4}$ is $\eta = 3 \cdot 10^{-10}$ corresponding to $0.01 \leq \Omega_B \leq 0.04$ (the width of this range is only due to the present uncertainty on the Hubble constant H_0 : $50 \leq H_0 \leq 100 \text{ km s}^{-1} \text{ Mpc}^{-1}$).

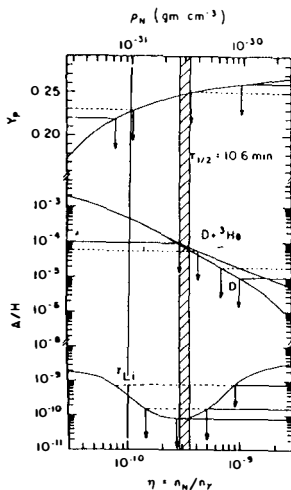


Figure 1. Calculations of the light element abundances made in the frame of the standard BBN model by Yang *et al.* (1984). The dashed domain indicates the η range ($\eta = n_B/n_\gamma$ i.e. the baryonic density relative to the photon density) compatible both with $Y_p = 0.24 \pm 0.01$ (Kunth, 1986) and with the Yang *et al.* 1984 prescription on $D/H < 10^{-4}$. One sees that the resulting is quite narrow $\eta = 3.2 \pm 0.2$ making such comparison fairly contrived.

In the frame of the standard BBN model, and given the fact that $Y_p < 0.25$ (Kunth, 1986) the only way to enlarge the possible range of η and therefore Ω_b is to assume that $(D + {}^3\text{He})/H_{\text{primordial}}$ can be larger than 10^{-4} . This implies that D is significantly destroyed during the galactic history. Our group (Delbourgo-Salvador et al., 1985, Vangioni-Flam and Audouze, 1988) have considered different possibilities to achieve that goal. There are (i) infall/outflow of processed material in the galactic disk, (ii) strong stellar mass losses occurring during the pre main sequence phase (Delbourgo-Salvador et al. 1985), (iii) a promising model is the chemical evolution scheme in which the rate of star formation is assumed to be varying with time (Vangioni-Flam and Audouze 1988). In this last model the rate of star formation is assumed to be large during the first $(0.5-2) 10^9$ years of galactic evolution. This assumption leads not only to a large D destruction but also to a proper account of the galactic evolution of heavier elements such as N, O, Fe and the s and r elements (Andreani et al. 1988).

To sum up : standard models of primordial nucleosynthesis provide most interesting constraints on the baryonic density of the Universe and the number of neutrino families. Regarding the baryonic density we claim that D needs to be thoroughly depleted during the galactic evolution and our preferred models with time varying rate of star formation like those of Vangioni-Flam and Audouze (1988) are well suited for that goal. Concerning the maximum number of neutrino families (3-4) it is interesting to note that a similar conclusion can be reached from the analysis of the neutrino fluxes generated by SN 1987A.

3. HIGH ENERGY PHOTON DECAY OF NON-BARYONIC PARTICLES

Standard models of primordial nucleosynthesis predict that $\Omega_b \sim 0.1$ while the dynamics of large scale structures of the Universe such as the current models of inflation imply much larger values for Ω . If Ω_b is very large the resulting D and ${}^3\text{He}$ abundances are much too low while those of ${}^4\text{He}$ and ${}^7\text{Li}$ are too high. The first possibility to consider is to assume the existence of massive unstable particles which would decay into high energy photons which in turn would partly photodisintegrate the surplus of ${}^4\text{He}$ and ${}^7\text{Li}$ into D and ${}^3\text{He}$. An important feature concerning the occurrence of such processes has been established by Lindley (1985). Such photodisintegration processes can only take place if the product $E_H \cdot E_{BB} < 1/50(\text{MeV})^2$ where E_H is the energy of the high energy photons and E_{BB} the energy of the thermal photons. Given the fact that E_H should be higher than 20-50 MeV to be able to induce such photodisintegration processes $E_{BB} \leq 4 \cdot 10^{-4} - 10^{-3}$ MeV which means that $t \geq 10^5 - 10^6$ sec.

As a consequence, particles like massive neutrinos and gravitinos with masses of a few hundred MeV and lifetimes of $10^5 - 10^6$ sec might decay into energetic photons able to partly photodisintegrate ${}^4\text{He}$ and ${}^7\text{Li}$ (see e.g. Audouze et al., 1985).

The possible influence of photinos on the early nucleosynthesis has been investigated by Salati et al., (1987). Let us summarize the main conclusions of their study :

(i) If photinos are stable, their mass has to be comprised between 5 and 8 GeV to lead to $\Omega=1$. If their mass is larger their contribution to the overall density of the Universe is negligible. If their mass is smaller, Ω would be much too large because their annihilation rate is so big that they would create too many fermion-antifermion pairs.

(ii) The physical situation is especially interesting if photinos are unstable. Figure 2 displays the constraints on their mass/lifetime coming from the early nucleosynthesis. Region II i.e. photinos massive enough with relatively low lifetime, corresponds to the physical conditions which respect the constraints coming from the early nucleosynthesis. Region I (light photinos with long lifetime) corresponds to the conditions which make photinos looking as another family of neutrinos, which would overproduce the ${}^4\text{He}$ abundance. Regions III, IV and V correspond to physical conditions where photinos would decay in high energy photons which would affect significantly the abundances of D, ${}^3\text{He}$ and ${}^4\text{He}$. This is therefore forbidden by the astronomical observations. In order to fulfill the conditions set up by the early nucleosynthesis, photinos have to be relatively massive and unstable.

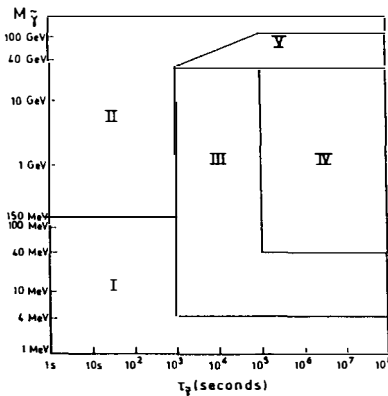


Figure 2 Photino mass $M_{\tilde{\gamma}}$ and lifetime $\tau_{\tilde{\gamma}}$ domains defined by the nucleosynthesis constraints for $\Omega=1$. Each domain is discussed in the text. The only allowed domain is domain II (low lifetime-high-mass) (from Salati et al., 1987).

When the different decay modes are envisaged for the photinos, these constraints on the lifetime induce further constraints on different parameters such as the supersymmetric breaking scale, the mixing parameter describing the lepton number violation or the vacuum expectation value of SUSY particles (Salati et al., 1987).

The decay into high energy photons of massive and unstable particles such as those predicted by the supersymmetry theories (see e.g. Fayet, 1984) can affect the outcome of the primordial nucleosynthesis. The observed abundances of the very light elements can be used to constrain the physical characteristics (mass, lifetime ...) of such particles.

More recently Dimopoulos et al., (1988a and b) have proposed a scenario involving the decay of some unstable massive non baryonic particles which would create large "hadron showers". These showers would result in reproducing quite satisfactorily the abundances of the light elements but also a quite large ${}^6\text{Li}$ primordial abundance such that ${}^6\text{Li}/{}^7\text{Li} \geq 10$. For many reasons based especially on the current abundance determinations of Li in the most metal poor stars, this model is found to be untenable in any reasonable model of galactic evolution (Audouze and Silk, 1988).

4. QUARK-HADRON PHASE TRANSITION AND EARLY NUCLEOSYNTHESIS

The possible influence of quark-hadron phase transition on the early nucleosynthesis has been envisaged in many recent papers (Applegate et al., 1987, Alcock et al., 1987, Audouze et al., 1988, Fuller et al., 1988). Around a temperature of 100 MeV the quarks confine and transform themselves into hadrons. As in a first order phase transition, during this very short period where $T_{BB} \sim 100$ MeV, there is the possibility of coexistence between the quark-gluon phase and the hadron phase. Because of the difference of the statistical weight between these two phases (the relativistic quarks have indeed a larger statistical weight than the non relativistic hadron), a natural segregation between a high density phase (the quark-gluon phase) and a low density phase (the hadron phase) takes place.

The contrast of density R (between these two phases) is simply given by :

$$R = \frac{n_b^q}{n_b^h} = \frac{\sqrt{\pi}^{-3/2}}{9} \frac{e^Z}{Z^{3/2}}$$

with $Z = m_n/T_c$, m_n is the mass of the nucleon and T_c is the temperature at which the phase transition occurs. This temperature T_c is related to a term B called the "bag constant" which expresses the negative pressure term coming from the quark confinement. If $T_c \sim 106$ MeV, $R = 120$ (the phase density contrast is large for a small bag constant such as the one predicted by the MIT model); if $T_c = 240$ MeV (large bag constant predicted by the chiral model), $R=3$.

This quark-hadron phase transition induces therefore density inhomogeneities : the quark zone which is a baryon rich zone which will become a proton rich zone while the hadron zone which is a baryon poor zone will become a neutron rich zone. This is because the neutrons have a diffusion mean free path which is much larger than that of the protons : the neutron density is constant while the overall baryon density is large in the former quark zone.

There are two basic parameters which fix the degree of inhomogeneity induced by this phase transition a) the baryon density contrast R and b) the fractional mass of the high density region f_v such that $\Omega_T = f_v \Omega_Q + (1-f_v) \Omega_H$, where Ω_T, Ω_Q and Ω_H are respectively the baryon cosmological parameters of the whole universe, the quark rich zone and the hadron rich zone. In the case of a total neutron diffusion the resulting abundances X_{el} of the light elements are given by Audouze et al., (1988).

$$X_{el} = X_{el}^1 f_v \frac{R + X_n(R-1)(f_v-1)}{1 + f_v(R-1)} + X_{el}^2 (1-f_v) \frac{1 + X_n f_v(R-1)}{1 + f_v(R-1)}$$

where X_n is the n/p ratio when the weak interactions stop and "freeze" this ratio. X_{el}^1 and X_{el}^2 are the resulting abundances in the high density region (1) and the low density region (2). These abundances depend on their relative densities Ω_B^1 and Ω_B^2 which are such that

$$\Omega_B^1 = \Omega_T \frac{R + X_n(R-1)(f_v-1)}{1 + f_v(R-1)}$$

and

$$\Omega_B^2 = -\Omega_T \frac{1 + X_n f_v(R-1)}{1 + f_v(R-1)}$$

For example, in the case of $\Omega_T = 0.01$ and $R = 10$ if $f_v = 0.2$, $\Omega_B^1 = 0.035$ and $\Omega_B^2 = 0.005$ (60 % of the light elements come from the dense zone) and of $f_v = 0.8$, $\Omega_B^1 = 0.012$ and $\Omega_B^2 = 2.5 \cdot 10^{-3}$ (98 % of the light elements come from the dense zone).

A first series of calculations have been reported by Audouze et al. (1988). They clearly show that ${}^7\text{Li}$ is significantly overproduced as soon as $\Omega > 0.05$ and $R > 5$. The abundance of D is also significantly decreased with respect to the standard case. All calculations performed so far in the frame of this model (Alcock et al., 1987, Applegate et al., 1987, Fuller et al., 1987, Malaney and Fowler, 1988, Salati et al., 1988) exhibit this conspicuous ${}^7\text{Li}$ overabundance (fig. 3). The basis of this explanation comes from the fact that ${}^7\text{Li}$ is overproduced at lower densities by the $T(\alpha, \gamma){}^7\text{Li}$ reaction and at higher densities by the ${}^3\text{He}(\alpha, \gamma){}^7\text{Be}$ reaction.

As a result the ${}^7\text{Li}$ abundance constitutes the most stringent constraint against models where the contrast R is higher than 3-5. The inhomogeneity of the Universe due to the quark-hadron is strongly limited by this specific abundance. Consequently

the high values of the bag constant $(250 \text{ MeV})^4$ predicted by the chiral model should be favoured compared to the low values predicted by the MIT bag model.

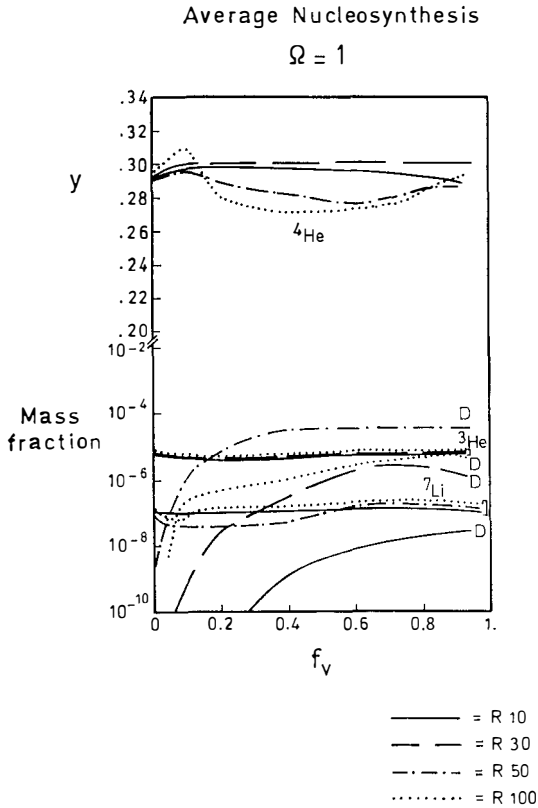


Figure 3. Resulting abundances of the very light elements in the frame of the quark-hadron phase transition model (from Salati et al., 1988). The calculations have been made for $\Omega_B = 1$ and $10 \leq R \leq 100$. In all cases one can notice that $X(^7\text{Li}) = 10^{-7}$ i.e. 200 times higher than its abundance in population II and 20 times higher than its highest stellar abundance. Many discrepancies arise also between the calculations and the observations for the other light elements. This clearly show that the contrast parameter R should be limited to its lowest values $R < 3-5$.

More recently an interesting proposal has been presented by Malaney and Fowler (1988) in an attempt to still reconcile $\Omega_b = 1$ with an inhomogeneous model taking into account this quark hadron phase transition. They argue that the neutrons can diffuse back from the neutron rich region to the proton rich one. In the proton rich region ${}^7\text{Li}$ is overproduced by the ${}^3\text{He}({}^4\text{He},\gamma){}^7\text{Be}$ reaction. The admixture of neutrons leads to the destruction of this ${}^7\text{Be}$ through the ${}^7\text{Be}(\eta,p){}^7\text{Li}(p,\gamma){}^4\text{He}$ chain. With a fairly narrow choice of f_v (fraction of mass in the dense region) values such that $f_v = 0.1-0.12$, Malaney and Fowler (1988) claim that if the fraction of neutrons which diffuse back to the high density region is $> 10^{-4}$ times the fraction present in the low density region ${}^7\text{Be}$ is then sufficiently destroyed. According to these authors this would avoid the ${}^7\text{Li}$ overproduction noticed in the other investigations. Nevertheless this optimistic view is challenged by two independent analyses performed by Terasawa and Sato (1988) and by Kurki-Suonio et al. (1988). They both consider also the same back-diffusion effect but their calculations clearly show that it is almost impossible to reconcile the outcome of this nucleosynthesis occurring in an inhomogeneous and diffusive medium with the observations of all the light elements.

5. SUMMARY

From these above remarks it appears that the best BBN model able to reproduce the observed abundances of the lightest elements are the simplest ones. One is still forced today to adopt a BBN model where $\Omega_B \leq 0.1$ and where the degree of inhomogeneity is low leading to the determination of a lower limit of T_c and consequently a lower limit of the value of the quark bag constant.

It is then pleasing to note that pure astronomical data like the primordial abundance of the light elements provide useful constraints on many parameters pertaining to the particle physics (number of families of leptons — mass and lifetime of some still hypothetical SUSY particles — physical characteristics of the quark confinement — coexistence temperature of the quark-hadron phase transition).

The research work reported here has been supported at least partly by CNRS and PICS n^o 18. We are most grateful to Marie-Christine Pelletan for her help in the presentation of this paper.

REFERENCES

- Alcock, C.R., Fuller, G.M. and Mathews, G.R., 1987, *Ap. J.*, **320**, 439
 Andreani, P., Vangioni-Flam, E. and Audouze, J., 1988, *Astrophys. J.* (in press, 15th Nov. issue)
 Applegate, J.H., Hogan, C.J. and Scherrer, R.J., 1987, *Phys. Rev. D*, **35**, 1151

- Audouze, J., 1987a in *Nucleosynthesis and Chemical Evolution of Galaxies*, eds B. Hauck, A. Maeder and G. Meynet, 16th Saas-Fee course, Geneva Observatory publication, p. 429
- Audouze, J., 1987b, in *Observational Cosmology*, eds A. Hewitt, G. Burbidge and L.Z. Fang, Reidel Dordrecht, p. 89
- Audouze, J., Delbourgo-Salvador, P., Reeves, H. and Salati, P., 1988, in *Origin and Distribution of the Elements*, ed. G. Mathews, World Scientific, p. 86
- Audouze, J., Lindley, D. and Silk, J., 1985, *Astrophys. J. Letters* 293, L53
- Audouze, J. and Silk, J., 1988, *Ap. J. Letters*, submitted
- Boesgaard, A.M. and Steigman, G., 1985, *Ann. Rev. Astron. Astrophys.* 23, 319
- Delbourgo-Salvador, P., Gry, C., Malinie, G. and Audouze, J., 1985, *Astron. Astrophys.* 150, 53
- Dimopoulos, S., Ezmailzadeh Hall L.J. and Starkman, G.J., 1988a, *Ap. J.* 330, 545
- Dimopoulos, S., Ezmailzadeh Hall L.J. and Starkman, G.J., 1988, in *Origin and Distribution of the Elements*, ed. G. Mathews, World Scientific, p. 116
- Fayet, P., 1984, in *Large Scale Structure of the Universe, Cosmology and Fundamental Physics*, 1st ESO CERN meeting, eds G. Setti and L. Van Hove, p. 35
- Fuller, G.M., Mathews, G.R. and Alcock, C.R., 1988, *Ap. J.* (in press)
- Kunth, D., 1986, *P.A.S.P.*, 98, 984
- Kurki-Suonio, H., Matzner, R.A., Centrella, J.M., Rothman, T. and Wilson, J.R., 1988, *Phys. Rev. D* (submitted)
- Lindley, D., 1985, *Astrophys. J.*, 294, 1
- Malaney, R.A. and Fowler, W.A., 1988, *Ap.J.* (in press)
- Salati, P., Delbourgo-Salvador, P. and Audouze, J., 1987, *Astron. Astrophys.*, 173, 1
- Salati, P., Delbourgo-Salvador, P., and Audouze, J., 1988, in preparation
- Sato, K., 1987, *Sendai Astronomiaj Raportoj*, 313, 171
- Terasawa, N. and Sato, K., 1988, preprint UT AP 77/1988
- Vangioni-Flam, E. and Audouze, J., 1988, *Astron. Astrophys.*, 193, 81
- Yang, J., Turner, M.S., Steigman, G., Schramm, D.N. and Olive, K., 1984, *Astrophys. J.*, 281, 493

LITHIUM AND THE NATURE OF DARK MATTER

Hubert Reeves, Service d'Astrophysique IRF CEN Saclay. F91191 Gif sur Yvette. Institut d'Astrophysique de Paris, F 75014, Paris.

**Abstract**

Limits on the value of critical temperature of the quark-hadron phase transition, evaluated by chiral perturbation calculations, are discussed in the frame of primordial nucleosynthesis. The yield of lithium is compatible with the Pop II data in approximately the same range as in the case of homogeneous baryonic density models (Ω_{B} between 0.01 and 0.10).

Taking into account various factors in the search for the initial abundance of the cosmological isotopes, it *appears very likely* that most of the baryonic matter is not luminous and that most of the dark matter is non-baryonic. However pushing all the uncertainties to their extremes, it seems also that we do not *necessarily* require baryonic dark matter and, 2) we do not *necessarily* require non-baryonic dark matter. The uncertainty in the value of the Hubble parameter remains one of the largest source of uncertainty in this analysis.

Chiral perturbation calculations and primordial lithium nucleosynthesis.

The low temperature behaviour of the quark condensate has been investigated with chiral perturbation calculations. (Gasser and Leutwyler 1987, 1988) (Leutwyler 1988). An expansion in power of the temperature, normalized to its $T = 0$ value, has been obtained. According to these authors, limits on the numerical value of the critical temperature of the chiral transition T_c (ch) can be estimated, even if the chiral perturbation calculations break down close to the transition temperature. The main justification is the fact that, in this temperature range, the partition function is dominated by the experimentally well-known properties of the pions.

The following limits are obtained. Assuming massless quarks, including tree, one-loop and two-loops graphs, a lower limit of T_c (ch) $> 180\text{MeV}$ is quoted. Assuming massive u , d , and s quarks, an upper limit of T_c (ch) $< 220\text{ MeV}$ is quoted (Gasser and Leutwyler 1988 and Leutwyler private communication).

QCD network calculations reported by Satz (87) show that, at low baryon chemical potential, the *confinement* and the *chiral* transitions are simultaneous. Therefore, in the context of the cosmological model, these limits should also apply to the confinement transition T_c (c)

Previous estimations of this parameter had been given by various authors. Wagoner and Steigman (1979) gave $170 < T_c < 360\text{ MeV}$. Olive (1981) gave $200 < T_c < 600$ from nuclear phenomenological data incorporated in a thermodynamic model. Satz (1985, 1987) from finite lattice calculations at zero baryonic number, quoted $150 < T_c < 200$.

In our previous work (Reeves 1986, Reeves et al 1988), in view of the large uncertainties on the value of T_c , our strategy was to use T_c as a free parameter and to try to constrain its value from the quark-lithium connection. It is now of interest, with the narrower T_c fork presented here, to rediscuss the subject differently.

Primordial lithium abundance.

Let us first recall that ${}^7\text{Li}$ has been observed (fig 1) in Pop II stars (Spite and Spite 1983 a and b, Spite et al 1987, Hobbs and Duncan 1987, Rebolo, Beckman and Molaro, 1987) which are presumed to represent an early stage of the life of our galaxy. As discussed in (Reeves and Richer 1988), both a stellar (Cayrel 1986, 1988) and a galactic cosmic ray origin can be eliminated as major contributors to the POP II ${}^7\text{Li}$ abundance, leaving the BBN origin as the most likely source.

The observed values of ${}^7\text{Li}/\text{H} = 1 \text{ to } 2 \times 10^{-10}$ correspond to the bottom of the dip of the lithium yield curve as a function of baryonic density in the standard (density homogeneous) model of Big Bang nucleosynthesis (BBN) (Beaudet and Reeves 1984, Yang et al 1984). In the case of a multiphase universe possibly resulting from the quark-hadron phase transition (Witten 1984, Applegate and Hogan 1984, Fuller et al 1987), the observed values lie the deepest part of the trench in the BBN lithium yield as a function of both the baryonic density and neutron to proton ratio. Because of this happy circumstance, ${}^7\text{Li}$ may be of great help in the study of the physics of the quark-hadron phase transition.

The small dispersion of lithium in Pop II stars (a factor of two) (fig 1 and 2) is the main argument in favor of the hypothesis that this lithium abundance has not suffered much depletion by processes associated with the stellar surfaces (Michaud 1986). Following the same logic, it appears reasonable to estimate that *the fractional depletion should not be larger as the observed dispersion*. In consequence we estimate an initial value of ${}^7\text{Li}/\text{H} = 3.0 \pm 1 \times 10^{-10}$.

Vauclair (1987), studying the effect of rotational mixing on stellar lithium, has argued that the depletion may have been larger and that the primordial value may be the same as for the Pop I stars (${}^7\text{Li}/\text{H} = 1.0 \times 10^{-9}$). It remains to be seen if the theory will be able to reproduce the small abundance dispersion displayed in figure 1. More work is being done on this subject.

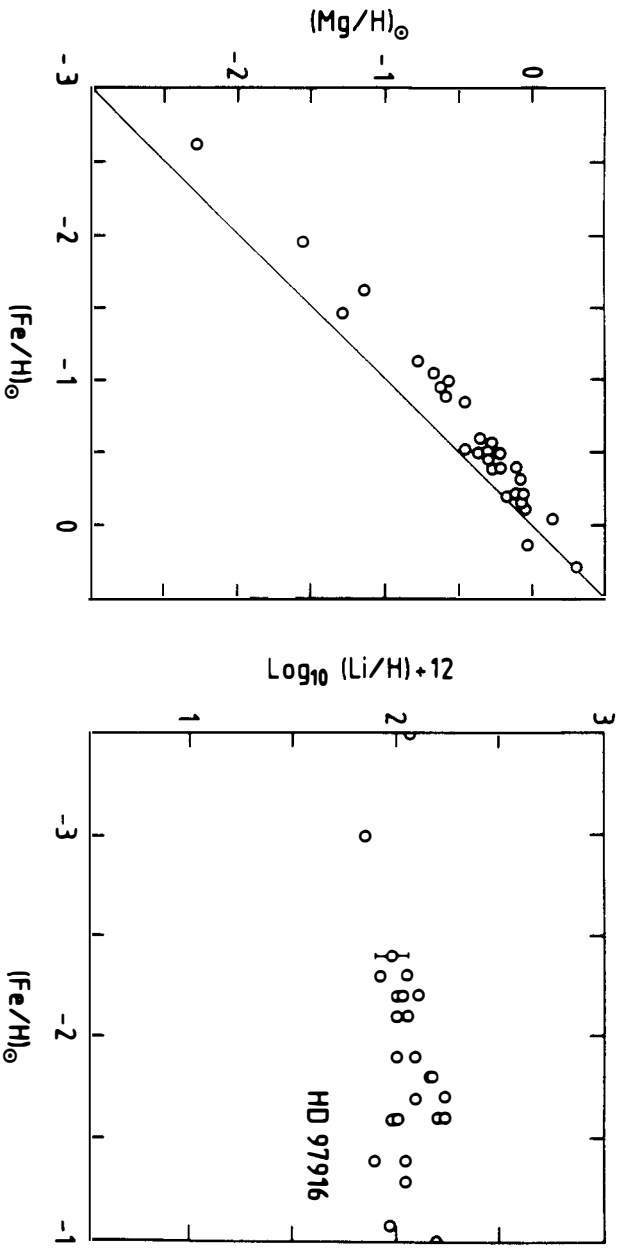


Fig 1 On the origin of Pop II lithium abundances: stellar- nucleosynthetic contribution.

The two figures show the correlation between iron abundances (in abscissa , normalized to the solar abundance) and the abundances of Pop II Li (on the left) and Mg (on the right) on a number of field stars (from R Cayrel , IAU Symposium no 1986).

Typically a product of stellar nucleosynthesis, Mg is seen to increase in steps with iron. The Pop II Li abundances appears to be independant of the amount of nucleosynthetic activity, suggesting a primordial origin.

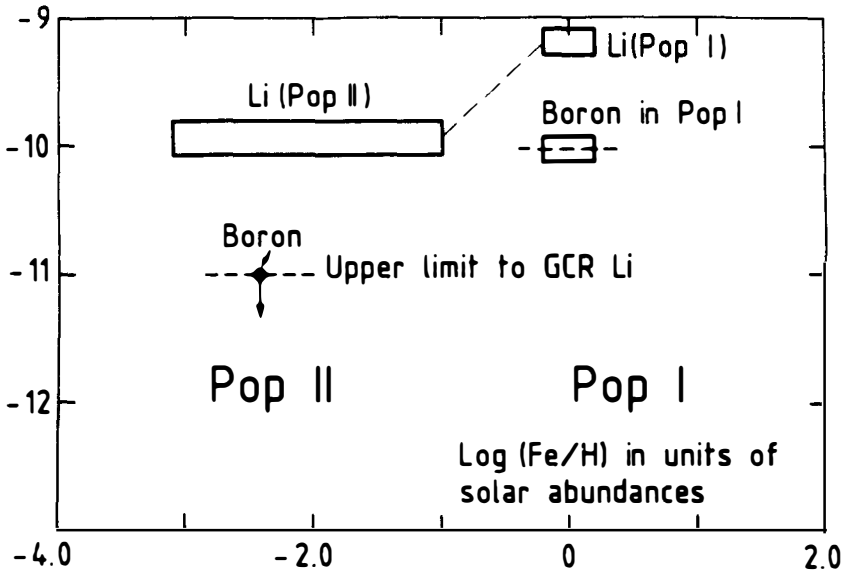


Fig 2 On the origin of Pop II lithium abundances: Galactic Cosmic Ray (GCR) contribution.

The figure displays the observations of stellar lithium and boron abundances (a pure GCR product) as a function of the iron abundances. For PopII we have only one upper limit of B abundance.

The GCR contribution to boron is quite similar to its contribution to lithium. The dashed line shows the upper limit of the GCR contribution to Li in PopII stars.

Baryon number contrast.

Fuller et al (1987) and Kapusta and Olive (1988) have calculated, with standard thermodynamic techniques, the ratio of the baryon numbers, $R(\mu_q) = (n_b^h) / (n_b^q)$ in the early hadronized (h) region and in quark sea (q) region for the case of chemical potential equilibrium ($\mu_b^q = \mu_b^h$; $3\mu_q = \mu_b$). Fuller et al treat the hadrons as free particles while Kapusta and Olive introduces a phenomenological hadronic potential. Their results are in agreement at low T_C value ($T_C < 150$ MeV) predicting large contrast values ($R \gg 10$). Above 160 MeV, however, the two calculations disagree. The contrast calculated by Fuller et al decreases gradually toward the value of one, and even below one. This last feature seems unphysical and justify the need for a more realistic treatment of the hadronic phase.

The effect of the hadronic potential is to level the contrast to values of seven to ten in the range $160 \text{ MeV} < T < 250 \text{ MeV}$. More accurate estimation of the effect of the hadronic potentials will require more sophisticated computations.

Baryon number equilibration.

One unresolved question is the approach of chemical potential (μ) equilibrium in the cosmic gas after the quark-hadron phase transition. We consider two possible cases.

A) Assume that the μ equilibrium is reached between the phases at the moment of Big Bang Nucleosynthesis (BBN).

Let us treat first the low T range. As discussed in Reeves (1987), the observed Pop stellar II lithium abundances restricts the baryonic density contrast R to be small. The possibility of early lithium depletion discussed in the last paragraph relaxes this constraint somewhat but not much. A lower limit of $150 \text{ MeV} < T_C$ is obtained, in agreement with the estimate from chiral perturbation calculations.

Can we reconcile the R values of seven to ten, obtained from the phenomenological hadronic potentials in the range $160 \text{ MeV} < T < 250 \text{ MeV}$, with the ${}^7\text{Li}$ observations in Pop II stars?

Excluding finely-tuned choices of the quark-hadron transition parameters, we find that, in the mean density range $\rho_B = 2.0 \text{ to } 5.0 \times 10^{-31} \text{ g/cm}^3$ ($\eta = 3.0$ to 8.0×10^{-10}), the BBN ${}^7\text{Li}$ yield averaged over the two phases is ${}^7\text{Li}/H \approx 3 \times 10^{-10}$, somewhat higher than in Pop II stars. *This can be reconciled with the observations if the initial lithium has been depleted by a factor of two or so by surface processes.* As discussed before, such a depletion is not incompatible with the observed dispersion of the ${}^7\text{Li}$ abundances in Pop II stars.

Taking into account the analysis of the cosmic abundance of D, ${}^3\text{He}$, and ${}^4\text{He}$ in the context of the effects of the quark-hadron phase transition (Reeves 1987, 1988) we select $\rho_B \approx 2.0 \text{ to } 5.0 \times 10^{-31} \text{ g/cm}^3$ as our best choice ($\eta = 3.0$ to 8.0×10^{-10}).

B) Now we relax the assumption of general chemical potential equilibrium and assume that this equilibrium is reached in each phase *but not between the phases* (μ_b^q is not equal to μ_b^h). Since the ratio of (m/T) is very small (μ/T) = 10^{-8} we can expand the baryon number density in (μ/T) :

$$R = R(\mu_{eq}) (\mu_b^q / \mu_b^h)$$

According to Fuller et al (1987) the degree of chemical potential equilibration depends upon the baryon transmission probability Σ_h across the phase boundaries. For values of Σ_h between 1 and 10^{-2} they find $R \approx R(\mu_{eq})$, while $R \gg R(\mu_{eq})$ at $\Sigma_h < 10^{-3}$. The fact that, in all cases, $R > R(\mu_{eq})$ shows that the lower limit $150 \text{ MeV} < T_c$ is valid even if full chemical potential equilibrium is not reached.

The strategy is now as follows. 1) Use the lithium data to find limits on R as discussed before. 2) Then use the chiral temperature limit calculations, $180 \text{ MeV} < T_c < 220 \text{ MeV}$ to obtain information on the baryon number diffusion

properties, as parametrized by the value of (μ_b^q / μ_b^h) at nucleosynthesis.

Without hadronic potentials we find $1 < (\mu_b^q / \mu_b^h) < 10$. The introduction of these potentials reduces this range to $1 < (\mu_b^q / \mu_b^h) < 2$

The Hubble parameter and the nature of dark matter.

The density of luminous matter in the universe is usually obtained in the following way. First integrate the average light emitted by galaxies. The value $L = 1.7 (+0.6) \times 10^8 h L_\odot / (\text{Mpc})^3$ is quoted by Tremaine and Binney in Galactic Dynamics, (1988), where h is the Hubble parameter in units of 100 km/sec/Mpc ($0.5 < h < 1$) and L_\odot is the solar luminosity ($4 \times 10^{33} \text{ erg/sec}$).

The average density of luminous matter ρ_L is given by: $\rho_L = L \times (M/L)$ where (M/L) is the mass to light ratio of luminous matter in solar units $(M_\odot/L_\odot) = 0.5 \text{ g/erg/sec}$. Numerically one finds: $\rho_L = 1.2 h^2 \times 10^{-32} (M/L) \text{ g/cm}^3$

In units of the critical density $\rho_C = 1.9 \times 10^{-29} h^2 \text{ g/cm}^3$ one gets: $\Omega_L = 6.1 \times 10^{-4} (M/L)$.

The estimated value of (M/L) averaged over the stellar luminosity function depends somewhat on the rather uncertain low-luminosity stellar extrapolation. Scalo (1986) has recently given a thorough discussion of this extrapolation. A value of ≈ 5 (mostly from elliptical galaxies) can be estimated (Rocca-Volmerange, private communication) from which we have $\Omega_L(\text{stars}) \approx 0.005$.

One should also consider the contribution from intergalactic gas emitting X rays in clusters. According to Sancisi (1988) the M/L ratio is appreciably larger (between 10 and 40) and the total contribution of this gas to universal density is rather poorly known. He quotes, for the sum of both contributions, a value $\Omega_L(\text{stars and Xray gas}) = 0.01$ with an uncertainty of a factor of two.

On the other hand, the density of clustered matter, required from different

dynamical considerations related to the motions of galaxies, has been established by various authors (Lynden-Bell 1988) to be in the range $\Omega_G = 0.1$ to 0.2 . The gap between the estimates of Ω_L and Ω_G defines the problem of the nature of the dark matter which is the subject of this section.

On the other hand, the success of standard BB nucleosynthesis gives an estimate of the baryonic density Ω_B of a few percent. The allowed range is further slightly narrowed by the effects of the quark-hadron transition as discussed previously.

Here, in the light of recent developments, I want to address two questions. 1) Could this dark matter be entirely non-baryonic? 2) Could this dark matter be entirely baryonic?

Is it still possible at this point to reconcile the luminous contribution with the baryonic contribution? What is the strength of the case for the existence of large scale baryonic dark-matter? One important uncertainty arises from the fact that while the BB nucleosynthesis defines a range of allowed baryonic density ρ_B , one needs the value of the Hubble parameter ($h = H_0$ in units of 100 km/sec/kpc) in order to compute Ω_B the baryonic density in units of the critical density. The range of h is usually given as $0.5 < h < 1$. Since $\rho_C = 1.9 \times 10^{-29} h^2 \text{ g/cm}^3$, an uncertainty of factor of four is introduced by the range of h . In this work I shall use $h = 0.75$ and discuss the effect of using rather $h = 0.5$ or 1 .

Could the dark matter be entirely non-baryonic?

For the Hubble parameter $h = 0.75$, $\Omega_L = 0.01$ corresponds to $\rho_B = 10^{-31} \text{ g/cm}^3$. At this density, the BB helium yield is $Y = 0.23$ quite in agreement with the observations.

An analysis of the effect of the quark-hadron transition, inducing an inhomogeneous density universe at the time of nucleosynthesis, gives, at a mean density of $\rho_B = 10^{-31} \text{ g/cm}^3$, an ${}^7\text{Li/H}$ yield $\approx 3 \times 10^{-10}$ not in contradiction

with the observations if the Pop I have suffered a minor amount of depletion. the observations. (This yield can be lowered by a fine adjustment of the parameters of the quark-hadron transition, a possibility that we do not consider here).

The real problem come from D (^3He is rather poorly observed). At $\rho_B = 10^{-31} \text{ g/cm}^3$, the D/H ratio is then 2.5×10^{-4} , ten to twenty times larger than the early solar system value. What can we say about D destruction during galactic evolution?

Such a decrease in the D abundance ratio implies that from *ninety to ninety five percent* of the present interstellar matter consists of processed matter which has been at least once astrated.

Such a large astration rate in the past galactic life would in principle be presently identifiable in a number of channels in relation with the stellar activity responsible for the D destruction . First by the *light* emitted by the stars which are still alive . Second by *heavy elements* generated by stars which are already dead . Third by the depletion of other light elements such as *lithium* which would also have suffered the postulated large astration rate. Fourth by the production of *spallation products* if the depletion of D is postulated to come from high energy particles.

Define $d(t)$ as the ratio of the primordial D/H ratio to the ratio at time t . Simple-minded models of chemical evolution using conventional wisdom and generally accepted hypotheses about the time variation of the stellar creation rate and luminosity function do not deplete D by more than fifty to sixty percent ($d < 3$) (Audouze and Tinsley 1976). For example the galactic evolution model of Rocca-Volmerange and Schaeffer(1988), where the latest data is used to modelize the abundance variation of C, O and Fe, gives $d = 2$. These hypotheses must be altered in some way to achieve larger D depletion.

This can be done, for instance, by biasing the early Initial Mass Function (IMF) toward the high mass range (the so-called bimodal star formation, Silk and Wyse 1984). This results in a rather high yield of metals per unit gas returned in space ($f_m \equiv \Delta Z / \Delta M$) and hence may result in an over-production of the heavy elements.

Alternatively one may consider an early increase in Star Formation Rate (SFR) without changing the (IMF) (Viangoni-Flam and Audouze 1987). Compared to the case discussed earlier, the metal overproduction problem is alleviated by the smaller average value of (f_m) coming from this distribution of stars. As a counterpart, small stars have a long life and many of them should still be visible in our sky.

At the other extreme, one could consider an generation of very large (and short-lived) objects processing a large amount of gas, without generating much metals (very low value of f_m).

Constraints

There are a number of observations from which some constraints can be derived.

1) The abundance of lithium in Pop II stars as a function of stellar metallicity puts some limits on the astration of galactic gas in the early days of the galaxy

2) A comparison between solar system and present D and ^3He abundance puts limits on the late rate of astration in the galactic gas.

3) The present stellar metallicity and the present luminosity function, interpreted in the framework of a model of galactic evolution, give limits on the evolutionary abundance curve of D throughout galactic life.

4) The observed ratios of $(\text{D}+^3\text{He}) / ^4\text{He}$ and $(\text{Li Be B}) / (\text{C N O})$ shows that the destruction of D by spallation reactions is negligible.

A) From PopII lithium. Recent data summarized in Cayrel (1986) show that the abundance of lithium in PopII stars varies by less than a factor of two when the iron abundance in the corresponding stars increase from less than 10^{-3} to ten percent of the solar value (fig 1). For stars with iron values from ten per cent to the solar value, lithium increases by a factor of ten. These observations gives information on the metal yield per unit mass of galactic matter returned to the gas in the early days of the galaxy ($f_m > 0.2$). Although this limit appears rather weak in comparison with the numbers usually derived from standard stellar nucleosynthesis model, nevertheless it limits the possibility of massive stellar objects eliminating D and ^7Li , for instance through strong stellar winds and later collapsing without metal formation.

(One alternative interpretation would invoke large fluxes of infalling matter on the galaxy in these early days, compensating the stellar lithium destruction. Needless to say, such an infalling material would also carry pristine D and make it even more difficult to reconcile the present D value, and a low baryonic density universe.)

B) Deuterium and helium-3 observations. The data is summarized in Boesgaard and Steigman 1985. Observations of interstellar clouds give a mean D/H value between 0.8 and 2×10^{-5} . The indirect evaluation obtained from helium in the early solar system gives D/H between 1.0 and 3×10^{-5} . Within the uncertainties, the two values are in agreement. This suggests that the depletion of D has been modest during the last five billion years. In terms of galactic evolution, these numbers limit the outflow of processed matter in the galaxy during this period.

C) From metal abundances and luminosity requirements. Vangioni-Flam and Audouze (1987) have investigated the possibility of obtaining large D depletion without overproducing the metals or overestimating the present galactic luminosity. Several recipes have been tested concerning the over-all rate of stellar formation or the alteration of the creation function. Their best result, in this respect, is obtained by an unmodified IMF coupled to a strong increase in overall activity (SFR) during the first two billion-years. In their best case, the D/H ratio is decreased to five percent of its initial value ($d = 20$) while the metal, early lithium and late D constraints are correctly met.

The main problem comes the resulting stellar luminosity function of the galaxy. The standard parameter here is $b(T_0)$: the ratio of the present stellar formation rate SFR to the time-averaged SFR (Scalo 1986) at T_0 the present age of the galaxy. From a summary of various observations, Scalo quotes an extreme lower limit of $0.18 < b(T_0)$ which, he writes, "comes from pushing all the uncertainties to their estimated limits". He personally favors the estimate $0.5 < b(T_0)$.

The model of Vangioni-Flam and Audouze (1987) quoted above results in an $b(T_0) = 0.15$, even lower than the extreme lower limit of Scalo. Furthermore it must be remembered that this discussion was based on the

assumption of $h = 0.75$. If $h = 0.5$ the requirement of D destruction amount to 99% of the initial value ($d = 100$), certainly too large in view of the last discussion. There would also be real problem with overproduction of ${}^7\text{Li}$ while ${}^4\text{He}$ would be OK. If $h = 1.0$ the required destruction correspond to a $d = 8$ still large but perhaps not in conflict with the $b(T_0)$ parameter constraint. The ${}^4\text{He}$ and ${}^7\text{Li}$ test would be OK.

Including the effects of the quark-hadron transition on the four cosmological isotopes, estimating the initial lithium as discussed in Reeves and Richer (88) and limiting the deuterium destruction by the Scalo estimate of the present to average star formation rate, we obtain a lower limit to the baryonic density : $\rho_b > 2 \times 10^{-31} \text{g/cm}^3$, corresponding to $\Omega_b > 0.01$ if $h = 0.75$. The upper limit $\Omega_L < 0.02$ quoted by Sancisi corresponds, for $h = 0.75$, to $\rho_b > 4 \times 10^{-31} \text{g/cm}^3$ in the hypothesis that all the baryonic matter is luminous. At this baryonic density the BBN is OK.

The conclusion is the following. The baryonic density obtained from BBN can still be reconciled with the luminous density but only by pushing some of the uncertainties to their extreme values ($\Omega_L = 0.02$ or $h = 1$ or $b(T_0) = 0.15$). More reasonably, we may estimate that more than fifty percent of the baryonic matter is invisible.

Do we require non-baryonic dark matter?

The *highest* baryonic density compatible with BBN, including the effects of the quark-hadron phase transition, is $5 \times 10^{-31} \text{g/cm}^3$, $\eta = 8 \times 10^{-10}$. This can only be reconciled with the *lowest* value of $\Omega_G = 0.1$, if $h = 1$.

Conclusions

The chiral perturbation calculations indicate that the quark-hadron phase transition takes place at a temperature for which a baryonic density contrast R between seven and ten can be expected at the moment of Big-Bang nucleosynthesis. This can be reconciled with the data of D, ${}^3\text{He}$, ${}^4\text{He}$ and ${}^7\text{Li}$ in a range a

baryonic density of $2 \text{ to } 5 \times 10^{-31} \text{ g/cm}^3$, corresponding to $\eta = 3 \text{ to } 8 \times 10^{-10}$ and Ω (baryonic) between 0,01 and 0,1.

The agreement between the lower limit for critical temperature obtained from the lithium data and from the chiral calculations is interesting and could be considered as another successful test of the Big-Bang theory.

The lithium data can be combined to the chiral perturbation calculation data to give information on the baryon number transmission probabilities across the density phases in the early universe.

The value of H_0 the Hubble parameter appears to play a crucial role in the determination of the nature of dark matter. At one hand of the range, if $h = 1$, the need for non-luminous baryonic matter can marginally be alleviated. For this, one requires also that the galactic evolution parameters be properly selected to insure a large depletion of D without over-production of metals, without overdestruction of the early Li or late D and without overestimation of the present stellar luminosity. Detailed galactic models shows that these constraints can be met only at the price of pushing the uncertainties at their extreme values.

At the other end of the range, for $h = 0.5$, the density of clustered matter Ω_G can marginally be reconciled with the baryonic component required for BBN.

Thus we have the same answer to the two questions: 1) Do we require baryonic dark matter? 2) Do we require non-baryonic dark matter? The common answer is: *probably yes, but not absolutely necessarily*. A narrowing of the allowed range of the Hubble parameter would have an important impact on our knowledge of the nature of dark matter.

Bibliography

- Alcock, C.R., Fuller, G.M., and Mathews, G.J., preprint UCRL 95896
1987
- Applegate, J.H., and Hogan, C. 1985 Phys. Rev. **D30** 3037.
Applegate, J.H., Hogan, C., and Sherrer R.J. 1987a Phys Rev., **D35**, 1151.
Audouze, J., and Tinsley, B.M. Ap. J. **192**, 487. 1974.
Baudet, G.; and Reeves H. 1984 Astr. Ap. **134**, 240.
Boesgaard, A., and Steigman, G., Ann. Rev. Astron. Astrophys. 1985.
Cayrel, R., I.A.U Symposium no 126 Cambridge 1986.
Cayrel, R., Proceedings of the Alpbach Summer school 1988.

Cayrel . R., Proceedings of the Alpbach Summer school 1988.
Fuller ,G.M., Mathews G.J., and Alcock, C.R. preprint,1987,

Gasser , J and Leutwyler, H., Light quarks at low temperature. Phys Lett B 184, 83 , 1988.

Gasser , J and Leutwyler, H., Thermodynamics of chiral symmetry. Phys Lett B 188, 477 , 1987.

Hobbs, L.M., and Duncan, D.K., Ap.J. **317**, 796, 1987. (Li in halo stars)

Kapusta,J.I., and Olive K.A. 1988 preprint

Leutwyler, H., QCD: low temperature expansion and finite -size effects. Proceedings of the Seillac Conference to appear in April 88.

Lynden -Bell , J., Third ESO-CERN conference, Bologna ,1988

Maurice, E., Spite., F., and Spite , M., Astron. Astrophys.**132**, **278** , 1984 (Li-7 / Li -6 ratio in old stars.)

Michaud,G., Fontaine, G, Beaudet, G. Ap.J. **282**, 206

Michaud, G., Ap. J. **302**, 650, 1986

Olive , K.A. 1981 Nucl. Phys. **B190** ,483.

Peebles, P.J.E. Physical Cosmology. Princeton University Press. 1971.

Rebolo, R., Beckman,,j., and Molaro, P., Astron, Astrophys. **172** L17 1987 (Li in G 64 -12)

Reeves . H., Varenna School "Confrontations between Observations and Theories in Cosmology" July 1987

Reeves, H., Delburgo-Salvador, P , Audouze, J. , and Salatti, P. to appear in European Journal of Physics may 88

Rocca-Volmerange ,B., and Schaeffer .R., Iron in the galaxy preprint 1988

Sale, K.E. and Mathews ,G.J. 1986 Ap.J. **309** L1

Sancisi, M., Third ESO-CERN conference, Bologna 1988.

Satz ,H., Ann. Rev. Nucl. Sci. **35** 1985

Satz .H ., Proceedings of the Strasbourg Symposium on the quark-hadron phase transition. . July 1987

Scalo ,J.M., Fundamentals of Cosmic Physics, **II** , 1 ,1986

Spite, M and Spite, F. 1983a Nature **297**, 483.

Spite, F. and Spite. M. 1983b Astr. Ap. , **115**, 337.

Spite, F., Spite, M., Peterson, R.C., and Chafee, F.H., Astron. Astrophys. **172** L9 1987, (Li in metal poor halo stars).

Tremaine, S., and Binney. J., Galactic Dynamics. Princeton University Press. 1987

Vangioni - Flam , E., and Audouze, J., Preprint 198 IAP Paris 1987.

Vauclair , S., Proceedings of Meudon IAU Symposium July 1987

Wagoner R.V. and Steigman ,G., Phys Rev D20 825 (1979)

Wyse, R., & Silk, J., Ap. J; Letters. 313, L11 1987.

Witten E., 1984 Phys. Rev. **D30** 272

Yang , J., Turner, M.S., Steigman, G., Schramm, D.N., and Olive, K, 1984, Ap.J. , **281**, 493

GENERATION OF FLUCTUATIONS FROM THE QUARK-HADRON
TRANSITION IN THE EARLY UNIVERSE

G.M. Fuller, G.J. Mathews, C.R. Alcock
Institute of Geophysics and Planetary Physics
Lawrence Livermore National Laboratory
University of California

Abstract

We present a model for the generation of isothermal baryon density fluctuations in the early universe associated with the quark-hadron transition. The model is based on thermal nucleation theory for the creation of bubbles of the new phase and on entropy conservation during the phase transition. We find that the baryon number transport characteristics together with the rapid motion of the phase boundary can result in baryon density fluctuations with amplitudes considerably larger than the chemical equilibrium limit. All of these results depend on uncertain quantities associated with the underlying QCD physics. We discuss how uncertainties in these quantities translate into uncertainties in the fluctuation amplitude, shape, and mean separation.

I. INTRODUCTION

Recent work¹⁻¹⁰⁾ has shown that isothermal baryon number fluctuations created during a first order phase transition associated with the quark-hadron transition can lead to primordial nucleosynthesis which is different than in the standard, homogeneous big bang. The details of this nucleosynthesis are still unclear, though it is clear that the light element abundances in these schemes depend on how neutron diffusion is handled before and during nucleosynthesis and on the detailed shape and spatial distribution of the fluctuations. This talk deals with the issue of fluctuation generation. The following talk will describe primordial nucleosynthesis calculations based on the fluctuation shapes and separations discussed here.

In the discussion of isothermal baryon number fluctuation generation to follow, we will first briefly describe the equation-of-state for each phase and outline a thermal nucleation model for the fluctuations before delving into an exposition of fluctuation generation.

II. EQUATION OF STATE

In what follows we will adopt a noninteracting particle equation of state for both the unconfined quark-gluon phase and the confined hadron phase. We have discussed this model in detail elsewhere⁷⁾ so here we will only give the salient results and comment on the applicability of the model.

For the deconfined quark-gluon plasma in the noninteracting model the thermodynamic potential is

$$\Omega_{\text{QG}} = -V \cdot T^4 \left[\frac{7\pi^2}{180} N_c N_f \left(1 + \frac{30}{7\pi^4} \left(\frac{\mu_Q}{T} \right)^2 + \frac{15}{7\pi^4} \left(\frac{\mu_Q}{T} \right)^4 \right) \right. \\ \left. - V \frac{\pi^2}{45} N_g T^4 \right. \\ \left. + V B \right] \quad (1)$$

where V is the volume of the system, T the temperature, N_c the number of colors (3), N_f the number of relativistic quark flavors (2 or 3), N_g the number of gluons (8), B the vacuum QCD energy, and $\mu_q = 1/3 \mu_b$ is the quark-baryon chemical potential.

Note that for the early universe $\mu_b/T \sim 10^{-8}$. In this dilute baryon number limit the baryon number density is

$$n_q \approx \frac{1}{9} N_c N_f T^3 \left(\frac{\mu_b}{T} \right). \quad (2)$$

For two relativistic quark flavors the total statistical weight in quarks and gluons is $g_q \approx 37$ and the contribution to the total pressure, energy density, and entropy density is

$$P_q \approx \frac{1}{3} g_q a T^4 - B \quad (3a)$$

$$\epsilon_q \approx g_q a T^4 + B \quad (3b)$$

$$S_q \approx \frac{4}{3} g_q a T^3 \quad (3c)$$

where $a \equiv \frac{\pi^2}{30}$. The justification for the use of a noninteracting equation of state in the strong coupling QCD limit is that the bag model of hadrons works¹²⁾. Another justification stems from deep inelastic lepton scattering experiments which indicate that quarks and gluons are relativistic¹³⁾. Recent finite temperature lattice QCD calculations¹⁴⁾ bear out the most important aspect of this approximation for our work: the baryon number concentration closely follows a Stefan-Boltzmann law.

For the confined, or hadronic, phase we again use a noninteracting model for the equation of state and we sum over all of the known mesonic and baryonic resonances. At low temperatures ($T < 120$ MeV) the statistical weight

is dominated by pions, $g_h \approx 3$, and useful approximations to our numerical results for the pressure, energy density, and entropy density for the confined phase are

$$P_h \approx \frac{1}{3} g_h aT^4 \quad (4a)$$

$$\epsilon_h \approx g_h aT^4 \quad (4b)$$

$$S_h \approx \frac{4}{3} g_h aT^3 \quad (4c)$$

At higher temperatures interactions between hadrons are important. These interactions tend to decrease the pressure and effective statistical weight of the hadron gas¹⁵⁾, with the result that the chemical equilibrium ratio of baryon densities in the quark and hadron phases which we present below is a lower limit to the actual ratio including interactions.

A dilute baryon number, low temperature limit approximation to the baryon number concentration in the hadron phase is

$$n_h \approx \left(\frac{g}{\pi}\right)^{1/2} T^3 \left(\frac{\mu_b}{T}\right) \left(\frac{m}{T}\right)^{3/2} e^{-m/T}, \quad (5)$$

where m is the mass of a nucleon. If separation of phases occurs in the early universe we expect that for some period (of order a Hubble time) the regions of different phase will be in thermodynamic equilibrium (nearly equal pressures and temperatures). We will argue below that the processes which transport baryon number across the phase boundary may be rapid enough to produce local chemical equilibrium at the boundary (equal baryon chemical potentials). If we define the ratio of the baryon density in the quark phase to the hadron phase as R , then in the chemical equilibrium limit,

$$R \equiv \frac{n_q}{n_h} \approx \frac{2}{9} \left(\frac{\pi}{8}\right)^{3/2} \left(\frac{T}{m}\right)^{3/2} e^{m/T_c}. \quad (6)$$

306

Our calculation for the equilibrium ratio, R , which includes a sum over all hadronic resonances, is shown in Figure 1.

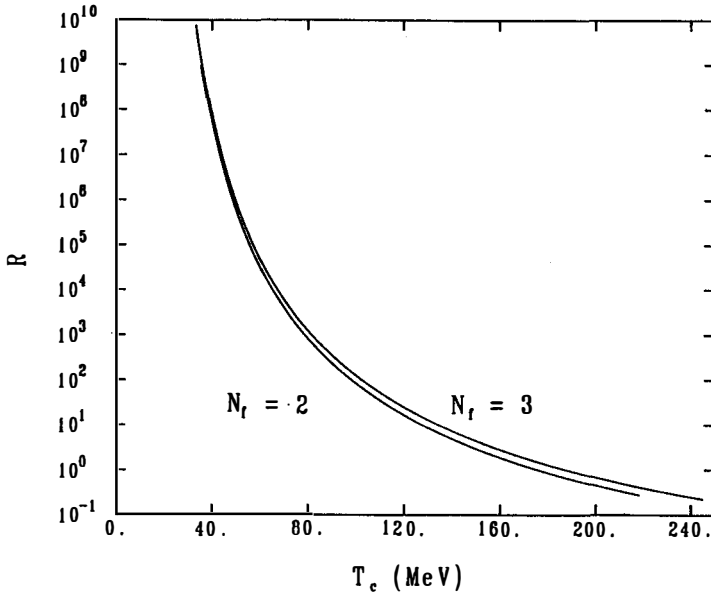


Fig. 1 The chemical equilibrium baryon ratio, R , as a function of coexistence temperature, T_c . Curves are shown for 2 and 3 relativistic quark flavors.

III. NUCLEATION

At high enough temperature the universe is filled with a deconfined quark-gluon plasma. As the universe expands the temperature drops until it becomes favorable to form bubbles of the new, confined phase. If a bubble of new phase with radius r_c appears it has free energy,

$$W = \frac{4\pi}{3} r_c^3 (P_q - P_h) + 4\pi \sigma r_c^2, \quad (7)$$

where σ is the surface-energy parameter. In the theory of spontaneous thermal nucleation¹⁶ the rate at which new phase appears is given by

$$P(\eta) \approx C T_c^4 \exp\left(\frac{-16\pi}{3} \frac{\sigma^3}{T_c L \eta^2}\right), \quad (8a)$$

where T_c is the coexistence temperature, L is the latent heat, C is a constant, and η is the supercooling parameter,

$$\eta \equiv \frac{T_c - T}{T_c}. \quad (8b)$$

We follow Kajantie and Kurki-Suonio¹⁷⁾ and assume that a bubble of new phase is accompanied by the formation of a shock. This shock heats the universe as it moves out, effectively transmitting the bubbles' latent heat to the outside medium of old phase. If the fraction of the volume of the universe which is unaffected by these shocks is f then we have shown that⁷⁾,

$$f(t) \approx \exp\left(-\int_{t_c}^{t_f} f(t') p(T') \frac{4}{3} \pi v_s^3 (t - t')^3 \left(\frac{T}{T'}\right)^3 dt'\right) \quad (9)$$

where t_c is the time when the universe first cools through coexistence, v_s is the shock velocity (which we take to be the sound speed) and t_f is the time when the universe is reheated to the coexistence temperature.

Equation (8) can be solved to yield the amount of supercooling,

$$\eta_f \approx 1.4 \frac{\sigma^{3/2}}{T_c^{1/2} L}, \quad (10)$$

where $\eta_f \approx 10^{-3}$ or 10^{-4} for a reasonable range of σ and T_c . An integration of the product of $p(t)$ and $f(t)$ yields the total number of nucleated bubbles of new phase per unit volume,

$$N_n = \int_{t_c}^{\infty} f(t) p(t) dt \quad (11)$$

The mean separation between the centers of nucleated bubbles, or nucleation scale is $\lambda \equiv N_n^{-1/3}$,

$$\lambda \approx 0.3 \frac{\sigma^{3/2} t}{T_c^{1/2} L} \quad (12a)$$

where t is the reheating time. Using the noninteracting equations of state presented in the last section we can show that

$$\lambda \approx (2 \times 10^6 \text{ m}) \frac{(\sigma/\text{MeV}^3)^{3/2}}{(T_c/\text{MeV})^{13/2}} \quad (12b)$$

We do not know either σ or T_c . A fair estimate is that $T_c \approx 100$ to 300 MeV, but σ may be between 0 and $B^{3/4}$. This means that λ may lie between 0 and the horizon scale (≈ 10 km).

IV. BARYON NUMBER TRANSPORT

After the universe has nucleated bubbles of hadrons and reheated back to the coexistence temperature, further spontaneous nucleation is suppressed on the timescale of the phase transition since the nucleation rate (equation 8a) is so small. As the universe continues to expand, the hadron phase grows in volume at the expense of the quark phase, releasing latent heat at a rate which keeps the temperature (and total entropy) constant until all of the universe is converted to confined phase. We will follow the transport of baryon number during this constant temperature epoch.

If $A(t)$ is the scale factor for the universe then the Einstein equation gives

$$\frac{\ddot{A}}{A} \approx \chi \left[\frac{\epsilon_h (1 - f_v) + \epsilon_q f_v}{B} \right]^{1/2} \quad (13a)$$

where f_v is the fraction of the volume of the universe in the quark-phase and x is a QCD expansion timescale⁷,

$$x = \frac{1}{143\mu \text{ sec}} (T_c / 100 \text{ MeV})^2 \quad . \quad (13b)$$

Energy-momentum conservation provides another constraint which, if the pressure is constant, is equivalent to total entropy conservation,

$$\frac{d}{dt} [A^3 (S_q f_v + S_h (1 - f_v))] \approx 0. \quad (14)$$

These equations can be solved to yield f_v as a function of time (Figure 2a) or, equivalently, the radius, r , of a typical bubble as a function of time (Figure 2b). Note that

$$f_v = \begin{cases} 4/3 \pi r^3 N_n \frac{V_0}{V} & f_v < \frac{1}{2} \\ 1 - 4/3 \pi r^3 N_n \frac{V_0}{V} & f_v \geq \frac{1}{2} \end{cases} \quad (15)$$

where V_0 is the volume of the universe at the end of reheating and V is the instantaneous value. In figure 2b we interpret r as the radius of a growing bubble of hadrons for $f_v \geq \frac{1}{2}$ and as the radius of a shrinking bubble of quark-gluon plasma for $f_v < \frac{1}{2}$. The approximation of spherical bubbles clearly makes sense at the beginning and end of the phase transition when surface energy may dominate, but may be overly simplistic near percolation.

Consider baryon number transport across a phase boundary, or wall, separating the quark phase from the hadron phase. If N_q and N_h are the comoving densities of baryon number in quarks and hadrons respectively then,

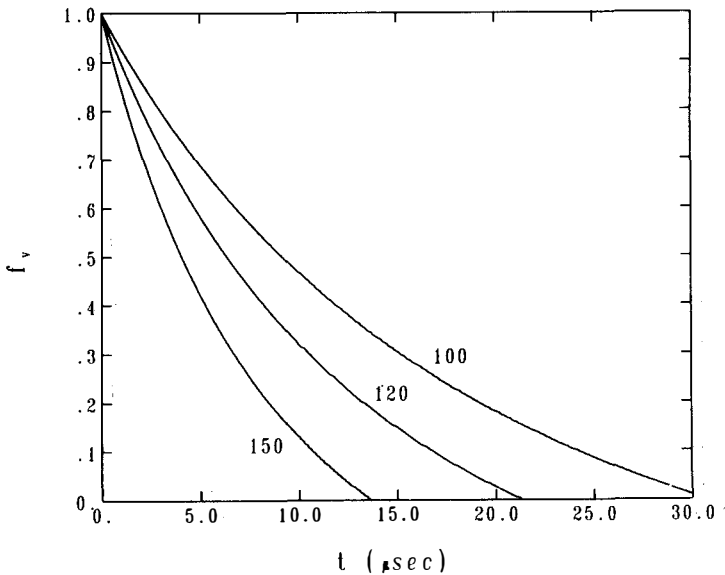


Fig. 2a The fraction of the volume of the universe, f_v , left in the unconfined quark phase as a function of time, t , during the constant temperature coexistence epoch. Curves for three different temperatures are shown: 100 MeV, 120 MeV, and 150 MeV.

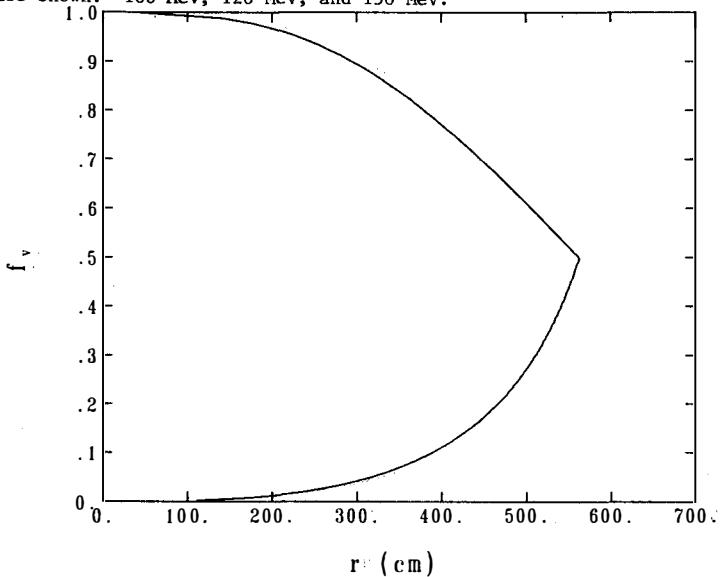


Fig. 2b The quark volume fraction f_v as a function of proper bubble radius r .

$$N_q = n_q f_v V \quad (16a)$$

$$N_h = n_h (1 - f_v) V \quad (16b)$$

where V is some proper volume. The rate at which baryon number is changing in each phase is given by

$$\dot{N}_q = -N_q \lambda_q + \left(\frac{f_v}{1 - f_v} \right) N_h \lambda_h \quad (17a)$$

$$\dot{N}_h = N_q \lambda_q - \left(\frac{f_v}{1 - f_v} \right) N_h \lambda_h \quad (17b)$$

where λ_q and λ_h are baryon number transport rates for quarks to hadrons and hadrons back to quarks respectively. These transport rates have been estimated previously⁷⁾ based on the flux of particles hitting the wall from each side.

$$\lambda_q \approx (1.115 \times 10^{14} \text{ s}^{-1}) \left(\frac{\text{MeV}}{T_c} \right) \left(\frac{\text{cm}}{r} \right) e^{-\frac{938 \text{ MeV}}{T_c}} \varepsilon_h \quad (18a)$$

$$\lambda_h \approx (3.00 \times 10^{10} \text{ s}^{-1}) \left(\frac{T_c}{312.7 \text{ MeV}} \right)^{1/2} \left(\frac{\text{cm}}{r} \right) \varepsilon_h, \quad (18b)$$

where ε_h will be defined presently.

Note that in the limit where equilibrium is obtained ($\dot{N}_q = 0$),

$$h = \lambda_h / \lambda_q. \quad (18c)$$

Detailed balance in equilibrium (equation 18c) can then be used to eliminate one of the unknown cross-sections in the transport rates in terms of the other. We have done this in equations 18ab to leave each rate proportional to ε_h , the probability that when a nucleon hits the wall it tunnels through to

evaporate into three quarks. Any attempt to estimate Σ_h is very model dependent⁷⁾ and therefore, not particularly believable: the largest it can be is unity; in reference 7 we estimate that $\Sigma_h \approx 10^{-3}$.

Equations 17ab leave out the crucial point that baryon number is not uniformly distributed in each phase, but in fact can diffuse toward or away from the bubble walls. We note two simplifying points: first, the chemical equilibrium timescale (inverse coefficient of λ_h) is short compared to the speed of the wall (roughly λ/t). Second, the speed of the wall is rapid compared to the baryon diffusion rate in the hadrons. This latter point follows by noting that the hadron diffusion length in a Hubble time is only 10^{-3} m and it is to be compared with λ which may be 1-1000 m. The generalization of equations 17ab to include diffusion away from the wall is,

$$\dot{N}_q = \frac{1}{dr} \{-N_q \lambda_q r/3 + N_h \lambda_h r/3 + 4\pi r^2 D_q v^2 (N_q/4\pi r^2)\} \quad (19a)$$

$$\dot{N}_h = \frac{1}{dr} \{N_q \lambda_q r/3 - N_h \lambda_h r/3 + 4\pi r^2 D_h v^2 (N_h/4\pi r^2)\} \quad (19b)$$

where dr is the width of a zone, and D_q and D_h are the baryon number diffusion constants for quarks and hadrons respectively.

In keeping with the two simplifying points given above we set $D_h = 0$ and in the solution to equation 19ab we demand that the ratio of the baryon number densities on either side of the phase boundary be R , the equilibrium ratio. We start the hadron bubbles at the end of reheating with the equilibrium baryon number concentration, and then integrate equations 19ab. We set $\Sigma_h = 1$. The relative baryon number densities ($n_h/n_q(0)$, where $n_q(0)$ is the comoving uniform baryon number density at the beginning of the phase transition), are shown in figure 3a as a function of $f_v^{1/3}$ for the beginning, middle ($t=15 \mu s$) and end ($t=30 \mu s$) of the phase transition. The $f_v^{1/3}$

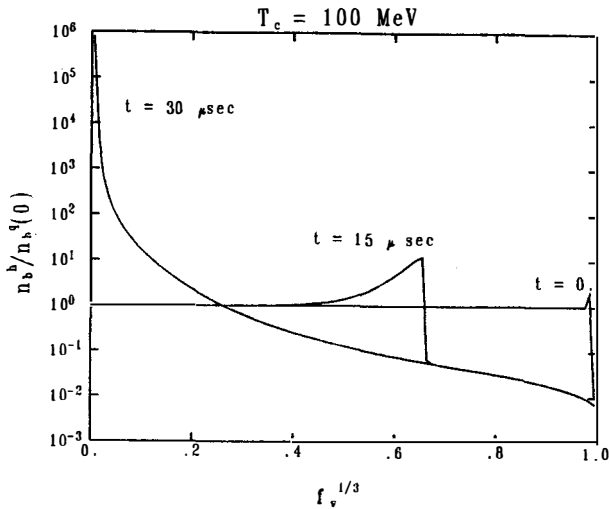


Fig. 3a The ratio of the baryon number density in the hadron phase to the comoving uniform baryon number density in the quark phase at the beginning of the phase transition as a function of $f_v^{1/3}$ (a measure of comoving fluctuation radius). Three times during the phase transition are shown: $t=0$, the end of nucleation; $t=15\mu\text{s}$, midway in the transition, and where we interpret densities to the left of the peak as being in quarks, to the right in hadrons; $t=30\mu\text{sec}$ the end of the transition. A coexistence temperature of 100 MeV is assumed.

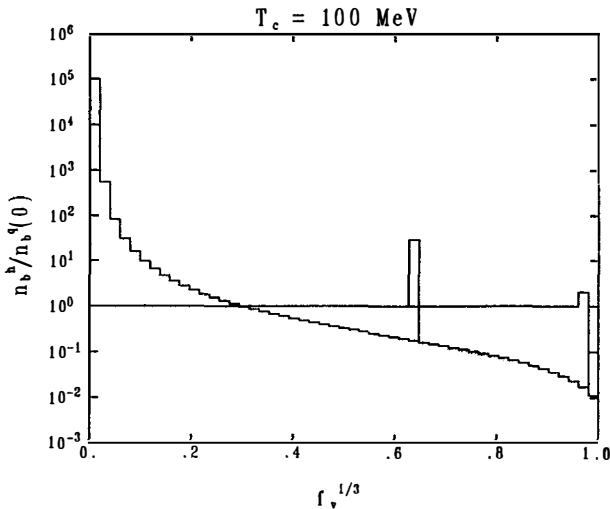


Fig. 3b Same as Fig. 3a but now the diffusion constant for quarks is set to zero.

parameter is essentially the comoving radius of a "Wigner-Seitz" cell centered on a fluctuation. During the phase transition, the baryon number density is in the quark phase to the left of the wall and is in the hadron phase to the right. With $T_c = 100$ MeV in this calculation the equilibrium jump condition at the wall is $R \approx 100$. Baryon number is concentrated in the shrinking bubble of quark gluon plasma because the surface area of the bubbles is going down rapidly and because the baryons can only be transported out of the quarks with the equilibrium ratio R . Near the end of the phase transition this equilibrium approximation will break down, most likely when the speed of the wall becomes of order the sound travel time across the bubble. At that point λ_q should diverge and cap off the peak. This calculation used $D_q = 4 \times 10^9 \text{ cm}^{-2} \text{ s}^{-1}$.

Figure 3b is the same as figure 3a except now $D_q = 0$. In this limit, baryon number piles up along the wall in the quark phase to the limit of the zoning. The net result is a fluctuation of smaller amplitude. It has been claimed that in the limit of $D_q = 0$ and infinitely fine zoning that the fluctuation amplitude should be limited⁹⁾ to R . We are currently investigating this but remain unconvinced because these claims are based on one-dimensional plane parallel calculations which admit a steady-state solution which does not exist in three dimensional geometry.

In figure 3c we repeat the calculation in (3a) but now reduce R to the value comensurate with $T_c = 200$ MeV in the noninteracting model ($R \approx 3$). Although the overall shape is relatively similar to that at $T_c = 100$ MeV, the amplitude is reduced by several orders of magnitude (but is still considerably larger than R). Finally, reducing Σ_h has the effect of narrowing and heightening the peaks.

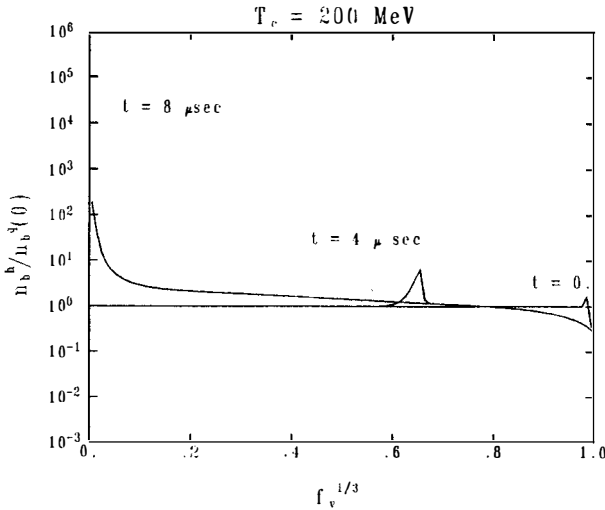


Fig. 3c Same as in Fig. 3a but now $T_c = 200 \text{ MeV}$. The times for the beginning ($t=0$), middle ($t=4\mu\text{s}$), and end ($t=8\mu\text{sec}$) of the phase transition are shown.

V. CONCLUSION

As we will see in the next talk¹¹⁾, the primordial nucleosynthesis associated with isothermal baryon number fluctuations may depend on the shape, amplitude, and mean separation of these fluctuations. The mean separation of these fluctuations depends on the latent heat associated with the phase transition and the unknown surface energy characterizing the phase boundary, σ . The fluctuation amplitude and shape depend on the equilibrium baryon number concentration ratio, R , the geometry of the bubbles, and the nucleon wall penetration probability, ϵ_n . In short there is a great deal of unknown physics associated with the characterization of fluctuations from the quark-hadron transition. For some values of these quantities the fluctuations

may be narrow and have amplitude considerably larger than the equilibrium concentration ratio, R .

VI. ACKNOWLEDGEMENTS

The authors would like to thank J. Audouze for the kind invitation to attend this workshop. Work performed under the auspices of the U.S. Department of Energy by the Lawrence Livermore National Laboratory under contract No. W-7405-ENG-48.

References

1. Witten, E., Phys. Rev. **D30**, 272 (1984).
2. Applegate, J.H., and Hogan, C., Phys. Rev. **D31**, 3037 (1985).
3. Sale, K.E., and Mathews, G.J., Astrophys. J. **309**, L1 (1986).
4. Applegate, J.H., Hogan, C., Scherrer, R.J., Phys. Rev. **D35**, 1151 (1987).
5. Malaney, R.A., and Fowler, W.A., Submitted to Astrophys. Journ. (1988).
6. Alcock, C.R., Fuller, G.M., and Mathews, G.J., Astrophys. Journ. **320**, 439 (1987).
7. Fuller, G.M., Mathews, G.J., Alcock, C.R., Phys. Rev. **D37**, 1380 (1988).
8. Audouze, J. et. al. (this conference proceedings)
9. Kurki-Suonio, H., et. al., Submitted to Phys. Rev. D (1988).
10. Reeves, H. (this conference proceedings)
11. Mathews, G.J., Fuller, G.M., Alcock, C., Kajino, T. (this conference proceedings).
12. Thomas, A.W., in "Advances in Nuclear Physics," ed. J.W. Negele and E. Vogt (Plenum, New York, 1983), **13**, 1.
13. Gross, D.J. and Wilczek, F., Phys. Rev. **D8**, 3633 (1973).
14. Gottlieb, S., et. al. Phys. Rev. Lett., **59**, 2247 (1987); and "Proceedings of the International Symposium on Field Theory on a Lattice" Saclay France, 1987, IUHET-138.
15. Olive, K. (this conference proceedings).
16. Landau, L.D. and Lifshitz, E.M., "Statistical Physics," (Pergamon, New York, 1969).
17. Kajantie, K. and Kurki-Suonio, H., Phys. Rev. **D34**, 1719 (1986).

THE EVOLUTION OF BARYON NUMBER DENSITY FLUCTUATIONS
BEFORE, DURING AND AFTER PRIMORDIAL NUCLEOSYNTHESIS

G. J. Mathews, G. M. Fuller, C. R. Alcock, and T. Kajino*
University of California
Lawrence Livermore National Laboratory
Livermore, CA 94550

ABSTRACT

We discuss the simultaneous evolution of weak and nuclear reactions along with baryon diffusion in isothermal fluctuations produced in the quark-hadron phase transition. We find that the resulting light-element nucleosynthesis is sensitive to the separation distance between fluctuations, although still consistent with observed light-element abundances (except possibly ${}^7\text{Li}$) for a reasonable range of separations between fluctuations. The heavy-element nucleosynthesis has been computed for all nuclei up to $A = 28$. It appears that an r-process "seed" abundance will be formed with a mass fraction of 10^{-12} to 10^{-10} . It is not yet clear whether this will lead to an overproduction of r-process abundances relative to that observed in metal-poor halo stars. The evolution of the fluctuations after nucleosynthesis is discussed and it is concluded that these fluctuations are not likely to collapse to form compact cold-dark-matter remnants, but are probably smoothed by baryon diffusion before recombination.

* Permanent Address, Department of Physics, Tokyo Metropolitan University, Setagaya, Tokyo 158 Japan

We have discussed in a previous talk¹⁾ how a first-order transition from quark-gluon plasma to confined hadronic matter could lead to pronounced isothermal baryon number density fluctuations. In this talk we concentrate upon how such fluctuations affect primordial nucleosynthesis and how they might evolve through and after the epoch of nucleosynthesis. The simple schematic treatment utilized in our earlier papers^{2,3)} involved simply forcing the neutron density to be homogeneous just before nucleosynthesis and neglected any effects of baryon diffusion thereafter. This was a convenient simplification for the purposes of a global parameter study. However, it has been pointed out^{4,5)} that baryon diffusion after the onset of primordial nucleosynthesis can be important. In particular, the inclusion of baryon diffusion may to some extent⁴⁾ avoid the problem of overproduced ${}^7\text{Li}$.

In the work reported here, we solve the baryon diffusion equation simultaneously with the weak and nuclear reaction rates from the time of the phase transition until after the epoch of nucleosynthesis. The rate of change of the density, n_i , of a given nuclear species, i , can then be written

$$\frac{\partial n_i}{\partial t} = \sum_{j,k,l} \left\{ N_i \frac{n_l^{N_l} n_k^{N_k}}{N_l! N_k!} N_A \langle \sigma_{lk} \rangle_j - \frac{n_i^{N_i} n_j^{N_j}}{N_i! N_j!} N_A \langle \sigma_{ij} \rangle_k \right\} + \nabla \cdot (D_i \nabla n_i) \quad (1)$$

where the summation is over all relevant nuclear and weak reactions of

the form:

$$N_i ({}^A_i Z_i) + N_j ({}^A_j Z_j) \dot{=} N_k ({}^A_k Z_k) + N_l ({}^A_l Z_l) . \quad (2)$$

The last term in Eq. (1) is the density dependent diffusion equation. For the work reported here it is sufficient to consider diffusion by baryons only while they appear as neutrons. Hence, the diffusion constants are taken to be zero except for the neutron for which

$$D_n^{-1} \approx D_{ne}^{-1} + D_{np}^{-1} , \quad (3)$$

where the proper diffusion constants for neutron-electron scattering, D_{ne} , and neutron-proton scattering, D_{np} , are taken from ref. 6.

Numerically, we have found that it is imperative to solve Eq. (1) implicitly. The finite differenced version of Eq. (1) appears as a nearly block diagonal matrix whose submatrices are connected via the diffusion matrix elements. Figure 1 shows an example of an eight zone discretized approximation to our calculated¹⁾ baryon density fluctuations as a function of comoving radial coordinate. Figure 2 shows how the neutron density in different zones varies as a function of time when the average separation between fluctuation centers is 40 m. Weak reaction decoupling occurs after about 1 sec when the temperature is ≈ 1 MeV. As one can see from this figure there is some baryon diffusion up to this time. However, after $t \approx 1$ sec when the neutrons are no longer rapidly converted into protons, the outer zones are able to approach equilibrium quickly after about 10 sec. The outer zones then remain in equilibrium. At $t \sim 200$ sec, the onset of nucleosynthesis causes a factor of 2 drop in the neutron density as the available protons are consumed. Afterwards, the neutron density decreases more gradually, and is essentially given by

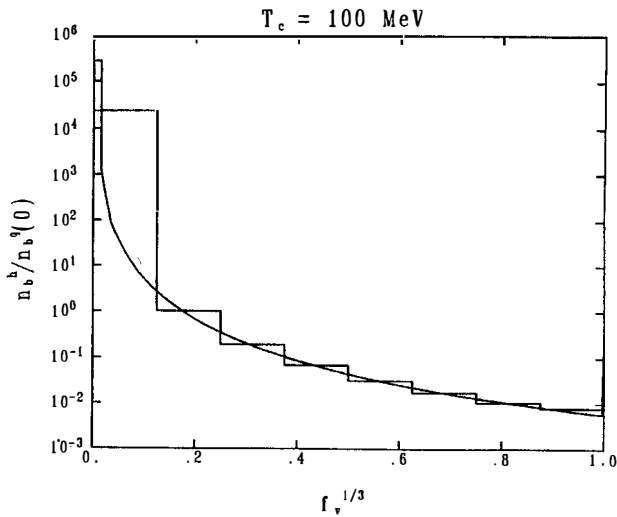


Fig. 1 An eight zone approximation (histogram) to a calculated (smooth curve) baryon density fluctuation, $n_b^h/n_b^q(0)$, as a function of the dimensionless comoving radial coordinate, $r_v^{1/3}$.

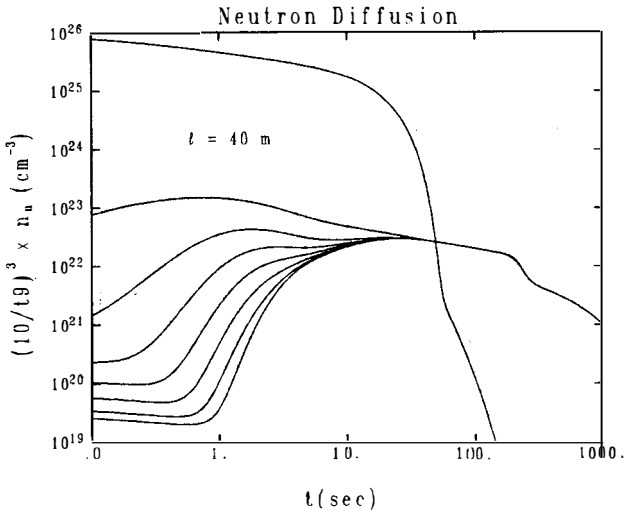


Fig. 2 Comoving neutron density as a function of time in different zones for a fluctuation similar to that shown in Fig. 1. The average separation, l , between fluctuations was taken to be 40 m for this calculation.

the timescale for neutron decay into protons which is required for further nucleosynthesis.

The innermost zone appears to evolve almost independently from the outer zones. The density in this zone remains high until $t \sim 10$ sec at which point the nucleosynthesis begins and the neutron density is quickly diminished as baryons are converted into ^4He . The reason that this zone does not efficiently communicate with the outer zones is due to its high baryon density. The resulting high neutron-proton scattering rate drastically shortens the baryon diffusion length.

The flow of neutrons among the zones is important for the resulting nucleosynthesis. The flow of neutrons into the inner high-density zone can reduce the overproduction of lithium via the $^7\text{Be}(n,p)^7\text{Li}(p,\alpha)^4\text{He}$ reaction.⁴⁾ On the other hand, the loss of neutrons from the outer low density zones will diminish the deuterium production there.

Given our calculated fluctuation shapes and diffusion constants, the amount of neutron flow is determined by the average separation between nucleation sites. Figure 3 shows an example of our calculated nucleosynthetic yields as a function of the separation between fluctuations. The optimum separation distance appears to be ~ 10 - 100 m at the time of the phase transition, which is comparable to our earlier estimates^{2,3)} based upon classical nucleation theory. For separations which are too close, < 10 m, ^4He and ^7Li are overproduced while ^2H and ^3He are underproduced. This is due to the flow of neutrons back into the high density zones after the onset of nucleosynthesis. For separations > 100 m, there is not enough neutron diffusion to produce significant ^2H in the low density zones. For the optimal conditions, ~ 30 m, ^7Li is overproduced at about six times the POP I Li abundance. This is a reduction by about a factor of 1 to 5 from the Li overproduction in our

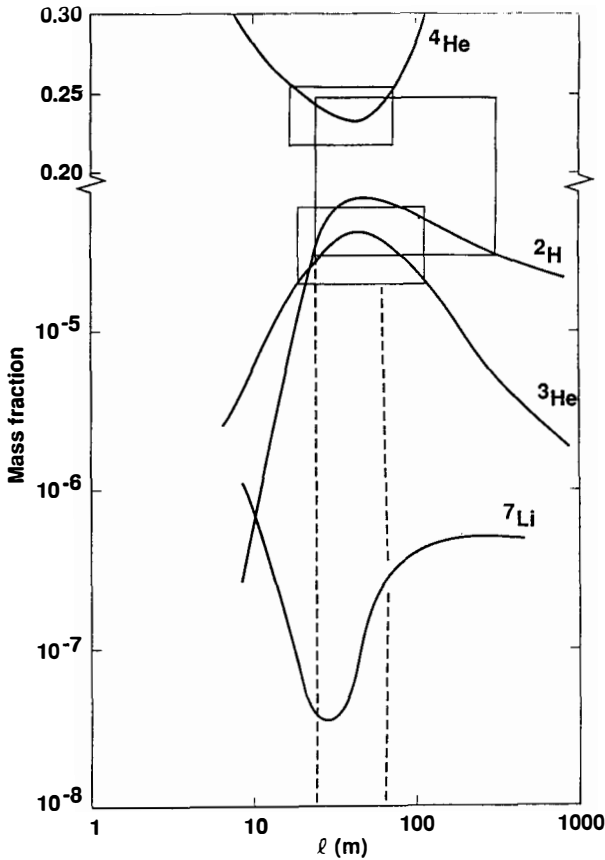


Fig. 3 Calculated average light-element nucleosynthesis yields as a function of fluctuation separation distance, l , for an $\Omega_b = 1$ universe. The squares show the regions consistent with observations. The dotted lines roughly indicate the region of common overlap for ${}^2\text{H}$, ${}^3\text{H}$, and ${}^4\text{He}$.

previous schematic model studies and reflects the importance of ${}^7\text{Be}$ destruction during nucleosynthesis.⁴⁾

Although our ${}^7\text{Li}$ abundance exceeds the observed POP I Li abundance for clusters < 5 Gyr old, it is not inconsistent with recent data⁷⁾ from the 10 Gyr old Pop I cluster, NGC188, which appears to show enhanced Li.

A decline in the observed galactic Li to a constant value for the past 5 Gyr could be easily understood as due to the combined effects of astration and infall in a galactic chemical evolution mode⁸⁾. We have also heard at this conference⁹⁾ that the apparent low value for lithium in POP II halo stars may be attributable to gradual destruction from a much higher initial Li abundance. Because of these considerations it appears to us that it would be premature to disregard cosmologies in which the universe is closed by baryonic dark matter on the basis of the predicted primordial lithium abundance.

With regard to nucleosynthesis, we are also studying the suggestion¹⁰⁾ of heavy-element formation via a primordial rapid-neutron-capture (r-) process which may have taken place in the neutron-rich zones after the buildup of CN and O elements. We have now extended the original nuclear reaction network in the big bang code to include nuclear species up to $A = 28$, including neutron capture paths for unstable elements with β -decay lifetimes > 1 ms. We are also in the process of connecting a classical¹¹⁾ r-process to this network to follow the buildup to heavier nuclei. What we have observed in the neutron rich zones is that a neutron capture flow path is quickly established which lasts for up to ~ 1000 sec after the onset of nucleosynthesis. This path flows through neutron rich nuclei with lifetimes ~ 1 min; e.g. $^{23}\text{Ne} \rightarrow ^{25}\text{Na} \rightarrow ^{27}\text{Mg}$. We see that seed material is built up with a mass fraction of $10^{-12} - 10^{-10}$ depending upon our assumptions about the neutron capture cross sections (i.e. direct radiative capture,¹²⁾ or Hauser-Feshbach estimates¹³⁾. Although results from our r-process network are not yet available we can calculate the expected r-process mass fractions, X_r , from our estimated seed abundances:

$$X_r \sim X_{\text{seed}} \times 2^n \quad ; \quad (4)$$

where n is the number of fission cycles.¹¹⁾ The number of fission cycles will be given by the ratio of the r -process time scale (~ 1000 sec from Fig. 2) to the sum of the β -decay lifetimes along the r -process path from $A \sim 100 - 300$. Along the neutron capture flow in our network, the β -decay lifetimes are ~ 1 min for nuclei with capture cross sections ~ 10 mb. Assuming an average capture cross section ~ 100 mb for heavy nuclei the corresponding β lifetime will be 10 sec. This implies a cycle time scale ~ 1000 sec. This is a long timescale for a true classical r -process and reflects the somewhat lower proper neutron-density ($< 10^{18}$ cm^{-3}) characteristic of our models. This lower neutron density in turn causes the flow path to fall closer to stability. Thus, we estimate that there will only be ~ 1 fission cycle. This means that the r -process mass fraction will only be $< 10^{-10}$. This is important since halo stars are observed¹⁴⁾ with r -process mass fractions as low as 10^{-10} . Thus, if there were many fission cycles, the r -process could be used as a constraint on inhomogeneous cosmologies.

Finally, we consider the dark matter issue: We would like to know whether or not the baryonic inhomogeneities predicted in this model could ever collapse to form dark matter remnants themselves. It appears that this is unlikely. If the separation between nucleation sites is $10 - 100$ m, then the total baryonic mass within a fluctuation is only $\sim 10^{15} - 10^{18}$ g. Since the baryonic pressure is large ($\approx n_b kT$) such objects could not be gravitationally bound until well past the epoch of recombination. On the other hand, as the photon and electron density decrease, the proton diffusion length will begin to exceed^{6,15)} the mean separation between nucleation sites after nucleosynthesis and well before recombination. Therefore, the only way that these fluctuations might form dark matter remnants is by a change in the equation of state as the baryons are compressed to very high density. Unfortunately, the mass of

these fluctuations is too low to balance the degeneracy pressure at nuclear matter densities so that they could not form "neutron stars." Even if these objects were compressed to form strange-matter quark nuggets, as originally proposed by Witten,¹⁶⁾ they would probably quickly evaporate.¹⁷⁾ It is also unlikely that these objects could be compressed to black holes. This would require a density far in excess of nuclear matter density. Therefore, these fluctuations are probably not a source of cold-dark-matter remnants.

ACKNOWLEDGEMENTS

Work performed under the auspices of the U.S. Department of Energy at Lawrence Livermore National Laboratory under contract number W-7405-ENG-48.

REFERENCES

- 1) G. M. Fuller, G. J. Mathews, and C. R. Alcock (this conference proceedings).
- 2) C. R. Alcock, G. M. Fuller, and G. J. Mathews, *Astrophys. J.*, 320, 439 (1987).
- 3) G. M. Fuller, G. J. Mathews, and C. R. Alcock, *Phys. Rev.*, D37, 1380 (1988).
- 4) R. A. Malaney and W. A. Fowler, submitted to *Astrophys. J.* (1988).
- 5) H. Kurki-Suonio, et. al., submitted to *Phys. Rev. D* (1988).
- 6) J. H. Applegate, C. T. Hogan, and R. J. Scherner, *Phys. Rev.* D35, 1151 (1987).
- 7) L. M. Hobbs and C. Pilachowski, *Ap. J.* (1988) in press.
- 8) J. Audouze, B. M. Tinsley, *Ann. Rev. Astron. & Astrophys.*, 14, 43 (1976).
- 9) S. Vauclair, (this conference proceedings).
- 10) J. H. Applegate, C. T. Hogan, and R. J. Scherrer, *Astrophys. J.*, 1988) in press.
- 11) G. J. Mathews and R. A. Ward, *Rept. Prog. Phys.* 48, 1371 (1985).
- 12) G. J. Mathews, et. al, *Astrophys. J.*, 270, 740 (1983).
- 13) S. E. Woosley, W. A. Fowler, J. A. Holmes, and B. A. Zimmerman, *Atomic Nucl. Data Tables*, 22, 371 (1978).
- 14) K. K. Gilroy, C. Sneden, C. A. Pilachowski, and J. J. Cowan, *Astrophys. J.*, 327, 298 (1988).
- 15) D. Seckel (private communication).
- 16) E. Witten, *Phys. Rev.* D30, 272 (1984).
- 17) C. R. Alcock and E. Farhi, *Phys. Rev.* D32, 1273 (1985).

ON THE MAGNITUDE OF BARYON DENSITY FLUCTUATIONS IN THE QUARK-HADRON
TRANSITION

Keith A. Olive
School of Physics and Astronomy
University of Minnesota
Minneapolis, MN 55455 USA

ABSTRACT

The baryon density contrast between the quark-gluon and hadron phases at the confinement transition is calculated. It is found that repulsive interactions among the hadrons at high temperatures and densities plays an important role. Instead of falling with increased transition temperature (as is the case in the absence of hadronic interactions) the contrast remains roughly constant with $(n_{B,Q})/(n_{B,H}) \geq 6$. This result has strong implications for big bang nucleosynthesis.

It has been suspected for some time that isothermal density perturbations might be produced during the quark-gluon to hadron confinement transition¹⁻¹⁰⁾. Recently the effects of such perturbations on big bang nucleosynthesis have been exploited^{3,4,6-11)}. Given a baryon density perturbation, differences in the diffusion lengths between neutrons and protons^{3,6)} prior to nucleosynthesis lead to inhomogeneities in the neutron to proton ratio. These inhomogeneities lead to changes in the calculated abundances of the light nuclei^{3,4,6,7)}. With exception of ⁷Li⁹⁾ calculated abundances can be made to agree with the observed abundances even for $\rho_B/\rho_C = \Omega_B = 1$ in contrast to standard big bang nucleosynthesis constraints¹²⁾ $0.01 \leq \Omega_B \leq 0.15$. These effects have been discussed in detail in this meeting¹³⁾.

The basic idea for generating a baryon density perturbation is that during the confinement transition at $T \approx 200$ MeV, quarks and gluons will condense, primarily into mesons; π , K , ρ , η etc. Baryons, and antibaryons will also be produced but their abundances are suppressed by a Boltzmann factor $\exp(-m/T_c)$. Because the nucleon mass $m_N > T_c$ baryons are difficult to produce. Assuming chemical equilibrium, it is possible to calculate²⁾ the net baryon density in both high density (Q) and low density (H) phases. For example, if one considers only the u and d quarks and neutrons and protons and a single quark chemical potential μ_Q and a hadron chemical μ_H then $3\mu_Q = \mu_H$ is our equilibrium condition. At very low net baryon density, the densities are to a very good approximation linear in μ so that

$$(n_B)_H \approx \frac{8\mu_H}{T} \left(\frac{m_N T}{2\pi}\right)^{3/2} e^{-m_N/T} \quad (1a)$$

$$(n_B)_Q \approx \frac{2}{9} \mu_H T^2 \quad (1b)$$

assuming massless quarks. The baryon density contrast $(n_B)_Q/(n_B)_H$ appears to be (exponentially) sensitive to the transition temperature T_c ,

$$\frac{(n_B)_Q}{(n_B)_H} \approx \begin{cases} 200, & T_c = 100 \text{ MeV} \\ 5, & T_c = 200 \text{ MeV} \end{cases} \quad (2)$$

We may now ask what happens if we include additional baryonic states. It was found²⁾ that including the first full baryon octet lowers the contrast to ≈ 4 at $T_c \approx 200$ MeV. Furthermore including all the known

baryon resonances⁷⁾ further lowers the contrast

$$\frac{(n_B)_Q}{(n_B)_H} = \begin{cases} 50, & T_c = 100 \text{ MeV} \\ 3, & T_c = 200 \text{ MeV} \end{cases} \quad (3)$$

Indeed at higher temperatures, it appears that the contrast falls below unity.

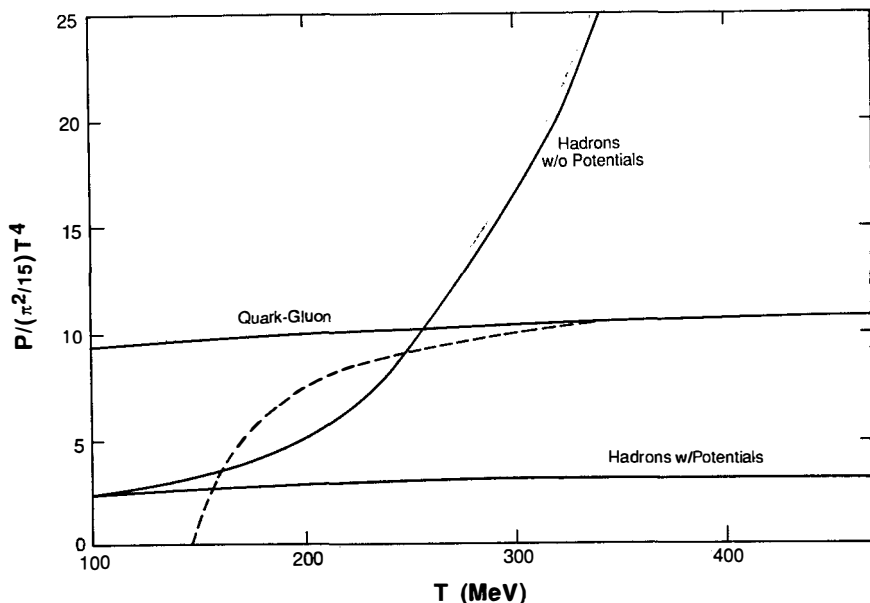


Figure 1.

It is necessary at this point to ask whether or not the above approach is thermodynamically consistent. Namely can we consider resonance states at high densities while neglecting their interactions. The answer to this question is no. Consider the P-T phase diagram in Figure 1, showing the (kinetic) pressure $P/(\pi^2/15)T^4$ (related to the number of degrees of freedom present) vs. temperature. The quark-gluon curve neglects Coulomb corrections which should be small. The total pressure in the quark-gluon phase is

$$p = p^{\text{kinetic}} - B \quad (4)$$

where B is the bag constant whose value determines T_c .

$$B = P_Q^{\text{kinetic}}(T_c) - P_H(T_c) \quad (5)$$

The contribution of B is shown by the dashed curve where $B^{1/4} = 230$ MeV and $T_c = 160$ MeV has been chosen. Consider first the curve labeled hadrons without potentials. This includes the full spectrum of known hadrons. At low temperatures ($T < T_c$), $P_H > P_Q$ and one is in the hadron phase. As we expect, at T_c the curves cross and $P_Q > P_H$ indicating a transition to the deconfined phase. But as the temperature continues to increase to $T \approx 260$ MeV, we see a second transition where $P_H > P_Q$ indicating a return to the hadron phase. (An exponential hadron mass spectrum would only aggravate this situation.) Clearly this description is not physical.

The problem is that we have been treating hadrons as free point-particles, which they are not. It was shown¹⁴⁾ that the inclusion of interactions in the form of mean field potentials can correct this errant thermodynamic behavior. Starting with a nucleon-nucleon potential such as the Reid potential¹⁵⁾, $U(r)$, integrating over all space leads to a potential energy per nucleon (\approx baryon) of the form¹⁴⁾

$$U(n) = K_N n \quad (6)$$

where $K_N = 680$ MeVfm³ for the Reid potential. A meson-meson potential based on a π - π interaction derived from Weinberg's effective lagrangian¹⁶⁾ can be put in the same form with a similar coefficient $K_\pi = 663$ MeVfm³. A baryon-meson interaction is not included. We expect a modification of these potentials by the bag model for the higher mass resonances¹⁷⁾

$$U = Kn(m/m_N)^2 \quad (7)$$

for masses $m > m_N$.

The potential energy is included in the density of states as follows¹⁴⁾: The number density of hadrons is given by

$$n = \sum_i \int dn_{q_i} \quad (8)$$

with

$$dn_{q_i} = (g_i/2\pi^2) [\exp(E_{q_i}/T) \pm 1]^{-1} q_i^2 dq_i \quad (9a)$$

$$E_{q_i} = (q_i^2 + m_i^2)^{1/2} + U(n) \quad (9b)$$

where g_i is the number of degrees of freedom of state with m_i . Because of the dependence on n in $d^3 q_i$, equation (8) must be solved self-consistently. Using the density of states in equation (9), thermodynamic quantities such as the energy density, pressure and entropy can be calculated¹⁴⁾. The pressure in the hadron phase with potentials is also shown in Figure 1. As one can see, the inclusion of interactions precludes a second "phase transition" at higher temperatures. At low temperatures, the effect of interactions is negligible because the densities are low enough so that $U \leq m_i$.

To compute the baryon density contrast we must integrate over the density of states given by equation (8) and specify the chemical potential μ_i . We consider three independent chemical potentials¹¹⁾ $\mu_u = \mu_c$, $\mu_e = \mu_\mu = \mu_\tau$, $\mu_\nu = \mu_{\nu_e} = \mu_{\nu_\mu} = \mu_{\nu_\tau}$ and $\mu_d = \mu_s = \mu_u + \mu_e - \mu_{\nu_e}$. We then compute a net number density for baryon number, lepton number and electric charge. A generic form for a net number density is given by

$$(\Delta n)_i = g_i \left(\frac{\mu_i}{T}\right) \int \frac{d^3 q_i}{(2\pi)^3} \frac{1}{\cosh(E_{q_i}/T) \pm 1} \quad (10)$$

where again the approximation that $\mu \ll T$ is made so that Δn is proportional to μ .

The chemical potentials are solved for by using the constraints that $\Delta n_q = 0$ (no net electric charge) and $\Delta n_L = \Delta n_B$ assuming B-L conservation. The three chemical potentials are then solved for in terms of the net baryon density Δn_B . This procedure is done in both the high and low density phases. In Figure 2, the (approximate) baryon density contrast is shown¹¹⁾ as a function of critical temperature T_c for both hadrons with and without potentials (the ratio $(A_{11})_Q/(A_{11})_H \approx (n_B)_Q/(n_B)_H$). Clearly there is a marked difference between the two cases. Whereas for hadrons without potentials the contrast falls exponentially, the contrast for hadrons with potentials remains large, $(n_B)_Q/(n_B)_H \geq 6$ for all values of T_c . Physically this just means that at high temperatures even though there are many possible baryonic states and the Boltzmann suppression is reduced, the density is so large that finite size effects through repulsive interactions still make it difficult to produce a baryon.

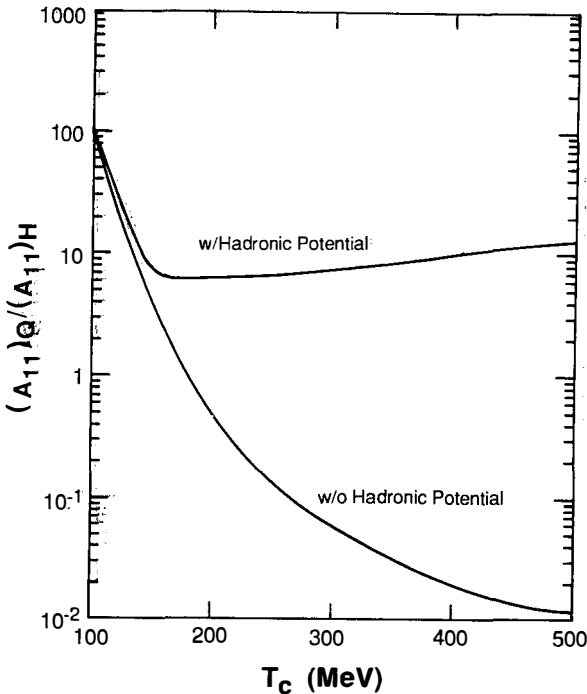


Figure 2.

The conclusion that we can draw from these results is clear. For perturbations formed during the confinement transition to have an effect on Big Bang nucleosynthesis the density contrast must be large and the distance scale of the perturbations must be large enough to avoid homogenization through proton diffusion. If we knew the distance scale and it is large, then nucleosynthesis and in particular the ${}^7\text{Li}$ abundance can be used as a constraint⁹⁾ on the baryon density contrast. Thus if the contrast falls with increasing T_c a constraint⁹⁾ could be placed on T_c . However, I believe that because such a limit is only possible in the absence of hadron potentials which implies a nonsensical phase diagram, one cannot place a limit on T_c . Instead if the density contrast is always relatively large, perhaps one can place a constraint on other details of the confinement transition. But because of our lack of knowledge on the details of the transition, such a constraint may be quite difficult to obtain.

ACKNOWLEDGEMENTS

The work described here was done in collaboration with J. Kapusta. Research was supported in part by DOE grant DE-AC02-83ER-40105 and by a Presidential Young Investigator Award.

REFERENCES

1. D.N. Schramm, M. Crawford and K.A. Olive, Proc. of the First Workshop on Ultra-relativistic Nuclear Collisions, ed. L.S. Schroeder (1979)241; M. Crawford and D.N. Schramm, Nature, 298(1982)538; C. Hogan, Phys. Lett. 133B, (1983)172.
2. E. Witten, Phys. Rev. D30, (1984)272.
3. J.H. Applegate and C.J. Hogan, Phys. Rev. D31 (1985)3037.
4. K.E. Sale and G.J. Mathews, Ap. J. 320 (1986)L1.
5. K. Iso, H. Kodama and K. Sato, Phys. Lett. 169B (1986) 337.
6. J.H. Applegate, C.J. Hogan and R.J. Scherrer, Phys. Rev. D35 (1987) 1151.
7. C. Alcock, G.M. Fuller and G.J. Mathews, Ap. J. 320 (1987) 439.
8. H. Kurki-Suonio, Drexel University preprint (1987).
9. H. Reeves, "The Quark-Lithium Connection" to appear in the Proceedings of the International School of Physics Enrico Fermi, Varonna, Italy 1987.
10. M.S. Turner, Fermilab preprint 87-155 (1987).
11. J. Kapusta and K.A. Olive, University of Minnesota preprint UMN-TH-647 (1988).
12. J. Yang, M.S. Turner, G. Steigman, D.N. Schramm, and K.A. Olive, Ap. J. 289 (1984)493.
13. J. Audouze, G.M. Fuller, G.J. Mathews and H. Reeves, these proceedings.
14. K.A. Olive, Nucl. Phys. B190 (1981)493; *ibid* B198 (1982)461.
15. See e.g. G.E. Brown and A.D. Jackson, The Nuclear-Nuclear Interaction (North-Holland, Amsterdam 1976).
16. S. Weinberg, Phys. Rev. 166 (1968)1568.
17. J. Kapusta and K.A. Olive, Nucl. Phys. A408 (1983)478.

VI. GRAVITATIONAL LENSES

DARK MATTER AND GRAVITATIONAL LENSING

Laurent Nottale

*Laboratoire d'Astrophysique Extragalactique et de Cosmologie.DAEC.
Observatoire de Paris-Meudon. F-92195 Meudon Principal Cedex.
France*



ABSTRACT. We consider two examples of gravitational lensing effects and their consequence for the nature and distribution of dark matter in the Universe. The first effect is variability by microlensing. The case of the OVV 0846+51W1 is recalled, with the conclusion that the sharp burst observed in its light curve may have been due to lensing by a compact object of the "Jupiter" mass in a foreground galaxy halo. The second effect is the creation of large gravitational arcs by the center of rich clusters of galaxies. We show how such structures may be eventually used to test General Relativity and to find extremely distant sources up to $z \approx 10$.

1. Introduction.

The various effects of gravitational lensing offer several methods to probe the distribution of matter in the Universe. Two physical contributions to the magnification of distant sources are to be considered: (i) the effects of shear due to masses exterior to a light beam; (ii) the effect of convergence of a light beam by matter interior to it. More generally one may demonstrate^{1,2,3,4}) that the matter term in the amplification formula yields the average effect of any distribution of mass. It depends on the surface density of matter foreground to a source and may be used in particular for comparison to statistical samples^{5,6,7,8}). The shear effect depends directly on the mass of the lens. Only the latter is considered in the present contribution, under two of its possible manifestations: variability due to compact objects in the halos of galaxies and formation of giant arcs by the central region of rich clusters of galaxies.

2. Microlensing and the mass of compact objects.

It was long ago realized^{2,9}) that the main observable effect of lensing by stars or compact objects in galaxies or galaxy halos (the so-called microlensing) may be variability, due to the passage of the lens in front of the line of sight of a distant object. I have proposed^{10,4}) that the microlensed objects were to be searched among the Optically Violently Variable (OVV) extragalactic objects, and exemplified this proposal by showing that all known properties of the QSO 0846+51W1 may be explained by this hypothesis¹⁰).

Arp et al.¹¹) report the following behaviour for this object of redshift 1.86: (i) It brightened in 1975 by ≈ 4 mag. in less than a month and then decreased by more than 1 mag. in two days. (ii) It lies only 12 arcs. south of a spiral galaxy of redshift 0.072, itself member of a group. (iii) The spectrum of this object is that of a BL Lac when brightest while broad QSO emission lines appear in its faintest phase. (iv) The optical spectral index vary with luminosity, the object being bluer at brightest level and redder at faintest level.

In this case, partly because the galaxy is a nearby one, lensing by the galaxy as a whole may be neglected and one may consider the theory of lensing by a point mass on an extended source (when the potential of the galaxy cannot be neglected, one expects two-peaks maxima in the light curve, see Refs.^{9,12,13}). If the source line-of-sight comes close enough to the lens, the total maximal amplification, rather than being infinite as in the point source case, is directly related to the critical radius r_c (see Eq.3.4) and to the source radius R ¹⁰):

$$\text{Amp}_{\max} \approx 2 (r_c/R) (D_s/D_d), \quad (2.1)$$

so that a highly hierarchically structured object like a QSO (continuum emission region of extent $\approx 10^{-4}$ - 10^{-3} pc, broad line region ≈ 0.1 -1 pc, narrow line region ≈ 100 pc) will be subjected to differential amplification by a microlens. The value of the critical radius

$$r_c \approx 2/3 \cdot 10^{-2} (M/M_\odot)^{1/2} \quad (2.2)$$

implies that only the continuum emission will be amplified, but not the lines. Due to a contrast effect, the spectrum of a QSO is then expected to turn to that of a BL Lac when magnified.

One of the potentially most important consequence of this model is that it allows to determine in a self-consistent way the mass of the compact object acting as a lens. Indeed a fit of the light curve yields a ratio of critical radius over relative line-of-sight velocity $r_0/v=50$ to 120 days. A reasonable range may be estimated for the velocity. Indeed the galaxy is an inclined spiral (axial ratio <0.5) and a lower value of the relative velocity of ≈ 300 km/s may be assumed. But the galaxy is member of a group, itself part of a larger structure, so that an upper value may be the maximal proper velocity of galaxies in clusters, of the order of 3000km/s. Using these values yields $r_0=10^{-4}$ to 10^{-3} pc and from Eq.(2.2) a lens mass $M=10^{-4}$ to $10^{-2} M_\odot$. This is a typical mass for compact objects of the "Jupiter" type, which have already been suggested as being the basic constituents of galaxy halos (see the contribution by K.M.Ashman in the present meeting). Moreover the assumption that a $\approx 10^{12} M_\odot$ halo is made with these objects allows to predict an average rate of 1 large burst every 10 to 50 years, a value quite consistent with observations of this particular object.

All the other characteristics of 0846+51 are accounted for by this hypothesis¹⁰⁾ as the colour variations (the red component might come from a host galaxy which is not amplified) or the rate of polarization, due to the differential amplification of a highly polarized region.

More generally, one may suggest that candidates for microlensing are to be searched among OVV's turning from QSOs to BL Lacs, having shown sharp bursts typical of amplification by lensing (e.g. 3C345, 0846+51, 3C446), and/or which are known to lie behind foreground matter, thanks to observation of absorption lines (e.g. 0235+16, 0420-014, 0735+178, 1308+326, 3C446), or better to direct imaging (0846+51, 0235+16, 0735+178,...). Note that our suggestion is consistent with the fact that all these objects are indeed the most eruptive among OVV's, the full range of their variability ranging from 3.3 to more than 4 magnitudes. New results concerning observations and detailed modelling of some of these objects have been recently obtained and will be presented elsewhere. Note that our proposal is somewhat different from the one which was formulated at about the same date by Ostriker and Vietri¹⁴⁾, who attempted to explain the BL Lac properties as due to lensing of already beamed OVV's and to errors in redshift determinations.

3. Possible implications of gravitational arcs.

3.1. Introduction.

The large luminous arc in A370 was discovered in September 1985¹⁵⁾ and followed by the observation of a second arc in the cluster 2244-02¹⁶⁾. The gravitational lens interpretation^{17,18)} allows to reproduce in details the observed configuration in A370^{18,19)}. It was recently definitively confirmed by the obtention of several spectra along the arc²⁰⁾, all of them yielding the same redshift 0.724, nearly two times that of the cluster, $z=0.374$. Moreover, nearly a hundred galaxy redshifts are known for the cluster²¹⁾, allowing a detailed comparison between the dynamical and "gravitational lensing mass".

Consider a virialized cluster of line-of-sight redshift dispersion $\sigma = \sigma_v/c$. Let $M(r)$ be the mass included into a cylinder of radius r centered on the cluster and set:

$$G M(r) c^{-2} r^{-1} \sigma^{-2} = K. \tag{3.1}$$

We get $K=3$ in the case of a Hubble spatial density profile $\rho(r) = \{1 + (r/r_0)^2\}^\beta$ with $\beta = -1$. More generally for $\beta \neq -1$, σ is a function of r and K is a slowly varying function of r , $K(r)$, with most of the time $K(r) \leq 3$ if virialization is assumed.

In the case of a symmetric mass distribution, the scalar bending angle is²²⁾:

$$\alpha = k G M(r) r^{-1} c^{-2}, \tag{3.2}$$

where $k=4$ in General Relativity but would be $=2$ in Newtonian theory. The special interest of gravitational arcs is that, lying nearly on the Einstein ring, several lens parameters collapse into one. Indeed the arc radius is given by:

$$r_0 = \alpha D, \tag{3.3}$$

where D is the usual distance term, $D = D_d D_{ds} / D_s$. We see from Eq.(3.2) that the arc radius is given by a generalisation of the usual point mass critical radius:

$$r_0 = \{k G c^{-2} M(r_0) D\}^{1/2}, \tag{3.4}$$

Hence Eq.(3.5) may be solved for r_0 or for M :

$$r_0^2 / M(r_0) = k G c^{-2} D. \tag{3.5}$$

4.2. A new test of General Relativity ?

Up to now one has not been able to use extragalactic gravitational lens effects to test Einstein's theory of gravitation, so that, while the value $k=4$ is now experimentally well established at the solar system scale, this is not the case for extragalactic distances. This is due to the fact that k appears in most expressions with G , M and r , and that masses and distances are often uncertain by a factor of 2 or more, and that no direct measurement of G is known at large distances. Gravitational arcs might constitute a unique tool in this respect. Indeed let $\phi = \alpha D_{ds} / D_s$ be the angular radius of a giant arc, combining equations (3.1) and (3.2) yields:

$$k = \phi K^{-1} \sigma^{-2} D_s / D_{ds}. \tag{3.6}$$

The remarkable result here is that G and H_0 have disappeared from this expression, which depends on directly observable quantities like ϕ , z_d , z_s and σ , and on dynamical analysis of the cluster (indeed the method relies on the assumption that the dynamical mass and the "gravitational lens" mass are identical).

Let us attempt to apply this test to the arc in A370. Its observed angular radius is $\phi = 25 \pm 2$ arcsec; the lens redshift is $z_d = 0.374$, the source redshift $z_s = 0.724$, from which the ratio D_s / D_{ds} varies in the range 2.50-2.67 when $q_0 = 0$ to 1. As well the density profile as the velocity dispersion profile (nearly independent from radius) are consistent with a Hubble law²³⁾ and one gets k in the following range:

$$k = 3.74 - 5.10 \quad (3/K) \tag{3.7}$$

Hence the Newtonian prediction $k=2$ seems to be excluded, unless an unreasonable value $K=6$ be adopted, while the expected value $K=3$ yields the GR prediction $k=4$, but at the scale of

≈200kpc. Our results are in agreement with the detailed gravitational lens model of refs. 19 and 24 who find consistent dynamical and lens masses, $M_D = M_L(1±0.2) = 3.10^{14} M_\odot$.

Gravitational arcs thus provide a unique tool to probe the amount and distribution of dark matter in rich clusters of galaxies. The agreement between the "gravitational lens mass" and dynamical mass in A370 corroborate the result that, in this cluster, dark matter is distributed mainly like galaxies with a M/L ratio of 60 to 100¹⁸⁻²¹).

4.3. Critical lensing mass.

Using the notations of Eq.(3.1) allows to write the mass able to create an arc as:

$$M_c = c^2 G^{-1} K^2 \sigma^4 k D. \tag{3.8}$$

As has been stressed in refs.4,5,25, the distance term D may be written under the form:

$$D = c/H_0 L(z_d) \{1 - \Delta(z_d)/\Delta(z_s)\} \tag{3.9}$$

where the optical distance $\Delta(z)$ and the function $L(z)$ have been defined by Nottale and Hammer⁵). While the final term $\{1-\Delta(z_d)/\Delta(z_s)\}$ quickly tends to 1 when the source moves away, the function $L(z_d)$ reaches a maximum $L=0.2$ for a lens redshift $z_d=0.75$. One finds :

q_0	z_{max}	L
0	$\sqrt{3}-1 = 0.73$	$1/3\sqrt{3} = 0.192$
1/2	$7/9 = 0.78$	$3^3/2^7 = 0.210$
1	$(1+\sqrt{13})/6 = 0.77$	0.221

Finally the critical mass for "arching" writes:

$$M_c = (c^3/GH_0) kLK^2 \sigma^4 \tag{3.10}$$

With $k=4$, $K=3$ and $L=0.2$, the numerical parameter $kLK^2=7.2$, and the critical mass is expressed only in terms of the cluster redshift dispersion σ and of the cosmological parameter (c^3/GH_0) , which is nothing but the "mass of the Universe" (e.g. the mass observable up to $z=+\infty$ in an Einstein-de Sitter Universe ($q_0=1/2$) is $M=4 c^3/GH_0$). Numerically one finds:

$$M_c = 3 \cdot 10^{14} M_\odot (\sigma_v/1500\text{km/s})^4 (K/3)^2 h_{100}^{-1} \tag{3.11}$$

This mass should be included in the corresponding arc radius :

$$r_o = 150\text{kpc} (\sigma_v/1500\text{km/s})^2 (K/3) h_{100}^{-1} \tag{3.12}$$

These numbers show that arcs may be created only by the richest "Coma like" clusters .

3.4. Arcs and the search for extremely distant objects.

In the case of a symmetric mass distribution in the lens, an arc is formed from an extended source (of radius R) slightly excentred with respect to the center of mass. The amplification for an arc subtending an angle θ is simply given by:

$$\text{Amp} = 1/2 (r_o/R) (D/D_d) \sin\theta/2, \tag{3.13}$$

D being the source angular diameter distance, $D(z)=cH_0^{-1}q_0^{-2}\{q_0z+1-q_0+(q_0-1)(1+2q_0z)^{1/2}\}$.

We decide to focus only on the large arcs, because of their clear morphological signature. Let $n=l/R=1/\sin\theta/2$ be an index of the angle subtended by an arc (e.g. $n=2:\theta=60^\circ$; $n=3:\theta=40^\circ$). The average amplification for all configurations yielding indices larger than n is:

$$\langle \text{Amp} \rangle = (1/n) (r_o/R) (D/D_d) \tag{3.14}$$

For example a cluster of the A370 type with a critical radius $r_c \approx 200 \text{ kpc}$ would magnify a distant source of 2 kpc radius by a factor of 100 ($\delta m = -5 \text{ mag}$), a 20 pc source by 10^4 , i.e. -10 mag. , and a QSO by -20 magnitudes. Thanks to the amplification, a source normally observable up to a luminosity distance L_0 becomes now observable up to:

$$L = L_0^2 (1+z)^{-2} (1/n) (r_c / R D_d) \tag{3.15}$$

since $L = D(1+z)^2$. But the larger the amplification, the smaller the probability of alignment. The final maximal distance up to which arcs may be expected to be observed results from a combination of these two opposite effects.

Let us attempt to estimate the probability of chance alignment. We first define a "volume" distance $d(z)$, such that the mass of the Universe contained in a sphere interior to redshift z be:

$$M(\leq z) = q_0 (c^3 / G H_0) d^3(z) \tag{3.16}$$

The expressions for $d(z)$ are respectively (we assume a zero cosmological constant):

$$\begin{aligned} q_0 \approx 0: & \quad d^3(z) = (3/2) \{ x (1+x^2)^{1/2} - \text{Argsh}x \} ; \quad x = z (1+z/2) / (1+z) \\ q_0 = 1/2: & \quad d^3(z) = 8 \{ 1 - (1+z)^{-1/2} \}^3 \\ q_0 = 1: & \quad d^3(z) = (3/2) \{ \text{Arcsin}x - x (1-x^2)^{1/2} \} ; \quad x = z / (1+z) \end{aligned} \tag{3.17}$$

The number surface density on the sky of a given population of objects of redshift $\leq z$ is then:

$$\Sigma = \Sigma_0 d^3(z) \tag{3.18}$$

Consider now a given line-of-sight (i.e. a point on the plane of the sky). The probability that the nearest object to that point be closer than an angular distance φ is:

$$P_1 = 1 - \exp(-\pi \Sigma_0 d^3 \varphi^2) \approx \pi \Sigma_0 d^3 R^2 D^{-2} n^2 \tag{3.19}$$

Let N_0 be the equivalent number of source objects which would lie in the range $[z=0, z=0.1]$ with the same comoving density (for example, one gets for galaxies $N_0 \approx 10^6$).

Let N_c be the total number of potential clusters capable of making arcs. It may be estimated by remembering that these clusters should be rich enough (Coma or A370-like, which are not more frequent than ≈ 1 cluster in $(100 \text{ Mpc})^3$) and should optimize the lensing function $L(z_d)$ (see refs.5, 25), so that $z_d \approx 0.2$ to 1. This yields $N_c \approx 10^4$.

Finally the expected number of giant arcs observable on the 4π sphere is:

$$N = 250 n^2 N_0 N_c d^3 R^2 D^{-2} \tag{3.20}$$

The extremal source redshift and radius we are looking for may be now found by writing that at least $N=1$ such arc should be observable. We will ask ourselves up to which redshift a source which would normally be observable up to $z=1$ becomes observable once lensed. To obtain our final result, let us specialize the Universe model.

* $q_0 \approx 0$: We have in that case $L \propto z(1+z/2)$, $L_0(z=1) = 1.5$, $D_d(z \approx 0.75) \approx 0.33$, $D = 0.5$ for $z > 1$ and $d^3 \approx 3z^2/8$. One finds:

$$N = 2.5 \cdot 10^3 N_0 N_c n^{3/2} r_0^{1/2} R^{3/2} \tag{3.21}$$

This yields the following critical source redshift and radius:

$$z_c = 18 [(L_0 / 1.5) \cdot (N_0 / 10^6) \cdot (N_c / 10^4)]^{1/6} (r_0 / 200 \text{ kpc})^{1/2} \tag{3.22}$$

$$R_c = 30 \text{ pc} [(L_0 / 1.5) \cdot (N_0 / 10^6) \cdot (N_c / 10^4)]^{-2/3} (3/n) (r_0 / 200 \text{ kpc})^{-1/3} \tag{3.23}$$

The nice result here is the power 1/6 describing the dependence of the critical redshift on our less well defined parameters, N_o and N_c . Even if their product was 100 times smaller than assumed, would the maximal redshift of arcs still be $z=10$.

* $q_o=1/2$: In that case $L=2z$, $D=2/z$, $D_d \approx 0.28$, $L_o(z=1)=1.17$, $d \approx D(1+z)$. One finds:

$$N = 4 \cdot 10^3 N_o N_c [(n/3) (L_o/1.17)]^{4/3} r_o^{2/3} R^{4/3} \tag{3.24}$$

$$z_c = 19 (L_o/1.17)^{1/3} [(N_o/10^6) \cdot (N_c/10^4)]^{1/4} (r_o/200\text{kpc})^{1/2} \tag{3.25}$$

$$R_c = 30\text{pc} [(N_o/10^6) \cdot (N_c/10^4)]^{-3/4} (3/n) (1.17/L_o) (r_o/200\text{kpc})^{-1/2} \tag{3.26}$$

The Einstein-de Sitter Universe is slightly less favorable than the open one, since $N_o N_c$ is to the power 1/4 instead of 1/6. But if this product was decreased by a factor of 100, the maximal redshift would still be $z=8$, obtained for $R=1\text{kpc}$.

3.5. *Expected number of arcs.*

Equations (4.21) or (4.24) may also be used to estimate the total number of arcs formed from a source of a given size that one may expect to discover on the whole sky. It is given in the following table for our two choices of $N_o N_c$ and for $q_o=0$ or $=1/2$.

R	$N_o \cdot N_c = 10^{10}$		$N_o \cdot N_c = 10^8$	
	$q_o=0$	$q_o=1/2$	$q_o=0$	$q_o=1/2$
30pc	1	1		
300pc	30	25		
600pc	90	54	1	
1kpc	150	100	2	1
3kpc	1000	600	11	4
10kpc	5000	2000	70	22

To conclude, one may expect to discover a large number of arcs formed from galaxies, detectable up to redshifts of the order of $z=5$. The total number found may be indicative of the cosmological model. Furthermore, if there existed at primeval epochs objects of the size of a galaxy stellar nucleus bright enough to be observable at $z=1$, at least one such object should be detectable as a gravitational arc up to $z=10$.

A last problem to be considered is that of surface brightness. The Etherington theorem²⁶ specifies that $B(1+z)^4$ is conserved in any Riemannian Universe. Thus the surface brightness of an object lying at redshift z is related to that of the same object at $z=1$, B_o , by :

$$B = B_o [2/(1+z)]^4 \tag{3.27}$$

This corresponds to a 2 mag./arcs² loss for $z=2$, 5 mag. for $z=5$ and 7 mag. for $z=10$. If indeed the present surface brightness limit of detection is ≈ 32 mag./arcs²(private comm.), the hereabove numbers correspond respectively to objects with $B=30$, 27 and 25 mag./arcs² at $z=1$. Hence a possible arc at $z=10$ should be detectable, but only at the extreme limit presently reached by the best detectors.

4. Discussion and conclusion.

Two particular examples of the use of gravitational lensing to probe dark matter have been described here. They were chosen in order to stress the huge range of mass scales that one may reach by such methods. Variability by microlensing points towards compact objects of Jupiter's mass ($\approx 10^{-3} M_{\odot}$) in galaxy halos, while giant arcs are made by $3.10^{14} M_{\odot}$ rich cluster centers. Both examples confirm the existence of dark matter, but in no larger amounts than given by dynamical methods ($\Omega \approx 0.1$) i.e. far from closing the Universe (see also the contribution on that subject by E. Turner in the present meeting).

Our suggestion that some sub-class of OVVs is the result of microlensing, first applied to the BL Lac object 0846+51, is now confirmed by observational studies and detailed modelling of similar objects, like 0235+16²⁷⁾ for which the same order of lens mass is found.

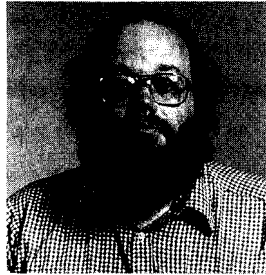
We also note that the statistical calculation presented hereabove may still be an underestimation of the actual number of potential arcs. Indeed we considered only arcs formed from spherically symmetric lenses, while dissymmetric potential wells (in particular bimodal ones, see e.g. ref.12) may be even more effective to create such shapes by merging of images. Now that we know that the richest clusters are just rich enough to produce shear effects as a whole, the systematic search for gravitational arcs seems very promising thanks to their clear morphological signature. However the confirmation that some extremely distant objects of $z \gg 5$ could be thus observable now depends on the difficult task of getting their spectra. The discovery of arcs reinforces our earlier suggestion⁵⁾ that rich clusters of galaxies of redshift 0.3-1.0 should be used as gravitational telescopes to scan the very distant Universe.

References

1. Weinberg, S., 1976, *Astrophys. J. Lett.*, **208**, L1
2. Young, P., 1981, *Astrophys. J.*, **244**, 756
3. Peacock, J.A., 1986, *Mon. Not. Roy. Astr. Soc.*, **223**, 113
4. Nottale, L., 1988, *Ann. de Phys.*, in the press
5. Nottale, L., Hammer, F., 1984, *Astron. Astrophys.*, **141**, 144
6. Hammer, F., Nottale, L., 1986, *Astron. Astrophys.*, **167**, 1
7. Nottale, L., Chauvineau, B., 1986, *Astron. Astrophys.*, **162**, 1
8. Nottale, L., 1987, *Annales de Phys.*, **12**, 241
9. Chang, K., Refsdal, S., 1979, *Nature*, **282**, 561
10. Nottale, L., 1986, *Astron. Astrophys.*, **157**, 383
11. Arp, H., Sargent, W.L.W., Willis, A.G., Oosterbaan, C.E., 1979, *Astrophys. J.*, **230**, 68
12. Schneider, P., Weiß, A., 1987, *Astron. Astrophys.*, **171**, 49
13. Grieger, B., Kayser, R., Refsdal, S., 1988, *Astron. Astrophys.*, in the press
14. Ostriker, J.P., Vietri, M., 1985, *Nature*, **318**, 446
15. Soucail, G., Fort, B., Mellier, Y., Picat, J.P., 1987, *Astron. Astrophys.*, **172**, L14
16. Lynds, R., Petrosian, V., 1986, *Bull. Astron. Am. Soc.*, **18**, 1014
17. Paczynski, B.P., 1987, *Nature*, **325**, 572
18. Soucail, G., Mellier, Y., Fort, B., Hammer, F., Mathez, G., 1987, *Astron. Astrophys.*, **184**, L7
19. Hammer, F., 1987, in *Third IAP Astrophys. Meeting*, "High redshift objects", eds Frontières, p. 467
20. Soucail, G., Mellier, Y., Fort, B., Mathez, G., Cailloux, M., 1987, *Astron. Astrophys.*, **191**, L19
21. Soucail, G., Mellier, Y., Fort, B., Cailloux, M., 1987, *Astron. Astrophys. Suppl.*, in the press
22. Young, P., Gunn, J.E., Kristian, J., Oke, J.B., Westphal, J.A., 1980, *Astrophys. J.*, **241**, 507
23. Fuchs, B., Materne, J., 1982, *Astron. Astrophys.*, **113**, 85
24. Hammer, F., Rigaut, F., in preparation
25. Nottale, L., 1987, in *Third IAP Astrophys. Meeting*, "High redshift objects", eds Frontières, p. 451
26. Etherington, I.M.M., 1933, *Phil. Mag.*, **15**, 761
27. Nottale, L., Hammer, F., le Fèvre, O., in preparation

DARK MATTER IN GRAVITATIONAL LENSES

Edwin L. Turner
Princeton University Observatory
Princeton, NJ 08544
USA



ABSTRACT

Recent results concerning four specific gravitational lens systems (2016+112, 2237+0305, 1635+267, and 2345+007) and two statistical gravitational lens null results are described with emphasis on the implications for dark matter. An attempt is made to state some of the general conclusions which can be drawn from the emerging field of gravitational lens studies of dark matter.

1. INTRODUCTION

The potential importance of gravitational lens studies for obtaining information on the abundance, distribution, and nature of dark matter is now widely appreciated¹. This paper will simply summarize a number of recent studies in this, as yet, only slightly explored area of investigation. The selection of specific results for discussion merely reflects an attempt to avoid duplication of Dr. Nottale's review elsewhere in this volume and my interests, familiarity, and judgements of importance; it is largely arbitrary.

Before turning to more specific issues, a few general remarks are in order. Gravitational lens systems are particularly good for studying dark matter because 1) the (gravitational) nature of the coupling makes them sensitive to all possible forms of dark matter, 2) they are potentially influenced by inhomogeneities in the dark matter on a wide range of mass scales ranging from that of massive planets to that of galaxy superclusters, and 3) they typically probe cosmological distance scales and thus automatically give "fair sample" measures. Unfortunately gravitational lens systems also have several severe disadvantages: They are quite rare requiring substantial resources or excellent luck just to be found. Moreover, it is often observationally challenging (particularly in terms of resolution and synoptic study) to obtain the detailed information needed to exploit them. The lensing object's mass distribution is often complex thus injecting undesirable model dependency into one's conclusions. Finally, there is the problem of contamination of samples of gravitational lens systems by physical pairs (or higher multiples) of quasars or other sources with similar properties. This last problem is seen as particularly pressing² at the moment and is given special attention in the remainder of this paper.

Gravitational lens studies are of two basic types: detailed modeling of individual lens systems and statistical analysis of large data sets in connection with the effects of many lensing events. Sections 2 through 4 discuss examples of the first type while sections 5 and 6 describe studies of the second type. Section 7 gives some general conclusions and comments.

2. THE DISTRIBUTION OF DARK MATTER IN THE 2016+112 LENS

The 2016+112 system has been studied in great detail^{3,4,5,6} and is effectively certain to be a real incidence of gravitational lensing. The system contains three images of a redshift 3.273 stellar radio source with an emission line spectrum resembling that of a typical quasar except that the lines are very narrow, unresolved in fact; two lensing galaxies including one with a measured redshift of 1.01; and two faint resolved emission line regions also at a redshift of 3.273. In addition to information on these components, there are very sensitive limits on the presence of additional images of the radio source and reasonably good limits on the brightness of any additional lensing objects.

Taken together this data makes detailed lens models of 2016+112 among the best constrained of known candidate lens systems. The acute angle between the lines connecting the two brightest images with the faint image and the center-of-light of the pair of lensing galaxies provides a particularly important constraint. Detailed models^{7,8} and some moderately model independent inferences⁴ have been published.

The implications of these models and inferences for dark matter can be stated in three points: First, the total required blue M/L ratio ($H_o=100$ km/s/Mpc, $q_o=1/2$) for the lensing galaxies is at least about $20 M_{\odot} / L_{\odot}$ with more typical values falling near $100 M_{\odot} / L_{\odot}$, values similar to those derived from studies of galaxy clusters, groups, and binaries⁹. Second, the total mass distribution is not identical to the observed light distribution in the lensing galaxies, again not a surprising result in view of other information on galaxy massive halos. Third, and more surprisingly, the center-of-mass in the lens cannot coincide with the observed center-of-light of the galaxies suggesting that the total dark matter distribution is not well described by a pure co-centric halo model. This last is an intriguing and novel result which deserves further investigation.

3. A UNIQUE LENS MODEL FOR 2237+0305

The gravitational lens 2237+0305 is unique among known systems in that the lensing object is at such a low redshift (~ 0.04) that it can be studied in great detail directly. In fact, it was discovered serendipitously during the course of the Center for Astrophysics Redshift Survey from routine spectroscopy of the nucleus of an ordinary survey galaxy¹⁰. The galaxy's nuclear light was found to be heavily contaminated with the light of several images of a redshift 1.69 quasar^{10,11}. Like 2016+112, this system is on the short list of objects which can be said to be real gravitational lenses with virtual certainty.

Optical images obtained under excellent seeing conditions of 2237+0305 have been extensively analyzed to derive the positions and brightnesses of four quasar images and to characterize the surface brightness distribution of the lensing galaxy^{12,13}. This observed surface brightness distribution has been used to construct a highly constrained detailed lensing model of the system which succeeds in explaining the positions and brightnesses of the images¹³.

This essentially unique model is a first for gravitational lens studies and has a number of important implications. Those relevant to dark matter include a nuclear (inner 500 pc) blue M/L ratio of $9.4 \pm 2.0 M_{\odot} / L_{\odot}$ indicating that the central region of this galaxy is almost certainly dominated by its visible stellar component being little affected by dark matter and the derivation of well determined microlensing optical depths which imply that the system should be almost ideally well suited to the study of this intriguing lensing phenomenon. Detection of microlensing events in this system would be an important first step toward realizing proposed¹⁴ gravitational lensing tests of the nature of the dark matter.

4. THE CONTROVERSIAL LENS CANDIDATES 1635+267 AND 2345+007

Although both 1635+267 and 2345+007 were initially regarded as strong candidates for being gravitational lens systems^{15,16} on the basis of spectroscopic similarity, the absence of any detectable lensing objects has more recently led to their being regarded as probable examples of misidentified physical pairs². Now, however, the weight of the evidence appears to be swinging

back toward supporting the lens hypothesis for both systems^{17,18}.

In the case of 2345+007, a recently published study¹⁷ of the system based on extremely high resolution images obtained on the CFHT at Mauna Kea has revealed that one of its two previously known components actually consists of at least two sub-components, one of which appears to be resolved. It is tempting to identify this newly discovered object as either an additional image of the source or, perhaps more likely, as the lensing object.

For the 1635+267 pair, a spectroscopic study¹⁸ has shown that the C III] and Mg II emission lines have strengths, widths, and profile shapes which match very accurately in the two objects and that the excess red light in the bright component (relative to the faint one) resembles the continuum emission of a redshift ~ 0.57 galaxy. Again these results appear to considerably strengthen the gravitational lens interpretation.

Both of these systems are quite interesting from the perspective of the dark matter problem. Both had been suggested as possible examples of systems containing dark lensing objects with M/L ratios of several hundred or more required to explain the absence of a detected lensing galaxy, a conclusion based on lens brightness limits which apply only well away from the observed source images. Clearly there is a lesson for the importance of using high quality data to search for lenses against the "glare" of source images and for not too rapidly abandoning the lens hypothesis. In the case of 1635+267 where there is an indication of the lens redshift, it is possible to infer a blue M/L ratio of $\sim 18 M_{\odot}/L_{\odot}$ and a total mass in the vicinity of $10^{12} M_{\odot}$; these numbers are more startling when the constraint that they must be projected onto the sky within a circle of radius 15 kpc is taken into account.

5. GRAVITATIONAL DISTORTION OF BACKGROUND GALAXY IMAGES

Tyson¹⁹ has pioneered a new technique for measuring the mean mass of galaxies out to substantial radii from the center. The idea is to look for the characteristic longitudinal stretching distortion of background galaxies produced by the gravitational field of foreground galaxies lying near the line-of-sight. The degree of this distortion depends directly upon

$M(<r)/r$ of the foreground galaxy where $M(<r)$ is the mass enclosed within radius r .

In a first application of this technique¹⁹, he has applied the technique statistically to a sample of 47,000 faint galaxies lying near some 12,000 bright galaxies and detected no such distortion as a function of angular separation. By applying a complex model which allows for such things as contamination by physical pairs, distributions of distances, K corrections, seeing, *et cetera*, this null result can be translated into an upper bound on galaxy masses on the assumption that *all bright galaxies have the same total masses*. This 2σ limit is quoted as $2.6 \times 10^{11} M_{\odot}$ within a radius of 65 kpc.

Although Tyson's analysis has been criticized²⁰ and clearly deserves carefully scrutiny, it is clearly a preliminary application of a potentially very important new technique which deserves further elaboration. It is worth noting that this preliminary result appears to be inconsistent with the predictions of the currently most popular theory of galaxy formation, $\Omega_0 = 1$ biased cold dark matter models. Whether or not one takes this conflict seriously, it demonstrates the potential of the method in a striking way.

6. A LIMIT ON POPULATIONS OF DARK MASSIVE OBJECTS

It has long been realized that the absence of detectable multiple images of cosmologically distant sources could be used to limit the abundance of lensing objects in the universe²¹. The type of lensing objects subject to such tests are determined of course by observational sensitivities, particularly resolution and dynamic range. Hewitt²² has recently carried out the first systematic application of this technique to a data sample obtained for such a purpose.

In this case a sample of carefully reduced VLA maps of uniform minimum quality were drawn from the first days of the VLA Lens Survey program²³ and classified into one of three categories: point sources, classical double lobed sources, and all other sources. A careful numerical calculation of the *detectable* lensing event cross sections for point mass and isothermal lensing objects was then made given the specific sensitivities of the VLA data. This allowed limits to be placed on putative lens populations given the assumption that only

sources in the third category could be the result of lensing.

Hewitt's results can be expressed as a limit on the contribution of 10^{11} to $10^{12} M_{\odot}$ point masses to Ω_0 of 0.4 and on the density of isothermal objects with velocity dispersions similar to those of bright galaxies of about 100 times that of observed galaxies. In my opinion, these are tremendously conservative limits since it is scarcely plausible that *all* observed radio structure beyond double lobes is due to lensing events; both limits could be reduced by a factor of ten with little fear of contradiction. This is probably the most robust and definite contribution of lens studies to date, namely that compact objects of roughly galaxy masses, however dark, cannot close the universe. This does not seem too surprising, but it is a hypothesis which could not otherwise be ruled out on empirical grounds.

7. CONCLUSIONS AND COMMENTS

It is probably too early in the gravitational lens study of dark matter to try to synthesize an integrated picture. Nevertheless, several important and intriguing results have emerged with varying degrees of certainty. These are enumerated below without further comment.

- 1) Gravitational potential wells associated with visible objects (galaxies and galaxy clusters) are not greatly outnumbered by those associated with any unknown (dark) class of objects of comparable masses and sizes.
- 2) The M/L ratios of typical galaxies are neither much smaller nor much larger than those derived by dynamical studies of rotation curves, binaries, and small groups.
- 3) The mass distribution in the neighborhood of bright galaxies does not closely follow the light (emissivity really) distribution on scales of $\gtrsim 10$ kpc.
- 4) The mass distribution in the regions of highest emissivity (galactic nuclei) is dominated by the luminous stellar component.

Of course, in a sense, the most important result is that we have a new tool to study dark matter which should continue to provide useful new insights for some time to come.

This work was supported by NSF grant AST86-18257. Conversations with several of my collaborators have contributed to this review.

REFERENCES

- 1) Canizares, C. R. 1987, in *Observational Cosmology: Proceedings of IAU Symposium No. 124*, eds. A. Hewitt, G. Burbidge, and L. Z. Fang (Dordrecht: D. Reidel), 729.
- 2) Blandford, R. D., and Kochanek, C. S. 1987, preprint; Shaver, P. A., Wampler, E. J., and Cristiani, S. 1987, *Nature*, **327**, 40.
- 3) Schneider, D. P., Gunn, J. E., Turner, E. L., Lawrence, C. R., Schmidt, M., and Burke, B. F. 1987, *A. J.*, **94**, 12.
- 4) Schneider, D. P., Gunn, J. E., Turner, E. L., Lawrence, C. R., Hewitt, J. N., Schmidt, M., and Burke, B. F. 1986, *A. J.*, **91**, 991.
- 5) Schneider, D. P., Lawrence, C. R., Schmidt, M., Gunn, J. E., Turner, E. L., Burke, B. F., and Dhawa, V. 1985, *Ap. J.*, **294**, 66.
- 6) Lawrence, C. R., Schneider, D. P., Schmidt, M., Bennett, C. L., Hewitt, J. N., Burke, B. F., Turner, E. L., and Gunn, J. E. 1984, *Science*, **223**, 46.
- 7) Narasimha, D., Subramanian, K., and Chitre, S. M. 1986, *Ap. J.*, **315**, 434.
- 8) Narasimha, D., and Chitre, S. M. 1988, preprint
- 9) Ostriker, J. P. 1987, in *Dark Matter in the Universe: Proceedings of IAU Symposium No. 117*, eds. J. Kormendy and G. R. Knapp (Dordrecht: D. Reidel), 85.
- 10) Huchra, J., Gorenstein, M., Kent, S., Shapiro, I. I., Smith, G., Horine, E., and Perley, R. 1985, *A. J.*, **90**, 691.
- 11) Tyson, J. A., and Gorenstein, M. 1985, *Sky and Telescope*, **70**, 319.
- 12) Yee, H. K. C. 1988, *A. J.*, **95**, 1331.
- 13) Schneider, D. P., Turner, E. L., Gunn, J. E., Hewitt, J. N., Schmidt, M., and Lawrence, C. R. 1988, *A. J.*, in press.
- 14) Gott, J. R. 1981, *Ap. J.*, **249**, 140.
- 15) Djorgovski, S., and Spinrad, H. 1984, *Ap. J. Lett.*, **282**, L1.
- 16) Weedman, D. W., Weymann, R. J., Green, R. F., and Heckman, T. M. 1982, *Ap. J. Lett.*, **255**, L5.
- 17) Nieto, J.-L., Roques, S., Llebaria, A., Vanderriest, Ch., Lelievre, G., di Serego Alighieri, S., Macchetto, F. D., and Perryman, M. A. C. 1988, *Ap. J.*, **325**, 644.
- 18) Turner, E. L., Hillenbrand, L. A., Schnieder, D. P., Hewitt, J. N., and Burke, B. F. 1988, *A. J.*, submitted.
- 19) Tyson, J. A. 1987, in *Theory and Observational Limits in Cosmology*, ed. W. R. Stoeger (Vatican City: Specola Vaticana), 441.
- 20) Kovner, I., and Milgrom, M. 1987, preprint.
- 21) Press, W. H., and Gunn, J. E. 1973, *Ap. J.*, **185**, 397.
- 22) Hewitt, J. N. 1986, Ph.D. Thesis, Massachusetts Institute of Technology.
- 23) Hewitt, J. N., Turner, E. L., Burke, B. F., Lawrence, C. R., Bennett, C. L., Langston, G. I., and Gunn, J. E. 1987, in *Observational Cosmology: Proceedings of IAU Symposium No. 124*, eds. A. Hewitt, G. Burbidge, and L. Z. Fang (Dordrecht: D. Reidel), 747.

PROBABILITY OF ELONGATED GALAXY IMAGES FROM CLUSTER LENSING

Robert J. Nemiroff and Avishai Dekel
Racah Institute of Physics
The Hebrew University of Jerusalem
Jerusalem, 91904
ISRAEL



ABSTRACT

Gravitational lensing by a cluster of galaxies can distort a background galaxy so that it appears unusually elongated. It is found that if the observer's detection thresholds for measuring an unusually elongated galaxy are axial ratio ≥ 5 and $z \leq 1$, then the probability of observation is about 1 in 50 clusters of velocity dispersion ≥ 1000 km/sec. It is also shown that such distorted galaxies are ≥ 10 times more likely than the currently observed giant arcs; the shorter the arc, the more probable it is to occur. Observation of these elongated galaxies could serve as a measure of the velocity dispersion of clusters of galaxies.

Large arcs near the centers of several clusters of galaxies have recently been reported. Probably the best documented case is that of A370, the first arc discovered ¹⁾. Since then, at least 5 other large arcs ²⁾ have been seen, most of which have not been formally reported yet.

Evidence is now mounting that the arc in A370 is an artifact of gravitational lensing. Spectra of the arc shows a spectral line that has been identified as the OII line ³⁾. If this identification is correct, the redshift of the arc is much greater than the redshift of the cluster - which leaves lensing as the only reasonable explanation ⁴⁾. In this paper we show that less elongated galaxies should be much more likely than the giant arcs observed, and we estimate the probability of their observation.

We assume that a cluster of galaxies is a smooth, spherical, isothermal lens acting alone. The character of the images of the known arcs is indicative of an isothermal distribution with small core radius, so we feel that this is a reasonable approximation. Such a lens has simple qualities⁵⁾. The following analysis will concentrate on the single most luminous image produced.

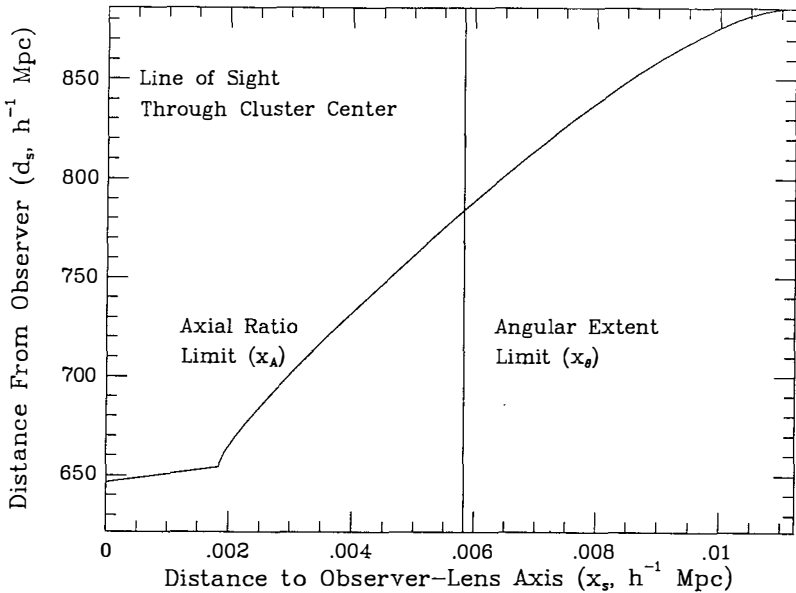


Figure 1: Detection volume boundaries.

The observer-lens-source geometry is shown schematically in Figure 1. Here d represents the angular-diameter distances to the source and x represents the distance from the source to the observer - lens axis. Two three-dimensional detection volumes are defined for a circular source of a given radius ⁶⁾. The cylindrical volume, with radius x_θ , is the space the source must fall into, behind the lens, so that the lens creates an image of it that covers a given fraction of a circle θ , or more. When the source is directly behind the lens, it is imaged into a complete circle. The conical volume, with radius x_A , is the axial ratio detection volume: it defines the space the circular source must fall into behind the lens to be distorted into a image with axial ratio A (major axis / minor axis) or greater. The detection volumes do not extend past the lens infinitely. The limit z_m is defined by the ability of the observer to distinguish the objects from the background.

In sum, the number of source galaxies in the source volume is given by

$$N = \int_{L_{min}}^{\infty} dL \Phi(L) \int_{D_{lens}}^{D_M} dD(z) [n(z)/n_o] \pi x^2$$

where L is the luminosity of source galaxies in terms of L_* , L_{min} is the minimum luminosity of galaxies considered (here = $0.1 L_*$), below which the surface brightness is assumed to drop sharply ⁷⁾, $\Phi(L)$ is the Schechter luminosity function (of the form $n_o L^{-\alpha} e^{-L}$ with $\alpha = 1.5$ and $n_o = 0.012$). D represents proper distance, $n(z)$ is the number density of sources along the line of sight (assumed to vary as $[1+z]^3$), and x represents the minimum proper radius of all the detection volumes being invoked.

Curvature, evolution, and K-corrections have been included in the determination of the value of z_m ⁸⁾, and we assumed a cosmology with $\Omega = 1$, and $H_o = 75 \text{ km sec}^{-1} \text{ Mpc}^{-1}$.

The results are summarized in Figure 2. Here $1/N$ represents how many clusters of galaxies of one-dimensional velocity dispersion $\sigma = 1000 \text{ km/sec}$ the observer has to inspect to have a 65 % chance of observing a distorted galaxy with the above $(A, \theta/\pi)$ or greater out to a redshift of z_m .

For example, if an observer can see galaxies out to a redshift of $z_m = 1$, then Figure 2 shows that the observer needs to observe on the average of 50 clusters to find a distorted galaxy with $A \geq 5$ and $\theta \geq \pi/10$.

One might take the $1/N$ estimates with some apprehension as a lot of assumptions went into them. They do, however, represent a fair guess of the parameters involved so we estimate this number to be correct to at least a factor of ten. The relative probability, however, is indisputable: *smaller arcs are more probable than larger arcs*. Figure 2 also shows that galaxies with $(A, \theta) = (5, \pi/10)$ are *relatively* much more likely than those like the giant arc in A370, with $(A, \theta) = (15, \pi/2)$, by more than a factor of ten - and this is the main point we wish to stress here.

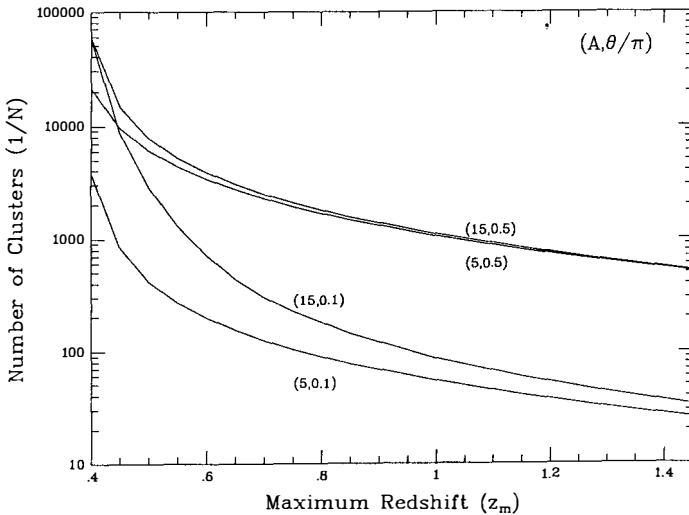


Figure 2: The probability of observing lensing.

The shorter the arc, the more probable it is by numerical factors of $\sin^2(\theta/2)$ and A^2 . When arcs get short enough, they look like elongated galaxies. If only long arcs are found, this would be a reason to disbelieve that the arcs are caused by gravitational lensing.

If large abundances of these elongated galaxies are found, they would be much more than a novel result of gravitational lensing: they could tell us the velocity dispersions of clusters of galaxies. By noting the redshifts of the cluster and the elongated galaxy, as well as the angular distance from the galaxy to the cluster center, one can directly calculate the one dimensional velocity dispersion. For example, using the known arc data for A370, it is straightforward to calculate that it's velocity dispersion is about 1400 km/sec.

REFERENCES

- 1) Lynds, R., and Petrosian, V. 1987a, *B.A.A.S.* **18**, 1014.
- 2) See, for example: Mellier, Y. et al. 1987, preprint.
- 3) Mellier, Y. 1988, preprint.
- 4) As predicted by: Paczynski, B. P. 1987, *Nature* **325**, 572.
- 5) See, for example: Turner, E. L., Ostriker, J. P., and Gott, J. R. III 1984, *Ap. J.* **284**, 1.
- 6) For a more complete description of the detection volumes necessary, see: Nemiroff R. J., and Dekel, A. 1988, *Ap. J.* submitted.
- 7) Dekel, A., and Silk, J. 1986, *Ap. J.* **303**, 39.
- 8) Empirically fit, assuming no density evolution, to the galaxy counts of Tyson J. A., and Jarvis, J. F. 1979, *Ap. J.* **230**, L153.

VII. STRINGS AND SOLITONS

DYNAMICAL EVOLUTION OF COSMIC STRINGS

FRANÇOIS R. BOUCHET

Department of Astronomy, University of California, Berkeley;
 and The Institute of Geophysics and Planetary Physics, Lawrence Livermore National Laboratory, Livermore;
 on leave from The Centre de Physique Théorique de l'Ecole Polytechnique, Palaiseau, France;
 and from The Institut d'Astrophysique de Paris, Paris, France.

In collaboration with D. P. BENNETT, Fermilab and U. of Chicago.



ABSTRACT

We have studied by means of numerical simulations the dynamical evolution of a network of cosmic strings, both in the radiation and matter era. Our basic conclusion is that a scaling solution exists, *i.e.* the string energy density evolves as t^{-2} . This means that the process by which long strings dump their energy into closed loops (which can gravitationally radiate away) is efficient enough to prevent the string domination over other forms of energy. This conclusion does not depend on the initial string energy density, nor on the various numerical parameters. On the other hand, the generated spectrum of loop sizes does depend on the value of our numerical lower cutoff (*i.e.* the minimum length of loop we allow to be chopped off the network). Furthermore, the network evolution is very different from what was assumed before¹²⁾, namely the creation of a few horizon sized loops per horizon volume and per hubble time, which subsequently fragment into about 10 smaller "daughter" loops. Rather, many tiny loops are directly cut from the network of infinite strings, and it appears that the only fundamental scale (the horizon) has been lost. This is probably because a fundamental ingredient had been overlooked, namely the kinks. These kinks are created in pairs at each intercommutation, and very rapidly, the long strings appear to be very "kinky". Thus the number of long strings per horizon is still of the order of a few, but their total length is fairly large. Furthermore, a large number of kinks favors the formation of small loops, and their sizes might well be governed by the kink density along the long strings. Finally, we computed the two-point correlation function of the loops and found significant differences from the work of Turok²⁰⁾.

Cosmic Strings are topologically stable linear defects that form in many grand unified theories (GUT) during a symmetry breaking phase transition in the early Universe. They might also be fundamental string remnants of an earlier phase (e.g. Piran, this volume). Contrary to monopoles and domain walls (the zero- and two-dimensional defects), they are not obviously a disaster for Cosmology. In fact, the idea that they might account for the formation of galaxies and large scale structure has recently generated a lot of interest. If the string tension μ is at the GUT scale (i.e. $\mu \sim (10^{16} G\epsilon V)^2$), they could provide appropriate seeds for the matter accretion in the matter era (or for the Ostriker-Thomson-Witten¹) explosions, if they are superconducting). Furthermore they have interesting observable signatures, like a non-zero residual of the millisecond pulsar timing measurements², or their gravitational lensing effects³, or the expected step-like discontinuities in the microwave background⁴). For the value of μ aforementioned (corresponding to $G\mu/c^2 \sim 10^{-6}$, G being Newton's constant), these might soon be detectable.

The physics of these objects is rather simple on a macroscopic scale. The equation of motion can be derived from the grand unified field theory, and is equivalent to the equations derived from the Nambu action (which is appropriate for fundamental strings), up to terms of the order of the transverse dimension of the string (typically 10^{-30} cm) divided by the local curvature radius (in the kiloparsec range for cosmological applications). In the following we use units such that $c \equiv 1$. But we occasionally include the c 's in order to make dimensions stand out more clearly, or to quote final results. In the Robertson-Walker metric $ds^2 = a^2(dr^2 - dx^2)$ where a is the expansion factor, the equation is⁵

$$\ddot{\mathbf{x}} + 2 \left(\frac{\dot{a}}{a} \right) \dot{\mathbf{x}}(1 - \dot{\mathbf{x}}^2) = \left(\frac{1}{\epsilon} \right) \left(\frac{\mathbf{x}'}{\epsilon} \right)', \quad (1)$$

in the gauge where $\dot{\mathbf{x}} \cdot \mathbf{x}' = 0$ (i.e. the velocity is perpendicular to the string). Dots denote derivatives with respect to conformal time τ , primes denote partial derivatives with respect to the string length parameter σ , and $\epsilon = \sqrt{\mathbf{x}'^2/(1 - \dot{\mathbf{x}}^2)}$ ($E = \mu a \int \epsilon d\sigma$ is thus the string energy). In the limit of zero expansion ($\dot{a} = 0$), Eq. 1 simply describes the evolution of a usual oscillating string. The term due to the expansion of the metric damps these oscillations by redshifting the velocities, and is efficient for structures of size comparable to, or larger than the horizon. The characteristic velocity is of order unity.

The only time when the Nambu equations are not sufficient to describe string evolution is when two strings interact, i.e. when they cross each other. This is the only time when the details of the fundamental field theory might play an important role. Numerical calculations^{6,7}) for the simplest string theories showed that in almost every case (i.e. for almost all relative velocities and angles) strings intercommute rather than pass through each other. Furthermore, it is expected on theoretical grounds that the intercommuting probability P controls the rate of relaxation of the string system but has no bearing on the existence of a scaling solution (see below), provided P is non zero. In the following we assumed $P=1$ to speed up the numerical calculation.

Since the strings oscillate, they gravitationally radiate, and closed loops can thus completely disappear. Various estimates^{8,9,10)} showed that the decay rate seemed to depend only weakly on the loop shape, so $\dot{E} = \mu \dot{l} \simeq 50G\mu^2$, where l is the length of the loop. For $G\mu \sim 10^{-6}$, the loop lifetime is of the order of $10^4 l$. This effect should thus be negligible in studying the string system evolution at the horizon scale, and is not incorporated in our numerical modeling.

Finally, at the time t_0 of the phase transition, the Higgs field orientations cannot be correlated on scales larger than the horizon, and thus the relative orientation of string segments should accordingly be uncorrelated at scales larger than ct_0 . One thus expects the string network at formation to be a collection of random walks with step size smaller than ct_0 . Most of the string length¹¹⁾ ($\simeq 75\%$) is in the form of infinitely long strings, which cannot subsequently radiate away, and are thus expected to survive indefinitely.

If one ignores the strings interaction, the evolution for the string energy per unit length $\epsilon = dl/d\sigma$ is obtained from Eq. 1

$$\dot{\epsilon} = -2(\dot{a}/a)\epsilon \dot{x}^2, \quad (2)$$

and by integration $\dot{E}/E = (\dot{a}/a)(1 - 2\langle v^2 \rangle)$, where $\langle v^2 \rangle$ is the velocity dispersion. Hence the evolution without interactions of the strings energy density $\rho_S \propto Ea^{-3}$ is

$$\dot{\rho}_S/\rho_S = -2(\dot{a}/a)(1 + \langle v^2 \rangle), \text{ and thus } \rho_S \propto a^{-2(1 + \langle v^2 \rangle)}. \quad (3)$$

Therefore ρ_S behaves as radiation only if $\langle v^2 \rangle = 1$, while $\langle v^2 \rangle = 1/2$ in flat space, and is even smaller in the expanding case. A non-interacting string system would rapidly come to dominate the energy density of the Universe, altering the growth rate of the expansion factor, and among other things, would disrupt the usual nucleosynthesis. The ‘‘Standard’’ scenario¹²⁾ holds that there is a scaling solution, *i.e.* $\rho_S \propto t^{-2}$, with a few length of rather straight strings per horizon volume, and horizon-size loops are produced at a rate of a few per horizon volume per Hubble time, this rate being large enough to insure a sufficient energy transfer onto loops. These ‘‘parent’’ loops then fragment into about ten daughter loops.

Kibble¹³⁾ and Bennett^{14,15)} studied this process analytically, by modeling the energy transfer mechanisms in terms of loop production and destruction functions. This is difficult, because the efficiency of the inverse process, namely the loop reconnections onto the long string network depends on the size of the objects formed. Larger loops have a larger cross section, and are more likely to reconnect. On the other hand, if their self-intersection probability is large enough, they will rapidly fragment, and daughter loops will reconnect less efficiently, which enhances the energy transfer onto loops that can ultimately radiate away. Even though the fate of the string system cannot be decided on pure analytical grounds, one can show that the strings will either come to dominate, or will converge toward a scaling solution. Misleading transients are likely to occur only when the reconnection process

is important. Also, the formalism provides a framework to analyze numerical results. As a matter of fact, by using this formalism, Bennett¹⁴⁾ showed that the simulation results of Albrecht and Turok¹⁶⁾ were inconsistent.

Thus, although much work has already been devoted to the cosmological implications of the strings existence, most of it is on fairly uncertain grounds, since the existence of a scaling solution must be postulated, as well as its expected properties (*e.g.* the loop size spectrum). Unfortunately, galaxy formation scenarios are rather dependent on the detail of the strings distribution. One would thus like to devise an accurate numerical code enabling to check the existence of the scaling solution, and obtain its characteristics, in particular the size spectrum, the loops velocities, and their correlation properties. Obviously the ultimate goal is to build a self-consistent kinetic model describing properly the strings network's evolution.

The numerical approach taken here is first to generate "reasonable" initial conditions, *i.e.* to create a string configuration which is a collection of random walks of given step-size ξ_0 in a box with periodic boundary conditions. To do so, we simply follow the procedure introduced by Vashaspati and Vilenkin¹¹⁾ for their numerical study of the phase transition. Nevertheless, the generated configurations do not have to be considered as faithful representations of the outcome of the phase transition. The procedure is rather a convenient device to generate initial conditions that embody the essential characteristics of a string configuration at any time, *i.e.* the absence of correlations on large scales, and the subsequent presence of infinite strings. Thus one should think of these conditions as out of equilibrium states used to study the possible relaxation toward a universal scaling solution. Indeed, this does not fix the horizon-size, which enables us to freely set the initial string energy density per horizon. The one improvement we made over the standard procedure was to round-off the corners (Fig. 1) in order to diminish the number of discontinuous derivatives the numerical program of evolution will have to cope with.

To evolve the strings, we start by sampling the strings with points initially regularly spaced and linked by "upstring" and "downstring" pointers so that neighboring points can be determined. The string position anywhere is then obtained by linear interpolation between the sampling points (a higher order interpolation scheme would be inappropriate, since the strings are far from smooth due to the kinks generated at each intercommutation). We then proceed by discretizing the equation of motion (Eq. 1). The system is evolved in time by a modified leapfrog scheme and spatial derivatives at mid-points are obtained by finite differences. We also evolve independently (with a semi-implicit scheme) the local energy density ϵ according to Eq. 2. The accuracy of the calculations is then checked by comparison with direct estimates of ϵ using the computed \dot{x} and x' . Each loop carries its own timestep satisfying the Courant condition, and our time-step halving routine preserves the $O(2)$ accuracy of the overall calculation.

To determine if two string segments crossed during the time step, we check the volume of the tetrahedron spanned by the four points on the two segments. If it changed sign during the step, the configuration is checked at the time the volume is zero, to see if a crossing did really occur (the positions of the points are extrapolated linearly between time steps). Also, the internal dynamics of loops is on a much smaller timescale than the displacement of complete loops. A given loop is thus checked for self-crossings at each of its individual timesteps, while the crossings between loops are checked only at each system timestep, when all loops are synchronized. When two segments have been determined to cross, we interchange partners, and average the positions and the velocities in the crossing region to help reduce the gauge condition violation.

One of the simulations we did was in a box $36\xi_0$ on a side, with an initial horizon size $H_0 = 2ct_0 = 14\xi_0$. It was evolved for 3.2 expansion factors (more than a factor of 10 in physical time), so that the final horizon size was $H = 45\xi_0$. The total number of strings increased from about 1000 at the beginning to about 16,500 at the end. The strings were sampled by about 350,000 points (which corresponds to 10 sampling points per initial correlation length ξ_0), and the calculation took about 40 cpu hours on a Cray-2. The evolution of the energy density in long strings ρ_{LS} (defined arbitrarily as being longer than $3.2ct$) multiplied by $(ct)^2/\mu$ is plotted in Fig. 2 as a function of the Horizon size in units of ξ_0 . At first strings are merely stretched. Then the loop production starts off, and a plateau is rapidly reached after an expansion by less than two ($a = H/H_0$). Such a fast relaxation justifies *a posteriori* the omission of gravitational decay corrections.

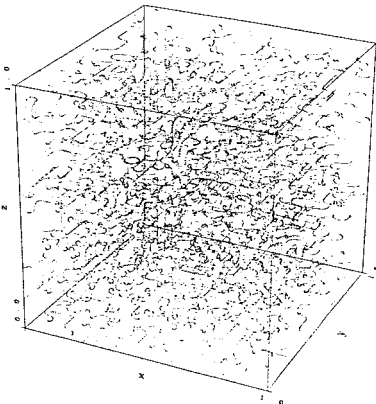


Figure 1

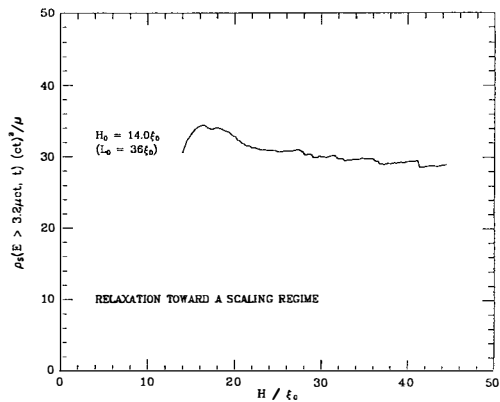


Figure 2

A lot of information can already be gained simply by looking at a carved out volume of the previous simulation. Since the only meter stick available to an observer is the horizon, we chose to display a volume of side ct (Fig. 3), which is thus an increasing fraction of the computational volume (*i.e.* from 0.7% initially to 23% finally). The snapshot presented is the final one when $H = 2ct = 45\xi_0$ ($L = 36\xi_0$). One notices immediately that long strings do appear relatively straight on the horizon scale, which does not mean they are smooth. On the contrary, one can easily see their

extremely “kinky” nature. It is also apparent that the majority of energy (almost 75% actually) is in the form of very small loops. Since the initial state had very little energy in small loops, this is graphic evidence that loop production actually succeeds in transferring large amounts of energy from the long strings to loops. Another striking feature is the total absence of horizon-sized loops; all the loops are much smaller than this.

In order to confirm the theoretical prediction that the scaling solution is stable, we thus evolved configurations with larger and smaller initial horizon-size H_0 , *i.e.* with different initial string energy densities. As is shown in Fig. 4, configurations with larger initial energy densities chop off many loops in order to lower the energy density in long strings ρ_{LS} , while in string-poor configurations more string-stretching and lower loop production rate yield an energy density increase. In other words, the scaling solution appears to be a stable point, and perturbed configurations quickly relax to a stationary state^{17,18}.

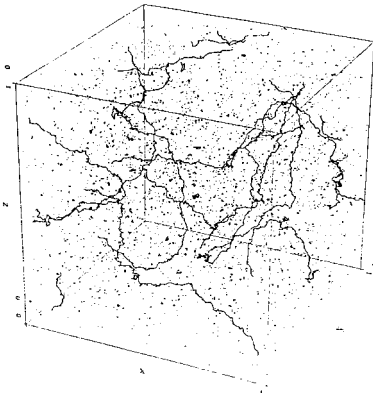


Figure 3

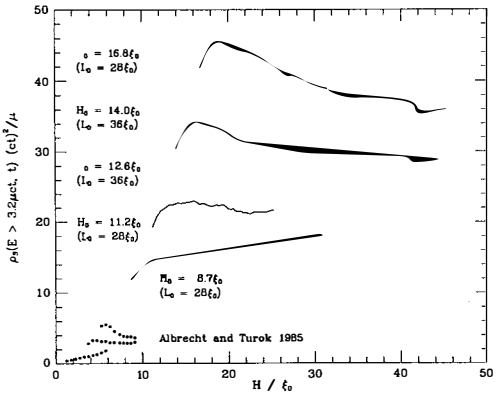


Figure 4

We checked the dependence of these results on our various numerical parameters, in particular the size of the computation box to check for boundary effects, the number of points per initial correlation length to determine possible sampling effects, as well as the time step requirements, or the value of our numerical lower cutoff. None of those but the last matters. This cutoff is implemented by requiring a minimal number of points for a loop to be allowed to chop off the network. We ran the simulation corresponding to the bottom curve of Fig. 4 ($H_0 = 8.7\xi_0$) with various cutoffs λ measured in units of the initial number of points per correlation length, *i.e.* per ξ_0 , since only their ratio is relevant. The results are shown in Fig. 5. Although the evolutions are different (after the first stretching period, the loop production burst is much more pronounced with a lower cutoff), it is reassuring to see the common trend toward larger energy densities appear. Since we checked that the energy in created loops is essentially independent of λ , the variations can be accounted for by the reconnection efficiency, which cannot indefinitely decrease. We therefore conclude that a scaling solution exists, and we can confirm the theoretical prediction that it is stable. However, there is

the possibility of significant systematic errors in our determination of ρ_{LS} , so we allow generous error bars¹⁹⁾ $\rho_{LS} = \zeta_{rad} \mu (ct)^{-2}$, with $\zeta_{rad} = 20 \pm 10$.

What does this imply in terms of energy transfer? Let us call $\dot{\rho}_T$ the rate of net energy transfer from the long strings into loops. One can thus modify Eq. 3 to take into account the total effect of the interactions

$$\dot{\rho}_{LS}/\rho_{LS} = -2(\dot{a}/a)(1 + \langle v^2 \rangle) - \dot{\rho}_T/\rho_{LS}, \quad (4)$$

and we know that the scaling is established in the radiation era when $\dot{\rho}_{LS}/\rho_{LS} = -4(\dot{a}/a)$. Thus $\dot{\rho}_{Trad} = \mu \zeta_{rad} (1 - \langle v^2 \rangle_{rad}) t^{-3}$. We measure $\langle v^2 \rangle_{rad} \simeq 0.45$, and the system thus transfers a length of about $11ct$ per ct^3 and per expansion time t .

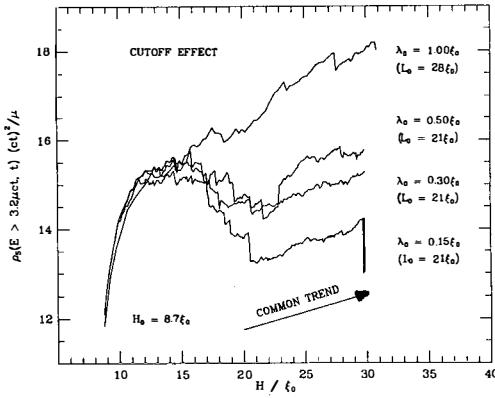


Figure 5

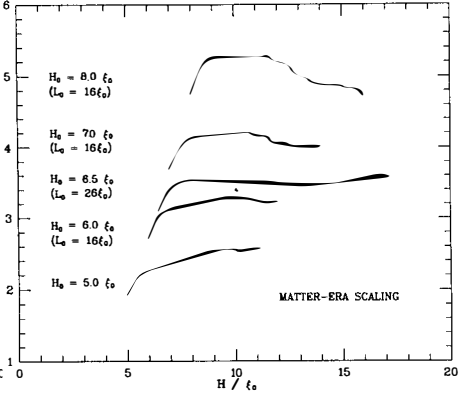


Figure 6

We performed a similar study of ρ_{LS} in the matter era (see Fig. 6). In this case, the relaxation is extremely fast, and we estimate the density at scaling to be such that $\zeta_{mat} = 3.5 \pm 1$, which is nearly a factor of ten smaller than in the radiation era. Since the scaling is now established for $\dot{\rho}_{LS}/\rho_{LS} = -3(\dot{a}/a)$, we have $\dot{\rho}_{Tmat} = (2/3)\mu\zeta_{mat}(1 - 2\langle v^2 \rangle_{mat})t^{-3}$. We measure $\langle v^2 \rangle_{mat} \simeq 0.40$. The system thus only transfers a length of about $0.45ct$ per ct^3 and per expansion time. Is this much lower energy density really surprising? Let us assume that the long string system may be characterized by a single scale L such that $\rho_{LS} = \mu L^{-2}$, *i.e.* the long strings are typically separated by L , and their characteristic interaction time is of the order of L^{-1} . One thus expects $\dot{\rho}_{Tmat}/\dot{\rho}_{Trad} = L_{mat}/L_{rad} = (\zeta_{rad}/\zeta_{mat})^{1/2}$. By comparison with our previous estimation, we get

$$\zeta_{mat} = \left(\frac{2}{3} \frac{1 - 2\langle v^2 \rangle_{mat}}{1 - \langle v^2 \rangle_{rad}} \right)^2 \zeta_{rad}, \quad (5)$$

which yields $\zeta_{mat} \sim 0.06\zeta_{rad} = 1.2$ in reasonable agreement with our direct measurement. Although quite simple, the model demonstrates the main difference between the scaling solutions in the matter and radiation eras: in the radiation era ζ must be large so that loop production proceeds at a rate

high enough for $\rho_{LS} \sim a^{-4}$ while in the matter era a much smaller ζ and lower loop production rate are required.

We now turn to the question of the loops distribution. What do we expect, once the scaling is established? Let us first assume that the network emits at time t_i in the radiation era χ loops of energy $E = \alpha \mu c t_i$ per ct_i^3 and per expansion time t_i , i.e. $dn(E, t_i) = \chi c dt_i / (ct_i)^4$. At a later time t , comoving volumes have expanded by $(t/t_i)^{3/2}$ and the number density has been redshifted accordingly: $dn(E, t) = \chi \alpha^{3/2} (E/\mu)^{-5/2} (ct)^{-3/2} d(E/\mu)$. The cumulative energy distribution in loops larger than some cutoff $E_c/\mu ct$ (corresponding to a length larger than some fixed fraction of ct) is then $\rho(E > E_c, t) = \int_{E_c}^{\infty} dE E dn(E, t)/dE$. In fact, one expects that loops are created in a range of sizes, so that one has to take $\chi = \chi(\alpha)$, and integrate over α . Thus

$$\rho(E > E_c, t) (ct)^2/\mu = \zeta_{rad} + \gamma (E_c/\mu ct)^{-1/2}, \text{ with } \gamma = 2 \int \chi(\alpha) \alpha^{3/2} d\alpha. \quad (6)$$

The energy density in long strings has been included in order to obtain the total cumulative energy density.

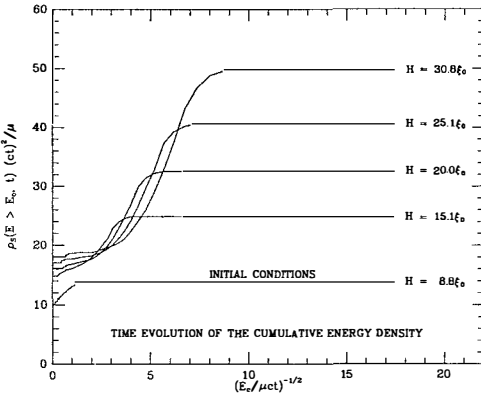


Figure 7

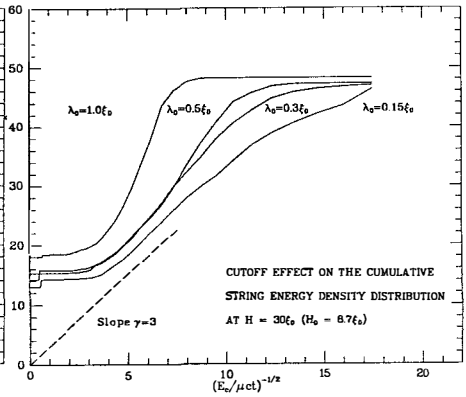


Figure 8

The time evolution of this cumulative energy distribution for the simulation corresponding to the lower curve of Fig. 4 is shown in Fig. 7. Times are labeled on the right by the current value of the horizon, and the bottom curve corresponds to the initial distribution, which is devoid by construction of loops smaller than $4\xi_0$, i.e. $(E_c/\mu ct_0)^{-1/2} \simeq 1$ since $H_0 = 2ct_0 = 8.7\xi_0$. One can recover on this graph the growth of the long string energy density as well as the appearance of a gap (flat curves on the left) which only translates our visual impression of the absence of loops of size comparable to the horizon. One also notes that the loop number density is indeed proportional to $E^{-5/2}$, as expected from Eq. 6. Nevertheless this is somewhat coincidental since our loop distribution is not yet in a true scaling regime. At smaller scales the straight lines turn over at the location of our cutoff (which is a decreasing fraction of the horizon since it requires a fixed number of points for a loop to be emitted).

Finally we note that on this graph the gravitational cutoff due to the finite lifetime of the loops would appear at $(E_c/\mu ct)^{-1/2} \simeq 100$.

To investigate the effect of the cutoff, we consider the distributions in simulations with the same initial conditions ($H_0 = 8.7\xi_0$), but different cutoff λ (the same simulations as in Fig. 5). The cumulative density distributions are compared at $H \simeq 30$ in Fig. 8. It is apparent that the slope γ depends on λ , although we might be close to cutoff independence since the slope variation seems to saturate for the lowest λ . This dependence is expected since the cutoff affects the size distribution of loops at birth $\chi(\alpha)$, and thus γ . How can it be then that ρ_{LS} is not affected more drastically? It turns out that the total energy dumped ($\propto \int \chi(\alpha) d\alpha$) is approximately constant. Everything happens as if, when the formation of small loops is forbidden, the network simply chops off larger loops in smaller number. If for instance the loop emission is controlled by the kinks (*e.g.* a piece of string chops off when it contains enough kinks to have a chance of looping back), then the kinks might travel a little further and cause the emission of a somewhat larger loop. Incidentally, two kinks are left over on the long string network, while more than two are taken away by the formed loop, thereby limiting the kink density on the long strings (but apparently at a rather high value).

Even though we do see a spectrum of loop sizes at birth, it is interesting to see what is the characteristic energy of the loops we form as well as how numerous they are. (The size defined as the *rms* radius R of the loops is simply a fixed fraction of the loop energy E , *i.e.* $E = \beta\mu R$, with $\beta \simeq 20$.) Approximating $\chi(\alpha)$ by $\chi(\alpha) = \bar{\chi}\delta(\alpha - \bar{\alpha})$, then $\gamma = 2\bar{\chi}\bar{\alpha}^{3/2}$. Our present results suggest $\gamma < 3$ (which implies $\nu \simeq \gamma/\beta^{3/2} < 0.03$ in the notation of Turok and Brandenberger¹²). By taking $\gamma = 3$, and recalling that the net energy transferred times $(ct)^2/\mu$ is $\bar{\chi}\bar{\alpha} = \zeta(1 - \langle v^2 \rangle) \simeq 11$, we get $\bar{\alpha} = (\gamma/2\zeta(1 - \langle v^2 \rangle))^2 \simeq 0.02$ and $\bar{\chi} \simeq 600$, *i.e.* we generate many tiny loops in contrast to the “standard scenario”. This is in qualitative agreement with our visual impression of Fig. 3 and the size gap in Fig. 8. Nevertheless the gap in Fig. 8 ends at $(E_c/\mu ct)^{-1/2} \simeq 4$ which corresponds to $\alpha \simeq 0.06$. This discrepancy simply denotes the oversimplification in approximating the spectrum by a δ function. One should also recall at this point that this cutoff study bears on simulations which have not yet reached the scaling regime and are thus still somewhat exploratory.

Even though the results concerning the loop sizes are still quantitatively quite uncertain, it is interesting to look at their correlation properties since it has been claimed²⁰ that the scenario naturally accounts for the correlation of clusters of galaxies and their scaling with richness^{21,22}. The richness scaling is such that the correlation functions ξ are similar for different cluster classes when distances are measured in units of the mean separation between the objects considered. This inter-object distance increases for rarer richer clusters thus enhancing the correlations. While difficult to explain otherwise, this scaling is a natural byproduct of the existence of only one fundamental scale (the horizon), in the cosmic string scenario (apart from the horizon size at equal matter and radiation density). Indeed, the correlation function at scaling should be a constant when distances are expressed

in units of ct , while the number of loops of a given size per horizon $(ct)^3 dn/dE$ should also be constant, which yields $\xi = f(r/(dn/dE))^{-1/3}$. What is not obvious on the other hand is the nature of $f(y)$, which should be $\sim 0.27y^{-1.8}$ to agree with the observations (note that this slope is not well constrained by the data, and was fixed to 1.8 to agree with the galaxy correlation function slope).

We have computed the correlation properties in the radiation era, and it turns out that the main conclusions does not seem to be affected by our cutoff λ . Our results are shown in figure 9 for the smallest cutoff simulation of Fig. 5 and 8. The open circles correspond to the correlation of loops at birth, *i.e.* their subsequent displacement was ignored. It follows quite closely the dash-dot line which corresponds to an y^{-2} fit to the cluster data and Turok's²⁰ results. If tiny loops are created along lines, dimensional analysis naturally yields the y^{-2} dependence. On the other hand, the match in amplitude came as a surprise, in accordance with Turok's²⁰ result. When we compute instead the correlations between all loops present at a given time in the simulation box, we obtain the curves labeled by squares (after 3.2 expansion factor) and filled circles (after 4.2 expansion factors), still in reasonable agreement with the observations. Nevertheless, when we extrapolated the loop positions to $a = 6.5$ by using their center of mass velocities, all correlations were pretty much washed out (filled triangles). This is because the loops have typically traveled further than their mean separation. We also tried to lower the loop center of mass velocities by an arbitrary factor to test the dependence of this negative conclusion on the precise computed velocity values. The correlations still tended to be washed out even after we decrease the velocities by a factor as large as two. Furthermore, our loops are born tiny and do not fragment very much, thus it is unlikely that spurious fragmentations might result in anomalously large velocities.

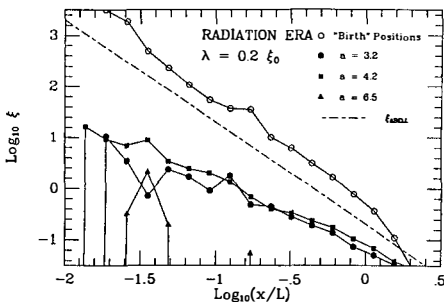


Figure 9

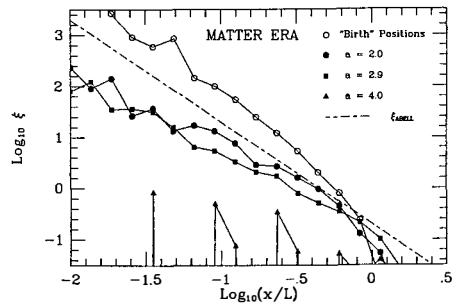


Figure 10

At this point, we might be tempted to conclude that the cosmic string model for galaxy formation does not do very well with the correlation functions for galaxies or Abell clusters. This would be premature, however, because most of the loops in our simulation are close enough to the lower cutoff in loop size so that they are artificially inhibited from fragmenting further. Thus, many

of these loops may be unphysical. When an attempt is made to use only the loops that are large enough so that they are probably physical, the correlation function does not seem to wash out quite so quickly, but the statistics are much worse. We also performed the same kind of analysis in the matter era (Fig. 10), and the results were slightly better (but the same caveat still applies).

In conclusion, we have proven that a scaling solution exists both in the radiation and the matter era. The long string energy density is measured to be $\rho_{LS} = \zeta(ct)^2/\mu$, with $\zeta_{rad} = 20 \pm 10$, and $\zeta_{mat} = 3.5 \pm 1$, and about $11ct$ of string length is transferred onto loops per $(ct)^3$ and per expansion time in the radiation era, this number being reduced to about $0.45ct$ in the matter era. Our results outline a scenario very different from the standard one: many tiny loops are directly chopped off the network with a dispersion of sizes. Correlations at birth are consistent with the observed ones in Abell's clusters. Nevertheless many issues remain to be resolved, in particular the effect of further lowering our numerical cutoff. Unfortunately, this cannot be done with our present algorithm, since at the end of a large simulation, we have only a few discretizing points per kink, which prevents any further reasonably accurate calculations. We are presently devising an improved algorithm to evolve the kinks analytically and later correct the evolution of the smooth component of the strings, hoping to be then able to settle the remaining questions. One might nevertheless speculate that this improvement will rather strengthen our present conclusions, since kinks will become even more prevalent.

This work was supported in part by the Theoretical Astrophysics Center at the University of California at Berkeley, and under the auspices of the U.S. Department of Energy by Lawrence Livermore National Laboratory under contractNo. W-7405-Eng-48.

REFERENCES

- 1) Ostriker, J.P., Thompson, C., and Witten, E. 1986, *Phys. Lett.*, **116b**, 141.
- 2) Hogan, C.J., and Rees, M.J. 1986, *Nature*, **311**, 109.
- 3) Vilenkin, A. 1981, *Phys. Rev. D*, **23**, 852.
- 4) Kaiser, N., and Stebbins, A. 1984, *Nature*, **310**, 391.
- 5) Turok, N., and Bhattacharjee, P. 1984, *Phys. Rev. D*, **29**, 1557.
- 6) Shellard, E.P.S. 1987, *Nucl. Phys. B*, **283**, 624.
- 7) Matzner 1988, *Texas U. preprint*.
- 8) Vashaspati, T., and Vilenkin, A. 1985, *Phys. Rev. D*, **31**, 3052.
- 9) Garfinkle, D., and Vashaspati, T. 1987, *Phys. Rev. D*, **36**, 2229.
- 10) Burden, C.J. 1985, *Glasgow U. Preprint 85-0745*.
- 11) Vashaspati, T., and Vilenkin, A. 1984, *Phys. Rev. D*, **30**, 2036.
- 12) Turok, N., and Brandenberger, R.H. 1986, *Phys. Rev. D*, **33**, 2175.
- 13) Kibble, T.W.B. 1985, *Nucl. Phys.*, **252**, 227.
- 14) Bennett, D.P. 1986a, *Phys. Rev. D*, **33**, 872.
- 15) Bennett, D.P. 1986b, *Phys. Rev. D*, **34**, 3592.
- 16) Albrecht, A., and Turok, N. 1985, *Phys. Rev. Lett.*, **54**, 1868.
- 17) Bouchet, F.R., and Bennett, D.P. 1987, Proceedings of the IAU Symposium 130, "Dark matter in the Universe", Balatonfured, Hungary.
- 18) Bennett, D.P., and Bouchet, F.R. 1987, Proceedings of the NATO-ASI meeting "The post-recombination Universe", Cambridge, England.
- 19) Bennett, D.P., and Bouchet, F.R. 1988, *Phys. Rev. Lett.*, **60**, 257.
- 20) Turok, N. 1985, *Phys. Rev. Lett.*, **55**, 1801.
- 21) Bahcall, N.A., and Soneira, R.M. 1986, *Astrophys. J.*, **270**, 20.
- 22) Klypin, A.A., and Kopylov, A.I. 1986, *Sov. Astron. Lett.*, **9**, 41.

**GLOWING HOT DARK MATTER
WITH OR WITHOUT
STRINGS ATTACHED**

Adrian L. Melott
Department of Physics and Astronomy
University of Kansas
Lawrence, Kansas 66045
USA



ABSTRACT

Neutrinos with a rest mass of order 30 eV may dominate the mass budget of the universe. There is increasing evidence for a substantial extragalactic flux of ionizing UV photons, which could be provided by neutrinos decaying with a lifetime of order 10^{24} sec. Some emission due to decay of local galactic halo material might be detected by the Extreme Ultraviolet Explorer, due to be launched in 1991. Previous arguments against such neutrinos as dark matter candidates are questioned and found to be fallible. Preliminary results on structure formation with massive neutrinos and cosmic strings suggest this is a promising model. Both hot and cold dark matter should be considered for direct detection.

I. INTRODUCTION

In a standard hot big bang cosmology, neutrinos of each type populate the universe with a mean density of order 110 cm^{-3} ; this is independent of mass for small masses such as we shall consider here¹⁾. A simple calculation shows that if one of the types of neutrinos had a mass of about 30 eV it would provide the critical density, just enough to make a flat Friedmann–Robertson–Walker universe. Such a mass cannot presently be excluded for the muon or tau neutrinos, although it may be excluded for the electron neutrino.

The formation of structure in a neutrino-dominated universe with ordinary density perturbations in the neutrinos proceeds from large to small. The free-streaming of the hot neutrinos damps out perturbations on small scales, leading to a well-known sharp cutoff in the power spectrum. Collapse of matter on such scales leads to a network of sheets and filaments, rather like that which has been observed on large scales²⁾.

Such neutrinos could decay to a lighter neutrino and a UV photon. This would explain a number of puzzling indications that there is a substantial extragalactic UV flux³⁾ which cannot be explained by conventional sources. Furthermore, a particle physics model which predicts such a decay rate simultaneously solves other astro-particle physics problems.⁴⁾

II. NEUTRINO CLUSTERING WITH ADIABATIC PERTURBATIONS

It is impossible to review the vast literature which has developed on neutrino clustering. I want to discuss what are often perceived as the three major problems of a neutrino-dominated universe: galaxy halo formation, the redshift of galaxy formation, and the correlation amplitude problem.

(a) It is generally assumed that there is a problem making galaxy halos, because the first dynamical event to take place in such a universe is the collapse of very long wavelength perturbations into sheets and filaments. The typical scale of such structures is that of a supercluster, 20–30 Mpc or so. An estimate of the velocity dispersion resulting from such

a collapse is 1000 km s^{-1} or more. Such particles would be too “hot” to ever cluster in a galaxy halo. Furthermore, one would expect the phase space density of the neutrinos to become “diluted” through phase-mixing. The success of the Tremaine–Gunn limit⁵⁾ depends on preserving the primordial phase space density.

A numerical study of neutrino clustering in pancaking⁶⁾ showed that these global approximations do not tell the whole story. One expects galaxies to form from the cooling of shocked gas in the center of the pancake. There is at this place after the collapse, a population of low-velocity neutrinos which have preserved their original phase-space density. The material is ideal for halo formation. The global average statements are true, but they do not apply to this crucial central region.

(b) A so-called “timing problem” is often mentioned in connection with these models. The general impression in the community is that galaxy formation begins only at the last minute. A related problem is the use of linear perturbation theory to estimate such things as microwave background fluctuations.

In Fig. 1, I show a graph from some recent work to illustrate this⁷⁾. In this simulation, which contains 262,144 particles and is scaled to be $128h^{-2} \text{ Mpc}$ on a side (where h is the Hubble constant in units of $100 \text{ km s}^{-1} \text{ Mpc}^{-1}$), I show the RMS density fluctuation inside the 64^3 cells (lower curve) and the maximum density anywhere in the simulation, plotted against redshift. The amplitude normalization is chosen so that the autocorrelation has a power-law slope 1.8 at $z = 0$.

Notice that (a) Even when the RMS fluctuation is $< 10^{-1}$, the upper curve breaks away, showing that non-gaussian behavior has begun for the peaks. (b) When the RMS fluctuations is about 0.2, the lower curve begins to grow faster than linear. This shows the danger in applying linear theory to these models.

What are our requirements for galaxy formation? Quasars are the earliest known nonlinearities. They are known to exist past a redshift of 4, with a mean spacing of something

like 50 Mpc, or about one per supercluster.⁸⁾ If we assume they have galactic masses, this is about one part in 3×10^4 . The inner parts of all galaxies, on the other hand, constitute about one part in 100 of the critical density. In Fig. 2 we see the number of cells whose density contrast has exceeded unity plotted as a function of z in the same simulation⁷⁾. We know from catastrophe theory⁹⁾ that there are density singularities inside these cells. By a redshift of 5 we have enough to account for QSOs, and by a redshift of 3 enough to account for galaxies. Arguments deriving from a timing problem¹⁰⁾ depend on collapsing entire cells (much more massive than galaxies) to zero volume. A comparison with Fig. 1 will show that the abundance of these density peaks is non-Gaussian. There is not a "timing problem".

(c) The last issue I wish to discuss here is the correlation length problem¹⁰⁾, which can be characterized as follows: we observe that the two-point correlation function of galaxies can be fit rather well by a power-law

$$\xi = \left(\frac{R_0}{R}\right)^\gamma, \quad (1)$$

where $\gamma \sim 1.8$ and $R_0 \sim 5h^{-1}\text{Mpc}$. When we do a neutrino simulation, the initial power spectrum is not a pure power-law, but has a sharp cutoff at a wavelength which scales as $(\Omega h^2)^{-1}$. In nonlinear evolution, the slope of ξ changes and we find a unique moment when $\gamma \sim 1.8$. At this time $R_0 \sim 4(\Omega h^2)^{-1} \text{Mpc}$. Requiring consistency with (1), we conclude $\Omega h \sim 0.8$, which is uncomfortably high but perhaps not inconceivable.

However, in the so-called "pancake theory"¹¹⁾ it is generally assumed that galaxies do not form everywhere, but only in the compressed areas. When the correlation function is calculated for this subset, the length $R_0 \sim 6(\Omega h^2)^{-1}\text{Mpc}$, implying $\Omega h \sim 1.25$, which seems to be excluded by age considerations. Unlike problems (a) and (b), this is well-founded in nonlinear numerical simulations, and all agree, given these assumptions. Let us point out several possible loopholes:

The simulations have included only dark matter. Assumptions have been made about galaxy formation. Three-dimensional numerical hydrodynamics with enough resolution to

follow the shocked gas from which galaxies form is at least one computer generation away. There may be surprises in the baryon distribution.

The dissipative processes involved in galaxy formation might give rise to explosions which could “smear out” the galaxy distribution.¹²⁾ “Antibiassing” might exist, in the sense that galaxy formation is suppressed in high-density areas.¹³⁾

It must be remembered that the simulations measure a mass-mass correlation. If the mass per galaxy were even modestly larger in cluster centers, this would strongly reduce the galaxy-galaxy correlation, which is sensitive to pair counts.

The correlation length in the simulations is rather stable, but there are signs that the observational value may reach $8 - 10h^{-1}\text{Mpc}$ with increased sample size.¹⁴⁻¹⁶⁾ Such values would drastically lower the estimate of Ωh from the simulations.

As we can see, there are numerous uncertainties associated with the correlation length problem. Since detailed comparison with nonlinear models eliminate the galaxy halo problem and the timing problem, I suggest that hot dark matter with adiabatic perturbations be carefully considered. After all, we know that neutrinos exist. Muon and tau neutrinos have only weak limits on their masses.

III. NEUTRINO CLUSTERING WITH COSMIC STRING LOOPS

Structure formation in a neutrino-dominated universe proceeds differently if we relax the assumption of adiabatic perturbations. If there are some “seeds” around to start galaxy formation which are not erased by neutrino free-streaming, they can trigger collapse of small-scale perturbations. One such possibility is cosmic string loops.

Metric perturbations induced by the strings induce density perturbations in the other components. I will report on preliminary results of a numerical treatment of large-scale structure in such a universe.¹⁷⁾

A distribution of loops of various masses is laid down with an r^{-2} correlation. These are given large random velocities. Their perturbations to the mean density grow according

to linear perturbation theory. This means that the Fourier components of these isocurvature perturbations grow very little outside the horizon. We take account of the effect of loop decay and the change in the neutrino Jeans length with time.

We also include a baryon contribution $\Omega_b h^2 = 0.02$. Baryon perturbations can grow after recombination, providing a “head start” for galaxy formation. Even if a loop decays, its baryon cloud may persist. As the neutrinos may only respond later, there is a natural separation of mass from light built in at the beginning.

Linear perturbation theory carries the model forward until the first resolved nonlinearity, when the PM code takes over. Given an assumed value of various string parameters such as the dimensionless $G\mu$, the present epoch is well-defined. We are able to match the values of γ and R_0 with reasonable string parameters.

In Figure 3 we see a slice of one of our numerical models. It displays interesting structure different from either CDM or HDM. The clusters are tighter and there are some isolated clusters not connected to the general network. The three-point correlation amplitude is much smaller than HDM. This model is much closer to the observed universe than strings + CDM, and deserves further study.

Figure 4 may provide some insight into the effect of non-Gaussian perturbations. I have taken the initial PM state of Fig. 3, and done a 3-dimensional Fourier analysis. Then, each component is multiplied by a random phase angle and an inverse transform done. This is evolved to become Fig. 4, which looks like other simulations with Gaussian perturbations. We intend to continue work on this promising model, and will report on it in the near future.

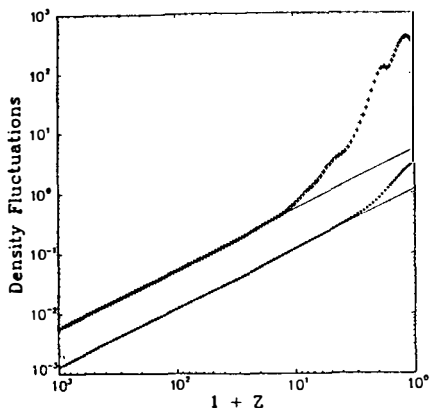


Fig. 1 A thin slice from a cosmic string+neutrino universe simulation. Note the condensations which are not connected to the filamentary structure.

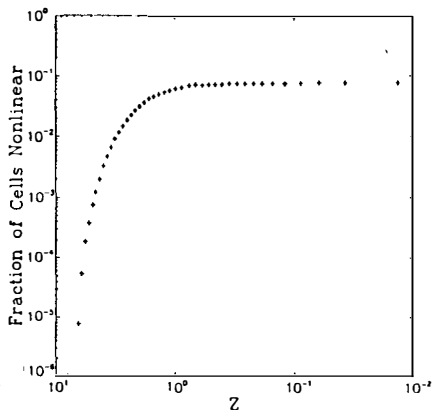


Fig. 2 The initial conditions of Fig. 1 were phase-randomized and then run for the same expansion factor as Fig. 1. This has the same power spectrum with different phase correlations. Note the absence of isolated lumps.

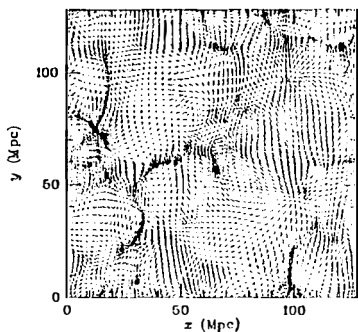


Fig. 3 In a hot dark matter universe with adiabatic perturbations the lower line is the RMS density fluctuations in the cells (see text) and the upper line is the maximum found in any cell. Note the deviation from Gaussian behavior when the RMS is still very small.

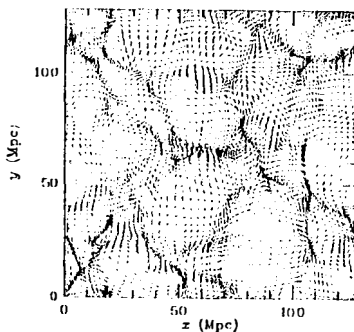


Fig. 4 The fraction of cells of density contrast greater than unity as a function of z . Some cells are nonlinear at $z=7$, and most action is complete by $z=1$.

IV. ACKNOWLEDGEMENTS

I am grateful to my collaborators Ed Bertschinger, Howard Bushouse, Joan Centrella, Jay Gallagher, Doug McKay, John Ralston, and Robert Scherrer for their talents. My part of this research has been supported by a Dudley Award, DOE Grant No. 85ER40214-A002, a NASA Astrophysics Grant, and University of Kansas General Research Allocation 3615-20-0038. The extremely time-consuming numerical simulations were performed on a Cyber 205 at the John von Neumann Computer Center as sponsored by the NSF Office of Advanced Scientific Computing under grant number NSF-863897.

REFERENCES

1. B. Lee and S. Weinberg, *Phys. Rev. Lett.* **39**, 165 (1977).
2. A.A. Klypin and S.F. Shandarin, *Mon. Not. R. Astron. Soc.*, **204**, 891 (1983).
3. A.L. Melott, D.W. McKay, and J.P. Ralston, *Ap. J. Lett.* **324**, L43 (1988).
4. J.P. Ralston, D.W. McKay, and A.L. Melott, *Phys. Lett.* **202B**, 40 (1988).
5. S. Tremaine and J.L. Gunn, *Phys. Rev. Lett.* **42**, 407 (1979).
6. A.L. Melott, *Ap. J.* **264**, 59 (1983).
7. J. Centrella, J. Gallagher, A. Melott, and H. Bushouse, *Ap. J.* submitted (1988).
8. R. Kron, personal communication (1987).
9. V.I. Arnold, S.F. Shandarin, and Ya. B. Zel'dovich, *Geophys. Astrophys. Fluid Dynamics* **20**, 111 (1982).
10. S.D.M. White, C. Frenk, and M. Davis, *Ap. J. Lett.* **274**, L1 (1983).
11. S.F. Shandarin and Ya. B. Zel'dovich, *Comments Ap.* **10**, 33 (1983).
12. S.F. Shandarin, in ESO-CERN Symposium (1984).
13. E. Braun, A. Dekel, and P. Shapiro, preprint (1987).
14. J. Einasto, A.A. Klypin, and E. Saar, *Mon. Not. R. Astron. Soc.* **219**, 457 (1986).
15. A. Oemler, personal communication (1987).
16. M. Geller, personal communication (1987).
17. E. Bertschinger, A.L. Melott, and R.J. Scherrer, in preparation (1988).

**FUNDAMENTAL STRINGS
AND
LARGE SCALE STRUCTURE FORMATION † ***

Tsvi Piran^a Jean Orloff ^{#,b} and Francois Englert^{a,b}

**a: The Racah Institute for Physics,
The Hebrew University, Jerusalem, ISRAEL**

**b: Service de Physique Théorique
Université Libre de Bruxelles,
B-1050 Brussels, BELGIUM**



ABSTRACT

Fundamental strings at high temperature may undergo a phase transition and form macroscopic objects which we call "Fundamental cosmic strings" These strings, like topological cosmic strings, provide a simple and efficient mechanism for the formation of large scale structures in the universe. We consider the astrophysical constraints on fundamental cosmic strings and examine the consistency between these constraints and the low energy phenomenology of string theories.

† talk given by T. Piran

* Supported in part by the Israel Foundation for Basic Research

Chercheur I.I.S.N

1: Introduction.

Aharonov, Englert and Orloff¹⁾ have recently shown that when the temperature approaches the Planck scale, the entropy available from the degeneracy of high mass states inflates the strings to energies much larger than the temperature. This may lead to a phase transition by which a huge string filling the whole space with constant average density is generated. The fact that such temperatures have probably been reached in the very early universe raises the interesting possibility that the macroscopic strings that form in this way “fundamental cosmic strings” may be responsible for seeding the large structure of the universe^{1,2)}. Indeed we shall see that, under not unreasonable assumptions, this macroscopic strings provide seeds for galaxies and clusters. Their distribution in mass and in space is quite similar to those indicated by numerical simulations of the evolution of topological cosmic strings³⁾. However the mechanism yielding the seeds can be totally different in the two scenarios and further could select one scenario or reject both of them.

We first review the cosmological hypothesis of reference 1. We then use the initial string distribution in the universe and assuming the existence of dark matter, we sketch the predicted large scale structure of the universe²⁾. Confrontation with observation yields an estimate of μ , the mass per unit length of the string, which is quite small. μ is related to the Regge slope, $\alpha' : \mu \simeq \alpha'^{-1}$, hence the required Regge slope is too large to be consistent with naive low energy phenomenology based on fundamental strings. This conclusion is strengthened by other more direct astrophysical observations quite independently of galaxy formation. Thus either our cosmological hypothesis is wrong or naïve low energy phenomenology is ruled out. These issues are discussed at the end of the paper.

2: The pre adiabatic era.

String theories involving only weakly coupled closed strings exhibit a high temperature phase characterized by the condensation of an infinite string¹⁾. This string takes up a finite average energy density and spans the space with a random walk of step size $\approx \alpha'^{1/2}$. It was suggested that, in the cosmological context, this phase is the ancestor of the adiabatic era: the infinite string with internal temperature provides the necessary correlation over the whole universe to fix the initial thermal state. In the semi-classical limit, the pre-adiabatic phase could be described by an exponential inflation with a Hubble constant H determined from thermal equilibrium at the Hawking temperature of the de Sitter space: $H/(2\pi) = \beta_0^{-1}$. Although a recent work of Turok⁴⁾

seems to corroborate this result, it is not clear whether the strong interaction with the gravitational background would not cause more dramatic quantum mechanical effects and invalidate a semi-classical description of the pre-adiabatic phase. We shall thus not commit ourselves to a detailed description of this phase. Our only tentative cosmological assumption will be that the initial state of the adiabatic expansion is given by a thermal distribution of closed string excitations at temperature $T = \beta_0^{-1}$ and critical density σ_c marked by the disappearance of the infinite string. Possible out of equilibrium remnants of the pre-adiabatic phase will be considered later on.

At $T = \beta_0^{-1}$ and $\sigma = \sigma_c$, the equilibrium distribution is given by “microscopic strings” which we call the (massless) radiation gas and an asymptotically scale invariant network of brownian shaped closed macroscopic strings^{1),2),5)}. The scale invariant distribution of the macroscopic strings is²⁾:

$$N(R)dR = \nu \frac{V}{R^3} \cdot \frac{dR}{R} \quad (1)$$

where

$$\nu = 0.016 \quad . \quad (2)$$

It is remarkable that for the string theories we have considered ν is a universal constant which does not depend on the generic string theory used but only on the number of non compact space-time dimensions $D \geq 4$. Namely (1), (2) are valid whether the internal degrees of freedom arise from a torus compactification of the bosonic string, of type II superstrings or of the heterotic string.

3: Strings in the adiabatic era.

We now turn to the cosmological evolution of the string network. Because of the expansion one expects decoupling of strings from the radiation gas in about one Hubble time. Therefore, we cannot dismiss a priori remnants of the pre-adiabatic phase in the form of infinite strings which would remain out of thermal equilibrium at the end of the transition to the adiabatic era: their disappearance depends on the detailed dynamics of the phase transition which we do not know. We therefore consider first the case of a system of fundamental strings which includes initially infinite strings.

The cosmological evolution of this universe is quite similar to the evolution of a universe containing a network of topological cosmic strings ^{#1} which was studied

^{#1} This follows from the similarity of the classical equations of motion for strings in a Robertson-Walker background metric.

numerically³). This evolution depends on p , the probability that two strings that cross each other intercommute. If $p = 0$ (no exchange of partners) the energy density of the infinite strings scales like matter and thus quickly dominates the energy density of the radiation filled universe. This catastrophe is avoided in the $p = 1$ case because infinite string cut themselves out, leaving about one segment of infinite string per horizon and forming closed strings of size comparable to the horizon size. In the radiation dominated era, the latter seem to be distributed in size (neglecting gravitational decay) according to

$$N_1(R, t) = V \nu_1 R^{-5/2} t^{-3/2} \quad (3)$$

where from numerical estimate³) $\nu_1 \approx 0.02$. These are the seeds from which galaxies and clusters can be formed. Note that in the result (3), the initial distribution of scale invariant closed string does not play a significant role. It is not clear whether the validity of (3) is contingent upon the hypothesis $p \approx 1$. Neither is it obvious that the closed strings formed in this way would not disappear by cutting themselves to very small rapidly decaying loops⁶). In any case, Eq. (3) can arise from infinite strings only as the result of a complicated dynamical process and the only informations we presently have rely heavily on numerical simulations.

On the other hand, if the adiabatic era indeed starts in thermal equilibrium at the critical density σ_c , there will be no infinite strings at that time. Such initial conditions are impossible in the context of topological strings but are rather natural within the framework of fundamental strings. This leads immediately to the seed distribution (3), *quite independently of the value of p* . Indeed strings larger than the horizon expand (their transverse size R grows like the Robertson-Walker scale factor $a(t) \sim t^{1/2}$ and stretch, their typical random walk step becoming of order t , the horizon size. Once they enter the horizon they stop expanding, oscillate and start decaying by emitting gravitational waves⁷). Neglecting gravitational decay (which can easily be taken into account), we get in the radiation dominated era, from (1):

$$N_1(R, t) = N(R) \frac{a^3(R)}{a^3(t)} = V \nu R^{-5/2} t^{-3/2}. \quad (4)$$

Remarkably enough, the analytic value (2) for ν agrees with the numerical data used for ν_1 in (3) so that the seed distributions coincide in the two scenarios. However in equation (4), self-intersections have been completely ignored. This would seem, at first sight to imply $p = 0$, but in fact it is not difficult to verify analytically that because of the scarcity of large loops in (1), the result (4) remains valid, up to factors of order 1 for all values of p between zero and one, provided closed strings inside the horizon do not self-intersect significantly.

4: Structure formation and other astrophysical constraints.

From $t = R$, the moment the closed string of size R entered the horizon, the scenario for structure formation follows the standard cosmic string scenario 7). In short, the string now begins to accrete dark matter while decaying; it eventually disappears, leaving a density contrast $\delta\rho/\rho$ which starts growing significantly after t_{eq} , the time when the density of matter and radiation are equal. The density and size of the different structures formed in this way (galaxies and clusters of galaxies) reflect the distribution of the corresponding seeds (4) whose mass are of order μR . From the observed density and mass of Abell clusters and bright galaxies one deduces 8) (in Planck units)

$$\mu \simeq 10^{-6}. \quad (5)$$

There is an uncertainty in this number by, say, an order of magnitude. However if μ is too small, then strings would not lead to formation of any large scale structure and if μ is too large, the resulting large scale structure would be quite different from the observed one (for instance cluster of galaxies would be much larger than they are).

Such a small value of μ contradicts naive phenomenology as it would lead to a comparable value of squares of gauge coupling constants at energy scales of order $\mu^{1/2}$; this is much too small to cope with reasonable renormalization group estimates of low energy values 9). Can this value be increased if despite the occurrence of the phase transition something went wrong in the assumption leading to structure formation? For instance, as already mentioned, every seed could disappear because of self intersections; or maybe there is no dark matter available to accrete at all. The answer is negative, as revealed by other astrophysical data, independent of galaxy formation, arising from gravitational interactions due to strings, namely gravitational radiation and various lensing effects.

The potentially strongest direct limit on the string parameters is due to the lack of residual noise in the timing of the millisecond pulsar due to the stochastic emission of gravitational waves by decaying strings 10). Upper limit to the noise in this pulsar sets a limit on $\mu^{1/2} \lesssim 10^{-3}(\alpha/T)^{1/4}$ where α is a numerical factor of order 2π and T is the observation time in years. While this limit is presently consistent with the value (5), the bound on μ is rapidly decreasing as the T increases. In fact if such random noise does not show up within a few years, the resulting limit would rule out any cosmic string mechanism for structure formation. Note that if string would disappear due to rapid self intersections, the decay to gravitational background could occur almost immediately after horizon crossing. The gravitational radiation is then redshifted by a factor of order $\mu^{1/2}$ and the constraint on μ would be correspondingly weaker: $\mu \lesssim 10^{-3}(\alpha/T)^2$.

The strongest other limits on the string parameters arise from the homogeneity of the microwave background. Both lensing effects¹¹⁾ and an interaction between the gravitational radiation field and the microwave radiation¹²⁾ lead to fluctuation in the microwave background. Since such fluctuations are not observed these effects yield additional upper limits to the string tension $\mu \lesssim 10^{-4}$. Finally, a group of double images would both identify the location of a large string and measure its tension. A tentative identification of such a line has been made¹³⁾ yielding results consistent with (5) but this identification is still uncertain at the moment.

5: Conclusions.

It is remarkable that the upper limits on μ obtained from the more direct astrophysical consideration are not very different from the actual parameters needed for the structure formation scenario. In any case $\mu \sim O(1)$ is excluded even if the structure formation scenario by strings would fail. Thus in the event that string theory is correct or at least represent a reasonable first approximation to the Planck scale physics, we are confronted with the following alternative: either the phase transition of reference 1 does not occur, or naive low energy phenomenology is wrong. We now examine the two issues.

There are several ways by which the phase transition could be avoided. Firstly it may just be an artifact of the weak coupling approximation. Second, as suggested by Witten, macroscopic fundamental string may be confined to boundaries of axion domain walls if anomalous superconductivity develops along the string¹⁴⁾. Third, an inflation which would take place after the phase transition would eliminate heavy macroscopic strings. However if the phase transition does occur we must have $\mu \lesssim 10^{-4}$ and fundamental strings would be the most natural agent for structure formation in particular because of the simplicity and of the possible success of the scenario without infinite strings. In this case, naïve phenomenology is untenable. This is not totally unexpected. Naïve phenomenological models rely on effective low energy lagrangians which relate directly the four dimensional gauge coupling e^2 to a universal string coupling g^2 . This relation would be reasonable if the dilaton would be the only scalar field with non-vanishing expectation value. However "compactification" to four dimensions may introduce mixing with new scalars and unbounded potentials. In this case genuine string corrections are required for stability and gauge couplings can be very different from the naïve value $e^2 \simeq \mu$.

Acknowledgments:

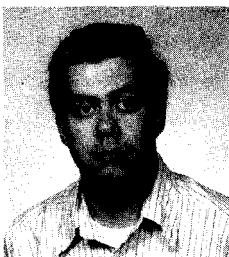
We are grateful to R. Brout, C. Gomez, H.P. Nilles, R. Parentani and D. Spergel for most informative and enjoyable discussions.

REFERENCES

- 1) Y. Aharonov, F. Englert and J. Orloff, *Phys. Lett.* **B199** (1987) 366.
- 2) F. Englert, J. Orloff and T. Piran, submitted to *Phys. Lett.* (1988).
- 3) T. Vachaspati and A. Vilenkin, *Phys. Rev.* **D30** (1984) 2036,
A. Albrecht and N. Turok, *Phys. Rev. Lett.* **54** (1985) 1868.
- 4) N. Turok, *Phys. Rev. Lett.* **60** (1988) 549.
- 5) D. Mitchell and N. Turok, *Phys. Rev. Lett.* **58** (1987) 1577.
- 6) D.P. Bennett and F. R. Bouchet, *Phys. Rev. Lett.* **60** (1988) 257, F. R. Bouchet, this volume.
- 7) See for instance N. Turok "Two Lectures on Cosmic String Theory of Galaxy Formation", Imperial College Preprint TP/87-88/19 to School on Cosmology and Particle Physics 1987.
- 8) N. Turok and R.H. Brandenberger, *Phys. Rev.* **D33** (1986) 2175.
- 9) M. Dine and N. Seiberg, *Phys. Rev. Lett.* **55** (1985) 366.
V. Kaplunovsky, *Phys. Rev. Lett.* **55** (1985) 1033.
- 10) C.J. Hogan and M.J. Rees, *Nature* **311** (1984) 109,
E. Witten, *Phys. Rev.* **D30** (1984) 272
- 11) N. Kaiser and A. Stebbins, *Nature* **310** (1984) 391
- 12) R.H. Brandenberger, A. Albrecht and N. Turok, *Nucl. Phys.* **B277** (1986) 605
- 13) L.L. Cowie and E.M. Hu, *Ap. J. Lett.* **318** (1987) 33.
- 14) E. Witten, *Phys. Lett.* **B153** (1985) 243.

LIMITING CURRENTS IN FERMIONIC
CONDUCTING COSMIC STRINGS

S. M. Barr
Bartol Research Institute
University of Delaware
Newark, Delaware 19716
USA



ABSTRACT

Recently there has been much interest in the possible effects of superconducting cosmic strings. Those effects which are of observational interest involve currents (in units where $\hbar = c = 1$) of grand unified scale (10^{15} GeV = 8×10^{20} Amps). We argue that in unified theories conducting strings of the fermionic type cannot achieve such currents because of scattering of current carriers via grand unified interactions. Currents are limited to be six to nine orders of magnitude lower than usually discussed.

Cosmic strings¹⁾ are of peculiar theoretical interest because (unlike monopoles or domain walls) they would always constitute, if the hypothesis of "intercommutation" is correct, a roughly fixed fraction of the mass density of the universe and hence leave a permanent imprint of physics at very early times, and thus at very high energies. So even if formed when $T \sim 10^{15}$ GeV they would have important consequences at times relevant to galaxy formation ($T \sim 1$ eV) and at the present time ($T \sim 1/4000$ eV). In 1985 Witten²⁾ showed that such strings can be superconducting and carry huge currents, thus opening up a whole range of possible, interesting electromagnetic effects³⁾.

There are two kinds²⁾ of superconducting strings: "bosonic" and "fermionic", referring to the nature of the current carriers. Our results⁴⁾ apply only to fermionic strings. In a string fermions can, because of topological "index theorems", have so-called "Jackiw-Rossi" zero modes⁵⁾, which propagate at the speed of light along the string. For a given species of particle these modes propagate only in one direction along the string, which depending on the form of its Yukawa coupling. Let us call the two directions the + and - directions, and say the i^{th} species of particle travels in the ϵ_i direction, $\epsilon_i = +$ or $-$. In the string the fermions are effectively massless, while away from the string they have their normal, in vacuo masses. If a bound fermion acquires momentum exceeding its in vacuo mass it will have sufficient energy to escape the string. The current carried by the i^{th} species is $\frac{1}{2\pi} q_i P_{Fi}$ where P_F is its (one-dimensional) Fermi momentum, usually assumed, for the reason just given, to be less than or equal to m_i . So $J_{\text{max}}(i) = \frac{1}{2\pi} q_i m_i$. If $m_i \sim 10^{15}$ GeV then $J_{\text{max}} \sim 10^{14}$ GeV $\sim 10^{20}$ Amps. ($\hbar = c = 1$). In fact, most of the observationally interesting effects³⁾ of conducting strings involve such huge currents being achieved.

Let us consider a toy model²⁾ where d , \bar{d} , e^- and e^+ move in the + direction and u , and \bar{u} move in the - direction. A possible source of dissipation is the charged weak interactions: $e_L^- + u_L \rightarrow \nu_L + d_L$. In the absence of scattering any applied emf (such as caused by the strings moving relativistically through a magnetic field) will produce a current in which $P_{Fi} \propto q_i \epsilon_i$. (The Lorentz force law says $P_i = \epsilon_i (q_i E)$.) One can show by simple arithmetic that if the emf is turned off weak interaction scattering will not be able to reduce the current to zero⁴⁾ because of the Pauli principle. If we only took account of electroweak interactions these strings would indeed be superconducting with J_{\max} given roughly by the typical fermion mass m_f . However,⁴⁾ in grand unified models the unified gauge interactions lead to very severe limits on the currents attainable. In our toy model one can have the $|\Delta B| = 1$ processes $e^- + u \rightarrow \bar{d} + \bar{u}$ and $d + u \rightarrow e^+ + \bar{u}$ mediated by charge - 4/3 gauge bosons. Now, simple arithmetic shows that if the applied emf is turned off, these GUT scattering processes will reduce the current to zero. How rapidly? If the fermions are the usual light quarks and leptons the time scale is the proton lifetime! However, in the cases of observational interest³⁾, where J and m_f are superlarge the fluxes are also superlarge and it turns out that for the gauge boson mass $M_x \sim 10^{16}$ GeV and J and $m_f \gtrsim 10^6$ GeV then $\tau_{\text{scat}} \ll t$ for all times for which $T \lesssim 10$ eV.

Given an applied emf arising from the string moving relativistically through a magnetic field B one finds that the current approaches a value J_{crit} which is always less than or equal to (for any fermion mass m_f) $J_{\max} = 10^6 \text{ GeV} \times (|B|/10^{-6}\text{G})^{1/6} \times (M_x/10^{16} \text{ GeV})^{2/3}$. ($10^6 \text{ GeV} \approx 8 \times 10^{11}$ Amps). To get currents of order 10^{14} GeV as required for most of the observationally interesting effects³⁾ discussed in the literature one would need $|\bar{B}| \sim 10^{42}$ Gauss! For detailed calculations of scattering

rates and bounds on currents see ref. 4.

In general one only expects to have fermion species of superlarge mass in theories with new interactions at superlarge scales, for instance grand unified theories. Our limits apply whenever there are gauge interactions corresponding to a group $G \supset SU(5)$, even if these occur at the Planck scale as in superstring models.

We have implicitly assumed that all the fermions are of comparable mass, m_f . If that is not true the analysis can be much more subtle (see the second paper of ref. 4). However, the qualitative conclusion is unaffected.

Finally, our analysis depends on the anomaly condition $\sum_{i=L} (q_i)^2 = \sum_{i=R} (q_i)^2$ being satisfied. However, any (global) string which fails to satisfy this will have a $U(1)$ global x $U(1)^2_{QED}$ anomaly. If $U(1)_{QED}$ is unified with $SU(3)_{QCD}$ as in all grand unified models, there will therefore be a $U(1)_{global}$ x $SU(3)^2_{QCD}$ anomaly as well. This implies the formation of "axion" domain walls when $T \cong 200$ MeV, and therefore that such strings will not be important at later times anyway.

It is fairly safe to conclude, then, that in essentially all interesting fermionic conducting strings the currents can never reach levels of observational interest because of scattering of charge carriers through unified gauge interactions.

REFERENCES

1. A. Vilenkin, Phys. Rep. a and references therein.
2. E. Witten, Nucl. Phys. B249, 557 (1985).
3. J. Ostriker, C. Thompson, and E. Witten, Phys. Lett. B181, 243 (1986); E. M. Chudnovsky, G. B. Field, D. N. Speigel, and A. Vilenkin, Phys. Rev. D34, 944 (1986); C. Hill, D. Schramm, and T. Walker, FERMILAB - Pub. - 86/146-T.
4. S. M. Barr, and A. M. Matheson, Phys. Rev. D36, 2905 (1987), Phys. Lett. B198, 146 (1987).
5. R. Jackiw, and P. Rossi, Nucl. Phys. B190, 681 (1981).

SOLITOGENESIS, CAN NON TOPOLOGICAL SOLITONS BE THE DARK MATTER?

Graciela Gelmini *

International School for Advanced Studies (SISSA/ISAS), Trieste - Italy

International Centre for Theoretical Physics (ICTP), Trieste - Italy

ABSTRACT

Solitogenesis is the primordial origin of non topological solitons (NTS). NTS are a wide class of stable extended classical objects, characterized by the presence of a conserved additive charge (such as a number of particles). Their stability is then guaranteed only if the energy of the NTS is lower than that of a collection of free particles with the same additive charge. We discuss the formation of NTS (within a particular model) in a second-order phase transition in the early Universe. The abundance, mass and characteristics of the NTS are model dependent. Even if their contribution to the energy density of the Universe is not compelling, it may easily be large. NTS may constitute the dark matter or, in any case, be cosmologically and astrophysically relevant.

*) On leave of absence from Dipartimento di Fisica, Università di Roma II, Tor Vergata, Via O. Raimondo, 00100 ROMA

Non-topological solitons (NTS) are a very wide type of stable extended objects, so wide that precisely this characteristic may limit the usefulness of the concept, in the sense of lacking of predictivity. The abundance, mass and characteristics of BNTS are model dependent, what may not seem appealing. However, the models in which NTS solutions appear are not rare and these solutions may have very characteristic properties, that may allow to distinguish them (as in the case of "soliton stars", for example). NTS can be cosmologically relevant, contributing a significant fraction of the present mass density of the Universe. To this last possibility refers this talk, based on work done with J. Friemann, M. Gleiser and E. Kolb ¹). The conclusion is that NTS may be relevant in cosmology and astrophysics and they open up an enormous variety of possibilities to be explored.

NTS solutions were introduced twenty years ago ^{2,3,4}) and reappeared recently as "quark nuggets" ⁵), "Q-balls" ⁶), "soliton stars" ⁷), "cosmic neutrino balls" ⁸). Let us start by defining what a non-topological soliton is. A soliton is any spatially confined and non dispersive solution of a field theory, i.e. a solution which has a finite non zero rest mass confined in a infinite region in space at all times ⁹). A wavepacket, formed through the superposition of planewaves does not remain confined for large times, i.e. is always dispersive and, therefore, is not a soliton. Historically, the name soliton referred at first to "indestructible solitons", such that their shape and velocity remain unchanged after a collision with another soliton ¹⁰). The first was the "solitary wave" in hydrodynamics, that Scott Russel followed on horseback after it formed in the water of a channel, in 1834. Indestructible solitons exist only in one space dimensions. In the wider sense of soliton used here, the indestructibility is not required and solitons appear in any number of space-dimensions. While the name "bound-state" applies historically to quantum systems, a "soliton" is actually a stable "bound state" that appears at a classical level. In order to have soliton solutions (in relativistic local field theories) there must be nonlinear couplings; otherwise the only solutions are plane waves. There are two types of solitons, according to the origin of their stability, topological and non-topological solitons:

i) Topological Solitons: the necessary condition for their existence is that there must be degenerate vacuum states. The soliton solution has different vacua at the boundaries. Thus the boundary condition at infinity for a soliton state is topologically different from that of the physical vacuum state. The stability of the topological soliton against decay into plane waves is ensured because of the different boundary conditions. Some of these solitons are cosmic walls, cosmic strings and magnetic monopoles (in 1, 2 and 3-space dimensions respectively) ¹²);

ii) Non Topological Solitons: the boundary condition at infinity for NTS's are the same as that for the physical vacuum state (there is no need for degenerate vacuum states, then). The necessary condition for their existence is that there should be an additive conservation law. The simplest such conserved additive charge corresponds to a particle number N . Thus one needs at least a complex bosonic or fermionic field, ϕ or ψ , such that ϕ , or ψ , carry $N=+1$ while ϕ^+ , or ψ^+ , carry $N=-1$, and $N \equiv dN/dt = 0$, i.e. the number of particles is conserved. Let us consider a soliton with conserved charge N and a set of plane waves (free particles) with equal charge, N . The stability of the N.T.S. depends on which solution has lower energy. Only if the energy of the N.T.S. is lower than the energy of a set of free particles with the same charge, the N.T.S. is stable. The NTS solutions can also (as the topological solitons) exist in any space dimensions.

Let us consider "soliton stars" ⁷⁾. The models, studied by T.D. Lee and collaborators, have a conserved particle number N carried either by a fermion or a boson field. This complex field is coupled to a bosonic real field σ . The real field has a potential, $U(\sigma) = (\frac{1}{2})m^2\sigma^2(1-\sigma/\sigma_0)^2$, with two degenerate vacua at $\sigma=0$ and $\sigma=\sigma_0$, which distinguish the outside and the inside of the NTS. An NTS is thus a bag with the σ_0 vacuum and N particles confined inside, the $\sigma=0$ vacuum outside and a wall where σ grows from 0 to σ_0 . The function of the σ field is simply to confine the N carrying particles inside the soliton. This is achieved if these particles have a σ -dependent mass, in such a way that they are massless inside the soliton and massive outside. The presence of the N particles confined inside the soliton is essential for its stability. Let us take, as an example, the case of a complex bosonic field ϕ . The total energy of the soliton consists of two contributions: the kinetic energy of the N -particles confined inside, $E_k = \pi N/R$, where R is the radius of the soliton (consider it as spherical) and the energy contained in the walls, $E_w = 4\pi sR^2$, where s is the mass of the wall per unit of area, $s \approx m \sigma_0^2 / 6$. The minimum energy, M , is obtained by varying the radius R , $(dE/dR) = 0$, with $E = E_k + E_w$. It is easy to see that, at the minimum, $M \sim N^{2/3}$. Since N free particles have an energy proportional to N , we see that for a large enough value of N , the energy M of the NTS is lower than that of a collection of free particles with equal N (i.e. the NTS is stable). A remarkable property of these NTS is their critical mass M_c , the mass necessary for the NTS to have the Schwarzschild radius, $R \approx 2 G M_c$, is of the order $M_c \approx M_p^4 / m^3$ where M_p is the Planck mass, $M_p \approx 10^{19}$ GeV. As an example, with $m \approx 3$ GeV, then $M_c \approx 10^{18} M_\odot$ (M_\odot is a solar mass) with $R \approx 10^5$ ly. For masses larger than M_c the NTS forms a black hole. These values M_c should be compared with approximately $5 M_\odot$ the maximum M_c allowed for usual stellar bodies. NTS "stars" may be much larger than usual stars without becoming black holes⁷⁾. In the case the $\sigma = \sigma_0$ vacuum

inside the soliton, has a positive vacuum energy density Λ with respect to the $\sigma=0$ vacuum outside, a volume contribution to the energy, $E_v = 4\pi \Lambda R^3/3$, should be added to the total energy. If this term is dominant with respect to E_w , as it is for sufficiently large N , the minimum energy is $M \sim N^{3/4}$, and in this case $M_c \sim M_p^3/\sqrt{\Lambda}$. This is the case considered below. A non degeneracy of the vacua inside and outside, $\Lambda > 0$ below, is necessary to form these NTS in a second order phase transition in the early universe [1]. The universe as a whole goes, then, to the "true" vacuum (the vacuum outside the NTS) leaving islands of the "false vacuum" (the vacuum inside the NTS), that are stabilized due to the presence of a sufficiently large number N of ϕ particles confined inside. Let us consider, then, the potential

$$U(|\phi|, \sigma) = \frac{\lambda}{8} (\sigma^2 - \sigma_0^2)^2 + h|\phi|^2 (\sigma - \sigma_0)^2 + \frac{\lambda}{3} (\sigma - \sigma_0)^3 \sigma_0 + \Lambda$$

The constant Λ is adjusted to have $U=0$ at the absolute minimum of the potential.

The formation of NTS in the early universe is, then, a problem of percolation of two vacua. As the temperature of the universe lowers below a critical temperature T_c , regions of space of characteristic size $V_\xi = 2\xi^3$, where ξ is the correlation length, fall into one of the two σ -minima, call them σ_0 and σ_1 (for "outside" and "inside"), with probabilities p_0 and p_1 . Evidently, if the two minima were degenerate, these probabilities would be equal $p_0=p_1=0.5$. With $\Lambda > 0$, σ_0 starts to be favoured, thus $p_0 > p_1$ (always $p_0+p_1=1$, of course). Actually, the values of p_0 and p_1 are not fixed at T_c , where the regions V_ξ fluctuate rapidly between $\sigma = \sigma_0$ and $\sigma = \sigma_1$. The probabilities remain fixed only at the Ginsburg temperature, T_G , at which these fluctuations freeze out. At $T_c \geq T \geq T_G$ the thermal transition rate of fluctuation of a volume V_ξ between the two minima is proportional to $\exp(-F_M/T)$, where $F_M = U_M V_\xi$ is the free energy of the fluctuations from one of the vacua to the maximum of the potential, U_M being the energy barrier that separates both vacua. As long as Γ is large, both vacua are in equilibrium and the relative population is given by the Boltzman formula, $p_1/p_0 = \exp(-\Delta F/T)$ where ΔF is the difference in free energy between a volume V_ξ of the σ_0 -vacuum and the same volume of the σ_1 -vacuum, $\Delta F = (U_0 - U_1) V_\xi$, (U_0, U_1 are the respective energy densities). For any temperature $T < T_G = F_M$, the rate Γ becomes exponentially small and each V_ξ remains in one of the two vacua definitively, with probability

$$p_1/p_0 = \exp(-\Delta F(T_G)/T_G) = \exp(-\Lambda/U_M)$$

The last equality holds when $U_0 - U_1 = \Lambda$, approximating the potential at T_G by the $T=0$ potential given above.

Lattice simulations show that if the probability of occupation per cell, p , is larger than a critical value, p_c , then an infinite cluster of those cells forms, while for $p < p_c$ only finite clusters do¹³⁾. In three space dimensions $p_c \approx 0.2$ to 0.3 , having different values for different types of lattice. For example $p_c = 0.31$ for a simple cubic lattice. When an infinite cluster forms it is said that the corresponding vacuum "percolates". Given the last value of p_c , the "false vacuum", σ_i , percolates whenever $\Lambda/U_M \leq 0.8$, what occurs when $\lambda_2/\lambda_1 \leq 0.13$. There are, then, two different scenarios, in one of them both vacua percolate, in the other only the "true vacuum", σ_0 , percolates. We consider only the cases with $\Lambda > 0$. If $\Lambda = 0$ ($h = \lambda_2 = 0$), the case of exact degeneracy, both vacua percolate, creating two infinite (and many finite) regions, with stable domain walls separating them. These walls soon dominate the energy density of the Universe, leading to contradictions with the observed isotropy of the cosmic background radiation (unless $\sigma_0 \leq 10\text{MeV}$)¹⁴⁾. Even a small energy density difference $\Lambda > 0$ causes regions of false vacuum to shrink, leading to the disappearance of the wall system^{12,15)} with the Universe everywhere in the true vacuum (that we want to be σ_0). There will still be isolated islands of the false vacuum, stabilized by the presence of a sufficiently large number N of ϕ -particles inside, that will be the NTS. This may happen in both scenarios.

First consider the case where $p_i < 0.31$. Since this is below percolation threshold, isolated bags of false vacuum are formed in the true vacuum "sea". If r is the number of false vacuum cells in a cluster ($r \approx (L/2\xi)^3$, where L is the cluster "diameter"), the density of r -clusters per lattice site is known¹³⁾ from Monte Carlo simulations to be $f(r) = br^{-1.5} \exp(-cr)$. The constants b and c are not known but are expected to be $b, c \approx 1$. The number density of r -clusters produced at $T = T_G$ is then simply $n(r) = f(r)/V_\xi$. Thus, the typical size of a false vacuum bubble is $L \sim 2\xi$, with larger bubbles exponentially suppressed.

Once formed the bubbles will be acted upon by several forces: 1) a surface tension due to the domain walls which tends to straighten out curved walls; 2) a vacuum pressure $p_{\text{vac}} = \Lambda$, which acts to collapse regions of false vacuum; 3) a thermal pressure p_ϕ due to the massless ϕ 's in the false σ_i (assuming these particles are confined) which tend to expand regions of this vacuum. The evolution of the system of domain walls and vacuum bubbles is quite complicated, and the dynamics depends upon ratios of coupling constants λ_1, λ_2 , and h . To elucidate a scenario for production of NTSs, we will assume two conditions are satisfied: (i) T_G is smaller than the mass of ϕ particles in the σ_0 vacuum (h is not too small), so that ϕ particles are trapped inside the σ_i domains at the Ginzburg temperature; (ii) $p_\phi = (\pi^2/45)T_G^4 \leq p_{\text{vac}} = \Lambda$, (i.e., λ_2 is not too

small) so that the thermal pressure due to the massless ϕ 's in the domain is always smaller than the vacuum pressure. (If condition (ii) is not satisfied, the σ_i domain will grow and possibly percolate; for this case, see the discussion below.) Given (i) and (ii), σ_i domains formed in the transition with $N \geq N_{\min}$ will survive to form stable NTSs, while those with $N \leq N_{\min}$ will evaporate and disappear. Since large domains of σ_i vacuum are exponentially rare for $p_i < p_c$, to first approximation the only surviving domains have $N = N_{\min} \cdot N_{\min}$, the minimum number of particles so that the NTS is stable, can be computed and with it, the present energy density of NTSs, can be computed¹¹.

The typical number of relativistic ϕ particles inside an r-cluster is $N(r) = r \eta_{\text{eff}} n_\phi V_\xi$, where η_{eff} is the effective excess ratio of particles over anti-particles and at T_G , $n_\phi \approx \zeta(3) T_G^3 / \pi^2$. Setting $N(r_{\min}) = N_{\min}$ gives $r_{\min} = N_{\min} \lambda_1^3 / \eta_{\text{eff}}$. We find the ratio between the number density of NTSs with $N(r_{\min})$ produced at the Ginzburg temperature to the entropy density $s = 2\pi^2 g_* T_G^3 / 45$ (with $g_* = 100$), and from it the present energy density of NTSs (with $N = N_{\min}$), $\rho_{\text{NTS}} = M_{\min} n(N_{\min})$. It contributes a fraction of closure density

$$\Omega_{\text{NTS}} h_0^2 = 5 \times 10^9 b \left(\frac{\eta_{\text{eff}}}{\lambda_1} \right)^{3/2} N_{\min}^{-3/4} \left(\frac{\Lambda}{\text{TeV}^4} \right)^{1/4} \exp[-c N_{\min} \lambda_1^3 / \eta_{\text{eff}}],$$

where h_0 reflects the uncertainty in the Hubble constant ($1 \geq h_0 \geq 1/2$). For example, if we set $b = c = 1$ and, take $\lambda_2 / \lambda_1 = 0.15$, then $N_{\min} = 18 \lambda_1 / h^2$ and the corresponding mass and radio are $M_{\min} = 46 (\lambda_1 / h^{3/2}) \sigma_0$, $R_{\min} = 1.7 h^{-1/2} \sigma_0^{-1}$. We consider two possibilities: a) If the effective asymmetry is comparable to the baryon asymmetry ($\eta_{\text{eff}} = 10^{-9}$) for the NTS density in the range $2 \times 10^{-3} \leq \Omega h_0^2 \leq$, we find the constraint $1.7 \times 10^{-5} \leq (\lambda_1^2 / h) \leq 2.5 \times 10^{-5}$ for $\sigma_0 = 1 \text{ TeV}$, and $4.2 \times 10^{-5} \leq (\lambda_1^2 / h) \leq 4.6 \times 10^{-5}$ for $\sigma_0 = 10^{12} \text{ TeV}$. The corresponding masses are $M_{\text{NTS}} = 0.2 h^{-1} \text{ TeV}$ and $M_{\text{NTS}} = 3 \times 10^{11} h^{-1} \text{ TeV}$. b) If $\eta_{\text{eff}} = 1$, for the NTS density to lie in the above range requires $1.0 \leq (\lambda_1^2 / h) \leq 1.2$ for $\sigma_0 = 1 \text{ TeV}$, and $1.6 \leq (\lambda_1^2 / h) \leq 1.7$ for $\sigma_0 = 10^{12} \text{ TeV}$. We note that since the density is exponentially sensitive to the ratio for fixed η_{eff} the range of parameter space for cosmologically significant NTSs is rather narrow. By the same token, the mass scale σ_0 required to produce abundant NTSs is essentially unconstrained.

Next we consider the case where both the vacua percolate, $0.31 < p_i < 0.69$. The Universe will be composed primarily of two interlocking infinite domains of complicated topology. The typical distance between the walls (the volume to surface ratio), as well as the typical curvature radius, is initially $L(t) = 2\xi(T_G)$.

We assume the early motion of the walls is dominated by the surface tension, which acts to rapidly (compared to the expansion time) increase the wall separation $L(t)$, until the vacuum pressure becomes comparable to the surface pressure, when $L(t) = L_0$. At this point, the vacuum pressure begins to accelerate

the walls into the false vacuum regions; since the curvature radius is of order the mean wall separation, the infinite σ_i domain will initially be pinched off into a series of finite σ_i bubbles of typical size L_o . The trapped charge in a typical bubble is thus $N(L_o) \simeq (4\pi/3)L_o^3 n_\phi(T_G)$. It can be computed ¹⁾ that $N(L_o)$ will be larger than N_{\min} if $h\lambda_1^3 \eta_{\text{eff}}^{1/2} / \lambda_2^2 \geq 160$. From condition (i) h must not be too small. We also note that if h is much larger than λ_1 and λ_2 , quantum corrections driven by the $h|\phi|^2 (\sigma - \sigma_o)^3 \sigma_o$ term might drastically change the form of the classical potential. To avoid this neither λ_1 nor λ_2 can be much smaller than h , and it is unlikely that the charge inside a bubble of radius L_o will exceed N_{\min} . As in the "below percolation case" stable, NTS will most likely be formed from rare large clusters consisting of many cells. The only qualitative difference in above and below percolation is that the effective cell size above percolation is L_o larger than ξ and r_{\min} , the minimum number of cells necessary for a cluster to have $N \geq N_{\min}$ is correspondingly smaller.

References

- 1) J. Frieman, G. Gelmini, M. Gleiser and E. Kolb, February 1988 preprint (SLAC-PUB-4538, FERMILAB-PUB-88/13-A).
- 2) G. Rosen, J. Math. Phys. **9**, 996 (1968).
- 3) R. Ruffini and S. Bonazzola, Phys. Rev. **187**, 1767 (1969).
- 4) R. Friedberg, T.D. Lee and A. Sirlin, Phys. Rev. **D13**, 2739 (1976); Nucl. Phys. **B115**, 1 (1976); **B115**, 32 (1976); R. Friedberg and T.D. Lee, Phys. Rev. **D15**, 1694 (1976).
- 5) E. Witten, Phys. Rev. **D30**, 272 (1984).
- 6) S. Coleman, Nucl. Phys. **B262**, 263 (1985).
- 7) T.D. Lee, Phys. Rev. **D35**, 3637 (1987); R. Friedberg, T.D. Lee and Y. Pang, Phys. Rev. **D35**, 3640 (1987); **35**, 3658 (1987); T.D. Lee and Y. Pang, Phys. Rev. **D35**, 3678 (1987); J.J. van der Bij and M. Gleiser, Phys. Lett. **194B**, 482 (1987).
- 8) B. Holdom, Phys. Rev. **D36**, 1000 (1987).
- 10) T.D. Lee, *Particle Physics and Introduction to Field Theory*, Harwood Academic Publisher, Chapter 7 (1981) and Phys. Rep. **23C**, 254 (1976).
- 11) A.C. Scott, F.Y.F. Chu and D.W. McLaughlin, Proc. IEEE **61**, 1443 (1973).
- 12) A. Vilenkin, Phys. Rep. **121**, 263 (1985).
- 13) D. Stauffer, Phys. Rep. **54**, 1 (1979).
- 14) Ya. B. Zel'dovich, I. Yu. Kobzarev and L.B. Okun, Zh. Eksp. Teor. Fiz. **67**, 3 (1974) [Sov. Phys. - JETP **40**, 1 (1975)].
- 15) T.W. Kibble, J. Phys. **A9**, 1387 (1986); P. Sikivie, Phys. Rev. Lett. **48**, 1156 (1982).

**VIII. STELLAR EVOLUTION
AND DARK MATTER (WIMPS)**



A Stellar Probe of Dark Matter Annihilation in Galactic Nuclei

Pierre Salati * †

*Department of Astronomy
University of California
Berkeley, California 94720*

Abstract

We investigate the evolution of main sequence stars which are embedded within a highly concentrated cloud of annihilating dark matter. Massive stars are not affected, but low mass stars are shifted to the red region of the Hertzsprung-Russell diagram. Stars inflate and become completely convective, moving upwards along the Hayashi track as if they were red giant stars, with their effective temperature dropping and their luminosity increasing. The required dark matter density is $\geq 10^6$ times that in the halo near the sun : such a high density could, and in certain models of galaxy formation should, be present in galactic nuclei. The formation of such nuclei in the early universe results in strongly enhanced baryonic dissipation : if the baryons fragment to form stars, the stellar collision cross-section is increased. The enhanced stellar collision rate means that formation of a central massive object, presumably a black hole, is likely to be inevitable. Independently of the mass of the dark matter particles, low mass stars can provide a unique probe of its degree of concentration.

*Miller Research Fellow at the University of California at Berkeley; also at LBL.

†On leave of absence from Laboratoire d'Annecy le Vieux de Physique des Particules, Chemin de Bellevue, BP 909, 74019 Annecy le Vieux Cedex, France and also from Université de Chambéry, 73000, Chambéry, France.

1. INTRODUCTION

Cold dark matter (CDM) denotes a generic species of weakly interacting particles that has been invoked to account for the matter density predicted by inflation. Inflationary cosmology predicts the spectrum of primordial density fluctuations. With CDM, these have provided a quantitative reconciliation of diverse observations of large scale structure, including the galaxy correlation function, the galaxy cluster distribution, the parameters of galaxy halos, galaxy peculiar velocities, and the isotropy of the microwave background. A direct test of the existence of CDM, and identification with a specific candidate particle, is therefore of considerable urgency. In what follows, we assume the CDM particles are massive relics of the early universe, and will not discuss the axion (a low mass option for CDM) : candidates include the lightest SUSY particle (e.g. photino or higgsino), massive neutrino, or more exotic relics from grand unification. These particles attain their present density via annihilation at very early epochs. Annihilations still occur today, albeit at a much slower rate, and the aim of this paper is to describe how CDM annihilation may modify stellar evolution in regions of high density CDM.

To commence, we note that galaxy formation in a CDM-dominated universe most probably results in production of a dense nucleus. We estimate the maximum density attainable in three ways.

Firstly, we note that density fluctuation growth effectively commences at the epoch of equality of matter and radiation densities, $1 + z_{eq} = 4 \cdot 10^4 \Omega h^2$. If non-linear seeds are present, such as expected in cosmic string or in isocurvature scenarios for galaxy formation, the collapse of the first shells of dark matter results in a density $\leq 200 \rho(z_{eq}) \sim 1.5 \times 10^{11} \Omega^4 h^8 \text{ GeV cm}^{-3}$. Cosmic string theory yields a dimension of $1 \sim 10$ pc for the loops that seed typical massive galaxies : this therefore represents the scale on which collapse first occurred. Subsequent accretion may tend to dilute this central density, especially if mergers occur between different condensation sites.

Secondly, we may note that collapse of sufficiently cold matter necessarily results in formation of a dense core. This is true for quasispherical collapse, and the final core density depends on the ratio of the initial thermal to potential energies $T_i/|W_i|$. According to numerical simulations by McGlynn (1984), $\rho_{core} \propto (T_i/|W_i|)^{-3}$. Since the final core satisfies $T/|W| = \frac{1}{2}$, we infer that the core density enhancement is $\sim 0.1 (T_i/|W_i|)^{-3}$. One might reasonably expect $T_i/|W_i| \sim 0.01$, corresponding to $v_i/\sigma_i \sim 0.1$ or $v_i \sim 20 \text{ km s}^{-1}$ for a protogalaxy, where v_i is the initial thermal speed and σ_i the initial escape velocity. Numerical simulations of tidal interactions between aggregates of mass points in an expanding universe find that $v_m/\sigma_i \sim 0.06$, where v_m is the maximum rotational velocity. In general, we would expect vortical and shearing motions to be comparable, so that $v_i \sim v_m$. Hence core enhancement by $\sim 10^5$ in density is not implausible for CDM collapse. With core

formation occurring at $z \leq 10$, as expected in the standard CDM model, one obtains $\rho_{core} \sim 10^5 \rho_i$ with $\rho_i \leq 200\rho(z \sim 10)$, or $\rho_{core} \sim 2.10^5 \Omega h^2 GeV cm^{-3}$. The core radius is $a_{core} \sim 2(T_i/|W_i|)a_i$, where a_i is the initial core radius : with $a_i \sim 10 kpc$, we obtain $a_{core} \sim 200 pc$. These parameters are consistent with the observed bulge of our galaxy : mass models yield a core density $\leq 200 M_\odot pc^{-3} \sim 8000 GeV cm^{-3}$ within the $\sim 150 pc$ core, and a substantial fraction of this density may be dark matter. Other galaxies with more luminous spheroids should have denser cores.

Thirdly, one can estimate the maximum CDM density attainable, subject to the restriction that annihilation is only just being initiated by the present epoch. The annihilation rate is known once the cosmological density of CDM is specified :

$$\langle \sigma v \rangle = 10^{-26} \Omega_x^{-1} cm^3 s^{-1}. \quad (1)$$

This rate is generic to any weakly interacting particle species. If we require the annihilation time of particles of mass m_x (in GeV) to exceed a Hubble time, we infer an upper bound on ρ_x , namely

$$\rho_x \leq m_x H_0 \langle \sigma v \rangle^{-1} \sim 3.10^8 m_x h GeV cm^{-3}. \quad (2)$$

Hence with $m_x \sim 10^3 GeV$, CDM densities of up to $\sim 10^{11} GeV cm^{-3}$ are attainable within a parsec-size core. With m_x in the $\leq 10 GeV$ range that most current detection schemes require, a CDM density of $\leq 10^9 GeV cm^{-3}$ is possible. Galaxy nucleus formation at $z \leq 30$ suggests $\rho_x \sim 10^7 GeV cm^{-3}$. One may compare these estimates with the solar neighborhood halo density of $\sim 0.3 GeV cm^{-3}$. Within our own galaxy, the paucity of low energy cosmic ray antiprotons suggests that $m_x \geq 6 GeV$, while the lack of a CDM associated galactic centre gamma ray flux argues that $\rho_x \leq 10^3 GeV cm^{-3}$ if $m_x \leq 10 GeV$ in the galactic bulge.

Nevertheless, much higher densities of CDM are possible in other galaxies. For example in M 31, there is strong evidence, unlike the situation for our galactic centre, for a central mass concentration within the inner 2 pc. While a $\sim 10^7 M_\odot$ black hole is one possible explanation, we will consider here the alternative that a central CDM cloud of densities $\sim 10^6 M_\odot pc^{-3}$ or $3.10^7 GeV cm^{-3}$ is present. More extreme CDM densities are clearly possible in nuclei where higher central masses are indicated. If the central black holes believed to power active nuclei were present at an early epoch in the universe, as observations of quasars at $z \geq 4$ suggest, the dissipative matter from which they formed could plausibly have left behind a dense relic cloud of CDM.

Our purpose (Salati and Silk, 1987) is to study the modification of stellar evolution within such dense clouds of slowly annihilating CDM. We shall show that stars catalyze the annihilation rate. This leads to observable consequences on the evolution of low mass

stars, as viewed in the cumulative light from distant galactic nuclei. Section 2 describes the evolution of a single star in the presence of an extreme concentration of CDM. In section 3, we describe a dynamical scenario for the evolution of a galactic nucleus containing stars and CDM.

2. INTERACTION OF A STAR WITH A HIGH CONCENTRATION OF ANNIHILATING DARK MATTER

In this section, we investigate the effects on main sequence stars of a large concentration of annihilating CDM. Our aim is to determine the evolution in the Hertzsprung-Russell diagram experienced by these stars. We approximate the structure of a main sequence star by a $n = 3$ polytropic model. In this scheme, once the mass of the star is fixed, all the relevant stellar quantities such as the central density ρ_c or the central temperature T_c only depend on the stellar radius. The stellar radius itself is not a free parameter since it is determined by the balance between the energy producing mechanisms and heat losses.

A. Energy production

The main source of energy for a star is obviously nuclear energy. For main sequence stars, both the pp chain and the CNO cycle come into play, and the energy production rate may be approximated by :

$$\epsilon_{nuc} = 0.6X_H^2 \rho \left(\frac{T}{1.5 \cdot 10^7 K} \right)^4 + 451X_H X_{CNO} \rho \left(\frac{T}{2 \cdot 10^7 K} \right)^{18} \text{ erg g}^{-1} \text{ s}^{-1}. \quad (3)$$

The first term on the right hand side refers to the pp chain, the second one to the CNO cycle. The pp chain is dominant for low mass stars. However, due to the strong temperature dependence, the CNO cycle overcomes the pp chain for massive stars. ϵ_{nuc} has to be integrated throughout the star in order to obtain the total nuclear luminosity :

$$L_{nuc} = \int_0^R 4\pi r^2 \rho(r) \epsilon(r) dr; \quad (4)$$

performing this integration for a $n = 3$ polytrope leads to :

$$\frac{L_{nuc}}{L_\odot} = 8.2X_H^2 \mu^4 \beta^4 \left(\frac{M}{M_\odot} \right)^6 \left(\frac{R_\odot}{R} \right)^7 + 368X_H X_{CNO} \mu^{18} \beta^{18} \left(\frac{M}{M_\odot} \right)^{20} \left(\frac{R_\odot}{R} \right)^{21}. \quad (5)$$

In this expression, μ is the mean molecular weight and β is the gas pressure to total pressure ratio which, for the $n = 3$ polytropic model, is assumed to be constant throughout the star.

The second energy source for the star is provided by the annihilation of CDM in the stellar core. When a star is trapped inside a very dense cloud of dark matter, it continuously captures CDM which accumulates in the stellar core and subsequently annihilates. A steady state is soon reached and equating the capture rate :

$$\Gamma_{\text{Capture}} = 10^{32} \text{ s}^{-1} \left(\frac{\rho_x}{1 M_\odot / \text{pc}^3} \right) \left(\frac{m_p}{m_x} \right) \left(\frac{300 \text{ km/s}}{V_x} \right) \left(\frac{M}{M_\odot} \right) \left(\frac{R}{R_\odot} \right) \times$$

$$\times \left\{ 1 + 0.16 \left(\frac{V_x}{300 \text{ km/s}} \right)^2 \left(\frac{M_\odot}{M} \right) \left(\frac{R}{R_\odot} \right) \right\} \text{Min} \left(1, \frac{\sigma_s M}{\sigma_\odot M_\odot} \left(\frac{R_\odot}{R} \right)^2 \right) \quad (6)$$

to the annihilation rate leads to the cosmion energy production rate :

$$\begin{aligned} \frac{L_x}{L_\odot} &= 4 \cdot 10^{-5} \left(\frac{\rho_x}{1 M_\odot / \text{pc}^3} \right) \left(\frac{M}{M_\odot} \right) \left(\frac{R}{R_\odot} \right) \left[1 + 0.16 \left(\frac{R}{R_\odot} \right) \left(\frac{M_\odot}{M} \right) \right] \times \\ &\times \text{Min} \left(1, \frac{\sigma_s M}{\sigma_\odot M_\odot} \left(\frac{R_\odot}{R} \right)^2 \right). \end{aligned} \quad (7)$$

Here σ_s is the scattering cross section of CDM particles off protons and $\sigma_\odot = 4.10 \cdot 10^{-36} \text{ cm}^2$ is the critical value of the cross section which corresponds in the case of the sun to a cosmion mean free path of the order of a solar radius. For large concentrations of cosmions, L_x turns out to be the dominant energy production luminosity.

B. Energy losses

Most stars on the main sequence have a substantial part of their structure governed by radiative losses. The luminosity of a star is dominated by the energy transport inside the outermost radiative layers. The global radiative luminosity is given by :

$$L_{\text{rad}}(\text{total})^{-1} = L_{\text{rad}}(\text{Kramers})^{-1} + L_{\text{rad}}(\text{electronic})^{-1} \quad (8)$$

with

$$\frac{L_{\text{rad}}(\text{Kramers})}{L_\odot} = \frac{0.57 (\mu\beta)^{7.5} \left(\frac{M}{M_\odot} \right)^{5.5} \left(\frac{R_\odot}{R} \right)^{0.5}}{(1 + X_H) \{ Z + 2.54 \cdot 10^{-3} (1 - Z) \}} \quad (9)$$

and

$$\frac{L_{\text{rad}}(\text{electronic})}{L_\odot} = \frac{160 (\mu\beta)^4 \left(\frac{M}{M_\odot} \right)^3}{(1 + X_H)}. \quad (10)$$

For low mass stars, the radiative luminosity is supplemented by convective losses from the surface. Assuming that the stellar surface has a low density, we have fitted the main sequence and obtained :

$$\frac{L_{\text{conv}}}{L_\odot} = 4.10^{-2} \left(\frac{M}{M_\odot} \right)^{0.356} \left(\frac{R}{R_\odot} \right)^{1.289}. \quad (11)$$

The energy production and loss rates reduce to functions of the stellar radius R which may be determined by solving the equation :

$$L_{\text{nuc}} + L_x = L_{\text{rad}} + L_{\text{conv}}. \quad (12)$$

Once the radius R has been determined, the effective temperature, one of the observable parameters, is given by :

$$T_{\text{eff}} = 5796 \text{ K} \left(\frac{L}{L_\odot} \right)^{0.25} \left(\frac{R_\odot}{R} \right)^{0.5}. \quad (13)$$

We have computed the luminosity and effective temperature of stars on the main sequence, and we have studied the dependence of these quantities on the dark matter abundance ρ_x . The stellar masses which we have considered range from $0.05 M_\odot$ up to $100 M_\odot$. We have varied the density of dark matter from 0 up to $10^6 M_\odot \cdot pc^{-3}$. Our results are displayed in the Hertzsprung-Russell diagram (Fig.1). Depending on the concentration of cosmions, we may distinguish two regimes :

- The standard situation is recovered for low concentrations of dark matter. In this case, the source of energy is provided by the nuclear reactions while the star loses energy through radiative transport. The stellar radius is obtained from :

$$L_{nuc} = L_{rad} . \quad (14)$$

- On the other hand, for large concentrations of dark matter, the annihilations of the cosmions trapped inside the core provide the star with a huge amount of heat. The star is unable to radiate away this additional energy and therefore inflates. As the stellar radius increases, the nuclear energy generation drops and vanishes as expected from the $(R/R_\odot)^{-4}$ (pp chain) and $(R/R_\odot)^{-21}$ (CNO cycle) dependence. Moreover, the star becomes convective. It stops inflating when the convective losses eventually overcome the CDM annihilation production of energy. In this regime, the stellar radius is given by :

$$L_x = L_{conv} . \quad (15)$$

In the absence of dark matter, we recover the standard main sequence. However as soon as ρ_x is increased, the main sequence departs from its standard location in the HR diagram. As can be seen from Figure 1, only the low mass stars are affected and accumulate along a vertical path which is just the Hayashi track. For large concentrations of dark matter, relation (15) leads to :

$$\frac{R}{R_\odot} = 1.1 \cdot 10^{-3} \left(\frac{\sigma_s}{\sigma_\odot} \rho_x \right)^{0.776} \left(\frac{M}{M_\odot} \right)^{0.5} , \quad (16)$$

which in turn implies that :

$$T_{eff} = 8750 K \left(\frac{\sigma_\odot}{\sigma_s \rho_x} \right)^{0.14} . \quad (17)$$

Therefore, in this regime, the effective temperature does not depend on the stellar mass and only exhibits a weak dependence on the cosmion density ρ_x .

- For $\rho_x \sim 10^4 M_\odot pc^{-3}$, we find that the structure of stars less massive than $\sim 0.5 M_\odot$ is significantly modified. These low mass stars gather along a vertical path in the HR diagram with a surface temperature ~ 2400 K and a luminosity enhancement of ~ 4 .

- For $\rho_x \sim 10^6 M_\odot \text{pc}^{-3}$, the structure of stars up to a mass $\sim 2 M_\odot$ is strongly modified. Their effective temperature drops to 1260 K and their luminosity is enhanced by ~ 200 .

3. ANNIHILATING DARK MATTER AND THE GALACTIC NUCLEUS

A star embedded within a highly concentrated cloud of annihilating dark matter strongly reacts by shifting upwards along the Hayashi track and becoming convective. We analyze now the effects of a highly concentrated dark matter core on the nucleus of the galaxy itself.

A. Stellar collisions.

Such a core initially contains a non-negligible amount of baryons which presumably condense into stars. An alternative is dissipation and collapse to form a central black hole. We shall show that even if the baryon matter fragments into stars, as seems more likely, the same fate awaits them : black hole formation is inevitable. What are the reactions of stars which have been embedded inside the DM cloud since its formation ? We have already described the behaviour of an individual star but we would like to address now the more general problem of the evolution of an entire stellar population.

To commence, we must determine the collision time t_{BHF} of these stars among themselves. Such collisions would disrupt the stars and induce collapse of the gas to form a central black hole. Stars which have formed inside the DM cloud are strongly affected by the presence of annihilating dark matter and behave as described in section 2. In particular, their radii increase according to relation (16). Therefore, the probability that they collide with each other is much greater than in ordinary galactic nuclei, leading to a fairly short collision time :

$$t_{BHF} = 2.10^{10} \left(\frac{\sigma_\odot}{\sigma_s} \right)^{1.552} M_8^{-1/3} \rho_6^{-2.72} \text{ yr} . \quad (18)$$

The mass of the core is estimated to be 10^7 - $10^8 M_\odot$ and is parametrized here by $M_8 10^8 M_\odot$, and ρ_6 is the core density expressed in units of $10^6 M_\odot \text{pc}^{-3}$. For simplicity, we have assumed that the stars of the galactic core contribute 1% to its total mass (our conclusions are independent of this assumption). The collision time is less than the age of the galaxy provided the dark matter density satisfies $\rho_6 \geq 1$. Then, we must compare t_{BHF} with the typical time t_{ann} associated with the annihilation of the dark matter core :

$$t_{ann} = 8.3 \times 10^{10} \left(\frac{m_x}{1 \text{ GeV}} \right) \left(\frac{10^{-26} \text{ cm}^3 \text{ s}^{-1}}{\langle \sigma_a v \rangle} \right) \rho_6^{-1} \text{ yr} . \quad (19)$$

The previous relations show that t_{BHF} depends much more sensitively than does t_{ann} on ρ_6 . In addition, for typical collision times less than the age of the universe, t_{ann} always is longer than t_{BHF} . Therefore, we are led to distinguish two regimes, depending on the dark matter density :

(1) - For $\rho_6 \leq 1$, stars embedded inside the dark matter core do not collide and have survived since their formation. As they formed, they accreted dark matter particles and

have until now been the seeds where CDM annihilation has been catalyzed. These objects have always been convective and appear today as red giant stars, located on a vertical path in the HR diagram. This is why they may provide us with a unique probe of the presence of annihilating dark matter at the centre of galaxies. We conclude that the observation of galactic cores and their luminosity to effective temperature relationship could provide us with an experimental test for the existence of annihilating dark matter. Note that this tests generic cold dark matter (other than sneutrinos), regardless of the candidate particle mass.

(2) - For $\rho_6 \geq 1$, stars borne in the galactic nucleus efficiently collide among themselves. The presence of such a high concentration of dark matter within the galactic core, by increasing the stellar radii, greatly enhances the collision rate of low mass stars. Many models of massive black hole formation rely on a high collision rate between stars to initiate the dissipation of matter and accelerate the collapse process (Shapiro and Teukolsky 1985). However the initial density required of stars is unrealistically high. A dark matter concentration in the early universe provides an alternative scheme for accelerating the stellar collision rate at a relatively modest density, similar to stellar densities in galactic nuclei and therefore not unexpected for any entrained dark matter component. Hence a high concentration of dark matter might trigger the formation of a black hole in the centres of galaxies. Despite its weak interaction with baryons, dark matter might therefore induce the formation of a giant black hole in galactic cores where the dark matter density exceeds the critical value $\rho_6 \sim 1$. Hence, annihilating non-baryonic dark matter would not only account for the missing mass in the universe, but could also provide a natural explanation of the massive black holes believed to power the intense activity of many galactic nuclei.

B. Dynamical friction.

We examine now the impact of a galactic core consisting of dark matter on the neighbouring stars. Is a star which crosses the galactic nucleus captured by the ambient dark matter ? Or, if the friction is not sufficient to trap the star, is the intruder at least affected by its travel inside the DM cloud and does it become convective ? To decide these questions, we must determine the typical time-scales that are relevant, namely the dynamical friction time t_f and the Kelvin time t_K , and compare them with the passing time t_p through the galactic core.

- The passing time t_p which is necessary for the star to cross the core is very short :

$$t_{\text{passing time}} = \frac{5140 \text{ yr}}{\rho_6^{1/2}} . \quad (20)$$

- When a star travels across the galactic core and is surrounded by a high concentration of dark matter, it experiences a damping force due both to dynamical friction and direct capture. For very large values of ρ_x up to $\rho_6 \sim 100$, we find that the dynamical friction

time associated with the damping experienced by the star is given by :

$$t_{friction} \sim \frac{5 \cdot 10^{10} M_{\odot}}{\rho_6^{1/2} M} \text{ yr} . \quad (21)$$

The stopping time t_f is much larger than the crossing time t_p . Since t_f exceeds t_p by seven orders of magnitude, any incoming star which crosses the galactic core just passes through as if the dark matter cloud was totally transparent.

• While it crosses the galactic centre, the star continuously captures dark matter particles which concentrate in its core and annihilate. The equilibrium time t_e , necessary for the star to equate the amount of its internal CDM annihilations to the capture rate, may be approximated, for main sequence stars (Bouquet and Salati, 1987), by :

$$t_{equilibrium} \simeq \frac{109}{\rho_6^{1/2}} \left(\frac{\sigma_{\odot}}{\sigma_s} \right)^{1/2} \left(\frac{10^{-26} \text{ cm}^3 \text{ s}^{-1}}{\langle \sigma_{ann} v \rangle} \right)^{1/2} \left(\frac{M}{M_{\odot}} \right)^{0.6} \left(\frac{m_p}{m_x} \right)^{1/4} \text{ yr} . \quad (22)$$

Equilibrium between capture and internal annihilation is therefore rapidly achieved.

• The energy produced by the annihilations is stored in the star which starts to move in the HR diagram. But in order to reach its new equilibrium state, the star must significantly increase its radius and has to wait for the annihilation energy to supplement the gravitational potential energy. The time scale for this process is the Kelvin time t_K , and it takes the star :

$$t_{Kelvin} \simeq \frac{7.9 \times 10^5}{\rho_6} \left(\frac{\sigma_{\odot}}{\sigma_s} \right) \log \left\{ \frac{R_f}{R_i} \frac{1 + 0.16 \frac{M_{\odot} R_i}{M R_{\odot}}}{1 + 0.16 \frac{M_{\odot} R_f}{M R_{\odot}}} \right\} \text{ yr} \quad (23)$$

to increase its radius from R_i to R_f . As t_K exceeds t_p by three orders of magnitude, it is not possible for a star which passes through the CDM galactic core to become convective and be displaced in the HR diagram. A much larger passage time would be necessary to perturb the stellar equilibrium and induce a significant change in the structure of the incoming star.

We therefore conclude that the presence of a highly concentrated core of CDM does not perturb the host galaxy. Neighbouring stars just pass through the galactic centre as if they travelled in empty space. The CDM cloud is unable to capture them. However, as previously shown, the galactic centre is perturbed. Dark matter triggers the formation of a massive black hole at the galactic centre and/or changes the low mass stars into bright red giants. Observations of galactic nuclei and their activity could provide evidence for the presence of dense clouds of annihilating non-baryonic matter.

REFERENCES

Bouquet, A. and Salati, P.; 1987, LPTHE-87-20, LAPP-TH-preprint-192/87, to appear in A&A.

McGlynn, T.; 1984, *Ap.J.*, **281**, 13.

Salati, P. and Silk, J.; 1987, *UCB-Astronomy preprint and LBL-24797*.

Shapiro, S.L. and Teukolsky, S.A.; 1985, *Ap.J.Letters*, **292**, L41.

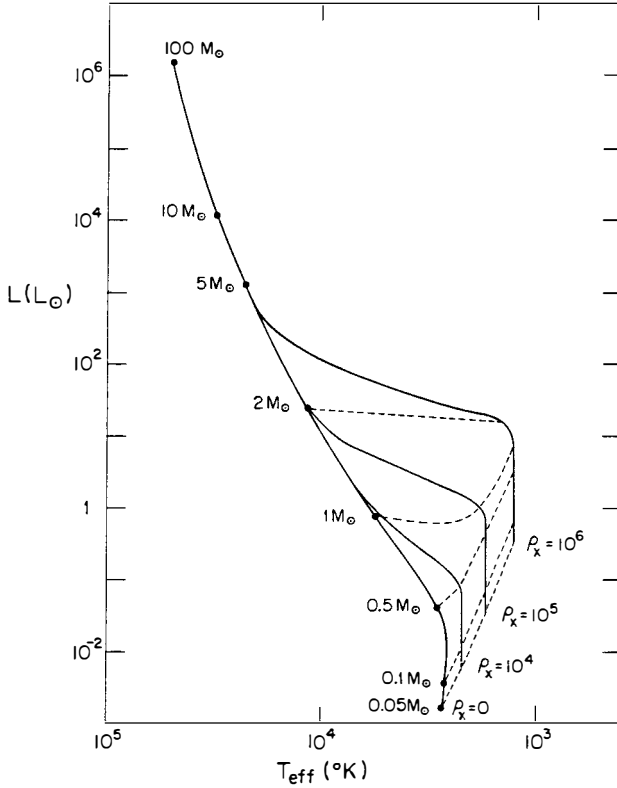


Figure 1

The main sequence is plotted in the Hertzsprung-Russell diagram. The CDM abundance is varied from $\rho_x = 0$ to $\rho_x = 10^6 M_\odot pc^{-3}$. The low mass stars are shifted in the red region of the HR diagram and gather along a vertical path. The transversal dashed lines correspond to the evolution of stars of different mass ($0.05 M_\odot$, $0.1 M_\odot$, $0.5 M_\odot$, $1 M_\odot$ and $2 M_\odot$) depending on the concentration ρ_x of dark matter.

WIMPS AND STELLAR STRUCTURE

Alain Bouquet

LPTHE, Université Paris VII, 75251 PARIS Cedex 05, France
and LAPP, BP909, 74019 ANNECY LE VIEUX Cedex, France

Jean Kaplan and François Martin

LPTHE, Université Paris VII, 75251 PARIS Cedex 05, France

Pierre Salati

LBL, University of California, BERKELEY, USA
and LAPP, BP909, 74019 ANNECY LE VIEUX Cedex, France



presented by A. Bouquet

ABSTRACT : We present the results of an analytic approximation to compute the effects of WIMPs on stellar structures in a self-consistent way. We examine in particular the case of the Sun and of horizontal branch stars.

1- Dark matter and the solar neutrino problem

It was suggested ^{1-10]} that dark matter could solve the long standing neutrino problem. The idea goes as follows : particles constituting the dark matter present ^{11]} in the halo of our Galaxy may be trapped when they cross the Sun, and accumulate in the course of time. Their number remains quite small, less than one per 10^{10} nuclei, nevertheless they can carry enough energy out of the core to cool it. If the central temperature decreases by a few percent, the flux of neutrinos coming from the decay of ^8B may go down by a factor 3 and agree with the experimental results of Davis ^{12]} and Kamioka ^{13]}. To play this role, dark matter particles must have a mass m_x larger than 4 GeV (otherwise they will quickly evaporate ^{8]} from the Sun), and a large mean free path, of the size of the radius of the Sun, to be able to carry energy away from the core. Such a large mean free path means that the particles interact weakly (hence the acronym WIMP which stands for Weakly Interacting Massive Particle), with a cross-section σ_i on nuclei ($i = \text{H, He, ...}$) of the order of a few picobarns (10^{-36} cm^2). Moreover, they must not annihilate by pairs, otherwise their density would be far too small ^{5]}, and this rules out many candidates for dark matter, such as the photino or a heavy neutrino (unless there is a cosmic asymmetry preventing an equal number of particles and antiparticles ^{14]}). Such requirements are difficult to fulfil, and many authors constructed particle physics models for these WIMPs ^{15-17]}. Once inside the Sun, WIMPs settle in the center, and their distribution is roughly barometric, that is :

$$n_x(r) = n_x(0) \exp\{-r^2/r_0^2\} \quad (1)$$

with a scale height r_0 :

$$r_0 = \left(\frac{3 k T_x}{2 \pi G \rho_c m_x} \right)^{\frac{1}{2}} \approx 0.04 R_{\text{sun}} \left(\frac{10 m_p}{m_x} \right)^{\frac{1}{2}} \quad (2)$$

The energy that they carry away is :

$$\epsilon_x(r) \approx 6 \text{ erg/g/s} \left(\frac{10 m_p}{m_x} \right)^{1.5} \left(\frac{\sigma_H}{1 \text{ pb}} \right)^2 \left(\frac{3}{2} \frac{r^2}{r_0^2} \right) e^{-r^2/r_0^2} \quad (3)$$

which is comparable to the nuclear energy produced in the core ($\epsilon_{\text{nuclear}} \approx 10 \text{ erg/g/s}$).

2- Effect on stellar structure

Since the energy carried out by WIMPs is nearly equal to the nuclear energy, the star must readjust its structure to take into account this energy drain. The best way to compute the effect of WIMPs on the stellar structure is to run a numerical code ^{7]}. This easily takes into

account the complexities of the structure and of the time evolution of the star. However, it takes a very long time on a big computer, and the physics is often not easily understood. An analytic approximation ^{18]} allows a fast study of many different stars, and a quick scan of the WIMP parameter domain (mass and cross-sections). However, only simple stellar structures can be studied, and there is no possibility to follow the time evolution.

Our analytic approximation makes use of the exponential decrease of the density of WIMPs (Equ. 1) : only the central part of the star is affected. We start from a stellar structure ^{19]}

without WIMPs, with given density profile $\rho_0(r)$ and temperature profile $T_0(r)$, solutions of the equations of hydrostatic equilibrium :

$$\frac{dP}{dr} = - \frac{G M(r) \rho(r)}{r^2} \quad (4)$$

and radiative equilibrium :

$$L_{\text{nuclear}} = L_{\gamma} \quad (5)$$

where

$$L_{\text{nuclear}} = \int 4\pi r^2 \rho(r) \epsilon_{\text{nuclear}} dr \quad (6)$$

$$L_{\gamma} = - \frac{64 \pi \sigma_{\text{Stefan}} T^3 r^2}{3 \kappa \rho} \frac{dT}{dr} \quad (7)$$

We add WIMPs as a small correction :

$$\rho_1(r) = \rho_0(r) + \delta\rho(r) \quad T_1(r) = T_0(r) + \delta T(r) \quad (8)$$

$$\delta\rho(r) = \delta\rho_c \cdot (\text{smooth function of } r) \cdot \exp\{-r^2/r_0^2\} \quad (9)$$

$$\delta T(r) = \delta T_c \cdot (\text{smooth function of } r) \cdot \exp\{-r^2/r_0^2\} \quad (10)$$

The equation of radiative equilibrium now takes into account the WIMPs luminosity L_x :

$$L_{\text{nuclear}} = L_{\gamma} + L_x \quad (11)$$

$$L_x = \int 4\pi r^2 \rho(r) \epsilon_x(r) dr \quad (12)$$

The key parameter is actually the ratio $X \equiv L_x(0) / L_{\gamma}(0)$. We look for the new

equilibrium state of the star. Our results were first obtained for small X (i.e. $X < 1$), but have been generalised since the Moriond meeting to any value of X [18]. When X increases, the X appearing in Eq.15 and 16 is replaced by an effective value $X_{\text{eff}} < X$, which remains small. For the core of the Sun :

$$X \approx 14 \left(\frac{10 m_p}{m_x} \right)^{1.5} \left(\frac{\sigma_H}{1 \text{ pb}} \right)^2 \quad (13)$$

We can expand the solutions around the center :

$$\begin{aligned} \rho(r) &= \rho_c \left(1 - A \frac{r^2}{R^2} + \dots \right) \\ T(r) &= T_c \left(1 - B \frac{r^2}{R^2} + \dots \right) \end{aligned} \quad (14)$$

We find that the temperature gradient is indeed lowered due to WIMP energy transport :

$$B \Rightarrow B (1 - X) \quad (15)$$

The central density increases, and the central temperature decreases :

$$\frac{\delta \rho_c}{\rho_c} \approx B \frac{r_0^2}{R^2} X \quad \frac{\delta T_c}{T_c} \approx - \frac{\delta \rho_c}{\rho_c} \quad (16)$$

Notice that it is **not** a homologous contraction of the stellar core. For the core of the Sun, these formulas lead to :

$$\frac{\delta T_c}{T_c} \approx - \left(\frac{10 m_p}{m_x} \right)^{2.5} \left(\frac{\sigma_H}{1 \text{ pb}} \right)^2 \quad (17)$$

This leads to a change in the total luminosity :

$$\frac{\delta L}{L} \approx - 0.05 \left(\frac{10 m_p}{m_x} \right)^4 \left(\frac{\sigma_H}{1 \text{ pb}} \right)^2 \quad (18)$$

The total luminosity of the Sun is well known, and if we require that it decreases by less than 1%, we get a lower bound on the WIMP mass :

$$m_x > 15 m_p \sqrt{\sigma_H / 1 \text{ pb}} \quad (18)$$

But then the decrease of the solar neutrino flux is too small : due to the larger temperature dependence of the ppIII chain, this decrease is larger than the decrease of the total luminosity, but (within our approximations) it is about 20 times larger only. This ratio depends weakly on the WIMP properties, and *if* we take this result seriously, it means that we cannot solve the solar neutrino problem and decrease the neutrino flux by 70% without decreasing too much the total luminosity.

3- Horizontal branch stars

Stars in the horizontal branch of the Hertzsprung-Russell diagram burn helium in their core, and hydrogen in a shell. In the helium core, the photon luminosity L_γ is less than 10% of the nuclear luminosity L_{nuclear} , and the core is convective. Renzini ^{20]} suggested that WIMPs could carry enough energy to stop convection. The amount of usable nuclear fuel is then lowered, because convection no longer brings fresh fuel to the center of the star, and the lifetime of the star on the horizontal branch is drastically reduced. Later, Spergel and Faulkner ^{21]} argued that the WIMP luminosity L_χ could never be larger than 10% of the nuclear luminosity. However, we showed ^{22]} that this affirmation rests on assumptions about the cross-sections on hydrogen and helium which are not necessarily true for many candidates (e.g. for the magnino ^{16]}), and on hypotheses on the halo density and velocity dispersion which are not necessarily true at different places of the Galaxy (e.g. at the center, the halo density is probably much larger than in the solar neighbourhood, and the WIMP accretion rate and their subsequent density in the core of stars is larger). It is therefore possible that WIMPs which are tailored to solve the solar neutrino problem also stop convection in HB stars. On the other hand, WIMPs may, here also, lead to a slight decrease of the central temperature of the HB star, which reduces the nuclear luminosity, and therefore the rate of fuel consumption: the lifetime may actually increase due to WIMPs!

References

- [1] G. Steigman, C.L. Sarazin, H. Quintana and J. Faulkner; *Astroph J.* **83**-1050 (1978)
- [2] D.N. Spergel and W.H. Press; *Astroph J.* **294**-663 (1985)
- [3] W.H. Press and D.N. Spergel; *Astroph J.* **296**-679 (1985)
- [4] L.M. Krauss; "*Cold dark matter candidates and the solar neutrino problem*" Harvard preprint HUTP-85/A008a, *unpublished*
- [5] L.M. Krauss, K. Freese, D.N. Spergel and W.H. Press; *Astroph J.* **299**-1001 (1985)
- [6] J. Faulkner and R.L. Gilliland; *Astroph J.* **299**-994 (1985)
- [7] R.L. Gilliland, J. Faulkner, W.H. Press and D.N. Spergel; *Astroph J.* **306**-703 (1985)
- [8] A. Gould; *Astroph J.* **321**-560 (1987)
- [9] A. Gould; *Astroph J.* **321**-571 (1987)
- [10] A. Bouquet and P. Salati; to appear in *Astronomy and Astrophysics*
- [11] J. Kormandy and G.R. Knapp; *Proc. IAU Symposium 117 "Dark matter in the universe"* (Reidel, 1987)
- [12] J.K. Rowley, B.T. Cleveland and R. Davis; in "*Solar neutrinos and neutrino astronomy*" (Homestake 1984) AIP Conf. Proc. 126
- [13] T. Kajita et al. (Kamiokande II coll.); talk at the XXIInd Rencontre de Moriond (Tran Than Van ed, Editions Frontières, 1987)
- [14] K. Griest and D. Seckel; *Nucl. Phys.* **B283**-681 (1987)
- [15] G. Gelmini, L. Hall and Lin; *Nucl. Phys.* **B281**-726 (1987)
- [16] S. Raby and G. West; *Nucl. Phys.* **B292**-793 (1987) and *Phys. Lett.* **200B**-547 (1988)
- [17] G.G. Ross and G.C. Segrè; *Phys. Lett.* **197B**-45 (1987)
- [18] A. Bouquet, J. Kaplan and F. Martin; to appear
- [19] D.D. Clayton; "*Principles of stellar evolution*" (University of Chicago Press, 1968)
- [20] A. Renzini; *Astronomy and Astrophysics* **171**-121 (1987)
- [21] D.N. Spergel and J. Faulkner; "*WIMPs in horizontal branch stars*", IAS Princeton preprint 1988
- [22] A. Bouquet, P. Salati and J. Silk; to appear

**REALISTIC HALO MODELS
AND THE DETECTION OF WIMPS**

David N. Spergel
The Institute for Advanced Study
Princeton, New Jersey, USA

and

Douglas O. Richstone
Department of Astronomy
University of Michigan, Ann Arbor, Michigan, USA



ABSTRACT

We construct realistic models for the galactic halo. We vary parameters in these models and explore the effects on the estimates of detector event rates. There is at a factor 4 uncertainty in the number of WIMPs captured by the Sun due to our ignorance of the local halo velocity distribution function and ambiguity in the local density of dark matter. The halo velocity distribution function influences both the event rate and the amplitude of the annual modulation in the event rate in direct detection experiments.

If the “missing mass” of the universe is composed of WIMPs, then planned experiments may detect these particles. Several speakers at this conference have described efforts to detect the recoil of WIMPs off of nuclei in a laboratory experiments, while several other speakers have reported on the search for annihilation products of WIMPs captured into the Sun. All of these speakers have had to assume a halo density and velocity distribution. This talk will explore how the ambiguity in our knowledge of the halo in their assumption and estimate how these uncertainties affect the predicted rates in these detectors. A subsequent paper will include more detailed calculations¹⁾.

In the first section of this talk, I describe the recipe for constructed spherical halo models. I will then discuss how varying the ingredients in the recipe alters (1) the event rate in laboratory detectors, (2) the capture rate in the Sun, (3) the seasonal modulation in the event rate and (4) the average recoil energy. I will then discuss the effect of relaxing the assumption of spherical symmetry on the predicted rates.

There are two ingredients needed to construct a spherical model for the galactic halo: (1) the density profile of the halo and (2) the velocity anisotropy of the halo as a function of radius. Measurements of the rotation velocity of gas in the disk is the major source of information about the density profile of our galactic halo. The galaxy’s flat rotation requires constant mass in each shell, $M(r) \propto r$. The disk and spheroid of our galaxy account for most of the mass in the central regions of our galaxy (inwards of 8 kpc), the unseen halo is responsible for most of the mass outside the solar circle. Caldwell and Ostriker²⁾ fit the halo density profile as:

$$\rho(r) = \frac{\rho_0}{1 + (r/r_c)^2} \quad (1)$$

with central density, $\rho_0 = 0.014M_\odot/\text{pc}^3$. and a core radius of $r_c = 7.8\text{Kpc}$. Caldwell

and Ostriker²⁾ estimate that there is a factor 2 uncertainty in local density of dark matter, $\rho(r_\odot)$. The halo density profile is truncated at a tidal radius, r_t . Observations of motions of nearby dwarf galaxies³⁾ and of high velocity stars in the solar neighborhood⁴⁾ imply a minimum tidal radius of 30 kpc.

While we can not yet directly observe or measure the components of the halo, we do know that its distribution function must be a solution of the collisionless Boltmann equation. (The galaxy is an equilibrium system.) The only additional constraint on the halo comes from stability considerations⁵⁾: the inner regions of the halo can not be dominated by radial orbits. These two constraints, however, permit considerable freedom in our choice of velocity distribution function. We will see that this freedom is a major source of ambiguity in any estimate of detector rates.

There are just two steps in the “Maximum Entropy” recipe⁶⁾: (1) calculate orbits in a logarithmic potential and (2) use a linear programming algorithm to populate the orbits with dark matter. This algorithm assures that the density profile satisfies equation (1) and maximizes a “profit” function, S . We use a profit function that rewards the maximum entropy solution:

$$S = - \int f(\vec{r}, \vec{v}) \log[f(\vec{r}, \vec{v})] d^3r d^3v + \alpha_r \int_{r_1}^{r_2} f(\vec{r}, \vec{v}) v_r^2 d^3r d^3v + \alpha_t \int_{r_3}^{r_4} f(\vec{r}, \vec{v}) v_t^2 d^3r d^3v \quad (2)$$

$f(\vec{r}, \vec{v})$ is the orbital distribution function. By varying α_r and α_t , we can encourage either large radial velocities, v_r , or large tangential velocities, v_t , at a given radius. We can also vary the rotation rate of the halo. By vary both the density profile (r_c and r_t) and the velocity anisotropy (through α_r and α_t), we explore the sensitivity of dark matter searches to astrophysical uncertainties.

A promising place to look for dark matter is in the Sun. (Always look for

your keys under the lamppost first!) If the halo is composed of WIMPs, then the Sun can capture these particles through their elastic collisions with nuclei. Press and Spergel⁷⁾ estimate the capture rate in the Sun of particles less massive than 40 GeV:

$$\dot{N}_{capt} = 8.8 \times 10^{29} \left(\frac{\rho}{10^{-2} M_{\odot}/\text{pc}^3} \right) \left(\frac{300 \text{ km/s}}{\langle 1/v \rangle^{-1}} \right) \left(\frac{m_x}{1 \text{ GeV}} \right) \min \left(\frac{\sigma}{\sigma_{crit.}}, 1 \right) \text{ s}^{-1} \quad (3)$$

σ is the WIMP-nucleon scattering cross-section and $\sigma_{crit} = 4 \times 10^{-36} \text{ cm}^2$. (See Gould⁸⁾ for a discussion of capture of more massive particles in the Sun or capture of particles by the Earth.) Once captured, these particles can annihilate into neutrinos and other end products⁹⁾⁻¹¹⁾. The neutrinos stream towards the Earth, where they can be detected in terrestrial experiments. Several speakers at this conference have described how the non-detection of these neutrinos place limits on SUSY halo dark matter.

Astrophysical uncertainties affect estimates of solar capture rates and weaken these limits. The local halo density is not well determined and the shape of the local velocity distribution function is unknown. We explore the influence of the velocity anisotropy on the capture rate by computing the geometric mean velocity in the frame of the Sun,

$$\langle 1/v \rangle \equiv \int \frac{d^3v}{|\vec{v} - \vec{v}_{\odot}|} f(v, \tau_{\odot}) \quad (4)$$

for each halo model. While figure (1a) shows that this velocity is insensitive to τ_c and τ_t , figure (1b) reveals that our ignorance of the velocity anisotropy is a source of a factor 2 uncertainty in the capture rate. This uncertainty should be included in any analysis of limits on halo SUSY particles from their annihilation in the Sun.

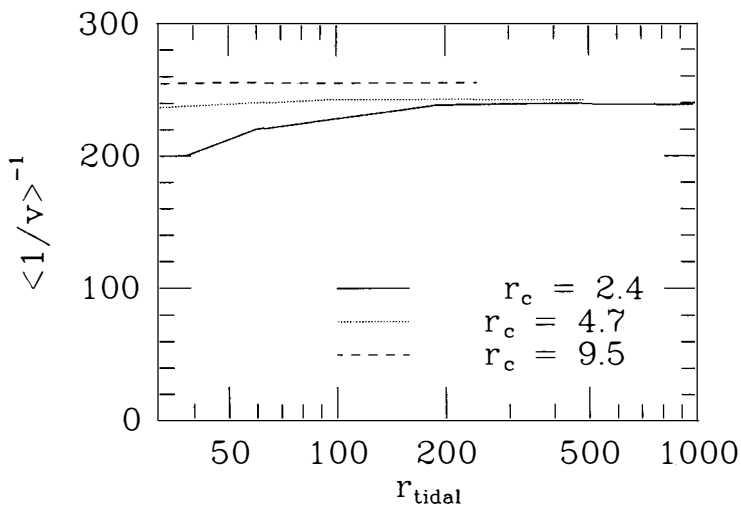


FIGURE 1A. The dependence of the geometric mean velocity in the frame of the Sun on the core and tidal radii of the halo model.

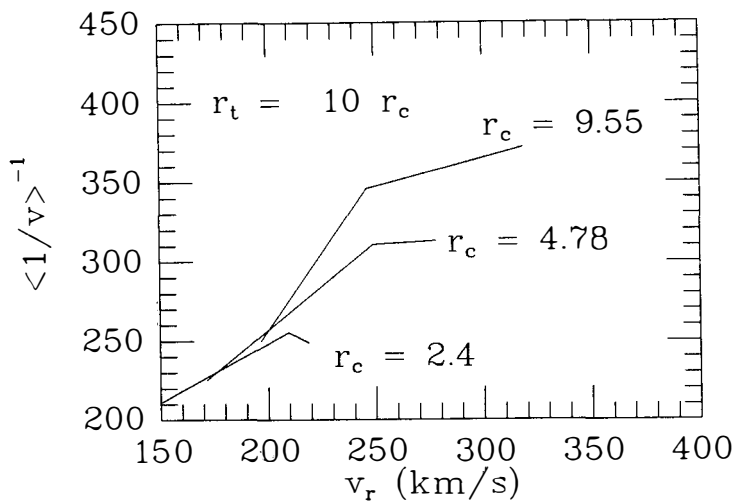


FIGURE 1B. The dependence of the geometric mean velocity in the frame of the Sun on the local halo radial velocity

Halo dark matter could also be detected directly in the laboratory¹²⁾⁻¹³⁾. WIMPs could scatter off of nuclei and these keV nuclear recoils could potentially be detected. Several speakers at this conference have described the exciting progress in developing laboratory experiments that could potentially see these recoils and find the dark matter. Both the rate of recoils and the energy of these recoils depend upon the local WIMP distribution function. We find that the largest astrophysical source of uncertainty is the factor 2 ambiguity in the estimate of halo density.

The earth's motion around the Sun produces an annual modulation in detector event rate¹⁴⁾. This modulation is due to variation in the earth's velocity relative to the rest frame of the halo. The amplitude of the modulation sets the size of the detector needed to establish the existence of halo WIMPs: requiring a 3σ effect over a 2 year experiment fixes the detector mass for a given cross-section.

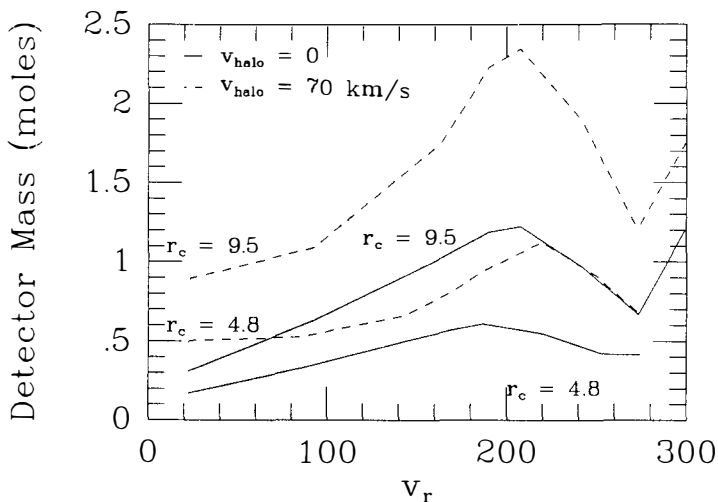


FIGURE 2. The minimum detector mass needed to observe a 3σ modulation effect in 2 years as a function of the mean local radial halo velocity. The figure is normalized to a local density of $0.01 M_{\odot}/\text{pc}^3$ and cross-section of 10^{-36}cm^2 .

Figure 2 shows the minimum detector mass needed to see this 3σ effect in a threshold detector (a detector that records the number of events above a fixed threshold). A detector with better energy resolution could be smaller; however, the astrophysical uncertainties would be similar.

Our ignorance of the velocity distribution function is again the largest source of astrophysical uncertainty. Unfortunately, no astronomical observation can remove this ambiguity. We will have to wait for experiment to reveal the local velocity anisotropy or rely on theoretical arguments and N-body simulations.

By assuming a spherical halo model, we ignored the possibility of a triaxial halo, the effect of the adiabatic growth of the disk on the halo^{15)–16)} and the interaction of dark matter with spiral arms and molecular clouds¹⁷⁾. All of these effects are likely to be beneficial to the experimentalist. They increase the local density of dark matter, which will enhance capture into the Sun and raise the event rate in laboratory experiments. Not all news is bad news!

ACKNOWLEDGMENTS

DNS is supported by NSF grant PHY-8620266 and NJ High Technology grant 88-240090-2.

REFERENCES

- 1) Richstone, D.O. and Spergel, D.N. in preparation.
- 2) Caldwell, J. and Ostriker, J.P., *Ap. J.*, **251**, 61 (1981).
- 3) Little, B. and Tremaine, S., *Ap. J.*, **320**, 493 (1987).
- 4) Carney, B. and Latham, D., *Astron. J.*, **93**, 116 (1987).
- 5) Barnes, J. Goodman, J.J. and Hut, P., *Ap. J.*, **300**, 112 (1986).

- 6) Richstone, D.O. and Tremaine, S., *Ap. J.*, **327**, 82 (1988).
- 7) Press, W.H. and Spergel, D.N., *Astrophys. J.*, **296**, 679 (1985).
- 8) Gould, A., *Ap. J.*, **321**, 571 (1987).
- 9) Silk, J., Olive, K. and Srednicki, M., *Phys. Rev. Lett.*, **53**, 624 (1985).
- 10) Gaiser, T.K., Steigman, G. and Tilav, S., *Phys. Rev. D*, **34**, 2206 (1986).
- 11) Hagelin, J.S., Ng, K.W. and Olive, K.A., *Phys. Lett.*, **100B**, 375 (1987).
- 12) Goodman, M. and Witten, E. *Phys. Rev. D* **31**, 3059 (1985).
- 13) Wasserman, I., *Phys. Rev. D*, **33**, 2071 (1986).
- 14) Drukier, A.K. , Freese, K. and Spergel, D.N. *Phys. Rev. D*, **33**, 3495 (1986).
- 15) Blumenthal, G., Flores, R., Primack, J. and Rees, M., *Ap. J.* , **301**, 27 (1986).
- 16) Ryden, B. and Gunn, J.E., in *Dark Matter in the Universe*, ed. G.R. Knapp and J. Kormendy, Reidel Pub. Co. (1987).
- 17) Dicus, D.A., Teplitz, D.C. and Teplitz, V.L., preprint.

**IX. DARK MATTER, SN 1987A
AND OTHER SUPERNOVAE**

POSSIBLE EVIDENCE FOR DARK MATTER FROM SN1987A

J. van der Velde
The University of Michigan
and
L.A.L. Orsay, France

ABSTRACT

The angular distribution of 19 events associated with SN1987A in the KAMIOKANDE and IMB detectors exhibits a forward peaking which appears to be inconsistent with their being due to neutrino interactions. The data could be explained by a new particle interacting coherently with the oxygen nucleus.

The energy spectrum, time interval, and number of events seen by KAMIOKANDE⁽¹⁾ and IMB⁽²⁾ in association with SN1987A appear to be in good agreement with the standard hypothesis that the data were due to neutrinos emitted from a blue giant supernova collapse.

The neutrino flux at the source can be estimated using cross sections calculated from the standard model of weak interactions in the energy range 10-50 MeV. These cross sections are shown in Fig. 1, calculated for 6800 tonnes of water in the IMB detector.⁽³⁾ It can be seen from Fig. 1 that the "inverse beta" reaction $\bar{\nu}_e + p \rightarrow e^+ + n$ dominates the relative cross sections in the energy range 10-40 MeV so that, assuming roughly equal numbers of the six known neutrinos and antineutrinos, the observed events will be dominated by the inverse beta reaction. Neutral-current interactions are invisible, and charged-current muon and tau reactions are below threshold at these energies. The total flux calculated under these assumptions is within a factor of 2 or 3 of that expected.

The energy-angle distribution of the 19 events is plotted in Fig. 2. It shows a tendency for the observed events (which appear to be electromagnetic showers) to peak in the direction away from the supernova. However, at most, one of the events is enough forward peaked to be due to scattering off electrons in the water. Angular errors due to multiple scattering and reconstruction are in the range of $10^\circ - 20^\circ$.^(1,2,4) The events are also not very isotropic, as would be expected from the inverse beta reaction which has an angular distribution given by $1 + A \cos \theta$, with $A = .05 - .15$, increasing with energy, in the range 10-40 MeV. A Smirnov-Cramer-von Mises (SCM) test on the angular distribution of the 19 events shown in Fig. 3 gives a probability of only 5×10^{-3} that it could have been a fluctuation from a parent $1 + .1 \cos \theta$ distribution.

It appears from Fig. 2 that there is a rather strong correlation of angle with energy. The IMB threshold was ~ 20 MeV (KAMIOKANDE's was 7.5 MeV) so that

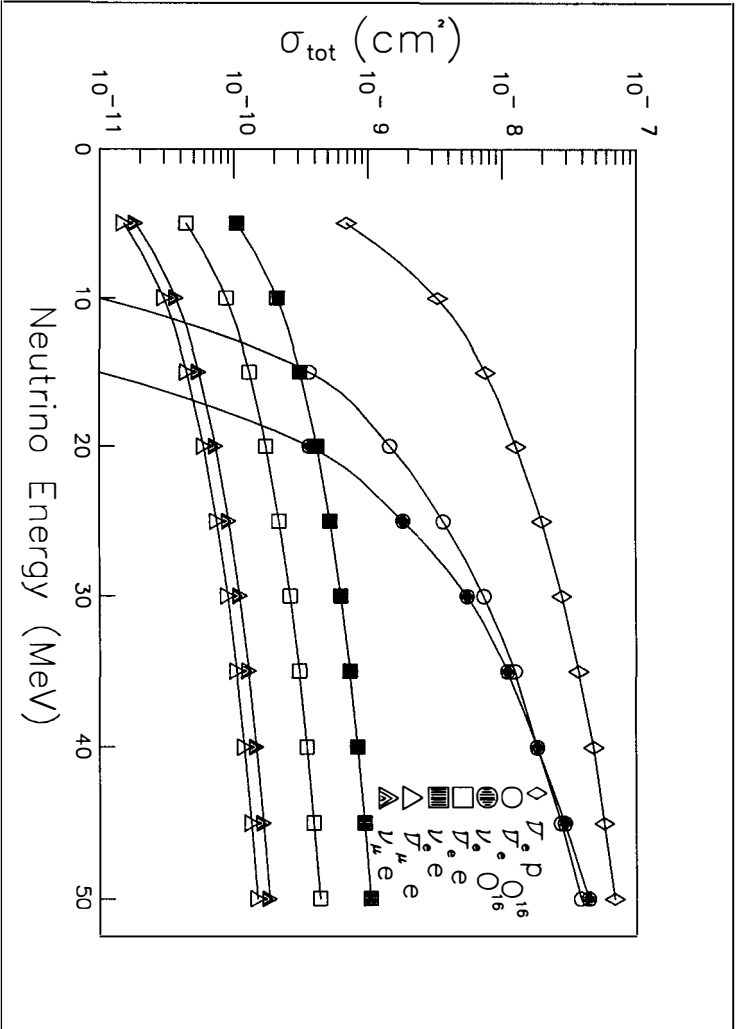


Fig. 1 Cross section of 6800 tonnes of water for various neutrino interactions.

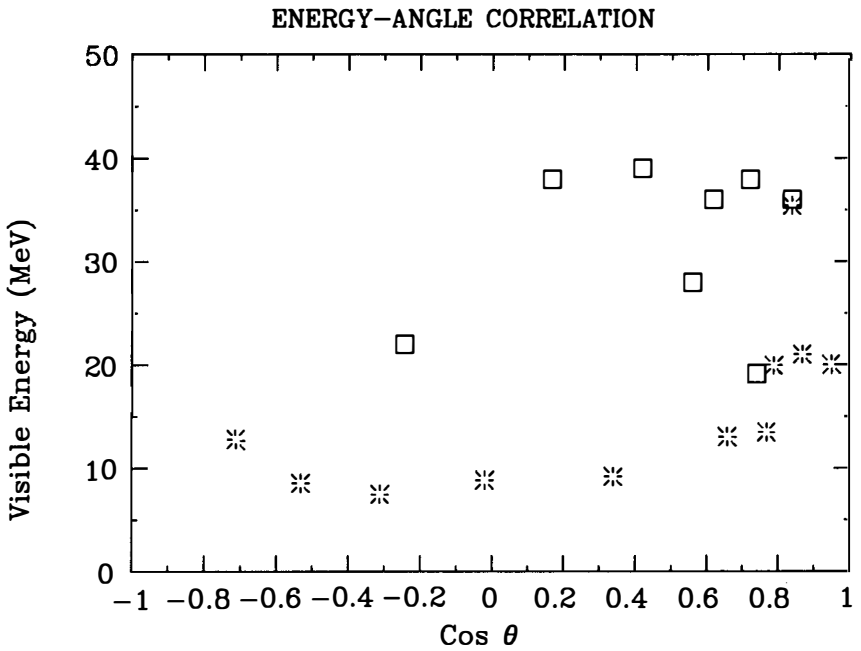


Fig. 2

Scatterplot of visible energy vs. $\cos \theta$ for 19 events seen in the KAMIOKANDE (stars) and IMB (squares) detectors. The angle θ is measured between a direction away from the supernova and the electromagnetic shower in the detector.

one can make an independent investigation of the combined angular distribution above 18 MeV. This is shown (shaded) in Fig. 3. An SCM test on that distribution gives a probability of 7×10^{-4} that it was a fluctuation from $1 + .2 \cos \theta^{(5)}$. If we attribute the most forward KAMIOKANDE event to $\nu - e$ scattering then these probabilities for the remaining events, become 1.3% and 0.2% respectively.

These small probabilities prompt us to look for alternative explanations for the data in Fig. 2, perhaps one that gives some correlation of forward peaking with increasing energy.

We note, first of all, that the answer does not seem to lie in the area of charged-current reactions off oxygen. These are considerably smaller than the inverse beta reactions (see Fig. 1) and, moreover, are expected to be backward peaked.⁽⁶⁾ In fact there seems to be no viable explanation for Fig. 2 (aside from a rare fluctuation) that involves conventional particles scattering off water.

In fact the energy-angle correlation seen in Fig. 2 is not unlike that which would be expected from particles scattering coherently off oxygen, in which the oxygen nucleus recoils in its ground state. Reactions of this type would be controlled by a form factor which we can characterize by $\exp(-q^2 R^2)$, where q is the four-momentum transfer and R is a typical oxygen radius. Since $q^2 \approx 4E^2 \sin^2 \frac{\theta}{2}$, where E = incoming beam energy (we assume $E \gg m$), such reactions can change from being nearly isotropic (at $E \ll R^{-1}$) to being very forward (at $E \gtrsim R^{-1}$).

A plot of $\exp(-q^2 R^2)$, for various E , and with $R^{-1} = 40 \text{ MeV} = (5f)^{-1}$, is shown in Fig. 4. A value of $R = (5 \pm 1)f$ gives a reasonable fit to the data of Fig. 2, and, we note, is in rather remarkable agreement with standard electromagnetic and nuclear form factors for oxygen. This is the main point we want to make.

The question then arises as to what particles could have scattered coherently off oxygen and become visible in the detectors. Neutrinos will scatter thus (see Fig. 5a)

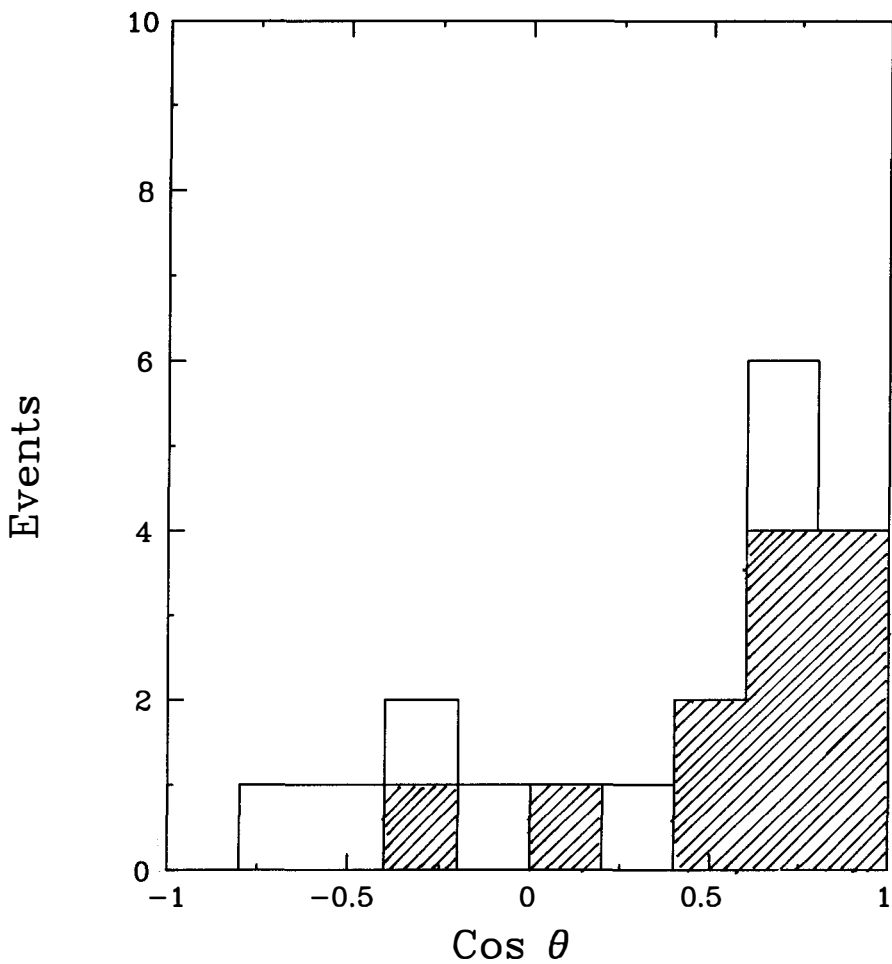


Fig. 3

Projection of Fig. 2, onto the $\cos \theta$ axis. Shaded events are above the IMB threshold.

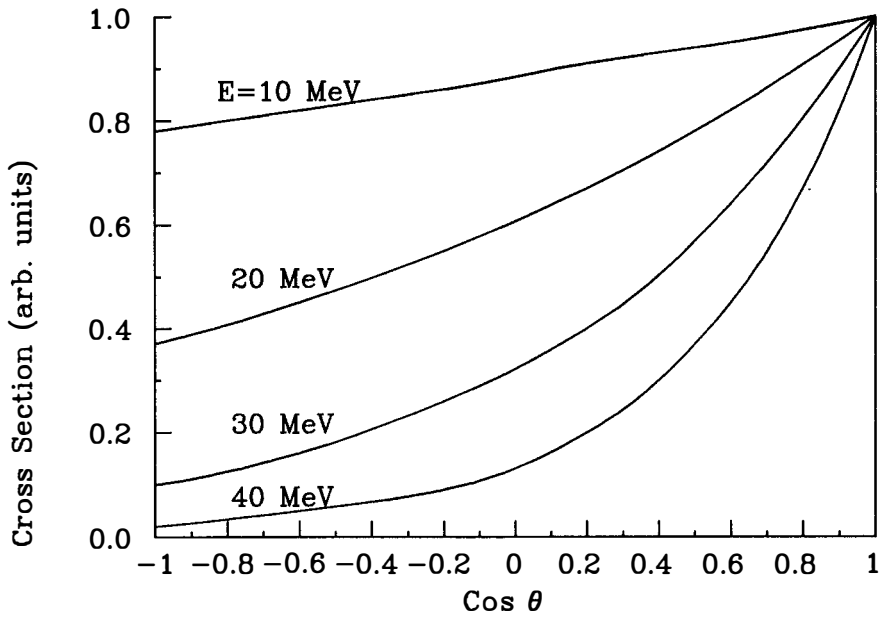


Fig. 4

Plots of the function $\exp(-q^2R^2)$ for various incoming particle energies (see text).

Curves are normalized to 1.0 at $\cos \theta = 1$.

but deposit virtually no energy. The outgoing particle(s) must produce something that looks like an electromagnetic shower in water.

We can hypothesize a particle which is neutral, which has $m \lesssim 20$ eV, and which interacts coherently off oxygen, giving an outgoing gamma ray. A Feynman diagram for such an interaction is shown in Fig. 5b. The exchange particle, Z' , should normally be heavy ($> .1$ GeV) so as not to make the reaction too forward peaked. However, Primakov-type process, with $X^0 \rightarrow \gamma\gamma$, might be a possibility. Another possibility, shown in Fig. 5c, would have the X^0 couple to something like $q\bar{q}$, one of which can then scatter coherently off oxygen via a strong interaction, e.g., π exchange. Such a particle could perhaps be a type of axion.⁽⁷⁾

At this juncture we should perhaps remind the reader that there is no direct evidence that neutrinos were produced in SN1987A. Presumably ν_e were produced during the prompt deleptonization of the star but, at most, one or two of the observed events are consistent with ν_e interactions. Most of the observed events appear to have been caused by particles in the 10-40 MeV range which were emitted over a time period of ~ 10 sec from a “hot soup” composed of several different particle types in a sort of quasi-equilibrium. The conditions at the core of such an event are not unlike those that existed at an equivalent temperature after the Big Bang. Any particles that have masses less than a few tens of eV will be in the “soup”. Their escape-depth and flux will depend on their cross section.

Since there is independent evidence for the existence of some unknown form of dark matter which was presumably made in large quantities in the Big Bang, we should not be surprised if similar matter was made in the “little bang” of a supernova collapse, provided its mass is smaller than ~ 1 MeV. Indeed, if particles with cross sections of the same magnitude as neutrinos exist in the eV range, it becomes a matter of calculation to determine how many of what were emitted and how many of what

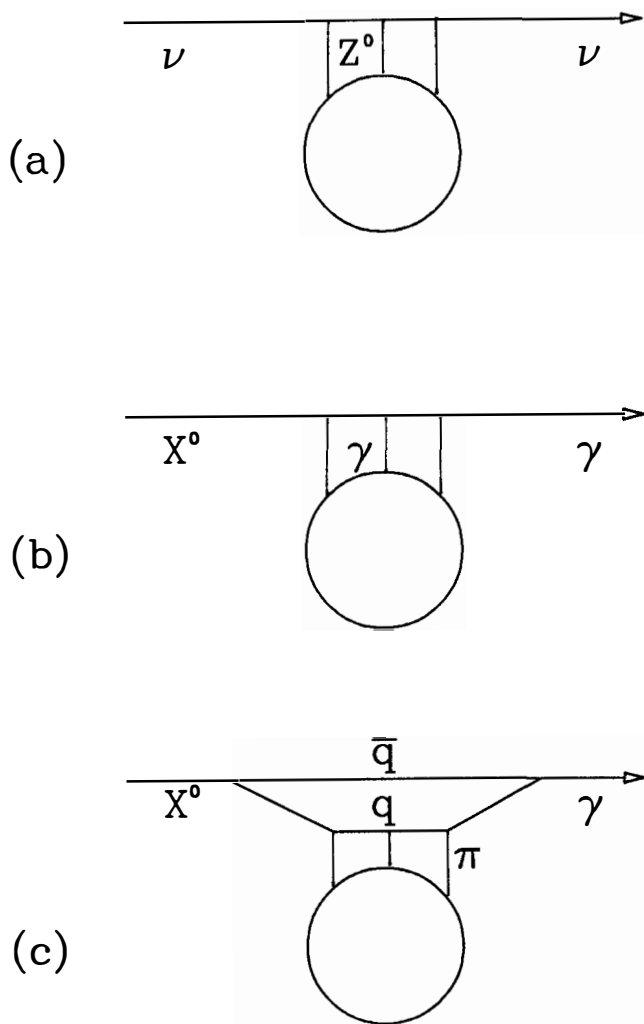


Fig. 5

Feynman graphs for various coherent reactions off oxygen. (b) and (c) represent possible graphs for the hypothetical X^0 particle.

interacted in the detectors.

Turning back to Figs. 2 and 4, it appears that all of the observed events could have been due to a new particle (X°) interacting coherently off oxygen (although some mixture of neutrinos is obviously allowed). If we assume that all were X° , we can estimate their cross section as follows.

The total energy emitted we take as $\sim 3 \times 10^{53}$ ergs, giving 2×10^{58} X° of 10 MeV each. This would give a flux at earth of $7 \times 10^{10}/\text{cm}^2$. An event rate in oxygen of 10 events/Ktonne then gives a cross section of 4×10^{-42} cm^2 coherently on an oxygen nucleus, or $\sigma_x = 4 \times 10^{-42}/256 = 1.6 \times 10^{-44}$ cm^2 per nucleon. This can be compared with a standard neutral current cross section of $\sim 3 \times 10^{-42}$ cm^2 at 10 MeV. Hence the X° cross section for the reaction



would be $\sim .01$ times standard weak neutral currents.

Of course, based on this one experiment, one cannot draw any firm conclusions as to the existence of new particles. Nevertheless, the odds against neutrinos causing the angular distribution are disturbingly high, and the correlation of the shape with the oxygen form factor is rather striking. If such X° particles do exist they will be difficult to produce and detect in the laboratory. They can perhaps be sought via their characteristic reaction (1) which is a dissipative neutral current. If relic X° exist in large quantities in the galactic halo then one might see them as monoenergetic photons from the reaction (1) with energy \approx equal to the X° rest mass. The wave length of such photons could be anything longer than $\sim 600\text{\AA}$, corresponding to the upper limit on X° mass of 20 eV derived from event arrival times in KAMIOKANDE and IMB detectors.

Time may (or may not) tell whether these speculations have any connection with reality. If large underground detectors are operating and record several hundred events from the next supernova in our galaxy, that should settle the question. Hopefully, we may not have to wait that long.

I would like to thank my colleagues in the IMB collaboration for all the hard work that led to these results. I am indebted to several colleagues, especially Dave Schramm and Arnon Dar, for helping me develop some of the ideas presented here. I am also grateful to the organizers of the conference, Jean Audouze and Tran Thanh Vanh, for the opportunity to attend and present these ideas.

References and Footnotes

- (1) K. Hirata, et al., *Phys. Rev. Lett.* **58**, 1490 (1987).
- (2) R.M. Bionta, et al., *Phys. Rev. Lett.* **58**, 1494 (1987).
- (3) We are indebted to C. Longuemare and D. Casper for Figure 1.
- (4) C.B. Bratton, et al., "Angular Distribution of Events from SN1987A", University of Michigan Preprint UM PDK 88-1, (to be published in *Phys. Rev. D*).
- (5) We use the asymmetry parameter .2 to include .1 from the expected inverse beta reaction at a mean energy of 25 MeV, and .1 from the angular bias (see ref. 4) of the IMB detector.
- (6) W.C. Haxton, "The Nuclear Response of Water Cerenkov Detectors to Supernova and Solar Neutrinos", University of Washington Preprint (1987), and references therein, and C. Longuemare (private communication).
- (7) M. Turner, "Axions from SN1987A", Fermilab-Pub-87/202-A, and references therein.

Neutrino Properties And The Neutrino Bursts From SN 1987A *

ARNON DAR AND SHLOMO DADO

Physics Department and Space Research Institute, Technion, Haifa, ISRAEL.

ABSTRACT

The neutrino observations of the supernova explosion SN 1987A in the Large Magellanic Cloud by the KAMIOKANDE II and IMB detectors suggest new limits on the mass, lifetime, electric charge, magnetic moment and mixing of electron neutrinos. These new limits imply that neutrino decay, neutrino electric charge, neutrino magnetic moment, neutrino mixing and the MSW effect apparently cannot solve the solar neutrino problem.

* Supported in part by the Technion Fund For Promotion Of Research and by the Israel Academy Of Sciences

Although the neutrino observations of the type-II supernova explosion SN 1987A in the nearby Large Magellanic Cloud by the KAMIOKANDE II (KII)¹ and by the IMB² detectors are in good agreement with theoretical estimates made prior to the discovery of the neutrino burst³, both the angular distribution and the time distribution of the events are somewhat puzzling: Too many events are pointing in the direction from SN 1987A, and there is a 9 seconds gap between event no. 9 and event no. 10 in KII. (Events nos. 10,11,12 could be background events. However, if they were produced by SN 1987A then the large time gap between events no. 9 and 10 could be real rather than a low probability statistical fluctuation.) Moreover, the KII first events seem to suggest a complete neutronization burst of energetic ν_e 's that preceded thermal emission⁴, while in the standard scenario of neutron star formation in type II supernovae explosions⁵ the neutronization in the infall stage by electron capture on protons bound in atomic nuclei, $e^-p \rightarrow n\nu_e$, is only moderate and lasts only for a short time ($\Delta t \sim 10$ ms) because of Pauli blocking by the trapped ν_e 's. The mean neutrino energy and the total binding energy released in this neutronization burst were predicted^{5,6} to be less than 15 MeV and 10^{51} ergs, respectively.

In order to estimate the magnitude of the neutronization burst and the effective temperatures of the neutrinos emitted by SN 1987A we assumed that the neutronization burst was followed by thermal emission of neutrinos of all known flavours ($\nu_e, \bar{\nu}_e, \nu_\mu, \bar{\nu}_\mu, \nu_\tau, \bar{\nu}_\tau$) in roughly equal proportions, and that the time-integrated neutrino fluxes from the explosion had approximately Fermi-Dirac distributions:

$$d\phi_{\nu_i}/dE = c_i E^2 / [1 + \exp(E/T_i)] . \quad (1)$$

We allowed different effective temperatures for the neutronization burst and for

the thermal emission and we assumed zero chemical potentials for the sake of simplicity. Using eq (1) and a maximum likelihood procedure⁷ we analyzed the neutrino signals of both K-II and IMB. Events were generated in the two detectors with probabilities proportional to $\rho(E_e, z)dE_e dz$, where $z = \cos\theta$ and

$$\rho = \sum N_t \int dE (d\phi_\nu/dE)\eta(E_e, z) d^2\sigma_{\nu t}/dE_e dz . \quad (2)$$

N_t is the number of target particles of type t , η is the detection efficiency, and the summation extends over all target particles and neutrino flavours. The standard electroweak cross sections which were used for νe scattering are listed in Table I. The cross sections for the charged current reactions were approximated (energies in MeV) as follows :

$$\sigma(\bar{\nu}_e p \rightarrow e^+ n) \simeq 8.86 \times 10^{-44} E_e^2 \simeq 8.86 \times 10^{-44} (E_{\bar{\nu}_e} - 1.3)^2 \text{ cm}^2 . \quad (3)$$

$$\sigma(\nu_e O^{16} \rightarrow e F^{*16}) \simeq 5 \times 10^{-44} E_e^2 \simeq 5 \times 10^{-44} (E_{\nu_e} - 26)^2 \text{ cm}^2 . \quad (4)$$

$$\sigma(\bar{\nu}_e O^{16} \rightarrow e^+ N^{*16}) \simeq 5 \times 10^{-44} E_e^2 \simeq 5 \times 10^{-44} (E_{\bar{\nu}_e} - 21)^2 \text{ cm}^2 . \quad (5)$$

The νe cross sections are sharply peaked forward⁸ while the charged current reactions on p and on O^{16} ⁹ are nearly isotropic. (We used the angular distributions given in Refs. 10,11 and the detectors efficiencies which were reported^{1,2} by K-II and by IMB.) The results of the maximum likelihood search applied to the joint results of K-II and IMB suggest the following:

(a) The neutrino bursts from SN 1987A consisted of a neutronization burst of $(7 \pm 4) \times 10^{56} D_{50}^2 \nu_e$'s with average energy $\bar{E}_{\nu_e} \simeq 3.15 T_{\nu_e} \simeq 33 \pm 8 \text{ MeV}$ and total energy $W_{\nu_e} \simeq (5 \pm 3) \times 10^{52} D_{50}^2 \text{ ergs}$, followed by a thermal emission of $(7 \pm 2) \times$

$10^{56} D_{50}^2 \bar{\nu}_e$'s with average energy $\bar{E}_{\bar{\nu}_e} \simeq 3.15 T_{\bar{\nu}_e} \simeq 15.4 \pm 3.7 \text{ MeV}$ and total energy $W_{\bar{\nu}_e} \simeq (2. \pm 0.3) \times 10^{52} D_{50}^2 \text{ ergs}$, where $D_{50} = D/50 \text{ kpc}$, D being the distance to SN 1987A¹⁰. Standard supernova theory^{5,6} predicts that most of the binding energy of the newly born neutron star is released by neutrino emission within the first 10 seconds after core collapse, and that only a small fraction ($\leq 1\%$) is released in gravitational waves and in kinetic and thermal energy of the expanding shell. Accordingly the energy released by SN 1987A within the first 12.6 seconds by the thermal burst is given approximately by $\sim 1.2 \times (N_\nu/3) \times 10^{53} D_{50}^2 \text{ ergs}$, where N_ν is the number of flavours of light neutrinos ($m_\nu c^2 \leq 10 \text{ MeV}$). Accelerator experiments and cosmological and astrophysical considerations yield $3 \leq N_\nu \leq 4$. Consequently, the total binding energy released in the neutronization and thermal bursts is $W \leq 2.4 \times 10^{53} D_{50}^2 \text{ ergs}$. Hence the standard equations of state of nuclear matter¹¹ suggest that SN 1987A produced a neutron star with $M_{NS} \leq 1.4 M_\odot$ and did not produce a black hole.

(b) The KII events suggest a complete neutronization burst: A typical white-dwarf like iron-core with $M_c \leq 1.4 M_\odot$ has a lepton number $L_e \sim 7 \times 10^{56}$. Consequently, lepton number conservation constrain a complete neutronization burst to contain $7 \times 10^{56} \nu_e$'s which is consistent with the number inferred from the KII results since¹⁰ $D_{50} = 1 \pm 0.15$.

(c) The mass of the neutrino satisfies $m_\nu c^2 \leq 3.4 \pm 1.1 \text{ eV}$ if the first KII event was produced by ν_e from the neutronization burst: The difference between the flight times of massive and massless neutrinos from a supernova explosion at a distance D to Earth in the limit $m_\nu c^2 \ll E_\nu$ is given by

$$\Delta t = (D/2c)(m_\nu c^2/E_\nu)^2. \quad (6)$$

This dispersion in arrival times of neutrinos of different energies can be used to measure the neutrino mass if one makes assumptions on the emission times¹². Various authors have assumed a smoothly varying function of time for the neutrino luminosity of SN 1987A and deduced¹³ a conservative upper bound $m_{\nu_e} < 15 \text{ eV}$. A lower limit can be derived from the assumption that the first KII event ($t = 0$, $E_e = 20 \pm 2.9 \text{ MeV}$, $\theta_e = 18^\circ \pm 18^\circ$) was produced by ν_e from the neutronization burst⁴ as suggested by its small electron recoil angle (if the time sequence of the events is included in the maximum likelihood analysis it yields that the first event recorded by K-II is most probably a $\nu_e e$ scattering event produced by a ν_e from the neutronization burst) while the third event ($t = 0.3 \text{ sec}$, $E_e = 7.5 \pm 2.0 \text{ MeV}$, $\theta_e = 108^\circ \pm 32^\circ$), as evident from its large electron recoil angle, is most probably a $\bar{\nu}_e p \rightarrow e^+ n$ interaction of a slower moving $\bar{\nu}_e$ which was emitted *later* in the thermal emission stage. Therefore, the difference between the flight times from SN 1987A to Earth of the ν_e and the $\bar{\nu}_e$ that produced events nos. 1 and 3, respectively, can only be shorter than the difference between their arrival times, at KII, i.e. $(D/2c)(m_{\nu_e} c^2)^2 (E_{\bar{\nu}_e}^{-2} - E_{\nu_e}^{-2}) \leq 0.3 \text{ sec}$. From conservation of energy and momentum it follows that $E_{\nu_e} \geq 20 \pm 2.9 \text{ MeV}$ and $E_{\bar{\nu}_e} = 8.9 \pm 2.0 \text{ MeV}$, which yields $m_{\nu_e} \leq 3.4 \pm 1.1 \text{ eV}$. Similiar bounds are obtained if one uses events no. 4 or no. 5 instead of no. 3. This $\sim 4 \text{ eV}$ upper bound is significantly smaller than those deduced by other authors¹⁴. It is also significantly smaller than the lower bound of 18 eV that has been deduced recently from new measurements¹⁵ of the electron spectrum near the end point in β decay of Tritium.

(d) The ν_e has a life time $\tau \geq 10^{13} m_{\nu_e} / E_{\nu_e}$: The idea of an unstable neutrino was proposed many years ago¹⁶ as a solution to the solar neutrino problem¹⁷. If ν_e 's are unstable and have a lifetime τ then the differential flux of ν_e 's at the detectors

should have been suppressed by a factor $e^{-m/E\tau}$, where t is the neutrino flight time from SN 1987A to earth. Assuming that the binding energy released by neutrinos from SN 1987A did not exceed 5×10^{53} ergs we obtained from the maximum likelihood analysis the above lower bound for the neutrino-lifetime. However it has been pointed out recently¹⁸ that if $\bar{\nu}_e$'s and ν_e 's are unstable but admixed significantly with other neutrinos which are stable, then they could have produced the observed neutrino signals from SN 1987A. This possibility is ruled out if KII has observed a complete neutronization burst, i.e. the maximal burst allowed by lepton number conservation.

(e) The neutrino electric charge satisfies $q_{\nu_e} < 2 \times 10^{-17}e$: If neutrinos have an electric charge q they are deflected by galactic and intergalactic magnetic fields and their path lengths and flight times from a supernova explosion to Earth depend on their energy. If they have a Boltzman energy distribution with temperature $T(\text{MeV})$ and if δt is the dispersion in their arrival times after a flight in a perpendicular magnetic field $B(\mu\text{G})$ along a path $D(10 \text{ kpc})$ then

$$q/e < 3 \times 10^{-12}(\delta t/t)^{1/2}T/BD. \quad (7)$$

Assuming a galactic magnetic field $B=1\mu\text{G}$ over a 10 kpc path, one obtains¹⁹ from the energy spread and the dispersion in arrival times of the neutrinos from SN 1987A that $q(\nu_e) < 2 \times 10^{-17}e$.

(f) The neutrino magnetic moment satisfies $\mu_{\nu_e} \leq 10^{-15}\mu_B$: An anomalous magnetic moment $\mu_{\nu_e} \simeq 10^{-10}\mu_B$, where μ_B is the Bohr magneton, has been suggested²⁰ as an explanation to the suppressed counting rate in the solar neutrino experiment and its apparent anticorrelation with the sun spot number²¹. However, a magnetic moment $\mu_{\nu} > 10^{-12}\mu_B$ will cause neutrino escape from the hot interior

of the protonneutron star with energies much larger²² than expected^{5,6}. Moreover, if $\mu_\nu > 2 \times 10^{-15} \mu_B$ then a magnetic field of the order $B \sim 10^{12}$ Gauss believed to be present near the surface of the protonneutron star will induce $\nu_L \leftrightarrow \nu_R$ precession. Thus the observed numbers of ν_L 's is only half the number of ν 's emitted by SN 1987A, and the inferred binding energy is twice that carried by the ν_L 's. But the inferred number of ν_e 's in the neutronization burst is the maximum number allowed by lepton number conservation (and the binding energy released by SN 1987A that was estimated by the KII group from their neutrino events is already about the maximum gravitational binding energy estimated for a neutron star) which imply that $\mu_{\nu_e} < 10^{-15} \mu_B$ ²³.

(g) Most of the MSW solutions²⁴ to the solar neutrino problem are ruled out: Resonant matter oscillation occur if the mass difference between the eigenvalues of the neutrino mass matrix $\Delta m^2 = m_1^2 - m_2^2$, satisfies $\cos 2\theta \Delta m^2 / 2E_\nu = \sqrt{2} G_F n_e$ where θ is the mixing angle, G_F is the Fermi coupling constant and n_e is the local electron density. Resonant oscillations inside the dense core require mass differences which are forbidden by reactor and accelerator experiments. Outside the core in the outer layers of the supergiant progenitor star, the neutrinos encounter densities that include the whole range of solar densities, and density gradients which are much more moderate. Consequently, the ν_e 's from the neutronization of the core of SN 1987A should have changed their flavours in the outer layers of the progenitor. If the first one or two events in K-II were generated by ν_e 's from a neutronization burst (it is very unlikely that they have been both generated by ν 's from the thermal burst because this would have required about 75 additional $\bar{\nu}_e p \rightarrow e^+ n$ events during the 0.107 sec between the first and second event.) then the ν_e 's from the neutronization burst did not flip their flavour in the mantle of

the progenitor. That is inconsistent with the MSW solutions to the solar neutrino problem, unless the ν_e 's flipped their flavour in the mantle of the progenitor and reflipped it back to ν_e in Earth²⁵ (SN 1987A is below the horizon at Kamioka. However, significant flavour flip can take place in Earth only for mixing parameters that satisfy²⁵ $E_\nu/\Delta m^2 \sim 3 \times 10^6 \text{ MeV}/\text{eV}^2$ and $\sin^2 2\theta \geq 2 \times 10^{-2}$.)

(h) The absence of a γ ray burst from SN 1987A following the ν bursts closed the window left by laboratory experiments and by astrophysical and cosmological observations²⁶ for the existence of massive neutrinos ($m_{\nu_h} > 1 \text{ MeV}$) that are mixed with ν_e : Mixing of a ν_h with ν_e induces muon-like decays $\nu_h \rightarrow \nu_e e^+ e^-$. The decay is accompanied by internal and external bremsstrahlung photons. If such ν_h 's exist Supernovae should then produce approximately $N_{\nu_h} \sim B \cdot N_{\nu_\mu} \nu_h$'s, where $B \sim 2.8(m/T)^{3/2} e^{-m/T}$ is the Boltzman factor and T is the temperature at the neutrinosphere for ν_μ emission. Those ν_h 's that decay outside the surface of the progenitor star produce a γ ray flux. From the fact that no significant flux of γ -rays with energies from 100 KeV to about 100 MeV above background has been observed²⁷ from SN 1987A since core collapse on Feb. 23.316 through April 9 we obtained²⁸ the lower bound $\tau_{\nu_h} \geq 10^5 \text{ sec}$ which closed the window for a significant mixing between ν_e and ν_h .

(i) The expected number of events due to the inferred neutrino fluxes from SN 1987A in the 90 tones Mont Blanc scintillator detector, in the 300 tones Baksan scintillator detector and in the 615 tones Homestake solar neutrino detector, are ~ 1 , ~ 3 , < 1 , respectively.

(j) If the 5 events observed by the Mont Blanc scintillator detector on February 23, 2:52:36:48 UT²⁹, i.e. about 5 hours before the KII and IMB signals, were generated by a neutrino burst from SN 1987A then the inferred neutrino flux

should have generated during the Mont Blanc signal 36 ± 12 events in K-II (taking into consideration the relative detection efficiency as function of energy and the fact that K-II contains 17 times more free protons) while no events were observed. Moreover, if the events observed by Mont Blanc were produced by neutrinos from SN 1987A then the inferred (via maximum likelihood analysis) binding energy released by SN 1987A in its "first bang" exceeded $2M_{\odot}c^2$. Such binding energy release is larger by more than an order of magnitude than the maximum binding energy released in the formation of a neutron star. Therefore it must be concluded that SN 1987A did not bang twice³⁰ and the Mont Blanc signal could not have been produced by thermal $\bar{\nu}_e$'s from SN 1987A.

Table I: Elastic Neutrino Cross Sections

$$d\sigma/dy = (G_F^2 m_e E_\nu / 2\pi) [A + B(1-y)^2] ; y = E_c/E_\nu$$

ν_i	A_i	B_i	$\sigma_i/E_\nu (10^{-44} \text{ cm}^2/\text{MeV})$
ν_e	$(2x_W + 1)^2$	$4x_W^2$	0.953
$\bar{\nu}_e$	$4x_W^2$	$(2x_W + 1)^2$	0.400
ν_μ, ν_τ	$(2x_W - 1)^2$	$4x_W^2/3$	0.140
$\bar{\nu}_\mu, \bar{\nu}_\tau$	$4x_W^2/3$	$(2x_W - 1)^2$	0.072

$$G_F^2 = 5.29 \times 10^{-44} \text{ cm}^2/\text{MeV}^2 ; x_W = \sin^2 \Theta_W = 0.232$$

REFERENCES

1. K. Hirata et al., Phys. Rev. Lett., 58, 1490(1987).
2. R.M. Bionta et al., Phys. Rev. Lett. 58, 1494(1987).
3. J.N. Bahcall et al., Nature 326, 135(1987), and references therein.
4. J. Arafune and M. Fukugita, Phys. Rev. Lett. 59, 367(1987); I. Goldman et al., Nature, 329, 134(1987); J. Arafune et al., Phys. Rev. Lett. 59, 1864(1987); D. Notzold, Physics Letters, 196B, 315(1987).
5. See e.g. J.R. Wilson et al., Ann. N.Y. Acad. Sci. 470, 267(1986); R. Mayle et al., Ap. J. 318, 244(1987); and references therein.
6. See e.g. S.W. Bruenn, Phys. Rev. Lett. 59, 938(1987), and references therein.
7. CERN minimization program "MINUIT" (CERN Library Program D506).
8. J.N. Bahcall, Rev. Mod. Phys. 59, 505(1987).
9. see e.g. J.B. Langworthy et al. Nuc. Phys. A280, 351(1977).
10. G.D. Vaucouleurs, Ap. J. 227, 380(1979); G. Tammann et al., Physical Cosmology (North Holland Pub. Co., 1980) p. 55.
11. See e.g. W.D. Arnett and L.B. Bowers, Ap. J. Suppl. 33, 415(1977) and references therein.
12. G.I. Zatsepin, JETP Lett. 8, 205(1968).
13. See e.g. J.N. Bahcall and D. Spergel, Phys. Lett. 200, 366(1988); Abbott et al., Boston Univ. Preprint BUHEP-87-24(July 1987); and references therein
14. see e.g. J.N. Bahcall and S.L. Glashow, Nature,326, 476(1987); W.D Arnett and J.L. Rosner, Phys. Rev. Lett. and Ref. 15.
15. J.F. Wilkerson et al. Phys. Rev. Lett. 58, 2023(1987).

16. J.N. Bahcall et al., Phys. Rev. Lett. 28, 316(1972); S. Pakvasa and K. Tennakone, Phys. Rev. Lett. 28, 1415(1972).
17. J.N. Bahcall et al., Rev. Mod. Phys. 54, 767(1982).
18. J.A. Frieman et al., SLAC Preprint SLAC-PUB 4261(1987); R.S. Raghavan et al, Preprint (July 1987).
19. G. Barbiellini and G. Cocconi, Nature 329, 21(1987).
20. M.B. Voloshin et al., Sov. J. Nucl. Phys. 44, 440(1986); L.B. Okun et al., Sov. J. Nucl. Phys. 44, 546(1986).
21. R. Davis Jr., Proc. 7th Workshop On Grand Unification, ICOBAN 86, Toyama Japan (April 1986).
22. A. Dar, IAS preprint, February 1987.
23. I. Goldman et al., Preprint TAUP 1543-87 (April 1987).
24. S.P. Mikheyev and A.Yu.Smirnov, Nuovo Cim. 9C, 17(1986); L. Wolfenstein, Phys. Rev. D17, 2369(1978).
25. A. Dar and A. Mann, Nature, 325, 790(1987); A.Dar et al., Phys. Rev. D35, 3607(1987); and references therein.
26. A. Dar et al., Phys. Rev. Lett., 58, 3246(1987) and references therein.
27. E.L. Chupp, Astronomical Circular 4365(April 13,1987).
28. A. Dar and S. Dado, Phys. Rev. Lett. 59, 2368(1987).
29. M. Aglietta et al., Europhysics Lett. 3, 1315(1987).
30. A. De Rujula, Phys. Lett. 193B, 514(1987).

THE NEUTRINO SIGNALS FROM SN1987A

Tsvi Piran
The Racah Institute for Physics,
The Hebrew University, Jerusalem, ISRAEL

and

David Spergel
The Institute for Advanced Study
Princeton, New Jersey, U.S.A.



ABSTRACT

We show that the Baksan data are consistent with the IMB and Kamiokande neutrino observations from SN1987a. All three data sets are compatible with a simple model for neutron star cooling. The gap in the Kamiokande data set is shown not to be statistically significant.

1: Introduction.

The detection of nineteen neutrinos from SN1987A in the Kamiokande and IMB detectors [1,2] marked the beginning of the era of extra-solar neutrino Astronomy. The analysis and reanalysis of these two signals generated far more papers than neutrinos. Rather than review this large literature, we present only an incomplete (and probably biased) list of references [3-7] and devote this paper to two outstanding questions: Is the Baksan data [8-10] compatible with the IMB and Kamiokande data? Is the gap in the arrival time in the Kamiokande data statistically significant? We will answer to the “yes” to the first question and “no” to the second question.

2: The Baksan Data.

Shortly after the announcement of the discovery of a burst of neutrinos signals from SN1987A in both IMB and Kamiokande experiments. the Baksan collaboration reported [8] that they detected of three events. These three events, observed in a 5.7 second interval that begins at 7 h 36 m 06 s (± 2 s), were within the timing errors of Kamiokande signal (11 events observed in 12.4 second interval starting at 7 h 35 m ± 1 minute), but some 25 seconds *after* the IMB signal (8 events observed in a 5.5 second interval beginning at 7 h 35 m 41 s ± 5 ms).

A revised inspection of the measurement in Baksan detector [9-10] reveal that there were five observed events, beginning at 7 h 36 m 11 s (the event at 7 h 36 m 06 s is believed to be noise) and lasting 9.1 seconds. In this analysis an error of up to -54 seconds was discovered in the Baksan time base. This error allows the Baksan data to be coincident with the IMB and Kamiokande detection. The efficiencies of the Baksan experiment is 8% at MeV, 50% at 10 MeV and 80% for $E > 12$ MeV [9-10]. This efficiencies are quite similar to those of Kamiokande. Is the detection of 5 events in a detector with 1.9×10^{31} free protons (Baksan) compatible with the detection of only 11 events in Kamiokande, an experiment with 1.5×10^{32} free protons?

In order to resolve this question, we performed a combined analysis of the Baksan, IMB and Kamiokande data. This analysis used the revised IMB energies and detection

efficiencies [2]. We assume in this analysis that all the events are antineutrino absorption. The fact that one or two of the events were probably neutrino scattering will not change our results in any significant way. We fit the observed data pairs (E_i, t_i) to a phenomenological model where the neutrino source is a black body ($F \propto T^3$) with an exponentially decaying temperature with a time scale τ :

$$F(t) = F_0 \exp(-3t/4\tau) \quad ,$$

$$T(t) = T_0 \exp(-t/4\tau) \quad .$$

$L_{\bar{\nu}_e}$ the antineutrino luminosity and $E_{\bar{\nu}_e}$, the antineutrino energy are:

$$L_{\bar{\nu}_e} = \frac{7\pi}{4} \sigma_B T^4 R^2 \quad 4\pi D^2 F(3.15T) \quad ,$$

$$E_{\bar{\nu}_e} = \int_0^\infty L_{\bar{\nu}_e} dt \quad ,$$

where R is the radius of the neutron star and D is the distance to the LMC. This analysis used maximum likelihood technique to fit this simple cooling black body model to all three data sets. (See Spergel et al. [5] for a discussion of the model and the statistical method).

The ‘‘maximum likelihood’’ parameters obtained from the combined analysis of all three data sets differ only slightly from those obtained in our earlier analysis of the Kamiokande and IMB events (the results presented here are based on the revised IMB efficiencies and energies):

Table 1. Maximum Likelihood Parameters (Cooling Black Body Model)

	Kam + IMB + Bak	Kam + IMB
T	$4.1^{+0.9}_{-0.6}$ MeV	$4.3^{+1.0}_{-0.7}$ MeV
R	29^{+13}_{-17} km.	24^{+12}_{-14} km.
τ	$5.0^{+1.9}_{-1.8}$ sec.	$4.5^{+1.6}_{-2.0}$ sec.
$E_{\bar{\nu}_e}$	$7.7^{+5.5}_{-3.3} \cdot 10^{52}$ ergs	$5.9^{+1.8}_{-3.3} \cdot 10^{52}$ ergs

The main change is that the high flux that is observed in Baksan raises the total flux by about 40%. The other parameters are almost unchanged. Using these parameters, the model predicts 4.8 events in IMB, 14.0 events in Kamiokande and 1.6 events in Baksan due to the burst of supernova neutrinos. In a 20 second interval, we expect an additional 0.6 background events in the Baksan detector [9]. The three data sets are consistent: five or more events should have been seen in Baksan at least 8% of the time.

3: The gap in the time of arrival data.

Probably the most puzzling feature of the SN1987A neutrino signal is the appearance of the 7 second gap in the Kamiokande neutrino signal: Eight events were observed in the 2 seconds prior to this gap and 3 events were observed in the subsequent 3.3 seconds. Several authors have argued that this gap is statistically significant and have proposed models that explain its origin [11-12]. The observation of 2 events in IMB in the center of the gap in Kamiokande argues strongly against the existence of a gap in the actual neutrino pulse. Moreover, we will show that even if the IMB data is ignored, the gap in the Kamiokande data set is not very significant.

We have produced some hundred thousand sets of simulated data from our best fit model for the neutrino pulse. Using this data we estimate the probability for a gap: In 11% of the simulations, there was at least a 7 second gap. This may underestimate the significance of the gap, since in these simulations the gap was usually between the final two events. In only $\approx 1\%$ of the simulations, there is a gap of 7 second or longer between the third to last and second to last events. In only $\approx 0.1\%$ of the simulations, there is a 7 second or longer gap between the fourth to last and the third to last events. Such simulations have been performed also by other groups. However, this statistic is, clearly ridiculously, a *posteriori*.

The K.S. test is a standard non-parametric statistical tool used to test if an observation differs in a statistically significant way from a model. The K.S. measure is the maximum distance between two curves: the cumulative number of events as a function of time in the data and the cumulative number of events as a function of

time in the model. Standard statistical techniques are used to assign a probability to the K.S. measure as a function of the number of data points. (See [13] for an implementation). Spergel et al. [5] used a two dimensional generalization of the K.S. test to argue that the arrival times and energies of the neutrino data is consistent with the simple cooling neutron star model.

However, as Sato and Suzuki [7] have stressed, the K.S. test is not a powerful statistic for detecting long gaps in the data: it does not distinguish between data in which the last event arrived 8 seconds after the first and data in which the last event arrived 80 seconds after the first. This weakness in the K.S. test has motivated us to develop a new statistic more sensitive to long delays in the data: we define the area between the two curves as the “area measure”. We compare the area measure of the Kamiokande data with the area measure obtained in several thousand simulations of synthetic data generated from the cooling neutron star model using the “maximum likelihood” parameters. In each simulation, we find the best fit parameters, calculate the area measure and then compare it to the area measure obtained for the Kamiokande data. In 4.4% of the simulations, the area between the curves for the simulated Kamiokande data exceeded the area between the curves for the real data. Since this test was designed *a posteriori* to look for gaps, this is further evidence that the gap is not statistically significant.

Our analysis used a model with exponential falling temperature and flux, if we had used a model with a power law fall off there would have been more events at late times. In models with power law tails, the probability for the gap would have increase. It does not seem necessary, however, to make even this mild modification of our simple model.

4. Conclusions

The Neutrino signal from SN1987A was a unique event. We were fortunate to observe it: both Kamiokande and IMB began operation in a mode that could capture these low energy neutrinos only a few month before the event. The signal itself was

just above the limiting sensitivity of these detectors: we would have missed this event had it occurred at twice the distance!

We have seen only 24 events in 3 detectors. The observation of such a small number of events is prone to statistical fluctuations and should be treated with care. Too often statistical noise is interpreted as a physical signal and colorful theories are constructed to explain this noise. Scientists calculate the *a priori* probability of an observation, argue that this probability is small and then provide a physical explanation. The assigned *a priori* probability ought to be multiplied by the fraction of the event space that has equal or greater “strangeness”. What is this factor? Given that physicists’ imagination is unbounded, and astrophysicists’ is even larger, this factor is transfinite.

We have demonstrated that a simple model, an exponentially cooling black body with a fixed radius, is compatible with the data. The observations are also compatible with theoretical predications obtained long before the supernova explosion [14]. It would have been exciting if these 24 neutrinos overturned Supernova theory, but this does not seem to have happened. We will have to build bigger experiments and wait for the next supernova to undermine our theoretical assumptions!

We thank J. N. Bahcall and I. Goldman for critical reading of the manuscript. D.N.S. thanks the Hebrew University for hospitality while this research was done. D.N.S. is supported by N.J. High Technology Grant 88-240090-2 and NSF grant PHY-8620266.

REFERENCES

1. Hirata, K., et al., Phys. Rev. Lett., **58**, 1490, 1987.
2. Bionta, R.M., et al., Phys. Rev. Lett., **58**, 1494, 1987; Bratton, C.B., et al., "Angular Distribution of Events from SN1987A", UM PDK 88-1, to appear in Phys. Rev D.
3. Bahcall, J.N., Dar A. and Piran T., Nature, **326**, 135, 1987.
4. Bahcall, J.N., Piran T., Press, W.H. and Spergel, D., Nature, **327**, 682, 1987.
5. Spergel, D., Piran T., Loeb, A., Goodman, J. and Bahcall, J.N., Science, **237**, 1471, 1987.
6. Arafune, J. and Fukugita, M., Phys. Rev. Lett., **59**, 367, 1987; Arafune, J. et al., Phys. Rev. Lett., **59**, 1964, 1987; Bludman, S.A. and Schneider, P.J., Ap. J. **326**, 265, 1988; Burrows, A. and Lattimer, J. M. Ap. J. Lett. **318**, L63, 1987; Dar, A. , to appear in the proceedings of the Supernova 1987A Intl. workshop. Fairfax, Virginia, Oct 1987. Dar, A. , to appear in the proceedings of the Supernova 1987A Intl. workshop. Fairfax, Virginia, Oct 1987. De Rujula A. Physics Letters, **193B**. 514, 1987; De Rujula A. This volume; Nussinov, I. et. al. Nature, **329**, 134, 1987; Sato, K. and Suzuki, H. Phys Rev. Lett, **58**, 2722, 1987; Sato, K. and Suzuki, H. Phys. Lett, **B196**, 267, 1987; Sato, K. and Suzuki, H. Publ. Astron. Soc. Japan. **39**. 521, 1987.
7. Sato, K. and Suzuki, H. to appear in the Proceeding of the 108 IAU colloquium. Sep 1987, Tokyo, Japan.
8. Pomansky, A., Recontres de Physique de Moriond. Les Arcs, 1987.
9. Alexeyev, E. N. et al., Phys. Lett. in press. 1988.
10. Alexeyev, E. N. et al. this volume. 1988.
11. Nakamura, T. and Fukugita, M. Proc of the ESO workshop on the Supernova 1987A, Danziger, I. J. ed. p. 355, 1987.
12. Kovner, I. Wietzmann Institute preprint. WIS-87/20 Phys., 1987.

- 13 Press, W. H et al Numerical Recipes, Cambridge University Press, Cambridge, England, 1985.
- 14 Baade, W. and Zwicky, F., *Proc. Nat. Acad. Sci.* , **20**, 254 (1934); Fowler, W. A. and Hoyle, F., *Ap. J. Suppl.* , **9**, 201 (1964); Colgate, S. A. and White, R. H., *Ap. J.*, **143**, 626 (1966); Arnett, W. D. , *Ann. Rev. Astron. Astrophys.* , **11**, 73 (1973); Bethe, H. A. et al., *Nuc. Phys.*,**A324**, 487 (1979); Bowers, R. L. and Wilson, J. R., *Ap. J. Suppl.*,**50**, 115 (1982); Arnett, W. D., *Ap. J.*, **263**, L55 (1983); Bethe, H. A. and Wilson, J. R., *Ap. J.*,**295**, 14 (1985); Burrows, A. and Lattimer, J. M., *Ap. J.*,**307**, 178 (1985); Wilson, J. R. et al, *Ann. N. Y. Acad. Sci.*,**470**, 267 (1986); Mayle, R., Wilson, J.R., and Schramm, D.N., *Ap.J.*, in press (1987).

GENERAL FEATURES OF NEUTRINO EXPLOSION DYNAMICS

REVEALED BY SUPERNOVA 1987A

S. A. Bludman and P. J. Schinder
Department of Physics, University of Pennsylvania
Philadelphia, Pa. 19104
USA



ABSTRACT

The general features of neutrino transport models for Type II supernova are reviewed, distinguishing the conditions necessary for a prompt shock or for a delayed shock explosion mechanism. The arrival times and energies of Supernova 1987A are consistent with iron core collapse to a neutron star and with known properties of neutrinos. A massive star collapse in our Galaxy, whether or not accompanied by an optical display, would test particular theories for supernova dynamics and for weak interactions.

I. IRON CORE COLLAPSE AND SUPERNOVA EXPLOSION DYNAMICS

A. Late Stages of Stellar Evolution. All of the general features of the quasistatic evolution of a nondegenerate star of mass M and radius R are determined by the virial theorem relating the mean kinetic and potential energies:

$$\langle 2K \rangle = - \langle V \rangle \sim GM^2/R, \quad E = \frac{1}{2} \langle V \rangle \sim - GM^2/2R.$$

For a nondegenerate star of N baryons of mass m_H ,

$$\langle K/N \rangle = \frac{3}{2} \langle kT \rangle \sim \frac{GM m_H}{R} \sim M^{2/3} \langle \rho \rangle^{1/3}$$

where $\langle \rho \rangle$ is the mean density. Four immediate consequences are:

- (1) In order to contract gravitationally, any star must radiate energy. In late stages of stellar evolution (carbon burning and later), the neutrino radiation dominates that by photons.
- (2) In nondegenerate stars, this energy loss leads to temperature increase. (Nondegenerate stars show a negative heat capacity.) If collapse continues, this temperature increase ignites successively nuclear fuels $H \rightarrow He \rightarrow C \rightarrow O\text{-Ne-Mg} \rightarrow Si\text{-S} \rightarrow Fe$.
- (3) Because of the temperature gradient between the center and surface, a star evolves an onion-skin structure with a large envelope of unburnt hydrogen, surrounding a He shell, surrounding a O-Ne-Mg shell...all the way up to Fe, if the star is massive enough to continue contracting.
- (4) Because nuclear burning rates increase rapidly with temperature, nondegenerate stars are gravitationally stable: any density perturbation is immediately corrected by a change in nuclear burning rate and in pressure. A degenerate star has, however, lost this stability: as long as it remains degenerate, its pressure is not responsive to temperature; as soon as the temperature rises enough to remove the degeneracy, the thermal pressure turns on explosively. The ignition temperature of each successive nuclear fuel increases with Z^2 . In low mass stars, a given fuel will ignite at low density, non-degenerately; this allows the star to evolve quiescently to the next stage of nuclear burning.

For $M < 8 M_{\odot}$, carbon ignition taking place while the electrons are degenerate, leads to nuclear explosion. For $8 M_{\odot} < M < 12 M_{\odot}$ (?), carbon burns non-degenerately, but O-Ne-Mg burning takes place explosively. For $12 M_{\odot}$ (?) $< M$, all fuels burn nondegenerately and the core can evolve quiescently all the way to Fe, the stablest of nuclei. Only these massive stars ($> 12 M_{\odot}$), ultimately producing type II supernovae by Fe core collapse, will be considered in this article. More particularly, we will concentrate on the collapse and explosion of this 1.2-2.0 M_{\odot} iron core, ignoring the

stellar mantle and envelope in which the supernova light is produced.

Evolutionary calculations⁽¹⁾ show that a star of main-sequence mass $M_{MS} = 13 M_{\odot}$ evolves a helium core of $M_{\alpha} = 3.3 M_{\odot}$ and an iron core of $M_{Fe} = 1.17 M_{\odot}$. At the center, the density is $\rho_c = 3 \times 10^{10} \text{ g cm}^{-3}$, the temperature is $T_c = 0.78 \text{ Mev}$, and the electron-baryon ratio is $Y_{ec} = 0.41$. During late stages of evolution, electron capture ($e^- + p \rightarrow \nu_e + n$) during quasistatic evolution has already neutronized iron from $Y_e = 0.46$ for Fe_{26}^{56} down to $Y_e = 0.41$ for a mixture of neutrino-rich Fe-Ni. Analysis of the light curve of Supernova 1987A shows that its progenitor was somewhat more massive: $M_{MS} = (15-20)M_{\odot}$, $M_{Fe} = (1.3-1.4)M_{\odot}$.

B. Core Collapse. Stripped of its surrounding onion-skins of lower mass elements, the iron core of the massive star would be a white dwarf. Although its mass exceeds the cold Chandrasekhar mass $M_{CH} = 5.75 Y_e^2 M_{\odot} = 1.01 M_{\odot}$, the iron core is supported against gravity by the thermal pressure of its nuclei and by semi-degenerate electrons. This heat content now reverses the exothermic reactions that produced the iron core in the first place by nuclear fusion. Initiated by endothermic thermal dissociation of the iron nuclei, followed by accelerated electron capture, the reduction in both thermal and degeneracy pressure support drives the core into runaway collapse. Even after neutrinos are trapped at $\rho_{TR} = 10^{12} \text{ g cm}^{-3}$, the cataclysmic collapse accelerates. The collapsing core separates into a subsonic inner core of mass $M_{HC} = 1.04 M_{Fe} (Y_L/Y_{ei})^2$, which collapses homologically, and a supersonic outer core of mass $M_{OVER} = M_{Fe} - M_{HC}$, which lags behind. Here Y_{ei} is the initial electron fraction and $Y_L = (Y_{ef}^{4/3} + 2^{1/3} Y_f^{4/3})^{3/4}$ is the effective lepton fraction of the trapped neutrinos and electrons.

Nuclear incompressibility halts the homologous collapse of the core when the central density reaches $\rho_b \sim (3-4) \times (\text{nuclear saturation density}) \sim 9 \times 10^{14} \text{ g cm}^{-3}$. The signal that the center has stopped propagates through the subsonic inner core, but cannot reach beyond the sonic point, outside of which the matter is falling faster than sound speed. Near this sonic point, which is just outside the edge of homology defined by the included mass M_{HC} , a pressure wave builds up that quickly steepens into a shock wave. The original source of this shock energy is the compressional energy, $E_{comp} \sim 7 \times 10^{51} \text{ ergs}$, of the compressed nuclear matter. The shock is nourished by the energetic matter falling through it and starts to propagate outwards.

The precise location of the sonic point or of the edge of the homology M_{HC} depends on the deleptonization that has transpired from initial electron fraction Y_{ei} to lepton fractions $Y_{\text{ef}}, Y_{\text{vf}}$ at bounce. As the shock wave propagates through the mass overlay M_{OVER} , it is depleted by neutrino radiation $E_{\nu}^{\text{rad}} \approx (2-4) \times 10^{51}$ ergs and by nuclear dissociation $E_{\text{diss}} = 8.5 (M_{\text{OVER}}/0.5 M_{\odot}) \times 10^{51}$ ergs.

C. Shock Propagation. The subsequent fate of the shock propagating through the overlay depends sensitively on neutrino radiation hydrodynamics and is still problematical. If (1) the nuclear matter is compressible enough at high density ρ_{b} to make the original shock energy E_{comp} large; (2) the infall deleptonization is small, so that M_{HC} lies far out; (3) the initial core mass is small, so that $M_{\text{OVER}} = M_{\text{Fe}} = M_{\text{HC}}$ is tolerably small, then the shock will traverse to the edge of the compact iron core with sufficient energy to eject a superficial layer of iron with kinetic energy $\sim 3 \times 10^{51}$ ergs, sufficient to power the optical display of the supernova envelope. This direct, essentially hydrodynamic mechanism, is called the prompt mechanism because if it succeeds, it operates on hydrodynamics time scales of tens of milliseconds.

Otherwise, the shock stalls at about 200-300 km. Because the tenuous matter outside this large radius is weakly bound gravitationally, it may be ejected, if the stalled shock is revived by neutrinos diffusing out of the hot inner core below and by matter still infalling from above. This mechanism is called the delayed or revived mechanism and operates on the time scale (~ 1 second) for neutrinos to diffuse out of dense matter.

Whether either the prompt or the delayed mechanism succeeds well enough to eject matter and power an optically visible supernova is still theoretically undecided. We will return to this question of neutrino explosion dynamics in the second lecture.

D. Prospectus. The gravitational energy ultimately released when an extended structure collapses down to a compact neutron star, is the neutron star binding energy of $(3-5) \times 10^{53}$ ergs. At least 99% of this energy emerges as neutrinos. Even if an optical supernova of 10^{49} ergs is formed, this requires conversion of only 1% of the $(3-5) \times 10^{53}$ ergs into ejected kinetic energy, which subsequently converts into light with another 1% efficiency. The optical supernova, dramatic as it is, is only a superficial phenomenon very sensitive to the neutrino-matter coupling at the edge of the iron core and the matter-light coupling in the surrounding stellar

envelope. The huge neutrino signal is, on the other hand, relatively insensitive to details.

What characterizes stellar collapse is this huge neutrino output in a few seconds. Indeed, Supernova 1987A shows us how a supernova can be optically weak, so that the true collapse rate may be seriously underestimated by the observed supernova rate. It also reminds us that massive stars may collapse to neutron stars with little or no light emission and that some collapses into black holes may radiate neutrino pulses, before they are engulfed by the event horizon.

If a neutron star remains, it must be very hot (~ 100 Mev) and must cool rapidly by neutrino radiation. It is these neutrinos from the hot nascent neutron star that were observed by Kamiokande II and IMB. We turn now to the analysis of the arrival times and energies of the $11 + 8 = 19$ neutrinos they observed. We will find that the sparse and uncertain neutrino signals from the cooling neutron star suffice to confirm remarkably the general features of the scenario we have just described, but not the details of any particular theoretical neutrino explosion mechanism.

II. ANALYSIS OF THE NEUTRINOS FROM SN 1987A

A. Neutrino Arrival Times and Energies. In our^(2,3,4) analysis of the Kamiokande II and IMB data we: (1) considered indiscriminately the complete sample of 19 neutrinos; (2) Ignored their angular distribution, which is consistent with isotropy. (Almost all the events captured in water would be expected to be $\bar{\nu}_e$ absorption ($\bar{\nu}_e + p \rightarrow e^+ + n$); only about one event would be expected to be $\nu_e + e^- \rightarrow \nu_e + e^-$. This might be the first forward-pointing event of Kamiokande II but, because we have no way of discriminating, we treated all 19 events as coming from the same $\bar{\nu}_e$ sample); (3) We set the neutrino mass equal to zero. The signal direction is consistent with $m_{\nu_e} < 17$ eV, which is also the laboratory limit.

We avoided the theorists' temptation to overinterpret these 19 events and did not pretend to discriminate among the 19 neutrinos. We assumed a thermal distribution of $N_0 \bar{\nu}_e$ with temperature T_S at time $t = 0$ at the source, and folded in the individual detector thresholds, efficiencies and energies and their uncertainties. We fit the thermal source cooling to the cooling function

$$T(t) = T_S \left(1 + \frac{at}{n}\right)^{-n} \quad (2.1)$$

where, for each n , the three parameters T_S , a , N_0 were determined from the data by maximum joint likelihood analysis. Special cases of the above form are: $a = 0$, constant temperature; $n = \infty$, exponential cooling at the

constant rate $\tau = a$; $n < \infty$, power law cooling, at the rate

$$\tau(t) \equiv - (d \ln t / dt)^{-1} = a^{-1} + t/n,$$

fast at the beginning, but protracted thereafter; $n = 1/2$, semi-degenerate Fermi gas whose heat content $E(t) \propto T^2$ is being black-body radiated $dE/dt = 4\pi R_V^2 \sigma T^4$ from some neutrinosphere fixed at (average) radius R_V .

Our best maximum likelihood fits to the combined Kamiokande-IMB data are given in Table 1 for each n , together with their (unnormalized) likelihoods. We see that:

- (1) The cooling models for various n have comparable likelihood. Any cooling source is 10^5 times more likely than a constant temperature source radiating for 12.4 seconds.
- (2) Our exponential fit yielding a fluence of $N_0 = 4.6 \times 10^{57} \bar{\nu}_e$ with energy $E = 6.7 \times 10^{52}$ ergs agrees with that of Spergel et al.⁽⁵⁾
- (3) Our $n = 1/2$ model (semidegenerate gas radiating from a black body of fixed radius), $T(t) = T_S (1 + 2at)^{-1/2}$, $T_3 = 4.1$ Mev, $a = 0.12 \text{ s}^{-1}$, $N_0 = 7.8 \times 10^{57} \bar{\nu}_e$, $E_0 = 8.0 \times 10^{52}$ ergs is three times more likely than the exponential model, for which there is no theoretical basis.
- (4) Allowing for six neutrino flavors, the total energy radiated $6 E_0 = (4-5) \times 10^{53}$ ergs, in good agreement with the binding energies of neutron stars of maximum mass calculated with various equations of state.
- (5) Because of the power-law tail to its cooling curve, the $n = 1/2$ model

n	a (s^{-1})	T_S , (Mev)	E_0 (10^{52} erg)	N_0 ($10^{57} \bar{\nu}_e$)	Max(J)
0.335	0.176	4.20	11.9	380.6	6.304
0.35	0.167	4.19	10.9	41.4	6.376
0.4	0.144	4.16	9.2	13.1	6.380
0.5	0.116	4.08	8.0	7.8	5.940
1.0	0.077	3.95	7.1	5.3	4.075
2.0	0.063	3.88	6.9	4.9	3.066
∞	0.052	3.84	6.7	4.6	2.197
-	0	3.33	5.7	3.4	10^{-5}

Table 1. Maximum joint likelihood fit of our cooling models $T = T_S (k + \frac{at}{n})^{-n}$. Special cases: $a = 0$, constant temperature, $n = \infty$, exponential; $n = \frac{1}{2}$ semidegenerate Fermi gas radiating as a black body.

gives E_0 and a neutron star binding energy 20% higher than that given by exponential cooling. This large binding energy suggests a large mass ($1.4 M_\odot$) iron core and a soft nuclear equation of state.

The probable errors in each of our best fits were 10% in T_s , 30% in E_0 and in N_0 , determined by running 750 Monte Carlo simulations of the two detectors.

The goodness-of-fit between our best fit $n = 1/2$ model and the separate Kamiokande II and IMB data sets is shown in Fig. 1. The top two curves show the cumulative distribution in arrival times, the bottom two curves the cumulative distribution in energies for the 11 Kamiokande II events and for the 8 IMB events. In each figure, the best fit is given by the central (dotted) curve, the 1σ and 2σ limits are shown by the surrounding pairs of long-dashed and short-dashed curves. Although Kamiokande seems to detect fewer and IMB more events than our best fits would have predicted, the observations at each detector agree with our best joint fit within 1σ . All our models would show almost the same goodness-of-fit.

B. Other Conclusions. Kamiokande II knew the absolute time of their data train only within one minute. We therefore estimated the time offset between the Kamiokande II and IMB data trains by Monte Carlo simulations and found that Kamiokande II lagged IMB by $0.1 + 0.5$ s. Our analysis of the data thus sets the Kamiokande clock within 0.5 seconds!

Besides the above continuous cooling models, we also considered models in which, as theoretically expected, a short heating period preceded the cooling. We found that such heating period in the observed data had to be shorter than 0.4 s.

By power spectrum analysis and by minimum residuals, we also showed that there were no significant periods in the Kamiokande II data, on any time scale.

The temperature of the $\bar{\nu}_e$ neutrinosphere is maintained by ν_e and $(\bar{\nu}_{\mu, \tau})$ diffusing out of the inner core over a few seconds. The total energy radiated, $6 E_0$, and the $\bar{\nu}_e$ number flux cooling time $(3a)^{-1} = (2.5-6)$ seconds we obtained, are consistent with neutrino diffusive cooling of a hot neutron star of time-averaged radius 35 ± 10 km.

The sparse and uncertain data from Kamiokande II and IMB are then consistent with the diffusive cooling of a hot neutron star remnant from the collapse of a $1.4 M_\odot$ iron core in a massive star. The observations are also consistent with laboratory bounds on the ν_e mass and with cosmological bounds on axion coupling, but no neutrino mass, neutrino oscillations, exotic neutrino interactions or exotic particles can be demonstrated from the

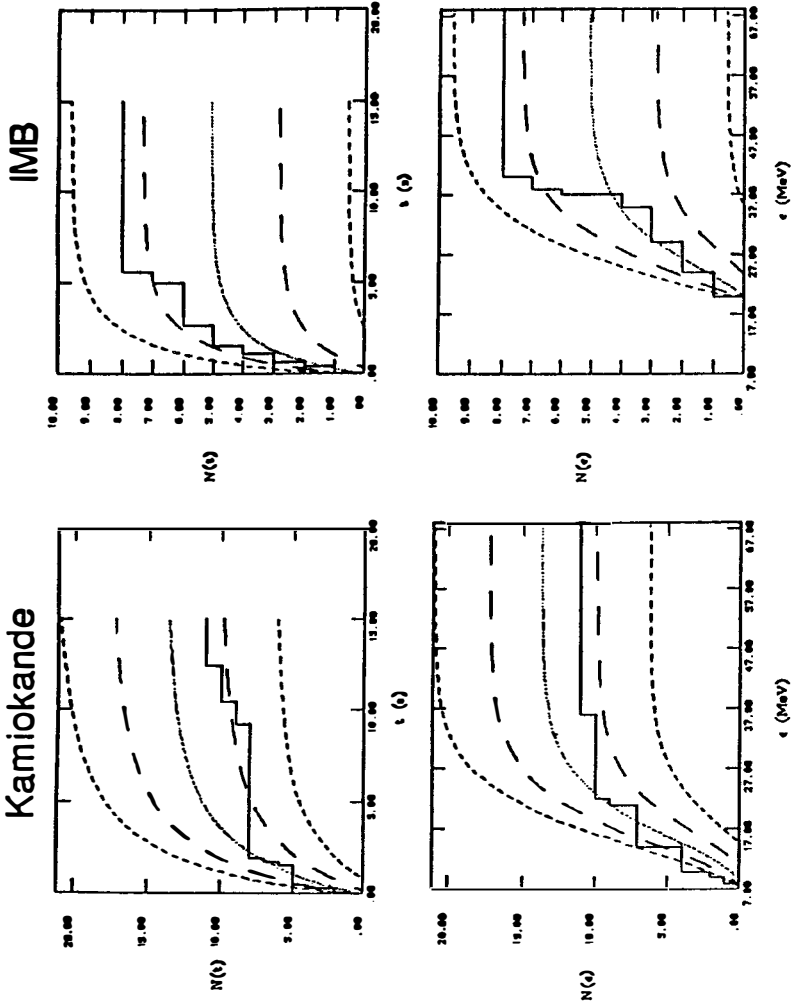


Fig. 1. Comparison of best fit $n = 1/2$ model with observations.

SN 1987A data. The data is also too sparse to show the detailed time structure that would test any particular neutrino explosion mechanism.

III. PROSPECTS FOR STELLAR COLLAPSES WITHIN OUR GALAXY.

Within our Galaxy, all stars more massive than $10 M_{\odot}$ die at a rate $1/50$ years, a value as small as $1/11$ years being estimated by Bahcall and Piran.⁽⁶⁾ These collapses may be to black holes as well as to remnant neutron stars or pulsars. Protracted mass accretion leading finally to black hole formation might be expected to produce a neutrino signal similar to SN 1987A, whether or not associated with optically visible supernova.

Any stellar collapse within our Galaxy, ten times closer than SN1987A in the Large Magellenic Cloud, would produce about 10^3 neutrinos in the existing Kamiokande-IMB detectors. With so many events, important particle physics and supernova physics would be learned.

A. Particle Physics. A sample of 10^3 supernova neutrinos would contain about $14 \left(\frac{v}{c}\right)_{\mu, \tau}$ whose masses could be determined from their time of flight

$$\Delta t = \left[\frac{m_{\nu}(\text{eV})}{E_{\nu}(\text{Mev})} \right]^2 \left(\frac{D}{5 \text{ kpc}} \right) 0.25 \text{ seconds}$$

from distance D. Indeed, if $\nu_{\mu, \tau}$ have masses below the cosmological bound, their masses could be directly measured only over astronomical flight paths.

B. Supernova Physics. A pulse of 10^3 neutrinos would show time structure (prompt neutronization burst over milliseconds, accretion heating and diffusive cooling over seconds) diagnostic for different theoretical neutrino explosion mechanisms. In some models⁷, the delayed explosion is preceded by gravitational oscillations of period 0.1 seconds, characteristic of the inner core density. If so, the same power spectrum analysis which revealed no periods in the 11 Kamiokande II events would reveal such 0.1 second periods provided their amplitude modulation $\geq 10\%$.

For these reasons, we look forward to the construction of dedicated supernova detectors and the coming Galactic supernova. Armed with the experience and confidence gained from Supernova 1987A, the new cadre of neutrino astrophysicists will be able to observe and analyze neutrino dynamics important to both supernova and particle physics.

This work is partially supported by the DOE contract EY-76-D-02-3071.

References

1. K. Nomoto, T. Shigeyama, and M. Hashimoto, in Proc. ESO Workshop on "SN 1987A" (ed. I. J. Danziger, ESQ: Garching (1987).
2. S. A. Bludman and P. J. Schinder, Ap. J. 326, 265 (1988).
3. P. J. Schinder and S. A. Bludman, in Proc. Fourth George Mason Fall Workshop in Astrophysics (Cambridge Univ. Press, 1988).
4. S. A. Bludman and P. J. Schinder in Proc. Workshop on Extrasolar Neutrino Astronomy (UCLA, 1987).
5. D. N. Spergel, T. Piran, A. Loeb, J. Goodman and J. N. Bahcall, Science 237, 1471 (1987).
6. J. N. Bahcall and T. Piran, Ap. J. (Letters) 267, L77 (1983).
7. R. Mayle, Ph.D. Thesis, University of California, Berkeley, 1986.

COMMENTS ON SN 1987A

Richard SCHAEFFER
*Service de Physique Théorique†
de Saclay
F-91191 Gif-sur-Yvette cedex*



The SN 1987A event in the large magellanic cloud was very surprising. A few days after its occurrence, it was obvious that the event should be classified as a type II supernova : Hydrogen was the dominant element, and the neutrino signal indicated the formation of a condensed object. The very likely explanation thus was that the event was due to the collapse of the iron core within a fairly heavy star, followed by an outward propagating shock. The surprises (ESO workshop, 1987), however, came from the magnitude of the luminous emission and the photospheric temperature that were pretty low for a typical SN event. Also, after a short underluminous plateau phase, the light emission started to be dominated by ^{56}Ni decay as is usually the case for an SNI. The progenitor was neither a white dwarf nor a red giant. Such a strange event, however, had been considered (Schaeffer, Cassé, Cahen 1987, SCC87) before the occurrence of SN 1987A.

† Laboratoire de l'Institut de Recherche Fondamentale du Commissariat à l'Énergie Atomique

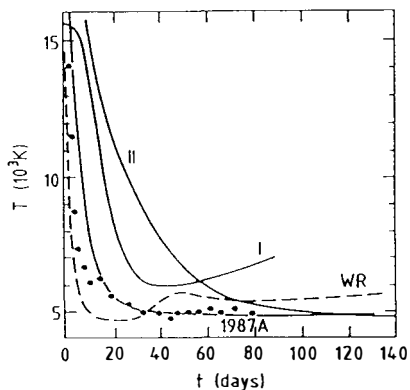
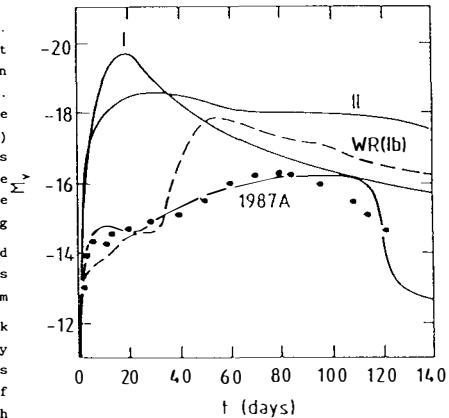
The faint light curve and the rapid decline of the temperature during the first days (Fig.1 and 2) can be explained by the compactness of the SN 1987A progenitor. Indeed (SCC87 and Schaeffer, Cassé, Mochkovich, Cahen 1987, SCMC87) the star is quite opaque under these conditions, and the luminous emission reduced. During its expansion, adiabatic cooling uses up all the available thermal energy that thus is not emitted in the form of light, but transformed into kinetic energy. Originally invoked for exploding Wolf-Rayet stars, this mechanism holds also for Sk 69202. The latter is obviously not a Wolf-Rayet star, but presents some similarities with such stars : it is small, compact and blue due to strong mass loss in the presupernova stage. The major difference is that its estimated initial mass ($15M_{\odot}$ - $20M_{\odot}$) is somewhat smaller than what is expected for Wolf-Rayet stars ($\sim 40M_{\odot}$ or more). The mass loss rate must have been fairly lower, since the outer layers were still hydrogen-dominated : at explosion the mass was still in the 10 - $15M_{\odot}$ range, as is now commonly admitted (SCMC87, Arnett 1987, Woosley et al 1988). The other difference is that Sk 69202 probably went through a red giant phase (Maeder 1987) before becoming a blue star whereas Wolf-Rayet stars do not. Nevertheless, the similarities

Fig. 1. :

Early light curve (SCMC87). The plateau phase during the first month was much fainter than expected for a typical SNI or SNI1. It was nearly of the same magnitude as the plateau calculated (SCC87) for exploding Wolf-Rayet stars (full curve, labelled SNI1). The bump after ~ 25 days in this case is due to $0.3M_{\odot}$ of ^{56}Ni decaying into ^{56}Co and ^{56}Fe . The dashed curve corresponds to the parameters of Sk 69202 ($15M_{\odot}$ mass, 310^{12}cm radius and $1.2 \cdot 10^{51}$ erg shock energy) with no Ni. The similarity of the Sk and Wolf-Rayet curves is due to the fact that, because of presupernova mass loss, both progenitors are massive but compact stars.

Fig. 2. :

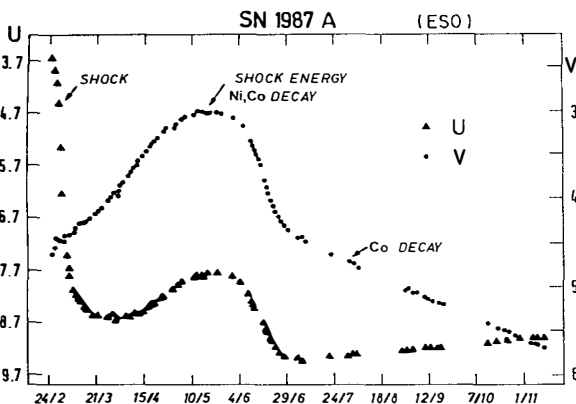
Temperature evolution (SCMC 87). The SN 1987A photospheric temperature is seen to be much lower than for an ordinary SNI or SNI1 event. It is nearly the same than for the SNI1 event calculated for a Wolf-Rayet progenitor (full curve). The dashed curve is the same calculation with the parameters of Sk 69202. As for the light curve, the similarity of the Sk and Wolf-Rayet curves is due to the fact that, because of presupernova mass loss, both progenitors are massive but compact stars.



in origine (a blue star that is small and compact because of mass loss) as well in the properties of the light curve (fainter, cooler) are striking, making both categories of explosion nearly the same. Due to the small fraction of the initial heat content that can be emitted as light, any late energy source will dominate the luminous emission after some time. The decay of ^{56}Ni and ^{56}Co is obviously of major importance. It was noted (SCC87, SCMC87) that masses of $0.3M_{\odot}$ would be overwhelmingly dominant, whereas an amount as low as $0.1M_{\odot}$ or even $0.05M_{\odot}$ could be visible. This also is a common feature of Wolf-Rayet explosions and SN 1987A. Other late energy sources such as the recombination energy of the electrons may play a role, but only if the initial ^{56}Ni content is lower than the above values. The SN 1987A light curve is compatible with $0.07M_{\odot}$ of ^{56}Ni (Woosley et al 1988) as can be inferred from the tail of the light curve (Fig. 3) and the observation of the γ -ray line due to the decay of ^{56}Co . Despite their similarities, the two kinds of events are usually classified into SNIb for Wolf-Rayet explosions, because of the lack of hydrogen, and into a new subclass, SNIib, for SN 1987A where hydrogen is present. Both kinds of events being due to massive stars are initiated by the collapse of the iron core of the progenitor and form a neutron star. It might thus be worthwhile to consider the classification of Chevalier (1986) that, after the suggestion (Chevalier 1976, Maeder and Lequeux 1982, Wheeler and Leveault 1985, Cahen et al 1985) that Wolf-Rayet stars might explode and could be SNIb's, introduced the new SNIII category to which SN 1987A may be rattaché, the light curve as well as the explosion mechanism being similar.

The SN 1987A thus is expected to explode via a core-collapse, the formation of a neutron star and a subsequent outward propagating shock. This is the mechanism that is believed to hold (Brown, Bethe, Baym 1981) for the SNI events. This explanation, however, is still questioned since

Fig. 3. :
Light curve (ESO) in the U and V bands. The narrow, prominent peak in the U band during the first days is characteristic of a shock hitting the star surface. The subsequent bump in the V band is mostly due to the radioactive decay of ^{56}Ni and ^{56}Co . The late time tail has an exponential slope that reflects quite accurately the Co lifetime.

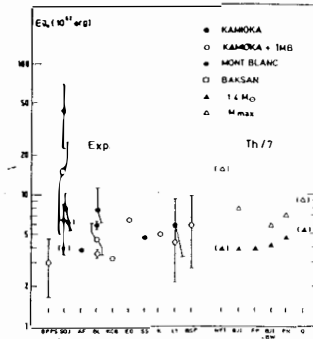


the numerical simulations do not produce an outward shock that is efficient enough to blow out the remainder of the progenitor (Baron, Cooperstein, Kahana 1985) unless an more or less arbitrary change is made in the compressibility of nuclear matter. Such a modification has received some justification (Brown and Osnes 1986) but is still criticized (Glendenning 1986, Pines et al 1988). We however follow the conclusion of the latter authors that consider the value obtained from nuclear excited states (Blaziot 1980) as still the more accurate determination of the compressibility. This value is close to the one to be used for supernovae. It is thus of primordial importance to note that the emergence of the shock is actually observed (Fig. 3) in the SN 1987A event. Without this shock, the bolometric light curve would be flat (Arnett 1982). During the first days, a prominent peak is present, as expected for this type of explosion. The observations thus tell us that the shock is indeed strong enough to get to the star's surface, and is very likely to be responsible for the explosion.

Finally, the neutrino signal was observed signal a few hours before the optical. The energy involved proves that a compact object was made at the outset of the supernova event. The signal, however was observed twice. First, the Mont-Blanc group reported an event, and five hours later the Kamioka, IMB and (marginally) the Baksan groups detected a neutrino signal. Only one neutrino burst was expected. The energy implied by the Mont-Blanc event, however, exceeds by an order of magnitude (Schaeffer, Declais, Jullian 1987) the one expected from any reasonable equation of state. This signal thus cannot be due to the formation of a neutron star. All groups having analysed the Kamioka and IMB events, on the other hand, find (Fig. 4) that this signal is compatible with a standard, $1.4M_{\odot}$,

Fig. 4. :

Energy in the emitted $\bar{\nu}_e$ pulse as implied by the various detections of the Mont-Blanc, Baksan, Kamioka and IMB groups. The initials refer to the various analysis of these events. The various theoretical models are those considered by Haensel and Proszynski 1982 (W.P.N. BJI) and Haensel et al 1986 (FP. SS), for a standard ($1.4M_{\odot}$) neutron star and for the largest possible stable star. The theoretical energies were kindly provided by P. Haensel (1988). The brackets indicate extreme equations of state.



neutron star made during the explosion. Together with the fact that the Mont-Blanc signal was not seen by the more sensitive Kamioka detector we are led to conclude that this signal was very likely not due to SN 1987A (I disagree with the conclusions drawn by De Rujula, 1987, that the detection by the Mont-Blanc and the non detection by Kamioka can be made compatible). Possible mechanisms have been suggested to reconcile the theory with the observation of a double bust (Hillebrandt et al 1987). Two possibilities were considered. Firstly a phase transition within the neutron star after a period of metastability. To meet the energy requirements of the first bust, a neutron star mass well above the Oppenheimer-Volkov limit is needed. It can be roughly estimated to be $\sim 5M_{\odot}$. For such masses, metastability may be present but during times that are typically milliseconds (Haensel and Schaeffer 1981), considerably shorter than the needed five hours delay. A second possibility considered by the former authors is a double system of

condensed stars, that due to dissipation collapses further five hours later. The excessive energy requirements of the Mont-Blanc neutrino detection make again this scenario very unlikely.

The occurrence of the SN 1987A event is thus consistent with the current theories of stellar evolution. It simply corresponds to a rather rare massive star explosion that could not have been recognised easily in outer galaxies. The observation of the neutrino signal, also, is consistent with the standard neutron star formation theories. This event provides the first confirmation of the core-collapse and shock mechanism for the explosion of the more massive stars.

REFERENCES

- Aglietta M. et al, 1987, Europhys. Lett 3, 1315
 Alexeyev E.N. et al 1987, JETP Lett. 45, 461
 Arafune J., Fukugita M., 1987, Phys.Rev.Lett. 59, 367
 Arnett W.D., 1982, AP.J. 253, 785
 Arnett W.D., 1987, AP.J 319, 136
 Bahcall J.M., Piran T., Press W.M., Spergel D.M., 1987, Nature
 Bahcall J.M., Spergel D.M., 1988, Phys.Lett. 200, 366
 Baron E., Cooperstein J., Kahana S., 1985, Nucl.Phys. A440, 744
 Baron E. Cooperstein J., Kahana S., 1985 Phys.Rev.Lett. 55, 126
 Bionta R.M et al, 1987, Phys.Rev.Lett. 58, 1494
 Blaizot J.P., 1980, Phys.Rep. 64, 171
 Brown G., Osnes E., 1986, Phys.Rev.Lett. 159, 1085
 Brown G., Bethe H.A., Baym G., 1981, Nucl.Phys. A375, 481
 Burrows S.A., Lattimer J.M., 1987, Ap.J. Lett
 Cahen S., Schaeffer R., Cassé M., 1985 3rd Astrophysical Moriond Meeting (Nucleosynthesis and Its Implication on Nuclear and Particle Physics, Ed.b.J.Audouze and N.Mathieu Dordrecht 1986: Reidel)
 Chevalier R.A, 1986, I.A.U. General Assembly Delhi (Highlights of Astronomy Ed. J.P. Swings, Dordrecht 1987, Reidel)
 De Rujula A., 1987, Phys.Lett. B193, 514
 Ellis J., Olive K.A., 1987, CERN-TM 4701/87
 ESO Workshop on the SN 1987A, 1987, Ed. I.J. Danziger
 Glendenning N., 1986, Phys.Rev.Lett. 57, 1120
 Haensel P., Proszynski M., 1982, Ap.J. 258, 306
 Haensel P., Schaeffer R., 1981, Nucl.Phys. A381, 519
 Haensel P., Zdunik J.L., Schaeffer R., 1986, A.A. 160, 251
 Hirata K. et al, 1987, Phys.Rev.Lett. 58, 1490
 Kahana S., Cooperstein J., Baron E., BNL 40012
 Kraus L.M, YIP 87-16
 Lattimer S.M., Yahil A., ACS Symposium, New Orleans 30 avril-4 septembre 1987
 Maeder A., 1987, ESO Workshop on the SN 1987A Ed.b.I.J.Danziger
 Maeder A., Lequeux J., 1982, A.A. 114, 409
 Matz S.M. et al, 1988, Nature 331, 416
 Pines D., Quader K.F., Wambach J., 1988, Nucl.Phys.A477, 365
 Sato K., Suzuki M., 1987, Phys. Rev.Lett. 58, 2722
 Schaeffer R., Cassé M., Cahen S., 1987, Ap.J.Lett. 316, L31
 Schaeffer R., Cassé M., Mochkovich R., Cahen S., 1987, A.A. Lett 184, L1
 Schaeffer R., Declais Y., Jullian S., 1987 Nature 330, 142
 Woosley S.E., 1988, Preprint UCRL 98001
 Woosley S.E., Pinto P.A., Ensmann L., 1988 Ap.J. 324

SIMULATION OF NEUTRINO TRANSPORT IN SUPERNOVAE

J.P. CHIEZE

C.E.A.

Centre d'Etudes de Bruyères-le-Châtel

Service P.T.N.

BP 12, F-91680 - Bruyères-le-Châtel, France

**ABSTRACT**

We present a simulation of neutrino transport in supernovae, in which the neutrino gas and the scattering medium are treated as two fluids exchanging energy and momentum. The method covers the whole range between the optically thick and thin regimes. We present some tests of the method, including energy transfer between matter and neutrinos and thermalization.

I INTRODUCTION

Neutrino transport plays a crucial role in Type II supernova theory. Due to the existence of neutral currents, neutrinos can participate efficiently to the dynamics of the collapse (the equation of state is governed by the leptonic fraction Y_l) and of the explosion (they provide an important energy store which may ultimately reinforce the stalled hydrodynamical shock¹⁾).

The neutrino transport problem is easily handled in the optically thick (diffusive) regime or the optically thin (free-streaming) regime. But the accurate treatment of the intermediate semi-transparent regime is much more difficult.

Neutrino trapping in a collapsing supernova core occurs at densities greater than $\rho \approx 10^{12} \text{ g cm}^{-3}$. By definition, the onset of trapping requires a careful treatment of the neutrino transport precisely in the semi-transparent regime. The situation is quite similar in the vicinity of the core bounce shock. It is therefore necessary to derive a technique able to deal with rapidly varying neutrino mean free path (both in time and space), in matter with complex motions, from free-streaming up to complete trapping.

Previous numerical simulations have made extensive use of flux-limiters^{2),3),4)}. The method presented here avoids, by construction, such difficulties and can be considered as exact within numerical accuracy⁵⁾.

II Simulation of Neutrino Transport

The neutrino mean free path in dense matter is dominated by elastic scattering on heavy nuclei. In matter of density ρ , composed of nuclei of atomic number A and neutron number N , the mean free path of neutrinos of energy E is:

$$\frac{\lambda_\nu}{1 \text{ cm}} = 4 \cdot 10^9 \frac{A}{N^2} \left(\frac{E}{1 \text{ MeV}} \right)^{-2} \left(\frac{\rho}{10^{11} \text{ g cm}^{-3}} \right)^{-1} \quad (1)$$

In order to avoid the numerical flaws which downgrade the resolution of the transfer differential equation, we keep close to the elementary physical processes which govern the problem. If we consider the diffusion on heavy nuclei, the neutrino gas behaves as a Lorentz gas. The properties of the flow are only governed by the differential macroscopic scattering cross section, proportional to $E^2(1 + \cos\theta)$, where θ is the scattering angle. The evaluation of energy and momentum transfer between the neutrino flow and supernova matter requires a self-consistent treatment of neutrino source terms and diffusion processes.

Source terms include neutrino production by electron capture both on free protons and heavy nuclei, and pair production in hot matter. Conversely, neutrinos are mainly absorbed by free neutrons.

Neutrino diffusion is due to inelastic scattering on electrons and coherent or incoherent scattering on nuclei and nucleons. Beta-reactions and, in a less extent, inelastic neutrino-electron scattering mediate the energy transfer between the neutrino gas and matter, while the (coherent) elastic scattering on nuclei dominates the opacity of dense stellar matter and thus governs the transport properties and momentum transfer.

Since neutrinos in the high density cores of supernovae form a degenerate Fermi gas, Pauli blocking factors are included.

The neutrino flow, distributed in a given number of energy bins (typically 10-30 energy bins), is streaming along a network of characteristics, with a large number of mesh points. Neutrino-matter interactions (elastic or inelastic scattering, neutrino emission and absorption) are regarded as source or sink terms operating along a given element of characteristic^{4),6),7)}.

i) By construction, the method conserves the total number of neutrinos.

ii) The method can accommodate any value of the cross-section (including $\sigma = 0$, i.e., free-streaming). It treats equally well and on the same footing the thin and thick regimes, and therefore, the transition between these two limiting cases. Both the isotropic diffusion limit and the highly anisotropic free-streaming limit can be handled with the same technique and with perfectly similar accuracy.

iii) Discontinuities in the matter density and therefore in the macroscopic cross-section do not raise any special difficulties, as opposed to what is encountered in partial differential equations. Hence, there is no need whatsoever to introduce flux limitation.

iv) The method is well suited for calculating physical quantities which result from the elementary scattering processes, such as momentum transfer. The evaluation of the momentum balance, for instance, is directly available at each step.

v) all the interactions are treated in the material comoving frame, and translated in a coordinate frame fixed with respect to the star.

Comparisons with Exact Solutions

Our first concern has been to check the accuracy of the method in cases where analytic solutions are available for comparison. These tests have been conclusive both in the case of vanishing cross section (free-streaming) and in the diffusive limiting regime in an infinite medium.

All calculations have been performed using units such that the neutrino velocity, the total extension and the total mass of the scattering medium are equal to 1. In all computations reported here, we used 300 mesh points within $R_0 = 1$ and to each mesh point is associated a set of 31 directions.

Fig. 1a) represents the analytical solution for a *freely expanding neutrino gas*. Fig. 1b) represents the simulation. The initial neutrino distribution $f(r, t = 0, \omega)$ is uniform and isotropic with $f = 1$ for $r \leq R_0$, and $f = 0$ for $r > R_0$. We plot the local total neutrino density $F(r, t) = \int_{-1}^{+1} f(r, t, \omega) d\omega$ as a function of the radius r for successive increasing values of the time t . At a given radius r the set of curves correspond to increasing values of the time $t_n = n\Delta t$ as one goes from the top to the bottom of the figures. The time interval between each curve is $\Delta t = \frac{R_0^3}{2c^3} = 0.05$.

Comparison of Fig. 1a) and 1b) shows the excellent agreement between the numerical and the analytical solutions. This is a test of the efficiency of the treatment of unscattered neutrinos.

At the beginning of the simulation, the neutrino density at the boundary of the initial (isotropic) distribution is reduced by a factor 2, since here, neutrinos which move in the

inward direction (half of their total number) are not replaced. This example shows that discontinuities in the *neutrino* distribution are correctly treated.

Another important feature of the exact solution is the transport to the center, of the initial singularity in the neutrino density distribution (at $t = 0, R = \frac{1}{2}$), at the time $t = \frac{R}{c} = \frac{1}{2}$. After that time, the central regions are no more replenished by incoming neutrinos, travelling from the outer regions.

At the center, the density suddenly drops from $F(0, \frac{1}{2} - \epsilon) = 1$ to $F(0, \frac{1}{2} + \epsilon) = 0$, where $\epsilon \ll 1$ as the time crosses $t = \frac{1}{2}$.

During the time interval $0 \leq t < \frac{1}{2}$ the neutrino density is uniform and equal to 1 inside a spherical region of steadily decreasing radius $r_1 = R - ct$. For $t \geq \frac{1}{2}$, a completely depleted region grows with radius $r_0 = c(t - \frac{1}{2})$. Neutrinos have completely leaved the region where they were initially confined at the time $t = 2\frac{R}{c} = 1$.

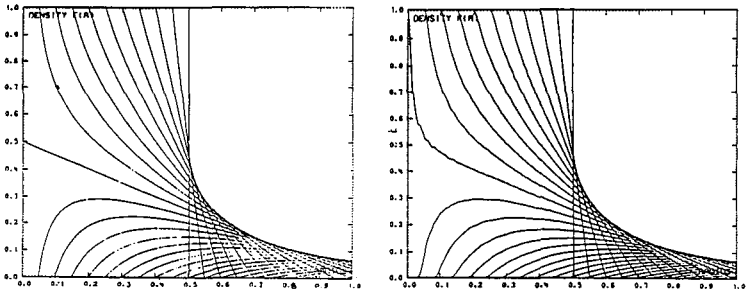


Fig. 1a: The analytical solution for free streaming neutrinos, for different times. Neutrinos are initially confined in a sphere of radius $R_0 = 0.5$ (arbitrary units), with an isotropic angular distribution. The total neutrino density is plotted on the vertical axis, normalised to its initial value.

Fig. 1b: The numerical solution for the same conditions as in Fig. 1a.

We turn now to the test of the *diffusive regime*. In this case, neutrinos are flowing along each characteristic element of the network. We consider an initial neutrino density of the form

$$f(r, t, \omega) = \frac{1}{2} (F(r, t) + 3\omega J(r, t)) \tag{2}$$

where $F(r, t) = \sin(kr)/kr \exp(-k^2 Dct)$ is the solution of the diffusion equation in spherical geometry and $J(r, t) = -D\nabla F(r, t)$ is the current density. We show on Fig. 2) the

numerical evolution of the total neutrino density: the simulation reproduces accurately the analytical solution. More precisely, the effective diffusion coefficient is $D_{eff} = \lambda/2.95$. The actual Eddington value is $D_{Edd} = \lambda/3$. This 1.7% difference is due to the finite neutrino mean free path actually used in the simulation ($\lambda = R(= 1)/200$).

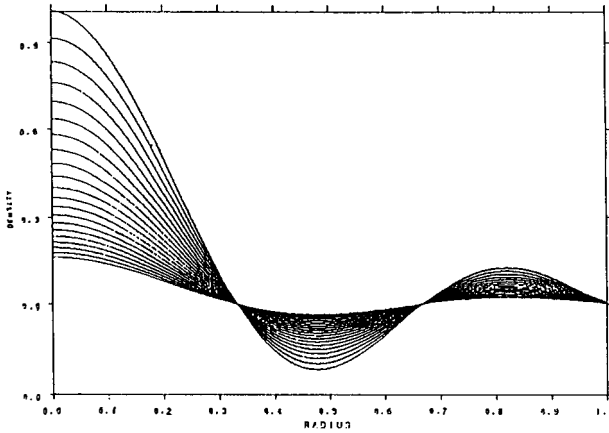


Fig. 2: Diffusive regime. The time dependent evolution of the third eigenmode of the diffusion equation.

The results presented in Fig. 2) are obtained using 31 discretized directions, but the same results are obtained when this number is reduced to 7.

Finally, Figs. 3 a,b) illustrate the neutrino flow crossing a density jump of a factor of 4, together with the net transfer of momentum from the neutrino gas to the scattering medium.

III Energy Exchanges

Neutrinos can locally gain or loss energy when they interact with electrons, nucleons, or nuclei which are infalling or expanding at relativistic velocities. Collisions with nuclei are treated in the comoving material frame. In the laboratory frame, attached to the center of the star, they result in a net energy transfer from matter to the neutrino gas ($-pdV$ work).

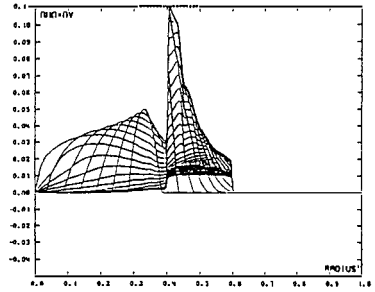
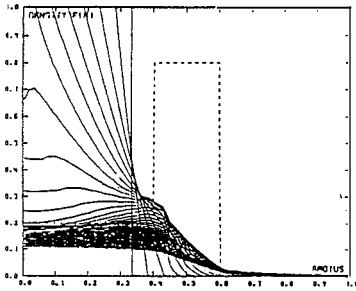


Fig. 3a: Discontinuous distribution of the scattering medium. Since the neutrino mean free path is inversely proportional to the density of scatterers, this case corresponds to $\lambda_m = \frac{1}{4}$ inside the core ($R < 0.4$) and $\lambda_m = \frac{1}{10}$ in the interval $0.4 \leq R \leq 0.6$.

Neutrinos escaping from the core are caught in a waiting line inside the diffusive barrier. Initially, some neutrinos are backscattered to the inner core whose depletion is slowed down.

Fig. 3b: Net momentum transfer from the neutrino gas to matter.

The neutrino energy distribution function is obtained in the rest frame as a function of the position in the star, the direction of propagation and time. It is given in terms of probability of occupation $f_\nu = f(\mathbf{r}, t, \Omega, \epsilon)$ of quantum states in the range $d^3\mathbf{r}d^3\mathbf{k}$, which is a relativistic invariant. It is defined by:

$$dn = (hc)^{-3} f_\nu \frac{1}{\beta} \frac{d\omega}{\beta^2} d\omega d\phi dV \epsilon^2 d\epsilon \tag{3}$$

where $\beta = v/c$ is the local velocity of the scattering material, $\epsilon = \hbar ck$, and where all other quantities have their usual meaning.

For practical purposes, only the energy occupation $f(\mathbf{r}, t, \epsilon)$, integrated over angles, is needed.

As an illustrative example, we present a short sketch of the diffusion of neutrinos in a collapsing stellar core, in the vicinity of the trapping density. The total mass of the core is $1 M_\odot$ with a uniform density of $\rho_0 = 10^{12} \text{ g.cm}^{-3}$. The infalling material (with an adiabatic exponent $\gamma = \frac{5}{3}$) is supposed to collapse homologously, so that the velocity field is linear and given by:

$$v(r, t) = \frac{2}{3} \frac{\Omega}{1 + \Omega t} r \tag{4}$$

where $\Omega = (6\pi G \rho_0)^{\frac{1}{2}} = 1122 \text{ s}^{-1}$.

The initial velocity at the edge of the infalling core is $v_0 \simeq \frac{c}{5}$. The neutrino gas is initially prepared as a zero temperature Fermi gas uniform and isotropic with a Fermi energy ($\epsilon_F = 10 \text{ MeV}$) over 90% of the core extension. We consider only elastic scattering in this example.

The evolution in space and time of the neutrino distribution functions $f(r, t, \omega, \epsilon)$ is followed up to a matter density $\rho = 2 \cdot 10^{12} \text{ g.cm}^{-3}$ just prior to complete trapping.

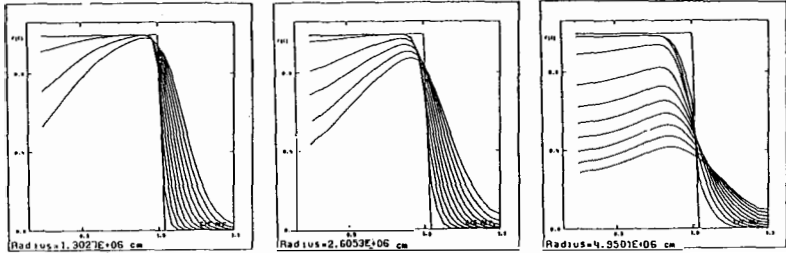


Fig. 4.a,b,c: The time dependent evolution of the probability of occupation of neutrino states with energy E for three (Eulerian) positions inside the collapsing core of a supernova - assuming no source terms. The vertical axis represents the occupation index $f(E)$. Since the distribution is not an equilibrium one, the occupation index is averaged over the azimuthal angles of the neutrino wave vector k , with $k = \frac{E}{\hbar c}$. $f = 1$ for a completely degenerate gas. On the horizontal axis, energies are in units of 10 MeV .

The dip which develops in the low energy tail of the spectrum is due to the escape of low energy neutrinos which have the largest mean free path. The high energy tail is fed by the relativistic compression of neutrinos near the Fermi surface. The initial infall velocity is about $\beta = 0.2$ in the outer core.

The probability of occupation $f(r, t, \epsilon)$ is given for different positions and times on Figs. 4a-c). The low energy part of the spectrum is steadily depleted because:

- i) low energy neutrinos have the largest mean free path,
- ii) down scattering has been ignored, according to the Lorentz gas approximation.

Collisions of neutrinos near the Fermi surface with relativistic nuclei feed the high energy tail of the spectrum with an efficiency increasing with the value of β , and so with the radius r . As a consequence of the homology of the collapse, the local Fermi energy evolves irrespective of the location and is inversely proportional to the radius of the star.

Neutrino production and absorption.

As already stated, the emission and the absorption of neutrinos are treated in the simulation as source or sink terms which operate along any neutrino elementary path of the characteristic network^(4),5),6),7).

Inelastic collisions.

The thermalisation of the neutrino gas is partly due to scattering on electrons. Fig. 5) shows the thermalisation of an initially fully degenerate ($T = 0$) neutrino gas, with a $\epsilon_F = 10 \text{ MeV}$ Fermi energy, interacting with a Maxwellian thermal bath of light particles ($m = m_e$) at a constant temperature ($T = 20 \text{ MeV}$) and density $n = 10^{33} \text{ cm}^{-3}$, which corresponds to $Y_e = 0.42$ for $\rho = 4 \cdot 10^9 \text{ g cm}^{-3}$.

In this example, both neutrino flow and thermalisation are mediated by inelastic scattering upon light particles.

Neutrinos are at first scattered out the Fermi surface while their temperature, initially zero, gradually increases and settles up to 20 MeV . At that time, due to the leakage of neutrinos, their chemical potential is about $\mu_F = -50 \text{ MeV}$ and constantly decreases.

During the relaxation phase, the energy neutrino spectrum can never be approximated, even crudely, by a Fermi-Dirac statistics.

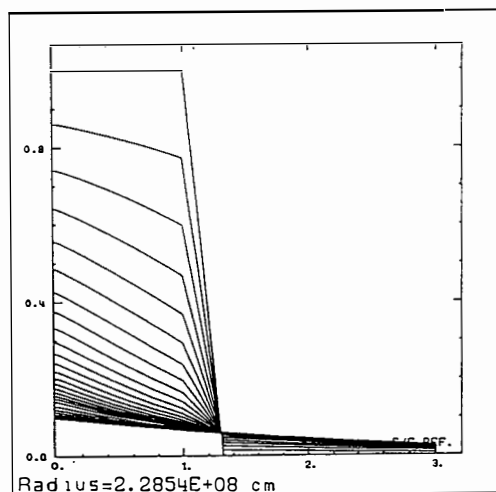


Fig. 5: Thermalisation of a neutrino zero temperature Fermi gas by a 20 MeV Maxwellian gas of light particles.

The method outlined in this paper allows the accurate calculation of neutrino production, absorption and transport during any phase of a Type II supernova explosion. The energy and momentum transfer from neutrinos to the supernova matter is a direct outcome of the calculation, as well as the emission spectra of all neutrino species.

ACKNOWLEDGEMENTS

This work is part of a Thesis by Ph. Mellor (Paris, 1988). It has been undertaken as part of the *PICS* no 18 "Nuclear Astrophysics" program. This is one publication of our group which includes J.L. Basdevant, P. Blottiau, J.P. Chièze and Ph. Mellor.

REFERENCES

- 1) Bethe, H.A. and Wilson, J.R. : 1985, *Astrophys. J.* **295**, 14
- 2) Arnett, W.D. : 1977, *Astrophys. J.* **218**, 815
- 3) Bowers, R.B. and Wilson, J.R. : 1982a, *Astrophys. J. Suppl.* **50**, 115
- 4) Bruenn, S. : 1985, *Astrophys. J. Suppl.* **58**, 771
- 5) Mellor, Ph., Chièze, J.P., and Basdevant, J.L. : 1988, *Astron. Astrophys.* **197**, 123
- 6) Fuller, G.M., Fowler, W.A. and Newman, M.J. : 1985, *Astrophys. J.* **293**, 1
- 7) Tubbs, D.L. and Schramm, D.N. : 1975, *Astrophys. J.* **201**, 467

THEORETICAL MECHANISMS FOR TYPE II EXPLOSION DYNAMICSS. A. Bludman¹Department of Physics, University of Pennsylvania
Philadelphia, PA. 19104
USA**ABSTRACT**

The prompt and delayed mechanisms for Type II supernova explosions are explained. Even with a low mass iron core ($1.17M_{\odot}$), a soft nuclear equation of state $K_0 (N = Z) = 180$ MeV, an underestimated free proton fraction ($W_s = 36$ MeV) and general relativity hydrodynamics, the prompt shock mechanism fails. This happens because, in a realistic description of neutrino transport, neutrino-electron downscattering leads to so much neutrino leakage ($Y_{LJ} \leq 0.37$) that the shock forms so far inside the iron core, that it cannot traverse the large overlay mass, without being arrested by nuclear dissociation and neutrino radiation. To see whether the stalled shock may later be revived on the neutrino diffusion time scale, we developed an implicit general relativistic Lagrangian hydrodynamics on polar-sliced time. This assures maximal coordinate singularity avoidance and maximal coverage of material zones.

¹Partially supported by DOE contract EY-76-D-02-3071

I. PROBLEMS WITH THE PROMPT EXPLOSION MECHANISM

A. Shock Formation in Stellar Collapse. Type II supernovae derive their energy from the gravitational collapse of the iron cores of massive ($> 12M_{\odot}$) single stars with the ultimate release of $\geq (1 - 3) \times 10^{53}$ ergs. Until nuclear densities are reached, these iron nuclei become moderately neutronized by electron capture ($e^{-} + p \rightarrow \nu_e + n$), the lepton fraction decreasing from $Y_{ei} = 0.41 - 0.42$ to $Y_{Lf} = 0.36 - 0.39$, but do not dissociate appreciably. Consequently, the average entropy per baryon increases only moderately, until the nearly adiabatic and homologous collapse of the inner core is suddenly stopped at some transnuclear density $\rho_b \sim 9 \times 10^{14}$ g cm $^{-3}$. When the ordered infall kinetic energy is suddenly thermalized, a shock wave forms at the edge of homology M_{HC} . The energy of this standing shock derives originally from the compressional energy of the compressed nuclear matter. The initial shock energy will be a maximum, therefore, if neutron-rich nuclear matter is relatively compressible at high density (small incompressibility $K_o(N=2Z)$), and if the bounce takes place at high density (general relativistic collapse nearly down to the event horizon for black hole formation).

The standing shock is fed by the continued accretion and thermalization of fast-infalling matter and begins to propagate outwards. While traversing the mass $M_{\bullet VER} = M_{Fe} - M_{HC} = 0.4 - 0.6M_{\odot}$ between the edge of homology and the edge of the iron core, the shock is dampened by neutrino radiation E_{ν}^{rad} and by dissociating iron nuclei. In order to reach the edge of the iron core and eject matter with sufficient kinetic energy ($\sim 10^{51}$ ergs) to form an optical supernova in the stellar envelope, it is therefore necessary that: (1) Neutron-rich nuclear matter have a comparatively low incompressibility K_o at high density; (2) The infall deleptonization $\Delta Y_L = Y_{ei} - Y_{Lf}$ be small so that the edge of homology which, in non-relativistic approximation, lies at $M_{HC} = 1.04M_{Fe}(Y_{e_f}^{\frac{4}{3}} + 2^{\frac{1}{3}}Y_{\nu_f}^{\frac{4}{3}})^{\frac{3}{2}}/Y_{ei}$, be far out; (3) The initial iron core mass M_{Fe} be small so that the overlay mass $M_{\bullet VER}$ be small.

B. Nuclear Equation of State. In order to see whether a prompt explosion could be obtained from stellar collapse under the apparently most favorable stellar conditions, Myra and Bludman (MB) ^(2,3) studied the relativistic collapse of a 1.17 M_{\odot} iron core ⁽⁴⁾, assuming the low value $K_o(N=Z) = 180$ MeV for symmetric nuclear matter corresponding to $K_o(N=2Z) = 140$ MeV for neutron-rich nuclear matter. Both these assumptions may indeed be overly optimistic: Interpretations⁽⁵⁾ of the Supernova 1987A light curve show that it came from a progenitor star of main sequence mass 15-20 M_{\odot} and iron core mass 1.3-1.4 M_{\odot} . Recent determinations of the incompressibility of symmetric nuclear matter, derived from giant monopole measurements, show⁽⁶⁾ $K_o(N=Z) = 290 \pm 20$ MeV, by the same Groningen group that had earlier reported $K_o = 210 \pm 30$ MeV. Glendenning⁽⁷⁾ has adduced other arguments for $K_o \sim 300$ MeV, from nuclear masses and radii, from heavy-ion flow measurements, and from neutron star masses. Nevertheless, in order to compare with Baron et al. (BBBCK) ⁽⁸⁾ who had reported strong $(1 - 2) \times 10^{51}$ ergs prompt explosions, we joined them in these two optimistic assumptions and in using the Cooperstein⁽⁹⁾ nuclear equations of state, with the Baron-Cooperstein-Kahana (BCK)⁽¹⁰⁾ extrapolation to densities above saturation density ρ_o .

$(N=2Z) = 2.4 \times 10^{14} \text{ g cm}^{-3}$, $P = (K_o \rho_o / 9\gamma)[(\rho/\rho_o)^\gamma - 1]$, $\gamma = 2.5$. The Cooperstein equation of state also contains a bulk-symmetry coefficient W_S , which directly controls the difference between neutron and proton chemical potentials and, therefore, the free proton fraction and the infall deleptonization ΔY_L . Cooperstein's code treats W_S as a free parameter, without compensating any change from $W_S = 31.5 \text{ MeV}$ in its calculation of the surface symmetry energy, so that for $W_S > 31.5 \text{ MeV}$, the proton fraction is underestimated.

C. Neutrino Radiation Hydrodynamics. The collapse of an iron core to a cold remnant neutron star releases $(3 - 5) \times 10^{53}$ ergs of gravitational binding energy, of which only 1% needs to be transferred to matter at the edge of the iron core in order to make a Type II supernova explosion. This makes the copious neutrino flux easy to estimate, but leaves the small neutrino-matter energy exchange as a delicate problem in neutrino radiation hydrodynamics. The neutrino neutral current scattering off nucleons and nuclei is almost energy conserving, while emission-absorption by charged currents and neutrino-electron scattering by charged and neutral currents (NES) thermalizes the neutrinos by exchanging energy with nucleons and electrons.

The crucial weak, energy-dependent neutrino-matter coupling transpires in a density regime where the neutrino transport is neither simply diffusive nor simply ballistic. Various approximations to the neutrino transport have been used: (1) BCK and BBCK describe the neutrino transport by a simple leakage scheme tuned to give average neutrino trapping at $1.0 \times 10^{12} \text{ g cm}^{-3}$; (2) MB use a multi-energy group flux-limited diffusion approximation including neutrino-electron scattering (NES) in a modified Focker-Planck approximation⁽¹¹⁾; (3) Bruenn⁽¹²⁾ applies a spherical harmonic approximation to the Boltzman transport equation.

None of these approximations is completely satisfactory in describing the delicate neutrino-matter coupling responsible for deleptonization during the infall and for shock wave damping and possible matter ejection after bounce. Our multi-group flux-limited diffusion approximation is only approximately generally relativistic and becomes inaccurate in the low density regime where delayed shock revival is supposed to take place. Our Focker-Planck approximation to NES, adapted from Bowers and Wilson⁽¹³⁾, gives accurate values for the trapped lepton number, but may underestimate the energy transfer from downscattering neutrinos to matter. Nevertheless, our transport and Bruenn's transport contain more physics than the BCK-BBCK leakage scheme, which neglects NES and the energy-dependence of neutrino trapping.

D. Generally Relativistic Explicit Hydrodynamics in Comoving Synchronous Gauge. All calculations of spherical collapse use Lagrangian hydrodynamics in which the coordinates comove locally with the matter. This (1) allows the matter equations to be directly integrated into conservation laws for energy, momentum, entropy and baryon number along matter trajectories; (2) Gives maximal matter coverage, because the comoving mass zones are concentrated where the matter is, not wasted where matter is absent or exceptionally diffuse. Of course, at shocks where the matter flow is discontinuous, Lagrangian coordinates become discontinuous.

These discontinuities are numerically smoothed out by introducing artificial viscosity.

In the prompt shock calculations we report^(2,3), we used explicit hydrodynamics, in which numerical stability requires that the difference equations advance by time steps smaller than the Courant time for a sound wave to traverse a mass zone. We also used (May-White) “synchronous” comoving space-time coordinates, which become singular as soon as any mass zone reaches a general relativity trapped surface.

E. Results. Table 1 presents BBBCK’s and our results, using the same equation of state ($K_o(N = Z) = 180 \text{ MeV}$; $\gamma = 2.5$, except in model 82) and general relativistic hydrodynamics, and similar low mass initial iron core configurations. BBBCK omit electron capture on nuclei and NES and treat neutrino transport by their leakage scheme, tuned to give average trapping at $1.0 \times 10^{12} \text{ g cm}^{-3}$. We treat neutrino transport by multi-group flux-limited diffusion approximation, including NES in Model 80 and nuclear capture in Model 79. In order to approximate the BBBCK trapping algorithm, we omit NES in our Models 77, 79, 81, 82 and omit electron capture on nuclei in Models 77, 81, 82. Except for BBBCK’s Models 59, 63, $W_s = 36 \text{ MeV}$, so that the free proton fraction and the amount of infall deleptonization is underestimated.

F. Conclusions. (1) The fate of the prompt shock is already determined by the trapped lepton fraction Y_{Lf} at bounce: For $Y_{Lf} > 0.37$, the edge of homology where the shock forms is far out, the overlay mass is small, and a prompt explosion is obtained. For $Y_{Lf} \leq 0.37$, either because of NES (Model 80) or because of a more reasonable higher proton fraction (Models 59), the prompt shock stalls; (2) The infall deleptonization down to Y_{Lf} depends, of course, on NES downscatter (present only in our model 80) and on the number of free protons capable of capturing electrons (underestimated in all but Models 59, 63). The Hashimoto-Nomoto presupernova configuration was given to us at a time when the electron-baryon ratio $Y_{ec} = 0.41$ at the center, so that electron capture by nuclei is already suppressed by neutron shell blockage over the bulk of the inner core: consequently our models 79 and 77, with and without nuclear capture, give identical results; (3) A soft nuclear equation of state with general relativity hydrodynamics does create an initially energetic shock wave: For $\gamma = 2.5$, nuclear bounce took place at $\rho_b \sim 9 \times 10^{14} \text{ g cm}^{-3}$; when we softened to $\gamma = 2$, bounce took place at $\rho_b = 14 \times 10^{14} \text{ g cm}^{-3}$ and, absent NES, a more energetic explosion took place; (4) If, to best approximate BBBCK (Model 62), we omit NES from our neutrino transport (Model 77), we can obtain strong explosions of 2×10^{51} ergs, as do BBBCK. When NES is properly included, however, we find (Model 80), even underestimating the free proton fraction, $Y_{Lf} = 0.37$ and a stalled shock; (5) NES is fatal to the prompt shock because it leads to infall deleptonization down to $Y_{Lf} = 0.37$. (Because our Focker-Planck approximation may underestimate neutrino downscatter in energy, NES may be even more harmful than we calculated.) After-bounce deleptonization down to $Y_L \leq 0.1$ is principally caused by enhanced electron capture in shock heated matter and not by NES downscatter. If we artificially stopped electron capture when Y_L reduced to 0.2, then, absent NES, we obtained a stronger shock. (6) The neutrino

Model	W_s (MeV)	Y_{LF} (10^{14} gm^{-3})	ρ_b (10^{51} erg)	E_{SH} (10^{51} erg)	E_{rad}^{V51} (10^{51} erg)	Y_{LF} (10^{14} gm^{-3})	ρ_b (10^{51} erg)	E_{SH} (10^{51} erg)	E_{rad}^{V51} (10^{51} erg)	Special Physics
59	29.3	0.365	9.8	0.0	0.0	Myra - Bludman Models: M G F L D A				Most free protons
63	34.0	0.375	9.8	1.4	4.6	$\underbrace{\hspace{10em}}$ Nuclear capture $Y_e > 0.2$				More free protons
62/77	36.0	0.385	9.8	2.1	2.1					
79	36.0	B B B C K Models								
81	36.0	Leakage Scheme				0.40	8.9	2.8	3.6	Soften to $Y = 2$ NES included
82	36.0	0.40	14	2.3	3.4					
80	36.0	0.37	8.0	0.0	4.0					

Table 1. General relativistic collapse of a low-mass iron core with Cooperstein-BCK equation of state. Baron et al. (left side) approximate neutrino transport by leakage scheme tuned to average trapping density $1.0 \times 10^{14} \text{ gm}^{-3}$. Myra and Bludman (right side) use multigroup flux-limited diffusion approximation. The free proton fraction is fixed by $W_s = 36 \text{ Mev}$ in all but Models 59, 63. Neutrino electron scattering is neglected in all but Model 80. The prompt shock stalls whenever $Y_{LF} < 0.37$ because of electron capture on free protons or neutrino-electron downscatter.

radiation loss is always about $(3.6-4.0) \times 10^{51}$ ergs in our calculations, irrespective of the success or failure of the prompt explosion. Neutrino loss history is therefore a poor diagnostic of explosion dynamics.

Even with a low mass iron core ($1.17M_{\odot}$), a soft nuclear equation of state K_0 ($N = Z$) = 180 MeV, an underestimated free proton fraction ($W_S = 36$ MeV), and general relativity hydrodynamics, the prompt shock mechanism fails. This happens because, in a realistic description of neutrino transport, neutrino-electron downscattering leads to so much neutrino leakage ($Y_{L_f} \leq 0.37$) that the shock forms so far inside the iron core, that it cannot traverse the large overlay mass, without being arrested by nuclear dissociation and neutrino radiation.

II. PROSPECTS FOR LATER REVIVAL OF THE STALLED SHOCK

A. Implicit Hydrodynamics. If the shock stalls on the hydrodynamic time scale (tens of milliseconds), it may⁽¹⁴⁾ still be revived by mass accretion and neutrino diffusive heating on a time scale (seconds) for neutrinos of all flavors to diffuse out of the hot core. In order to economically follow the core evolution through this quasistatic stage of shock revival and later neutrino cooling, we must take much longer numerical time steps than the Courant time step allowed in explicit hydrodynamics.

Schinder⁽¹⁵⁾ has written a May-White general relativity hydrodynamic code in which the equations are differenced implicitly(GRIMP). An implicit code is always numerically stable, but escapes the Courant time step restriction at the cost of solving a set of non-linear equations self-consistently at each time step. Because these large matrices of differential coefficients are anyway inverted numerically, we have followed Richard Bowers and Tom Oliphant at Los Alamos National Laboratory, in also calculating the many differential coefficients numerically.

B. Improved General Relativity: Polar Slicing of Space-Time. Almost all previous general relativistic hydrodynamic calculations have used the comoving "synchronous" coordinates of May and White, in which the radial coordinate is the areal radius $R = (area/4\pi)^{1/2}$. These coordinates become singular everywhere as soon as a horizon is reached anywhere. We want to study stellar core collapses right up to black hole formation, because these produce initial shocks of maximum energy. Besides collapses into remnant neutron stars, we also want to consider protracted collapses into a black hole, where the infalling matter lingers just outside the horizon, before relatively slowly accreting enough mass to be drawn across the horizon. If the lingering is protracted enough, before being swallowed up by the black hole, we expect some neutrino radiation to escape to infinity. Neutrino-signalled stellar collapses may therefore be more frequent than neutron-star formation.

For these reasons, we have also shifted from the Schwarzschild areal radius coordinate R to a new comoving polar-sliced coordinate $r(R, t)$ by the coordinate shift $dR = R' dr + \dot{R} dt = R'(dr + \beta' dt)$, where $' = \partial/\partial t, \dot{t} = \partial/\partial r$. In the two gauges

$$ds^2 = -\alpha^2 dt^2 + (dR/\Gamma)^2 + R^2 d\Omega^2 = -(\alpha^2 - \beta_r \beta^r) dt^2 + 2\beta_r dr dt + (R'/\Gamma)^2 dr^2 + R^2(r, t) d\Omega^2$$

Both space-time coordinates are polar-sliced, meaning that the trace of the transverse part of the intrinsic curvature of the space-like surfaces vanishes. Schwarzschild coordinates are not co-moving but are Gaussian normal, meaning that the slicings (space-like surfaces $t = \text{constant}$) are everywhere normal to the velocity field of Eulerian observers. In our new comoving polar-sliced gauge, from one slicing to the next, the constant coordinate lines are shifted from the normal by $\dot{R}dt = \alpha U dt$, depending on the material velocity U as well as the lapse α . The lapse vanishes exponentially near the apparent horizon (outermost trapped surface) so that evolution freezes near the apparent horizon while continuing elsewhere, until as $t \rightarrow \infty$, matter everywhere reaches the apparent horizon. Our polar-sliced coordinates therefore avoid coordinate singularities while allowing maximum coverage of the domain of outer communication outside of the trapped surfaces. Because they are comoving, these coordinates also allow maximum coverage of material zones.

Our polar-sliced comoving adiabatic hydrodynamic code (GRIPOS) has passed several critical tests⁽¹⁵⁾ and has been generalized by Schinder⁽¹⁷⁾ to include neutrino radiation transport. Even if black holes form ultimately, we are ready to pursue spherical stellar collapse for many time steps. We hope that the prompt shock that stalled in hydrodynamic time scales ultimately revives on the diffusive time scale.

References

1. K. A. Van Riper, *Ap. J.* **232**, 558 (1979); **326**, 235 (1988); K. A. Van Riper, and W. D. Arnett, *Ap. J. (Letters)* **225**, L129 (1978).
2. G. S. Myra and S. A. Bludman, Neutrino Transport and the Prompt Mechanism for Type II Supernovae, UPR-0352T, submitted to *Ap. J.*
3. S. A. Bludman, *Phys. Reports* (1988), in press.
4. M. Hashimoto and K. Nomoto, *Physics Reports* (1988), in press.
5. W. D. Arnett, *Ap. J.* **319**, 136 (1987); T. Shigeyama, K. Nomoto and M. Hashimoto, *Astr. Ap.* (1987); S. E. Woosley, P. A. Pinto and L. Ensmann, *Ap. J.* **324**, 466 (1988).
6. M. M. Sharma, W. T. A. Borghols, S. Brandenberg, S. Crona, J. H. Meier, A. van der Woode and M. N. Harakek (preprint KVI-689, Groningen).
7. N. K. Glendenning, *Phys. Rev. C* (1988).
8. E. A. Baron, H. A. Bethe, G. E. Brown, J. Cooperstein and S. Kahana, *Phys. Rev. Lett.* **59**, 736 (1987).
9. J. Cooperstein, *Nucl. Phys.* **A429**, 527 (1985).
10. E. A. Baron, J. Cooperstein, and S. Kahana, *Phys. Rev. Letters* **55**, 126 (1985); *Nucl. Phys.* **A440**, 744 (1985).

11. E. S. Myra, S. A. Bludman, Y. Hoffman, I. Lichtenstadt, N. Sack and K. A. Van Riper, *Ap. J.* **318**, 744 (1987).
12. S. W. Bruenn, *Ap. J. Suppl.* **58**, 771 (1985); *Ap. J.* **62**, 331 (1986), private communication (1988).
13. R. L. Bowers and J. R. Wilson, *Ap. J. Suppl.* **50**, 115 (1982).
14. J. R. Wilson in Numerical Astrophysics, ed. J. Centrella, J. LeBlanc and R. Bowers (Jones and Bartlett, Boston, 1985); H. A. Bethe and J. R. Wilson, *Ap. J.* **295**, 14 (1985).
15. P. J. Schinder, S. A. Bludman and T. Piran, *Phys. Rev.* **D37**, 2722 (1988).
16. S. A. Bludman and P. J. Schinder, Theoretical Significance of Detecting Neutrinos from Supernova 1987A, UPR-0326T; *Ap. J.* **326**, 265 (1988).
17. P. J. Schinder, General Relativistic Radiation Hydrodynamics and Neutrino Transport in Polar Sliced Space-Time, UPR-0351T, submitted to *Phys. Rev. D*.

AUTHOR INDEX

ALCOCK C.R.	303, 319	MARIS H.J.	75
ASHMAN K.M.	141	MARTIN F.	413
ATHANASSOULA E.	231	MATARRESE S.	211
AUDOUBE J.	277	MATHEWS G.J.	251, 303, 319
BARR S.M.	389	MAUROGORDATO S.	199
BENNETT D.P.	361	MELISSINOS A.C.	113
BIENAYMÉ O.	239	MELOTT A.L.	373
BLUDMAN S.A.	461, 487	MOSKOWITZ B.	113
BOUCHET F.R.	205, 361	NEMIROFF R.J.	355
BOUQUET A.	413	NEZRICK F.	113
CALDWELL D.O.	55	NOTTALE L.	339
CARR B.J.	141	OLIVE K.A.	33, 329
CHIEZE J.P.	477	ORLOFF J.	381
COLAFRANCESCO S.	211	PELLEGRINI P.S.	151
COWAN J.J.	251	PERRET-GALLIX D.	85, 95
CRANE P.	171	PIRAN T.	381, 453
CRÉZÉ M.	239	PRODELL A.	113
DA COSTA L.N.	151	REEVES H.	287
DADO S.	429	REPHAELI Y.	123
DALY R.A.	133	RICH J.	43
DAR A.	429	RICHSTONE D.O.	419
DE PANFILIS S.	113	ROBIN A.C.	239
DEKEL A.	355	ROGERS J.	113
DELBOURGO-SALVADOR P.	277	SADOLET B.	55, 63
EISBERG R.M.	55	SALATI P.	277, 403, 413
ENGLERT F.	381	SASLAW W.C.	171
FOWLER W.	113	SCHAEFFER R.	177, 471
FULLER G.M.	303, 319	SCHINDER P.J.	461
GELMINI G.	393	SCHRAMM D.N.	251
GONZALEZ-MESTRES L.	85, 95	SEIDEL G.M.	75
GOULDING F.S.	55	SEMERTZIDIS Y.	113
GRUMM D.M.	55	SILK J.	3
HALAMA H.	113	SMITH A.R.	55
HAYWOOD J.W.	261	SMOOT G.	123
HEGYI D.J.	261	SPERGEL D.N.	419, 453
KAJINO T.	319	TARTAGLIA M.A.	105
KAPLAN J.	413	THUAN T.X.	161
KRAUSS L.M.	23	TURNER E.L.	347
KUNTH D.	219	VAN DER VELDE J.	429
LACHIÈZE-REY M.	187, 199	VAUCLAIR S.	269
LANOU R.E.	75	WITHERELL M.S.	55
LUCCHIN F.	211	WUENSCH W.	113

LIST OF PARTICIPANTS

ALEXEIEV A.	Moscow, USSR
AMRAM Philippe	Obs. Marseille, France
ASHMAN Keith	Queen Mary Coll., London, UK
ATHANASSOULA Evangelina	Obs. Marseille, France
AUDOUZE Jean	Inst. Astrophys., Paris, France
BARR Stephen	Bartol Res. Inst., Newark, USA
BLOTIAU Patrick	CEA, Villeneuve st Georges, France
BLUDMAN Sidney	Pennsylvania Univ., Philadelphia, USA
BOSMA Albert	Obs. Marseille, France
BOUCHET Francois	California Univ., Berkeley, USA
BOUQUET Alain	LAPP, Annecy, France
BRACCESI Alessandro	Osserv. Astron., Bologna, Italy
CALDWELL David	California Univ., Santa Barbara, USA
CARTER Brandon	Obs. Meudon, France
CASPER David	Boston Univ., USA
CESARSKY Catherine	Astrophys., Saclay, France
CHAPELLIER Maurice	Phys. Solides, Orsay, France
CHARDIN Gabriel	DPhE, Saclay, France
CHIEZE Jean-Pierre	CEA, Bruyères le Châtel, France
COLAFRANCESCO Sergio	Padova Univ., Italy
COOPER Susan	MIT, Cambridge, USA
CORON Noel	LPSP, Verrieres, France
CRANE Philippe	ESO, Garching, FRG
DA COSTA Luiz	Observ. Nacional, Rio de Janeiro, Brasil
DALY Ruth	IOA, Cambridge, UK
DAR Arnon	Haifa, Israel
DE BERNARDIS Paolo	La Sapienza Univ., Roma, Italy
DEKEL Avishai	Hebrew Univ., Jerusalem, Israel
DE RUJULA Alvaro	CERN, Geneva, Switzerland
FOCARDI Paola	Bologna Univ., Italy
FULLER George	Livermore Nat. Lab., USA
GELMINI Graciela	ICTP/ISAS, Trieste, Italy
GONZALES-MESTRES Luis	LAPP, Annecy, France
HEGYI Dennis	Michigan Univ., Ann Arbor, USA
JABIOL Marie-Antoinette	DPhPE, Saclay, France
JAUNEAU Louis	LAL, Orsay, France
KAPLAN Jean	Phys. Theorique, Paris Univ., France
KRAUSS Lawrence	Yale Univ., New Haven, USA

KUNTH Daniel
 KUZNIK Bernd
 LACHIEZE-REY Marc
 LANOU Robert
 LLOYD OWEN David
 MASI Silvia
 MATHEWS Grant
 MAUROGORDATO Sophie
 MELCHIORRI Francesco
 MELLOR Phillip
 MELOTT Adrian
 MORIN Stephane
 MOSCA Luigi
 MOSCOSO Luciano
 NEMIROFF Robert
 NOTTALE Laurent
 OLIVE Keith
 ORLOFF Jean
 PERRET-GALLIX Denis
 PILKHUN Hartmut
 PIRAN Tsvi
 REEVES Hubert
 RENZINI Alvio
 REPHAELI Yoel
 RICH James
 ROBIN Annie
 RONNBACK Jari
 SADOULET Bernard
 SALATI Pierre
 SCHAEFFER Richard
 SCHUHL Alain
 SILK Joseph
 SIROUSSE-ZIA Haydeh
 SPERGEL David
 SYGNET Jean-Francois
 TAKITA Masato
 TARLE Gregory
 TARTAGLIA Michael
 TRIAY Roland
 TRIN XUAN Thuan
 TURNER Edwin
 VAN DER VELDE Jack
 VAUCLAIR Sylvie
 WUENSCH Walter

Inst. Astrophys., Paris, France
 Wuppertal, FRG
 Astrophys., Saclay, France
 Brown Univ., Providence, USA
 LAL, Orsay, France
 La Sapienza Univ., Roma, Italy
 Livermore Nat. Lab., USA
 Astrophys., Saclay, France
 La Sapienza Univ., Roma, Italy
 CEA, Villeneuve St Georges, France
 Kansas Univ., Lawrence, USA
 Obs. Marseille, France
 DPhPE, Saclay, France
 DPhPE, Saclay, France
 Hebrew Univ., Jerusalem, Israel
 Obs. Meudon, France
 Minnesota Univ., Minneapolis, USA
 Univ. Libre, Bruxelles, Belgium
 LAPP, Annecy, France
 Karlsruhe Univ., FRG
 Hebrew Univ., Jerusalem, Israel
 Astrophys., Saclay, France
 Bologna Univ., Italy
 Tel Aviv Univ., Israel
 DphPE, Saclay, France
 Obs. Besancon, France
 Obs. Uppsala, Sweden
 California Univ., Berkeley, USA
 California Univ., Berkeley, USA
 Phys. Theorique, Saclay, France
 Phys. Solides, Orsay, France
 California Univ., Berkeley, USA
 Inst. H. Poincare, Paris, France
 Inst. for Adv. Study, Princeton, USA
 Inst. Astrophys., Paris, France
 Tokyo, Japan
 Michigan Univ., Ann Arbor, USA
 Michigan State Univ. East Lansing, USA
 Phys. Theorique, Marseille, France
 Inst. Astrophys., Paris, France
 Princeton Univ., USA
 Ann Arbor, USA
 Obs. Toulouse, France
 Rochester Univ., New York, USA